Synthesis of Novel Polysiloxanes and Silsesquioxanes with High Refractive Index by Utilizing Alkoxysilane Precursors with Polycyclic Aromatic Substituents

Dissertation

zur Erlangung des Grades

des Doktors der Naturwissenschaften

der Naturwissenschaftlich-Technischen Fakultät

der Universität des Saarlandes

von

Max Florian Briesenick

Saarbrücken

2025

Tag des Kolloquiums: 02.10.2025

Dekan: Prof. Dr.-Ing. Dirk Bähre

Berichterstatter: Prof. Dr. Guido Kickelbick

Prof. Dr.-Ing. Markus Gallei

Akad. Mitglied: Dr. Carsten Präsang

Vorsitz: Prof. Dr. Marc Schneider

Die vorliegende Arbeit wurde in der Zeit von September 2018 bis Mai 2022 an der Universität des Saarlandes im Institut für anorganische Festkörperchemie im Arbeitskreis von Prof. Dr. Guido Kickelbick angefertigt.

"Failure is simply the opportunity to begin again, this time more intelligently."

Henry Ford

Danksagung

Ich möchte mich bei allen bedanken, die mich während meiner Doktorarbeit begleitet haben und mir stets mit Rat und Tat zur Seite standen.

Zuerst möchte ich mich bei Prof. Dr. Guido Kickelbick für die Möglichkeit bedanken, die Doktorarbeit in seiner Arbeitsgruppe anfertigen zu können. Des Weiteren möchte ich mich für seine wissenschaftliche Unterstützung, sowie die zahlreichen Gespräche bedanken, bei denen nicht nur Probleme angesprochen werden konnten, sondern die oftmals zu neuen Ideen führten. Besondere Erwähnung soll hier auch finden, dass mir stets die Freiheit gegeben wurde, meine eigenen Ideen zu verfolgen und meine Arbeit in die von mir gewünschte Richtung zu lenken.

Des Weiteren möchte ich mich bei Prof. Dr. Gerhard Wenz bedanken, der sich selbst kurz vor seiner Rente, noch zu meiner wissenschaftlichen Begleitung bereit erklärt hat.

In diesem Zusammenhang gilt mein besonderer Dank Prof. Dr.-Ing. Markus Gallei, der meine wissenschaftliche Begleitung im Anschluss übernommen hat. Ebenso möchte ich ihm für die Begutachtung meiner Publikation und dieser Arbeit danken.

Nicht zuletzt möchte ich der ganzen Arbeitsgruppe für das großartige Arbeitsklima danken, welches mehr als einmal dabei geholfen hat die steten Herausforderungen einer Doktorarbeit zu meistern und auch Rückschläge teils mit Humor zu nehmen. Ich möchte mich ebenfalls für die interessanten Gespräche und die Bereitschaft bedanken mir immer bei jeder Art von Problem zu Helfen. Besonders bedanken möchte ich mich bei Dr. Nils Steinbrück für die Einarbeitung in das Thema meiner Doktorarbeit. Ebenfalls besonders danken möchte ich Svenja Pohl, die auf Grund eines sehr ähnlichen Forschungsgebiets stets die ideale Ansprechpartnerin war, immer ein offenes Ohr hatte und meine Probleme sowie gelegentliche Frustration wohl besser als viele andere nachvollziehen konnte.

Ich möchte zudem Stefan Blank für seine Hilfe bei der Reparatur der Messgeräte und seine teils kreativen Problemlösungen danken, die die Lebenszeit von so manchem Gerät verlängert haben. Ebenfalls bedanken möchte ich mich bei Sylvia Beetz, die nicht nur unsere Pumpen wartet, sondern auch mehr als einmal diverse Bauteile für mich hergestellt hat und mir hierbei stets mit Rat und Tat zur Seite gestanden hat.

Abschließend möchte ich mich bei meiner Familie bedanken, die es mir überhaupt erst ermöglicht hat zu studieren und mich bei meiner Doktorarbeit zu jeder Zeit und ohne Druck unterstützt hat.

List of Publications

High-Refractive-Index Polysiloxanes Containing Naphthyl and Phenanthrenyl Groups and Their Thermally Cross-Linked Resins.

Briesenick, M.; Gallei, M.; Kickelbick, G. *Macromolecules* **2022**, 55, 4675-4691. https://doi.org/10.1021/acs.macromol.2c00265

Synthesis and Hydrogen-Bond Patterns of Aryl-Group Substituted Silanediols and -triols from Alkoxy- and Chlorosilanes.

Kannengießer, J.-F.; Briesenick, M.; Meier, D.; Huch, V.; Morgenstern, B.; Kickelbick, G. *Chem. Eur. J.* **2021**, *27*, 16461-16476.

https://doi.org/10.1002/chem.202102729

Multi-Pulse Agglomeration Effects on Ultrashort Pulsed Direct Laser Interference Patterning of Cu.

Müller, D. W.; Lößlein, S.; Pauly, C.; Briesenick, M.; Kickelbick, G.; Mücklich, F. *Appl. Surf. Sci.* **2023**, *611*, 155538.

https://doi.org/10.1016/j.apsusc.2022.155538

Single-Step Production of Photocatalytic Surfaces via Direct Laser Interference Patterning of Titanium.

Fox, T.; Delfino, P. M.; Cortés, F.; Pauly, C.; Müller, D. W.; Briesenick, M.; Kickelbick, G.; Mücklich, F. *ChemNanoMat* **2023**, 9, e202300314. https://doi.org/10.1002/cnma.202300314

Rapid Synthesis of a Green Emitting Phosphor by Sulfidation of Intermetallic EuAl₂ and Its Use in a Hybrid Material.

Gießelmann, E. C. J.; Engel, S.; Pohl, S.; Briesenick, M.; Rüthing, L. P.; Kloos, C.; Koldemir, A.; Schumacher, L.; Wiethölter, J.; Schmedt auf der Günne, J.; Kickelbick, G.; Janka, O. *Chem. Mater.* **2025**, *37*, 97–108.

https://doi.org/10.1021/acs.chemmater.4c02093

Zusammenfassung

Silikone finden zunehmend Anwendung in optischen Materialien, wie zum Beispiel als Verkapselungsmaterial für Leuchtdioden (LEDs) oder als Kontaktlinsen in Form von Silikon-Hydrogel. Trotz einer hohen Transparenz, sowie exzellenter chemischer und thermischer Stabilität limitiert ein niedriger Brechungsindex ihre Anwendung. Im ersten Teil der vorliegenden Dissertation wurden daher neuartige polycyclische aromatische Dialkoxysilane verwendet, um deren Einfluss auf den Brechungsindex der mittels Hydrolyse und Kondensation erhaltenen Silikonharze zu untersuchen. Hierbei konnte eine deutliche Erhöhung des Brechungsindex, hohe thermische Stabilität und Transparenz, jedoch auch ein Verflüssigen bei hohen Temperaturen beobachtet werden. Im zweiten Teil dieser Arbeit wurde daher das zuvor erfolgversprechendste Silikonharz auf verschiedene Arten nachvernetzt. Das bei zwei Silikonen auf diese Art deutlich besser ins Netzwerk eingebaute polycyclische Dialkoxysilan verhindert ein Verflüssigen bei hohen Temperaturen und ermöglicht somit einen Einsatz Hochtemperaturanwendungen. Zuletzt wurden sogenannte "polyhedral oligomeric silsesquioxanes" (POSS) mit den bereits zuvor verwendeten polycyclischen aromatischen Gruppen mittels Tetrabutylammoniumfluorid (TBAF) oder KOH hergestellt. Bei allen Ansätzen konnten POSS-Systeme erhalten, jedoch nur der T₈-POSS mit 1-Naphthylgruppen an allen Ecken rein hergestellt und mittels Kristallstruktur bestätigt werden.

Abstract

Silicones are becoming increasingly popular in optical materials, for example as encapsulation material for light-emitting diodes (LEDs) or as contact lenses in the form of silicone hydrogel. Despite their high transparency and excellent chemical and thermal stability, a low refractive index limits their application. In the first part of this dissertation, novel polycyclic aromatic dialkoxysilanes were therefore used to investigate their influence on the refractive index of silicone resins obtained by hydrolysis and condensation. A significant increase in the refractive index, high thermal stability and transparency, but also liquefaction at high temperatures were observed. In the second part of this work, the previously most promising silicone resin was therefore post-crosslinked in various ways. The polycyclic dialkoxysilane, which is now much better integrated into the network in two of the silicones, prevents liquefaction at high temperatures and thus enables use in high-temperature applications. Finally, so-called 'polyhedral oligomeric silsesquioxanes' (POSS) containing the previously used polycyclic aromatic groups were prepared using tetrabutylammonium fluoride (TBAF) or KOH. POSS systems could be obtained in all approaches, but only the T₈-POSS with 1-naphthyl groups at all corners could be produced purely and was confirmed by means of crystal structure.

List of Abbreviations

ATR Attenuated Total Reflectance

BCF Tris(pentafluorophenyl)borane ($B(C_6F_5)_3$)

CP-MAS NMR Cross Polarization-Magic Angle Spinning Nuclear Magnetic Resonance

 D_4 Octamethylcyclotetrasiloxane

D₅ Decamethylcyclopentasiloxane

DBTA Di-*n*-Butyltin Diacetate

DBTDL Dibutyltin dilaurate

DCM Dichloromethane

DMA Dynamic Mechanical Analysis

DMDMS Dimethyldimethoxysilane

DMSO Dimethyl Sulfoxide

DOC Degree of Condensation

DPDMS Diphenyldimethoxysilane

DSC Differential Scanning Calorimetry

ECHA European Chemicals Agency

EN Electronegativity

FTIR Fourier Transform Infrared

HPLC High-Performance Liquid Chromatography

HMPA Hexamethylphosphoramide

HOTf Trifluoromethanesulfonic acid

HRI High Refractive Index

HTPDMS Hydroxyl-Terminated Polydimethylsiloxane

IR Infrared

LED Light-Emitting Diode

LEE Light Extraction Efficiency

LM Loss Modulus

LPS Ladder-Like Polysiloxanes

MALDI - FTICR Matrix-Assisted Laser Desorption/Ionization - Fourier-Transform Ion

Cyclotron Resonance

MALDI-TOF Matrix-Assisted Laser Desorption/Ionization - Time of Flight

MAS NMR Magic Angle Spinning Nuclear Magnetic Resonance

MG Melting Gel

NMR Nuclear Magnetic Resonance

OLED Organic Light-Emitting Diode

OPS Octaphenylsilsesquioxane

PDMS Polydimethylsiloxane

PhMG Polyphenylsilsesquioxane Melting Gel

PMPS Polymethyl Phenyl Siloxane

PNMs Polymer Nanostructured Materials

POSS Polyhedral Oligomeric Silsesquioxane

PS Polystyrene

PTMS Phenyltrimethoxysilane

PXRD Powder X-ray Diffraction

Refractive Index RI

ROP Ring Opening Polymerization

Room Temperature Vulcanizing RTV

SEAC Committee for Socio-Economic Analysis

SEC Size Exclusion Chromatography

SM Storage modulus

SVHCs Substances of Very High Concern

TBAF Tetrabutylammonium Fluoride

TEOS Tetraethoxysilane

Glass transition temperature T_{g} **TGA**

Thermogravimetric Analysis

TG-FTIR Thermogravimetric-Fourier Transform Infrared

THF Tetrahydrofuran

TIR **Total Internal Reflection**

TMOS Tetramethoxysilane

TP Tubular Polysiloxane

UV-vis Ultraviolet-Visible

YAG:Ce Cerium-Doped Yttrium Aluminum Garnet

ΥI Yellowness Index

Table of Contents

1	The	oret	ical Background	1
	1.1	Ge	neral Overview of Silicones	1
	1.2	Bin	ding Theory and Characteristics in Silicones	3
	1.3	Syr	nthesis of Monomers	5
	1.3.	1	Organochlorosilanes	5
	1.3.	2	Alkoxysilanes	6
	1.3.	3	Grignard Reaction	8
	1.4	Syr	nthesis of Silicones via Hydrolysis and Condensation	10
	1.5	Diff	ferent Types of Silicones	14
	1.5.	1	Linear Siloxanes	15
	1.5.	2	Cyclic Siloxanes	17
	1.6	Cro	oss-Linking and Coupling Reactions	18
	1.6.	1	Mizoroki-Heck Reaction	18
	1.6.	2	Piers-Rubinsztajn Reaction	19
	1.6.	3	Hydrosilylation	21
	1.7	Sils	sesquioxanes	23
	1.7.	1	Caged Structures	23
	1.7.	2	Ladder-Like Structures	26
	1.8	Me	lting Gels	29
	1.9	Cha	aracterization and Property Analysis of Silicones	31
	1.9.	1	Structural Analysis and Characterization	31
	1.9.	2	Thermal Properties and Characterization	36
	1.9.	.3	Optical Properties and Characterization	36
	1.9.	4	Refractive Index (RI)	37

2	Aims an	d Scope of this Work41			
3	Results	and Discussion45			
	3.1 High	h-Refractive-Index Polysiloxanes Containing Naphthyl and Phenanthrenyl			
	Groups an	d their Thermally Cross-Linked Resins45			
	3.1.1	Abstract			
	3.1.2	Introduction			
	3.1.3	Results and Discussion			
	3.1.4	Experimental Section			
	3.1.5	Conclusions			
	3.2 Pos	t-Cross-Linking of Siloxane/Silsesquioxane Mixtures Containing Polycyclic			
	Aromatic (Groups to Modify their Softening Behavior for Usage in High-Temperature			
	Application	าร 81			
	3.2.1	Abstract81			
	3.2.2	Introduction			
	3.2.3	Results and Discussion			
	3.2.4	Experimental Section			
	3.2.5	Conclusions			
	3.3 Syn	thesis of Polyhedral Oligomeric Silsesquioxanes (POSS) Containing			
Polycyclic Aryl Groups					
	3.3.1	Abstract111			
	3.3.2	Introduction111			
	3.3.3	Results and Discussion			
	3.3.4	Experimental Section			
	3.3.5	Conclusions143			
4	Conclus	ions and Outlook145			
5	Reference	ces149			
6	Supporti	Supporting Information			

6.1 I	High-Refractive-Index Polysiloxanes Containing Naphthyl and Phenanthrenyl				
Groups	and their Thermally Cross-Linked Resins189				
6.1.1	Dialkoxysilanes189				
6.1.2	Polysiloxanes/Silsesquioxanes200				
6.2 I	Post-Cross-Linking of Siloxane/Silsesquioxane Mixtures Containing Polycyclic				
Aromat	ic Groups to Modify their Softening Behavior for Usage in High-Temperature				
Applications					
6.2.1	Synthesis of Dimethoxyphenyl-(1-naphthyl)silane231				
6.2.2	Differential Scanning Calorimetry (DSC)232				
6.2.3	Thermal Treatment Experiment				
6.2.4	Dynamic Mechanical Analysis (DMA)234				
6.2.5	Nuclear Magnetic Resonance (NMR) Spectroscopy236				
6.2.6	Fourier Transform Infrared (FTIR) Spectroscopy248				
6.2.7	Powder X-ray Diffraction (PXRD)249				
6.2.8	Ultraviolet-visible (UV-vis) Spectroscopy250				
6.3	Synthesis of Polyhedral Oligomeric Silsesquioxanes (POSS) Containing				
Polycyclic Aryl Groups					
6.3.1	Trialkoxysilanes252				
622	Sileogguiovanos				

1 Theoretical Background

1.1 General Overview of Silicones

Siloxanes are also known by the term "silicone" which was introduced by Frederick S. Kipping at the beginning of the 20th century.¹ In 1904 he prepared organosilicon compounds by using the Grignard reaction and discovered that the condensation of silanols leads to siloxanes and polysiloxanes. He thought of these substances as carbon analogues or "silicones" doubting they would play a major part in future developments due to their limited variety and inertness. In addition, he did not assign great importance to the investigation of silanols due to their low stability.² In the 1930s James F. Hyde produced silicone resins for impregnating and coating glass building on Kipping's work.³,4

In 1941 and 1942, Eugene Rochow⁵ and Richard Müller⁶ independently developed a method for the production of methylchlorosilanes in the United States and Germany, respectively. These methylchlorosilanes are the starting compounds for silicone synthesis.⁷

For a long time it was an exclusively American industry and only started to flourish in Germany and England after the second world war.⁸ The growing interest in this field can best be seen in the increasing demand for siloxane products over the years as more than 150.000 applications had been registered until 2015.⁷ The amount of siloxanes produced rose from 2 million tons to 7.4 million tons between 2002 and 2017 with only a slight decline in 2019 to 6.75 million tons.⁹⁻¹¹ Large manufacturers of siloxanes for example include Wacker Chemie (Germany), Dow Corning (USA), Shin-Etsu Chemical (Japan), Evonik Industries (Germany), and many more.⁷

Siloxanes are widely used by adults, children, and infants as about 50% of skin care products contain at least one type of silicone. Since they differ in particle size, molecular weight, shape and physico-chemical properties, there is a discussion on their effect on safety and risk of application. Therefore, the Committee for Socio-economic Analysis (SEAC) of the European Chemicals Agency (ECHA) agreed to various restrictions regarding the use of octamethylcyclotetrasiloxane (D_4) and decamethylcyclopentasiloxane (D_5) in 2016 as well as adding those substances to the list of Substances of Very High Concern (SVHCs) in 2018.

Silicones are used in optoelectronic and optical applications, for example, due to their high flexibility, good film-forming ability and optical transparency. These include organic light emitting diodes (OLEDs), organic photovoltaic devices and elastic optoelectronic devices, as they are required for biomedical, mountable and wearable applications. Linear silicones such as polydimethylsiloxane (PDMS) show high optical transparency and a homogeneous morphology, while cross-linked systems display high elongation at break, tensile strength and Young's modulus.¹²

Their flexibility, elasticity and high biocompatibility also make them interesting for optical fibre coatings, ¹³ while their low viscosity, stress-relieving properties and heat resistance are useful in light guides. ¹⁴ Other applications include lenses, ¹⁵ optical fibres, ¹⁶ optical diffusers, ¹⁷ optical adhesives ¹⁸ and optical sensors. ¹⁹

1.2 Binding Theory and Characteristics in Silicones

Silicones are hybrid organic-inorganic polymers with a backbone of alternating silicon and oxygen atoms and can be linear or branched (**Figure 1**).²⁰ Their widespread use is due to their positive characteristics like thermal stability, electronically inertness, high dielectric constants and low toxicity,²¹ as well as their chemical stability, flexibility, self-healing abilities, high thermal insulation^{22,23} and their tensile strength which among others is related to the degree of condensation.²⁴

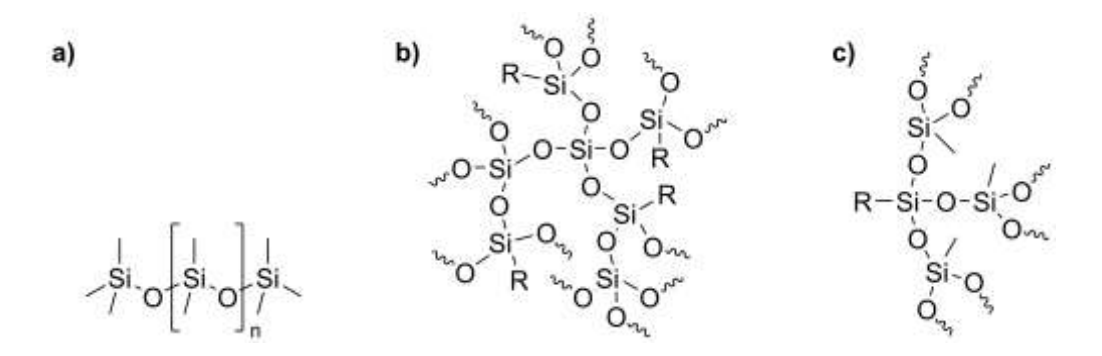


Figure 1: Different silicone structures, a) linear, b) branched, c) distinct branches.

Some of the properties of silicones can be attributed to the special characteristics of the Si-O bond. The Si-O bond length (1.64 Å) is longer than the C-C bond length (1.53 Å) which is caused by the larger atomic radius of the silicon atom (1.17 Å) compared to the carbon atom (0.77 Å). Furthermore, the bond angle of the Si-O-Si bond is wider than that of the C-O-C bond which is caused by the partial double bond character of the Si-O-Si bond compared to the sp³ hybridized C-O-C bond. A result of this larger bond angle is a lower energy barrier for the rotation of the organic groups on the silicon atom and therefore a higher flexibility of the silicone backbone. 25,26 Hydroxyl-terminated polydimethylsiloxane (HTPDMS) for example has a Si-O-Si bond angle of 143° which is much larger than the tetrahedral bond angle of 110°.27 Furthermore, the Si-O bond shows a substantial ionic character (~40 %), leading to its shortening compared to theoretical values.²⁶ The ionic character is caused by the high difference in electronegativity between the silicon atom $(EN_{Si} = 1.7)$ and the oxygen atom $(EN_O = 3.5)$ compared to the carbon atom for example $(EN_C = 2.5)$. This high polarity of the Si-O bond together with the high electron density at the oxygen atom ensures better π -backbonding of oxygen to the silicon. Furthermore, the backbonding into $\sigma^*(Si-R)$ orbitals causes a competition between electron donation towards electrophiles and Si-O bond stabilization, which lowers the basicity and also weakens the Si-C bonds. ^{26,28} In addition, the Si-O and Si-O-Si bond show a much higher bond dissociation energy (460 kJ mol⁻¹ and 422 kJ mol⁻¹) compared to the C-O bond (345 kJ mol⁻¹) which results in high thermal stability. ^{25,26} This stability can be further increased by incorporating phenyl groups, as these are not only more difficult to oxidize than methyl groups, for example, but also cause a steric hindrance that makes it more difficult to degrade the Si-O bond. ²⁹ Epoxy resins for example, which contain C-C as well as C-O bonds, show good optical transparency and low gas permeability but have low refractive indices and undergo heat-induced yellowing. Silicones on the other hand provide excellent thermal stability against said yellowing, therefore replacing epoxides for example as LED encapsulation materials. ^{30,31}

Most properties of silicones can be modified via the organic groups, such as phenyl groups for example, which are very frequently used. In polymethyl phenyl siloxane (PMPS), the amount of phenyl groups increases the dielectric constant or electrical breakdown strength and diphenyl silicone elastomers show better radiation resistance and thermal stability than dimethyl silicone elastomers. The phenyl groups increase the monomeric friction, the refractive index and, as the comparison of polydiphenyl siloxanes with polydimethyl siloxanes shows, can cause an increase in the decomposition temperature.

An important part of silicones are their functional groups at the end of the chains which determine their use as they change their characteristics. Alkyl-terminated PDMS can for example can be used as lubricant due to local changes in surface energy.³⁷ PDMS terminated with groups like hydroxy, alkoxy, hydrido and vinyl groups is called "telechelic". Telechelic hereby describes polymers which can further polymerize or undergo polymer-like reactions due to their reactive chain ends. This changes the structure of the polymer while its degree of polymerization is not changed. These end-groups originate from initiators or terminating agents, not from the used monomers. If the polymers have the same reactive groups at both chain ends, they are called homotelechelic, if they have different groups at each chain end, they are called heterotelechelic.¹¹

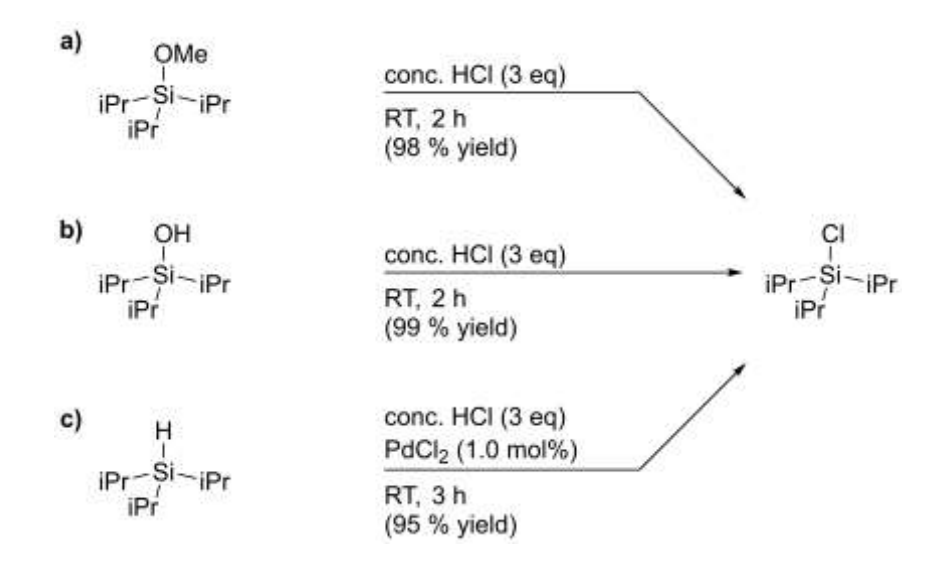
1.3 Synthesis of Monomers

1.3.1 Organochlorosilanes

Up to this day organochlorosilanes are mainly produced on an industrial scale by the already mentioned Müller–Rochow process, which was developed independently by E. Rochow^{5,38} and R. Müller⁶ in the early 1940s. In this copper catalyzed process elementary silicon is reacted with chloroalkanes in fluidized bed reactors leading mainly to hydrido-, methyl-, ethyl- and phenylchlorosilanes. When producing methylchlorosilanes by the Müller–Rochow process (**Scheme 1**) the main reaction (a) leads to dimethyldichlorosilane as the main product, as well as other methylchlorosilanes (b and c) and hydride-containing silanes (e) as side products, the latter of which are important raw materials for hydrosilylation reactions. ^{11,39,40} Furthermore, organochlorosilanes can be produced by using Grignard reactions, hydrosilylation or radical additions. ^{41–44}

Scheme 1: Müller-Rochow process for the preparation of methylchlorosilanes.

Trialkylchlorosilanes with large alkyl groups, such as isopropyl groups, can be used as protecting groups and can be prepared by chlorination of alkoxysilanes, silanols or hydrosilanes (**Scheme 2**).⁴⁵



Scheme 2: Synthesis of triisopropylchlorosilane from a) triisopropylmethoxysilane, b) triisopropylhydroxysilane, c) triisopropylsilane.

Other reactions include, for example, the synthesis of tetrachlorosilane from tetramethoxysilane by adding hydrochloric acid, acetonitrile and various catalysts such as LiCl, ZnCl₂, FeCl₃ and hexamethylphosphoramide (HMPA)⁴⁶ or the more specialized preparation of chlorosilanes from fluoroalkylsilanes.⁴⁷

If protic compounds such as water are present, organochlorosilanes can hydrolyze, which can be used to synthesize polymeric silicones with cyclic or linear structures, for example.^{48–50}

1.3.2 Alkoxysilanes

In a similar way to chlorosilanes, E. Rochow also developed a process to produce tetramethoxysilane from silicon and methanol using a copper catalyst (**Scheme 3**).^{51,52}

Scheme 3: Synthesis of tetramethoxysilane from methanol and silicon.

As in the production process for chlorosilanes, some side reactions can also occur here, some of which can lead to the formation of water and thus to hydrolysis and condensation of the previously formed products.⁵³

Another possibility for their synthesis is the conversion of chlorosilanes into alkoxysilanes using alcohols in the presence of bases such as pyridine or a tertiary amine (**Scheme 4**). This reaction can also be used to protect alcohols.⁵⁴

$$\begin{array}{c} CI \\ -Si \end{array} + ROH \xrightarrow{Et_3N} \begin{array}{c} OR \\ -Si \end{array} + HC$$

Scheme 4: Reaction of a silicon halide with an alcohol to form a Si-O bond, used to synthesize a new silane or to protect an alcohol.

Tetraalkoxysilanes can also be produced by direct syntheses starting from SiO_2 .⁵⁵ Base-catalyzed reactions with diols (**Scheme 5**, **a**),⁵⁶ alcohols (**Scheme 5**, **b**)⁵⁷ or dialkyl carbonates (**Scheme 5**, **c**) are used for this purpose.⁵⁸

 $\textbf{Scheme 5:} \ Syntheses \ of \ tetraalkoxysilanes \ from \ SiO_2 \ and \ a) \ diols, \ b), \ alcohols \ and \ c) \ dialkyl \ carbonates.$

Another method to form Si-O bonds is dehydrogenative coupling, a one-step and atom economical approach also known as dehydrogenative silylation. ^{59,60}

Furthermore, compounds that have a double bonded silicon, such as silenes and disilenes, can react with alcohols and water via a nucleophilic addition to form silanols and alkoxysilanes, respectively. 61-63

Another special case is the synthesis of alkoxysilanes using mechanochemistry, which has increased in recent years. This involves grinding silicon with alcohols and using various metals like copper (**Scheme 6**).^{64,65}

a) Si
$$\frac{ROH}{250 \text{ °C, 1 h, 7.5 g}}$$
 $\frac{OR}{RO - \text{Si-OR}} + 2 \text{ H}_2$
 $\frac{1)}{R} = \text{Me (100 \% yield)}$
b) Si + 4 ROH $\frac{Cu}{RT, 2 \text{ h}}$ $\frac{OR}{RO - \text{Si-OR}} + 2 \text{ H}_2$
 $\frac{1}{RO} = \text{RO (7 yield)}$
1) R = Me (7 yield)
2) R = Et (51 % yield)

Scheme 6: Mechanochemical synthesis of alkoxysilanes using different metals as catalysts.

1.3.3 Grignard Reaction

The Grignard reaction was discovered by Victor Grignard in 1900.^{66,67} This reaction is mainly used to form carbon-carbon bonds between an organomagnesium species, the so-called Grignard reagent, and an electrophilic substrate and can be applied to a wide variety of compounds.⁶⁷

However, the Mg/Br exchange is quite slow and therefore requires high temperatures, which are incompatible with many functional groups and can lead to unwanted by-products in the case of electron-rich aromatic bromides. A further development of the classic Grignard reaction is therefore the use of the so-called turbo Grignard reagent (*i*PrMgCl*LiCl), which accelerates the Mg/Br exchange considerably (**Scheme 7**). ^{68,69}

$$R = FI, CI, Br, CN, CO2R, OMe$$

$$MgCI*LiCI$$

$$E^{+}$$

$$R = PhCHO, PhCOCI, CIPPh2, ...$$

Scheme 7: Turbo-Grignard reaction, utilizing the increased reactivity of *i*PrMgCl*LiCl compared to magnesium. Adapted from reference [68].

By utilizing reagents of this type, it is also possible to convert chlorosilanes into other chlorosilanes using Grignard coupling and HCl (**Scheme 8**).⁴⁵

Scheme 8: Grignard coupling reaction to modify chlorosilanes.

The Grignard reaction can also be used to prepare silanes like trimethoxy-(1-naphthyl)silane (**Scheme 9**, **a**) or trichloro-(1-naphthyl)silane (**Scheme 9**, **b**) of which the former was also used in this work.^{70,71} As the silicon-chlorine bond is very reactive, chlorosilanes can easily be hydrolyzed by moisture, resulting in gaseous hydrochloric acid, which is toxic and poses a health and safety risk. As this not only decomposes alcohols, but also leads to condensation, a Lewis base must also be used as an acid scavenger.⁷²⁻⁷⁴

a)
$$\frac{\text{Mg, I}_2, \text{Et}_2\text{O}}{1. \text{ 45 min, reflux}} \qquad \frac{\text{Si}(\text{OMe})_4, \text{Et}_2\text{O}}{1. \text{ -5 to } 23 \text{ °C}} \qquad \frac{\text{Si}(\text{OMe})_4, \text{Et}_2\text{O}}{1. \text{ -5 to } 23 \text{ °C}} \qquad \frac{\text{MgBr}}{2. \text{ RT, over night}} \qquad \frac{\text{MeO}^{-\text{Si}} - \text{OMe}}{\text{MeO}}$$
b)
$$\frac{\text{Mg, I}_2, \text{THF}}{\Delta} \qquad \frac{\text{SiCI}_4, \text{THF}}{1. \text{ RT}} \qquad \frac{\text{SiCI}_4, \text{THF}}{2. \text{ RT, over night}} \qquad \frac{\text{CI}^{-\text{Si}} - \text{CI}}{\text{CI}} \qquad \frac{\text{CI}^{-\text{CI}} - \text{CI}}{\text{CI}} \qquad \frac{\text{CI}$$

Scheme 9: Synthesis of a) trimethoxy-(1-naphthyl)silane and b) trichloro-(1-naphthyl)silane using a Grignard reaction.

In addition to the example just shown, numerous other alkoxy- and chlorosilanes were produced utilizing Grignard reactions (**Figure 2**).^{70,75–77}

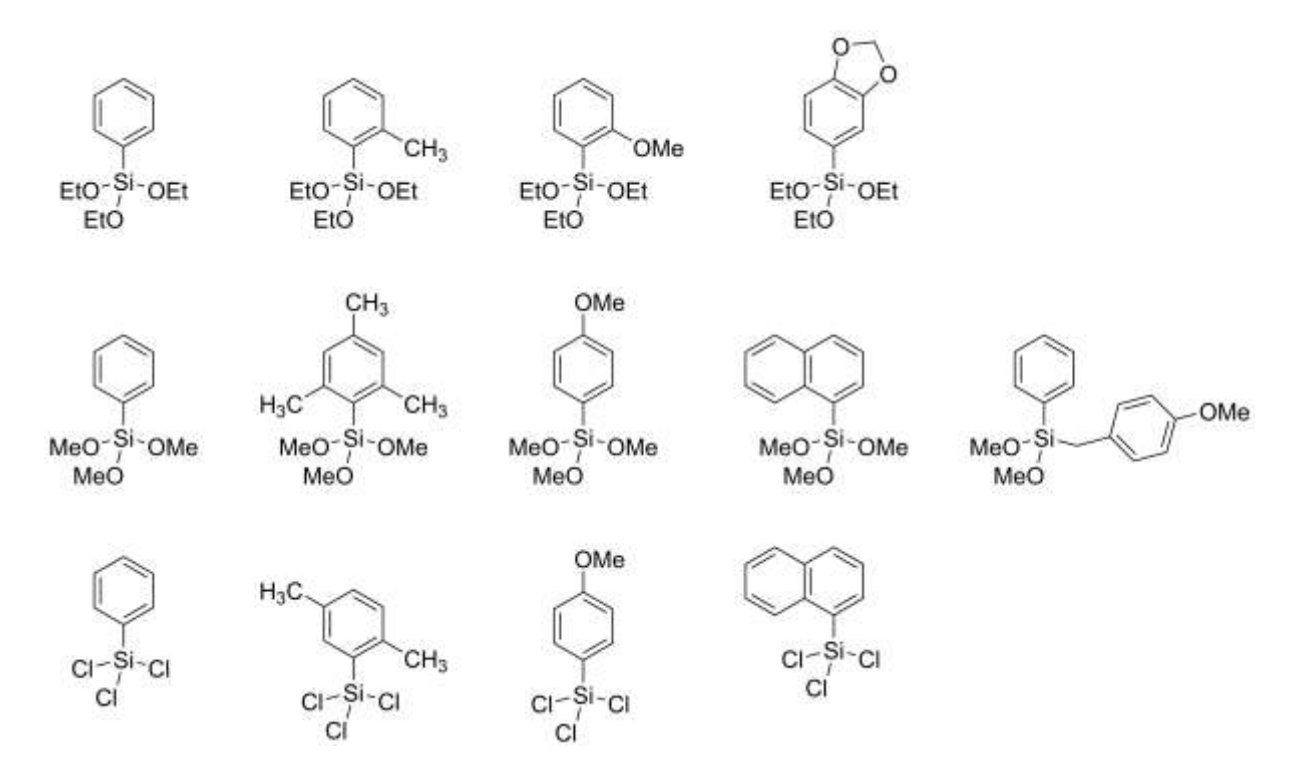


Figure 2: Exemplary structures of alkoxysilanes and chlorosilanes.

1.4 Synthesis of Silicones via Hydrolysis and Condensation

Silicones are usually produced from chlorosilanes or alkoxysilanes by means of a polycondensation reaction. As they are used in this work, the hydrolysis and condensation of alkoxysilanes, which can be acid- or base-catalyzed, is discussed in more detail below. In both acid-catalyzed reactions (**Scheme 10**, **a**), the alkoxy group (hydrolysis) or hydroxyl group (condensation) is first protonated, followed by a nucleophilic attack by water or another silanol. Hydrolysis hereby produces a silanol, while condensation results in a Si-O-Si bond. In the base-catalyzed reaction (**Scheme 10**, **b**), a nucleophilic attack of OH⁻ (hydrolysis) or Si-O⁻ (condensation) takes place with the formation of a 5-fold coordinated intermediate with subsequent elimination of OH⁻ or OR⁻. The relative reaction rates of both reactions are pH dependent. For example, while hydrolysis for Si(OR)₄ is slowest at approx. pH 7, this is the case for the condensation reaction at approx. pH 4.5. ^{78,79}

Scheme 10: Synthesis of silicones via hydrolysis and condensation, a) acid catalyzed, b) base catalyzed.

The silanols produced during hydrolysis can react with alkoxysilanes, which is why hydrolysis and condensation cannot be separated from each other.⁸⁰ The reaction rate of the alkoxy group herby is determined by the chain length of the alkoxide, decreasing with longer chains.81 Furthermore, the ratio of alkoxysilane, water and the corresponding alcohol influences the behavior of the solutions. 82,83 If an acid catalyst is used, the first

hydrolysis will increase the difficulty of any subsequent hydrolysis at the same silicon atom favoring linear silicones while a base catalyst facilitates the subsequent hydrolysis on the same silicon atom leading to branched structures. Herthermore, the substituents on the silicon atom also play an important role. In an acid catalyzed reaction, the nucleophilic attack of water on the silicon atom is the rate determining step which occurs via an SN₂ mechanism. Here, silicon compounds with methyl instead of methoxy groups react faster, as these have a +I-effect. The opposite is true for basic catalysis, where a high electron density reduces the reaction rate. When different groups are compared in this process, those with less steric hindrance react faster. He same silicon

Hydrolysis and condensation can be observed by liquid NMR, as has been done for example with tetraethoxysilane (TEOS) using ¹H NMR (**Figure 3**). ⁸⁸ The methylene moiety of the ethoxy group causes a quartet which shifts slightly downfield because of the hydrolysis and even further depending on the degree of condensation as it was observed for methyltrimethoxysilane. ⁸⁹ The Si-OH moiety of the silanol formed during the hydrolysis can be difficult to detect because of their fast exchange with water or a quickly occurring condensation. In this case the decreasing methoxy signal of the alkoxysilane or the corresponding alcohol which is formed can be studied. ⁹⁰ It is also possible to detect monohydrolyzed or higher hydrolyzed species. Nevertheless, it is still possible to see and integrate the Si-OH signals if, for example, a condensation of silanols is carried out without solvent. ⁹¹

Furthermore, it is possible to see and quantify the organic groups present on the silicon atom in addition to the alkoxy groups. The former can be used to determine the composition of the final polymer, ⁹² while the latter is suitable for obtaining an impression of the progress of the hydrolysis. ^{93,94}

Another commonly used application for ¹H NMR spectroscopy is the reaction control of hydrosilylation reactions. The quantification of the hydrogen atoms and vinyl groups used for cross-linking allows a statement on how far the reaction has progressed. ^{95–98}

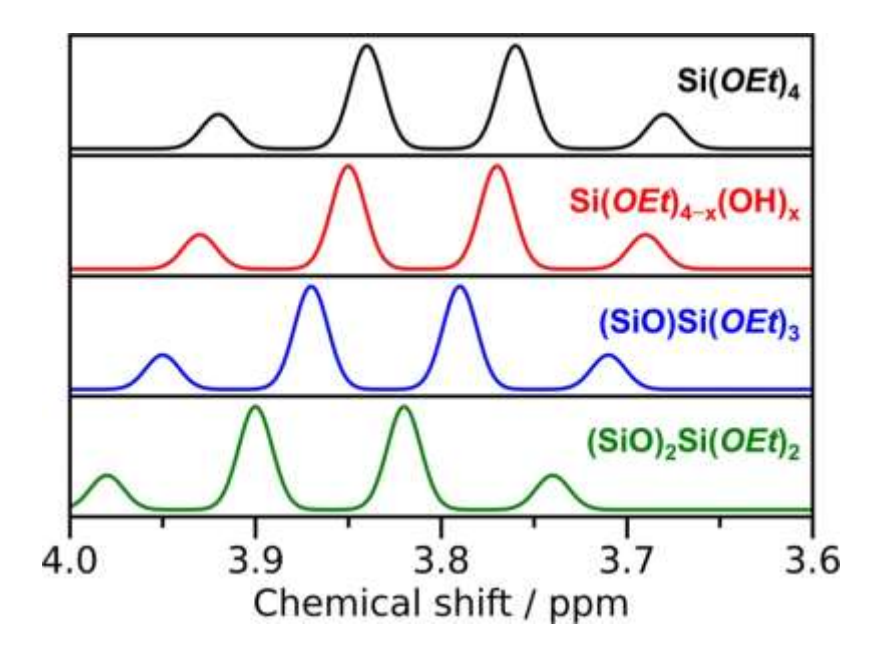


Figure 3: ¹H NMR of the methylene moiety of the ethoxy group during hydrolysis and condensation of TEOS. Reproduced with permission from Springer Nature.⁹⁹

1.5 Different Types of Silicones

The hydrolysis and polycondensation of di-, tri- and tetrafunctional silanes leads to the formation of three-dimensional silicones and silsesquioxanes which include linear, cyclic, and ladder-like structures, as well as cages and partial cages (**Figure 4**) and influence the characteristics of the final polymer.^{28,100}

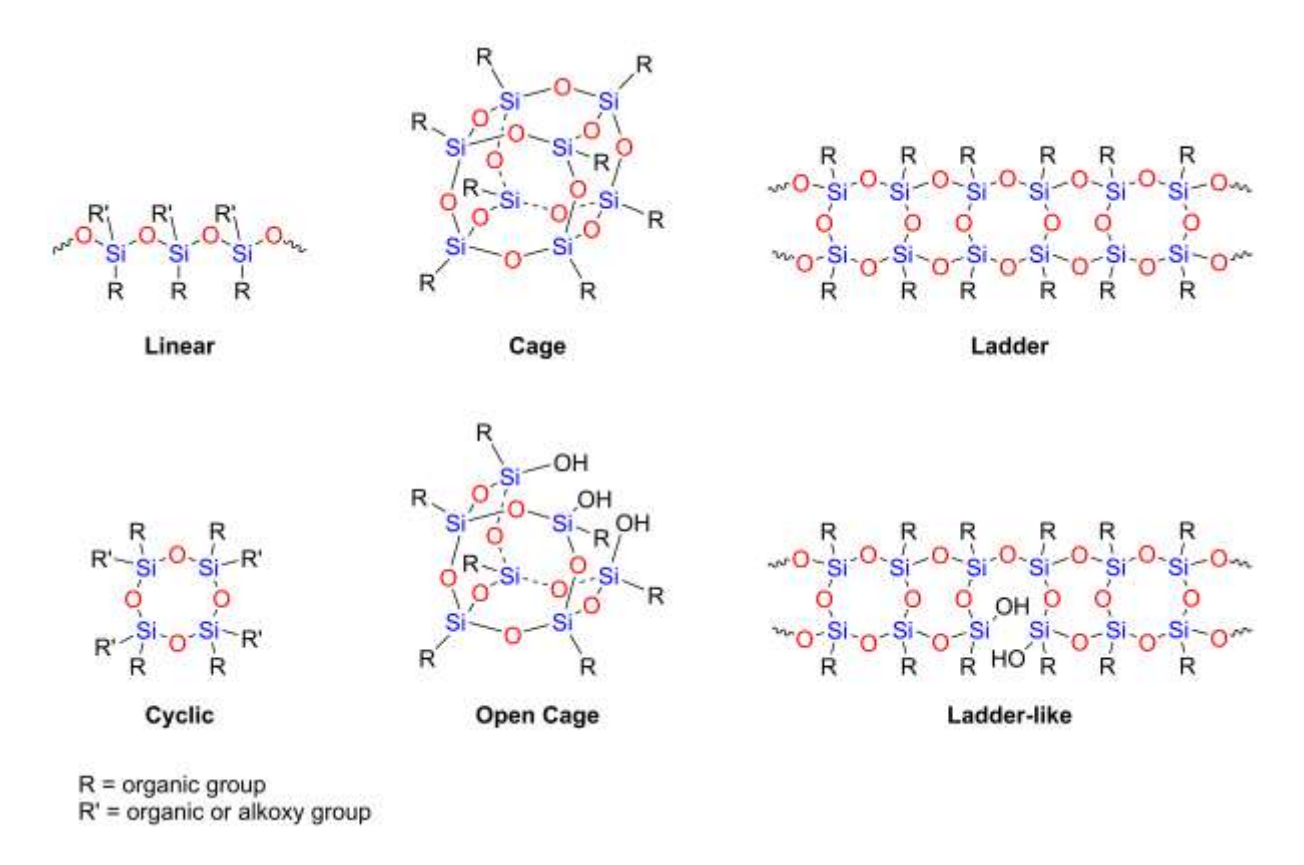


Figure 4: Possible structures of silicones after polycondensation of di-, tri- and tetrafunctional silanes. Adapted from reference [99].

In general, silicones can be found in many different applications which include antifoaming agents, lubricants, cosmetics, and coatings,¹⁰¹ as well as in the construction sector, medicine and electronics.^{102,103} They can also be used in insulating materials, spreading agents, implants, adhesives, sealants and in drug delivery systems.^{104–107} Other possible applications include protective coatings,^{108,109} microelectronics,¹¹⁰ lithography,¹¹¹ photoimaging¹¹² and nanotechnology.^{113,114}

A more detailed insight into properties, applications and syntheses is provided below for the individual structure types.

1.5.1 Linear Siloxanes

Linear siloxanes consist of chains in which oxygen atoms and silicon atoms alternate. In addition, two organic residues are attached to each silicon atom and three to the terminals (**Figure 5**).

$$R = \text{organic groups}$$

Figure 5: Exemplary representation of a linear siloxane.

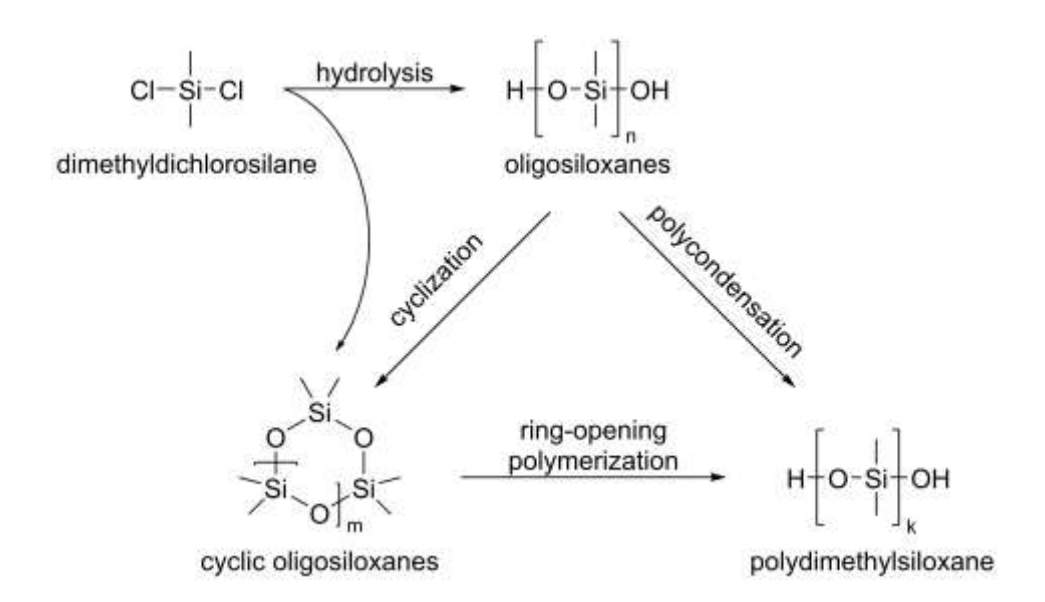
They have many interesting properties and are therefore used in a wide range of products. Linear siloxanes are characterized by only small changes in their viscosity and elastic modulus over a wide temperature range. Copolymers of dimethylsiloxanes and siloxanes with large groups show excellent fluidity at low temperatures and do not crystallize but stiffen and become hard glasses. Furthermore, dimethylpolysiloxanes exhibit high thermal stability, which makes them suitable for use at high temperatures of up to 250 °C. Linear siloxanes also have high oxidation resistance, low surface tension and interfacial tension. Their water-repellent properties are used as films on metals, ceramics and textiles. They can also be used for insulation, as dielectric materials or lubricants in the form of silicone fluids and rubbers. 115 The high flexibility and low surface energy of polydimethylsiloxanes for example stems from the low steric hindrance of the methyl groups on the silicon atoms of the siloxane backbone which also make them adhesive. Therefore, they are used as carrier or coating material for flexible electronics, biomedical devices or soft robotics. 116 Poly(dimethyl diphenyl siloxanes) on the other hand can be used as adhesives for high temperature service, lubricants or as packing material for chromatographic columns due to their thermal stability.³⁶

1.5.1.1 Synthesis

The partial ionic character of the Si-O bond can be used to synthesize and modify silicones by so-called "equilibration" or "redistribution" reactions in the presence of acids or bases.^{11,26} Many processes have been established and are still developed to

obtain linear siloxanes in the industry. ^{117–120} The properties of linear siloxanes can also be manipulated easily by changing the functional units resulting in a wide selection of linear polysiloxane-based hosts. An example is the attachment of carbazole or triphenylamine units showing good overall performance. ^{121–123}

Hydroxy-terminated PDMS, for example, can be synthesized by hydrolysis and condensation reactions of organochlorosilanes or by ring opening polymerization (ROP) of cyclic polyorganosiloxanes (**Scheme 11**). The former is not well controlled and leads to siloxanes with broad polydispersity while the latter enables more control and therefore makes it possible to obtain siloxanes with tailored molecular weights. For this reason, it is also used in the industry and there is a variety of suitable initiators, end-capping agents, and additives. Neutralizing the basic or acidic catalyst is very important since it can lead to degradation of the polymer. 124



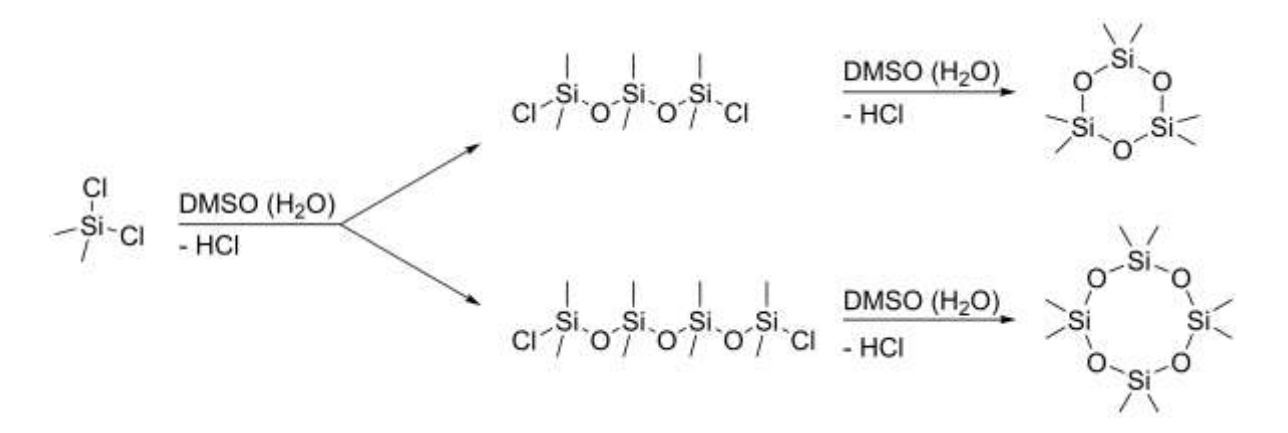
Scheme 11: Different synthesis routes for OH-terminated polydimethylsiloxane (PDMS). Adapted from reference [11].

1.5.2 Cyclic Siloxanes

Cyclic siloxanes are inert, colorless, odorless, volatile and have a soft feel. They also show thermal stability, chemical inertness and low surface tension. A wide variety of consumer products contain linear and cyclic siloxanes and thus contribute to human exposure. They can be found in electronics, furniture, cosmetics, skin lotions, hair-care products, kitchen appliances, health-care products and medical applications. 125 As they are very volatile, have a long half-life in air and a high octanol-water partition coefficient, they can be transported over long distances and accumulate in the organism. 126,127 Furthermore, studies with rats have displayed harmful effects of D_4 and D_5 and are therefore regulated in many countries. 127,128

1.5.2.1 Synthesis

The cracking of siloxane polymers at high temperatures leads to cyclic compounds while octamethylcyclotetrasiloxane (D_4) in turn serves as a starting material for the production of polymeric siloxanes. Hexamethylcyclotrisiloxane and larger cyclic siloxanes, for example, can be synthesized by hydrolysis of dichlorodimethylsilane (**Scheme 12**) in which the DMSO reacts with the produced HCl. 129



Scheme 12: Synthesis of hexamethylcyclotrisiloxane and larger siloxanes by hydrolysis of dichlorodimethylsilane.

Another example for the production of cyclic siloxanes is the synthesis of all-cistetrasiloxycyclotetrasiloxanes from trimethoxysilanes¹³⁰ or their synthesis from chlorosilanes such as dichlorosilane (**Scheme 13**).⁴⁹

CI-Si-CI DCM, H₂O RT, overnight
$$H$$
-Si O H Si -O Si -H $n = 1-6$ $n = 7-19$ in traces

Scheme 13: Synthesis of hydride containing cyclic siloxanes from the corresponding dichlorosilane.

1.6 Cross-Linking and Coupling Reactions

Reactions such as the Mizoroki-Heck reaction, the Piers-Rubinsztajn reaction or the hydrosilylation can be used to produce silane monomers as well as to form hybrids from silicones, modify existing silicones and to form new ones. The Mizoroki-Heck reaction, which tolerates for example vinyl groups and Si-OMe groups, has already been used to produce pyrene substituted octavinylsilsesquioxane and stilbenevinylsilsesquioxanes, as well as σ - π -conjugated polymers from divinyl silane and dibromo carbazole compounds. The Piers-Rubinsztajn reaction catalyzes the reaction between Si-H and alkoxy groups to form Si-O bonds without the silicones undergoing redistribution and can therefore be used for the synthesis of discrete siloxane structures such as siloxane-triarylamine hybrids. Transition-metal-catalyzed hydrosilylation, which involves the addition of an Si-H bond to a double or triple bond, is one of the most important industrial applications for the production of silane coupling agents or cross-linked silicones. 135,136

1.6.1 Mizoroki-Heck Reaction

The Mizoroki-Heck reaction is a palladium-catalyzed cross-coupling reaction between an unsaturated carbon-carbon bond (such as a vinyl group) and an aryl halide (**Scheme 14**).¹³¹

$$R = A$$
 Alkyl, alkenyl, alkynyl, aryl, alkoxyl $X = Cl$, Br, I

Scheme 14: Mizoroki-Heck Reaction.

A somewhat more specialized application is the coupling of cyclic siloxanes with each other via fluorene units (**Scheme 15**).¹³²

Scheme 15: Synthesis of a conjugated polymer using the Mizoroki-Heck reaction.

1.6.2 Piers-Rubinsztajn Reaction

The Piers-Rubinsztajn reaction can be used to produce silane monomers, which for example involves a reaction between a silicon hydride and an aryl or alkyl which contains a hydroxyl or alkoxy group (**Scheme 16**, **a**). It is catalyzed by tris(pentafluorophenyl)borane ($B(C_6F_5)_3$ or BCF) which is a strong Lewis acid (**Scheme 16**, **b**). The Piers–Rubinsztajn reaction only needs low catalyst loadings and produces no significant by-products besides gaseous hydrocarbons which must be handled with some caution. Many different silanes including small molecules and polymers can be produced with this reaction. ^{21,133,134,137} Many other chemical functionalities are tolerated by it and also alkoxysilanes will react under these conditions. ^{138,139}

b)
$$B(C_6F_5)_3 = BCF = F_5$$

Scheme 16: Piers-Rubinsztajn reaction, a) reaction, b) catalyst. Adapted from reference [21].

However, it can also be used as an end-capping reaction (**Scheme 17**, **a**), 140 to modify linear siloxanes (**Scheme 17**, **b**) 141 or to cross-link polysiloxanes (**Scheme 17**, **c**). 142

Scheme 17: Different ways to use the Piers-Rubinsztajn reaction to a) end-cap siloxanes, b) modify siloxanes and c) cross-link siloxanes.

1.6.3 Hydrosilylation

The last reaction to modify siloxanes is the hydrosilylation reaction. Here a silicon-carbon bond is formed by adding a silicon hydride (Si-H) to a carbon–carbon double bond. The formation of the product typically follows the anti-Markovnikov addition (**Scheme 18**, **a**) while the reaction itself is catalyzed by platinum-based catalysts, rhodium, nickel, and other transition metals. The two most common platinum catalysts are the Karstedt's catalyst and Speier's catalyst (**Scheme 18**, **b**). 135,143

Scheme 18: Hydrosilylation, a) reaction, b) catalysts. Adapted from reference [21].

In addition to the production of siloxane monomers, hydrosilylation can also be used to modify siloxanes on or in their backbone (**Scheme 19**). 97,144,145

Scheme 19: Hydrosilylation reaction to a) modify the siloxane backbone itself, b) modify the groups at the silicon atoms.

However, one of the main applications is the cross-linking of linear siloxanes, which can take place according to or against Markovnikov's rule, resulting in an α or β product, respectively (**Scheme 20**, **a**)¹³⁶ and can be done in various ways (**Scheme 20**, **b** and **c**). 146,147

Scheme 20: Hydrosilylation reactions to cross-link linear siloxanes.

1.7 Silsesquioxanes

1.7.1 Caged Structures

Siloxanes consisting of only trifunctional silanes can for example form caged structures which have the general formula $(RSiO_{1.5})_n$. They can have 8, 10, 12 or more silicon atoms and are categorized as T_8 , T_{10} , T_{12} and so on, respectively (**Figure 6**). 99,148,149

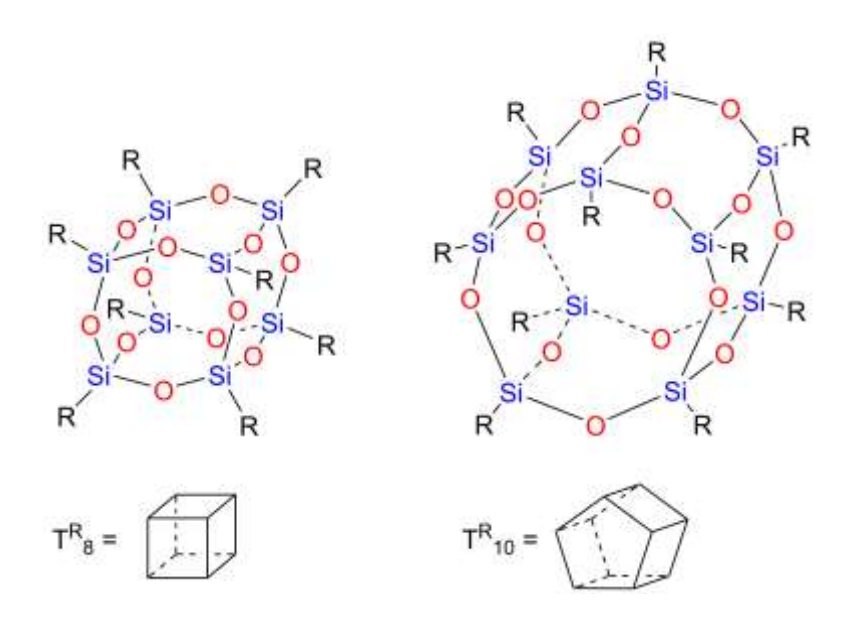


Figure 6: Exemplary structures of T_8 and T_{10} systems.

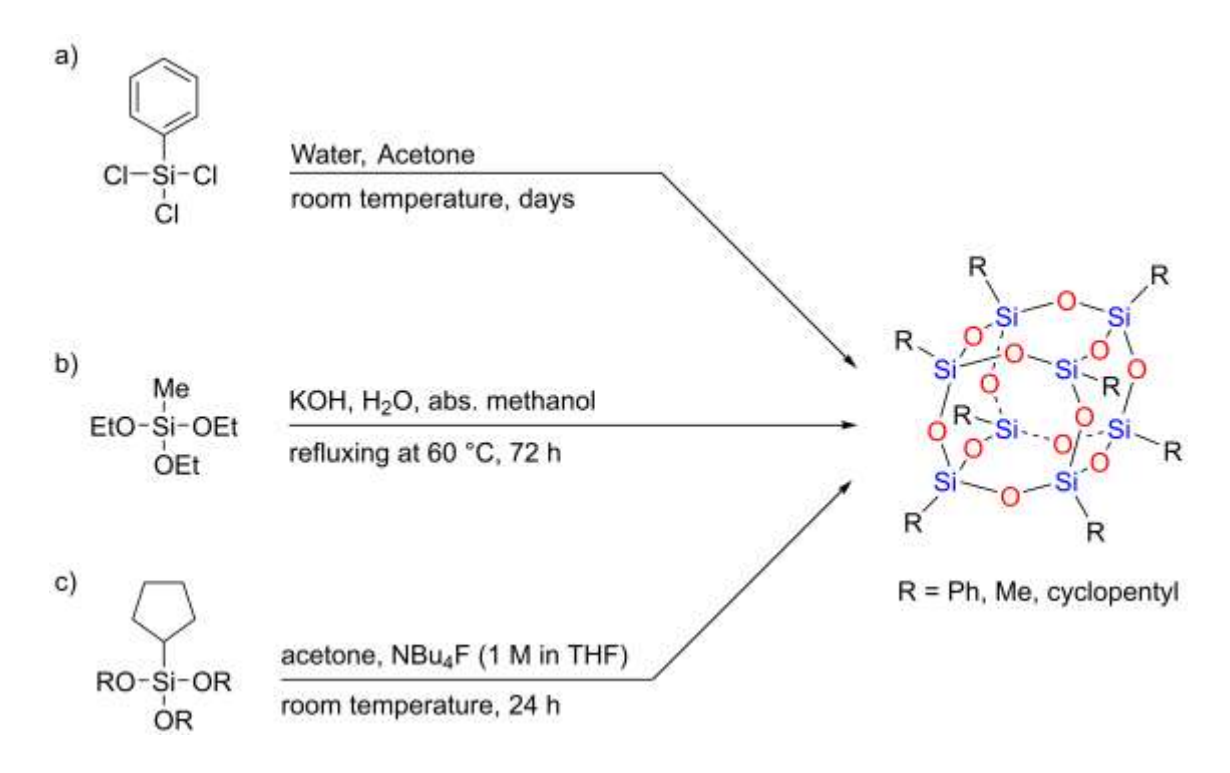
These so called polyhedral oligomeric silsesquioxanes (POSS) can be functionalized on their edges with organic groups influencing their properties, such as thermal stability or solubility. These groups can also contain carrier-transporting moieties or chromophores enabling them to combine the advantages of a small-molecule and polymer light-emitting materials. This leads to high purity and solution processability making them interesting for electrophosphorescent devices. POSS-containing polymers can also be used for LEDs due to an improved external quantum efficiency, color stability and thermal stability. They also increase excimer formation and lead to more brightness. 151-154

These cage-like silsesquioxanes can be used as hybrid materials for catalysis, biomedical devices, drug delivery systems, dental applications, nanocomposites, photoactive materials and tissue engineering scaffolds due to their antimicrobial efficacy and biocompatibility. They can be adjusted in terms of their biodegradability and can

therefore be used for various tissues. ^{50,155} POSS can also be incorporated into a polymer matrix by means of copolymerization, grafting, reactive blending or physical mixing. They form so-called polymer nanostructured materials (PNMs), which can replace traditional filled polymers or polymer compositions. Further interesting properties include thermal and oxidation stability, surface durability, non-toxicity, biostability and improved mechanical properties, which make them interesting as flame-retardants, membranes and adhesives, as well as for drug delivery systems, medical imaging techniques and photodynamic therapy. ^{156,157} Furthermore, water-soluble POSS can be used as sensors or for monitoring biological activities. ¹⁵⁸

1.7.1.1 Synthesis

POSS systems can be produced from either trichlorosilanes (**Scheme 21, a**)¹⁵⁹ or trialkoxysilanes. While the addition of acetone and water is often sufficient for trichlorosilanes, trialkoxysilanes are usually synthesized using catalysts such as KOH (**Scheme 21, b**),¹⁶⁰ TBAF (**Scheme 21, c**),¹⁶¹ trifluoromethanesulfonic acid (HOTf)¹⁶² or dibutyltin dilaurate (DBTDL).¹⁶³ A wide variety of groups such as phenyl, methyl, ethyl, vinyl, hexyl and cyclohexyl groups have already been used.¹⁶¹ The difficulty in producing these compounds is finding the right reaction conditions. While the reaction proceeds very slowly under acidic conditions and leads to poor yields, very basic reactions can lead to cleavage of the cages. Refluxing in acetone with inorganic salts can also lead to a partial rearrangement of the T₈ cages to T₁₀ or T₁₂.¹⁶⁴



Scheme 21: Synthesis routes for POSS using, a) trichlorosilanes, water and acetone, b) trialkoxysilanes and KOH, c) trialkoxysilanes and TBAF.

In addition to the symmetrical systems just mentioned, there are also non-symmetrical POSS systems in which not all corners carry the same group. These can be asymmetrically functionalized either by polycondensation of trifunctional monomers or starting from incomplete cages by means of corner capping, using phenyl, naphthyl, phenanthrenyl or pyrenyl groups, for example. 71,165

They can be further divided into functional and nonfunctional silsesquioxanes. Functional silsesquioxanes have one or more functional groups like vinyl, allyl or methacryl groups and can be prepared from trialkoxysilanes or trihalogen silanes. Nonfunctional silsesquioxanes do not possess functional groups but instead contain alkyl or aryl groups like phenylsilsesquioxane or methylsilsesquioxane.¹⁰⁰

Cage structures have been studied extensively in 29 Si NMR. T_8^R cages for example show one single signal in 29 Si solution NMR spectroscopy since every silicon atom has the same environment. When the substituent is an alkyl group the signal is at -65 to -70 ppm or it is at -77 to -83 ppm when the substituent is an aryl group. 99,148,166 The same applies to T_6^R and T_{10}^R cages. Exchanging the organic group at one corner ($T_8^{R7R'}$) typically leads to three signals with a 3:3:1 area ratio. T_{12}^R cages on the other hand have two potential isomers

with D_{2d} and D_{6h} symmetries (**Figure 7**) and therefore display two signals. ^{148,149,167} When the Si-O-Si bond angle increases, the signal in the ²⁹Si NMR shifts toward a higher magnetic field. ¹⁶⁸ Many different cages and their chemical shifts in ²⁹Si NMR have been studied. ^{162,164,168–171}



Figure 7: Structures of T_{12}^R , a) less symmetrical structure (D_{2d}), b) higher symmetrical structure (D_{6h}). Each corner represents one silicon atom, and each edge represents one oxygen atom. Adapted from reference [149].

Even though ladder-like polysilsesquioxanes, which are discussed in the following chapter, cannot be attributed to ²⁹Si NMR as well as cages they show a sharp signal which is all the sharper the more regular the structure is. Structural defects on the other hand can be seen as shoulder peaks. ^{172,173}

1.7.2 Ladder-Like Structures

Another type of structure based on trifunctional silanes are ladder-like silsesquioxanes 174 which possess the same general formula $(RSiO_{1.5})_n$ as caged structures. 175 They show excellent thermal and chemical stability, as well as high resistance to various types of degradation due to their double-chain structure. 176

The integration of ladder-like polysiloxanes (LPS) can significantly improve the performance of various materials, such as gas separation membranes, electronics, micro/nano-pattern, imprinting, photonics or LED encapsulations. Furthermore, they can be used as coatings for dental materials due to their antibacterial effects, as well as to produce various structures. These include mesomorphic LPSs and tubular polysiloxanes (TPs), which are used in liquid crystal displays or nonlinear optical materials, as well as block copolymers synthesized by using the hydroxyl groups in ladder-like polysiloxanes. 178–180

1.7.2.1 Synthesis

One way to synthesize ladder-like silsesquioxanes is to form dimers from trichlorosilanes such as $PhSiCl_3$ which subsequently form a ladder superstructure and are then condensed to a silsesquioxane (**Scheme 22**). 172

Scheme 22: Formation of a ladder-like silsesquioxane from phenyltrichlorosilane.

An example for their formation based on prefabricated building blocks is the synthesis of a pentacyclic ladder siloxane using cis-1,3,5,7-cyclotetrasiloxanetetraol (${}^{i}PrSi(OH)O)_{4}$ as a precursor (**Scheme 23**). ¹⁸¹

Scheme 23: Synthesis of pentacyclic ladder siloxane.

There are also syntheses that can yield silsesquioxanes with ladder-like, as well as caged structures. One example is the base-catalyzed hydrolysis and polycondensation reaction using phenyltrimethoxysilane (PTMS) and K_2CO_3 (**Scheme 24**). Depending on the initial PTMS concentration both structure types can be obtained.

Scheme 24: Synthesis of ladder-like and cage structured polyphenylsilsesquioxanes.

1.8 Melting Gels

Melting gels are a special form of siloxanes, which are produced from di- and trialkoxysilanes in a condensation reaction. These organically modified silica gels are rigid at room temperature, soften and flow at elevated temperatures around 110 °C and consolidate at even higher temperatures. After condensation they can be repeatedly softened at elevated temperatures, while once consolidated they are permanently rigid since their cross-linking is complete. 183,184 This is due to the fact that consolidation increases the reactivity of the retained hydroxyl groups, allowing the cross-linking to proceed to a degree where an irreversible network is formed that is permanently rigid. 184 The softening behavior was first observed by Matsuda et al. 185,186 and mislabeled as "melting", hence their name. 184 Their consolidation temperature can vary between 130 °C and 200 °C depending on the used organic groups and their composition. 183,187 Simplified, their synthesis can be done in three steps. In the first step water, HCl, alcohol and the trialkoxysilane are mixed and stirred in a closed vessel. In the second step the dialkoxysilane diluted in alcohol is added to the mixture and further stirred in the closed vessel. Lastly ammonia is added and stirred again before opening the vessel, heat treatment, washing and a second heat treatment to obtain the condensed gels which can be reversibly softened. 183,188 One of the first of these syntheses was done by Masai et al. on siloxane hybrid gels containing methyl and phenyl groups. 189

In this work a simplified version of the melting gel synthesis was applied by using only hydrochloric acid. The addition of the base to neutralize the hydrochloric acid is no longer carried out, which saves the washing step at the end. Furthermore, all alkoxysilanes were already added in the first step. This results in three slightly different steps (**Figure 8**). In the first step all monomers, aqueous HCl and methanol are added, heated, and stirred in a closed vial. In the second step the vial is opened and transferred into a beaker where gelation takes place by evaporation of water and methanol. In the third step, the samples are heated in a vacuum oven to obtain the condensed gels which can be reversibly softened. Lastly, consolidation is carried out in an oven at 200 °C to obtain permanently rigid samples.

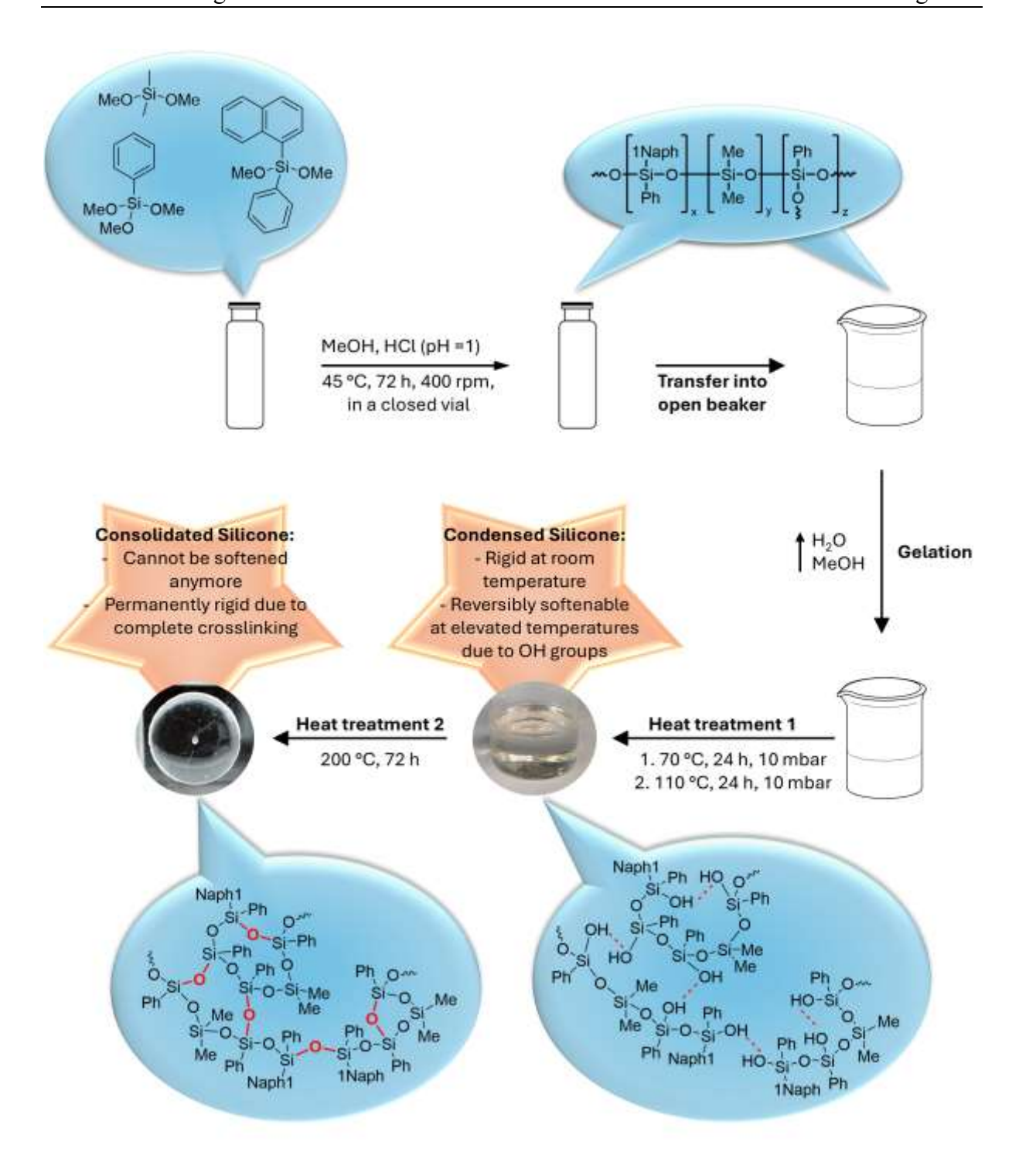


Figure 8: General synthesis of the silicones (Melting Gels) used in this work.

1.9 Characterization and Property Analysis of Silicones

Silicones and silsesquioxanes as well as their different structures can be studied using a wide variety of characterization methods like nuclear magnetic resonance (NMR) spectroscopy, fourier transform infrared (FTIR) spectroscopy, Powder X-ray Diffraction (PXRD), Ultraviolet-visible (UV-vis) Spectroscopy, Fluorescence Spectroscopy, Matrix-Assisted Laser Desorption/Ionization Time of Flight (MALDI-TOF) spectrometry, Size Exclusion Chromatography (SEC), Differential Scanning Calorimetry (DSC), Thermogravimetric Analysis (TGA) and Refractive Index (RI) measurements. While some of these methods like DSC, TGA and refractive index measurements are used to gain more knowledge about properties like glass transition temperature (Tg), thermal stability or the refractive index, 190,191 other methods like PXRD, Fluorescence spectroscopy, MALDI-TOF spectrometry and SEC provide first insights into their structure, aggregation, molecular weight/size and polydispersity index. 182,192-194 However, NMR and IR spectroscopy provide by far the greatest insight into the structure of silicones and the incorporation of their respective monomers into the network as their chemical shift in the NMR and wavenumber in the IR depend on the substituents attached to them such as organic, alkoxy, and hydroxy groups. 195

1.9.1 Structural Analysis and Characterization

1.9.1.1 Liquid Nuclear Magnetic Resonance (NMR) Spectroscopy

A particularly useful method for analyzing the incorporation of the individual monomers into the silicone is ²⁹Si NMR spectroscopy since their chemical shift depends on their structure and substituents and has been done on a wide variety of silicones. ^{18,196,197} Depending on the number of oxygen atoms that are attached to the silicon atom the structural units are called M-, D-, T- or Q-units (**Figure 9**). The superscript number next to the letter represents the integration into the silicone network. Q⁰ for example would be an uncondensed tetraalkoxysilane, while Q¹ would describe a tetraalkoxysilane where one alkoxy or Si-OH group has formed a Si-O-Si bond. Therefore, Q⁴ would be a tetraalkoxysilane that is completely integrated into the network without any alkoxy or Si-OH groups left. ^{99,195}

As it has been shown in other publications liquid ²⁹Si NMR studies should be conducted using relaxation agents like chromium(III)acetylacetonate, allowing for their quantification. ^{198–200}

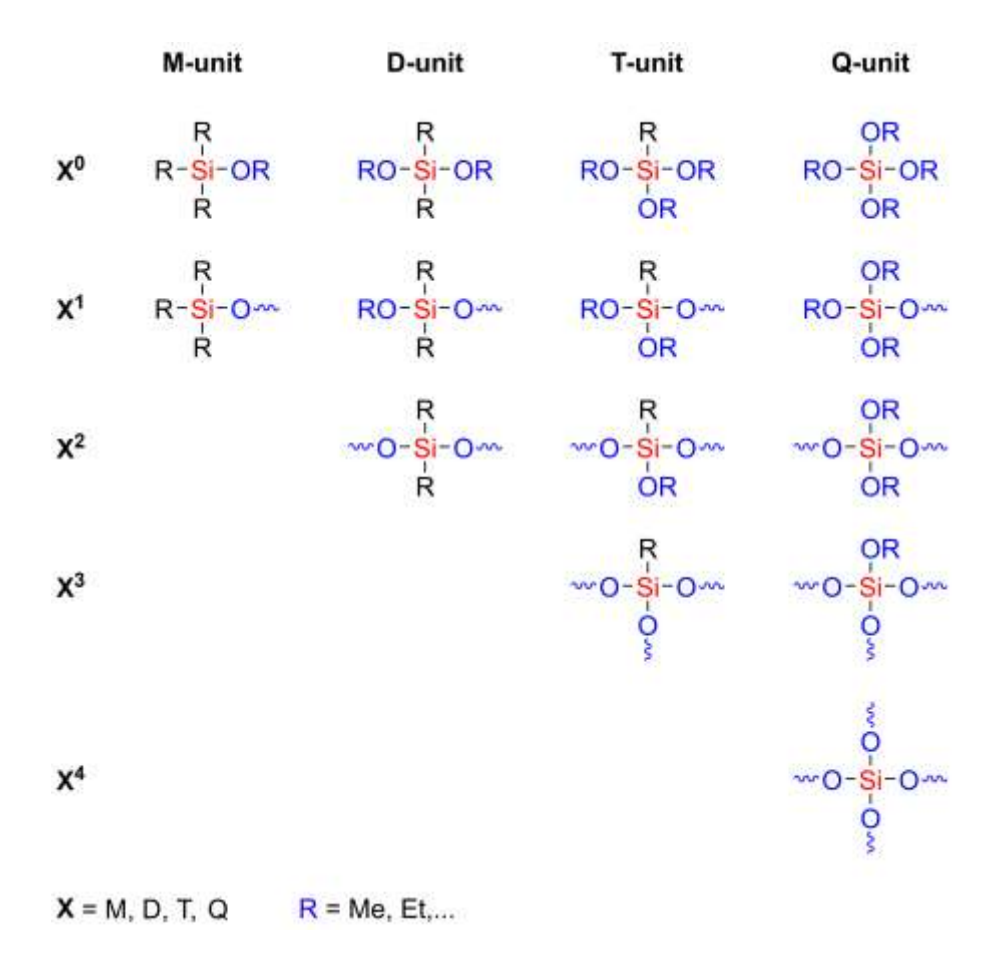


Figure 9: M-, D-, T- and Q-unit structures of silicones.

If the hydroxyl groups in the hydrolysis of tetraethoxysilane are now also taken into account, the ²⁹Si NMR shows even more signals (**Figure 10**) which show an upfield shift with an increasing number of siloxy groups bonded to silicon atoms and a downfield shift with an increasing number of silanol groups. ^{198,201–204} This is due to the shielding effect of the p-orbital of oxygen to the d-orbital of silicon when bonding. ^{99,205} Furthermore, their structural properties are influenced by this type of bonding. ^{28,206} The chemical shift of the silanol group for example can be altered by interactions with a solvent as can be seen for the chemical shift of (¹BuO)₃SiOH which is 4 ppm lower in a high-polarity solvent like DMSO-d₆ than in a low-polarity solvent like CDCl₃. Presumably the solvents prevent the formation of hydrogen bonds between two silanols or a silanol and an alkoxide. ²⁰⁷ The

signal in the NMR also changes upon strain. Small structures like cyclotrisiloxanes and T_6 cages appear at lower magnetic field than larger structures like cyclotetrasiloxanes and T_8 cages and this also follows suit for even larger structures. 167,208,209

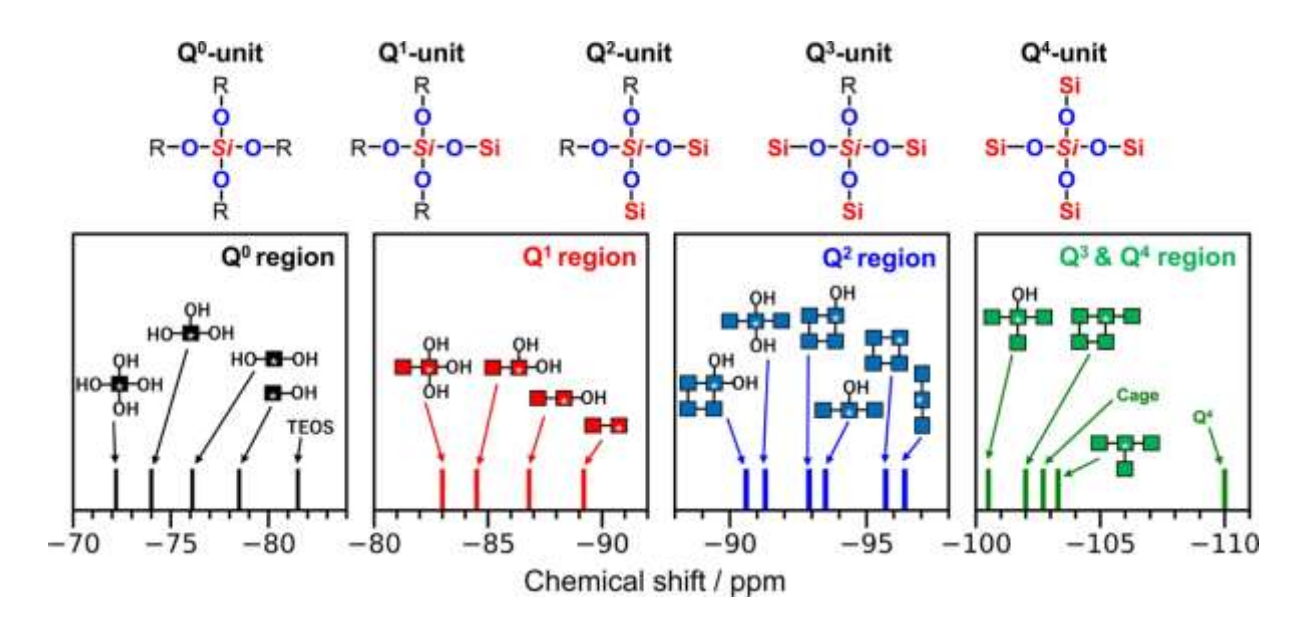


Figure 10: ²⁹Si NMR of different hydrolyzed and condensed TEOS structures. Reproduced with permission from Springer Nature. ⁹⁹

1.9.1.2 Solid-state Nuclear Magnetic Resonance (NMR) Spectroscopy

²⁹Si solid-state NMR spectroscopy can be used to study silicones that cannot be dissolved after condensation and is especially useful to determine the degree of condensation (DOC) and to distinguish between M-, D-, T- and Q-units, as well as study their integration into the silicone network.²¹⁰ Since ²⁹Si solid-state NMR spectra of silicones often show overlapping peaks, spectral deconvolution is used to retrieve these peaks. In this way, the incorporation of the monomers and the chemical environment of the silicon atoms can be investigated.²¹¹ This approach has been widely applied for various silicones to study for example silanols in silicas²¹² or the distribution of silanol hydroxyl groups on silica particles.²¹³ It has also been used to determine the composition of polysiloxane hybrids²¹⁰ or to distinguish between different Si environments in hybrid glasses.²¹⁴ Further examples include siloxane hybrid materials,²¹⁵ organosiloxanes²¹⁶, silsesquioxanes²¹⁷ and silicones.^{218–220}

A distinction can be made between Cross-Polarization Magic-Angle-Spinning Nuclear Magnetic Resonance (CP/MAS NMR) spectroscopy and Magic-Angle-Spinning Nuclear Magnetic Resonance (MAS NMR) spectroscopy. The former method transfers magnetic polarization from abundant nuclei (e.g. ¹H) to rare nuclei (e.g. ¹³C or ²°Si) to enhance the signal from the rare nucleus. ¹²¹ It has to be mentioned that the ²°Si-¹H cross-polarization efficiency decreases when the Si-H distance increases and therefore signals are not quantitative. This is especially the case for highly cross-linked species as the ²°Si nuclei are far away from protons. ²²²²,²²²³ MAS NMR spectroscopy on the other hand measures the silicon nucleus directly, leading to quantitative results but increasing the measuring time and decreasing the quality of the spectrum, like the signal to noise ratio due to the low natural abundance and long spin lattice relaxation time of ²°Si. ²²²⁴

1.9.1.3 Fourier Transform Infrared (FTIR) Spectroscopy

FTIR spectroscopy is a valuable method to determine the substituent groups and structures of silicones as well as the Si-O-Si bond and therefore the success of the condensation reaction and was done for numerous silicones. ^{18,190,225,226} In addition to condensation, hydrolysis can also be observed by the reduction of the Si-OCH₃ band and the simultaneous appearance of the Si-OH and methanol bands. ²²⁷ Especially the Si-O-Si stretching vibrations of silicones and silsesquioxanes are important to determine their structures (**Figure 11**). Silicones with random structures are comprised of various structures including linear, branched, ladder-like, cyclic, strained cyclic, and cage-like structures and therefore their Si-O-Si stretching vibration appears as a broad band at 1000-1150 cm⁻¹. ⁹⁹ Linear, branched and cyclic structures can generally be found between 1000-1150 cm⁻¹, while a decrease in the Si-O-Si bond angle leads to a shift of that band to smaller wavenumbers. ^{136,174,228-230} At 1100-1140 cm⁻¹, Si-O-Si networks of cages appear as a sharp and strong band. ^{173,182,231-233} Ladder- and ladder-like silsesquioxanes show two bands at around 1150 and 1050 cm⁻¹, ^{173,182,234} while 4-fold siloxane rings (the cyclic (Si-O)₄ moiety) are seen as a band at ~550 cm⁻¹. ²³⁵⁻²³⁷

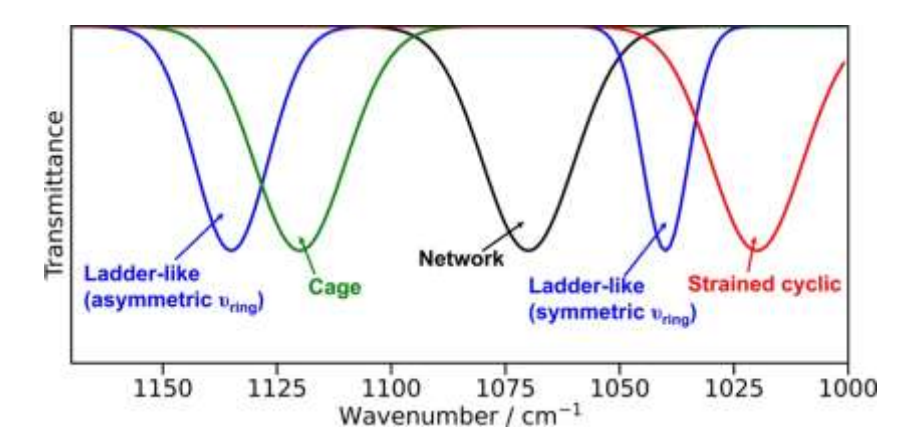


Figure 11: Si-O-Si bands of different siloxane structures. Reproduced with permission from Springer Nature. 99

The position of the Si-O-Si band in cages can differ between different IR methods like the KBr pellet, the solution, and the ATR method, as was seen for octa(3-mercaptopropyl) octasilsesquioxane showing bands at 1109 cm⁻¹ for the KBr and 1077 cm⁻¹ for the ATR method. This is the case because the ATR method maintains certain crystallographic phases while they collapse in the KBr pellet method. ^{99,238,239} The Si-OH band in Q units appears at around 960 cm⁻¹ while for D and T units it appears at 920-890 cm⁻¹, which is due to the formation of hydrogen bonds. ^{99,240,241} Furthermore, the O-H bond of silanols can be seen in the form of an absorption band at 3750-3200 cm⁻¹. ²⁴⁰⁻²⁴²

1.9.1.4 Further Structural Analysis Methods

PXRD measurements are another method to gain more insight into the structures of silicones. If ladder-like structures are present, two reflexes can be identified at 2θ around 8° and 20°. The first reflection (d₁) describes the chain-to-chain distance, which is the width of the superstructure, while the second reflex (d₂) describes the thickness of the ladder, which is the chain-to-chain distance within the ladder. The ratio of d₁ to d₂ shows the regularity of the structure. ^{182,193,243}

During condensation, the cross-linking increases the molecular weight of the silicones, which makes it possible to monitor the reaction, for example, by SEC, GPC or MALDI-TOF. 96,244-249 While a reduction in cross-link functionality results in a lower elastic modulus, an increase in cross-linking leads to a reduction in elasticity. Furthermore, increasing the molecular weight can lead to a higher viscosity of the reaction medium and thus a lower reaction rate. 244,250

1.9.2 Thermal Properties and Characterization

Silicone resins can withstand temperatures of over 1000 °C and are therefore used, for example, as binders for ceramic frit coatings.²⁵¹ They can also form a silica residue during combustion, which protects the underlying polymer surface and thus serves as a selfextinguisher.²⁵² In addition to the protective SiO₂ layer, alkyl groups of silicones are oxidized at high temperatures and form Si-O-Si bonds, which provide additional stability.²⁵³ In the field of highly refractive silicones, decomposition temperatures between 283 and 442 °C are known. 190,254-256 A higher degree of condensation, such as occurs during the consolidation of melting gels, an increased cross-linking density and bulky, rigid groups, such as phenyl groups, increase the thermal stability. This can be demonstrated by a higher T₉₅ value and char residues. On the other hand, silicones that still have OH groups show a reduced thermal stability, as these cause degradation via a back-biting mechanism. 183,190,196,257 Another important parameter is the glass transition temperature (Tg), which reflects an interval in the transition from the liquid to the glassy state and is influenced, for example, by the viscosity, the dielectric constant and other mechanical properties. In relation to silicones, the Tg also depends on the degree of cross-linking and should increase with increasing oxygen bridges between the silicon atoms and thus during consolidation.²⁵⁸

1.9.3 Optical Properties and Characterization

Both UV light and free radicals produced at high temperatures cause yellowing of the silicones, which can be detected using yellowness index measurements. This helps to determine the long-term stability and describes the color change from clear/white to yellow. These measurements can be carried out over a long period of time and a wide temperature range using colorimeters and UV-vis spectrometers.^{256,259–261}

As silicones are used in many optical materials, such as displays, organic light-emitting diodes and microlens components, a high level of transparency is required. This is usually measured in a range between 200 and 800 nm using a UV-vis spectrometer, whereby round and square shaped samples as well as samples on glass slides and films are used. 18,254,262-264

In order to avoid the toxicity, poor processability and sometimes high costs of some fluorescent materials, silicones with fluorescent properties are being developed as coatings, for light emitting diodes or luminescent solar collectors. Aromatic groups can herby lead to excimer formation and π - π stacking, which helps to obtain materials with a homogeneous morphology and can therefore be advantageous for photovoltaic devices. 192,265-267

1.9.4 Refractive Index (RI)

As already mentioned at the beginning, this work aims to increase the refractive index by means of polycyclic aromatic groups. The refractive index (RI) is a dimensionless property defined as (eq. 1)

$$n = \frac{c_0}{c} \tag{1}$$

Where c_0 is the speed of light in vacuum and c is the speed of light in the medium.²⁶⁸

The RI depends on temperature, pressure, density and the wavelength or frequency of the incident light and has been extensively studied. $^{269-274}$ It can be measured by using ellipsometry, $^{275-277}$ thin film analysis 274,278 or an Abbe refractometer. 190,279

A high RI can have many advantages for example in optical materials or photonic devices, where materials can be thinner with an increase in RI.²⁸⁰

One other widespread application that requires a high refractive index (HRI) are light emitting diodes (LEDs). Here HRI encapsulants are of great importance to reduce the total internal reflection (TIR) at the interface of the LED chip enabling light to be refracted through the packaging material. ¹⁹⁰ As soon as light from a medium with a high refractive index like a LED chip (n_1) enters a medium with a lower refractive index like a silicone (n_2) and its angle of incidence (θ_i) is greater than the critical angle (θ_c), TIR occurs (**eq. 2**). This causes the light to be reflected back into the medium with the higher refractive index (**Figure 12**). ²⁸¹

$$\theta_c = \sin^{-1}\left(\frac{n_2}{n_1}\right) \tag{2}$$

This means that the deflection angle on a light-entering surface must be the same as on a light-exiting surface of the same lens in order to avoid reflection loss.²⁸² That in turn increases the so-called light extraction efficiency (LEE) which is defined as the number of photons emitted into free space per second divided by the number of photons emitted from the active region per second.²⁸³

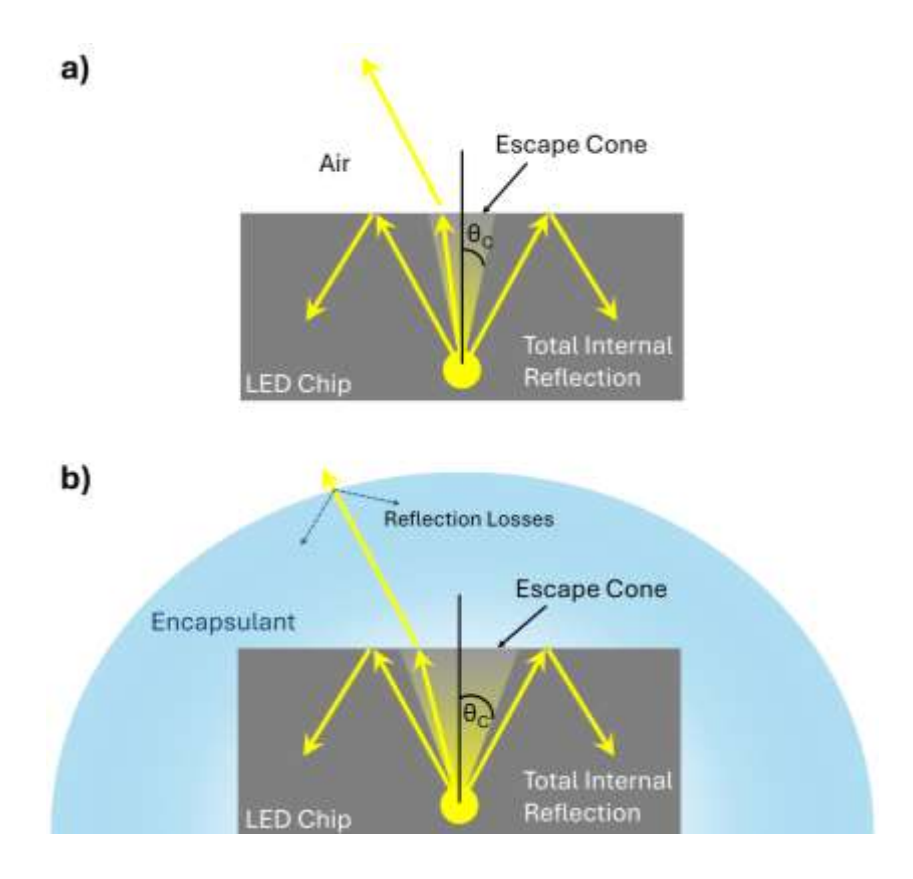


Figure 12: LED escape cone, a) in air, b) with encapsulation. Adapted from references [284,285].

The refractive index of LED chips is in the range between 2.5 and 3.5, while it is 1.83 for cerium-doped yttrium aluminum garnet (YAG:Ce) yellow phosphor which is used in white light-emitting diodes (w-LEDs). Silicones on the other hand usually only have a RI of 1.4 to 1.5. In order to increase efficiency, the refractive index of the silicones must therefore be increased. The RI can be calculated using the Lorentz-Lorenz equation (eq. 3)

$$n_D = \sqrt{\frac{1 + 2R/V_M}{1 - R/V_M}} \tag{3}$$

where R is the molar refraction, n_D is the refractive index at 589 nm and V_M is the molar Volume.

The molar Volume in turn can be determined by (eq. 4)

$$V_M = M/\rho \tag{4}$$

where M is the molecular weight and ρ is the density. Therefore, it can be seen that the molar refraction, the molecular weight, and the density of the precursors used for the polymer synthesis are of utmost importance.²⁸⁷

In recent years, numerous attempts have been made to increase the refractive index of silicones. One frequently used method, for example, is the incorporation of nanoparticles, whereby TiO_2 (RI = 1.596-2.01)^{288–290} and ZrO (RI ≈ 1.55)^{291,292} are usually used. In addition, titanium and zirconium atoms are also incorporated into the silicone network by using titanium and zirconium alkoxides instead of silicon alkoxides (RI = 1.58-1.60). $^{30,293-296}$

The use of aromatic substituents, such as phenyl and carbazole groups, also leads to an increase in the refractive index, whereby these can be located both as a substituent on the silicon atom (RI = 1.580, 1.49) 95,297 and in the Si-O-Si network (RI = 1.60) 254 itself. Finally, the additional incorporation of heteroatoms such as oxygen (RI = 1.60) 298 , sulfur (RI = 1.58 - 1.665) 255,277,298,299 and nitrogen (RI = 1.56) 190 was also investigated.

The refractive index is usually measured at 25 °C and at different wavelengths, such as 589 nm or 622 nm, in a soft or solid state using an Abbe refractometer. It is important to consider, that the refractive index depends on both the wavelength and the temperature. 18,190,300,301 In the solid state, however, a contact liquid such as monobromonaphthalene is required. Alternatively, solid samples can also be analyzed as films using an ellipsometer. 191,302,303

A selection of monomers and polymers and their refractive indices is shown below (**Table 1** and **Table 2**).

Table 1: Selection of monomers including their refractive indices.

Monomers	n _D ²⁵	RI @20 °C (Commercial)
Methyltrimethoxysilane	1.3690304	1.371305
Dimethyldimethoxysilane	1.3699304	1.369 ³⁰⁶
Phenylmethyldimethoxysilane	1.4769304	1.4694307
Diphenyldimethoxysilane	1.5404304	1.5447308
Phenyltrimethoxysilane	1.4710 ³⁰⁴	1.4734 ³⁰⁹
Phenyltriethoxysilane		1.4718 ³¹⁰
Phenyltrichlorosilane		1.523 ³¹¹

Table 2: Selection of commercially available and synthesized silicones including their refractive indices.

Polymers	RI	Wavelength	source
		/nm	
Silanol terminated polydimethylsiloxane,	1.402		Gelest ³¹²
35-45 cSt			
Silanol terminated polydimethylsiloxane,	1.403		Gelest ³¹³
3,500 cSt			
Poly(methylphenylsiloxane), 450-550 cSt	1.5365		Sigma-
			Aldrich ³¹⁴
Methacryl-diphenyl-polysiloxane	1.54-1.61	633	292
S-TiO₂/silicone nanocomposite (1 wt%)	1.56-1.60		289
Coumarin-based polysiloxane	1.559-	633	315
	1.603		
Ladder-like diphenylsiloxane-bridged	1.59	633	316
methacryl-phenyl-siloxane	1.61	450	
3-mercaptopropylmethyldimethoxysilane	1.55-1.65	589	255
containing silicone-oligomer			
Bromine containing organic-inorganic	1.54-1.61	632	317
polysiloxanes			

2 Aims and Scope of this Work

Silicone resins with a high refractive index are used today in a variety of applications, such as encapsulants for light emitting diodes (LEDs), anti-reflective optical coatings and contact lenses. The efficiency of an LED, for example, increases the closer the refractive indices of the chip or conversion phosphor and the silicone-containing packaging material are, with the former being very high and the latter rather low. Packaging materials with a high refractive index are therefore required to increase the efficiency and thus the luminous efficacy.

The aim of this work is to produce transparent, thermally stable and processable silicone resins with a high refractive index by using polycyclic aromatic groups, as well as to produce polyhedral oligomeric silsesquioxanes (POSS) with said groups as possible fillers. For this purpose, the influence of polycyclic aromatic groups on characteristics like the transparency, refractive index, thermal stability and processability of the fully consolidated silicone resins was investigated in a total of three studies.

1. Aim:

 Development of a thermally stable and highly refractive silicone resin using polycyclic aromatic groups from previously self-synthesized highly refractive index dialkoxysilanes.

Objectives:

- Synthesis of novel dialkoxysilanes with polycyclic aromatic groups and verification of their structure by NMR and FTIR spectroscopy, as well as elemental analysis.
- 2. Investigation of these monomers regarding further properties such as absorption maximum, excimer formation and refractive index using UV-vis and fluorescence spectroscopy, as well as refractive index measurements.
- 3. Preparation of highly refractive silicone resins from the previously produced dialkoxysilanes by means of hydrolysis and condensation reaction.

- Determination of the influence of different organic groups on their structure and size using NMR, FTIR and fluorescence spectroscopy, as well as PXRD, MALDI-TOF and SEC.
- 5. Determination of the influence of different organic groups on their transparency and thermal properties using UV-vis spectroscopy, DSC and TGA.
- 6. Determination of the influence of different organic groups on the refractive index using an Abbe refractometer.

2. Aim:

2. Further improvement of the previously produced, most promising high refractive index silicone resin by means of post-cross-linking to achieve a better cross-linking, which prevents liquefaction at high temperatures, in order to increase the possible field of application.

Objectives:

- 1. Post-cross-linking of the most promising sample with various additives.
- Determination of the influence of different organic groups and additives on the structure and cross-linking of the newly obtained samples using NMR and FTIR spectroscopy, as well as PXRD.
- 3. Determination of the influence of different organic groups and additives on their thermal properties using DSC and UV-vis spectroscopy, as well as TGA.
- Determination of the influence of different organic groups and additives on the viscoelastic properties and thus possible liquefaction at high temperatures using DMA.
- 5. Analysis why post-cross-linking with certain additives leads to significantly better results.

3. Aim:

3. Synthesis of novel POSS systems containing polycyclic aromatic groups.

Objectives:

- Synthesis of novel trialkoxysilanes with polycyclic aromatic groups and verification of their structure by NMR and FTIR spectroscopy, as well as elemental analysis.
- Investigation of the produced trialkoxysilanes with regard to further properties such as absorption maximum, excimer formation and refractive index by means of UV-vis and fluorescence spectroscopy, as well as refractive index measurements.
- 3. Preparation of POSS systems from these trialkoxysilanes using synthesis routes known from literature.
- 4. Determination of the influence of different polycyclic aromatic groups on their structure and size using NMR, FTIR and fluorescence spectroscopy, as well as single X-ray crystallography, MALDI-FTICR and SEC.
- 5. Determination of the influence of different polycyclic aromatic groups on their thermal properties using DSC and TGA.

3 Results and Discussion

The results of this doctoral thesis are summarized in the following chapters in the form of publications, whereby the first chapter has already been published.

Briesenick, M.; Gallei, M.; Kickelbick, G. High-Refractive-Index Polysiloxanes Containing Naphthyl and Phenanthrenyl Groups and Their Thermally Cross-Linked Resins. *Macromolecules* **2022**, *55*, 4675-4691. https://doi.org/10.1021/acs.macromol.2c00265.

3.1 High-Refractive-Index Polysiloxanes Containing Naphthyl and Phenanthrenyl Groups and their Thermally Cross-Linked Resins

3.1.1 Abstract

High-refractive-index polysiloxanes containing naphthyl, phenanthrenyl, phenyl, and methyl groups have been synthesized using a polycondensation reaction starting from substituted di- and trialkoxysilanes. The obtained polymers comprised linear siloxane and partially cross-linked silsesquioxane units and showed optical transparencies of up to 99 % at a thickness around 120 µm and high refractive indices of up to 1.622. The polymeric structures contained stabilized silanol groups that were further cross-linked at increased temperatures of 200 °C resulting in the formation of hybrid inorganic-organic resins. These typical thermal treatments at 200 °C for 72 h kept the transparencies as high as 98% and slightly lowered the RIs to values up to 1.610. A detailed structure evaluation of the resulting systems showed, depending on the size of the polycyclic aromatic substituent, excimer formation, which is based on weak interactions of the aromatic groups in the polymeric material. After thermal consolidation, glass transition temperatures of the cross-linked systems were in the range of 18-74 °C depending on the composition. Thermal stabilities of the final resins reached higher values than commonly used siloxane resins up to 470 °C. The final materials are potential resins for hightemperature optical applications.

3.1.2 Introduction

High-refractive-index (HRI) polymer-based materials are of great interest in optoelectronic applications, for example, as encapsulants for light emitting diodes (LEDs),31 organic electroluminescent devices,318 anti-reflective optical coatings,319 and immersion lithography.³²⁰ The refractive index (RI) of such systems is usually controlled through specific polarizable functional groups in the polymer chain or by the formation of nanocomposites of highly refractive inorganic nanoparticles in an organic polymer matrix. 31,276,321,322 Systems containing merely polarizable groups usually show RIs below 1.80, while the formation of nanocomposites can reach values higher than 1.80.323 Polyamides with ortho-linked sulfide or sulfoxide linkages, for example show RIs of up to 1.7401 at a wavelength of 633 nm.³²⁴ The introduction of thiazole and naphthalene units as well as thioether linkages into polyamides resulted in values of up to 1.7701 at 633 nm. ³²⁵ Poly(methylmethacrylate) (PMMA)-titania hybrid thin films reveal RIs in a range of 1.505-1.867 at 633 nm depending on the titania content,²⁷⁸ while highly aromatic, carbazole-based methacrylates possess RIs of 1.63.326 More examples of high RI polymers include a poly(propylene trithiocarbonate) (RI = 1.78),³²⁷ naphthyl-containing polyferrocenes (RI = 1.82 at 589 nm), 328 and a polymer with thioester and thioacetal structure (RI = 1.94 at 193 nm).329 Many of these systems have a limited optical transparency and low thermal stabilities or show photochemical side reactions such as yellowing at increased lifetimes. Some of these disadvantages can be overcome using silicone resins. These are usually two-component systems that cross-link via hydrosilylation reactions of vinyl- and hydride group containing oligo- and polysiloxanes.¹³⁶ Generally, siloxane resins feature high mechanical flexibility, high thermal stability, and excellent optical transparency, 322 as well as the option to introduce organic groups that can provide additional emission properties, such as fluorescent dyes. 330 One of the drawbacks of many commercially available polysiloxanes is their quite low RI.³³¹ Increasing the refractive index of such materials can, for example, increase the efficiency of LEDs if they are used as encapsulation materials.^{286,332} Already reported methods for such an increase for polysiloxanes are the incorporation of ZrO₂²⁷⁶ or ZnS nanoparticles.321 Another route is the partial substitution of methyl against phenyl groups, which can lead to an RI up to 1.55-1.57.298 Additional incorporation of heavier elements such as phosphorus or halogen atoms is also an effective method to increase

the RI.³¹⁶ However, modifications with halogen atoms often decrease stability to light, heat, or chemical reagents, resulting in discoloration and degradation of mechanical properties of the polymers.³³³

In general, the refractive index depends on the electron density and its polarizability and can be deduced from the Lorentz-Lorenz equation (eq. 3).

$$n_D = \sqrt{\frac{1 + 2R/V_M}{1 - R/V_M}} \tag{3}$$

where R is the molar refraction, n_D is the refractive index at 589 nm and V_M is the molar Volume. The molar Volume is given in **eq. 4**

$$V_M = M/\rho \tag{4}$$

where M is the molecular weight and ρ is the density. This equation shows that the RI correlates with the molar refraction, molecular weight, and the density of the molecules used as precursors for the polymers. The molar refraction is particularly high for aromatic groups, halogen, and sulfur atoms. In aromatic systems, the size of the delocalized electron system has a significant effect on the RI. While a phenyl group, for example, has a molar refraction of 25, a naphthyl group shows a value of 43. Hence, polycyclic aromatic groups as substituents in siloxanes can result in a significant increase of the RI. At the same time, however, other properties of the polymer, such as the viscosity, are drastically changed.

Recently, we were able to show that hybrid siloxane/silsesquioxane polymers are an excellent one-component alternative to traditional two-component polysiloxane resins for optical applications. These materials show thermoplastic behavior up to a specific temperature and behave like thermosets above this temperature. This means they can be reversibly softened in a certain temperature range. If this temperature range is exceeded, the siloxanes can no longer be softened or dissolved. Furthermore, the systems show high optical transparency and thermal stability. In the study presented here, we synthesized one new dialkoxysilane and reinvestigated two others already studied in our group containing 1-naphthyl, 2-naphthyl, or 9-phenanthrenyl groups and an additional phenyl group as substituents. These monomers were applied as precursors

in a polycondensation reaction together with diphenyldimethoxysilane or dimethyldimethoxysilane as well as phenyltrimethoxysilane to form polysiloxanes with a partial condensation between single chains.³³⁴ We investigated the optical and thermal properties of the resulting materials with respect to their potential application in optoelectronic devices.

3.1.3 Results and Discussion

3.1.3.1 Synthesis and Characterization of Dialkoxysilanes

The purpose of this study is to show how the extension of the delocalized π electron system in the substituents on the Si atom to the polycyclic aromatic substituents naphthalene and phenanthrene affects the properties of polysiloxane/polysilsesquioxane systems. 334,335 Based on previous studies on alkoxysilanes with polycyclic aromatic substituents, we synthesized several naphthyl- and phenanthrenyl group substituted monomers for polycondensation reactions. 74,191 The effect of isomeric attachment of the same aromatic group to the polymer backbone on the final material properties was investigated using 1-naphthyl or 2-naphthyl substituents. Furthermore, we focused only on the phenyl group as the second substituent at the Si atom of the substituted alkoxysilane monomers, since a methyl group would result in a lower RI.336 dialkoxysilanes were prepared by Grignard reactions between 1- or 2-bromonaphthalene or 9-bromophenanthrene and trimethoxyphenylsilane (Scheme 25). Dimethoxyphenyl-(1-naphthyl)silane and dimethoxyphenyl-(9-phenanthrenyl)silane hereafter referred to as 1-NaphPhSi(OMe)₂ and 9-PhenPhSi(OMe)₂, respectively, formed as a white solid, while dimethoxyphenyl-(2-naphthyl)silane hereafter referred to as 2-NaphPhSi(OMe)₂ was obtained as a viscous colorless liquid. All compounds were obtained in high purity and yields between 54 % and 68%.

R ₁	Overall Yield [%]
1-naphthyl	66
2-naphthyl	68
9-phenanthrenyl	54

Scheme 25: General synthetic route of the dialkoxysilanes using a Grignard reaction.

The molecular structures of all dialkoxysilanes have been verified using ¹H, ²⁹Si, ¹H, ²⁹Si HMBC, and ¹³C NMR as well as IR-spectroscopy and elemental analysis (see **Figure S 1 – Figure S 13** and **Table S 1**). All signals are in good agreement with previously reported spectra of similar compounds. ^{337–341}

UV-vis spectroscopy revealed the typical absorption bands of aromatic groups connected to a silicon atom (see Figure S 14).342 The absorption maxima for 1-NaphPhSi(OMe)₂, 2-NaphPhSi(OMe)₂ and 9-PhenPhSi(OMe)₂ were found at 284, 272 and 258 nm, respectively. It must be mentioned here that the absorption maxima of naphthalene and phenanthrene are at approx. 220 and 260 nm, respectively. 343,344 While the absorption maximum of 9-PhenPhSi(OMe)₂ therefore corresponds very well with that of phenanthrene, 1-NaphPhSi(OMe)₂ probably only shows a local maximum, as the absorption of all samples below 250 nm was too strong for further evaluation. The observable signals in turn show an increasing blue shift in the row 1-naphthyl, 2-naphthyl and 9-phenanthrenyl. For optical applications, it is often important to know the fluorescent behavior, which also helps to understand potential aggregation phenomena particularly in the case of compounds containing polycyclic aromatic substituents. Therefore, we applied fluorescence spectroscopy on all three dialkoxysilanes as a dilution series in DCM to investigate their potential to form excimers and to determine their Stokes shift (see Figure S 15 – Figure S 17). The experiments were performed at an excitation wavelength of 290 nm, which provided the highest intensities in the resulting emission spectra in previous experiments. For 1-NaphPhSi(OMe)2, two peaks are visible.

The peak at a lower wavelength can be assigned to molecular fluorescence, while the broad peak at a higher wavelength, which decreases with further dilution, can be attributed to excimer fluorescence.³⁴⁵ The sharp peak resulting from molecular fluorescence shifts from 331 nm to 342 nm with increasing concentration. Naphthalene can self-assemble to form J-aggregates, which show a shift to higher wavelengths and sharpening of peaks.³⁴⁶⁻³⁴⁸ 2-NaphPhSi(OMe)₂ shows the same peak of molecular fluorescence as 1-NaphPhSi(OMe)₂ at 341 nm, but not shifted to smaller wavelengths, as well as a second signal with a maximum at 356 nm. While the broad band at higher wavelengths indicative of excimer fluorescence is not visible, the broad tailing of the second band, which decreases with lower concentrations, could be due to ground state aggregation.¹⁹² It can be concluded that the isomerism has an influence on the aggregation behavior in case of naphthyl-substituted alkoxysilanes. 9-PhenPhSi(OMe)₂ shows a similar but less pronounced emission behavior like 2-NaphPhSi(OMe)₂ with a shift to higher wavelengths typical for the phenanthrene group.^{349,350}

The main reason for incorporating the naphthyl and phenanthrenyl systems in the polymer structures was to increase the RI. Hence, the RI of the dialkoxysilanes was determined at 20 °C and 589 nm. The RI for the liquid monomer 2-NaphPhSi(OMe)₂ can be obtained by standard measuring procedures. For the solid monomers 1-NaphPhSi(OMe)₂ and 9-PhenPhSi(OMe)₂, the RI was studied applying a calibration curve method of different concentrated solutions to extrapolate the RI of the pure substances (for further details, see Supporting Information).²⁵⁵ The obtained refractive indices of 1-NaphPhSi(OMe)₂, 2-NaphPhSi(OMe)₂ and 9-PhenPhSi(OMe)₂ are 1.602, 1.594 and 1.671, respectively (see **Figure S 18** and **Table S 2**), which is rather high compared with other alkoxyphenylsilanes generally ranging from 1.471 to 1.540.³⁰⁴ The samples show that replacing the 1-naphthyl for a 2-naphthyl substituent has no influence on the RI and therefore constitutional isomerism does not play a role for the RI.

3.1.3.2 Polymers

1-NaphPhSi(OMe)₂, 2-NaphPhSi(OMe)₂, and 9-PhenPhSi(OMe)₂ were polymerized together with phenyltrimethoxysilane and dimethyldimethoxysilane or diphenyldimethoxysilane as comonomers. All polycondensation reactions have been

carried out under HCl catalysis applying tetrahydrofuran (THF) as solvent to obtain partially cross-linked polysiloxanes (**Scheme 26** and **Table 3**). The abbreviations for the sample names are composed as follows: MG refers to melting gel and Naph1 indicates the monomer used, while Ph and Ph₂/Me₂ denote phenyltrimethoxysilane and diphenyldimethoxysilane/ dimethyldimethoxysilane, respectively. Post treatment in a vacuum drying oven at 70 and 110 °C resulted in the removal of methanol and water, which are side products of the condensation reaction. Polycondensation of single siloxane units commonly leads to a ring-chain equilibrium, which cannot be excluded in our case. However, we showed in a previous study that the final properties of the resin are not influenced by these ring structures. We addressed the formation of such ring structures in a study of the formation of phenyl-group-containing melting gels. The possible formation of poly(THF), which can be catalyzed under acidic conditions, was not observed at any stage of the preparation.

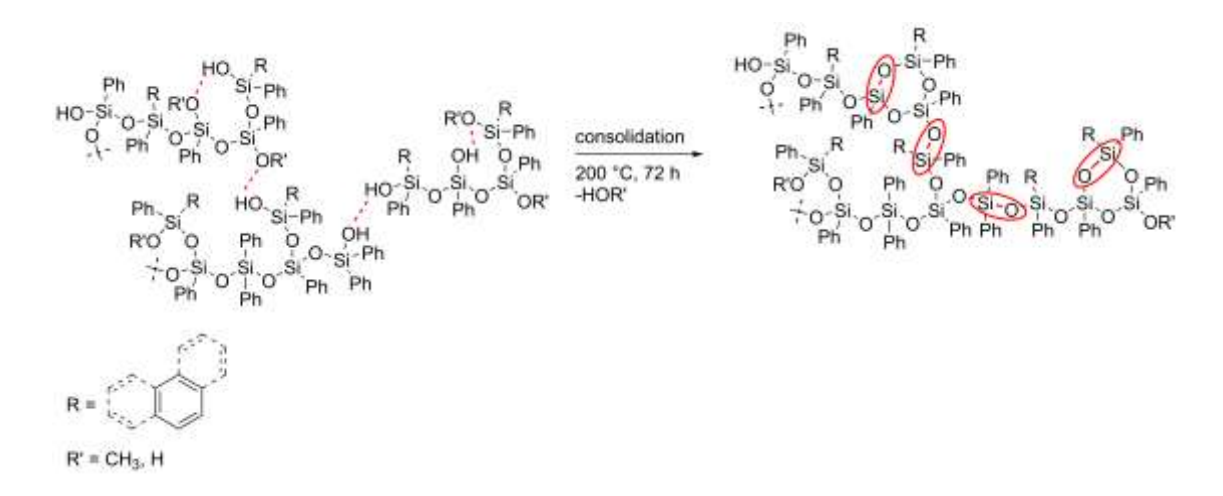
1
$$O-Si-O' + 2$$
 $O-Si-O' + 1$ $O-Si-O'$ $O-Si-O' + 1$ $O-Si-O'$ $O-Si-O' + 1$ $O-Si-O$

Scheme 26: Condensation reaction of alkoxysilanes to cross-linked HRI polysiloxanes.

Table 3: Summary of all synthesized polysiloxanes and their abbreviations.

R (1 eq)	PhSi(OMe)₃	Ph ₂ Si(OMe) ₂	Me ₂ Si(OMe) ₂	Abbreviation
1-naphthyl	(1 eq)	(2 eq)	×	MGNaph1_Ph_Ph2
	(1 eq)	*	(2 eq)	MGNaph1_Ph_Me2
2-naphthyl	(1 eq)	(2 eq)	×	MGNaph2_Ph_Ph2
	(1 eq)	*	(2 eq)	MGNaph2_Ph_Me2
9-phenantrenyl	(1 eq)	(2 eq)	×	MGPhen9_Ph_Ph2
	(1 eq)	*	(2 eq)	MGPhen9_Ph_Me ₂

The synthesis was based on previously reported synthetic procedures, which resulted in reversibly meltable hybrid glasses that consolidated at elevated temperatures (see Figure S 19).³³⁴ The ratio between the monomers (Table 3) was chosen because preliminary studies showed that this ratio should result in crack-free cross-linked materials after consolidation. Since the phenyl and polycyclic aromatic groups contained in the polysiloxane already greatly increase the molar friction and thus the viscosity, the amount of phenyltrimethoxysilane as the cross-linker was kept low. A systematic variation of the additional dialkoxysilanes compared to the polycyclic aromatic ones was to study the influence of phenyl and methyl groups on the properties of the final polymer and resin, such as optical transparency, reversible melting behavior, consolidation, and structure.^{334,335} After polycondensation, a partially cross-linked structure is expected, which shows non-condensed silanol and methoxy groups stabilized by intra- or intermolecular hydrogen bonds. After consolidation in an oven at 200 °C for 72 h, these groups react with each other to form a structure with a higher degree of condensation (Scheme 27).



Scheme 27: Polysiloxane structure before and after consolidation.

3.1.3.3 Nuclear Magnetic Resonance (NMR) Spectroscopy

Since the polymers after polycondensation as well as those after consolidation were still soluble, NMR spectroscopy was performed before and after consolidation to verify their structure (see **Figure S 20 – Figure S 49**) and to identify differences between the two states. Based on the findings regarding the solubility of the consolidated products, it can

already be concluded that the degree of cross-linking in the consolidated systems is not as high as in previous systems with smaller aromatic units. Former resins did not show any solubility after consolidation.

¹H NMR and ¹³C NMR of the polycondensation products revealed all expected signals. 335,352 After consolidation the peaks attributed to the methoxy groups decrease while the other peaks become broader and more uniform, indicating further condensation. ²⁹Si NMR spectroscopy in solution revealed the typical D- and T-signals according to the used monomers, 291,335,338 which were further confirmed by 1H 29Si HMBC spectroscopy and is shown exemplary for MGNaph1_Ph_Ph2 and MGNaph1_Ph_Me2 (Figure 13), and all other spectra are found in Figure S 20 – Figure S 49. Even though the signals in the ²⁹Si NMR cannot be integrated to obtain further information, some trends are visible. The unconsolidated MGNaph1_Ph_Ph2 shows D1- and D2- as well as T1- to T³-signals, while the consolidated sample shows no T¹-signals MGNaph1_Ph_Me2 shows no T1 peak even before consolidation and the D1 peak of dimethyldimethoxysilane is almost not visible. This indicates that the condensation is more progressed at this stage. Considering that the only difference in both polymers is the exchange of the diphenyl- for the dimethylsilane, this can be taken as an indication that the substitution pattern of the monomers has an influence on the consolidation process. Interestingly, the four other polymers show no difference between the consolidated and unconsolidated state.

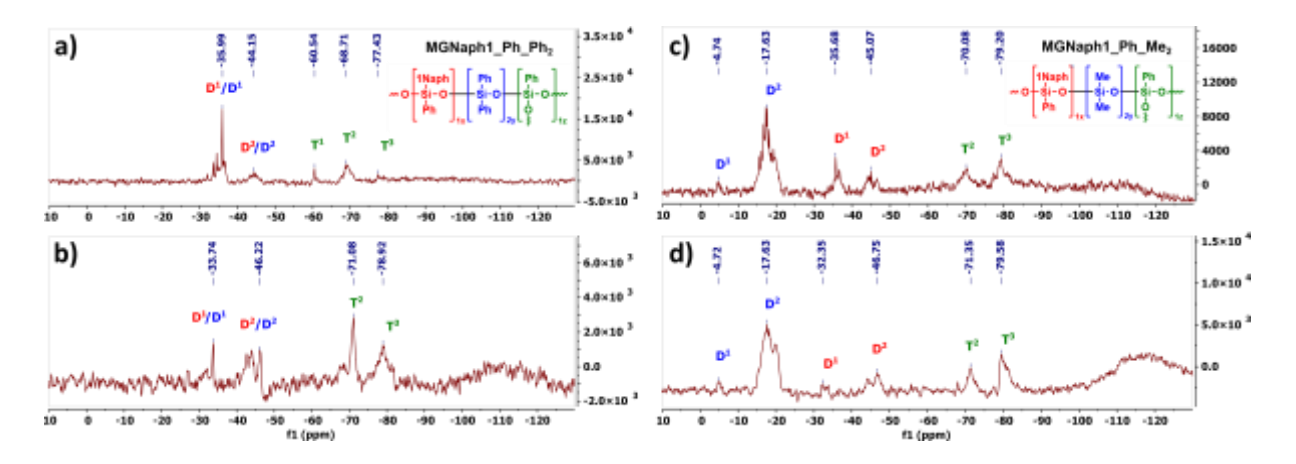


Figure 13: ²⁹Si NMR of MGNaph1_Ph_Ph₂ a) unconsolidated, b) consolidated and MGNaph1_Ph_Me₂ c) unconsolidated, d) consolidated.

3.1.3.4 Cross Polarization-Magic Angle Spinning Nuclear Magnetic Resonance (CP-MAS NMR) Spectroscopy

One way to quantify the degree of cross-linking after consolidation is ²⁹Si CP-MAS NMR spectroscopy, which was performed on all six consolidated samples (see Figure S 50 -Figure S 55). All samples show the expected shifts for each alkoxysilane monomer. It must be pointed out that in case of the diphenyldialkoxysilane containing samples, the D-signals of the latter monomers overlap with those of the polycyclic aromatic substituted monomers. Contrary, in cases in which dimethyldimethoxysilane was used as a comonomer, the samples show two D signal regions denominated D and D'. Phenyltrimethoxysilane shows two shifts at around -70 ppm (T2) and -78 ppm (T3) while dimethyldimethoxysilane and diphenyldimethoxysilane show shifts at around -6 ppm $(D^{\prime 1})$ and -19 ppm $(D^{\prime 2})$ and -33 ppm (D^{1}) and -45 ppm (D^{2}) , respectively. ^{335,353} Exemplary ²⁹Si CP-MAS NMR spectra are shown for MGNaph1_Ph_Ph₂, MGNaph2_Ph_Me₂, MGPhen9_Ph_Ph2 and MGPhen9_Ph_Me2 (Figure 14). Comparing MGNaph1_Ph_Ph2 and MGPhen9_Ph_Ph2 (Figure 14, a and c) with each other reveals that after consolidation, the T²- and T³-signals are almost identical while MGNaph1_Ph_Ph₂ shows a significantly lower D² signal. Considering the only difference in both polysiloxanes are the 1-naphthyl and 9-phenanthrenyl groups, it can be concluded that the latter is more cross-linked. Comparing both 9-phenanthrenyl containing samples, the ratio of the D-signals at -33.1 and -44.8 ppm (blue and purple) stayed almost the same, indicating that diphenyldimethoxysilane and 9-PhenPhSi(OMe)₂ show a similar condensation behavior. The dimethyldimethoxysilane shows almost exclusively D'2-signals, while the ratio of the T² and T³-signals is exactly reversed compared to the only phenyl-substituents containing samples. This leads to the assumption that the dimethyldimethoxysilane shows a higher degree of cross-linking. Examining the samples MGNaph2_Ph_Me₂ and MGPhen9_Ph_Me2 (Figure 14, b and d) the D'-signals (orange and green) from dimethyldimethoxysilane as well as the T-signals from phenyltrimethoxysilane are almost identical. The only difference is in the D-signals resulting from the polycyclic monomer indicating further condensation of 2-NaphPhSi(OMe)₂.

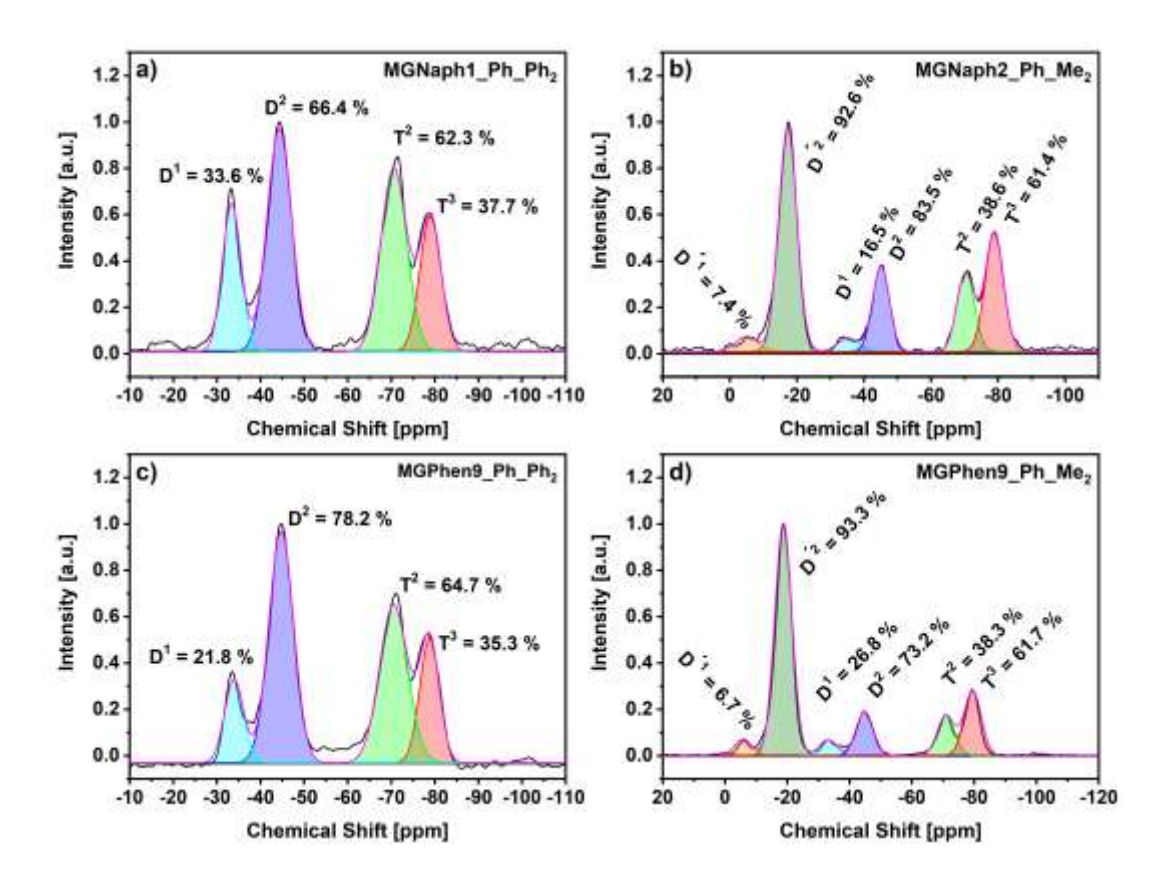


Figure 14: ²⁹Si CP-MAS NMR spectra of the consolidated polysiloxanes. a) MGNaph1_Ph_Ph₂, b) MGNaph2_Ph_Me₂, c) MGPhen9_Ph_Ph₂, d) MGPhen9_Ph_Me₂.

Based on the ²⁹Si CP-MAS NMR spectra, the degree of condensation (DOC) can be determined according to equation 5 (**Table 4** and **Table S 3**). ²⁹¹

$$DOC = \frac{D^{1} + 2D^{2} + D^{'1} + 2D^{'2} + T^{1} + 2T^{2} + 3T^{3}}{2 \cdot (D^{1} + D^{2} + D^{'1} + D^{'2}) + 3 \cdot (T^{1} + T^{2} + T^{3})}$$
(5)

From these calculations, the following condensation tendency can be formulated 2-naphthyl > 9-phenanthrenyl \geq 1-naphthyl. These results demonstrate that constitutional isomerism has an influence on the reactivity during the polycondensation process.

Table 4: Calculated degree of condensation for all oligosiloxanes.

Oligosiloxane	DOC/%
MGNaph1_Ph_Ph ₂	80.8
MGNaph1_Ph_Me ₂	89.7
MGNaph2_Ph_Ph ₂	83.5
MGNaph2_Ph_Me2	91.1
MGPhen9_Ph_Ph2	82.7
MGPhen9_Ph_Me ₂	89.7

3.1.3.5 Powder X-ray Diffraction (PXRD)

PXRD measurements were used to gain additional insight into the structures of the networks and were performed on the diphenyl containing oligosiloxanes after consolidation. These should show more inter- and intramolecular interactions, as they consist exclusively of aromatic groups. Similar to measurements already performed in our group on related systems, the obtained PXRD patterns show two reflections at 2θ around 8 and 20° (see **Figure S 56** and **Table S 4**).³³⁴ The first reflection (d_1) can be ascribed to the chain-to-chain distance of ladder-like structures or the ladder width of the superstructure, while the second reflection (d_2) indicates its thickness.^{182,193} Since the ratio of both reflections shows the structural regularity, it can be concluded that the obtained structures show a certain regularity.²⁴³ In contrast to our previous work, not only trimethoxy- but also dimethoxysilanes were incorporated into the oligosiloxane. Therefore, it can be assumed that the regular, possibly ladder-like structures are limited to certain domains.

3.1.3.6 Fourier Transform Infrared (FTIR) Spectroscopy

FTIR spectra of the polymers (**Figure 15** and **Figure S 57** – **Figure S 58**) show the expected signals of the aromatic groups at around 3070 cm⁻¹ (v_{asym} CH), 3049 cm⁻¹ (v_{sym} CH), 1591 cm⁻¹ (v_{asym} CH), 1429 cm⁻¹(v_{asym} CH) and 739, 716 and 694 cm⁻¹ (Ar-Si-Ar) as well as the

methyl groups at 2962 cm⁻¹ (v_{asym} CH₃) and 2902 cm⁻¹ (v_{sym} CH₃). 340,354 The stretching vibration of the Si-O-Si bond from 1119 cm⁻¹ to 995 cm⁻¹ belongs to the newly formed network and is a proof of a successful condensation. 190 Furthermore, the absorption band of the methoxy group at 1188 cm⁻¹ cannot be detected anymore.²²⁷ Considering the liquid ¹H and ¹³C NMR spectra before consolidation show nearly no methoxy groups and the ¹³C CP-MAS NMR spectrum after consolidation shows no methoxy groups, this is a further proof that the network was successfully formed.²²⁷ A first indication of how far the condensation has progressed is the absorption band of Si-OH from 925 cm⁻¹ to 827 cm⁻¹ and is shown exemplary for MGNaph1_Ph_Ph2 and MGNaph1_Ph_Me2 (**Figure 15**).³⁴⁰ This band can only be observed for the unconsolidated MGNaph1_Ph_Ph2 and disappears upon consolidation, showing that this sample is less condensed than MGNaph1_Ph_Me₂. Two important signals, which are shown in the FTIR spectrum, are the absorption bands of the isolated silanols from 3704 to 3521 cm⁻¹ (v(OH_{isolated})) and the mono-hydrogenbonded silanols from 3498 to 3126 cm⁻¹ (v(OH_{H-bonded})), which develop during the hydrolysis step in the polycondensation reaction.³⁵⁵ Prior to consolidation, the latter is more pronounced when diphenyldimethoxysilane (green curve) is included instead of dimethyldimethoxysilane (red curve), also indicating a less advanced condensation. Comparing the polysiloxanes before and after consolidation, this band disappears completely, indicating that the OH-groups continue to condense during the consolidation, which is also reflected in the higher glass-transition temperatures shown later. This would also prove that the condensation reaction proceeds further during the consolidation. The more advanced condensation of Me₂Si(OMe)₂ compared to Ph₂Si(OMe)₂ can be explained by a closer look on the acid-catalyzed sol-gel process, which is divided into hydrolysis and condensation. Under acidic conditions, the first is the rate-determining step due to the nucleophilic attack of water on the silicon atom and proceeds according to an S_N2 mechanism.^{80,85} Its reaction rate is thereby determined by the +I-effect and steric hindrance. The methyl groups provide a greater +I-effect as well as less steric hindrance. Effects of exchanging substituents on the silicon atom on hydrolysis and condensation were already extensively described in literature. 81,86,87

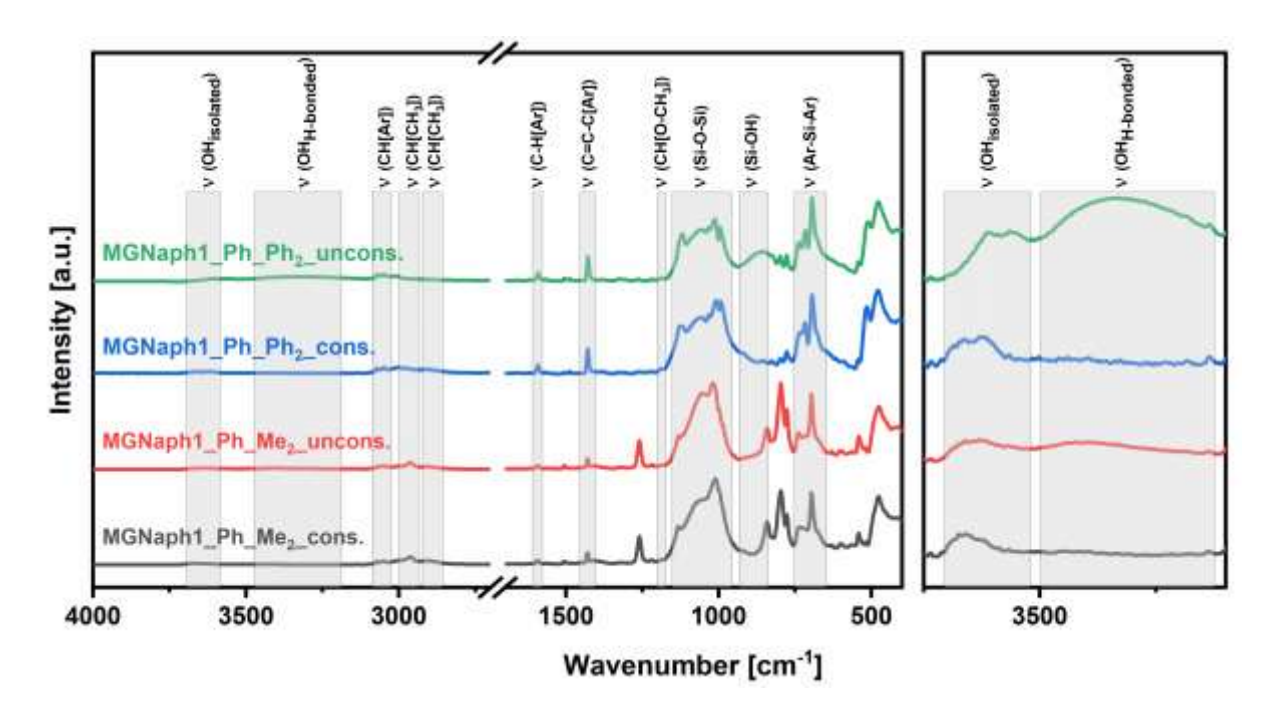


Figure 15: FTIR spectra of both MGNaph1_Ph_Me₂ before (red) and after (black) and MGNaph1_Ph_Ph₂ before (green) and after (blue) consolidation.

3.1.3.7 Ultraviolet-visible (UV-vis) Spectroscopy

Important properties of polysiloxanes used in optoelectronic devices are transparency, resistance against yellowing, and overall thermal stability. When polysiloxanes are exposed to high temperatures and UV light, bonds can be broken, creating free radicals that lead to yellowing, which also reduces transparency.²⁵⁹ The long-term optical stability can be determined by the yellowness index (YI), which can be determined using UV-vis spectroscopy and that describes the color change from clear/white to yellow.²⁶⁰ We performed measurements on all samples for approximately $120 \,\mu m$ thick films doctor-bladed on glass slides. Measurements were carried out before and after consolidation and after an additional 72 h and 168 h at 200 °C. The additional thermal steps can lead to a change in film thickness (Figure 16 and Figure S 59 - Figure S 60). All samples show a transmittance at 450 nm between 98 and 99 % before consolidation, which decreases by 1 to 2 % after thermal treatment (Figure 16, a). The only exception is MGPhen9_Ph_Ph2, which cracked after consolidation during cooling to room temperature, which explains the high drop in transmittance of 6%. Cracking of this sample compared to the others is based on the purely aromatic content and the phenanthrenyl group, both making the final polymer very brittle. Furthermore, it is worth mentioning that the polysiloxanes with 2-naphthyl showed a slightly higher decrease in transmittance than 1-naphthyl, which could be due to the different bonding of the naphthyl group. The transmittance of all oligosiloxanes decreases upon further thermal treatment for 3 d and 7 d. MGNaph1_Ph_Ph2, MGNaph2_Ph_Me2 and MGPhen9_Ph_Ph2, hereby show the biggest decrease of almost 10 %. For MGNaph1_Ph_Ph2 and MGPhen9_Ph_Ph2, this can be attributed to the cracking of the sample. Apart from this, their transmittances are decreasing only slowly. The smallest transmission loss is observed for MGNaph1_Ph_Me2 and MGPhen9_Ph_Me2 with only 2.3 and 2.7 %, respectively. Based on the samples containing dimethylsilanes, none of which cracked, the following series for thermal stabilities based on transmittance can be obtained: 1-naphthyl > 9-phenanthrenyl > 2-naphthyl. YI measurements confirm this trend for the afore mentioned silanes (Figure 16, b). Before consolidation, all samples show similar YI being the highest for 9-phenanthrenyl. After thermal treatment 2-naphtyl containing oligosiloxanes show the highest increase in YI. Siloxanes with dimethylsilane reveal the same or a lower YI before and after thermal treatment than those with diphenylsilane. MGNaph2_Ph_Me2 hereby is an exception having a significantly higher YI than MGNaph2_Ph_Ph2 after thermal treatment. In the literature, it is known that phenyl groups can undergo temperature-induced oxidation in air.31 This would explain the increase in YI at prolonged times at 200 °C, while the methyl groups seem to play only a minor role. YI measurements in literature have been carried out on various silicones in a time range between 1 and 1200 h and temperature ranges from room temperature to 200 °C, thereby increasing by values of up to 21.31,260,261,356

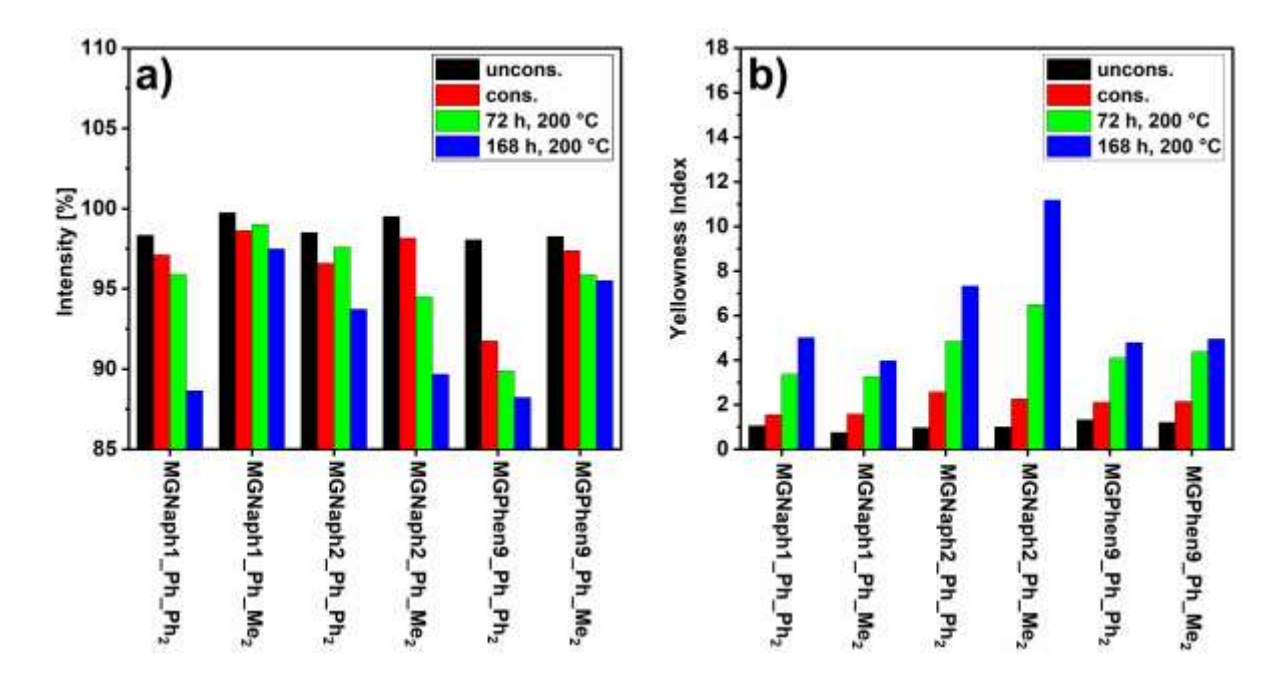


Figure 16: UV-vis measurements of all oligosiloxanes: a) transmittance and b) YI.

3.1.3.8 Fluorescence Spectroscopy

Fluorescence spectroscopy was performed on the unconsolidated siloxanes to investigate potential π - π -interactions of the polycyclic aromatic systems expressed in the formation of excimers (see Figure S 61 - Figure S 66), which can be shown by a concentration-dependent study of the diluted condensed materials and exemplified for MGNaph1_Ph_Ph2 and MGPhen9_Ph_Ph2 (Figure 17). If excimers are present, a broad peak should appear, which decreases with increasing in dilution.357 For MGNaph1_Ph_Ph2, two bands were detected. The signal at 342 nm is the one that is also observed for the monomer 1-NaphPhSi(OMe)₂ also shifting to lower wavelengths upon further dilution. The second peak at 398 nm shows no shift but decreases with increasing dilution, which is due to excimer fluorescence. 345,358-360. The same behavior can be observed for MGNaph1_Ph_Me2 as well as the 2-naphthalene containing siloxanes only varying slightly in wavelength. Comparing 1-naphthyl and 2-naphthyl, the excimer formation is less pronounced for the latter. Considering the lower decrease of the excimer band at high dilutions, intramolecular excimer formation seems to be a factor. Since the obtained oligosiloxanes are networked with PhSi(OMe)₃ and not just linear, the intramolecular excimer formation should arise from neighboring aromatic groups rather than from the formation of loops. Clarification on this however would need further

investigation. MGPhen9_Ph_Ph2 shows only the three close peaks originating from the phenanthrenyl group, which has already been observed in 9-PhenPhSi(OMe)₂ and can therefore be attributed to molecular fluorescence. The slight decrease in intensity with further dilution could possibly be attributed to ground-state aggregation.¹⁹² A similar observation is made for MGPhen9_Ph_Me2. It was not possible to measure the whole dilution series for all siloxanes due to a constant increase in intensity with further dilution, which eventually reached the detector limit. The Stokes shifts (see Figure S 61 - Figure S 66) of all samples show that excitation and emission are heavily overlapping, especially for the 9-phenanthrenyl systems. This is a sign for self-quenching phenomena and would explain the increase in intensity with further dilution. Diluting even further, the intensity of the spectra should decrease again since less molecules become available for absorption and subsequent emission.³⁶¹ Interestingly, even though the larger aromatic system of the phenanthrenyl group compared to the naphthalene group should in theory lead to more aggregation, no excimer fluorescence is observed. 362 This phenomenon was already investigated in the literature. According to Förster, the stability of the excited dimer mainly results from the resonance force between excited and unexcited molecules of the same kind, which is much weaker for phenanthrene than it is for naphthalene.³⁶³ In summary, it can be concluded that 1-naphthyl shows the highest tendency for dimerization and therefore the formation of excimers followed by 2-naphthyl, while 9-phenanthrenyl shows no aggregation tendency at all.

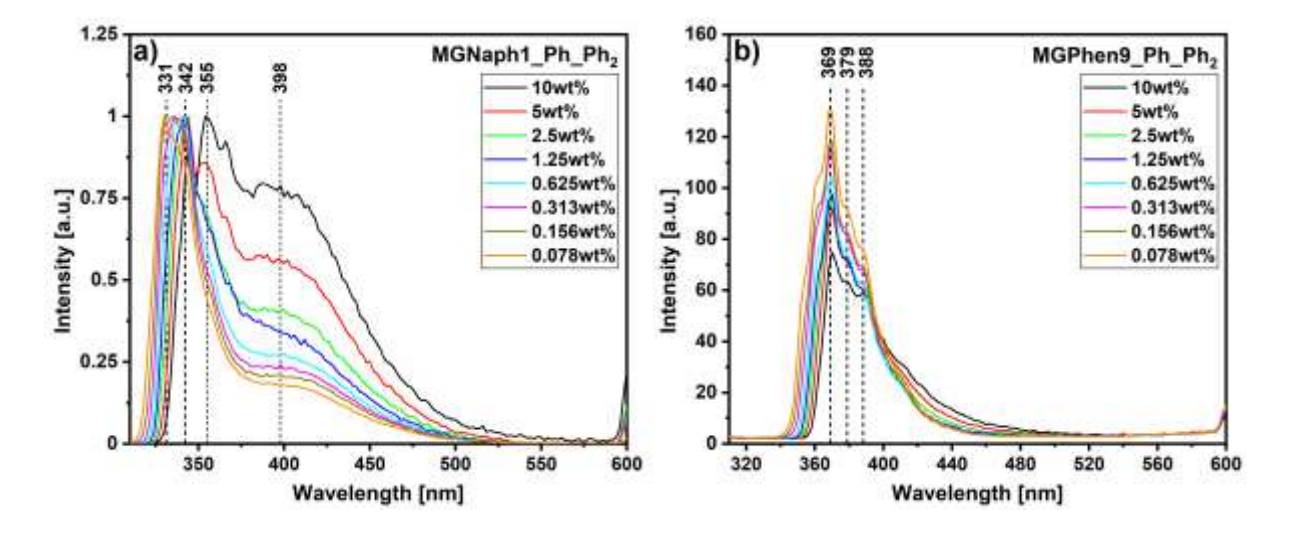


Figure 17: Fluorescence spectra of a dilution series of a) MGNaph1_Ph_Ph₂ and b) MGPhen9_Ph_Ph₂ in DCM with an excitation wavelength of 300 nm.

3.1.3.9 Matrix-Assisted Laser Desorption/Ionization Time of Flight (MALDI-TOF)

The molecular weight and therefore the size of a polymer as well as any low-molecularweight species influence the properties and characteristics of the polymer. To gain an insight into these characteristics, we used MALDI-TOF measurements (see Figure S 67 -Figure S 72). MALDI-TOF measurements of MGNaph1_Ph_Ph2 and MGPhen9_Ph_Ph2 (Figure 18) show a range in molecular weight up to 1600 and 2000 m/z, respectively, and are therefore oligosiloxanes rather than polysiloxanes. It should be noted that a matrix was used for these measurements, which can be found up to 800 m/z, preventing analysis up to this region. This is supported by the ²⁹Si CP-MAS NMR of MGPhen9_Ph_Ph₂ that shows a slightly higher condensation than for MGNaph1_Ph_Ph2 with DOCs of 83 and 81 %, respectively. The dimethyl containing polysiloxanes are roughly reaching the same values as the samples with diphenylsilane. Considering the monomer Me₂Si(OMe)₂ has less molecular weight then Ph₂Si(OMe)₂, oligosiloxanes containing the former should have more repeat units. They also show a higher DOC. This can also be deduced from the ²⁹Si CP-MAS NMR results showing higher ratios of T³ to T² as well as very high ratios of D'² to D'1 of the samples with Me₂Si(OMe)₂ as monomers. The mass fragments of all monomer units are present in the spectra, proving that all monomers were incorporated in the polymeric structures. Furthermore, for MGNaph1_Ph_Ph2 certain oligomers can be identified as, for example at 892, 963 and 1013 m/z. During the ionization in these measurements, H⁺ ions can accumulate on the oligomers, increasing their molecular weight slightly. Since the consolidated oligosiloxanes are still soluble, we exemplary carried out MALDI-TOF measurements on the consolidated MGNaph1_Ph_Ph2 (see Figure S 73). The molecular weight now reaches up to 2400 m/z and therefore has increased significantly, indicating further condensation during the consolidation.

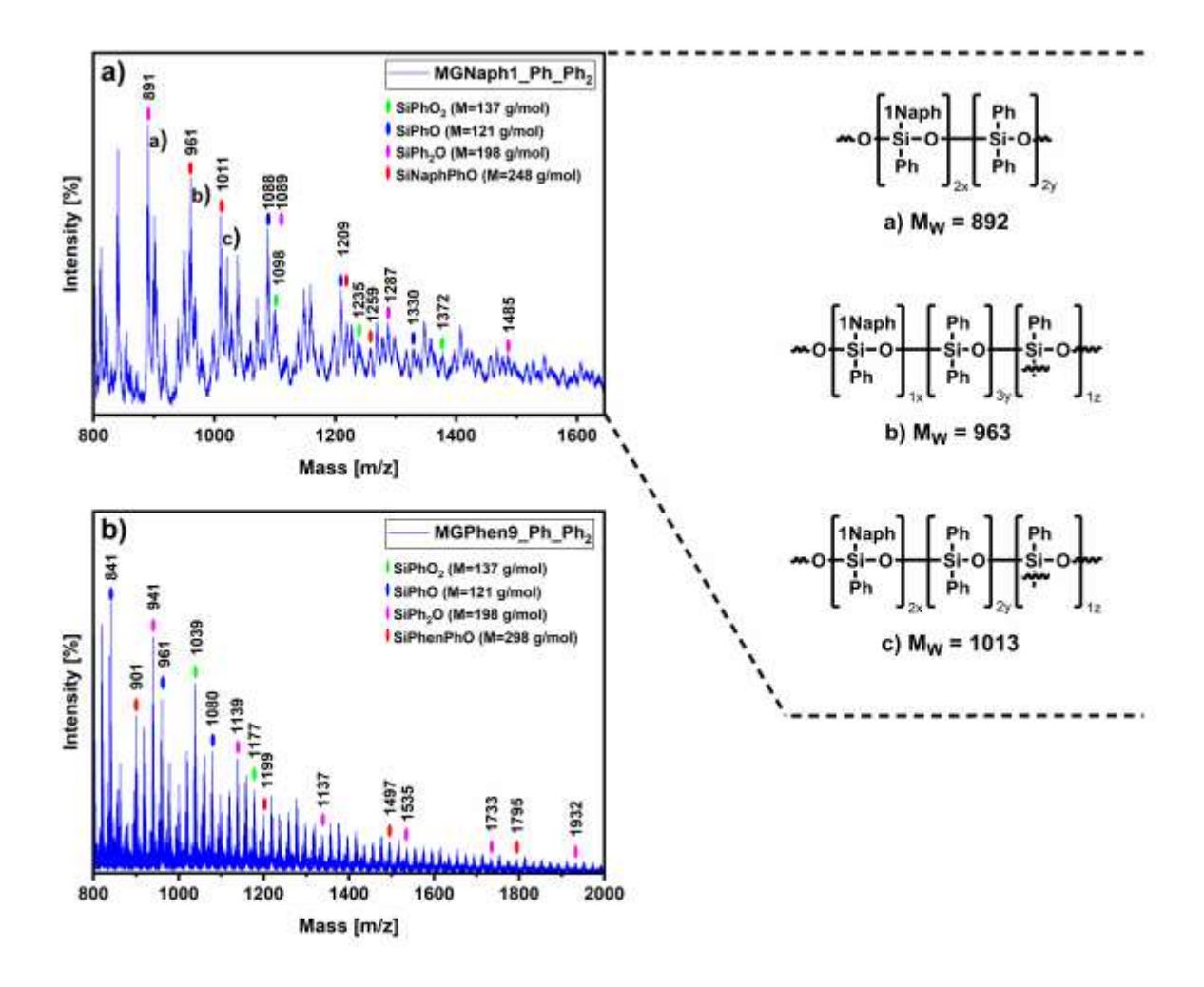


Figure 18: MALDI-TOF measurement of a) MGNaph1_Ph_Ph2 and b) MGPhen9_Ph_Ph2.

3.1.3.10 Size Exclusion Chromatography (SEC)

Size exclusion chromatography experiments were performed on MGNaph1_Ph_Ph2 and MGNaph1_Ph_Me2 (see **Figure S 74** and **Table S 5**) using a UV detector. The chromatogram of MGNaph1_Ph_Ph2 taken with polystyrene (PS) as standard shows only one broad peak with two maxima in a range of 300-1200 g mol $^{-1}$ with an average molecular weight (M $_{\rm w}$) of 790 g mol $^{-1}$ and a polydispersity index (D) of 1.174. The chromatogram for MGNaph1_Ph_Me2 shows one broad peak from 300 to 1500 g mol $^{-1}$ with an average molecular weight (M $_{\rm w}$) of 1212 gmol $^{-1}$ and a D of 1.428. Both oligosiloxanes have roughly the same size distribution with no monomers being present. It also shows that oligomers rather than polymers were obtained during the condensation process confirming the MALDI-TOF mass spectrometry measurements. Even though the PS standard which was used differed with respect to the hydrodynamic volume in THF compared with our systems, the molecular weight is in the same range as already shown by the MALDI-TOF

measurements. In contrast to the MALDI-TOF experiments, no interfering matrix is present in these investigations. Thus, low-molecular-weight species below 800 g mol⁻¹ can be observed. We cannot exclude that also ring formation occurred during the polycondensation reaction, which would lead to small organo cyclotrisiloxanes or cyclotetrasiloxanes. However, these ring systems cannot be specifically detected with the instrumental methods used in our studies.

3.1.3.11 Differential Scanning Calorimetry (DSC)

DSC measurements show the expected reversible thermoplastic behavior of melting-gellike structures with a distinct melting process. 183 Repetitive heating and cooling was applied to the samples to obtain hysteresis curves investigating the repeatability of the melting process for the unconsolidated samples as well as their glass transition temperature (Tg) (Figure 19). It can be concluded that all oligosiloxanes are reversibly changes in their T_g's. All samples meltable without condensed with diphenyldimethoxysilane show a higher $T_{\rm g}$ then their dimethyldimethoxysilane counterparts, which is a literature-known phenomenon.³⁶⁴ It should also be mentioned that the T_g increases further with larger aromatic substituents, which can be seen as the phenanthrenyl containing oligosiloxanes exhibit higher values then the naphthyl derivates. Comparing MGNaph1_Ph_Ph2 with MGNaph2_Ph_Ph2 or MGNaph1_Ph_Me2 with MGNaph2_Ph_Me2 it becomes obvious that 2-naphthyl leads to a lower Tg then 1-naphthyl. This could be due to the different binding leading to less steric hinderance and less free volume.365 The steric demand of the two groups differently attached to the siloxane backbone can result in different degrees of freedom of the polymer chains and consequently in variations of the association efficiency (Scheme 28). The measured Tg's, in general, range from -14.5 °C (MGNaph2_Ph_Me₂) to 21.8 °C (MGPhen9_Ph_Ph₂). Generally, the Tg's for polysiloxanes can range from around -115 to 56 °C depending on the groups present, the amount of di- and trialkoxysilanes, and their ratio. 183,184,298,366

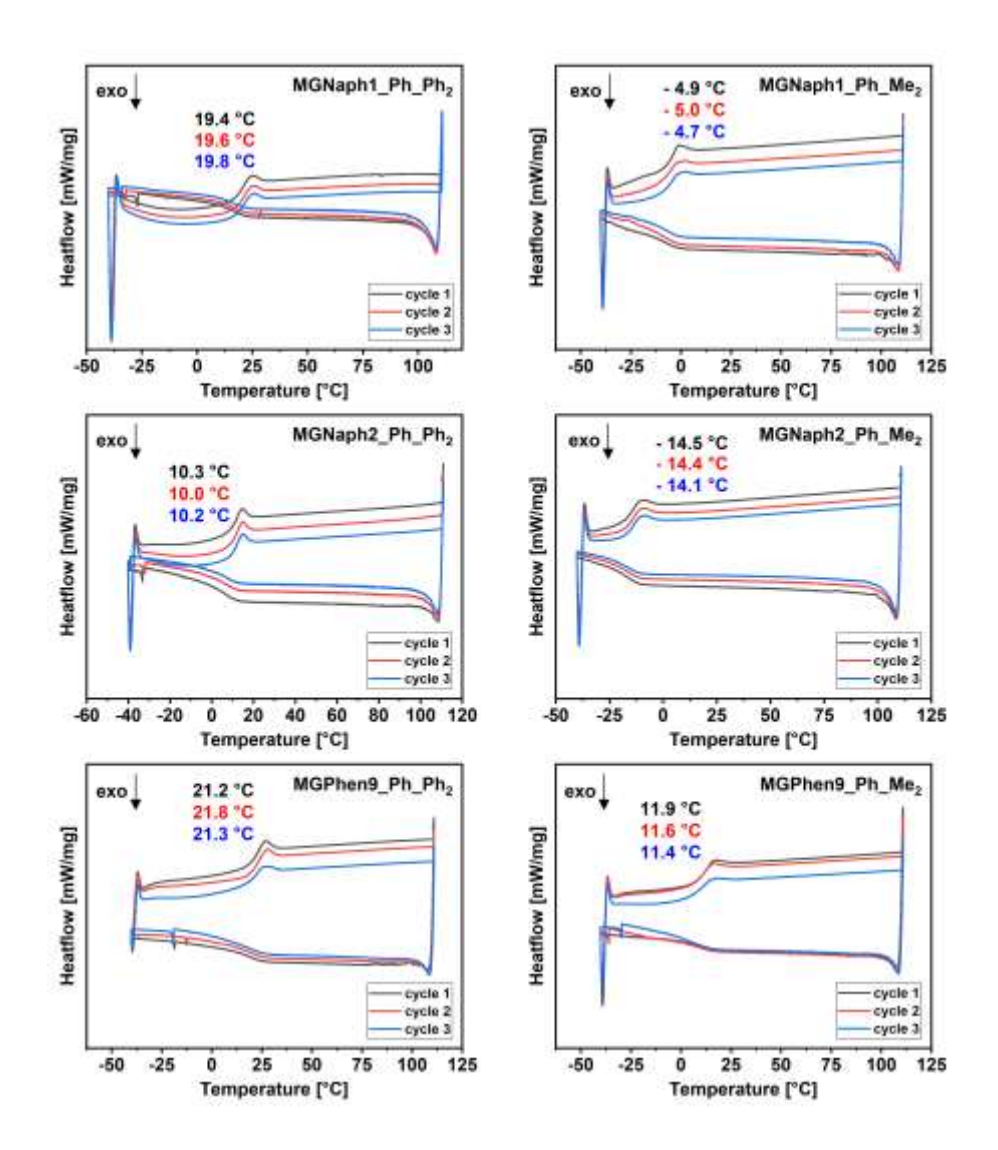


Figure 19: Hysteresis curves of all oligosiloxanes before consolidation. Every sample was measured three times.

Scheme 28: Differences in steric hinderance of 1-naphthyl and 2-naphthyl in a) MGNaph1_Ph_Ph_2 and b) MGNaph2_Ph_Ph_2.

Usually, consolidation of phenyl structures is obtained upon heating to 200 °C for 24 h. 183 However, for the here described more sterically demanding polycyclic aromatic groups, longer consolidation times are necessary; therefore, we heated our samples at 200 °C for 72 h (Figure 20). Successfully consolidated materials do not show any Tg since the crosslinking should lead to an irreversible dense network formation, resulting in the loss of a softening temperature. 183,184 Upon thermal treatment, the $T_{\rm g}$ of all oligosiloxanes further increased, which shows that the condensation process continues. For almost all oligosiloxanes, the general trend already discussed for the unconsolidated samples continues in that the Tg increases from 2-naphthyl to 1-naphthyl to 9-phenanthrenyl. It also increases for the corresponding oligosiloxanes from those containing dimethyldimethoxysilane to those containing diphenyldimethoxysilane. The only exception is MGNaph2_Ph_Me2, which now shows the second highest $T_{\rm g}\mbox{ of all}$ oligosiloxanes. This could possibly be due to the higher degree of condensation of the 2-naphthyl monomer compared to the 9-phenanthrenyl monomer as already observed in the ²⁹Si CP-MAS spectra as well as the highest DOC of all samples. Unfortunately, all supposedly consolidated samples still show a T_g, proving that no complete consolidation was achieved. This could be due to the steric hindrance originating from the polycyclic aromatic groups and high aromatic content in general. Incomplete consolidation is also

evidenced by the overall low T^3 signals in the ²⁹Si CP-MAS NMR spectra. None of the measured T_g increases from one cycle to another which can be taken as an indication that the consolidation process is complete. The T_g 's obtained after consolidation are quite low in some cases. The highest values being reached at 74 °C for the purely aromatic phenanthrenyl containing polymer, which makes them appear unfavorable for high temperature applications. In summary, although all polysiloxanes undergo further condensation by heating them to 200 °C, the condensation process cannot complete to a point where the T_g disappears.

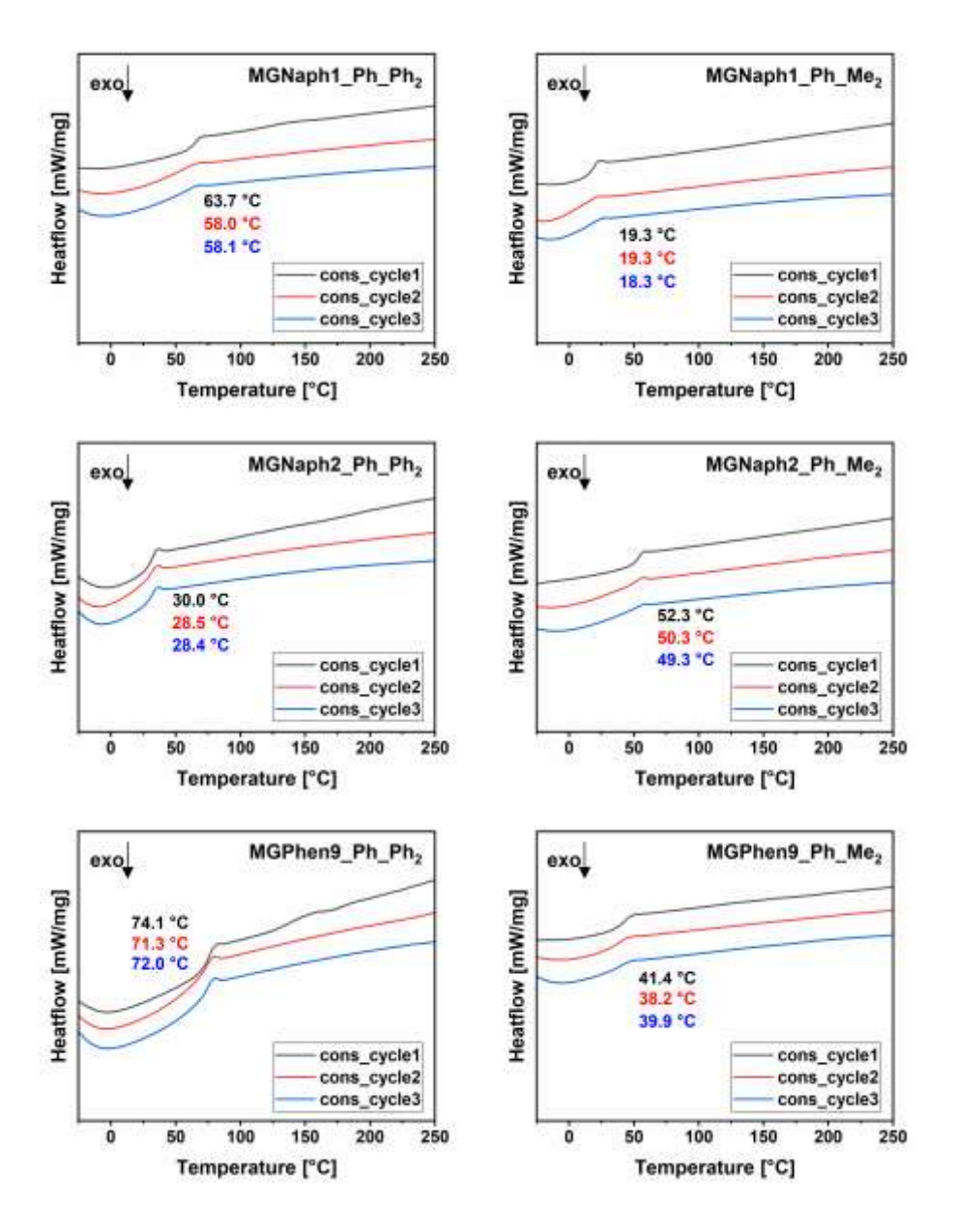


Figure 20: DSC curves of all oligosiloxanes after consolidation. Every sample was measured three times.

3.1.3.12 Thermogravimetric Analysis (TGA) and TG-FTIR

Thermogravimetric analysis (TGA) was performed to evaluate the thermal stability of the polysiloxanes as well as study their decomposition behavior. For this purpose, all oligosiloxanes before and after consolidation were heated up to 800 °C under oxygen (Figure 21). For the unconsolidated samples, the T₉₅ values range from 222 to 306 °C with residual masses between 15.95 and 29.22 %. Oligosiloxanes with dimethyldimethoxysilane show а higher residual mass than those with diphenyldimethoxysilane due to the lower molecular weight of the methyl groups compared to the phenyl groups. Within each group, no logical sequence can be determined. This could be due to a different degree of condensation and thus different amounts of water and methanol released during heating. Another possibility would be the formation of cyclic structures during the condensation reaction, which would also evaporate at elevated temperatures. It is clearly visible that the polycyclic group has a strong influence on the T_{95} values with 2-naphthyl providing the highest and 9-phenanthrenyl the lowest values. For samples containing the same polycyclic group, Me₂Si(OMe)₂ seems to lead to equal or lower values than Ph₂Si(OMe)₂.^{367,368} Before consolidation, the first mass loss should be due to evaporation of water and methanol formed during the ongoing condensation at higher temperatures. 369 This would lead to the assumption that the oligosiloxanes containing 9-phenanthrenyl are least condensed and thus release the most water and methanol followed by 1-naphthyl and 2-naphthyl. To investigate this further, TG-FTIR studies were applied using MGNaph1_Ph_Ph2 (Figure 22). The TG and Gram Schmidt curves (Figure 22, b) show four mass loss steps at 164, 309, 572 and 679 °C. As already assumed, the first mass loss at 164 °C is due to water and methanol. At 309 °C (Figure 22, c), the IR shows water and the typical signals of aromatic compounds, indicating the breakage of Si-C bonds and release of benzene and naphthalene. A distinction between both is not possible due to their strong similarity. 370-³⁷³ At 572 °C (**Figure 22, c**), the same absorption bands as before can be seen. Additionally, a band at 1429 cm⁻¹ (Si-Ph) and a broad band from 1128 to 1012 cm⁻¹ (Si-O-Si) are appearing, both signifying the existence of small condensed species. Considering the amount of dialkoxysilanes, these should be cyclic structures. 374,375 At 679 °C (Figure 22, c), the previously observed bands have almost disappeared and a strong CO₂ band can be observed indicating further decomposition of the oligosiloxane.

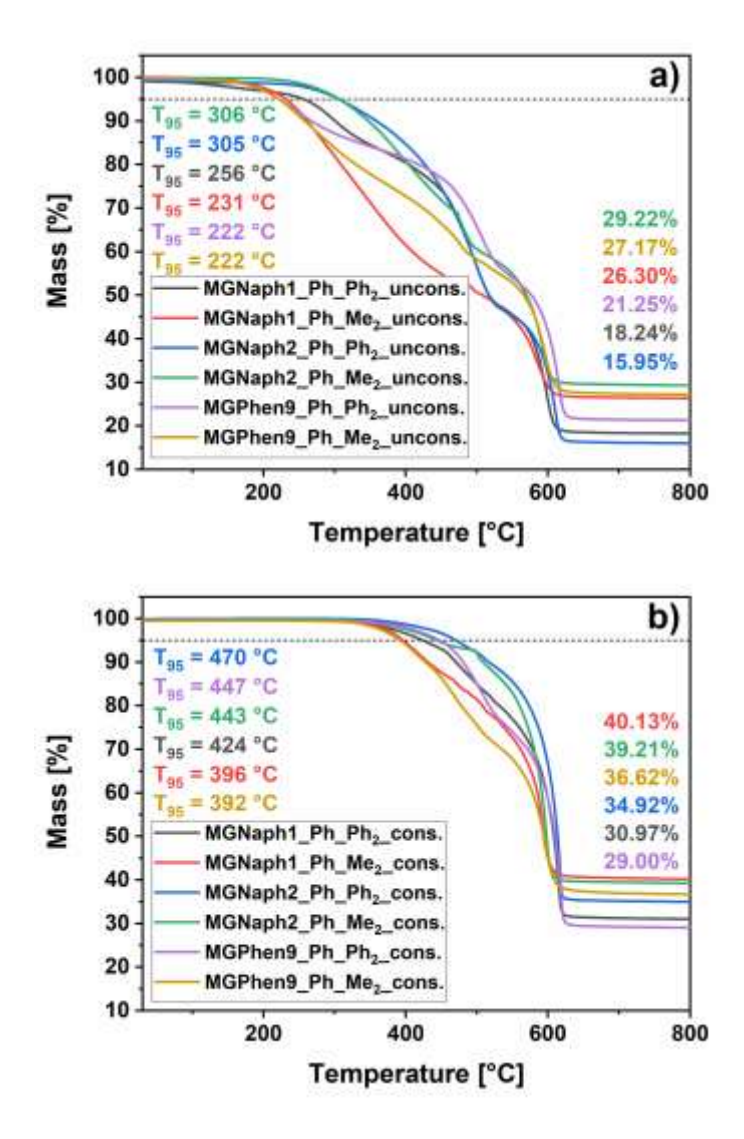


Figure 21: TGA curves of all polysiloxanes a) before and b) after consolidation.

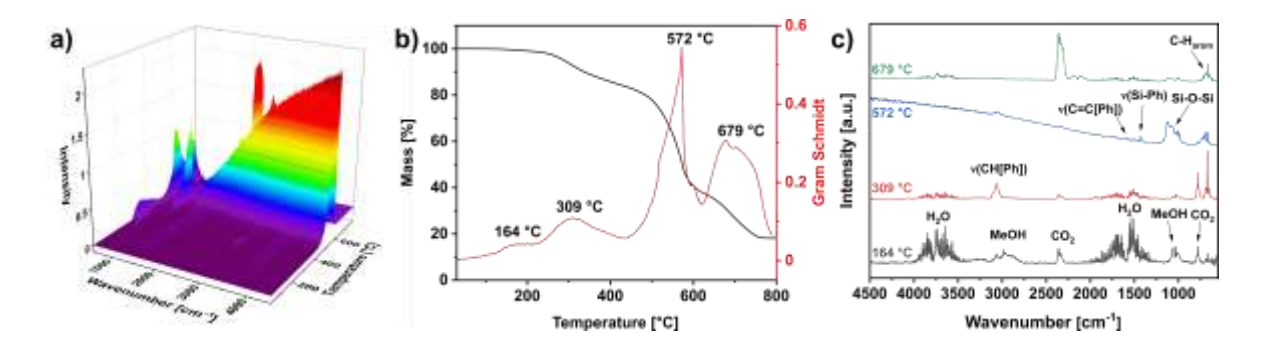


Figure 22: TG-FTIR measurements of MGNaph1_Ph_Ph₂. a) 3D plot, b) TG and Gram Schmidt curves, c) IR at 164, 309, 572 and 679 °C.

The appearance of cyclic species during the thermal decomposition of polymers is a well-known phenomenon and can be explained by a backbiting mechanism (**Scheme 29**). ^{228,368}

R = 1-naphthyl, phenyl, OR

Scheme 29: Cyclization reaction due to backbiting and release of cyclic species shown exemplary on MGNaph1 Ph Ph₂.

The consolidated oligosiloxanes show a different order than the unconsolidated ones in terms of the residual mass as well as T_{95} values. For the residual mass, the same trend as for the unconsolidated samples can be seen. In general, dimethyldimethoxysilane show higher values than those with diphenyldimethoxysilane due to the lower molecular weight of the methyl groups. After consolidation, the residual mass within these two groups decreases with the polycyclic group enlarging from naphthyl to phenanthrenyl as expected. MGNaph2_Ph_Ph2 hereby has a higher residual mass then MGNaph1_Ph_Ph2, indicating a higher ratio of silicon to organic and therefore a higher degree of condensation. This is also evident in the higher proportion of D² and T³ signals in the ²⁹Si CP-MAS spectra. The T₉₅ values are in no clear order. MGNaph2_Ph_Ph₂ shows the highest value at 470 °C, while MGPhen9_Ph_Me2 has the lowest at 392 °C. It seems that phenyl groups lead to higher thermal stability than methyl groups for the respective polycyclic monomer, which is in good agreement with the literature.367,368 Among the polycyclic aromatic groups, thermal stability tends to be highest for 2-naphthyl, although this may also be due to the slightly increased cross-linking degree also visible in the ²⁹Si CP-MAS spectra. In general, it can be concluded that the obtained cured oligosiloxanes show very high thermal stabilities. Other siloxanes consisting mainly of phenyl and methyl groups show T₉₅ values between 340 and 460 °C, ^{190,254,277,316} while the polysiloxanes containing polycyclic aromatic groups previously synthesized in our group showed values up to 370 °C.191

3.1.3.13 Refractive Index (RI)

Polymers with a high RI are important for many applications like prisms, lenses, or optical fibers.324 The RI was measured via the afore mentioned calibration curve method (see Figure S 75 – Figure S 76) before and after consolidation (Table 5). To achieve a high RI, a siloxane needs to contain groups with a high molar refraction, which in turn increases with more polarizable groups and a higher overall density. Systems with conjugated π -bonds also increase the refractive index. Other factors that have to be considered for an increase in RI are a low molecular volume and an improved molecular packing, which can be influenced by the steric demand of the used groups.²⁸⁰ For the unconsolidated samples, the RI increases from naphthyl to phenanthrenyl due to the latter having a higher molar fraction, while there is no difference between the 1-naphthyl and 2-naphthyl groups. Interestingly, the RI decreases upon consolidation for the samples with 1-naphthyl and 9-phenanthrenyl groups. One explanation could be the condensation reaction considering it leads to more "glass like" structures and the SiO₂ in glass has a RI of only 1.463, which is significantly lower than that of our polymers.³⁷⁶ A second possible explanation could be the cleavage of the methoxy and hydroxy groups during condensation. Both methyl and hydroxy groups should have a higher molar refraction than the Si-O-Si unit obtained by condensation.³⁵ Interestingly, the RI of both oligosiloxanes containing the 2-naphthyl group increases after consolidation and for MGNaph2_Ph_Ph2 even reaching the highest value of all samples. A definitive explanation for this observation cannot be given at this point. Possibly, the sterically less hindered 2-naphthyl group leads to a stronger reduction of the molar volume (V_M) during consolidation than the other polycyclic residues. According to the Lorentz-Lorenz equation (eq. 3), this would lead to an increase in the refractive index. The sterically less bulky 2-naphthyl groups could also lead to an improved molecular packing, which in turn would decrease the molar volume and therefore increase the RI. 377,378 Similar attempts to increase the RI by modification of the organic residues at the silicon backbone or the backbone itself gave similar or lower RIs, whereby higher RIs were obtained by the addition of sulfur. Further improvements were made by adding metal atoms such as germanium or tin as well as by using halogenated polycyclic aromatics or preparing siloxanes consisting of only polycyclic groups. It should be noted that while the former is

not a pure siloxane, the latter has no known characteristics other than its refractive index. (**Table 6**).

Table 5: Refractive indices of the polymers before and after consolidation.

	RI, unconsolidated	RI, consolidated
MGNaph1_Ph_Ph₂	1.603 ± 0.001	1.598 ± 0.001
MGNaph1_Ph_Me₂	1.559 ± 0.002	1.557 ± 0.001
MGNaph2_Ph_Ph₂	1.600 ± 0.003	1.610 ± 0.001
MGNaph2_Ph_Me₂	1.560 ± 0.002	1.585 ± 0.001
MGPhen9_Ph_Ph₂	1.622 ± 0.002	1.603 ± 0.003
MGPhen9_Ph_Me ₂	1.585 ± 0.003	1.575 ± 0.001

Table 6: Comparison of refractive indices of different polysiloxanes.

	RI	Wavelength /nm	Source
This work	1.610	589	
Our previous work	1.63	622	191
adamantane-based phenyl epoxy-silicone	1.565		190
Siloxane-Sulfide Polymer	1.665	546	277
Polysiloxane-Silphenylene Hybrimer	1.59	520	254
Epoxy Modified Methyl Phenyl Silicone Resin	1.5367		379
Thiol-Ene Polymers	1.703	546	380
Halogenated functional resins	1.770	633	381

3.1.4 Experimental Section

3.1.4.1 Materials

Magnesium chips (99.9+%, Acros Organics), 1-bromonaphthaline (97%, abcr GmbH), 2-bromonaphthalene (98%, BLD Pharmatech Ltd), 9-bromophenantherene (99.83%, BLD Pharmatech Ltd), and phenyltrimethoxysilane (97%, abcr GmbH) were used without further purification. THF (99.8 % HPLC grade, Fischer Chemical) was purified in a MBraun SPS-5 solvent purification system. All dialkoxysilane syntheses were carried out under

inert atmosphere. For polymer synthesis dimethoxydiphenylsilane (97%, Alfa Aesar), dimethyldimethoxysilane (97%, abcr GmbH), phenyltrimethoxysilane (97%, abcr GmbH), and THF (99.8 % HPLC grade, Fischer Chemical) were used without further purification. Hydrochloric acid (pH 1) was diluted from conc. HCl (for analysis, ACS BerndKraft) using demineralized water.

3.1.4.2 Instrumentation and Characterization Methods

NMR spectra in solution were carried out on an Avance III HD 400 MHz spectrometer (Bruker Corporation, Billerica, USA) with 400.13 MHz for ¹H NMR spectra, 100.62 MHz for ¹³C NMR spectra and 79.49 MHz for ²⁹Si NMR spectra. All NMR samples were prepared in chloroform-d (CDCl₃). ²⁹Si spectra of the polymers were analyzed after subtraction of a blanc spectrum measured in the same type of tube as the samples containing only chloroform-d (CDCl₃) to remove the glass peak using TopSpin (4.1.1, 2020, Bruker BioSpin GmbH).

CP-MAS NMR spectra were recorded on an Avance III HD-Ascend 400WB spectrometer (Bruker Corporation, Billerica, USA) using 4 mm inner diameter ZrO₂ rotors with a 13 kHz rotation frequency. The resonance frequencies were 100.67 MHz for ¹³C and 79.53 MHz for ²⁹Si NMR spectra. All spectra except for the ²⁹Si CP-MAS NMR were plotted in MestReNova v14.2.1-27684 using the apodization function to adjust the signal-to-noise ratio, while the ²⁹Si CP-MAS spectrum was analyzed with OriginPro 2021b and integrated using a Gaussian function. For MGNaph1_Ph_Me₂ it was only possible to record a ²⁹Si CP-MAS spectrum with half of the normal number of scans. Due to its lower viscosity and the rotation, the sample was pressed upward against the inner wall of the rotor, causing the lid to loosen and the measurement had to be stopped.

Fourier transform infrared (FTIR) spectra were recorded in attenuated total reflectance mode (ATR) on a Vertex 70 spectrometer (Bruker Optics, Ettlingen, Germany) from 4500 to 400 cm⁻¹ for the monomers but only shown from 3250 to 400 cm⁻¹ due to the absence of other signals at higher wavenumbers and from 4000 to 400 for the unconsolidated samples, each with a resolution of 4 cm⁻¹ and 16 scans.

Elemental analysis was performed on a Vario Micro cube (Elementar Analysensysteme GmbH, Langenselbold, Germany).

UV-vis transmission measurements of the monomers were performed in a quartz glass cuvette with 1 cm thickness, diluted in dichloromethane from 200 to 800 nm but only

presented from 230 to 500 nm due to the absorption of the quartz class at low wavelengths and the absence of other signals at high wavelengths. All oligosiloxanes were doctor bladed onto glass slides at a thickness of approximately 120 μ m, heated to 110 °C for 5 min in an oven to ensure a uniform film and measured after cooling. The measurement range was from 200 to 800 nm but is only presented from 300 to 800 nm due to the absorption of the class slides at low wavelengths. Consolidation of the oligosiloxanes was performed in a vacuum oven at 200 °C for 24 h to prevent blistering and then for an additional 72 h at 200 °C in an oven. Further thermal treatment was also done in an oven at 200 °C for an additional 7 days, and measurements were taken after 3 and 7 days. All transmittance measurements were performed on a Lambda 750 instrument (Perkin Elmer Inc., Shelton, USA) equipped with a 100 mm integration sphere with 2 nm increments and 0.2 s integration time. Yellowness index measurements were performed on the same samples at the same time intervals as the transmittance measurements from 380 to 780 nm, with 10 nm increments and 0.24 s integration time using the same instrumental setup.

Fluorescence measurements for all samples were performed in a quartz glass cuvette with 1 cm thickness, diluted in dichloromethane on a fluorescence spectrometer FP-6500 (Jasco, Pfungstadt, Germany). All emission spectra were recorded with a band width of 3 nm, a response time of 0.5 s, and a scanning speed of 200 nm min⁻¹. The excitation wavelengths of the monomers and oligosiloxanes for the emission spectra were 290 and 300 nm, respectively. Excitation spectra were recorded in the same manner with emission wavelengths of 360, 370 and 400 nm for 1-NaphPhSi(OMe)₂, 2-NaphPhSi(OMe)₂ and 9-PhenPhSi(OMe)₂ as well as 360 nm for 1- and 2-naphthalene and 390 nm for 9-phenanthrene containing oligosiloxanes.

Thermogravimetric measurements (TG) were carried out applying a TGA/DSC STARe System 1 (Mettler-Toledo, Schwerzenbach, Switzerland) applying a heating rate of 10 K min⁻¹ between 25 and 800 °C using an oxygen gas flow of 40 mL min⁻¹.

Refractive indices were measured as a dilution series (see Supporting Information) on an Abbemat 350 (Anton-Paar OptoTec GmbH, Seelze-Letter, Germany) at a wavelength of 589 nm and 20 °C.

TG-FTIR measurements were performed using the above-mentioned Bruker Vertex 70 spectrometer coupled to a TG F1 Iris (NETZSCH-Gerätebau GmbH, Selb, Germany). Each

FTIR spectrum was performed in the wavenumber range $550-4500 \, \text{cm}^{-1}$ and by averaging 16 scans with a spectral resolution of $4 \, \text{cm}^{-1}$. TGA was performed under a constant flow of N_2 (32 mL min⁻¹) and O_2 (8 mL min⁻¹) with a heating rate of 20 K min⁻¹ to a maximum of 800 °C. During the measurements, the samples were placed in an open alumina crucible. Differential scanning calorimetry (DSC) was performed with a DSC 204 *F1 Phoenix* calorimeter (NETZSCH-Gerätebau GmbH, Selb, Germany) using aluminum crucibles with pierced lids under nitrogen/oxygen-flow (40/60 mL min⁻¹) applying a heating rate of 10 K min⁻¹. The temperature range was -40 to 200 °C to measure the T_g of the consolidated and -40 to 110 °C to determine repeatability of the melting process of the unconsolidated samples. The value of the glass transition temperature (T_g) was taken by determining the center point of the glass event.

MALDI-TOF measurements were carried out on a 4800 Plus MALDI tandem TOF (AB Sciex, Darmstadt, Germany) in linear mode with a neodym YAG laser (353 nm) and analyzed with Data Explorer Software (4000 Series Explorer). The samples were dissolved with a dithranol-matrix solved in 70 % TFA and 30 % water, placed on a plate, and left to dry. Then, 1 μ L AgTFA solved in THF was added and the samples were measured.

Size exclusion chromatography (SEC) was performed with a PSS SECcurity2 system composed of a 1260 IsoPump-G7110B (Agilent Technologies, Santa Clara, CA, USA) and a 1260 VW-detector G7162A at 270 nm (Agilent Technologies) at 25 °C, with THF as the mobile phase (flow rate 1 mL min⁻¹) on an SDV column set (SDV 10³, SDV 10⁵, SDV 10⁶) from PSS (Polymer Standard Service, Mainz, Germany). Calibration was carried out using PS standards (from PSS).

Powder X-ray diffraction (PXRD) patterns of the pulverized samples were recorded at room temperature on a D8-A25-Advance diffractometer (Bruker AXS, Karlsruhe, Germany) in Bragg-Brentano θ - θ geometry (goniometer radius, 280 mm) with Cu K α radiation (λ = 154.0596 pm). A 12 μ m Ni foil working as a K $_{\beta}$ filter and a variable divergence slit were mounted at the primary beam side. A Lynxeye detector with 192 channels and a variable slit diaphragm in front of it was used at the secondary beam side. Experiments were carried out in a 2 θ range of 3–40° with a step size of 0.013° and a total scan time of 1 h. The recorded data was evaluated using TOPAS 5.0 (Bruker AXS, 2014, Karlsruhe, Germany) software, with the observed reflections being treated via single-line fits.

3.1.4.3 Synthesis of Dialkoxysilanes

All three dialkoxysilanes were synthesized and purified according to modified literature procedures. 70,382 All temperatures were taken from the heating block.

Dimethoxyphenyl-(1-naphthyl)silane (1-NaphPhSi(OMe)₂)

A 1000 mL three-necked round bottom flask equipped with a reflux condenser, a dropping funnel, and a gas inlet was charged under a nitrogen atmosphere with magnesium chips (12.32 g, 506.8 mmol, 1.5 eq) and 400 mL abs THF and heated to 45 °C. 1-bromonaphthalene (71.04 g, 343.1 mmol, 1 eq) was diluted with 50 mL abs THF in the dropping funnel and added dropwise over a period of 30 minutes. The reaction mixture was stirred at 60 °C for 2 h. Phenyltrimethoxysilane (201.78 g, 1017.6 mmol, 3 eq) was added to a 1000 mL Schlenk flask, which was charged under nitrogen atmosphere, cooled to -10 °C using an ethanol/nitrogen bath, and the still-hot reaction mixture was added via cannula. The solution was stirred overnight and allowed to warm up to room temperature.

After the solvent was removed, 400 mL n-hexane was added to the residue, refluxed for 10 minutes, and decanted after cooling to room temperature. 200 mL n-hexane was added to the remaining residue, refluxed for 10 minutes, and filtered while hot. The combined organic solvents were subsequently removed with a rotary evaporator and in high vacuum. The crude product was distilled by fractionating distillation: 1. Fraction (1.0x10⁻² mbar, 80 °C) was excess phenyltrimethoxysilane, 2. fraction (1.2x10⁻² mbar, 160 °C) was the desired product. The product was allowed to solidify overnight, crushed, and then washed with cold ethanol and precipitated from the filtered ethanol to gain a total yield of 66.8 g (yield: 66 %) of a white crystalline solid.

¹**H NMR:** (400 MHz, CDCl₃) δ 8.30-8.24 (phenyl/naphthyl, m, 1H), 8.06-8.01 (phenyl/naphthyl, dd, J = 6.8, 1.4 Hz, 1H), 7.98-7.93 (phenyl/naphthyl, dt, J = 8.2, 1.1 Hz, 1H), 7.89-7.84 (phenyl/naphthyl, m, 1H), 7.73-7.68 (phenyl/naphthyl, m, 2H), 7.55-7.50 (phenyl/naphthyl, dd, J = 8.2, 6.8 Hz, 1H), 7.48-7.44 (phenyl/naphthyl, m, 2H), 7.44-7.41 (phenyl/naphthyl, m, 1H), 7.40-7.34 (phenyl/naphthyl, m, 2H), 3.67 (OCH₃, s, 6H) ppm.

²⁹**Si NMR** (79 MHz, CDCl₃) δ -27.65 ppm.

¹³**C NMR** (101 MHz, CDCl₃) δ 137.20, 136.36, 134.80, 133.40, 133.07, 131.35, 130.46, 130.17, 128.86, 128.36, 128.09, 126.52, 125.73, 125.20, 51.11 ppm.

CHN: calc. C: 73.43 %, H: 6.16 %; found C: 73.21 %, H: 5.78 %

Dimethoxyphenyl-(2-naphthyl)silane (2-NaphPhSi(OMe)₂)

Dimethoxyphenyl-(2-naphthyl)silane was synthesized in the same manner as dimethoxyphenyl-(1-naphthyl)silane. After removing the solvent of the combined filtrates, the crude product had to be purified by Kugelrohr distillation (2.5x10⁻² mbar, 200 °C) and yielded 68.4 g (68 %) of a viscous colorless liquid.

¹**H NMR:** (400 MHz, CDCl₃) δ 8.33-8.25 (phenyl/naphthyl, m, 1H), 7.96-7.85 (phenyl/naphthyl, m, 3H), 7.81-7.70 (phenyl/naphthyl, dd, J = 7.9, 1.6 Hz, 3H), 7.61-7.41 (phenyl/naphthyl, m, 5H), 3.74 (OCH₃, s, 6H) ppm.

²⁹**Si NMR** (79 MHz, CDCl₃) δ -28.76 ppm.

¹³**C NMR** (101 MHz, CDCl₃) δ 136.47, 135.01, 134.53, 132.94, 132.30, 130.57, 130.42, 129.71, 128.55, 128.13, 127.87, 127.38, 127.03, 126.12, 51.12 ppm.

CHN: calc. C: 73.43 %, H: 6.16 %; found C: 73.30 %, H: 6.39 %

Dimethoxyphenyl-(9-phenanthrenyl)silane (9-PhenPhSi(OMe)₂)

Dimethoxyphenyl-(9-phenanthrenyl)silane was synthesized in the same manner as dimethoxyphenyl-(1-naphthyl)silane. After filtration of the twice refluxed solution, the crude product crystallized in the filtrate. It was filtered off again, recrystallized from n-hexane, and yielded 53.9 g (54 %) of a crystalline white solid.

¹**H NMR:** (400 MHz, CDCl₃) δ 8.78-8.70 (phenyl/phenanthrenyl, m, 2H), 8.47-8.43 (phenyl/phenanthrenyl, s, 1H), 8.38-8.33 (phenyl/phenanthrenyl, dd, J = 8.1, 1.3 Hz, 1H), 8.04-7.99 (phenyl/phenanthrenyl, dd, J = 7.9, 1.5 Hz, 1H), 7.82-7.77 (phenyl/phenanthrenyl, dt, J = 6.6, 1.6 Hz, 2H), 7.77-7.70 (phenyl/phenanthrenyl, ddd, J = 8.3, 7.0, 1.5 Hz, 1H), 7.69-7.62 (dddd, J = 8.3, 7.0, 2.7, 1.3 Hz, 2H), 7.61-7.54

(phenyl/phenanthrenyl, ddd, J = 8.2, 6.9, 1.3 Hz, 1H), 7.50-7.39 (phenyl/phenanthrenyl, m, 3H), 3.75 (OCH₃, s, 6H) ppm.

²⁹**Si NMR** (79 MHz, CDCl₃) δ -27.54 ppm.

¹³C NMR (101 MHz, CDCl₃) δ 139.08, 134.80, 134.72, 132.97, 131.76, 131.06, 130.51, 130.11, 129.47, 129.10, 128.87, 128.12, 127.93, 126.92, 126.75, 126.41, 123.07, 122.60, 51.12 ppm.

CHN: calc. C: 76.71 %, H: 5.85 %; found C: 76.07 %, H: 5.68 %

3.1.4.4 Polymers

All oligosiloxanes were prepared according to a modified literature procedure. 184 Therefore, a general synthetic route is described. The monomers and exact ratios can be found in the text.

Condensation and Consolidation of the Oligosiloxanes

All di- and trialkoxysilanes as well as THF (150 %v/w related to the mass of all monomers, 1.5 mL of THF would be used for a combined mass of all monomers of 1 g) and HCl (pH=1; one equivalent of HCl for every methoxy group of the monomers was used, 1 eq of PTMS would require 3 eq of HCl, also the molar mass of water was used for the calculations due to its dilution) were added into a vial, which was then closed and stirred for 72 h at 45 °C and 400 rpm. The reaction mixture was then transferred into a beaker and stirred until stirring was no longer possible. THF, methanol, and water were removed first in vacuum at room temperature until no more bubbling could be seen, then in a vacuum drying oven for 24 h at 70 °C and 24 h at 110 °C at 10 mbar. The transparent polysiloxanes were then allowed to cool to room temperature before further characterization.

Consolidation of the oligosiloxanes was done in a vacuum oven at 200 °C for 24 h to prevent blistering and to remove any volatile components that may be present, followed by an additional 72 h at 200 °C in an oven to finish the consolidation process.

3.1.5 Conclusions

Three dialkoxysilanes containing polycyclic aromatic groups were synthesized and characterized. These compounds exhibit high refractive indices, making them promising precursors for HRI siloxanes. Six oligosiloxanes containing naphthalene and phenanthrene groups as well as phenyl and methyl groups were prepared and characterized from the dialkoxysilanes, three of them containing exclusively aromatic groups. By FTIR spectroscopy, it was shown that only methoxy and hydroxy groups that had already formed hydrogen bonds after condensation were integrated into the siloxane network. These groups are important for a further cross-linking during the consolidation process. CP-MAS NMR spectroscopy also revealed a decreasing reactivity sequence from 2-naphthyl via 9-phenanthrenyl to 1-naphthyl in the condensation reaction. Furthermore, it was found that the refractive index of oligosiloxanes containing 1-naphthyl and 9-phenanthrene decreased during consolidation and that of 2-naphthyl increased, possibly due to a decrease in molar volume due to lower steric demand. All samples exhibit glass transition temperatures up to 74 °C after consolidation. In addition, high thermal stability could be demonstrated, which is characterized by T₉₅ values of up to 470 °C of the cured samples. Furthermore, the oligosiloxanes show a high transparency of up to 99 %, which decreases only by 2-10 % depending on the sample even after 1 week at 200 °C. However, it should be noted that the samples gradually turn yellow at this temperature and the pure aromatic oligosiloxanes tend to crack. Almost all measurements showed that the constitutional isomerism of the 1- and 2-naphthyl samples has an influence on the properties of the prepared oligosiloxanes. For example, 2-naphthyl shows a higher condensation tendency, higher T₉₅ values, and a higher RI but also less excimer formation and stronger yellowing upon thermal treatment. The Tg and RI showed unexpected features as 2-naphthyl has a higher RI than 1-naphthyl after consolidation and its Tg depends strongly on the comonomer used. All samples also show high refractive indices of up to 1.610, making them promising materials for optoelectronic applications.

Acknowledgments

The authors thank Blandine Boßmann for recording and analyzing the size exclusion chromatograms, Dr. Klaus Hollemeyer for the MALDI-TOF measurements, Dr. Michael Zimmer for the CP-MAS NMR measurements, Susanne Harling for the elemental analysis, Prof. Dr. Gregor Jung for the possibility to use the fluorescence spectrometer and Viktoria Kiefer for the help with these measurements. Instrumentation and technical assistance for this work were provided by the Service Center X-ray Diffraction, with financial support from Saarland University and German Science Foundation (project number INST 256/349-1). The authors thank Dr. Oliver Janka for the support in the collection of the X-ray diffraction data presented in this paper.

3.2 Post-Cross-Linking of Siloxane/Silsesquioxane Mixtures Containing Polycyclic Aromatic Groups to Modify their Softening Behavior for Usage in High-Temperature Applications

3.2.1 Abstract

High-refractive-index hybrid siloxane/silsesquioxane materials containing phenyl, methyl, and polycyclic aromatic groups synthesized by condensation of the corresponding alkoxysilanes are often not completely cross-linked after thermal crosslinking, most likely due to the steric demand of the incorporated aromatic groups. For many potential applications of such materials, for example in optical applications, a rigid structure is required. In this study we conducted a systematic analysis of the post-crosslinking strategy with various additives. These include dimethyldimethoxysilane, diphenyldimethoxysilane and phenyltrimethoxysilane, as well as the organotin condensation catalyst di-n-butyltin diacetate (DBTA). The highest thermal stability of up to 453 °C was achieved with a high amount of phenyltrimethoxysilane. A transparency of up to 99 % even after prolonged times at 200 °C with only little yellowing on the other hand was achieved with diphenyldimethoxysilane. Even though all of the consolidated siloxane/silsesquioxane mixtures showed glass transition temperatures up to 68 °C according to DSC and up to 124 °C according to dynamic mechanical analysis (DMA) only the two samples post-cross-linked with phenyltrimethoxysilane diphenyldimethoxysilane reached a rubbery plateau during heat treatment instead of becoming liquid indicating a higher rigidity. It was shown that the number of phenyl groups, the cross-linking density, the structural regularity and the degree of condensation (DOC) are important to obtain high-temperature stable siloxanes. The most important characteristic however is the complete incorporation of the monomer carrying the sterically demanding naphthyl group into the sample during the consolidation. All of the above-mentioned characteristics but especially the incorporation of the naphthyl group containing monomer are positively influenced by post-cross-linking.

3.2.2 Introduction

Siloxanes are used in a wide variety of applications from architecture, health care industry and aerospace to optical applications like organic light-emitting diodes (OLEDs) and displays and are even tested in biomedicine as intraocular lenses. 95,254,294,297,379 Their widespread use is due to their excellent properties like flexibility, biocompatibility and gas permeability.³⁶⁶ They also show high transparencies as well as thermal stability and stability against UV radiation, are shock resistant and possess good adhesion properties.^{277,291,294,316,379} One major downside for optical applications like LEDs is their comparatively low refractive index (RI) which is commonly between 1.4 and 1.5.²⁹² Several routes are described in literature to increase the RI, such as the incorporation of polycyclic aromatic groups or titanium or zirconium containing compounds into the siloxane network. 191,291,293,294,383 While the former increases the friction and therefore the viscosity of the siloxane, the latter can lead to agglomeration and thus to light scattering which is particularly unfavorable for optical applications.^{34,384} As shown in previous studies, siloxanes with various structures can be produced in many different ways, 11,174,193,379,385,386 one of which is, for example, the use of diphenylsilanediol and trialkoxysilanes to achieve a high refractive index.31,190,387 By using acid-catalyzed hydrolysis and condensation reactions of aromatic di- and trialkoxysilanes, so-called melting gels can be produced, as has already been done in our group. 334,335,383 After condensation these materials can reversibly soften at temperatures around 110 °C. Once they have been treated at temperatures higher than 110 °C for a longer time they consolidate. This means the cross-linking is complete and the melting gels can no longer The consolidation be softened. temperature hereby depends their composition. 183,184,187

In previous studies we applied an acid-catalyzed condensation reaction between di- and trialkoxysilanes containing methyl, phenyl and polycyclic aromatic groups, which resulted in siloxane/silsesquioxane hybrids with high refractive indices 383 that also exhibit excellent thermal stability and high transparency. We were also able to show that, for example, the isomerism between 1- and 2-naphthyl influences the formation of excimers, thermal stability, and the glass transition temperature (T_g), but has only a minor influence on the refractive index of the resulting material. Despite these advantages, however, prolonged exposure to high temperatures results in slight yellowing and liquefaction of

all samples, which makes them unsuitable for high-temperature applications such as encapsulation materials in LEDs, which can reach temperatures of up to 120 °C. 388 To the best of our knowledge this behavior is exclusive to materials featuring polycyclic aromatic substituents, as systems containing phenyl groups yield hard materials upon consolidation. Even with phenyl groups, it is known that a large number of them leads to less bridging oxygens resulting in weak interactions between siloxane networks which in turn is necessary to prevent softening, 389 while also creating steric hindrance to the crosslinking process which in turn leads to higher consolidation temperatures. 184 It is therefore reasonable to conclude that the polycyclic aromatic groups are responsible for the lack of consolidation as the final degree of cross-linking cannot be achieved. Hence, we considered if subsequent post-cross-linking applying small reactive molecules could lead to an enhanced cross-linking of the materials. For this approach we decided to use methyl and phenyl containing di- and trialkoxysilanes as they are commonly used in melting gel synthesis.¹⁸³ Another method to condensate siloxanes is by using alkyltin carboxylates like di-n-butyltin diacetate (DBTA), which is known to vulcanize a mixture of siloxanes within a day under ambient conditions involving the formation of Si-O-Sn bonds.^{390,391} All of these approaches can change the properties of these siloxanes as they can be adjusted by the organic groups, the amount of substitutions on the alkoxide, the chain length, as was shown for dimethylsilphenylene dimethylsiloxane oligomers for example, or their structure itself. 140,183,392-394 Therefore, studies were carried out to show the effect of post-cross-linking with the afore mentioned methods on different characteristics of the final siloxanes like thermal stability and cross-linking density.

3.2.3 Results and Discussion

For the following studies we selected NaphMG from our previous investigations for post-cross-linking experiments, which contains 1-naphthyl groups, as it showed the lowest T_g but at the same time excellent processability and exceptional thermal stability after consolidation. This system is composed of a 1:2:1 mixture of dimethoxyphenyl-(1-naphthyl)silane, dimethyldimethoxysilane and phenyltrimethoxysilane (see **Scheme 30**). The synthesis of the model system followed the protocol outlined in our prior study. 383 All monomers were combined in a closed headspace vial with methanol and aqueous

HCl (9 eq, pH = 1) and stirred at 45 °C for 72 hours. Subsequently, the reaction mixture was transferred to a beaker for gelation, followed by further condensation in a vacuum-drying oven at 110 °C for 24 h. The subsequent consolidation was carried out for 72 h at 200 °C in a drying oven. The resulting siloxane was hard at room temperature but could still be liquefied at elevated temperatures. The synthesis of dimethoxyphenyl-(1-naphthyl)silane can be found in the Supporting Information.

Scheme 30: Synthesis of the siloxane NaphMG.

Contrary to phenyl silsesquioxane melting gels (PhMG) incomplete consolidation in these samples was observed through the presence of a higher proportion of residual silanol and methoxy groups in the infrared spectrum, along with remaining methoxy groups in the NMR analysis (**Figure 23**).

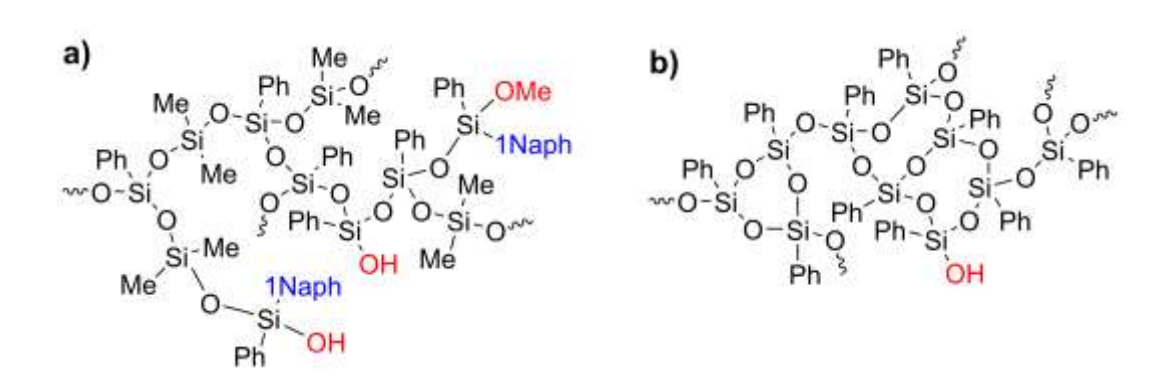


Figure 23: Incomplete cross-linking of NaphMG (a) compared to PhMG (b) after consolidation, shown by the larger number of hydroxyl groups, as well as methoxy groups still present.

In order to condense the remaining groups and thus achieve improved material properties regarding stiffness and Tg, as well as liquefication behavior and yellowing at high temperatures, a comparative study of various post-cross-linking methods of the partially condensed but insufficiently consolidated NaphMG sample was carried out (Scheme 31). As a first method, we post-cross-linked via dialkoxysilanes, which can react with available silanol groups by a condensation reaction. We used dimethyldimethoxysilane (DMDMS) and diphenyldimethoxysilane (DPDMS) for this purpose, as they are commonly used in melting gel synthesis and lead to a more flexible cross-linking compared to trialkoxysilanes due to the presence of only two reactive groups for condensation (**Scheme 31, a** and **b**). Another cross-linking agent that was investigated is phenyltrimethoxysilane (PTMS). In contrast to the previously used molecules, a trialkoxysilane can achieve a higher cross-linking density as it can crosslink with three groups (Scheme 31, c). In order to rule out the possibility that only the increase in cross-linking density is responsible for any improvements in properties such as liquefaction at high temperatures, a direct approach was also chosen. In a single step, a sample with the same cross-linking density was produced as for post-cross-linking with PTMS (Scheme 31, e). Finally, we compared the addition of alkoxysilane cross-linking agents with the use of di-n-butyltin diacetate (DBTA), which is known as a condensation catalyst (Scheme 31, d).

Scheme 31: Post-cross-linking of NaphMG with various alkoxysilanes and di-*n*-butyltin diacetate (**a-d**) and the direct approach (**e**). The numbers before each alkoxysilane represent the used equivalents related to NaphMG and therefore translate to the composition of the final siloxane.

The abbreviations of the resulting samples are as follows: MG refers to Melting Gel, Naph, Me_2 , Ph_2 , Ph and Sh denote 1-Naph $PhSi(OMe)_2$, DMDMS, DPDMS, PTMS and di-n-butyltin diacetate, respectively. The last part of each abbreviation indicates the difference between the samples. The sample which was prepared directly from the monomers without post-cross-linking was labeled $NaphMG_5Ph_d$, whereas 5Ph refers to the amount of cross-linker used, and d stands for the direct preparation.

The partially condensed but not yet consolidated NaphMG was still soluble and was therefore dissolved in MeOH and then either monomers and HCl (**Scheme 31, a** to **c**) or di-*n*-dibutyltin diacetate (**Scheme 31, d**) were added for further condensation. The samples were afterwards stirred at elevated temperatures, gelled, and further

condensed at elevated temperatures (**Figure 24**). Given the toxicity of the organotin compound, all heat treatments of the samples before consolidation were performed in opened headspace vials in a heat block in the fume hood, as opposed to a vacuum drying oven as had been used previously. This method ensures comparability of all samples. Consolidation was performed in a drying oven under air (**Scheme 31, a** to **c, e**), with the exception of the organotin compound (**Scheme 31, d**), which was consolidated in a tube furnace under wet argon to facilitate the safe removal of potentially harmful substances. Wet argon was chosen as the atmosphere because polycondensation with organotin compounds does not work under anhydrous conditions.³⁹⁰ All resulting consolidated siloxane/silsesquioxane mixtures were hard at room temperature with the exception of NaphMG_2Me₂ which was still viscous.

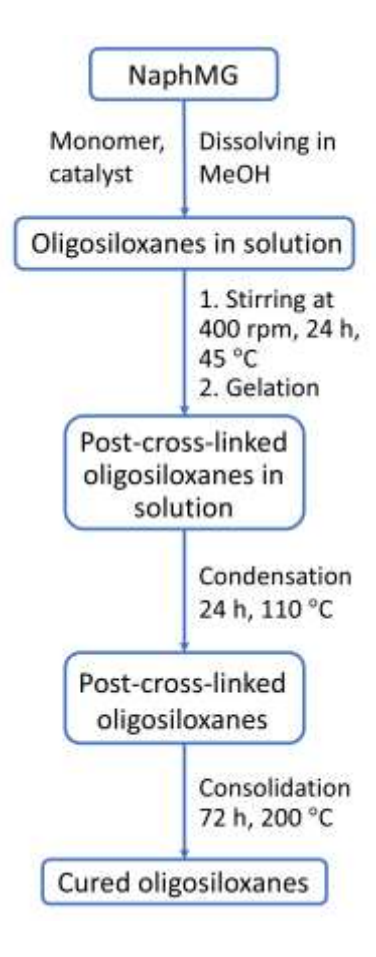


Figure 24: Synthesis and consolidation of all siloxanes.

At 200 °C, all consolidated samples turned into a liquid state, except for NaphMG_2Ph₂ and NaphMG_4Ph which were softened, retaining their elasticity. To further investigate these findings, we used DSC and dynamic mechanical analysis (DMA) measurements

and performed a series of heat treatment experiments at different temperatures in an oven. These analyses were intended to provide information about the T_g , the elasticity, and the softening behavior of our samples. We then attempted to correlate the obtained observations to possible differences in their structure by carrying out NMR, FTIR and PXRD measurements. Finally, we evaluated the transparency and thermal stability of our siloxanes by UV-vis spectroscopy and TGA measurements.

3.2.3.1 Differential Scanning Calorimetry (DSC)

We employed differential scanning calorimetry (DSC) to determine the $T_{\text{\scriptsize g}}$ after consolidation. Each sample was measured within the temperature range of 40 °C to 250 °C, except for NaphMG_2Me₂, which was limited to 100 °C due to its anticipated low T_g (**Table 7** and **Figure S 77**). Typically, systems containing only phenyl and/or methyl groups are consolidated over a period of 24 hours at temperatures up to 200 °C. Given the steric hindrance of the naphthyl groups, which influences the cross-linking reaction, and to maintain consistency with our previous methodology, we have extended the consolidation time to 72 hours at 200 °C.383 Successful consolidation should result in a non-detectable T_g , as a result of enhanced cross-linking rendering the samples permanently rigid. 183,184 A first comparison of the post-cross-linked samples with the initial sample NaphMG shows that all methods have a significant influence on the Tg and either lead to a strong increase or strong decrease. The comparison between NaphMG_2Ph2 and NaphMG_2Me2 shows that the replacement of phenyl by methyl groups in the pristine samples leads to a significant decrease in Tg from 68 °C to -34 °C, which is in line with expectations. 364,365 Further investigation of NaphMG_Sn and of the initial sample NaphMG shows that the use of an organotin catalyst leads to an increase in T_g from 5 °C to 19 °C, indicating improved cross-linking. Similarly, there are large differences in T_g values between NaphMG_4Ph and NaphMG_5Ph_d, which are 33 °C and 67 °C respectively, indicating structural differences after their consolidation. NaphMG_2Ph2 and NaphMG_5Ph_d exhibit the highest Tg values of all samples at 68 °C and 67 °C, respectively. It is worth noting that although both samples contain a similar amount of phenyl groups, their different cross-linking densities indicate that the influence of the bulky phenyl groups predominates in the determination of their Tg.

Comparing the T_g values of other cured polysiloxanes containing methyl, phenyl and carbazole groups in various ratios, which typically range between -83 °C and 56 °C, NaphMG_2Ph2 and NaphMG_5Ph_d exhibit relatively high T_g s. ^{183,184,366} Since melting gels no longer soften after consolidation, the presence of a T_g after attempted consolidation is an indication that it was not complete. ^{183,184,395,396} Generally, cross-linking in siloxane networks can be hindered by sterically demanding substituents on the silicon atoms, which means that higher consolidation temperatures could be required. ¹⁸³ It could even be possible that the exceptionally bulky naphthyl groups hinder successful consolidation completely.

Table 7: Glass transition temperatures of the siloxane samples. Each sample was measured three times and the mean value of the three measurements is given.

Siloxane	T _{g, average} (°C)
NaphMG_2Me ₂	-34.3
NaphMG_2Ph₂	67.8
NaphMG_4Ph	33.1
NaphMG_5Ph_d	66.7
NaphMG	5.3
NaphMG_Sn	19.3

3.2.3.2 Thermal Treatment Experiments

Since the DSC measurements still showed a T_g for all samples after consolidation, the question now arose as to whether the samples only soften at high temperatures or if they liquefy. A first, quick investigation in this regard was carried out using thermal treatment experiments. We conducted this investigation by grinding all solid specimens into powders and subjecting them to incremental heating up to 200 °C in 25 °C increments, with each step lasting 20 minutes (see **Figure S 78**). Our observations reveal distinct thermal responses among the samples: NaphMG_Sn exhibits an initial liquefication at approximately 100 °C, followed by NaphMG_5Ph_d at 150 °C, while NaphMG_2Ph₂ and NaphMG_4Ph demonstrate no signs of liquefication, even at the maximum temperature of 200 °C.

It is noteworthy that NaphMG_4Ph and NaphMG_5Ph_d show a significantly different behavior despite having the same composition. While the former has a significantly lower T_g, it remains solid even at high temperatures, in contrast to the latter. This discrepancy emphasizes that the measured T_g values indicate temperatures at which the mobility of the polymer chains increases rather than the onset of liquefaction. It also shows that post-cross-linking exerts a significant influence on the softening behavior of the samples, effectively preventing them from transitioning into a liquid state at elevated temperatures. Consequently, it can be affirmed that we have successfully synthesized two siloxanes capable of maintaining their solid state, even at 200 °C.

3.2.3.3 Dynamic Mechanical Analysis (DMA)

Dynamic mechanical analysis (DMA) of the samples was performed using oscillatory rheometric measurements by placing the samples between two plates and oscillating the upper one with a frequency of 1 Hz and an amplitude of 5 %. To assess viscosity, storage modulus (SM), and loss modulus (LM) across various temperatures,³⁹⁷ the samples were initially heated to either 150 °C or 200 °C, followed by a temperature reduction to 35 °C (**Figure 25** and **Figure S 79** - **Figure S 80**).

As the viscosity of the samples varied greatly, the starting temperatures had to be adjusted to minimize the risk of the samples losing contact with the plates due to too low viscosity at higher temperatures. In addition, it was essential to start the measurements at high temperatures, as most samples were rigid and solid at room temperature, which increased the risk of breakage. This was particularly observed in the case of NaphMG_5Ph_d, which is therefore only presented from 200 °C to 100 °C. The loss factor tan δ was calculated from the storage and loss modulus, and by identifying the peak maximum in the resulting curves, the T_g could be determined (see **Figure 25**, **c** and **d**). ^{397,398} In the case of NaphMG, the T_g increases from 43 °C to 74 °C due to consolidation and further increases to 80 °C due to the additional use of DBTA (NaphMG_Sn). This indicates an advancing condensation, which leads to an increasingly dense network. It can also be seen that the increasingly low viscosity of the unconsolidated sample NaphMG at high temperatures has repeatedly led to loss of contact with the plates, resulting in high peaks. Despite an increase in viscosity and storage modulus upon

consolidation (Figure 25, a and b and Figure S 79 and Table S 6) as was shown for NaphMG, their Tg's remain relatively low. As expected, NaphMG_2Me2 exhibits the lowest viscosity and storage modulus among all samples (Figure 25, a and b and Figure S 79), as methyl groups favor a lower modulus, while phenyl groups increase the stiffness.³⁹⁹ Firstly, this means that the measurement could only be carried out from 150 °C to avoid contact loss with the plates. On the other hand, it was not possible to determine a $T_{\rm g}$ in the investigated temperature range. As this sample was already very soft at room temperature, additional cooling would most likely have been necessary to determine its T_g. However, such a measurement was not possible with our experimental setup. The tan δ curves of NaphMG_2Ph₂ and NaphMG_4Ph reveal T_gs of 124 °C and 67 °C, respectively in contrast to the Tgs from the DSC measurement which were 68 °C and 33 °C, respectively. These experiments show that a modification with DPDMS leads to a higher T_g than the use of PTMS. NaphMG_5Ph_d was only measured from 200 °C to 100 °C, as it was too hard at lower temperatures and would very likely have shattered due to the rotation of the plates. This sample shows no peak in the observed temperature range but a steadily increasing curve. It is noticeable that the Tgs obtained by DMA are much higher than those obtained by DSC. The results of DMA measurements differ from those obtained by DSC because DMA measurements take into account the change in modulus versus temperature, which is a bulk phenomenon and therefore not uniformly distributed. It therefore takes into account the effects of temperature on the chains. A similar trend, namely a higher Tg in the DMA measurements, has already been observed in the literature. 400 In summary, the following sequence of measured T_g 's results: NaphMG_2Ph₂ > NaphMG_Sn > NaphMG_cons. > NaphMG_4Ph > NaphMG_cond. If one also considers the Tg's of NaphMG_5Ph _d and NaphMG_2Me2, which are very likely too high or too low for our measurement in the applied temperature range, the following can be determined. Further condensation by means of consolidation and DBTA leads to an increase in Tg, while post-cross-linking with additional phenyl or methyl groups leads to the highest or lowest Tg's, as already described in the literature.³⁹⁹ Only the rather low Tg of NaphMG_4Ph cannot be explained and may have something to do with the post-crosslinking compared to the direct synthesis of NaphMG_5Ph_d. At this point it should be mentioned once again that the measurements were not carried out as usual with a

precisely measured sample body clamped in a measuring device, such as a rod or a thin plate, but with tablet-shaped samples and an oscillating measuring plate.

Comparing the viscosities at 200 °C (**Figure S 79** and **Table S 6**) NaphMG_4Ph shows the highest values by far, followed by NaphMG_2Ph₂, NaphMG_Sn and NaphMG_5Ph_d. The same trend was observed for the storage modulus (**Figure 25**, **a** and **b**). NaphMG_4Ph reaches the highest rubbery plateau of all samples already at around 130 °C, followed by NaphMG_Sn reaching the third highest plateau at 160 °C and NaphMG_2Ph₂ reaching the second highest plateau at around 190 °C, while NaphMG_5Ph_d does not reach a rubbery plateau at all, which shows that the former three keep their elasticity at high temperatures and form a cross-linked structure.^{397,401} This was also confirmed during the thermal treatment experiment. Interestingly NaphMG_Sn did turn liquid during this experiment either because it has the lowest elastic modulus of the three samples reaching a rubbery plateau or because the thermal treatment experiment was done with grinded samples instead of tablet shaped and compressed samples as in the DMA.

In summary the dynamic mechanical analysis showed an increase in viscosity and storage modulus by adding phenyl groups or increasing the cross-link density which was to be expected since it is known that the modulus of elastomer increases with increasing cross-link density. 402,403 By comparing NaphMG_4Ph and NaphMG_5Ph_d it was also shown that post-cross-linking seems much more favorable to obtain siloxanes that are elastic and not liquid at high temperatures. Consequently, it was possible to prepare three samples which show a rubbery plateau at 200 °C and therefore should keep their elasticity.

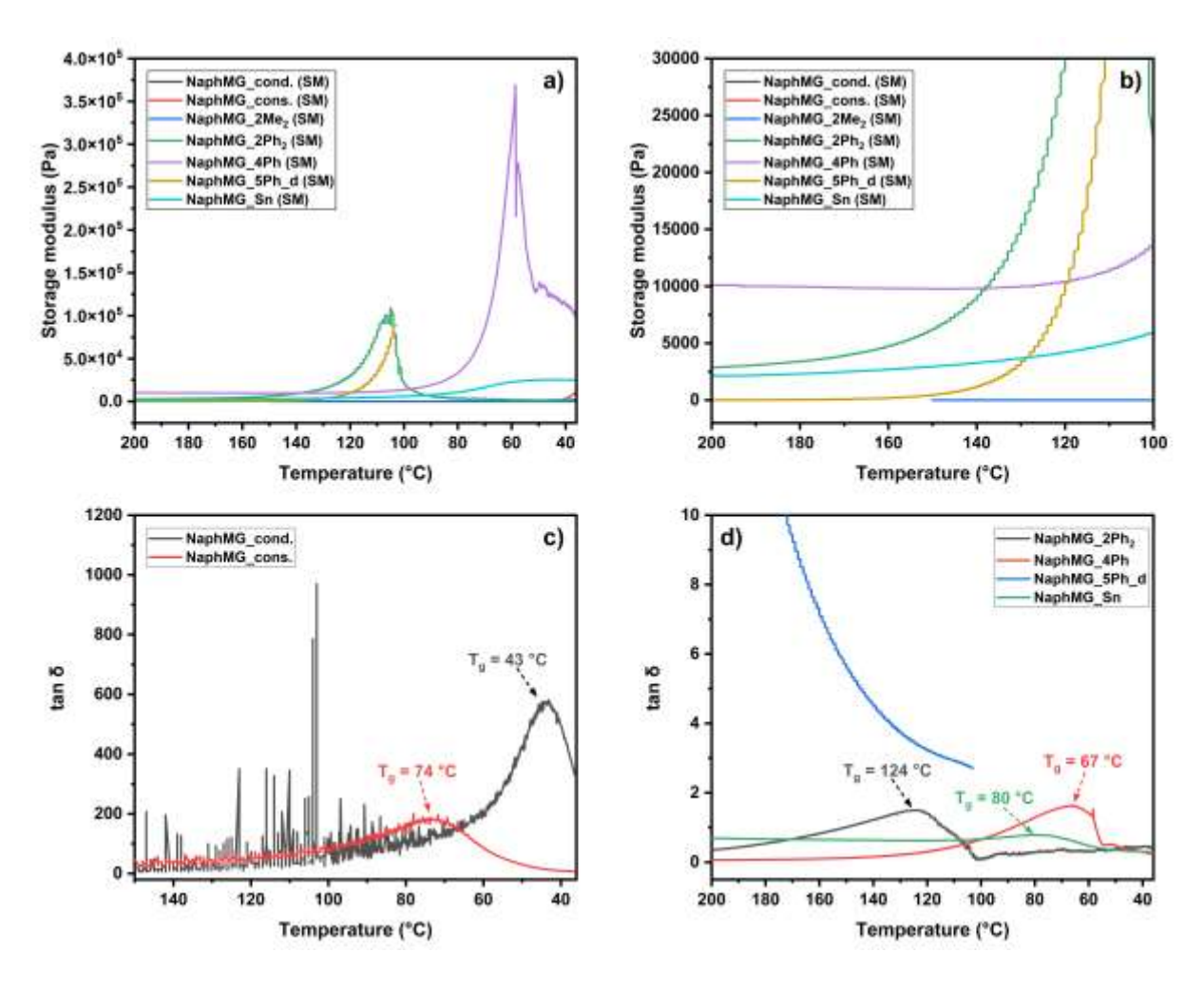


Figure 25: DMA measurements of all siloxanes. a) storage modulus, b) storage modulus (zoomed in), c) tan δ of NaphMG_cond. (black) and NaphMG_cons. (red), d) tan δ of NaphMG_2Ph₂ (black), NaphMG_4Ph (red), NaphMG_5Ph_d (blue) and NaphMG_Sn(green).

3.2.3.4 Nuclear Magnetic Resonance (NMR) Spectroscopy

Since our consolidated samples behaved very differently in the previous measurements, we applied NMR spectroscopy to investigate potential correlations between the degree of condensation (DOC) and the observed T_gs of the samples, as well as their liquefaction behavior. Therefore, we used ²⁹Si- and ¹³C CP-MAS NMR spectroscopy and ²⁹Si- and ¹³C SP-MAS spectroscopy for samples NaphMG_2Ph₂, NaphMG 4Ph NaphMG_5Ph_d, as well as ²⁹Si solution NMR measurements for samples NaphMG_cond., NaphMG_cons. and NaphMG_2Me2. NaphMG_Sn could neither be measured in liquid nor solid form, as it was not soluble in any solvent and due to its still slightly deformable consistency, pushing the lid of the rotor in the solid-state NMR upwards, which meant that uniform rotation was not possible. Furthermore, the DOC of

all samples was determined (for further details see Supporting Information). When comparing the results obtained by ²⁹Si CP-MAS and ²⁹Si SP-MAS NMR spectroscopy (Table 8 and Figure S 81 - Figure S 101 and Table S 7) it becomes obvious that the differences in the signals corresponding to each monomer, as well as for the DOC in general are only minor and could also stem from the fitting of the spectra themselves. Therefore, only the ²⁹Si CP-MAS spectra were used for further comparison as they display a better resolution which can be fitted more precisely. Interestingly the obtained DOCs (**Table 8**) indicate that any form of post-cross-linking does in fact decrease the DOC. This would suggest that the additional aromatic groups and the higher cross-link density could play a more important role for the viscosity and softening characteristics after consolidation, especially since phenyl groups increase the monomeric friction and therefore viscosity.³⁴ Furthermore, this was also seen in the polyphenylsilsesquioxane melting gel (PhMG) from previous studies, which did not soften after consolidation, despite having a DOC of 83 %.334. Looking at NaphMG_2Me2 and NaphMG_2Ph2 the former shows a higher DOC. This is in accordance with our hypothesis that smaller substituents at the Si atom result in a better cross-linking. In the case of the monomer DMDMS we expect steric and electronic effects to be the reason for the increased DOC.85-⁸⁷ Comparing the DOCs of NaphMG_4Ph and NaphMG_5Ph_d indicates that post-crosslinking leads to a higher DOC. The signal of 1-NaphPhSi(OMe)₂ (D², purple) for these two samples is particularly interesting (Figure 26). It is almost 20 % higher for NaphMG_4Ph, which indicates that the post-cross-linking actually causes the remaining Si-OH groups on the sterically hindered 1-NaphPhSi(OMe)₂ to react further as we intended and is also observed for NaphMG_2Ph₂. This in turn increases the number of bridging oxygens, which reduces their softening.³⁸⁹ Considering all observations this shows that a high DOC is important for properties such as high viscosity and no liquefication in the final siloxane but that other factors also play an important role as the highest DOC was obtained for NaphMG_2Me₂ which is soft even at room temperature. Therefore, it can be concluded that aromatic groups, cross-linking density and in our case the incorporation of sterically demanding groups into the siloxane network are also crucial. For the latter we proved that post-cross-linking is much more effective which seems to be the key to prevent liquification upon high temperatures.

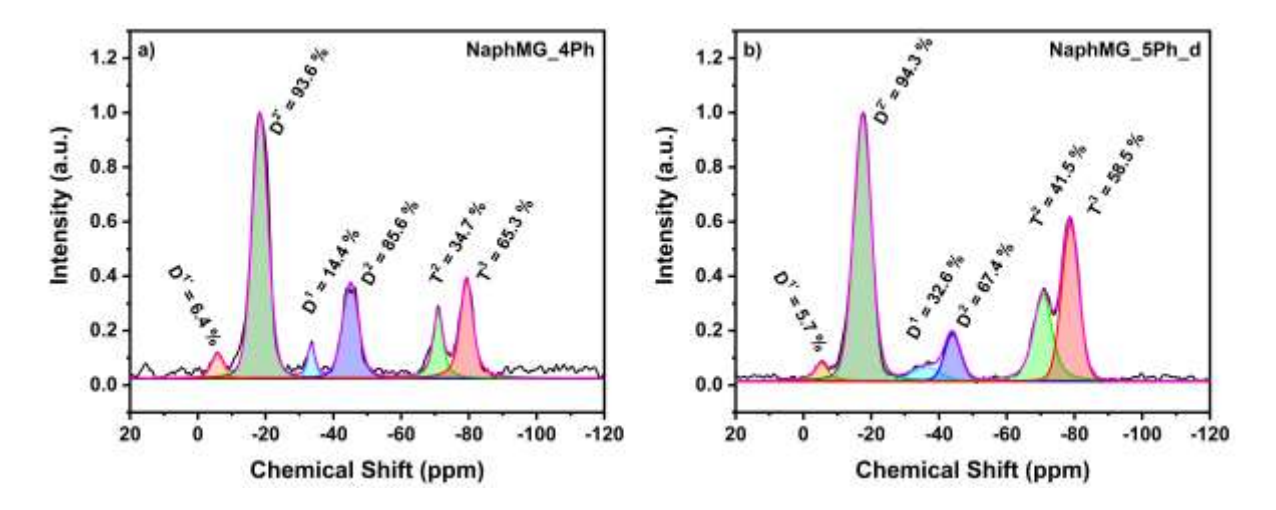


Figure 26: Integrated ²⁹Si CP-MAS NMR of a) NaphMG_4Ph and b) NaphMG_5Ph_d.

Table 8: Degree of condensation (DOC) for all siloxanes calculated from different NMR methods.

	²⁹ Si SP-MAS	²⁹ Si CP-MAS	²⁹ Si Liquid NMR
	DOC /%	DOC /%	DOC %
NaphMG_cond.	-	-	88.8
NaphMG_cons.	-	-	93.7
NaphMG_2Me₂	-	-	93.4
NaphMG_2Ph₂	94.8	91.0	-
NaphMG_4Ph	92.0	92.1	-
NaphMG_5Ph_d	87.6	88.6	-
NaphMG_Sn	-	-	-

3.2.3.5 Fourier Transform Infrared (FTIR) Spectroscopy

FTIR spectroscopy was performed on all samples as an additional characterization method to further study their condensation behavior, as well as the remaining hydroxy and methoxy groups (**Figure 27** and **Figure S 102** and **Table S 8**). Besides the aromatic groups and the methyl groups, the Si-O-Si stretching vibration can be found in form of two absorption bands, one from 1131 cm⁻¹ to 996 cm⁻¹ and the other one at 798 cm⁻¹ indicating a successful network formation. This is further supported by the missing band of the methoxy groups at 1188 cm⁻¹. ^{190,227,354} During the condensation process hydrolyzation plays an important role. Therefore the absorption bands at 3712 cm⁻¹ to 3575 cm⁻¹ (v(OH_{isolated})), 3500 cm⁻¹ to 3120 cm⁻¹ (v(OH_{H-bonded})) and 920 cm⁻¹ to 890 cm⁻¹ (v(Si-OH)) are

of great importance. ^{227,355} After the consolidation with additives there are no hydrogen bonded hydroxyl groups (3500 - 3120 cm⁻¹) left indicating that the condensation is finished. ^{334,383} Comparing all samples only NaphMG_2Me₂ and NaphMG_Sn show no isolated OH groups anymore, leading to the assumption that these have the highest DOC. For NaphMG_2Me₂ this can be attributed to electronic and steric effects also mentioned in the last chapter. ^{81,86} NaphMG_Sn was further condensed with an organotin catalyst which are known for room temperature vulcanizing (RTV) of siloxanes and therefore could explain the better condensation. In summary it can be said that the FTIR spectra show a successful condensation of all samples which was also seen in the ¹³C CP-MAS NMR spectra which show either no remaining or only very small signals of methoxy groups.

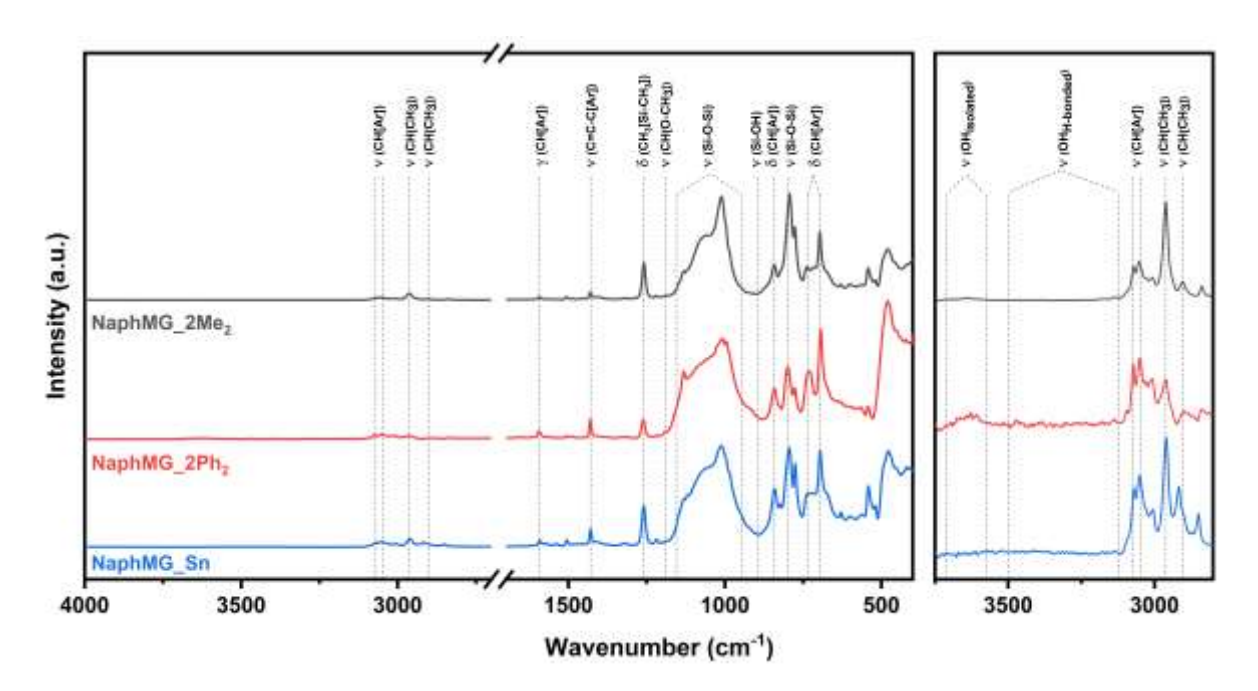


Figure 27: FTIR spectra of the consolidated samples NaphMG_2Me₂ (black), NaphMG_2Ph₂ (red) and NaphMG_Sn (blue). Left: full spectrum, right: enlarged area.

The afore mentioned Si-O-Si absorption band (1131 – 996 cm⁻¹) can be used to gain more insight into the structures that could have formed inside the network (**Figure 28**). Since our samples are random networks formed of three to four different monomers no clear statement can be made but only trends can be identified. For better comparison all spectra were normalized using the Si-CH₃ absorption band (1261 cm⁻¹). The broad band ranging from 1115 cm⁻¹ to 1037 cm⁻¹ shows linear, branched, and cyclic structures and is not of much interest since they are random and cannot be further analyzed. The

absorption bands at 1131 cm⁻¹ and 1012 cm⁻¹ on the other side can be attributed to ladder like structures⁹⁹ where the band at higher wavenumbers gets more intense when the regularity of the structure increases.^{182,243} For our samples this would mean that the amount of ladder like structures and therefore the structural regularity is highest for NaphMG_2Ph₂, NaphMG_5Ph_d and NaphMG_4Ph which also contain the highest amount of phenyl groups. This shows that a higher aryl content leads to more regular structures which most likely can arrange better in a solid sample resulting in no liquification in the case of NaphMG_2Ph₂ and NaphMG_4Ph at higher temperatures. However, since NaphMG_5Ph_d did turn liquid at higher temperatures the high number of oxygen bridges from the better incorporated 1-NaphPhSi(OMe)₂ shown in the NMR seem to be more important than the structural regularity.

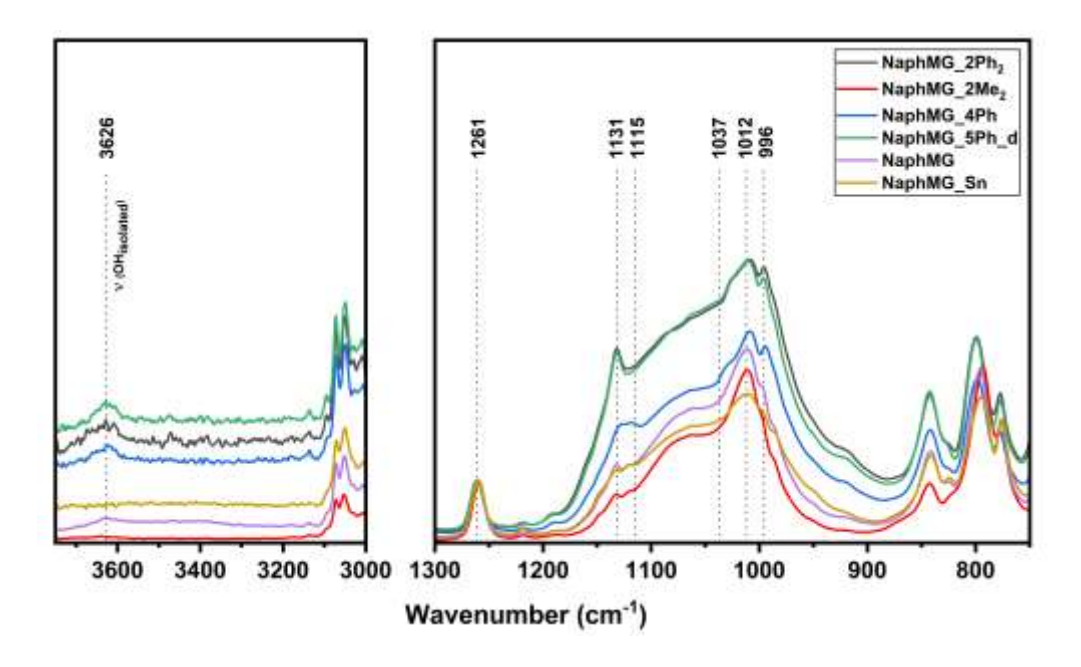


Figure 28: FTIR measurements of all samples. Left: zoomed into the OH band, right: zoomed into the Si-O-Si band.

3.2.3.6 Powder X-ray Diffraction (PXRD)

We applied PXRD measurements to obtain additional insight into the intra- and intermolecular spacing of our partly ladder-like structured siloxanes. Two main peaks are identified in such polymers, one around 7° 2θ (d_1), corresponding to the chain-to-chain distance, and a second one around 19° 2θ (d_2) that is attributed to the intra-chain distance or the average thickness of the ladder. The ratio of their heights (R=I(d_1/d_2)) indicates the structural regularity of the ladder-like siloxane which increases

for higher d₁ values.^{182,193,243} All samples were measured in one piece without being pulverized (Figure 29 and Figure S 103 - Figure S 104). The first reflex increases from NaphMG_cond. to NaphMG_cons. to NaphMG_Sn. This shows an ongoing consolidation process which leads to more Si-O-Si bonds by condensing free hydroxy and methoxy groups, herby decreasing irregularities. For the former two this was already seen via the DOC in the NMR spectra. The increasing DOC during the consolidation process leads to a denser and more rigid structure resulting in an increase in d₁ from 0.73 to 0.95 nm for these three samples. Masai et al. and Klein et al. for example also use a condensation method in which an acid is added first, followed by a base to complete hydrolysis and further cross-linking. 183,189 An increase in d_1 from 0.80 to 1.04 nm, as well as in its intensity from NaphMG_2Me₂ to NaphMG_2Ph₂ indicates an increase in structural regularity and rigidity due to higher phenyl content, possibly due to π - π stacking. In addition to the IR spectra, where the increasing phenyl content showed more ladder-like structures and therefore a higher structural regularity this time a clear trend can be seen. NaphMG_2Ph₂ shows the highest regularity, followed by NaphMG_4Ph, while NaphMG_5Ph_d displays almost no regularity despite having the same amount of aryl groups. It seems that structural regularity decreases if high amounts of PTMS are reacted at once as well as with increased cross-link density. The corresponding d_1 positions of these three samples show the same trend indicating a denser, more rigid structure which also gets supported by the NMR spectra showing an increasing DOC from NaphMG_5Ph_d to NaphMG_4Ph. The values of the d_2 reflexes of all samples representing the intra-chain distance or thickness of the ladder are almost identical, which was to be expected, considering the ladders are always comprised of Si-O-Si bonds. In summary the PXRD measurements show that the regularity of the siloxanes seems to increase with the amount of phenyl groups but decreases with cross-link density, at least when the same amount of phenyl groups is present. Furthermore, adding PTMS to an existing siloxane seems to increase the regularity compared to adding all monomers at the start.

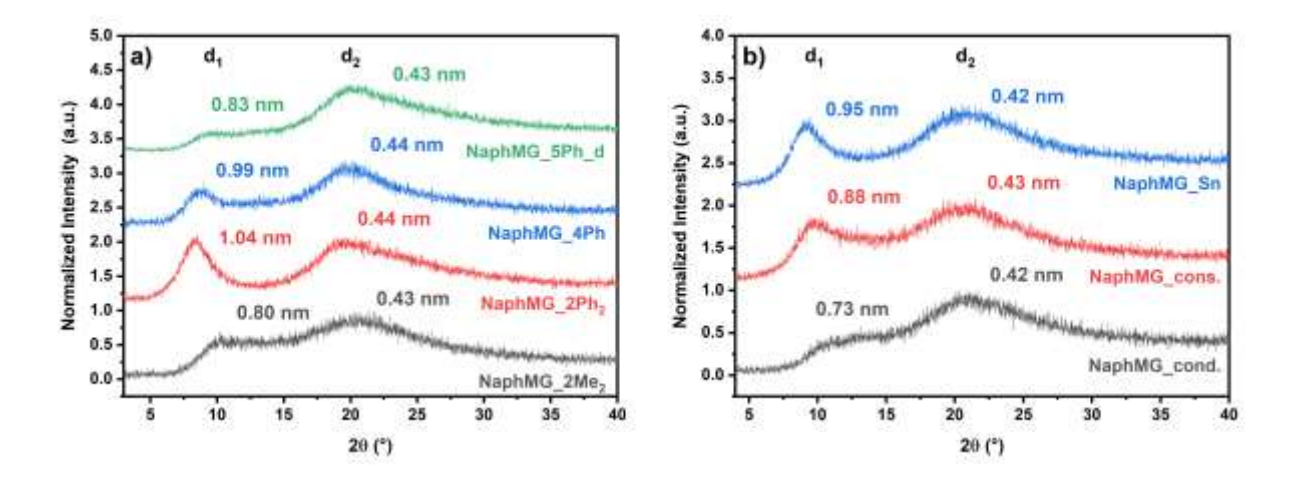


Figure 29: PXRD measurements of all samples directly as tablets. a) NaphMG_2Me₂ (grey), NaphMG_2Ph₂ (red), NaphMG_4Ph (blue) and NaphMG_5Ph_d (green), b) NaphMG_cond. (grey), NaphMG_cons. (red) and NaphMG_Sn (blue).

3.2.3.7 Ultraviolet-Visible (UV-vis) Spectroscopy

We studied the thermal stability and optical transparency of our siloxanes by measuring their transparency and yellowness index (YI) via UV-vis spectroscopy. The YI hereby describes the change from clear/white to a yellow color²⁶⁰ and plays an important role regarding thermal stability, since high temperatures as well as UV light can lead to the creation of free radicals causing yellowing of the material.²⁵⁹ All samples were doctor bladed onto glass slides after their condensation at a thickness of approximately 120 μ m, heated in a vacuum drying oven for 24 h at 200 °C to remove any blistering, consolidated for 72 h at 200 °C and were kept for an additional 3 as well as 7 days at 200 °C in an oven (see Figure 30 and Figure S 105 - Figure S 106). Due to the toxicity of the organotin catalyst, NaphMG_Sn was only measured after condensation, consolidation and after 7 d at 200 °C in a tube furnace (see experimental part). At 450 nm all samples show transmittances of 98 % or higher after condensation. After vacuum drying and consolidation the transmittance for NaphMG_5Ph_d decreased the most, which can be attributed to the cracking of the sample due to its high PTMS content. In comparison, no cracks are visible for NaphMG_4Ph even though it has the same ratio of monomers. All other transmittances stayed the same or increased, which can be attributed to the films becoming slightly thinner during consolidation. Comparing all completely heat-treated samples, with the exception of NaphMG_5Ph_d, those having higher phenyl ratios seem to lose less transmittance. This is consistent with literature, according to which phenyl groups increase thermal stability in siloxanes. 367,368 This is attributed to the fact that the phenyl group is difficult to oxidize and that it forms a steric hindrance against the degradation of the Si-O unit by ring degradation.²⁹ If comparing the sample that was not further post-cross-linked (NaphMG) with the sample that was post-cross-linked using tin (NaphMG_Sn), it can be seen that the decrease in transmission of both samples after an additional 7 days at 200 °C is almost identical. The tin catalyst therefore does not appear to have a negative influence on thermal stability in terms of transmission. The YI measurements (Figure 30, b) show a very similar trend to the extent that samples with higher phenyl content show less yellowing which was to be expected. Since all samples are transparent, loss in transmittance should mainly stem from yellowing. NaphMG_2Ph2 which already had the highest transparency, now also shows the least yellowing. Comparing NaphMG_2Ph₂ and NaphMG_4Ph with NaphMG_2Me₂, NaphMG and NaphMG_Sn higher amounts of phenyl groups seem to reduce yellowing which is consistent with the statement above that phenyl groups lead to higher thermal stabilities. A comparison of the samples NaphMG and NaphMG_Sn also shows an almost identical yellowness index, which again shows that the tin catalyst does not appear to have a negative influence on the thermal stability. In summary both measurements show that phenyl groups increase the thermal stability of siloxanes by showing higher transmittances and leading to less yellowing after heat treatment. Additionally, post-cross-linking (NaphMG_4Ph) compared to reacting all monomers at once (NaphMG_5Ph_d) seems to be beneficial not only to obtain siloxanes which keep their elasticity at high temperatures but also in terms of transmittance and avoidance of cracks.

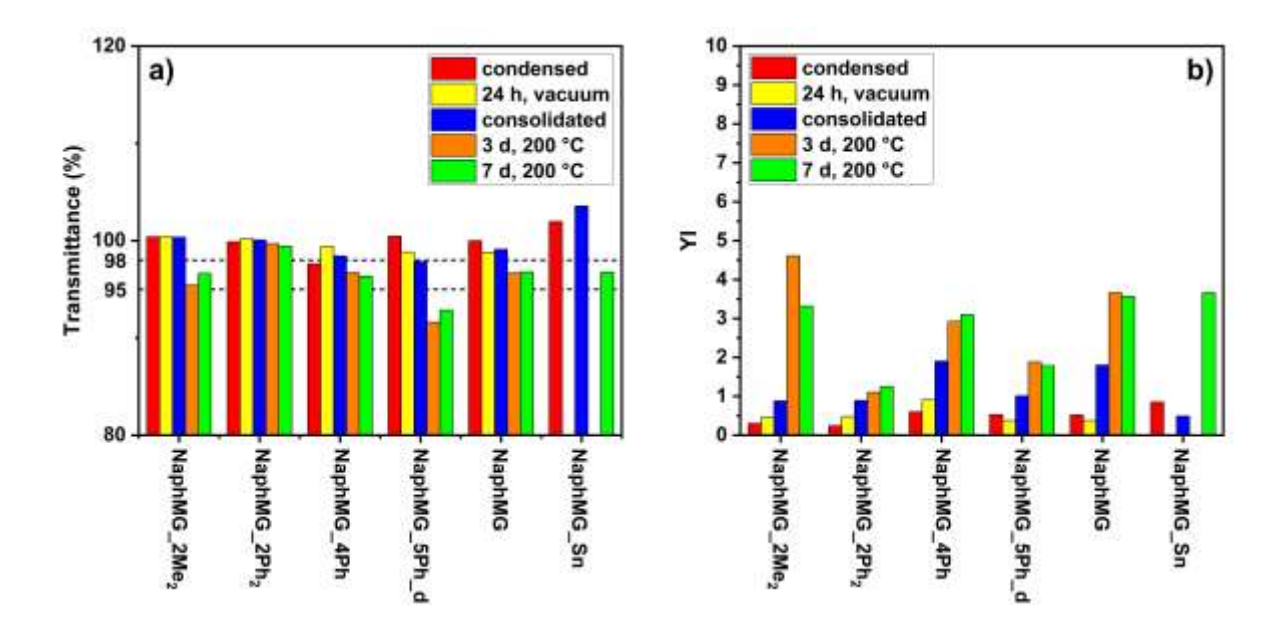


Figure 30: UV-vis measurements of the obtained samples at different heat treatment steps. a) Transmittance, b) Yellowness Index (YI).

3.2.3.8 Thermogravimetric Analysis (TGA)

To further evaluate the thermal stability and decomposition behavior of our siloxanes thermogravimetric analysis (TGA) was performed. All samples were heated up to 800 °C under oxygen with a heating rate of 10 K min⁻¹ (**Figure 31**, **Table 9**). NaphMG shows a T₉₅ value of 374 °C. Further cross-linking using an organotin catalyst (NaphMG_Sn) leads to a slight decrease to 361 °C while adding DMDMS (NaphMG_2Me₂) does not change it. Using DPDMS (NaphMG_2Ph₂) or PTMS (NaphMG_4Ph and NaphMG_5Ph_d) on the other hand increases the T₉₅ value to 419 °C, 390 °C and 453 °C, respectively. This shows that aromatic groups convey higher thermal stability³⁶⁸ and that while Si-O-Si chains consisting of only D² units are susceptible to thermal rearrangement degradation, complex structures have better thermal stability.³⁶⁷

All samples show two decomposition steps. The first is around 410 to 460 °C and the second between 540 and 570 °C. Only NaphMG_Sn shows a very broad first decomposition step between 310 to 500 °C. These two decomposition steps were already observed for the samples in our previous work and further analyzed via TG-FTIR measurements. These studies led to the conclusion that during the first decomposition step aromatic groups are released due to Si-C bond cleavage. During the second decomposition step small condensed species, possibly cyclic structures, were detected.

Comparing the first decomposition step for NaphMG_4Ph and NaphMG_5Ph_d, the former shows much more Si-C bond cleavage, possibly due to different structures that may have formed which also explains the lower T_{95} value.

Residual masses exhibit the same general trend as the T₉₅ values. NaphMG_5Ph_d shows the highest value, followed by NaphMG_2Ph2, while NaphMG has by far the lowest residual mass with only 14 % which is due to the low amount of cross-linking. 374,404 Further cross-linking with the organotin catalyst (NaphMG_Sn) leads to a significant increase of the residual mass to 35 %. Comparing NaphMG_2Me₂ and NaphMG_2Ph₂, the latter has a higher residual mass although the sample has more carbon incorporated. One possible explanation could be the slightly lower degree of condensation, while another reason for this could be found in the structure. Looking at the two decomposition steps of these two samples it can be seen that NaphMG_2Me2 lost most of its mass due to Si-C bond cleavage compared to NaphMG_2Ph2. It is known from literature that the insertion of phenyl groups increases the thermal stability of siloxanes. In addition the thermooxidative stability of methyl group containing siloxanes is poor due to the oxidation of Si-CH₃ at relatively low temperatures, which leads to the breaking of this bond. 405-409 Similar to the T₉₅ values, NaphMG_4Ph also shows a lower residual mass than NaphMG_5Ph_d which can also be explained by a significantly higher Si-C bond cleavage. In summary the number of aromatic groups as well as the cross-linking density play an important role for the thermal stability of siloxanes. We also observed that the preparation route has a significant influence on their structures and thus on their decomposition behavior.

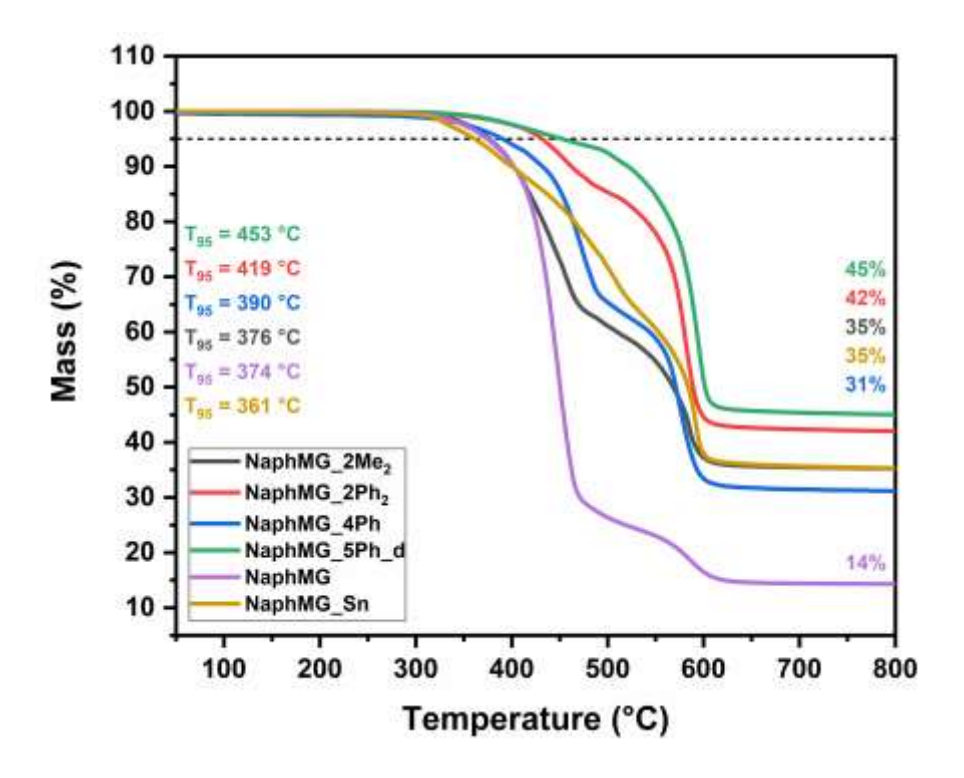


Figure 31: TGA measurements of all samples including T_{95} values and residual masses, measured under oxygen.

Table 9: TGA measurements of all siloxanes including residual masses, decomposition temperatures and mass losses.

	T ₉₅	Residual	Decomp	Mass	Decomp	Mass
	(°C)	mass (%)	osition 1	loss 1	osition 2	loss 2
			(°C)	(%)	(°C)	(%)
NaphMG_2Ph ₂	419	42	440	15	540	42
NaphMG_2Me₂	376	35	450	41	560	23
NaphMG_4Ph	390	31	460	36	540	32
NaphMG_5Ph_d	453	45	410	9	560	45
NaphMG	374	14	440	74	570	11
NaphMG_Sn	361	35	310-500	13/23	560	28

3.2.4 Experimental Section

3.2.4.1 Materials

Dialkoxysilane synthesis was carried out under inert atmosphere. Magnesium chips (99.9+%,Acros Organics), 1-bromonaphthaline (97%, abcr GmbH) and phenyltrimethoxysilane (97%, abcr GmbH) were used without further purification. THF (99.8 % HPLC grade, Fischer Chemical) was purified in a MBraun SPS-5 solvent purification system (M. Braun Inertgas-Systeme GmbH, Garching, Germany). For polymer synthesis dimethoxydiphenylsilane (97%, Alfa Aesar), dimethyldimethoxysilane (97%, abcr GmbH), phenyltrimethoxysilane (97%, abcr GmbH), di-n-butyltin diacetate (for synthesis, Merck-Schuchardt) and MeOH (98 %, BCD Chemie GmbH) were used without further purification. Hydrochloric acid (pH 1) was diluted from conc. HCl (for analysis, ACS BerndKraft) using demineralized water.

3.2.4.2 Instrumentation and Characterization Methods

Solid state CP-MAS NMR spectra were recorded on an Avance III HD – Ascend 400WB spectrometer (Bruker Corporation, Billerica, USA) using 4 mm inner diameter ZrO_2 rotors with 13 kHz rotation frequency. The resonance frequencies were 100.67 MHz for ^{13}C and 79.53 MHz for ^{29}Si NMR spectra. Solid state SP-MAS NMR spectra were recorded with the same instrumental setup.

NMR spectra in solution were recorded on an Avance III 300 MHz spectrometer (Bruker Corporation, Billerica, USA) with 59.63 MHz for ²⁹Si NMR spectra. The NMR samples were dissolved in chloroform-d (CDCl₃) and 10⁻² mol/l chromium(III)acetylacetonate as a relaxation agent was added. All spectra except for the integrated solid state ²⁹Si CP-MAS and integrated solid state ²⁹Si SP-MAS spectra, were plotted in MestReNova (v14.2.0-26256, Mestrelab Research, Santiago de Compostela SPAIN) using the apodization function to adjust the signal to noise ratio. The ²⁹Si solution NMR spectra were also adjusted using a Multipoint Baseline Correction. The solid state ²⁹Si CP-MAS and ²⁹Si SP-MAS spectra were analyzed with OriginPro (Version 2021b. OriginLab Corporation, Northampton, MA, USA) and integrated using a Voigt function.

Fourier transform infrared (FTIR) spectra were recorded in attenuated total reflectance mode (ATR) on a Vertex 70 spectrometer (Bruker Optics, Ettlingen, Germany) from

4500-400 cm⁻¹ for the consolidated siloxanes but only shown from 4000-400 cm⁻¹ due to the absence of other signals at higher wavenumbers, each with a resolution of 4 cm⁻¹ and 16 scans.

Powder X-ray diffraction (PXRD) patterns of the tablet shaped samples were recorded at room temperature on a D8-A25-Advance diffractometer (Bruker AXS, Karlsruhe, Germany) in Bragg-Brentano θ - θ geometry (goniometer radius 280 mm) with Cu Ka radiation (λ = 154.0596 pm). A 12 μ m Ni foil working as a K $_{\beta}$ filter and a variable divergence slit were mounted at the primary beam side. A Lynxeye detector with 192 channels and a variable slit diaphragm in front of it was used at the secondary beam side. Experiments were carried out in a 2 θ range of 3–40° with a step size of 0.013° and a total scan time of 1 h. The recorded data was evaluated using TOPAS 5.0 (Bruker AXS, 2014, Karlsruhe, Germany) software, with the observed reflections being treated via single-line fits and a background of 5 but no sample displacement.

For UV-vis transmittance measurements all siloxanes were doctor bladed onto glass slides (Microscope Slides, VWR, Radnor, Pennsylvania, USA) at a thickness of approximately 120 μ m, heated to 110 °C for 5 minutes in an oven to ensure a uniform film and measured after cooling. The measurement range was from 250 to 800 nm but is only presented from 300 to 800 nm due to the absorption of the class slides at low wavelengths. Consolidation of the siloxanes was performed in a vacuum drying oven at 200 °C for 24 h to prevent blistering and then for an additional 72 h at 200 °C in a drying oven. Further thermal treatment was carried out in a drying oven at 200 °C for an additional 7 days and additional measurements after 3 and 7 days. Consolidation of NaphMG_Sn was performed in a tube furnace under wet argon at 200 °C for 72 h, while thermal treatment was performed under synthetic air $(N_2/O_2: 16/4)$ for an additional 7 d at 200 °C. All transmittance measurements were performed on a Lambda 750 instrument (Perkin Elmer Inc., Shelton, USA) equipped with a 100 mm integration sphere with 2 nm increments and 0.2 s integration time. Yellowness index measurements were performed on the same samples at the same time intervals as the transmittance measurements from 380 to 780 nm, with 10 nm increments and 0.24 s integration time using the same instrumental setup.

Thermogravimetric measurements (TG) were carried out applying a TGA/DSC STARe System 1 (Mettler-Toledo, Schwerzenbach, Switzerland) applying a heating rate of 10 K min⁻¹ between 25 and 800 °C using an oxygen gas flow of 40 ml min⁻¹.

Differential scanning calorimetry (DSC) was performed with a DSC 204 *F1 Phoenix* calorimeter (NETZSCH-Gerätebau GmbH, Selb, Germany) using aluminum crucibles with pierced lids under nitrogen/oxygen-flow (40/60 mL min⁻¹) applying a heating rate of 10 K min⁻¹. The temperature range was -100 to 250 °C, depending on the sample and each sample was measured three times and averaged. The value of the glass transition temperature (T_g) was determined at the center point of the glass event.

Thermal treatment experiments were conducted with all solid samples by grinding them into powder and placing them on Teflon molds. They were heated in 25 °C steps from 50 to 200 °C for 20 minutes at each step in an oven.

Dynamic mechanical analysis (DMA) was performed using a MCR-301 rheometer with a CTD-450 convection heating system (Anton Paar GmbH, Graz, Austria) in oscillatory mode with a plate–plate geometry using a 25 mm PP25 measuring plate, an amplitude of 5 %, a frequency of 1 Hz and a normal force value of 0. The samples were cooled from 150 °C or 200 °C to 35 °C with a cooling rate of 0.03 °C s⁻¹ depending on the viscosity to prevent them from losing contact with the upper plate.

Synthesis of NaphMG and NaphMG_5Ph_d

The synthesis of NaphMG and NaphMG_5Ph_d was carried out applying a similar approach. The amount of monomers, catalyst and solvent is documented in **Table 10**. All monomers were weighed into a 50 mL headspace vial, dissolved in methanol and HCl (pH = 1) was added. After closing the headspace vial, the solution was stirred at 400 rpm at 45 °C for 72 h. The headspace vial was opened to gel over night at room temperature and then heated to 110 °C for 24 h in a heat block.

Table 10: Equivalents of all monomers, solvent, and catalyst for the syntheses of NaphMG and NaphMG_5Ph_d. ^{a)} 150 %v/w of MeOH was used related to the mass of all monomers combined (1.5 mL of MeOH would be used if the mass of all monomers combined was 1 g). ^{b)} One equivalent of aqueous HCl for every methoxy group was used (1 eq of PTMS would require 3 eq of HCl, also the molar mass of water was used for the calculations due to its dilution).

Sample	1-NaphPhSi(OMe) ₂	DMDMS	PTMS	MeOH	HCl (pH 1)
NaphMG	1 eq	2 eq	1 eq	a)	9 eq ^{b)}
NaphMG_5Ph_d	1 eq	2 eq	5 eq	a)	21 eq ^{b)}

Synthesis of NaphMG_2Me₂, NaphMG_2Ph₂, NaphMG_4Ph and NaphMG_Sn

Synthesis of NaphMG_2Me₂, NaphMG_2Ph₂ and NaphMG_4Ph were carried out in a similar manner as already described above but with different amounts of solvent and HCl. The amount of added monomer, catalyst and solvent is documented in **Table 11**. In a 50 mL headspace vial NaphMG (1 eq) was dissolved in methanol, the respective monomer and HCl were added, and the vial closed. After stirring at 400 rpm for 24 h at 45 °C, the headspace vial was opened to gel overnight at room temperature. After that the siloxanes were further condensed for 24 h at 110 °C in a heat block.

Synthesis of NaphMG_Sn was done in a slightly different way. In a 50 mL headspace vial NaphMG (1 eq) was dissolved in methanol, di-*n*-butyltin diacetate (DBTA) was added and the vial closed. After stirring at 400 rpm for 24 h at 45 °C, the headspace vial was opened so that the reaction mixture could gel overnight at room temperature. After that, the sample was further condensed for 24 h at 110 °C in a heat block.

Table 11: Equivalents of all monomers, solvent, and catalyst used for the siloxane syntheses. ^{a)} 200 %v/w of MeOH was used related to the mass of NaphMG (2 mL of MeOH would be used for 1 g of NaphMG). ^{b)} Half an equivalent of HCl for every methoxy group of the monomer was used (1 eq of PTMS would require 1.5 eq of HCl, also the molar mass of water was used for the calculations due to its dilution). ^{c)} Related to the mass of NaphMG.

Sample	Monomer	MeOH	HCl (pH 1)	DBTDA
NaphMG_2Me ₂	DMDMS (2 eq)	a)	2 ^{b)}	
NaphMG_2Ph₂	DPDMS (2 eq)	a)	2 ^{b)}	
NaphMG_4Ph	PTMS (4 eq)	a)	6 ^{b)}	
NaphMG_Sn		a)		2 wt% ^{c)}

Consolidation of the Siloxanes

All siloxanes except for NaphMG_Sn were consolidated for 72 h at 200 °C in a drying oven to obtain the cured siloxanes. Due to its toxicity NaphMG_Sn was consolidated for 72 h at 200 °C in a tube furnace under wet argon.

3.2.5 Conclusions

Various siloxanes were synthesized by adding dimethyldimethoxysilane, diphenyldimethoxysilane, phenyltrimethoxysilane or di-n-butyltin diacetate to an already condensed but not consolidated siloxane to obtain samples with a high degree of condensation and with an increased rigidity at high temperatures, preventing them from liquefying. The obtained polymers therefore contained naphthyl groups, as well as different amounts of phenyl and methyl groups and varied in their cross-linking density. Since only two of them (NaphMG_2Ph2 and NaphMG_4Ph) showed the desired properties, all samples were analyzed via NMR, IR and PXRD measurements to gain more insights into structural issues related to the observed characteristics. All studies revealed that not only the amount of phenyl groups and the cross-linking density play an important role for their characteristics but that post-cross-linking an already existing siloxane is more effective than reacting all monomers at once in terms of usability at high temperatures. This was confirmed in NMR studies showing that post-cross-linking is not only beneficial to achieve a higher DOC but above all excels at integrating sterically demanding alkoxysilanes such as 1-NaphPhSi(OMe)₂ into a siloxane network. This creates more bridging oxygens resulting in stronger interactions between siloxane networks which in turn is necessary to prevent them from liquefying. The consolidated siloxanes showed high transparencies of up to 99 % even after a week at 200 °C, little yellowing, T₉₅ values of up to 453 °C and T_g's between -34 and 68 °C according to DSC measurements while dynamic mechanical analysis revealed higher glass transition temperatures up to 124 °C. The storage modulus also showed that three samples had a rubbery plateau at 200 °C indicating that they were still elastic but not liquid which was confirmed for two of the samples by a thermal treatment experiment in an oven heating them up to 200 °C. These two siloxanes are thus potentially suitable for high-temperature applications. Therefore, we were able to show that post-cross-linking a siloxane affects

DOC, structure, thermal stability, transmittance and $T_{\rm g}$, as well as viscosity and elasticity and is beneficial to prepare samples which show less cracking at room temperature and stay elastic at high temperatures.

Acknowledgments

The authors thank Dr. Michael Zimmer and Elias Gießelmann for the CP-MAS and SP-MAS NMR measurements. Instrumentation and technical assistance for this work were provided by the Service Center X-ray Diffraction, with financial support from Saarland University and German Science Foundation (project number INST 256/349-1). The authors thank Dr. Oliver Janka for the support in collecting the X-ray diffraction data presented in this paper.

3.3 Synthesis of Polyhedral Oligomeric Silsesquioxanes (POSS) Containing Polycyclic Aryl Groups

3.3.1 Abstract

Polyhedral oligomeric silsesquioxanes (POSS) containing polycyclic aromatic groups exhibit exceptional chemical, thermal, and photochemical stability, making them suitable for numerous applications such as sensors and optical devices. In this study, POSS derivatives containing 1-napthyl, 2-naphthyl and 9-phenantrenyl groups were prepared via two distinct approaches. Initially, trialkoxysilanes were synthesized from the corresponding polycyclic aromatic bromides using a Barbier-type reaction. Subsequent condensation to POSS derivatives was achieved either by refluxing the monomers with potassium hydroxide or by using tetrabutylammonium fluoride (TBAF). Only the first method successfully yielded T₈ 1-naphthyl POSS, while the other methods produced compounds with varying cage sizes and possibly higher molecular weight species, as indicated by silicon NMR, as well as MALDI-FTICR. The successful formation of 1-naphthyl POSS using the KOH method was confirmed by NMR, IR, and single crystal X-ray crystallography. Further characterization through fluorescence spectroscopy, DSC and TGA revealed no excimer formation, a high thermal stability (T_{onset} = 453.6 °C) and a melting point of 311 °C.

3.3.2 Introduction

Silsesquioxanes with the general formula $(RSiO_{1.5})_n^{100}$ can form different structures like cages, open cages, 166,410 ladder-type oligomers 411,412 , nanoparticles 413,414 and star-shaped structures. 415,416 A typical example for a cage-like silsesquioxane is the T₈ POSS with a cubic structure and the formula $R_8Si_8O_{12}$. Herein the substituents R are placed at each corner and are either hydrogen atoms or other organic groups like for example alkyl, alkylene, aryl, or arylene substituents with or without further functional groups attached 100,148 and allow for easy functionalization. 417 These organic groups make POSS compatible with polymers, surfaces or biological systems and can also be designed to be reactive or unreactive. 150 Their incorporation into polymers can be achieved by chemical cross-linking and copolymerization, attaching them through covalent bonds or by

blending.418 These systems show high thermal and mechanical stability,419,420 high oxidative resistance and gas permeabilities, 421-423 are hydrophobic or hydrophilic and have the ability to aggregate. 424 They possess high biocompatibility, little cytotoxicity 425,426 and can improve thermal and mechanical properties in polymers, 427,428 as well as reduce flammability. 429 Therefore, possible applications for POSS based composites are fluorescence sensors, coating materials, drug delivery systems, organic semiconductors and medical applications. 430431,432 Within a polymer they can also lower cross-link density since they add a substantial volume to the polymer or can act as centers of a local crosslinked network and hereby increase or decrease the RI, 150,433 whereas the RI of the cubes themselves is generally around 1.5.433 Different sized POSS structures with various organic groups have been already synthesized (**Figure 32**). 71,159,162,434–442 While symmetric POSS systems, such as octaphenylsilsesquioxanes, facilitate crystalline packing due to their high symmetry and low dipole moment, they often lead to poor solubility in organic solvents and a neutral response to mechanical shear. These limitations can be overcome by asymmetric POSS systems in which at least one corner carries a different organic group (**Figure 32**).⁷¹ POSS systems also offer the ideal opportunity to introduce polycyclic groups into various systems. They exhibit high thermal and photochemical stability, high fluorescence, tunable luminescence and low toxicity, which makes them interesting for example as sensors for biological imaging and sensing, for LEDs and as optical switches.442-444

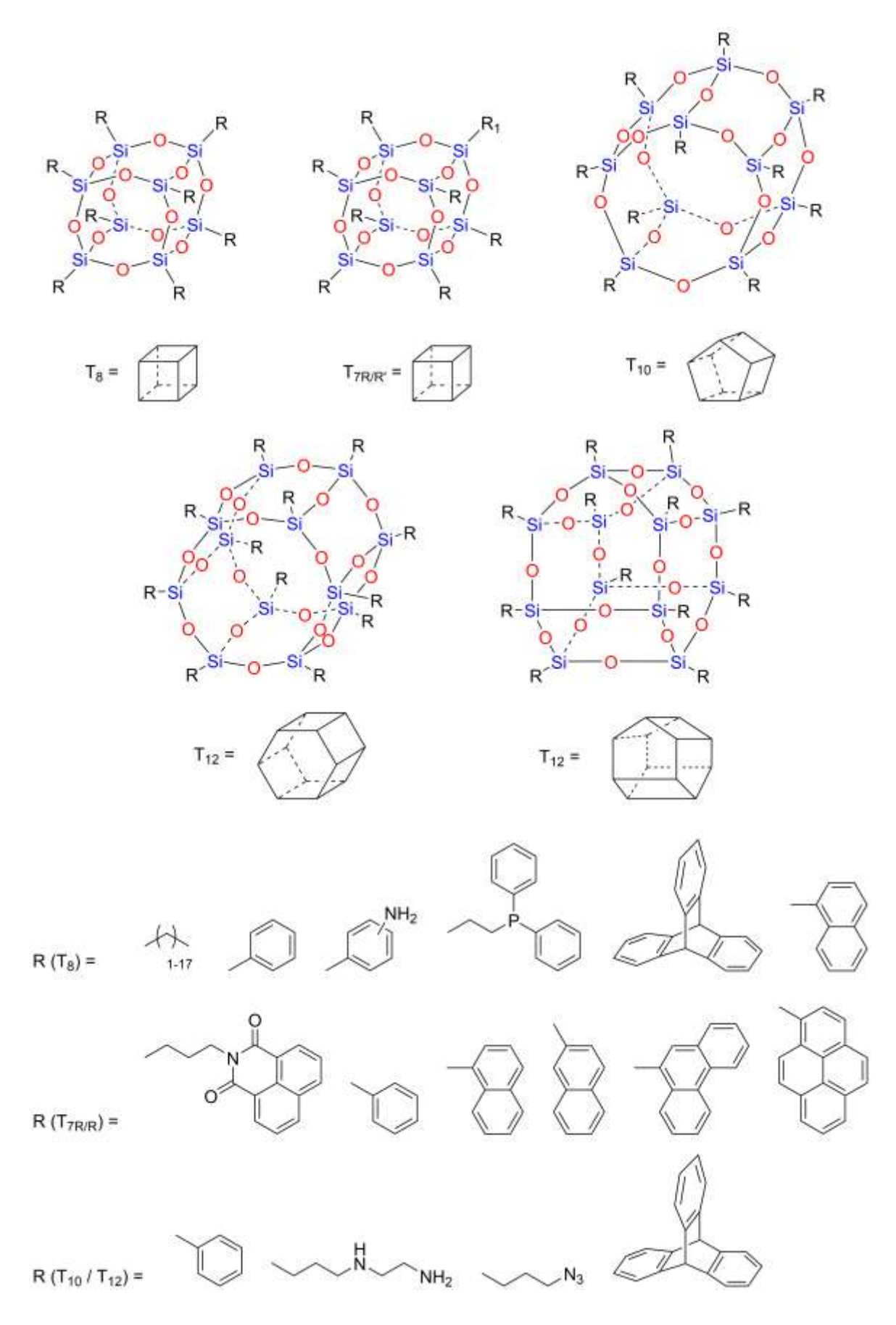


Figure 32: Presentation of several POSS systems and their possible organic groups.

In general, there are two major methods to synthesize POSS systems. The first method is the new formation of Si-O-Si bonds by assembling silsesquioxanes from monomers with the general formula RSiX₃ where R is a chemically stable substituent like methyl, phenyl or vinyl and X is a reactive substituent like Cl, OH or OR. The second method is their formation from linear, cyclic, or polycyclic siloxanes which are derived from the RSiX₃-type. ¹⁵⁰ Furthermore, they can be formed by sol-gel reactions ⁴⁴⁵ like hydrochloric acid and trimethoxysilane in methanol⁴⁴⁶ or trichloroalkylsilane in ethanol and water.⁴⁴⁷ The yield, reaction rate and degree of oligomerization hereby depend on the concentration of the initial monomer, solvent, substituents R and X, catalyst, reaction temperature, water addition and solubility of the formed oligomers. Monofunctional POSS are produced by corner-capping an open cage which contains three residual Si-OH groups with a trifunctional monomer and can be synthesized by kinetic controlled condensation of for example cyclohexyltrichlorosilane. Depending on the monomer this method can lead to various types of products like styryl-substituted-, aminosubstituted- or norbornyl POSS. 448-451 Multifunctional POSS on the other hand are synthesized by hydrolysis and condensation of trialkoxysilanes or trichlorosilanes. 150 A well-known representative is the phenyl POSS which for example can be synthesized from phenyltrichlorosilane and benzyl trimethyl ammonium hydroxide. 452-454 Another way to form POSS systems from phenyltrialkoxysilanes is by using different bases like KOH, TBAF or KF. When using TBAF, fluoride ions are used to catalyze the formation of the corresponding POSS systems, whereby the fluoride ions must subsequently be removed again using CaCl₂, for example. KF, on the other hand, is used together with crown ethers such as 1,4,7,10,13,16-hexaoxacyclooctadecane (18-crown-6) due to its poor solubility. These crown ethers not only help to dissolve KF in polar and non-polar, aprotic solvents, but also reduce the strong solvation forces acting on the fluoride ion to produce a "naked" fluoride, which should be able to react as a nucleophile and base. This "naked" fluoride attacks the silicon atoms as a nucleophile and causes rearrangements of the skeleton and thus does not serve to hydrolyze the alkoxy groups. 160,164,455-457

POSS systems containing various organic groups have been extensively studied for many years. However, in case of polycyclic aromatic systems until now only POSS were synthesized were one corner was modified with a naphthyl group, as well as the T_8 1-naphthyl POSS from 1-naphthyltrichlorosilane. While the former are asymmetric POSS,

which differ in their properties from symmetric systems, the T₈ 1-naphthyl cage was mainly investigated for its architecture, decomposition and thermal properties. 71,434,442 Therefore, we wanted to extend these studies to symmetric POSS systems consisting purely of 1-naphthyl, 2-naphthyl or 9-phenanthrenyl groups, to investigate their fluorescence behavior and also to compare possible differences due to the isomeric attachment regarding the 1-naphthyl and 2-naphthyl group. Furthermore, by using trimethoxysilanes as opposed to trichlorosilanes, we wanted to investigate new possible reaction pathways to produce POSS systems. To this end, in the present study we have tried to synthesize POSS systems from trimethoxysilanes containing 1-naphthyl, 2-naphthyl and 9-phenanthrenyl groups by reaction with KOH as well as TBAF.

3.3.3 Results and Discussion

The precursors for the POSS systems, i.e. trimethoxysilanes with polycyclic aromatic groups, were prepared by Barbier-type reactions between 1- or 2-bromonaphthalene or 9-bromophenanthrene and tetramethoxysilane (TMOS) (**Scheme 32**). Trimethoxy-(1-naphthyl)silane and trimethoxy-(2-naphthyl)silane hereafter referred to as 1-NaphSi(OMe)₃ and 2-NaphSi(OMe)₃ formed as colorless liquids, while trimethoxy-(9-phenanthrenyl)silane hereafter referred to as 9-PhenSi(OMe)₃ was obtained as a white solid. All compounds were obtained in high purity and yields between 31 and 63 %.

R ₁	Overall Yield [%]
1-naphthyl	61
2-naphthyl	63
9-phenanthrenyl	31

Scheme 32: General synthetic route of all three trialkoxysilanes using a Barbier-type reaction.

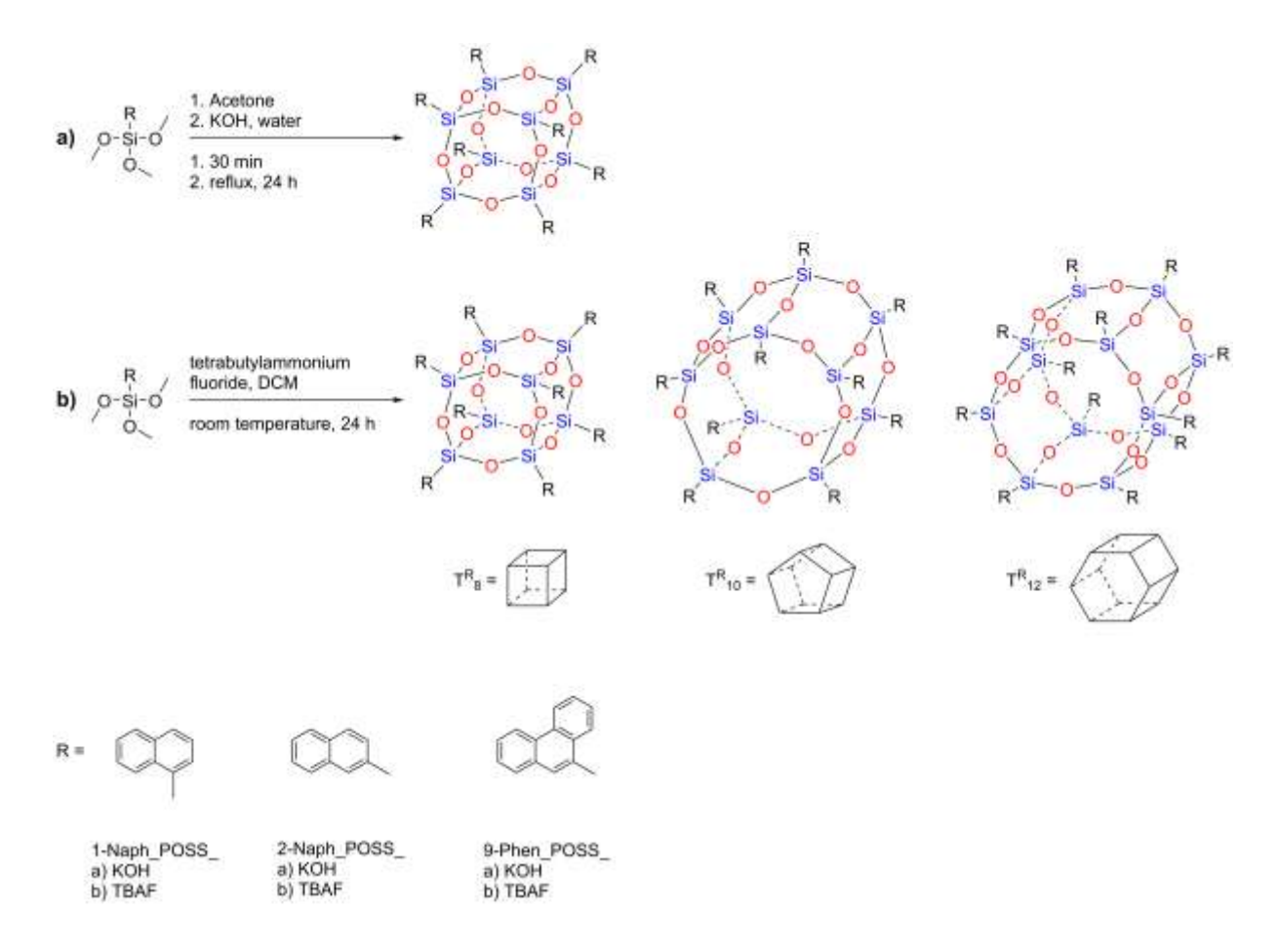
The molecular structures of all trimethoxysilanes have been verified using ¹H, ²⁹Si, ¹H-²⁹Si HMBC, and ¹³C NMR spectroscopy as well elemental analysis and IR-spectroscopy (see **Figure S 107 – Figure S 119** and **Table S 9**). All signals are in good agreement with similar literature known compounds.^{72,340,341}

UV-vis spectroscopy shows the typical absorption bands of naphthalene and phenanthrene, as well as similar compounds where aromatic groups are bound to a silicon atom (see Figure S 120).342 The absorption maxima of 1-NaphSi(OMe)3, $2-NaphSi(OMe)_3$ and $9-PhenSi(OMe)_3$ are at 284, 278 and 256 nm, respectively and thereby show an increasing blue shift. In previous studies dialkoxysilanes with polycyclic aromatic groups revealed excimer formation, which might have an influence on ordering phenomena during condensation reactions. Therefore, we investigated the three trimethoxysilanes for the same phenomena using fluorescence spectroscopy (see Figure S 121 - Figure S 123). The concentration dependent excimer formation for the three synthesized trimethoxysilanes was studied using a dilution series in dichloromethane at an excitation wavelength of 290 nm for 1-NaphSi(OMe)₃ and 2-NaphSi(OMe)₃ and 340 nm for 9-PhenSi(OMe)₃. The fluorescence spectra revealed for 1-NaphSi(OMe)₃ only one broad peak at 339 nm for high concentrations, which can be attributed to the molecular fluorescence of naphthalene. 345,348 With an increase in dilution this peak shifts to lower wavenumbers, getting sharper and more detailed. The latter part was already observed by Nishimura et al. for α -naphthalene, 458 as well as similar compounds. 459 Instead of a broad peak at around 410 nm which would show excimer formation a broad tailing of the peaks can be observed. Since it decreases with lower concentrations it can be attributed to ground state aggregation. 192 2-NaphSi(OMe)₃ shows the same peak at 338 nm which is due to the molecular fluorescence of naphthalene. Interestingly two more peaks can be seen at 323 and 352 nm. While the former increases with decreasing concentration, the latter shows the opposite behavior. In their form they resemble the peak of 1-NaphSi(OMe)₃ at low concentrations. The opposite behavior has already been observed for naphthalene 460,461 and a somewhat similar behavior in an anthracene derivative, with the latter being attributed to static quenching.⁴⁶² Furthermore, no excimer formation or ground state aggregation can be seen. The fluorescence spectra of 9-PhenSi(OMe)₃ only shows the peaks typical for the phenanthrene group. 350,463 The first peak at 349 nm interestingly also increases with decreasing concentration. Comparing now the spectra of the diluted samples with those of the pure samples, one can recognize a band at approx. 400 nm in all undiluted samples, which indicates excimer fluorescence. This behavior was already observed in poly(acetoxy-p-phenylene vinylene), for example, when the fluorescence of the solid film was compared with that of a diluted sample 464 and even more clearly in a thiophene-flanked pyrene carbon analogue. Here, a dilute solution showed mainly monomer fluorescence, while the solid sample showed considerable excimer fluorescence. This was attributed to closely adjacent molecules in the solid phase, which allow excimer formation due to a large molecule-to-molecule overlap area. From this it can be concluded that, in contrast to the dialkoxysilanes already investigated, none of the trialkoxysilanes shows excimer formation in dilution, but only in pure form.

Polycyclic aromatic groups usually also have a large influence on the refractive index (RI) of substances, which can be also used to generate high RI sol-gel materials. 191,383,466,467 We measured the RI of all three trialkoxysilanes at 20 °C and 589 nm. 9-PhenSi(OMe)₃ is a solid compound at room temperature. Its melting point of 86 °C (Figure S 124) was too high to be measured on our refractometer. Therefore, it could only be measured by applying a calibration curve method, which already proofed reliable in our previous studies on dialkoxysilanes (see Figure S 125 and Table S 10).383 To stay consistent and obtain comparable results we decided to measure all three samples with this method. In short this means that different concentrated solutions of 1-NaphSi(OMe)₃ and 2-NaphSi(OMe)₃ in toluene and 9-PhenSi(OMe)₃ in THF were prepared, measured, and plotted. In the linear equation of the resulting calibration curve, x was set as 100 to simulate the pure substance and calculated. The obtained refractive indices of 1-NaphSi(OMe)₃, 2-NaphSi(OMe)₃ and 9-PhenSi(OMe)₃ are 1.554, 1.541 and 1.615, respectively. These values are high compared to those of standard trialkoxysilanes like phenyltrimethoxysilane (1.4710) or benzyltriethoxysilane (1.4628).³⁰⁴ Furthermore, it can be seen that the constitutional isomerism of the naphthyl groups does not play a significant role for the refractive index.

3.3.3.1 Condensation of Trimethoxysilanes

2-NaphSi(OMe)₃ and 9-PhenSi(OMe)₃ 1-NaphSi(OMe)₃, condensed were silsesquioxanes using two different methods. In the first method KOH and acetone were applied under reflux for 24 h. This method has proven its suitability in the synthesis of octaphenylsilsesquioxane, octamethylsilsesquioxane and fluorodecyl POSS. 160,232,468 The second method was using DCM and tetrabutylammonium fluoride (TBAF) while stirring the mixture at room temperature for 24 h (Scheme 33) which has already been done to synthesize T_8 , T_{10} and T_{12} phenylsilsesquioxanes. While the former method strongly favors T_8 cages with yields between 81 % and 95 %, 160,232 the latter tends to lead to all three cage sizes. 456 To study the obtained structures NMR, IR, MALDI-FTICR and SEC measurements were performed. Additionally, the successfully synthesized POSS structure was confirmed by single crystal X-ray crystallography and further studied using UV-vis and fluorescence spectroscopy, as well as DSC and TGA measurements.



Scheme 33: Condensation reactions of trialkoxysilanes to form POSS systems, including their abbreviations. a) using KOH and acetone, b) using TBAF and DCM.

3.3.3.2 Nuclear Magnetic Resonance (NMR) Spectroscopy

As already mentioned, different sized cages as well as partially open structures or random polysiloxanes can form during the synthesis. Liquid NMR spectroscopy was performed to study the obtained products (see Figure 33 and Figure S 126 - Figure S **143**). After the successful synthesis the ¹H and ¹³C NMR should show only sharp peaks in the aromatic region without any remaining methoxy signal, while the ²⁹Si NMR is supposed to show only one signal for the T₈ cube.²³² Additional peaks can result from larger cages or open structures. 438,469 It can be seen that only 1-Naph_POSS_KOH was formed exclusively as a T₈ cage as it shows sharp signals in the ¹H and ¹³C NMR as well as only one signal in the ²⁹Si NMR at -77.26 ppm which corresponds well with octaphenylsilsesquioxane (OPS) at -78.3 ppm.²³² The other POSS systems show very little to no peaks for the methoxy groups in the ¹H NMR and multiple signals in the ²⁹Si NMR which can result from low molecular weight species, cages of various sizes and open cages for example. 2-Naph_POSS_KOH shows four silicon signals which could be based on a mixture of T_8 , T_{10} and T_{12} cubes, especially since the latter can result in more than one signal. The T_{10} phenyl POSS shows a signal at -79.6 ppm while the T_{12} phenyl POSS displays two signals at around -79.5 ppm and -81.5 ppm. 440,456 Therefore the observed signals at -77.76 ppm and -79.14 ppm could belong the T_8 and T_{10} species, respectively. Another possibility would be one closed and one open T₈ POSS since the open cage would lead to three signals with the one for the silicon atoms next to the hydroxy groups being more downfield shifted than the others. For OPS with one corner missing this results in signals at -69.05, -77.55 and -78.52 ppm. 470 However, as these signals differ significantly from those observed for 2-Naph_POSS_KOH, this possibility can be ruled out. Also considering no hydroxy or methoxy signals are present in the ¹H and ¹³C NMR, it seems more likely that the previously mentioned mixture of T₈ and T₁₀ cages is present. For 9-Phen_POSS_KOH a lot of signals in the ²⁹Si NMR can be found, which leads to the assumption that many different species may be present. The highest signals at -77.75 ppm, -79.13 ppm and -78.35 ppm could originate from T_8 and T_{12} cages. For 1-Naph_POSS_TBAF the signals at -69.37 ppm, -77.87 ppm and -78.04 ppm could stem from an open T₈ cage, while the signals at -77.20 ppm, -76.17 ppm and -78.69 ppm could belong to closed T₈ and T₁₂ cages, respectively. 2-Naph_POSS_TBAF shows three signals at -78.83 ppm, -80.98 ppm and -78.94 ppm which could be attributed to T_{12} and T_{8} cages.

Lastly, 9-Phen_POSS_TBAF shows signals at -69.07 ppm, -77.93 ppm and -78.54 ppm potentially stemming from open T_8 cages, as well as a signal at -77.66 ppm from closed T_8 cages. In general, further purification by recrystallizing and subsequent column chromatography of the supernatant could help to separate different sized cages and polymeric products which was not possible due to time constraints.²³¹

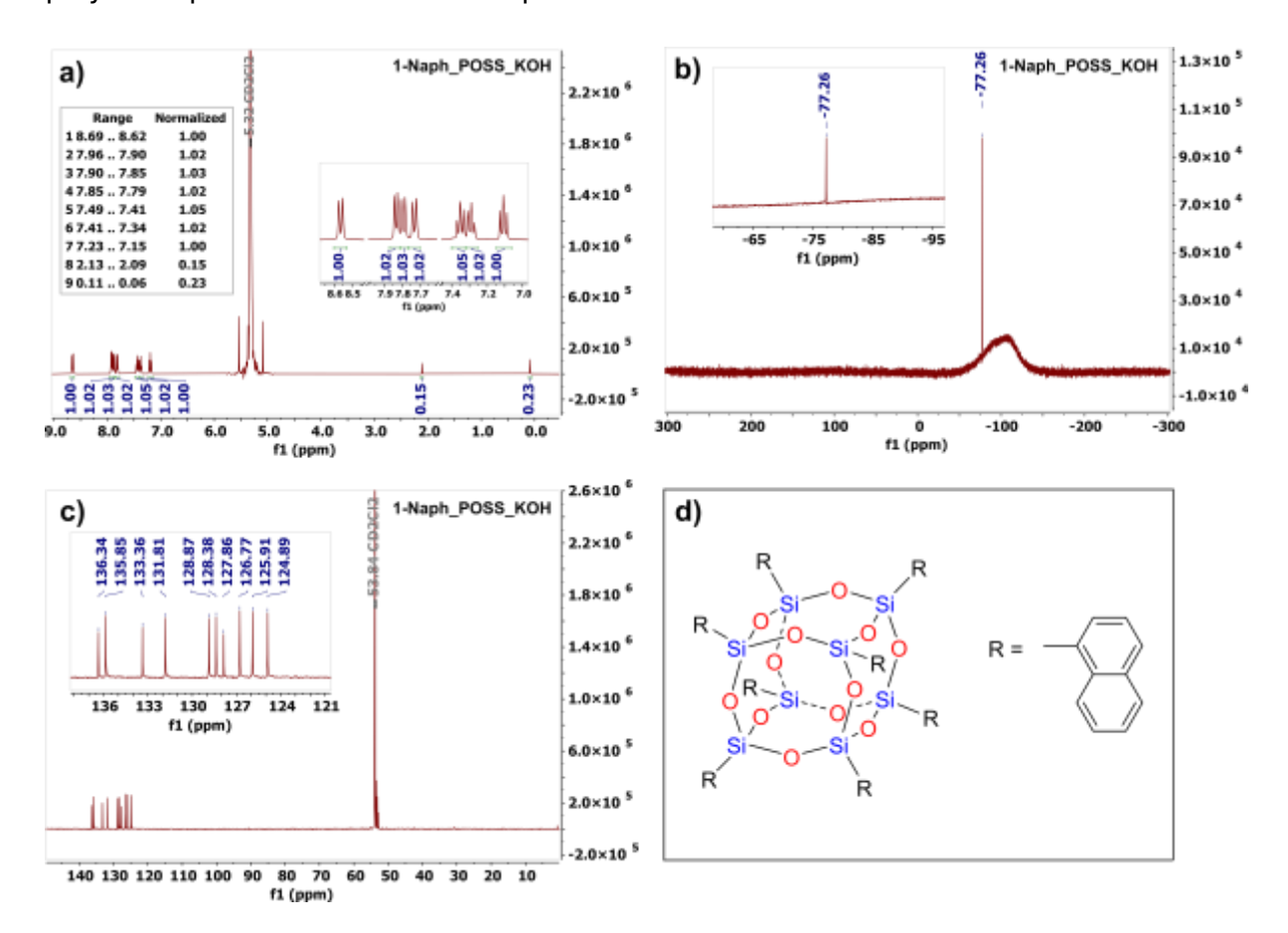


Figure 33: NMR spectra of 1-Naph_POSS_KOH in CD₂Cl₂. a) ¹H NMR (400.13 MHz), b) ²⁹Si NMR (79.49 MHz), c) ¹³C NMR (100.62 MHz), d) Illustration of 1-Naph_POSS_KOH.

3.3.3.3 Fourier transform Infrared (FTIR) Spectroscopy

FTIR spectra of the POSS systems (**Figure 34**) show the expected signals of the aromatic groups at around 3100-2950 cm⁻¹ (v(CH)_{Ar}), 1650-1480 cm⁻¹ (v/ δ (C=C)_{Ar}) and 770-680 cm⁻¹ (v(CH)_{Ar}) as well as the vibration of the Si-O-Si bond from 1200 to 950 cm⁻¹. The typical absorption bands for the methoxy groups that were present in the trialkoxysilanes at 2836 and 1183 cm⁻¹ as well as the broad OH absorption bands between 3700 and 3100 cm⁻¹ cannot be observed anymore.^{340,341,354,355,471} Therefore, it can be concluded that all methoxy groups have been hydrolyzed and the condensation has progressed to such an

extent that almost no hydroxy groups are present. The very weak Si-OH absorption band at around 896 cm⁻¹ can be observed in all samples except for 1-Naph_POSS_KOH and 1-Naph_POSS_TBAF.²²⁷ This is consistent with the previous observation that complete hydrolysis has taken place and condensation has progressed to such an extent that only cages, ladders, partially open cages, or other very high condensed species should exist. As already mentioned, the only exceptions being 1-Naph_POSS_KOH and 1-Naph_POSS_TBAF, where the former shows no additional signals in the silicon NMR indicating that no open cages or highly condensed species are present and the latter shows only very small signals, especially compared to the other samples. The most important signal in identifying POSS systems in the IR is the form of the Si-O-Si band which allows to determine the species of polysiloxane/network. While ladder-like polysilsesquioxanes show two absorption peaks at 1150 and 1050 cm⁻¹ due to the asymmetrical horizontal (Si-O-Si) and vertical (Si-O-Si-R) siloxane bond, cages show only one peak at around 1100 cm⁻¹ due to the Si-O-Si vibration band, depending on the organic group. 182 It should also be mentioned that silsesquioxanes can rearrange from ladder-like structures to caged structures, thereby changing from the afore mentioned two absorption bands to one.⁴⁷² While a broad absorption band at around 1100 cm⁻¹ indicates other species, such as cycles, ladders or random networks, 99 no further statement can be made about the size of the cages or if they are open or closed. 232,438,439,456,469,473 This sharp peak was only observed for 1-Naph_POSS_KOH and also supports the conclusion from the NMR that only this substrate was successfully obtained in the form of pure cages. For the remaining samples this band is wider or shows more peaks indicating together with die Si-OH band that other species are present and therefore also confirming the NMR results.

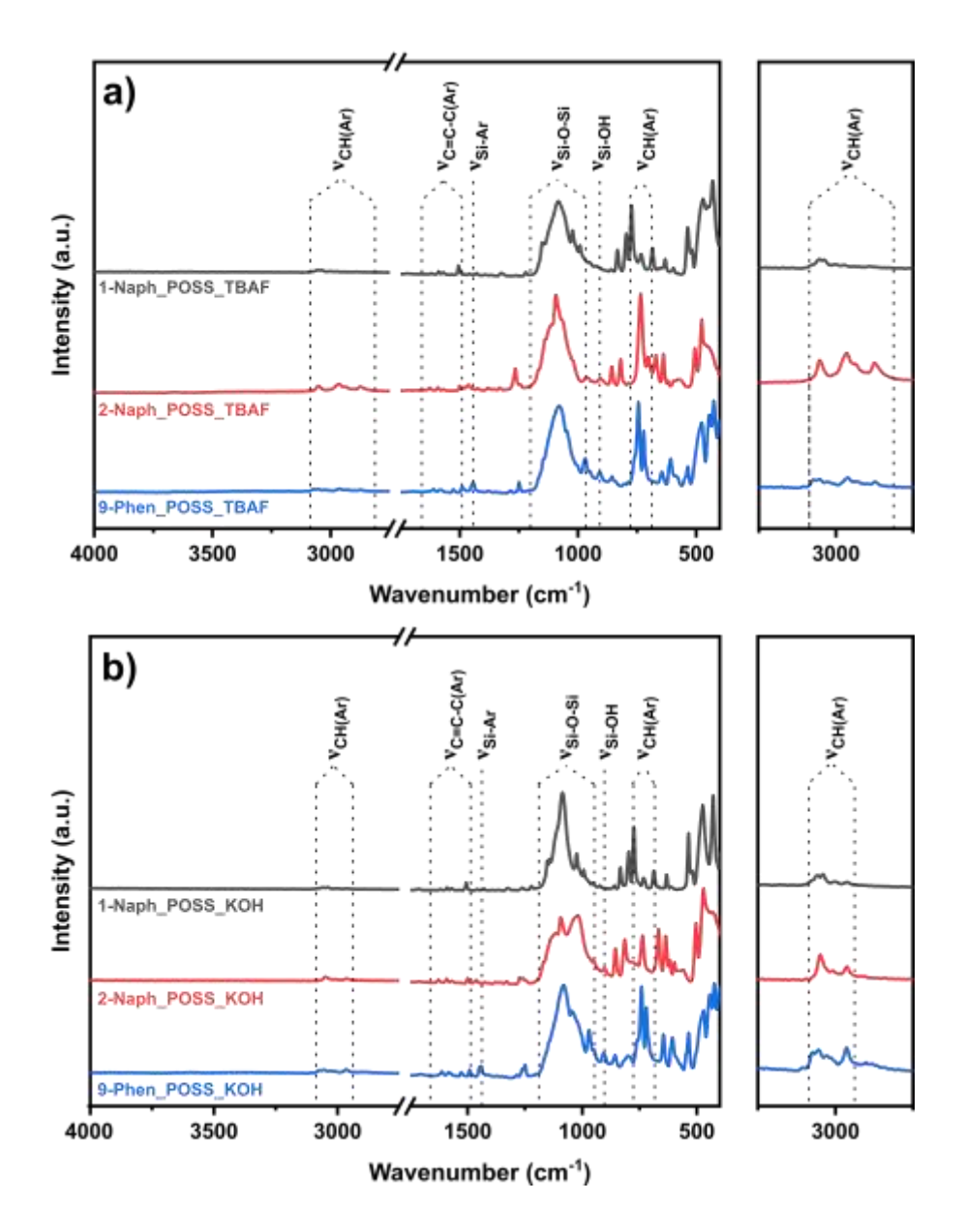


Figure 34: FTIR spectra of a) 1-Naph_POSS_TBAF (black), 2-Naph_POSS_TBAF (red) and 9-Phen_POSS_TBAF (blue) and b) 1-Naph_POSS_KOH (black), 2-Naph_POSS_KOH (red) and 9-Phen_POSS_KOH (blue).

3.3.3.4 Matrix-Assisted Laser Desorption/Ionization Fourier-Transform Ion Cyclotron Resonance (MALDI - FTICR) Mass Spectrometry

MALDI-FTICR measurements were used to gain more insight into the sizes of the synthesized samples and therefore possible T_8 , T_{10} , T_{12} or even larger cages as well as other high molecular weight species that might have formed (Figure 36). For 1-Naph_POSS_KOH two mass peaks at 1457 m/z and 1473 m/z were found in the spectra. These belong to the T₈ cage with added sodium which is omnipresent in MALDI spectra⁴⁷⁴ and added potassium stemming from the KOH used in the synthesis, respectively and are further proof that this POSS was successfully formed. For 2-Naph_POSS_KOH among all signals only one mass at 2532 m/z can be identified which belongs to the corresponding T_{14} cage with added sodium. This cage can either have D_{3h} symmetry, which results in a total of three signals in the ^{29}Si NMR, or $C_{2\nu}$ symmetry, which results in five signals (**Figure 35**).¹⁶⁸ ²⁹Si Assuming D_{3h} symmetry, the three signals in the NMR at -77.76 ppm, -78.36 ppm and -79.14 ppm can thus be explained.

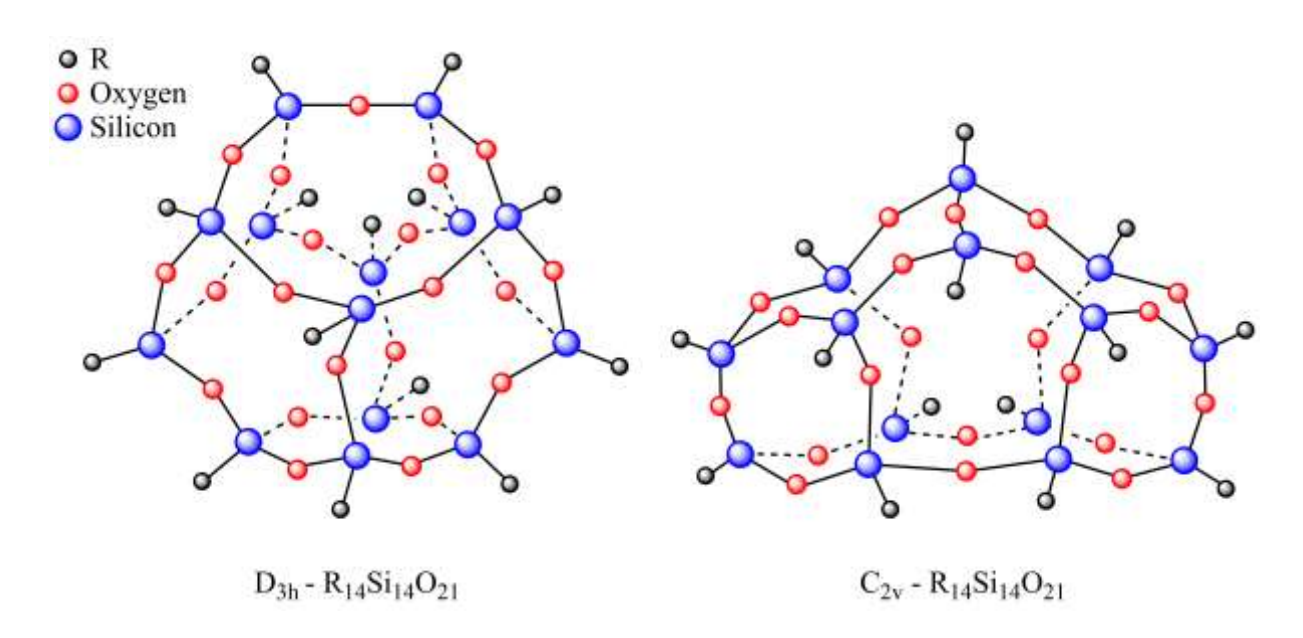


Figure 35: Depiction of the two different symmetries of the T₁₄ cage.

For 9-Phen_POSS_KOH among all signals again only one at 1942 m/z can be identified which belongs to the T_8 cage with additional silver, originating from the silver trifluoroacetate used in the matrix. Therefore, the other signals in the 29 Si NMR could belong to high molecular weight species which cannot be identified any further. Looking

at the samples synthesized with TBAF and starting with 1-Naph_POSS_TBAF three signals corresponding to the T_8 cage (1434 m/z [M], 1457 m/z [M+Na⁺] and 1542 m/z [M+Ag⁺]) and one signal corresponding to the T₁₀ cage (1815 m/z [M+Na⁺]) can be observed. Both cages lead to one signal in the silicon NMR. This would explain two of the five signals but due to their proximity to each other no direct assignment can be made. 168,475 The most prominent signal at -77.20 ppm could be attributed to the T₈ cage as it has the same chemical shift as for the T₈ cage of 1_Naph_POSS_KOH. 2-Naph_POSS_TBAF shows signals for the T₁₀ cage (1792 m/z [M], 1815 m/z [M+Na $^{+}$]) and the T₁₂ cage (2151 m/z [M], 2174 m/z [M+Na $^{+}$]). Considering that the T_{10} cage shows one and the T_{12} cage two signals in the silicon NMR, all three signals in the silicon NMR for 2-Naph_POSS_TBAF can be explained. For 9-Phen_POSS_TBAF a total of six signals can be identified. Three belong to the T₈ cage $(1853 \text{ m/z} [\text{M+F}^-], 1906 \text{ m/z} [\text{M+THF}], 1942 \text{ m/z} [\text{M+Ag}^+])$ and the other three belong to the T_{10} cage (2312 m/z [M+F⁻], 2316 m/z [M+Na⁺], 2401 [M+Ag⁺]). Since each cage leads to one signal in the silicon NMR only two of the five signals can be explained. In general, it seems that the synthesis with TBAF leads to different sized cages for each sample ranging from T_8 to T_{12} while the synthesis with KOH leads only to one cage size per synthesis which was either T₈ or T₁₄. This was also seen in studies were the KOH approach yielded the T₈ OPS with yields of 81 % and 95 %, respectively, while the synthesis with TBAF led to T₈, T₁₀ and T_{12} phenyl POSS systems. 160,232,456 Looking at the two approaches separately, it is noticeable that 1-naphthyl and 9-phenanthrenyl each lead to cages of the same size, namely T₈ and T₁₀, while 2-naphthyl leads to larger cages in both cases. A possible explanation for this can be found in two recent theoretical studies, which show that the Si-O bond length decreases with increasing cage size. 476,477 This can be observed by looking at the Si-O bond lengths for octaphenyl POSS (1.618 - 1.626 Å)⁴⁷⁸ compared to dodecaphenyl POSS (1.604 - 1.618 Å), 479 or for styryl-functionalized POSS, where the average bond length also decreases from T_8 (1.617 Å) to T_{10} (1.610 Å) to T_{12} (1.60 Å). ¹⁴⁹ This would bring the organic groups closer together and could possibly explain why the sterically less demanding 2-napthyl group forms larger cages.

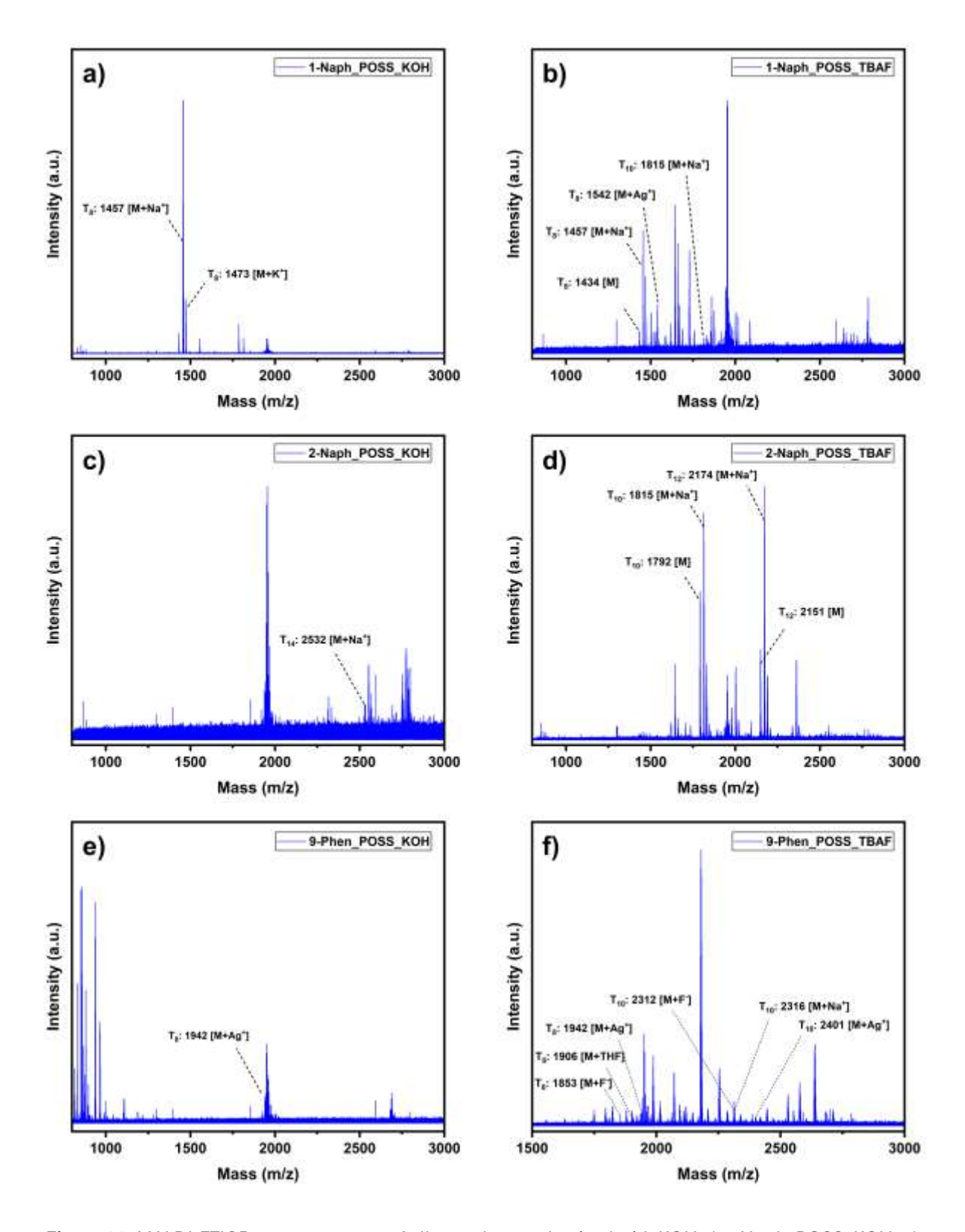


Figure 36: MALDI-FTICR measurements of all samples synthesized with KOH a) 1-Naph_POSS_KOH, c) 2-Naph_POSS_KOH, e) 9-Phen_POSS_KOH and synthesized with TBAF b) 1-Naph_POSS_TBAF, d) 2-Naph_POSS_TBAF, f) 9-Phen_POSS_TBAF.

3.3.3.5 Size Exclusion Chromatography (SEC)

Size exclusion chromatography experiments were performed on all POSS systems to get more insight into their size distribution and their polydispersity index value (\mathcal{D}) using an RI detector (Figure 37). Even though polystyrene was used as a standard which is quite different with respect to the hydrodynamic volume in THF compared with our POSS systems, the obtained θ values can still be used to estimate if many substances of different sizes were obtained and to compare if the molecular weight is in the same range as already shown by the MALDI-FTICR measurements. The *Đ* value for all samples is very narrow, ranging from 1.05 to 1.12 indicating very little molar mass distribution. This displays that mostly POSS systems, namely T₈-, T₁₀- and T₁₂ cages, or structures of similar size should have formed. The average molecular weight (Mw) ranges from 815 to 1401 g mol⁻¹. T₈ cages of 1-Naph_POSS and 2-Naph_POSS have a molecular weight of 1434.00 g mol⁻¹ and that of 9-Phen_POSS has one of 1834.48 g mol⁻¹. Considering the afore-mentioned shortcomings of this method, those results are in good agreement with our expectations. Only 9-Phen_POSS_KOH stands out since it not only shows a larger polydispersity index value at 2.86 but also a much larger average molecular weight at 144 790 g mol⁻¹. It seems that in this synthesis in particular, in addition to the T₈ cage, substances with different sizes and generally more polymeric structures were formed, which has not yet been noticed in the MALDI-FTICR measurements, as these are only possible up to 3000 m/z in our setup. These results in general are in good agreement with the MALDI-FTICR measurements which showed between one and three different sized cages for each sample as well as signals mostly in a range of 1000 to 2000 m/z indicating that not many different species were formed. Since the MALDI-FTICR measurements in our case can only be done up to 3000 m/z no more statements regarding the large average molecular weight of 9-Phen_POSS_KOH can be made.

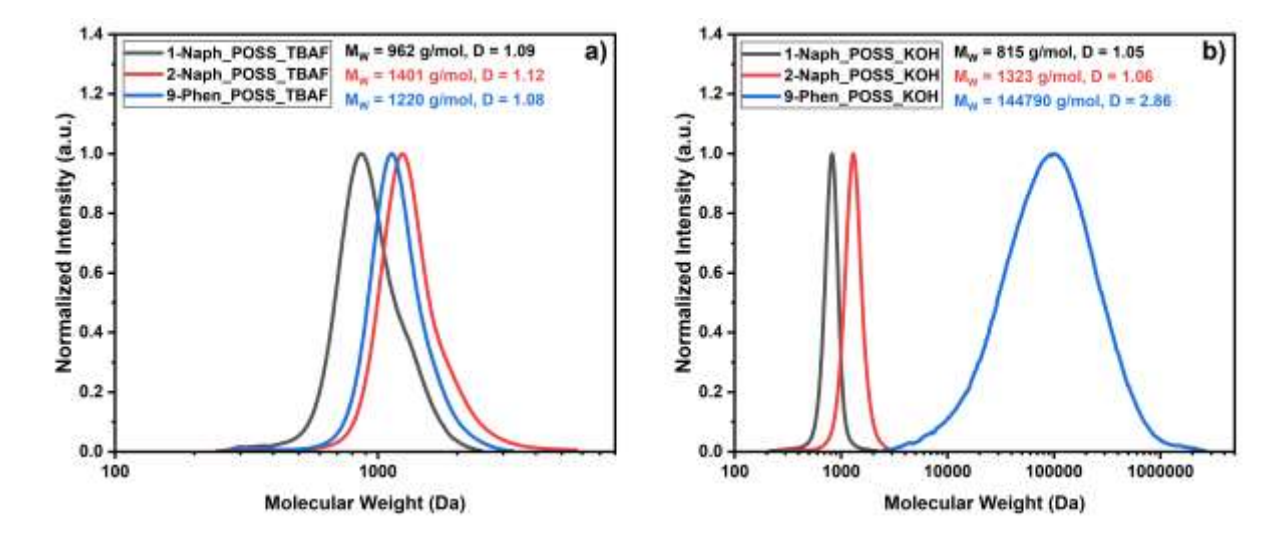


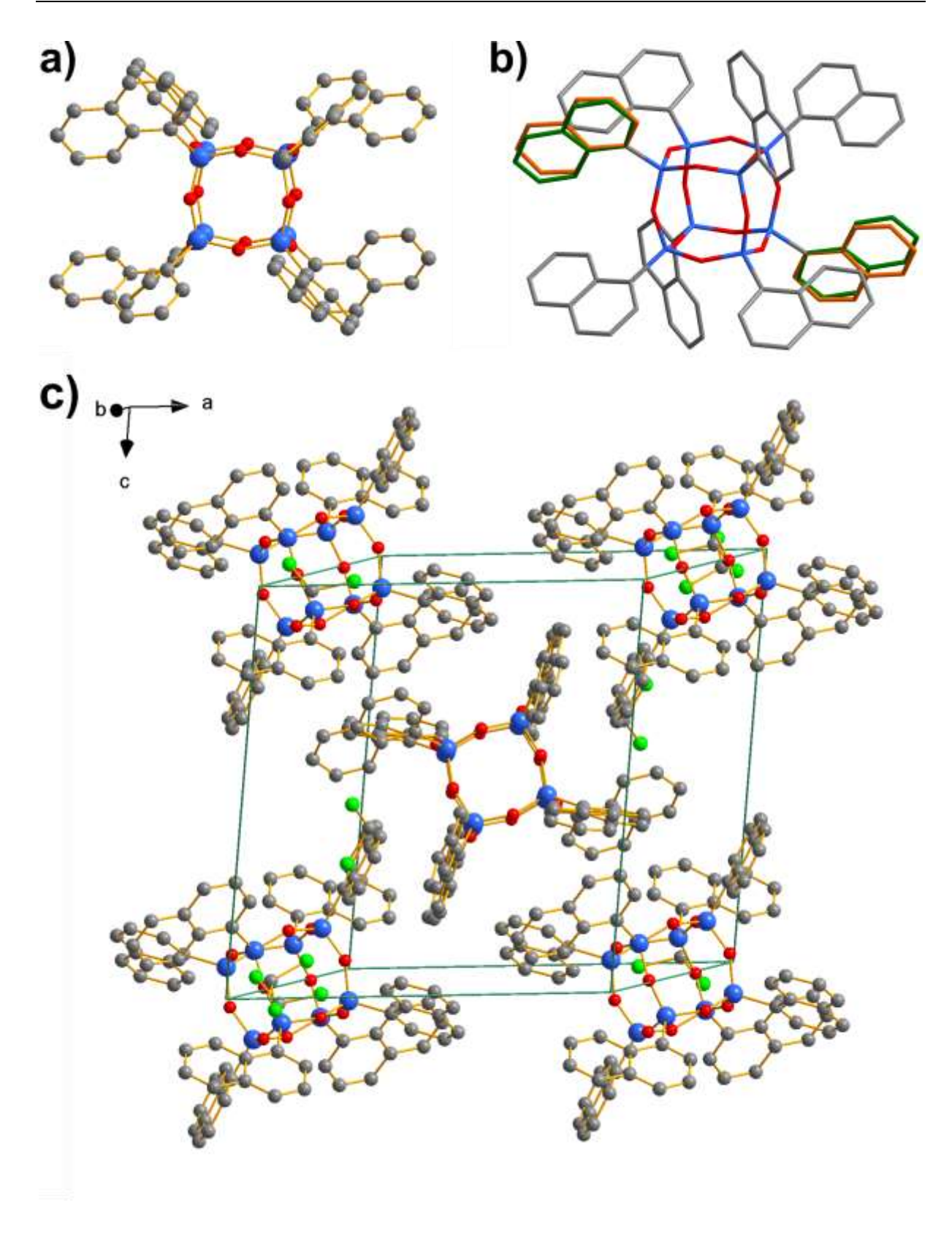
Figure 37: SEC profiles for a) all three POSS systems synthesized via TBAF and b) all three POSS systems synthesized via KOH, measured on a RI detector.

3.3.3.6 Single Crystal X-ray Crystallography

We obtained single crystals of 1-Naph_POSS_KOH by dissolving the powder in DCM and subsequently evaporating the solvent slowly but not completely (Figure 38 and Table S 11 - Table S 16). Single crystals of 1-Naph_POSS_KOH were investigated by X-ray diffraction experiments at 133(2) K. The compound was found to crystallize in the triclinic crystal system with space group $P\overline{1}$. The measured values for the Si-O bond length (161.0 to 162.1 pm; average 161.6 pm), the Si-C bond length (183.9 to 185.0 pm; average 184.5 pm), the Si-O-Si bond angle (145.0 to 153.8°; average 149.4°) and the O-Si-O bond angle (107.0 to 109.6°; average 108.3°) are very close to the values known in the literature for similar compounds such as octaphenylsilsesquioxane¹⁵⁹ or styryl functionalized silsesquioxane¹⁴⁹ and only bit more fluorine differ а from octaphenylsilsesquioxane480 which can be attributed to the fluorine within the cage (Table 12). In addition, the O-Si-O bond angle matches almost exactly a tetrahedral angle suggesting that the sterically more demanding 1-napthyl group has no major influence on these values. Furthermore, each unit cell contains a total of two cages, which do not show any π - π interactions. There are two non-equivalent cages in the lattice in which two opposing naphthyl groups differ in their orientation (Figure 38, b). This has already been observed in styrene functionalized silsesquioxanes and was attributed to the fact that these were formed to enable optimal packing in the solid state.¹⁴⁹ Furthermore, two dichloromethane molecules from the solvent used to crystallize the cage can be seen.

Table 12: Characteristic bond distances and angles for 1-naphthyl functionalized T_8 POSS, as well as phenyl functionalized T_8 silsesquioxane with and without fluorine and styryl functionalized T_8 silsesquioxane as comparison.

	1-Naph-T ₈	Ph-T ₈ ¹⁵⁹	Ph-T ₈ fluoride ⁴⁸⁰	Styryl-T ₈ ¹⁴⁹
Bond lengths [pm]				
Si-O (min)	161.0	160.6	162.1	160.3
Si-O (max)	162.1	161.8	162.8	163.1
Si-O (average)	161.6	161.2	162.5	161.7
Si-C (min)	183.9	182.8		182.7
Si-C (max)	185.0	183.9		185.2
Si-C (average)	184.5	183.4		184.1
Bond angles [°]				
Si-O-Si (min)	145.0	144.7	139.1	138.6
Si-O-Si (max)	153.8	151.6	143.4	161.5
Si-O-Si (average)	149.4	148.2	141.2	149.1
O-Si-O (min)	107.0	108.0	112.4	107.5
O-Si-O (max)	109.6	109.9	113.6	110.2
O-Si-O (average)	108.3	109.0	113.0	109.1



 $\label{eq:Figure 38:} \textbf{Figure 38:} Single X-ray structure of 1-Naph_POSS_KOH. a) single T_8 cube, b) single T_8 cube in order to highlight the two differently oriented naphthyl groups and c) unit cell .$

3.3.3.7 Further Purification and Separation Attempts

Having shown that only 1-Naph_POSS_KOH was successfully synthesized in pure form, further efforts towards obtaining pure POSS systems were made. We tested several washing procedures to purify the crude products as well as column chromatography, which is a known method to separate larger cages from smaller ones. All separation efforts were tested with 9-Phen_POSS_KOH and 9-Phen_POSS_TBAF as a model system. Both showed broad Si-O-Si signals in the IR spectra and impurities in the NMR spectra.

The attempted purification by washing was done with 9-Phen_POSS_KOH, using ethanol and acetone and characterized by FTIR (**Figure 39**). As already mentioned, POSS systems show only one narrow peak at around 1100 cm⁻¹. Therefore, the changes to this band were observed during the washing procedure. Washing with acetone only removes a few byproducts as the shoulder in the absorption band at 1084 cm⁻¹ gets smaller, while additional washing with ethanol does not seem to lead to further improvements.

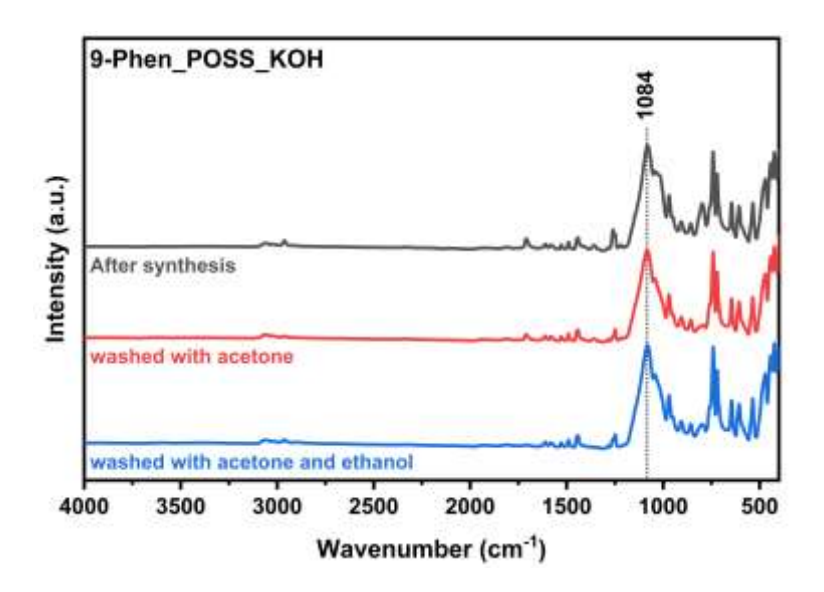


Figure 39: FTIR measurements of 9-Phen_POSS_KOH. After synthesis (black), washed with acetone (red) and washed additionally with ethanol (blue).

All substrates synthesized using TBAF showed signals in the ²⁹Si NMR, which could result from a variety of very highly condensed species in addition to the desired cages. Therefore, 9-Phen_POSS_TBAF was used for column chromatography hoping that any of those structures would remain on the silica due to their hydroxy groups. To investigate the suitability of column chromatography for purification, a thin layer chromatography

was carried out using pure DCM as eluent, showing one spot which did not move at all and one spot moving with the solvent front. Hence, a column chromatography using pure DCM was done and characterized by NMR (**Figure S 144**). It can be seen from the ¹H and ¹³C NMR that some byproducts were successfully removed in that almost all aliphatic signals disappeared. The silicon NMR on the other hand shows the same number of signals as before the column chromatography with only slight variations in their intensity, which means that no silicon compounds were removed. This leads to the conclusion that either other purification and separation steps are needed to remove everything besides the desired cages or that only cages are left. As already mentioned in the beginning further separation could possibly be achieved by dissolving the substrate and slowly precipitating it again, followed by evaporation of the resulting supernatant and purification by column chromatography using a gradient.²³¹ However, as this method requires a lot of time and experience, it could unfortunately not be carried out in the remaining time available.

3.3.3.8 Further Characterization of 1-Naph_POSS_KOH

Since the previously described purification attempts did not lead to pure substrates further characterization was carried out only with 1-Naph_POSS_KOH.

Even though we saw no excimer formation for any of the used trialkoxysilanes, we decided to also investigate the fluorescence properties of 1-Naph_POSS_KOH using a dilution series in dichloromethane (**Figure 40** and **Figure S 145**). Since the excitation wavelength for the monomer was 290 nm it was kept for the POSS system. It can clearly be seen that the diluted POSS system shows the exact same fluorescence behavior as its diluted monomer 1-NaphSi(OMe)₃ in that only the fluorescence of the naphthyl groups can be seen at high concentrations. This peak also shifts to lower wavelengths and becomes sharper and more detailed with further dilution. Furthermore, no excimer formation can be observed which would be indicated by a broad peak at around 400 nm as we observed in our previous work.³⁸³ In contrast to its undiluted monomer 1-NaphSi(OMe)₃, the undiluted POSS system shows no excimer fluorescence, which suggests that there is no overlap of the naphthyl groups.⁴⁶⁵

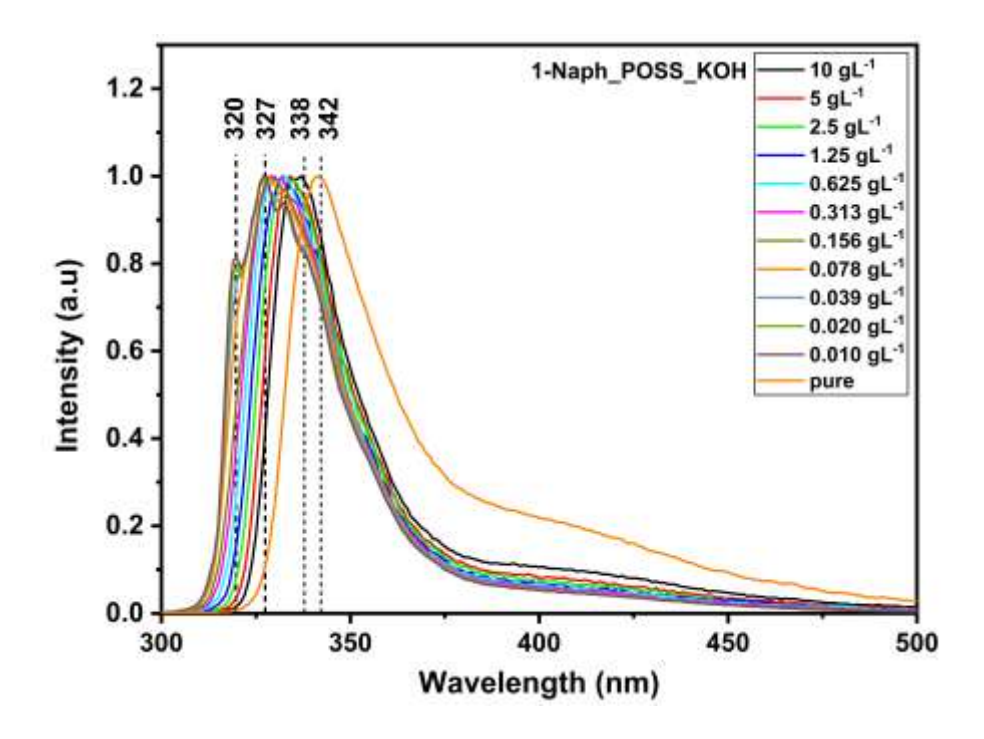


Figure 40: Fluorescence spectra of a dilution series of 1-Naph_POSS_KOH in DCM with λ_{ex} = 290 nm.

Furthermore, we also investigated the absorption properties of 1-Naph_POSS_KOH (**Figure 41**). It can be seen that its absorption spectrum looks exactly like 1-NaphSi(OMe)₃ with its maximum at 284 nm which is due to the naphthyl group.

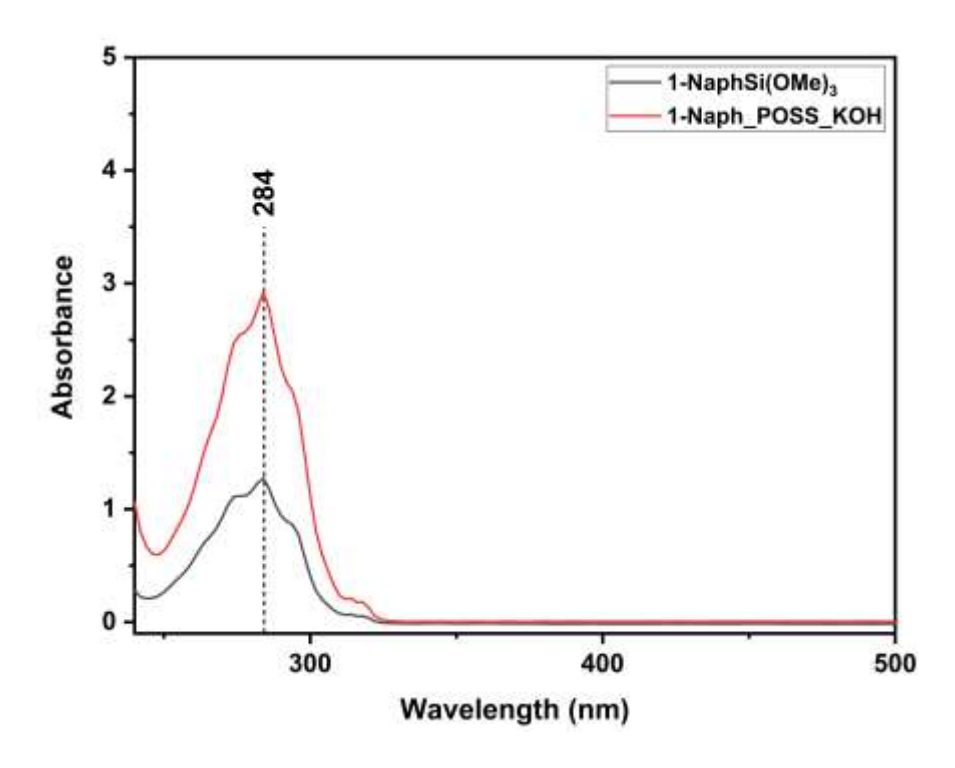


Figure 41: UV-vis spectrum of 1-Naph_POSS_KOH (red) and 1-NaphSi(OMe)₃ (black) as comparison.

Thermogravimetric analysis (TGA) was performed to analyze the thermal stability as well as the decomposition behavior of 1-Naph_POSS_KOH. Therefore, the sample was heated up to 900 °C under air (Figure 42, a and Table 13). It can be seen that the sample has a high thermal stability (Tonset of 453.6 °C) which is very close to that of polyhedral oligomeric octaphenylsilsesquioxane (OPS) which is at 465 °C.481 1-Naph_POSS_KOH also shows three mass losses at 483.9 °C, 572.2 °C and 649.7 °C with mass losses of 17.0 %, 19.6 % and 29.5 %, respectively. In comparison, Zhang et al. observed an onset temperature of 474.0 °C and three mass losses at 519.5 °C, 581.6 °C and 628.1 °C with mass losses of 61.6 %, 6.5 % and 15.7 %, respectively for OPS. According to their research the first mass loss occurs due to sublimation, the second one due to sublimation, detachment of phenyl groups and destruction of caged structures, while the third mass loss is due to the oxidation of the residual organic part into carbon monoxide and carbon dioxide. 482 As the present DSC measurement was only carried out up to 400 °C, sublimation can unfortunately not be checked. The temperatures for the three mass losses are close to those observed in our system, except for the first step, which could be due to the presence of naphthyl instead of phenyl groups.

Looking at the masses of the individual decomposition steps compared to OPS, differences become clear. While the highest mass loss in OPS occurs in the first stage through sublimation, 1-Naph_POSS_KOH shows the highest mass loss in the third stage, which is the oxidation of the organic groups into carbon monoxide and carbon dioxide. The sterically demanding naphthyl groups could make sublimation in the first stage much more difficult, but due to their significantly higher molecular weight they lead to a higher mass loss during decomposition. Closer analysis is not possible due to the proximity of the individual decomposition stages to each other. DSC measurements which were performed under a nitrogen/oxygen-flow (40/60 mL min⁻¹) applying a heating rate of 10 K min⁻¹ revealed a melting point of 1-Naph_POSS_KOH of 311 °C (**Figure 42, b**).

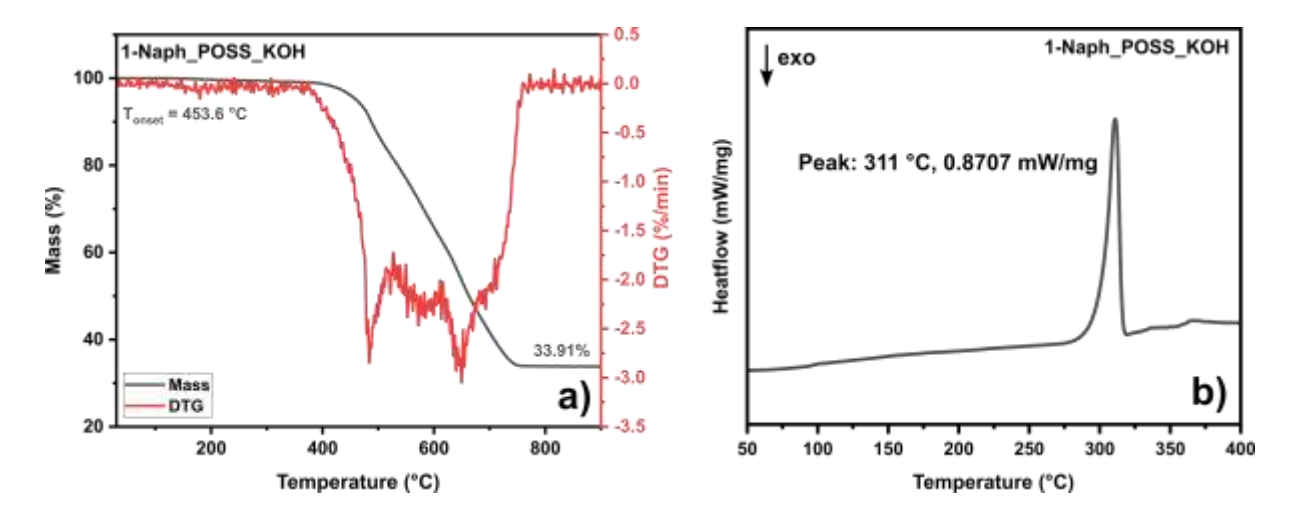


Figure 42: a) TGA measurement of 1-Naph_POSS_KOH under air, mass loss (black) and DTG (red), b) DSC measurement of 1-Naph_POSS_KOH under air.

Table 13: TGA data of 1-Naph_POSS_KOH under air. T_{max}: Temperature at maximum mass loss rate.

Tonset	T _{max1}	T _{max2}	T _{max3}	1 st mass loss	2 nd mass loss	3 rd mass loss
/°C	/°C	/°C	/°C	/%	/%	/%
453.6	483.9	572.2	649.7	17.0	19.6	29.5

3.3.4 Experimental Section

3.3.4.1 Materials

All trimethoxysilane syntheses were carried out under inert atmosphere. Magnesium chips (99.9+%, Acros Organics), 1-bromonaphthalene (97%, abcr GmbH), 2-bromonaphthalene (98%, BLD Pharmatech Ltd), 9-bromophenantherene (99.83%, BLD Pharmatech Ltd), tetramethoxysilane (98%, abcr GmbH) and n-hexane (for synthesis, BCD Chemie GmbH) were used without further purification. THF (99.8% HPLC grade, Fisher Chemical) was purified in a MBraun SPS-5 solvent purification system (M. Braun Inertgas-Systeme GmbH, Garching, Germany). For POSS synthesis acetone (97%, BCD Chemie GmbH), KOH (Fisher Chemical), anhydrous ethanol (99.5%, Thermo Fisher Scientific), DCM (99%, Fisher Scientific) and TBAF (1M in THF, TCI chemicals) were used without further purification. For column chromatography DCM (99%, Fischer Scientific) and silica gel 60 (particle size 0.063 – 0.200 nm (70 – 230 mesh ASTM), Merck) were used.

3.3.4.2 Instrumentation and Characterization Methods

NMR spectra in solution were carried out on an Avance III HD 400 MHz spectrometer (Bruker Corporation, Billerica, USA) with 400.13 MHz for ¹H NMR spectra, 100.62 MHz for ¹³C NMR spectra and 79.49 MHz for ²⁹Si NMR spectra. All NMR trialkoxysilane samples were prepared in chloroform-d (CDCl₃) and all POSS samples were prepared in CD₂Cl₂. All spectra were plotted in MestReNova (v14.2.0-26256, Mestrelab Research, Santiago de Compostela SPAIN).

Fourier transform infrared (FTIR) spectra were recorded in attenuated total reflectance mode (ATR) on a Vertex 70 spectrometer (Bruker Optics, Ettlingen, Germany) from 4500-400 cm⁻¹ for the trialkoxysilanes but only shown from 3500-400 cm⁻¹ due to the absence of other signals at higher wavenumbers and for the POSS systems from 4000-400 cm⁻¹, each with a resolution of 4 cm⁻¹ and 16 scans.

Elemental analysis was performed on a Vario Micro cube (Elementar Analysensysteme GmbH, Langenselbold, Germany).

UV-vis absorption measurements of the trialkoxysilanes were performed in a quartz glass cuvette with 1 cm thickness, diluted in dichloromethane from 236 to 800 nm in 2 nm steps, but only presented from 236 to 500 nm due to the absence of other signals at high wavelengths. 1-Naph_POSS_KOH was measured with the same setup from 200 to 800 nm but only presented from 240 to 500 nm due to strong absorption at low wavelengths and the absence of other signals at high wavelengths. All UV-vis measurements were performed on a Lambda 750 instrument (Perkin Elmer Inc., Shelton, USA) equipped with a 100 mm integration sphere with 2 nm increments and 0.2 s integration time.

Fluorescence measurements of all samples were performed in a quartz glass cuvette with 1 cm thickness, diluted in dichloromethane or in pure form in a quartz glass tube with a diameter of 2 mm on a FluoroMax 4 spectrofluorometer (Horiba Scientific, Kyoto, Japan). The excitation wavelength for the emission spectra of 1-NaphSi(OMe)₃ and 2-NaphSi(OMe)₃ were 290 nm, while 9-PhenSi(OMe)₃ was measured at 340 nm. Excitation spectra of the trimethoxysilanes were recorded in the same manner with emission wavelengths of 350, 340 and 370 nm for 1-NaphSi(OMe)₃, 2-NaphSi(OMe)₃ and 9-PhenSi(OMe)₃, respectively. The emission and excitation spectra of 1-Naph_POSS KOH

were measured with the same setup at an excitation wavelength of 290 nm and an emission wavelength of 350 nm.

Thermogravimetric Analysis (TGA) was performed on a TG F1 Iris (Netzsch-Gerätebau GmbH, Selb, Germany) under a constant flow of N_2 (16 mL min⁻¹) and O_2 (4 mL min⁻¹) as purge gas and N_2 (20 mL min⁻¹) as protective gas with a heating rate of 10 K min⁻¹ from 25 °C to 900 °C. During the measurements, the samples were placed in an open alumina crucible.

Differential scanning calorimetry (DSC) was performed with a DSC 204 *F1 Phoenix* calorimeter (NETZSCH-Gerätebau GmbH, Selb, Germany) using aluminum crucibles with pierced lids under nitrogen/oxygen-flow (40/60 mL min⁻¹) applying a heating rate of 10 K min⁻¹ and a cooling rate of 15 K min⁻¹ in a temperature range between 50 to 400 °C for 1-Naph_POSS_KOH and in a temperature range from 40 to 150 °C for 9-PhenSi(OMe)₃. The value of the melting point was taken by determining the peak maximum.

MALDI-FTICR measurements were carried out on a 4800 Plus MALDI tandem TOF (AB Sciex, Darmstadt, Germany) in linear mode with a neodym YAG laser (353 nm) and analyzed with Data Explorer Software (4000 Series Explorer) and DCTB/Ag triflate was used as a matrix.

Size exclusion chromatography (SEC) was performed with a PSS SECcurity2 system composed of a 1260 IsoPump-G7110B (Agilent Technologies, Santa Clara, CA, USA) and a 1260 VW-detector G7162A at 270 nm (Agilent Technologies) at 25 °C, with THF as the mobile phase (flow rate 1 mL min⁻¹) on an SDV column set (SDV 10³, SDV 10⁵, SDV 10⁶) from PSS (Polymer Standard Service, Mainz, Germany). Calibration was carried out using PS standards (from PSS).

For X-ray crystallography the data set was collected using a Bruker D8 Venture diffractometer with a microfocus sealed tube and a Photon II detector. Monochromated Mo_{Kα} radiation (λ = 71.073 pm) was used. Data were collected at 133(2) K and corrected for absorption effects using the multi-scan method. The structure was solved by direct methods using SHELXT⁴⁸³ and was refined by full matrix least squares calculations on F² (SHELXL2018⁴⁸⁴) in the graphical user interface Shelxle⁴⁸⁵. All non H-atoms were located in the electron density maps and refined anisotropically. C-bound H atoms were placed

in positions of optimized geometry and treated as riding atoms. Their isotropic displacement parameters were coupled to the corresponding carrier atoms by a factor of 1.2 (CH, CH₂). During the structure refinement, disorder of one of the eight naphthalene groups (C62A-C70A, C62B-C70B) and of one of the two dichloromethane solvent molecules were split over two positions. Their occupancy factors refined to 0.50(1) and 0.78(1), respectively.

Refractive indices of the trialkoxysilanes were measured as a dilution series (for further information see results and discussion part) on an Abbemat 350 (Anton-Paar OptoTec GmbH, Seelze-Letter, Germany) at a wavelength of 589 nm and 20 °C. The refractive index of 1-Naph_POSS_KOH could not be determined since it was insoluble.

Column chromatography was done with a mixture of silica gel and DCM as stationary phase and DCM as mobile phase/eluent.

3.3.4.3 Syntheses of Trimethoxysilanes

The corresponding trimethoxysilanes were prepared in a similar way as the dialkoxysilanes in our previous studies^{74,383} which was derived from literature.^{70,382}

Trimethoxy-(1-naphthyl)silane (1-NaphSi(OMe)₃)

To a 1000 mL three-necked round bottom flask equipped with a reflux condenser, a dropping funnel and a gas inlet which was flame-dried under vacuum and back-filled with argon 7.37 g magnesium chips (303.2 mmol, 1.5 equiv.), 90 mL tetramethoxysilane (604.5 mmol, 3 eq) and 270 mL abs THF were added and heated to 45 °C. 43.36 g 1-bromonaphthalene (209.4 mmol, 1 eq) was diluted with 60 mL abs THF in the dropping funnel, added dropwise over a period of 30 minutes and stirred at 60 °C for 2 h. The solution was then stirred overnight and allowed to cool to room temperature.

After the solvent was removed 260 mL n-hexane were added to the residue, refluxed for 10 minutes, and decanted while still hot. 130 mL n-hexane were added to the remaining residue, refluxed for 10 minutes, and filtered while hot. The combined organic solvents and tetramethoxysilane were removed in high vacuum. The crude product was distilled $(1.2 \times 10^{-2} \text{ mbar}, 120 \, ^{\circ}\text{C})$ to yield 31.9 g (61 %) of a colorless liquid.

¹**H NMR:** (400.13 MHz, CDCl₃) δ 8.36-8.30 (naphthyl, d, J = 8.3 Hz, 1H), 8.03-7.95 (naphthyl, dd, J = 14.4, 7.5 Hz, 2H), 7.91-7.86 (naphthyl, d, J = 8.1 Hz, 1H), 7.61-7.55 (naphthyl, m, 1H), 7.55-7.49 (naphthyl, t, J = 7.4 Hz, 2H), 3.70 (OCH₃, s, 9H) ppm.

²⁹**Si NMR** (79.49 MHz, CDCl₃) δ -52.67 ppm.

¹³**C NMR** (100.62 MHz, CDCl₃) δ 137.04, 136.20, 133.31, 131.39, 128.72, 128.28, 127.69, 126.61, 125.74, 125.00, 50.76 ppm.

CHN: calc. C: 62.87 %, H: 6.49 %; found C: 62.70 %, H: 5.53 %

Trimethoxy-(2-naphthyl)silane (2-NaphSi(OMe)₃)

To a 1000 mL three-necked round bottom flask equipped with a reflux condenser, a dropping funnel and a gas inlet which was flame-dried under vacuum and back-filled with argon 7.38 g magnesium chips (303.5 mmol, 1.5 equiv.), 90 mL tetramethoxysilane (604.8 mmol, 3 eq) and 270 mL abs THF were added and heated to 45 °C. 41.81 g 2-bromonapthalene (201.9 mmol, 1 eq) was dissolved with 70 mL abs THF in the dropping funnel, added dropwise over a period of 30 minutes and stirred at 60 °C for 2 h. The solution was then stirred overnight and allowed to cool to room temperature.

After the solvent was removed 260 mL n-hexane were added to the residue, refluxed for 10 minutes, and decanted while still hot. 130 mL n-hexane were added to the remaining residue, refluxed for 10 minutes, and filtered while hot. The combined organic solvents and tetramethoxysilane were removed in high vacuum. The precipitated crude product was distilled $(1.0 \times 10^{-2} \text{ mbar}, 150 \, ^{\circ}\text{C})$ to yield 31.4 g (63 %) of a colourless liquid.

¹**H NMR:** (400.13 MHz, CDCl₃) δ 8.39-8.32 (naphthyl, d, J = 1.0 Hz, 1H), 8.02-7.94 (naphthyl, m, 2H), 7.94-7.89 (naphthyl, dd, J = 8.1, 1.8 Hz, 1H), 7.85-7.79 (naphthyl, dd, J = 8.1, 1.1 Hz, 1H), 7.63-7.53 (naphthyl, m, 2H), 3.76 (OCH₃, s, 9H) ppm.

²⁹**Si NMR** (79.49 MHz, CDCl₃) δ -54.11 ppm.

¹³**C NMR** (100.62 MHz, CDCl₃) δ 136.38, 134.52, 132.83, 130.14, 128.38, 127.74, 127.38, 126.99, 126.83, 126.05, 50.84 ppm.

CHN: calc. C: 62.87 %, H: 6.49 %; found C: 63.28 %, H: 5.88 %

Trimethoxy-(9-phenanthrenyl)silane (9-PhenSi(OMe)₃)

To a 1000 mL three-necked round bottom flask equipped with a reflux condenser, a dropping funnel and a gas inlet which was flame-dried under vacuum and back-filled with argon 6.28 g magnesium chips (258.4 mmol, 1.5 eq), 75 mL tetramethoxysilane (504.0 mmol, 3 eq) and 200 mL abs THF was added and heated to 45 °C. 42.92 g 9-bromophenanthrene (166.9 mmol, 1 eq) was dissolved with 70 mL abs THF in the dropping funnel, added dropwise over a period of 30 minutes and stirred at 60 °C for 2 h. The solution was then stirred overnight and allowed to cool to room temperature.

After the solvent was removed 220 mL n-hexane were added to the residue, refluxed for 10 minutes, and decanted while still hot. 110 mL n-hexane were added to the remaining residue, refluxed for 10 minutes, and filtered while hot. The combined organic solvents and tetramethoxysilane were removed in high vacuum. The crude product was washed with hot methanol and filtered to gain a yield of 15.6 g (31 %) of a white powder.

¹**H NMR:** (400.13 MHz, CDCl₃) δ 8.77-8.68 (phenanthrenyl, m, 2H), 8.39-8.34 (phenanthrenyl, m, 1H), 8.31 (phenanthrenyl, s, 1H), 8.00-7.94 (phenanthrenyl, dd, J = 7.9, 1.4 Hz, 1H), 7.75-7.60 (phenanthrenyl, m, 4H), 3.72 (OCH₃, s, 9H) ppm.

²⁹**Si NMR** (79.49 MHz, CDCl₃) δ -52.71 ppm.

¹³**C NMR** (100.62 MHz, CDCl₃) δ 139.16, 134.52, 131.79, 130.95, 130.13, 129.40, 129.11, 128.03, 127.13, 126.78, 126.57, 126.54, 123.07, 122.62, 50.98 ppm.

CHN: calc. C: 68.42 %, H: 6.08 %; found C: 67.73 %, H: 5.45 %

3.3.4.4 Syntheses of POSS Systems using KOH

All syntheses were done according to literature procedure. 232

1-Naph_POSS_KOH

In a 50 mL round-bottom flask equipped with a reflux condenser and a magnetic stirrer trimethoxy-(1-naphthyl)silane (5.02 g, 20.21 mmol) and acetone (25 mL) were charged and stirred for 30 min. Afterwards, deionized water (1 mL) and KOH (0.04 g) were added. Then the mixture was refluxed for 24 h. The crude product was filtered and washed with

anhydrous ethanol to remove any unreacted substances followed by drying in a vacuum oven at 120 °C for 8 h to yield 1.95 g (54 %) of 1-Naph-POSS_KOH as a white powder.

¹**H NMR:** (400.13 MHz, CD₂Cl₂) δ 8.69-8.62 (naphthyl, d, J = 8.5 Hz, 1H), 7.96-7.90 (naphthyl, dd, J = 6.8, 1.2 Hz, 1H), 7.90-7.85 (naphthyl, d, J = 8.4 Hz, 1H), 7.85-7.79 (naphthyl, d, J = 8.4 Hz, 1H), 7.49-7.41 (naphthyl, ddt, J = 8.1, 6.8, 1.3 Hz, 1H), 7.41-7.34 (naphthyl, tt, J = 7.0, 1.4 Hz, 1H), 7.23-7.15 (naphthyl, ddd, J = 8.1, 6.8, 1.1 Hz, 1H) ppm.

²⁹**Si NMR** (79.49 MHz, CD_2Cl_2) δ -77.26 ppm.

¹³**C NMR** (100.62 MHz, CD₂Cl₂) δ 136.34, 135.85, 133.36, 131.81, 128.87, 128.38, 127.86, 126.77, 125.91, 124.89 ppm.

CHN: calc. C: 67.01 %, H: 3.94 %; found C: 65.80 %, H: 4.01 %

2-Naph_POSS_KOH

In a 50 mL round-bottom flask equipped with a reflux condenser and a magnetic stirrer trimethoxy-(2-naphthyl)silane (5.00 g, 20.13 mmol) and acetone (25 mL) were charged and stirred for 30 min. Afterwards, deionized water (1 mL) and KOH (0.04 g) were added. Then the mixture was refluxed for 24 h. The crude product was filtered and washed with anhydrous ethanol to remove any unreacted substances followed by drying in a vacuum oven at 120 °C for 8 h to yield 1.49 g (41 %) of crude product as a white powder.

¹**H NMR:** (400.13 MHz, CD_2Cl_2) δ 9.16-7.73 (naphthyl, m, 3H), 7.71-6.06 (naphthyl, m, 4H) ppm.

²⁹**Si NMR** (79.49 MHz, CD_2Cl_2) δ -79.14, -78.36, -77.76, -75.87 ppm.

¹³**C NMR** (100.62 MHz, CD₂Cl₂) δ 138.52, 133.72, 131.33, 130.44, 128.97, 128.01, 125.88, 123.21, 122.02 ppm.

9-Phen_POSS_KOH

In a 50 mL round-bottom flask equipped with a reflux condenser and a magnetic stirrer trimethoxy-(9-phenanthrenyl)silane (5.02 g. 16.82 mmol) and acetone (20 mL) were charged and stirred for 30 min. Afterwards, deionized water (0.84 mL) and KOH (0.03 g) were added, and the mixture was refluxed for 24 h. The crude product was filtered, washed with anhydrous ethanol to remove any unreacted substances followed by drying in a vacuum oven at 120 °C for 8 h to yield 1.90 g (49 %) of crude product as a white powder.

¹**H NMR:** (400.13 MHz, CD_2Cl_2) δ 9.13-7.80 (phenanthrenyl, m, 4H), 7.70-6.84 (phenanthrenyl, m, 4H), 6.79-6.25 (phenanthrenyl, m, 1H) ppm.

²⁹**Si NMR** (79.49 MHz, CD_2Cl_2) δ -79.43, -79.13, -78.35, -77.90, -77.75, -76.72, -75.87 ppm.

¹³**C NMR** (100.62 MHz, CD₂Cl₂) δ 139.21, 134.00, 131.80, 130.57, 129.46, 127.69, 126.64, 122.90 ppm.

3.3.4.5 Syntheses of POSS Systems using TBAF

All syntheses were done according to literature, while the purification was changed. 161

1-Naph_POSS_TBAF

In a 500 mL round-bottom flask trimethoxy-(1-naphthyl)silane (3.01 g, 12.12 mmol), DCM (276 mL) and TBAF (6.9 mL, 1 M in THF, 6.9 mmol) were added and stirred for 24 h at room temperature. The reaction mixture was evaporated to 1/3 of its volume using a rotary evaporator. Afterwards the crude product was precipitated in an ice bath using EtOH, filtered, washed with cold EtOH, and dried under vacuum to afford 0.68 g (31 %) of crude product as a white powder.

¹**H NMR:** (400.13 MHz, CD_2Cl_2) δ 8.82-7.59 (naphthyl, m, 4H), 7.56-6.55 (naphthyl, m, 3H) ppm.

²⁹**Si NMR** (79.49 MHz, CD₂Cl₂) δ -78.69, -78.04, -77.87, -77.20, -76.17, -69.37 ppm.

¹³**C NMR** (100.62 MHz, CD₂Cl₂) δ 136.27, 135.79, 133.29, 131.75, 128.80, 128.31, 127.79, 126.70, 125.84, 124.81 ppm.

2-Naph_POSS_TBAF

In a 500 mL round-bottom flask trimethoxy-(2-naphthyl)silane (3.03 g, 12.21 mmol), DCM (276 mL) and TBAF (6.9 mL, 1 M in THF, 6.9 mmol) were added and stirred for 24 h at room temperature. The reaction mixture was evaporated to 1/3 of its volume using a rotary evaporator. Afterwards the crude product was precipitated in an ice bath using EtOH, filtered, washed with cold EtOH, and dried under vacuum to afford 0.80 g (37 %) of crude product as a white powder.

¹**H NMR:** (400.13 MHz, CD₂Cl₂) δ 8.37-5.94 (naphthyl, m, 7H) ppm.

²⁹**Si NMR** (79.49 MHz, CD₂Cl₂) δ -80.98, -78.94, -78.83 ppm.

¹³**C NMR** (100.62 MHz, CD₂Cl₂) δ 136.14, 134.67, 132.92, 129.94, 128.50, 127.73, 126.35 ppm.

9-Phen_POSS_TBAF

In a 500 mL round-bottom flask trimethoxy-(9-phenanthrenyl)silane (2.49 g, 8.35 mmol), DCM (191 mL) and TBAF (4.8 mL, 1 M in THF, 4.8 mmol) were added and stirred for 24 h at room temperature. The reaction mixture was evaporated to 1/3 of its volume using a rotary evaporator. Afterwards the crude product was precipitated in an ice bath using EtOH, filtered, washed with cold EtOH, and dried under vacuum to afford 0.61 g (32 %) of crude product as a white powder.

 1 H NMR: (400.13 MHz, CD₂Cl₂) δ 9.12-7.90 (phenanthrenyl, m, 4H), 7.79-6.49 (phenanthrenyl, m, 5H) ppm.

²⁹Si NMR (79.49 MHz, CD₂Cl₂) δ -78.54, -77.93, -77.66, -75.88, -69.07 ppm.

¹³**C NMR** (100.62 MHz, CD₂Cl₂) δ 138.87, 134.09, 132.01, 130.83, 130.72, 129.58, 127.02, 126.81 122.74 ppm.

3.3.4.6 Further Purification Attempts

The first purification was attempted by washing 9-Phen_POSS_KOH. Therefore, the substrate was first washed with acetone and afterwards washed with ethanol.

The second purification was done by column chromatography. 1 g of 9-Phen_POSS_TBAF was dissolved in as little dichloromethane as possible, put on the column which was filled with a mixture of silica gel and DCM and washed from the column using pure dichloromethane as eluent/mobile phase. The product was then precipitated with ethanol, filtered and dried to yield 0.62 g (62 %) of a white powder.

3.3.5 Conclusions

Three trimethoxysilanes containing 1-naphthyl, 2-naphthyl and 9-phenanthrenyl groups have been successfully synthesized using a Barbier-type reaction. NMR and IR spectroscopy, as well as elemental analysis confirmed the molecular structures while UV-vis measurements showed the expected absorptions. Fluorescence spectroscopy revealed no excimer formation for any of the three diluted trimethoxysilanes but for all three pure samples while refractive index measurements showed high refractive indices of up to 1.615 for 9-PhenSi(OMe)₃. Furthermore, POSS systems were produced from all three trimethoxysilanes using either KOH or TBAF leading to a total of six samples. While all samples show cages in the MALDI-FTICR measurements ranging from T_8 to T_{14} only 1-Naph_POSS_KOH could be synthesized as a pure compound according to NMR studies. This successful synthesis was further proven by single crystal X-ray crystallography and thus further characterized. While fluorescence spectroscopy showed no excimer formation, DSC measurements displayed a melting point of 311 °C and thermogravimetric analysis showed an onset temperature of 453.6 °C and also revealed three decomposition steps.

Acknowledgments

The authors thank Blandine Boßmann for recording and analyzing the size exclusion chromatograms, Dr. Mathilde Laird for the MALDI-FTICR measurements, Dr. Michael Zimmer for the NMR measurements and Susanne Harling for the elemental analysis. Instrumentation and technical assistance for this work were provided by the Service Center X-ray Diffraction, with financial support from Saarland University and German Science Foundation (project number INST 256/506-1).

4 Conclusions and Outlook

In this thesis, di- and trialkoxysilanes have been synthesized containing naphthyl and phenanthrenyl groups using a Grignard reaction, as well as a Barbier-type reaction. The dialkoxysilanes were then condensed into high refractive index siloxanes using an acid catalyzed condensation reaction. These novel siloxane oligomers were then investigated for their structural, thermal, optical and rheological properties, as well as their refractive indices. Additionally, the corresponding trialkoxysilanes were studied towards their potential to form polyhedral oligomeric silsesquioxanes (POSS) using two different literature known methods. The research objectives are described in more detail below and the corresponding observations are drawn.

In the first chapter three high refractive index dialkoxysilanes were synthesized as monomers containing 1-naphthyl, 2-naphthyl and 9-phenanthrenyl groups using a Grignard reaction. Their characterization with liquid NMR, UV-vis and IR spectroscopy, as well as elemental analysis confirmed their molecular structure. Additionally, fluorescence spectroscopy of the molecules showed excimer formation for the 1- and 2-naphthyl groups and refractive index measurements revealed high refractive indices up to 1.671 for the 9-phenanthrenyl group. Afterwards, these dialkoxysilanes were condensed together with either dimethyldimethoxysilane or diphenyldimethoxysilane, as well as phenyltrimethoxysilane in an acid catalyzed hydrolysis and condensation reaction to produce oligosiloxanes containing naphthyl or phenanthrenyl, phenyl and methyl groups. Various characterization methods were used to study the properties of the obtained polymeric samples as well as to gain more insight into the condensation reaction itself. CP-MAS NMR spectroscopy has shown that the incorporation of the polycyclic dialkoxysilanes during consolidation decreases from 2-naphthyl to 1-naphthyl to 9-phenanthrenyl, which can be attributed to their steric hindrance and constitutional isomerism. FTIR spectroscopy also revealed that only hydrogen-bonded hydroxy groups in the condensed polymeric samples will form covalent bonds during the consolidation process and therefore contributing to the siloxane network, while isolated hydroxy groups will not react any further. Furthermore, it was observed that the constitutional isomerism between 1-naphthyl and 2-naphthyl influences nearly all characteristics of the samples like thermal stability, glass transition temperature and excimer formation but only slightly the refractive index. Overall, it was possible to prepare oligosiloxanes with polycyclic aromatic groups that show high thermal stabilities, high transparencies, and very high refractive indices of up to 1.610 making them promising materials for optoelectronic applications. The only downside was a slight yellowing of the samples upon prolonged times at 200 °C, as well as the fact that they did not achieve a sufficiently high degree of cross-linking during consolidation and therefore liquefy at high temperatures, limiting them to low temperature applications.

The aim of the second chapter was to increase the degree of cross-linking of the systems obtained in the first chapter to such an extent that the samples remain solid even at high temperatures in order to make them interesting for high-temperature applications. Our initial thesis was that the samples liquefied at high temperatures due to an insufficient cross-linking caused by the sterically demanding polycyclic aromatic groups. Therefore, we post-cross-linked the most promising sample from our first study, which contained 1-naphthyl groups, with dimethyldimethoxysilane, diphenyldimethoxysilane, phenyltrimethoxysilane and dibutyltin diacetate to achieve a sufficient degree of cross-linking. To ensure that it is not the increased cross-linking density due to the addition of phenyltrimethoxysilane, but the post-cross-linking that is responsible for the sample remaining stable at high temperatures, another sample with the same cross-linking density prepared without post-cross-linking. was directly diphenyldimethoxysilane or phenyltrimethoxysilane to the already existing 1-naphthyl containing oligosiloxane resulted in two samples that still soften a little but do not turn liquid anymore at 200 °C while keeping their thermal stability and high transparency. The improved elastic properties at high temperatures were shown by dynamic mechanical analysis and thermal treatment in an oven. Additional characterization methods were used to gain more insight into the relationship between the properties of the samples and their structure. Solid state NMR revealed a much better incorporation of the sterically demanding naphthyl monomer into the siloxane network, which is the main reason for the significantly improved rheological behavior at high temperatures. In addition to NMR spectroscopy, both FTIR spectroscopy and PXRD measurements have shown that high cross-link density and aromatic groups play an important role for structural regularity, which is also a reason for the improved elasticity and increased viscosity at high temperatures and was not the case for the sample produced without post-cross-linking.

It can therefore be stated that it was possible to produce siloxanes that soften only slightly at high temperatures while keeping their elasticity. Furthermore, they form significantly fewer cracks after consolidation, while properties such as high thermal stability and high transparency were retained.

In the last chapter an attempt was made to prepare T₈ POSS systems containing 1-naphthyl, 2-naphthyl and 9-phenanthrenyl groups at all corners. For this purpose, trialkoxysilanes with the corresponding groups were first prepared using a Barbier-type reaction and their structure was investigated by NMR and IR spectroscopy, as well as elemental analysis. Contrary to the dialkoxysilanes from the first chapter fluorescence spectroscopy revealed that the trialkoxysilanes only showed excimer formation in their pure form, but not diluted, while also displaying refractive indices up to 1.615 for trimethoxy-(9-phenanthrenyl)silane. From these trialkoxysilanes POSS systems were prepared by using either potassium hydroxide (KOH) or tetrabutylammonium fluoride (TBAF). By reacting trimethoxy-(1-naphthyl)silane with KOH the corresponding T₈ cage was successfully synthesized and confirmed by NMR and IR spectroscopy, as well as single crystal X-ray crystallography. This POSS system was further characterized and showed no excimer formation, an onset temperature of 453.6 °C and a melting point of 311 °C. According to MALDI-FTICR measurements all other reactions lead to cages ranging from T₈ to T₁₄ but could not be purified in the given time frame of this work.

In summary, it can be stated that in the present work oligomeric siloxanes with high thermal stability and transparency, as well as a high refractive index were successfully prepared by hydrolysis, condensation and consolidation from the corresponding and previously self-synthesized monomers. Due to their high refractive index, high thermal stability and very low softening at high temperatures, these materials can be used in a variety of optoelectronic applications such as LEDs, anti-reflective optical coatings or immersion lithography and also in materials such as contact lenses. For example, they could increase the efficiency of LEDs or ensure that contact lenses become thinner in order to make them more comfortable to wear. In the field of LEDs in particular, it is also interesting to note that the constitutional isomerism plays an important role for almost all properties of siloxanes, but only very little in terms of the refractive index, which makes it possible to adjust their properties without heavily changing the refractive index.

The realization that post-cross-linking and the timing of the addition of the individual monomers significantly changes the properties of a siloxane despite the same monomer ratios in the final polymer is of great importance. In the future, this could open up far more possibilities for adapting siloxanes to given requirements than has been the case to date. The studies shown here can also serve as a starting point for experiments to further optimize the systems shown, whether by varying the monomers, their ratio to each other or the order in which they are added.

Finally, the studies on POSS systems with polycyclic aromatic groups have shown that these can be successfully synthesized in different cage sizes using already known methods. This lays the foundation for further experiments on their synthesis, purification and the separation of different cage sizes from each other.

As a result, it can be stated that high refractive index siloxanes with high thermal stability and transparency were successfully obtained, which are suitable for high-temperature applications due to their processability and good rheological properties. In addition, successful experiments on POSS systems with polycyclic groups on every corner were carried out, laying the foundation for further studies.

5 References

- (1) Kipping, F. S. XXII.-Organic Derivatives of Silicon. Part II. The Synthesis of Benzylethylpropylsilicol, Its Sulphonation, and the Resolution of the Dl-Sulphonic Derivative into Its Optically Active Components. *J. Chem. Soc. Faraday Trans.* **1907**, 91, 209–240.
- (2) Kipping, F. S. The Bakerian Lecture Organic Derivatives of Silicon. *Proc. R. Soc. Lond. A Math. Phys. Sci.* **1937**, 159 (896), 139–148. https://doi.org/10.1098/rspa.1937.0063.
- (3) Shand, E. B.; Hyde, J. F. Fibrous Glass Textile Material For Electrical Insulation, US2209850A. **1940**.
- (4) Hyde, J. F. Glass Building Unit Joining Method, CA355761. 1936.
- (5) Rochow, E. G.; Schenectady, N. Y. Preparation of Organosilicon Halides, US2380995A. **1941**.
- (6) Müller, R. Verfahren Zur Herstellung von Kohlenstoff-Silicium-Halogenverbindungen. VEB Silikonchemie, DD Pat **1953**, 5348.
- (7) Mojsiewicz-Pienkowska, K.; Jamrógiewicz, M.; Szymkowska, K.; Krenczkowska, D. Direct Human Contact with Siloxanes (Silicones) Safety or Risk Part 1. Characteristics of Siloxanes (Silicones). *Front. Pharmacol.* **2016**, 7 (MAY), 1–8. https://doi.org/10.3389/fphar.2016.00132.
- (8) Rochow, E. G. The Chemistry of Silicones. *Sci. Am.* **1948**, *179* (4), 50–53. https://doi.org/www.jstor.org/stable/10.2307/24945903.
- (9) Tran, T. M.; Abualnaja, K. O.; Asimakopoulos, A. G.; Covaci, A.; Gevao, B.; Johnson-Restrepo, B.; Kumosani, T. A.; Malarvannan, G.; Minh, T. B.; Moon, H.-B.; others. A Survey of Cyclic and Linear Siloxanes in Indoor Dust and Their Implications for Human Exposures in Twelve Countries. *Environ. Int.* **2015**, *78*, 39–44. https://doi.org/10.1016/j.envint.2015.02.011.
- (10) Xiang, X.; Liu, N.; Xu, L.; Cai, Y. Review of Recent Findings on Occurrence and Fates of Siloxanes in Environmental Compartments. *Ecotoxicol. Environ. Saf.* **2021**, *224*, 112631. https://doi.org/10.1016/j.ecoenv.2021.112631.
- (11) Köhler, T.; Gutacker, A.; Mejía, E. Industrial Synthesis of Reactive Silicones: Reaction Mechanisms and Processes. *Org. Chem. Front.* **2020**, *7* (24), 4108–4120. https://doi.org/10.1039/D0QO01075H.
- (12) Miroshnichenko, A. S.; Neplokh, V.; Mukhin, I. S.; Islamova, R. M. Silicone Materials for Flexible Optoelectronic Devices. *Materials* **2022**, *15* (24), 8731. https://doi.org/10.3390/ma15248731.
- (13) Janani, R.; Majumder, D.; Scrimshire, A.; Stone, A.; Wakelin, E.; Jones, A. H.; Wheeler, N. V.; Brooks, W.; Bingham, P. A. From Acrylates to Silicones: A Review of Common Optical Fibre Coatings Used for Normal to Harsh Environments. *Prog. Org. Coat.* **2023**, *180*, 107557. https://doi.org/10.1016/j.porgcoat.2023.107557.

- (14) Hu, C. C.; Zheng, Y. J.; Hsu, Y. F.; Ye, Z. T. Design and Application of Liquid Silicone Rubber Light Guide in Compact Automotive Headlamps. *Int. J. Optomechatronics* **2024**, *18* (1), 2343407. https://doi.org/10.1080/15599612.2024.2343407.
- (15) Maffli, L.; Rosset, S.; Ghilardi, M.; Carpi, F.; Shea, H. Ultrafast All-Polymer Electrically Tunable Silicone Lenses. *Adv. Funct. Mater.* **2015**, *25* (11), 1656–1665. https://doi.org/10.1002/adfm.201403942.
- (16) Ballato, J.; Hawkins, T.; Foy, P.; Stolen, R.; Kokuoz, B.; Ellison, M.; McMillen, C.; Reppert, J.; Rao, A. M.; Daw, M.; others. Silicon Optical Fiber. *Opt. Express* **2008**, *16* (23), 18675–18683. https://doi.org/10.1364/OE.16.018675.
- (17) Wang, J.-H.; Lien, S.-Y.; Ho, J.-R.; Shih, T.-K.; Chen, C.-F.; Chen, C.-C.; Whang, W.-T. Optical Diffusers Based on Silicone Emulsions. *Opt. Mater.* 2009, *32* (2), 374–377. https://doi.org/10.1016/j.optmat.2009.09.005.
- (18) Pan, Z.; Li, S.; Cai, C. The Preparation of a Novel Silicone Optical Adhesive with Low Hardness and High Refractive Index. *Silicon* **2025**, *17* (1), 63–74. https://doi.org/10.1007/s12633-024-03183-6.
- (19) Frank, G.; Askari, S.; Raschdorf, K.; Khosravi, S.; Kwon, B. K.; Shadgan, B. The Effects of Silicone Enclosure Colour on the Function of Optical Sensors. *Biology* (*Basel*). **2022**, *11* (6), 932. https://doi.org/10.3390/biology11060932.
- (20) Morgan, J.; Chen, T.; Hayes, R.; Dickie, T.; Urlich, T.; Brook, M. A. Facile Synthesis of Dendron-Branched Silicone Polymers. *Polym. Chem.* **2017**, *8* (18), 2743–2746. https://doi.org/10.1039/c7py00260b.
- (21) Kamino, B. A.; Bender, T. P. The Use of Siloxanes, Silsesquioxanes, and Silicones in Organic Semiconducting Materials. *Chem. Soc. Rev.* **2013**, *42* (12), 5119–5130. https://doi.org/10.1039/c3cs35519e.
- (22) Kodama, S.; Miyamoto, Y.; Itoh, S.; Miyata, T.; Wada, H.; Kuroda, K.; Shimojima, A. Self-Healing Lamellar Silsesquioxane Thin Films. *ACS Appl. Polym. Mater.* **2021**, 3 (8), 4118–4126. https://doi.org/10.1021/acsapm.1c00592.
- (23) Zhang, C.; Qu, L.; Wang, Y.; Xu, T.; Zhang, C. Thermal Insulation and Stability of Polysiloxane Foams Containing Hydroxyl-Terminated Polydimethylsiloxanes. *RSC Adv.* **2018**, *8* (18), 9901–9909. https://doi.org/10.1039/C8RA00222C.
- (24) Takamura, N.; Gunji, T.; Hatano, H.; Abe, Y. Preparation and Properties of Polysilsesquioxanes: Polysilsesquioxanes and Flexible Thin Films by Acid-Catalyzed Controlled Hydrolytic Polycondensation of Methyl-and Vinyltrimethoxysilane. J. Polym. Sci., Part A: Polym. Chem. 1999, 37 (7), 1017– 1026. https://doi.org/10.1002/(SICI)1099-0518(19990401)37:7<1017::AID-POLA16>3.0.CO;2-F.
- (25) Liu, Y.; Luan, X.; Feng, Y.; Tan, X.; Han, Y.; Sun, X. Self-Adhesive Epoxy Modified Silicone Materials for Light Emitting Diode Encapsulation. *Polym. Adv. Technol.* **2017**, *28* (11), 1473–1479. https://doi.org/10.1002/pat.4024.
- (26) Yilgör, E.; Yilgör, I. Silicone Containing Copolymers: Synthesis, Properties and Applications. *Prog. Polym. Sci.* **2014**, 39 (6), 1165–1195.

- https://doi.org/10.1016/j.progpolymsci.2013.11.003.
- (27) Ananda kumar, S.; Denchev, Z.; Alagar, M. Synthesis and Thermal Characterization of Phosphorus Containing Siliconized Epoxy Resins. *Eur. Polym. J.* **2006**, *42* (10), 2419–2429. https://doi.org/10.1016/j.eurpolymj.2006.06.010.
- (28) Dankert, F.; von Hänisch, C. Siloxane Coordination Revisited: Si-O Bond Character, Reactivity and Magnificent Molecular Shapes. *Eur. J. Inorg. Chem.* **2021**, *2021* (29), 2907–2927. https://doi.org/10.1002/ejic.202100275.
- (29) Zielecka, M.; Rabajczyk, A. Silicone Nanocomposites with Enhanced Thermal Resistance: A Short Review. *Materials* **2024**, *17* (9), 2016. https://doi.org/10.3390/ma17092016.
- (30) Kim, Y. H.; Bae, J.-Y.; Jin, J.; Bae, B.-S. Sol-Gel Derived Transparent Zirconium-Phenyl Siloxane Hybrid for Robust High Refractive Index LED Encapsulant. *ACS Appl. Mater. Interfaces* **2014**, 6 (5), 3115–3121. https://doi.org/10.1021/am500315y.
- (31) Kim, J.-S.; Yang, S.; Bae, B.-S. Thermally Stable Transparent Sol-Gel Based Siloxane Hybrid Material with High Refractive Index for Light Emitting Diode (LED) Encapsulation. *Chem. Mater.* **2010**, *22* (11), 3549–3555. https://doi.org/10.1021/cm100903b.
- (32) Yu, Y.; Zhao, Y.; Huang, B.; Ji, Y.; Zhao, Y.; Zhang, Z.; Fei, H.-F. Effect of Phenyl Side Groups on the Dielectric Properties and Dielectric Behavior of Polysiloxane. *Polymer* **2022**, *249*, 124865. https://doi.org/10.1016/j.polymer.2022.124865.
- (33) Duan, S.; Li, Z.; Liu, Y.; Zhao, N.; Li, Z. Preparation of Robust Diphenyl Silicone Elastomers with Enhanced Mechanical Properties and Thermal-Aging Resistances by Using Phosphazene as Catalyst. *Polymer* **2023**, *272*, 125855. https://doi.org/10.1016/j.polymer.2023.125855.
- (34) Zolper, T. J.; Jungk, M.; Marks, T. J.; Chung, Y.-W.; Wang, Q. Modeling Polysiloxane Volume and Viscosity Variations with Molecular Structure and Thermodynamic State. J. Tribol. 2014, 136 (1), 011801-1-011801–011812. https://doi.org/10.1115/1.4025301.
- (35) Brunchi, C. E.; Filimon, A.; Cazacu, M.; Ioan, S. Properties of Some Poly(Siloxane)s for Optical Applications. *High Perform. Polym.* **2008**, *21* (1), 31–47. https://doi.org/10.1177/0954008308088737.
- (36) Deshpande, G.; Rezac, M. E. The Effect of Phenyl Content on the Degradation of Poly(Dimethyl Diphenyl) Siloxane Copolymers. *Polym. Degrad. Stab.* **2001**, *74* (2), 363–370. https://doi.org/10.1016/S0141-3910(01)00186-0.
- (37) Urata, C.; Masheder, B.; Cheng, D. F.; Miranda, D. F.; Dunderdale, G. J.; Miyamae, T.; Hozumi, A. Why Can Organic Liquids Move Easily on Smooth Alkyl-Terminated Surfaces? *Langmuir* **2014**, *30* (14), 4049–4055. https://doi.org/10.1021/la500548v.
- (38) Rochow, E. G. The Direct Synthesis of Organosilicon Compounds. *J. Am. Chem. Soc.* **1945**, *67* (6), 963–965.
- (39) Clarke, M. P. The Direct Synthesis of Methylchlorosilanes. J. Organomet. Chem.

- **1989**, 376 (2–3), 165–222. https://doi.org/10.1016/0022-328X(89)85131-9.
- (40) Yuan, W.; Smirnov, P.; Oestreich, M. Custom Hydrosilane Synthesis Based on Monosilane. *Chem* **2018**, *4* (6), 1443–1450. https://doi.org/10.1016/j.chempr.2018.03.017.
- (41) Burkhard, C. A.; Rochow, E. G.; Booth, H. S.; Hartt, J. The Present State of Organosilicon Chemistry. *Chem. Rev.* **1947**, *41* (1), 97–149.
- (42) Klokov, B. A. Continuous and Batch Organomagnesium Synthesis of Ethyl-Substituted Silanes from Ethylchloride, Tetraethoxysilane, and Organotrichlorosilane for Production of Polyethylsiloxane Liquids. 2. Continuous One-Step Synthesis of Ethylethoxy-and Ethylchlorosilane. *Org. Proc. Res. Dev.* **2001**, *5* (3), 234–240. https://doi.org/10.1021/op000100p.
- (43) Beckmann, J.; Dakternieks, D.; Duthie, A.; Floate, S. L.; Foitzik, R. C.; Schiesser, C. H. Chiral Organochlorosilanes Derived from Terpenes: Diastereoselective Hydrosilylation of Methylene Bicyclo [2.2.1] Heptanes with HSiMe_nCl_{n-2} (N= 0-2). *J. Organomet. Chem.* **2004**, 689 (5), 909–916. https://doi.org/10.1016/j.jorganchem.2003.12.021.
- (44) Andrianov, K. A.; Kurakov, G. A.; Khananashvili, L. M. The Reaction of 1, 3-Dioxolane with Organochlorosilanes. *Bull. Acad. Sci. USSR, Div. Chem. Sci.* **1964**, *13*, 2148–2150.
- (45) Masaoka, S.; Banno, T.; Ishikawa, M. The Synthesis of Chlorosilanes from Alkoxysilanes, Silanols, and Hydrosilanes with Bulky Substituents. *J. Organomet. Chem.* **2006**, 691 (1–2), 174–181. https://doi.org/10.1016/j.jorganchem.2005.08.028.
- (46) Roberts, J. M.; Eldred, D. V; Katsoulis, D. E. Synthesis of SiCl₄ from Gaseous HCl and Si(OMe)₄. Reaction Development and Kinetic Studies. *Ind. Eng. Chem. Res.* **2016**, 55 (6), 1813–1818. https://doi.org/10.1021/acs.iecr.5b04720.
- (47) Ishikawa, M.; Toyoda, E.; Ishii, M.; Kunai, A.; Yamamoto, Y.; Yamamoto, M. Synthesis of Chlorosilanes from (Fluoroalkyl) Silanes, Bis(Silyl)Benzenes, and α,ω-Dihydropolysiloxanes. *Organometallics* **1994**, *13* (3), 808–812.
- (48) Seyferth, D.; Prud'homme, C. C. Linear Polysiloxanes from Dichlorosilane. *Inorg. Chem.* **1984**, *23* (26), 4412–4417.
- (49) Seyferth, D.; Prud'homme, C.; Wiseman, G. H. Cyclic Polysiloxanes from the Hydrolysis of Dichlorosilane. *Inorg. Chem.* **1983**, *22* (15), 2163–2167.
- (50) Liu, Y.; Chaiprasert, T.; Ouali, A.; Unno, M. Well-Defined Cyclic Silanol Derivatives. *Dalton Trans.* **2022**, *51* (11), 4227–4245.
- (51) Rochow, E. G. Methyl Silicate from Silicon and Methanol. *J. Am. Chem. Soc.* **1948**, 70 (6), 2170–2171.
- (52) Rochow, E. G.; Schenectady, N. Y. Preparation of Tetramethyl Silicate, US2473260A. **1949**.
- (53) Temnikov, M. N.; Krizhanovskiy, I. N.; Anisimov, A. A.; Bedenko, S. P.; Dementiev,

- K. I.; Krylova, I. V; Milenin, S. A.; Maksimov, A. L.; Egorov, M. P.; Muzafarov, A. M. Direct Synthesis of Alkoxysilanes: Current State, Challenges and Prospects. *Russ. Chem. Rev.*, **2023**, *92* (7). https://doi.org/10.59761/RCR5081.
- (54) Purkayastha, A.; Baruah, J. B. Synthetic Methodologies in Siloxanes. *Appl. Organometal. Chem.* **2004**, *18* (4), 166–175. https://doi.org/10.1002/aoc.607.
- (55) Putro, W. S.; Lee, V. Y.; Sato, K.; Choi, J.-C.; Fukaya, N. From SiO₂ to Alkoxysilanes for the Synthesis of Useful Chemicals. *ACS Omega* **2021**, 6 (51), 35186–35195. https://doi.org/10.1021/acsomega.1c05138.
- (56) Laine, R. M.; Furgal, J. C.; Doan, P.; Pan, D.; Popova, V.; Zhang, X. Avoiding Carbothermal Reduction: Distillation of Alkoxysilanes from Biogenic, Green, and Sustainable Sources. *Angew. Chem. Int. Ed.* **2016**, *55* (3), 1065–1069. https://doi.org/10.1002/anie.201506838.
- (57) Fukaya, N.; Choi, S. J.; Horikoshi, T.; Kataoka, S.; Endo, A.; Kumai, H.; Hasegawa, M.; Sato, K.; Choi, J.-C. Direct Synthesis of Tetraalkoxysilanes from Silica and Alcohols. *New J. Chem.* **2017**, *41* (6), 2224–2226. https://doi.org/10.1039/c6nj03897b.
- (58) Ono, Y.; Akiyama, M.; Suzuki, E. Direct Synthesis of Tetraalkoxysilanes from Silica by Reaction with Dialkyl Carbonates. *Chem. Mater.* **1993**, *5* (4), 442–447.
- (59) Pramanik, S.; Fernandes, A.; Liautard, V.; Pucheault, M.; Robert, F.; Landais, Y. Dehydrogenative Silylation of Alcohols Under Pd-Nanoparticle Catalysis. *Chem. Eur. J.* **2019**, *25* (3), 728–732. https://doi.org/10.1002/chem.201803989.
- (60) Zhu, J.; Chen, S.; He, C. Catalytic Enantioselective Dehydrogenative Si-O Coupling to Access Chiroptical Silicon-Stereogenic Siloxanes and Alkoxysilanes. *J. Am. Chem. Soc.* **2021**, *143* (14), 5301–5307. https://doi.org/10.1021/jacs.1c01106.
- (61) Veszprémi, T.; Takahashi, M.; Hajgató, B.; Kira, M. The Mechanism of 1,2-Addition of Disilene and Silene. 1. Water and Alcohol Addition. *J. Am. Chem. Soc.* **2001**, *123* (27), 6629–6638. https://doi.org/10.1021/ja0040823.
- (62) Raabe, G.; Michl, J. Multiple Bonding to Silicon. Chem. Rev. 1985, 85 (5), 419–509.
- (63) Davidson, I. M. T.; Wood, I. T. Kinetics of Addition of 2-Methyl-2-Silapropene to Methyl Trimethylsilyl Ether. *J. Chem. Soc., Chem. Commun.* **1982**, No. 10, 550–551. https://doi.org/10.1039/C39820000550.
- (64) Temnikov, M. N.; Anisimov, A. A.; Zhemchugov, P. V; Kholodkov, D. N.; Goloveshkin, A. S.; Naumkin, A. V; Chistovalov, S. M.; Katsoulis, D.; Muzafarov, A. M. Mechanochemistry a New Powerful Green Approach to the Direct Synthesis of Alkoxysilanes. *Green Chem.* 2018, 20 (9), 1962–1969. https://doi.org/10.1039/c7gc03862c.
- (65) Miura, Y.; Kashiwagi, T.; Fukuda, T.; Shichiri, A.; Shiobara, T.; Saitow, K. Near-Room-Temperature Synthesis of Alkoxysilanes and H₂ via Mechanochemical Ball Milling. *ACS Sustainable Chem. Eng.* **2022**, *10* (49), 16159–16168. https://doi.org/10.1021/acssuschemeng.2c04086.
- (66) Grignard, V. Sur Quelques Nouvelles Combinaisons Organométalliques Du

- Magnésium et Leur Application Àdes Synthèses d'alcools et d'hydrocarbures. *COMPTES RENDUS DES SÉANCES L'ACADÉMIE DES Sci.* **1900**, 1322–1324.
- (67) Peltzer, R. M.; Gauss, J.; Eisenstein, O.; Cascella, M. The Grignard Reaction Unraveling a Chemical Puzzle. *J. Am. Chem. Soc.* **2020**, *142* (6), 2984–2994. https://doi.org/10.1021/jacs.9b11829.
- (68) Krasovskiy, A.; Knochel, P. A LiCl-Mediated Br/Mg Exchange Reaction for the Preparation of Functionalized Aryl- and Heteroarylmagnesium Compounds from Organic Bromides. *Angew. Chem. Int. Ed.* **2004**, *43* (25), 3333–3336. https://doi.org/10.1002/anie.200454084.
- (69) Ziegler, D. S.; Wei, B.; Knochel, P. Improving the Halogen–Magnesium Exchange by Using New Turbo-Grignard Reagents. *Chem. Eur. J.* **2019**, *25* (11), 2695–2703. https://doi.org/10.1002/chem.201803904.
- (70) Visco, M. D.; Wieting, J. M.; Mattson, A. E. Carbon-Silicon Bond Formation in the Synthesis of Benzylic Silanes. *Org. Lett.* **2016**, *18* (12), 2883–2885. https://doi.org/10.1021/acs.orglett.6b01223.
- (71) Moore, B. M.; Ramirez, S. M.; Yandek, G. R.; Haddad, T. S.; Mabry, J. M. Asymmetric Aryl Polyhedral Oligomeric Silsesquioxanes (ArPOSS) with Enhanced Solubility. J. Organomet. Chem. 2011, 696 (13), 2676–2680. https://doi.org/10.1016/j.jorganchem.2011.03.035.
- (72) Wakabayashi, R.; Sugiura, Y.; Shibue, T.; Kuroda, K. Practical Conversion of Chlorosilanes into Alkoxysilanes without Generating HCl. *Angew. Chem. Int. Ed.* **2011**, *50* (45), 10708–10711. https://doi.org/10.1002/anie.201104948.
- (73) Jean, P. A.; Gallavan, R. H.; Kolesar, G. B.; Siddiqui, W. H.; Oxley, J. A.; Meeks, R. G. Chlorosilane Acute Inhalation Toxicity and Development of an LC50 Prediction Model. *Inhal. Toxicol.* 2006, 18 (8), 515–522. https://doi.org/10.1080/08958370600686093.
- (74) Kannengießer, J.-F.; Briesenick, M.; Meier, D.; Huch, V.; Morgenstern, B.; Kickelbick, G. Synthesis and Hydrogen-Bond Patterns of Aryl-Group Substituted Silanediols and -Triols from Alkoxy- and Chlorosilanes. *Chem. Eur. J.* **2021**, *27* (66), 16461–16476. https://doi.org/10.1002/chem.202102729.
- (75) Manoso, A. S.; Ahn, C.; Soheili, A.; Handy, C. J.; Correia, R.; Seganish, W. M.; DeShong, P. Improved Synthesis of Aryltrialkoxysilanes via Treatment of Aryl Grignard or Lithium Reagents with Tetraalkyl Orthosilicates. *J. Org. Chem.* **2004**, 69 (24), 8305–8314. https://doi.org/10.1021/jo048667h.
- (76) Tacke, R.; Bentlage-Felten, A.; Linoh, H.; Magda, S. Sila-Pharmaka, 34. Mitt.[1]. Sila-Analoga Des Triparanols Und Ethamoxytriphetols: Synthese Sowie Pharmakologische Und Toxikologische Eigenschaften. *Zeitschrift für Naturforsch. B* **1986**, *41* (5), 649–654. https://doi.org/10.1515/znb-1986-0518.
- (77) Biedermann, J.; Wilkening, H. M. R.; Uhlig, F.; Hanzu, I. Electrochemical Properties of Arylsilanes. *Electrochem. commun.* **2019**, *102*, 13–18. https://doi.org/10.1016/j.elecom.2019.03.010.

- (78) Sfameni, S.; Rando, G.; Plutino, M. R. Sustainable Secondary-Raw Materials, Natural Substances and Eco-Friendly Nanomaterial-Based Approaches for Improved Surface Performances: An Overview of What They Are and How They Work. Int. J. Mol. Sci. 2023, 24 (6), 5472. https://doi.org/10.3390/ijms24065472.
- (79) Schubert, U. Sol-Gel-Chemie: Einfach Und Doch Kompliziert. *Chem. Unserer Zeit* **2018**, *52* (1), 18–25. https://doi.org/10.1002/ciuz.201700792.
- (80) Osterholtz, F. D.; Pohl, E. R. Kinetics of the Hydrolysis and Condensation of Organofunctional Alkoxysilanes: A Review. *J. Adhes. Sci. Technol.* **1992**, 6 (1), 127–149. https://doi.org/10.1163/156856192X00106.
- (81) Schmidt, H.; Scholze, H.; Kaiser, A. Principles of Hydrolysis and Condensation Reaction of Alkoxysilanes. *J. Non-Cryst. Solids* **1984**, 63 (1–2), 1–11. https://doi.org/10.1016/0022-3093(84)90381-8.
- (82) Sakka, S.; Kamiya, K.; Makita, K.; Yamamoto, Y. Formation of Sheets and Coating Films from Alkoxide Solutions. *J. Non-Cryst. Solids* **1984**, 63 (1–2), 223–235. https://doi.org/10.1016/0022-3093(84)90401-0.
- (83) Glaser, P. M.; Pantano, C. G. Effect of the $H_2O/TEOS$ Ratio upon the Preparation and Nitridation of Silica Sol/Gel Films. *J. Non-Cryst. Solids* **1984**, 63 (1–2), 209–221. https://doi.org/10.1016/0022-3093(84)90400-9.
- (84) Klein, L. C. Sol-Gel Processing of Silicates. *Ann. Rev. Mater. Sci.* **1985**, *15*, 227–248. https://doi.org/10.1146/annurev.ms.15.080185.001303.
- (85) Leyden, D. E.; Atwater, J. B. Hydrolysis and Condensation of Alkoxysilanes Investigated by Internal Reflection FTIR Spectroscopy. *J. Adhes. Sci. Technol.* **1991**, 5 (10), 815–829. https://doi.org/10.1163/156856191X00233.
- (86) Chambers, R. C.; Jones, Jr, W. E.; Haruvy, Y.; Webber, S. E.; Fox, M. A. Influence of Steric Effects on the Kinetics of Ethyltrimethoxysilane Hydrolysis in a Fast Sol-Gel System. Chem. Mater. 1993, 5 (10), 1481–1486. https://doi.org/10.1021/cm00034a018.
- (87) Tan, B.; Rankin, S. E. Study of the Effects of Progressive Changes in Alkoxysilane Structure on Sol-Gel Reactivity. *J. Phys. Chem. B* **2006**, *110* (45), 22353–22364. https://doi.org/10.1021/jp060376k.
- (88) Turner, C. W.; Franklin, K. J. Studies of the Hydrolysis and Condensation of Tetraethylorthosilicate by Multinuclear (¹H, ¹⁷O, ²⁹Si) NMR Spectroscopy. *J. Non-Cryst. Solids* **1987**, 91 (3), 402–415. https://doi.org/10.1016/S0022-3093(87)80349-6.
- (89) Liu, J.; Kim, S. D. Polycondensation Behavior of Methyltrimethoxysilane Studied by NMR Spectroscopy. J. Polym. Sci., Part B: Polym. Phys. 1996, 34 (1), 131–140. https://doi.org/10.1002/(SICI)1099-0488(19960115)34:1<131::AID-POLB11>3.0.CO;2-F.
- (90) Dubitsky, Y.; Zaopo, A.; Zannoni, G.; Zetta, L. ¹H NMR Study of the Hydrolysis of Vinyltrialkoxysilanes. *Mater. Chem. Phys.* **2000**, 64 (1), 45–53. https://doi.org/10.1016/S0254-0584(99)00251-5.

- (91) Kannengießer, J.-F.; Morgenstern, B.; Janka, O.; Kickelbick, G. Oligo-Condensation Reactions of Silanediols with Conservation of Solid-State-Structural Features. Chem. Eur. J. 2024, 30 (16), e202303343. https://doi.org/10.1002/chem.202303343.
- (92) Hao, X.; Jeffery, J. L.; Le, T. P. T.; McFarland, G.; Johnson, G.; Mulder, R. J.; Garrett, Q.; Manns, F.; Nankivil, D.; Arrieta, E.; others. High Refractive Index Polysiloxane as Injectable, in Situ Curable Accommodating Intraocular Lens. *Biomaterials* **2012**, *33* (23), 5659–5671. https://doi.org/10.1016/j.biomaterials.2012.04.052.
- (93) Helary, G.; Sauvet, G. Heterofunctional Condensation of Alkoxysilanes and Silanols-II. Synthesis of Linear Poly(Aminoalkylsiloxane)S. *Eur. Polym. J.* **1992**, *28* (1), 37–41. https://doi.org/10.1016/0014-3057(92)90234-S.
- (94) Lavrencic Stangar, U.; Sassi, A.; Venzo, A.; Zattin, A.; Japelj, B.; Orel, B.; Gross, S. IR and NMR Time-Resolved Studies on the Hydrolysis and Condensation of Methacryloxyalkylsilanes. J. Sol-Gel Sci. Technol. 2009, 49, 329–335. https://doi.org/10.1007/s10971-008-1882-1.
- (95) Fan, X.; Cao, X.; Shang, X.; Zhang, X.; Huang, C.; Zhang, J.; Zheng, K.; Ma, Y. A Transparent Cyclo-Linear Polyphenylsiloxane Elastomer Integrating High Refractive Index, Thermal Stability and Flexibility. *Polym. Chem.* 2021, 12 (36), 5149–5158. https://doi.org/10.1039/d1py00688f.
- (96) Ji, J.; Ge, X.; Liang, W.; Pang, X.; Liu, R.; Wen, S.; Sun, J.; Chen, X.; Ge, J. Synthesis of High Molecular Weight Vinylphenyl-Con Taining MQ Silicone Resin via Hydrosilylation Reaction. *Coatings* 2019, 9 (10), 605. https://doi.org/10.3390/coatings9100605.
- (97) Racles, C.; Alexandru, M.; Bele, A.; Musteata, V. E.; Cazacu, M.; Opris, D. M. Chemical Modification of Polysiloxanes with Polar Pendant Groups by Co-Hydrosilylation. *RSC Adv.* **2014**, *4* (71), 37620–37628. https://doi.org/10.1039/c4ra06955b.
- (98) Brown, L. C.; Giles, S. L.; Daniels, G. C.; Romanczyk, M.; Ananth, R. Iridium-Catalyzed Hydrosilylation of Polymeric Olefins: Moving beyond Platinum-Based Catalysts for Surfactants. *Ind. Eng. Chem. Res.* 2024, 63 (21), 9329–9335. https://doi.org/10.1021/acs.iecr.4c00048.
- (99) Sato, Y.; Hayami, R.; Gunji, T. Characterization of NMR, IR, and Raman Spectra for Siloxanes and Silsesquioxanes: A Mini Review. *J. Sol-Gel Sci. Technol.* **2022**, *104*, 36–52. https://doi.org/10.1007/s10971-022-05920-y.
- (100) Baney, R. H.; Itoh, M.; Sakakibara, A.; Suzuki, T. Silsesquioxanes. *Chem. Rev.* **1995**, 95, 1409–1430.
- (101) Kekevi, B.; Berber, H.; Yildirim, H. Synthesis and Characterization of Silicone-Based Surfactants as Anti-Foaming Agents. *J. Surfact. Deterg.* **2012**, *15* (1), 73–81. https://doi.org/10.1007/s11743-011-1277-0.
- (102) Kassu, A.; Powers, K.; Petway, W.; Sharma, A. Fourier Transform Infrared Characterization of Construction Joint Sealants. *J. Civil Eng. Mater.App.* **2020**, *4* (3), 155–160. https://doi.org/10.22034/jcema.2020.237399.1029.

- (103) Poojari, Y. Silicones for Encapsulation of Medical Device Implants. *Silicon* **2017**, 9 (5), 645–649. https://doi.org/10.1007/s12633-017-9603-4.
- (104) Meals, R. N. Silicones. *Ann. N. Y. Acad. Sci.* **1965**, *125* (1), 137–146. https://doi.org/10.1111/j.1749-6632.1965.tb45384.x.
- (105) Zepeda-Velazquez, L.; Macphail, B.; Brook, M. A. Spread and Set Silicone-Boronic Acid Elastomers. *Polym. Chem.* **2016**, *7* (27), 4458–4466. https://doi.org/10.1039/c6py00492j.
- (106) Kappel, R. M.; Klunder, A. J. H.; Pruijn, G. J. M. Silicon Chemistry and Silicone Breast Implants. *Eur. J. Plast. Surg.* **2014**, *37*, 123–128. https://doi.org/10.1007/s00238-013-0914-4.
- (107) Ho, K. Y.; Dodou, K. Rheological Studies on Pressure-Sensitive Silicone Adhesives and Drug-in-Adhesive Layers as a Means to Characterise Adhesive Performance. *Int. J. Pharm.* **2007**, 333 (1–2), 24–33. https://doi.org/10.1016/j.ijpharm.2006.09.043.
- (108) Owen, M. J. The Surface Activity of Silicones: A Short Review. *Ind. Eng. Chem. Prod. Res. Dev.* **1980**, *19* (1), 97–103.
- (109) Jemmett, A. E. Chemical Behaviour of Siloxanes at Metal Interfaces. *Tribology* **1968**, *1* (3), 173–177. https://doi.org/10.1016/S0041-2678(68)80528-7.
- (110) Yamada, Y. Siloxane Modified Polyimides for Microelectronics Coating Applications. *High Perform. Polym.* **1998**, *10* (1), 69–80. https://doi.org/10.1088/0954-0083/10/1/009.
- (111) Wang, P.-I.; Nalamasu, O.; Ghoshal, R.; Ghoshal, R.; Schaper, C. D.; Li, A.; Lu, T.-M. Novel Photocurable Epoxy Siloxane Polymers for Photolithography and Imprint Lithography Applications. *J. Vac. Sci. Technol. B* **2008**, *26* (1), 244–248. https://doi.org/10.1116/1.2834559.
- (112) Kärkkäinen, A. H. O.; Rantala, J. T.; Maaninen, A.; Jabbour, G. E.; Descour, M. R. Siloxane-Based Hybrid Glass Materials for Binary and Grayscale Mask Photoimaging. *Adv. Mater.* **2002**, *14* (7), 535–540. https://doi.org/10.1002/1521-4095(20020404)14:7<535::AID-ADMA535>3.0.CO;2-T.
- (113) Celio, H.; Lozano, J.; Cabibil, H.; Ballast, L.; White, J. M. Self-Assembly of Fluid-Filled KHCO₃ Microfibers. *J. Am. Chem. Soc.* **2003**, *125* (11), 3302–3310. https://doi.org/10.1021/ja021419n.
- (114) Jiang, Y.; Tian, C.; Yao, J.; Wu, W.; Ning, N.; Tian, M.; Zhang, L. Nano-Silica/Polydimethyl(Methylvinyl)Siloxane Dielectric Elastomer Generator with High Generating Energy Density, High Efficiency and Long Fatigue Life. *Chem. Eng. J.* **2022**, *439*, 135339. https://doi.org/10.1016/j.cej.2022.135339.
- (115) Warrick, E. L.; Hunter, M. J.; Barry, A. J. Polymer Chemistry of the Linear Siloxanes. *Ind. Eng. Chem.* **1952**, *44* (9), 2196–2202.
- (116) Yi, B.; Wang, S.; Hou, C.; Huang, X.; Cui, J.; Yao, X. Dynamic Siloxane Materials: From Molecular Engineering to Emerging Applications. *Chem. Eng. J.* **2021**, *405*, 127023. https://doi.org/10.1016/j.cej.2020.127023.

- (117) Sato, M.; Furuya, M.; Maruyama, M. Method for the Preparation of Diorganopolysiloxane End-Blocked with Silanolic Hydroxy Groups, US5475077A. 1995.
- (118) Petersen, L. P. Process for the Continuous Manufacture of Siloxane Polymers, US4250290A. **1981**.
- (119) Ottlinger, R.; Reitmeier, R. Method for Preparing Linear Organopolysiloxanediols, US4762937A. **1988**.
- (120) Itoh, K.; Shinohara, T.; Kizaki, H.; Tanaka, S.; Satou, Y.; Umemura, K. Method of Producing Dimethylpolysiloxanes, US5473037A. **1995**.
- (121) Sun, D.; Fu, Q.; Ren, Z.; Li, W.; Li, H.; Ma, D.; Yan, S. Carbazole-Based Polysiloxane Hosts for Highly Efficient Solution-Processed Blue Electrophosphorescent Devices. *J. Mater. Chem. C* **2013**, *1* (34), 5344–5350. https://doi.org/10.1039/c3tc31108b.
- (122) Sun, D.; Yang, Z.; Ren, Z.; Li, H.; Bryce, M. R.; Ma, D.; Yan, S. Oligosiloxane Functionalized with Pendant (1,3-Bis(9-Carbazolyl)Benzene)(MCP) for Solution-Processed Organic Electronics. *Chem. Eur. J.* **2014**, *20* (49), 16233–16241. https://doi.org/10.1002/chem.201402374.
- (123) Sun, D.; Yang, Z.; Sun, X.; Li, H.; Ren, Z.; Liu, J.; Ma, D.; Yan, S. Synthesis of Triphenylamine Based Polysiloxane as a Blue Phosphorescent Host. *Polym. Chem.* **2014**, *5* (17), 5046–5052. https://doi.org/10.1039/c4py00450g.
- (124) Rupasinghe, B.; Furgal, J. C. Degradation of Silicone-Based Materials as a Driving Force for Recyclability. *Polym. Int.* **2022**, *71* (5), 521–531. https://doi.org/10.1002/pi.6340.
- (125) Horii, Y.; Kannan, K. Survey of Organosilicone Compounds, Including Cyclic and Linear Siloxanes, in Personal-Care and Household Products. *Arch. Environ. Contam. Toxicol.* **2008**, *55* (4), 701–710. https://doi.org/10.1007/s00244-008-9172-z.
- (126) Yucuis, R. A.; Stanier, C. O.; Hornbuckle, K. C. Cyclic Siloxanes in Air, Including Identification of High Levels in Chicago and Distinct Diurnal Variation.

 Chemosphere 2013, 92 (8), 905–910. https://doi.org/10.1016/j.chemosphere.2013.02.051.
- (127) Lee, D.; Park, M.-K.; Lee, I.-S.; Choi, S.-D. Contamination Characteristics of Siloxanes in Coastal Sediment Collected from Industrialized Bays in South Korea. *Ecotoxicol. Environ. Saf.* **2019**, *182*, 109457. https://doi.org/10.1016/j.ecoenv.2019.109457.
- (128) Bletsou, A. A.; Asimakopoulos, A. G.; Stasinakis, A. S.; Thomaidis, N. S.; Kannan, K. Mass Loading and Fate of Linear and Cyclic Siloxanes in a Wastewater Treatment Plant in Greece. *Environ. Sci. Technol.* **2013**, *47* (4), 1824–1832. https://doi.org/10.1021/es304369b.
- (129) Le Roux, C.; Yang, H.; Wenzel, S.; Grigoras, S.; Brook, M. A. Using "Anhydrous" Hydrolysis to Favor Formation of Hexamethylcyclotrisiloxane from

- Dimethyldichlorosilane. *Organometallics* **1998**, *17* (4), 556–564. https://doi.org/10.1021/om970953e.
- (130) Unno, M.; Endo, H.; Takeda, N. Synthesis and Structures of Extended Cyclic Siloxanes. *Heteroat. Chem.* **2014**, *25* (6), 525–532.
- (131) Ren, Z.; Yan, S. Polysiloxanes for Optoelectronic Applications. *Prog. Mater. Sci.* **2016**, 83, 383–416. https://doi.org/10.1016/j.pmatsci.2016.07.004.
- (132) Naga, N.; Miyanaga, T.; Wang, Y.; Nakano, T. Synthesis and Properties of σ-π Conjugated Porous Polymers Obtained with Mizoroki-Heck Reaction of Tetra Vinyl Cyclic Siloxane with Dibromo Fluorene. *J. Polym. Sci.* **2020**, *58* (17), 2301–2309. https://doi.org/10.1002/pol.20200268.
- (133) Kamino, B. A.; Grande, J. B.; Brook, M. A.; Bender, T. P. Siloxane-Triarylamine Hybrids: Discrete Room Temperature Liquid Triarylamines via the Piers-Rubinsztajn Reaction. *Org. Lett.* **2011**, *13* (1), 154–157. https://doi.org/10.1021/ol102607v.
- (134) Kamino, B. A.; Mills, B.; Reali, C.; Gretton, M. J.; Brook, M. A.; Bender, T. P. Liquid Triarylamines: The Scope and Limitations of Piers-Rubinsztajn Conditions for Obtaining Triarylamine-Siloxane Hybrid Materials. *J. Org. Chem.* **2012**, *77*(4), 1663–1674. https://doi.org/10.1021/jo2020906.
- (135) Zaranek, M.; Pawluc, P. Markovnikov Hydrosilylation of Alkenes: How an Oddity Becomes the Goal. *ACS Catal.* **2018**, *8* (10), 9865–9876. https://doi.org/10.1021/acscatal.8b03104.
- (136) Nyczyk, A.; Paluszkiewicz, C.; Hasik, M.; Cypryk, M.; Pospiech, P. Cross-Linking of Linear Vinylpolysiloxanes by Hydrosilylation FTIR Spectroscopic Studies. *Vib. Spectrosc.* **2012**, 59, 1–8. https://doi.org/10.1016/j.vibspec.2012.01.002.
- (137) Gretton, M. J.; Kamino, B. A.; Brook, M. A.; Bender, T. P. The Use of Piers-Rubinsztajn Conditions for the Placement of Triarylamines Pendant to Silicone Polymers. *Macromolecules* **2012**, *45* (2), 723–728. https://doi.org/10.1021/ma202041u.
- (138) Grande, J. B.; Thompson, D. B.; Gonzaga, F.; Brook, M. A. Testing the Functional Tolerance of the Piers-Rubinsztajn Reaction: A New Strategy for Functional Silicones. *Chem. Commun.* **2010**, *46* (27), 4988–4990. https://doi.org/10.1039/c0cc00369g.
- (139) Rubinsztajn, S.; Cella, J. A. A New Polycondensation Process for the Preparation of Polysiloxane Copolymers. *Macromolecules* **2005**, *38* (4), 1061–1063. https://doi.org/10.1021/ma047984n.
- (140) Brook, M. A. New Control Over Silicone Synthesis Using SiH Chemistry: The Piers-Rubinsztajn Reaction. *Chem. Eur. J.* **2018**, *24* (34), 8458–8469. https://doi.org/10.1002/chem.201800123.
- (141) Szawiola, A. M.; de Melo Souza, N.; Lessard, B. H.; Bender, T. P. Phenoxylated Siloxane-Based Polymers via the Piers-Rubinsztajn Process. *Polym. Int.* **2017**, 66 (9), 1324–1328. https://doi.org/10.1002/pi.5396.

- (142) Fawcett, A. S.; Grande, J. B.; Brook, M. A. Rapid, Metal-Free Room Temperature Vulcanization Produces Silicone Elastomers. *J. Polym. Sci., Part A: Polym. Chem.* **2013**, *51* (3), 644–652. https://doi.org/10.1002/pola.26414.
- (143) Tondreau, A. M.; Atienza, C. C. H.; Weller, K. J.; Nye, S. A.; Lewis, K. M.; Delis, J. G. P.; Chirik, P. J. Iron Catalysts for Selective Anti-Markovnikov Alkene Hydrosilylation Using Tertiary Silanes. *Science*. **2012**, *335* (6068), 567–570. https://doi.org/10.1126/science.1214451.
- (144) Putzien, S.; Nuyken, O.; Kühn, F. E. Functionalized Polysilalkylene Siloxanes (Polycarbosiloxanes) by Hydrosilylation-Catalysis and Synthesis. *Prog. Polym. Sci.* **2010**, 35 (6), 687–713. https://doi.org/10.1016/j.progpolymsci.2010.01.007.
- (145) Guida-Pietrasanta, F.; Boutevin, B.; Nuyken, O. Polysilalkylene or Silarylene Siloxanes Said Hybrid Silicones. In *Inorganic polymeric nanocomposites and membranes*. *Advances in Polymer Science*; Springer, Berlin, Heidelberg, **2005**; pp 1–27. https://doi.org/10.1007/b104479.
- (146) Kownacki, I.; Marciniec, B.; Macina, A.; Rubinsztajn, S.; Lamb, D. Catalytic Activity of Iridium Siloxide Complexes in Cross-Linking of Silicones by Hydrosilylation. *Appl. Catal. A: Gen.* **2007**, *317* (1), 53–57. https://doi.org/10.1016/j.apcata.2006.09.037.
- (147) Islamova, R. M.; Dobrynin, M. V; Ivanov, D. M.; Vlasov, A. V; Kaganova, E. V; Grigoryan, G. V; Kukushkin, V. Y. Bis-Nitrile and Bis-Dialkylcyanamide Platinum(II) Complexes as Efficient Catalysts for Hydrosilylation Cross-Linking of Siloxane Polymers. *Molecules* **2016**, *21* (3), 311. https://doi.org/10.3390/molecules21030311.
- (148) Cordes, D. B.; Lickiss, P. D.; Rataboul, F. Recent Developments in the Chemistry of Cubic Polyhedral Oligosilsesquioxanes. *Chem. Rev.* **2010**, *110* (4), 2081–2173. https://doi.org/10.1021/cr900201r.
- (149) Laird, M.; Van Der Lee, A.; Dumitrescu, D. G.; Carcel, C.; Ouali, A.; Bartlett, J. R.; Unno, M.; Wong Chi Man, M. Styryl-Functionalized Cage Silsesquioxanes as Nanoblocks for 3-D Assembly. *Organometallics* **2020**, *39* (10), 1896–1906. https://doi.org/10.1021/acs.organomet.0c00119.
- (150) Li, G.; Wang, L.; Ni, H.; Pittman Jr., C. U. Polyhedral Oligomeric Silsesquioxane (POSS) Polymers and Copolymers: A Review. *J. Inorg. Organomet. Polym.* **2001**, *11*, 123–154. https://doi.org/10.1023/A:1015287910502.
- (151) Xiao, S.; Nguyen, M.; Gong, X.; Cao, Y.; Wu, H.; Moses, D.; Heeger, A. J. Stabilization of Semiconducting Polymers with Silsesquioxane. *Adv. Funct. Mater.* **2003**, *13* (1), 25–29. https://doi.org/10.1002/adfm.200390000.
- (152) Lee, J.; Cho, H.-J.; Jung, B.-J.; Cho, N. S.; Shim, H.-K. Stabilized Blue Luminescent Polyfluorenes: Introducing Polyhedral Oligomeric Silsesquioxane. *Macromolecules* **2004**, *37* (23), 8523–8529. https://doi.org/10.1021/ma0497759.
- (153) Yang, X.; Froehlich, J. D.; Chae, H. S.; Harding, B. T.; Li, S.; Mochizuki, A.; Jabbour, G. E. Efficient Light-Emitting Devices Based on Platinum-Complexes-Anchored Polyhedral Oligomeric Silsesquioxane Materials. *Chem. Mater.* **2010**, *22* (16),

- 4776-4782. https://doi.org/10.1021/cm101314b.
- (154) Yang, X.; Froehlich, J. D.; Chae, H. S.; Li, S.; Mochizuki, A.; Jabbour, G. E. Efficient Light-Emitting Devices Based on Phosphorescent Polyhedral Oligomeric Silsesquioxane Materials. *Adv. Funct. Mater.* **2009**, *19* (16), 2623–2629. https://doi.org/10.1002/adfm.200900050.
- (155) Ghanbari, H.; Cousins, B. G.; Seifalian, A. M. A Nanocage for Nanomedicine: Polyhedral Oligomeric Silsesquioxane (POSS). *Macromol. Rapid Commun.* **2011**, 32 (14), 1032–1046. https://doi.org/10.1002/marc.201100126.
- (156) Lichtenhan, J. D.; Pielichowski, K.; Blanco, I. POSS-Based Polymers. *Polymers* **2019**, *11* (10), 1727. https://doi.org/10.3390/polym11101727.
- (157) Ozimek, J.; Pielichowski, K. Recent Advances in Polyurethane/POSS Hybrids for Biomedical Applications. *Molecules* **2022**, *27* (1), 40. https://doi.org/10.3390/molecules27010040.
- (158) Tanaka, K.; Chujo, Y. Unique Properties of Amphiphilic POSS and Their Applications. *Polym. J.* **2013**, *45* (3), 247–254. https://doi.org/10.1038/pj.2012.154.
- (159) Hossain, M. A.; Hursthouse, M. B.; Malik, K. M. A. Octa(Phenylsilasesquioxane) Acetone Solvate. *Acta Crystallogr. B: Struct. Sci. Cryst. Eng. Mater.* **1979**, *35* (9), 2258–2260. https://doi.org/10.1107/S0567740879008992.
- (160) Zhang, D.; Shi, Y.; Liu, Y.; Huang, G. Influences of Polyhedral Oligomeric Silsesquioxanes (POSSs) Containing Different Functional Groups on Crystallization and Melting Behaviors of POSS/Polydimethylsiloxane Rubber Composites. *RSC Adv.* **2014**, *4* (78), 41364–41370. https://doi.org/10.1039/c4ra07242a.
- (161) Bassindale, A. R.; Liu, Z.; MacKinnon, I. A.; Taylor, P. G.; Yang, Y.; Light, M. E.; Horton, P. N.; Hursthouse, M. B. A Higher Yielding Route for T₈ Silsesquioxane Cages and X-Ray Crystal Structures of Some Novel Spherosilicates. *Dalton Trans.* **2003**, *3* (14), 2945–2949. https://doi.org/10.1039/b302950f.
- (162) Imai, K.; Kaneko, Y. Preparation of Ammonium-Functionalized Polyhedral Oligomeric Silsesquioxanes with High Proportions of Cagelike Decamer and Their Facile Separation. *Inorg. Chem.* **2017**, *56* (7), 4133–4140. https://doi.org/10.1021/acs.inorgchem.7b00131.
- (163) Bagheri, H.; Soofi, G.; Javanmardi, H.; Karimi, M. A 3D Nanoscale Polyhedral Oligomeric Silsesquioxanes Network for Microextraction of Polycyclic Aromatic Hydrocarbons. *Microchim. Acta* **2018**, *185* (9), 418. https://doi.org/10.1007/s00604-018-2950-z.
- (164) Koželj, M.; Orel, B. Synthesis of Polyhedral Phenylsilsesquioxanes with KF as the Source of the Fluoride Ion. *Dalton Trans.* **2008**, 5072–5075. https://doi.org/10.1039/b804224a.
- (165) Calzaferri, G.; Marcolli, C.; Imhof, R.; Törnroos, K. W. The Monophenylhydrosilasesquioxanes PhH_{n-1}Si_nO_{1.5n} Where N= 8 or 10. *J. Chem. Soc., Dalton Trans.* **1996**, No. 15, 3313–3322.

- (166) Wang, X.-M.; Guo, Q.-Y.; Han, S.-Y.; Wang, J.-Y.; Han, D.; Fu, Q.; Zhang, W.-B. Stochastic/Controlled Symmetry Breaking of the T₈-POSS Cages toward Multifunctional Regioisomeric Nanobuilding Blocks. *Chem. Eur. J.* **2015**, *21* (43), 15246–15255. https://doi.org/10.1002/chem.201502125.
- (167) Sato, N.; Tochigi, K.; Kuroda, Y.; Wada, H.; Shimojima, A.; Kuroda, K. Synthesis and Crystal Structure of Double-Three Ring (D3R)-Type Cage Siloxanes Modified with Dimethylsilanol Groups. *Dalton Trans.* **2019**, *48* (6), 1969–1975. https://doi.org/10.1039/c8dt04244f.
- (168) Agaskar, P. A.; Klemperer, W. G. The Higher Hydridospherosiloxanes: Synthesis and Structures of $H_nSi_nO_{1.5n}$ (n = 12, 14, 16, 18). *Inorganica Chim. Acta* **1995**, *229* (1–2), 355–364. https://doi.org/10.1016/0020-1693(94)04266-X.
- (169) Rikowski, E.; Marsmann, H. C. Cage-Rearrangement of Silsesquioxanes. *Polyhedron* **1997**, *16* (19), 3357–3361. https://doi.org/10.1016/S0277-5387(97)00092-2.
- (170) Fasce, D. P.; Williams, R. J. J.; Méchin, F.; Pascault, J. P.; Llauro, M. F.; Pétiaud, R. Synthesis and Characterization of Polyhedral Silsesquioxanes Bearing Bulky Functionalized Substituents. *Macromolecules* **1999**, *32* (15), 4757–4763. https://doi.org/10.1021/ma981875p.
- (171) Haouas, M.; Falaise, C.; Martineau-Corcos, C.; Cadot, E. Cyclodextrin-Driven Formation of Double Six-Ring (D6R) Silicate Cage: NMR Spectroscopic Characterization from Solution to Crystals. *Crystals* **2018**, *8* (12), 457. https://doi.org/10.3390/cryst8120457.
- (172) Zhang, Z.-X.; Hao, J.; Xie, P.; Zhang, X.; Han, C. C.; Zhang, R. A Well-Defined Ladder Polyphenylsilsesquioxane (Ph-LPSQ) Synthesized via a New Three-Step Approach: Monomer Self-Organization-Lyophilization—Surface-Confined Polycondensation. *Chem. Mater.* **2008**, *20* (4), 1322–1330. https://doi.org/10.1021/cm071602l.
- (173) Seki, H.; Kajiwara, T.; Abe, Y.; Gunji, T. Synthesis and Structure of Ladder Polymethylsilsesquioxanes from Sila-Functionalized Cyclotetrasiloxanes. *J. Organomet. Chem.* **2010**, 695 (9), 1363–1369. https://doi.org/10.1016/j.jorganchem.2010.02.008.
- (174) Abe, Y.; Gunji, T. Oligo- and Polysiloxanes. *Prog. Polym. Sci.* **2004**, *29* (3), 149–182. https://doi.org/10.1016/j.progpolymsci.2003.08.003.
- (175) Koleżyński, A.; Jastrzkebski, W.; Szczypka, W.; Kowalewska, A.; Nowacka, M.; Sitarz, M. The Structure and Bonding Properties of Chosen Phenyl Ladder-like Silsesquioxane Clusters. *J. Mol. Struct.* **2013**, *1044*, 314–322. https://doi.org/10.1016/j.molstruc.2012.12.013.
- (176) Wang, R.; Rong, T.; Cao, G. S.; Jia, X. W.; Zhang, Z. P.; Rong, M. Z.; Zhang, M. Q. Synthesis and Synergetic Effects of Ladder-like Silsesquioxane/Epoxy Compositional Gradient Hybrid Coating. *Prog. Org. Coat.* **2019**, *130*, 58–65. https://doi.org/10.1016/j.porgcoat.2019.01.037.
- (177) Shang, X.; Cao, X.; Ma, Y.; Kumaravel, J. J.; Zheng, K.; Zhang, J.; Zhang, R. Diphenylsiloxane-Bridged Ladder-like Hydrido-Polysiloxane and the Derivatisation

- by Triphenylsiloxy Substitution. *Eur. Polym. J.* **2018**, *106*, 53–62. https://doi.org/10.1016/j.eurpolymj.2018.07.006.
- (178) Park, S.; Kim, J.-Y.; Choi, W.; Lee, M.-J.; Heo, J.; Choi, D.; Jung, S.; Kwon, J.; Choi, S.-H.; Hong, J. Ladder-like Polysilsesquioxanes with Antibacterial Chains and Durable Siloxane Networks. *Chem. Eng. J.* **2020**, 393, 124686. https://doi.org/10.1016/j.cej.2020.124686.
- (179) Zhou, Q.; Yan, S.; Han, C. C.; Xie, P.; Zhang, R. Promising Functional Materials Based on Ladder Polysiloxanes. *Adv. Mater.* **2008**, *20* (15), 2970–2976. https://doi.org/10.1002/adma.200800580.
- (180) Ostanin, S. A.; Kalinin, A. V; Bratsyhin, Y. Y.; Saprykina, N. N.; Zuev, V. V. Linear/Ladder-like Polysiloxane Block Copolymers with Methyl-, Trifluoropropyland Phenyl-Siloxane Units for Surface Modification. *Polymers* **2021**, *13* (13), 2063. https://doi.org/10.3390/polym13132063.
- (181) Unno, M.; Suto, A.; Matsumoto, H. Pentacyclic Laddersiloxane. *J. Am. Chem. Soc.* **2002**, *124* (8), 1574–1575. https://doi.org/10.1021/ja0173876.
- (182) Choi, S.-S.; Lee, A. S.; Hwang, S. S.; Baek, K.-Y. Structural Control of Fully Condensed Polysilsesquioxanes: Ladderlike vs Cage Structured Polyphenylsilsesquioxanes. *Macromolecules* **2015**, *48* (17), 6063–6070. https://doi.org/10.1021/acs.macromol.5b01539.
- (183) Klein, L. C.; Jitianu, A. Organic-Inorganic Hybrid Melting Gels. *J. Sol-Gel Sci. Technol.* **2010**, *55*, 86–93. https://doi.org/10.1007/s10971-010-2219-4.
- (184) Jitianu, A.; Amatucci, G.; Klein, L. C. Phenyl-Substituted Siloxane Hybrid Gels That Soften below 140°C. *J. Am. Ceram. Soc.* **2009**, 92 (1), 36–40. https://doi.org/10.1111/j.1551-2916.2008.02841.x.
- (185) Katagiri, K.; Hasegawa, K.; Matsuda, A.; Tatsumisago, M.; Minami, T. Preparation of Transparent Thick Films by Electrophoretic Sol Gel Deposition Using Phenyltriethoxysilane-Derived Particles. *J. Am. Ceram. Soc.* **1998**, *81* (9), 2501–2503. https://doi.org/10.1111/j.1151-2916.1998.tb02653.x.
- (186) Matsuda, A.; Sasaki, T.; Hasegawa, K.; Tatsumisago, M.; Minami, T. Thermal Softening Behavior and Application to Transparent Thick Films of Poly(Benzylsilsesquioxane) Particles Prepared by the Sol-Gel Process. *J. Am. Ceram. Soc.* **2001**, *84* (4), 775–780. https://doi.org/10.1111/j.1151-2916.2001.tb00740.x.
- (187) Jitianu, A.; Doyle, J.; Amatucci, G.; Klein, L. C. Methyl Modified Siloxane Melting Gels for Hydrophobic Films. *J. Sol-Gel Sci. Technol.* **2010**, 53, 272–279. https://doi.org/10.1007/s10971-009-2087-y.
- (188) Kakiuchida, H.; Takahashi, M.; Tokuda, Y.; Masai, H.; Kuniyoshi, M.; Yoko, T. Viscoelastic and Structural Properties of a Phenyl-Modified Polysiloxane System with a Three-Dimensional Structure. *J. Phys. Chem. B* **2006**, *110* (14), 7321–7327. https://doi.org/10.1021/jp0573543.
- (189) Masai, H.; Takahashi, M.; Tokuda, Y.; Yoko, T. Gel-Melting Method for Preparation

- of Organically Modified Siloxane Low-Melting Glasses. *J. Mater. Res.* **2005**, *20*, 1234–1241. https://doi.org/10.1557/JMR.2005.0151.
- (190) Tong, L.; Feng, Y.; Sun, X.; Han, Y.; Jiao, D.; Tan, X. High Refractive Index Adamantane-Based Silicone Resins for the Encapsulation of Light-Emitting Diodes. *Polym. Adv. Technol.* **2018**, 29 (8), 2245–2252. https://doi.org/10.1002/pat.4335.
- (191) Meier, D.; Huch, V.; Kickelbick, G. Aryl-Group Substituted Polysiloxanes with High-Optical Transmission, Thermal Stability, and Refractive Index. *J. Polym. Sci.* **2021**, 59 (20), 2265–2283. https://doi.org/10.1002/pol.20210316.
- (192) Ganesan, P.; Van Lagen, B.; Marcelis, A. T. M.; Sudhölter, E. J. R.; Zuilhof, H. Siloxanes with Pendent Naphthalene Diimides: Synthesis and Fluorescence Quenching. *Org. Lett.* **2007**, *9* (12), 2297–2300. https://doi.org/10.1021/ol070562o.
- (193) Zhang, W.; Wang, X.; Wu, Y.; Qi, Z.; Yang, R. Preparation and Characterization of Organic-Inorganic Hybrid Macrocyclic Compounds: Cyclic Ladder-like Polyphenylsilsesquioxanes. *Inorg. Chem.* **2018**, *57* (7), 3883–3892. https://doi.org/10.1021/acs.inorgchem.7b03264.
- (194) Zhao, Y.; Xu, L.; He, Y.; Feng, Z.; Feng, W.; Yan, H. Nonconventional Aggregation-Induced Emission Polysiloxanes: Structures, Characteristics, and Applications. *Aggregate*. **2024**, *5* (2), e471. https://doi.org/10.1002/agt2.471.
- (195) Issa, A. A.; Luyt, A. S. Kinetics of Alkoxysilanes and Organoalkoxysilanes Polymerization: A Review. *Polymers* **2019**, *11* (3), 537. https://doi.org/10.3390/polym11030537.
- (196) Zhan, X.; Liu, H.; Zhang, J.; Cheng, J.; Lin, X. Comparative Study of Silicone Resin Cured with a Linear and a Branched Cross-Linking Agent. *Ind. Eng. Chem. Res.* **2014**, 53 (11), 4254–4262. https://doi.org/10.1021/ie403010s.
- (197) Zhan, X.; Zhang, J.; Cheng, J.; Shi, L.; Lin, X. Synthesis, Characterization, and Cure Kinetics Analysis of High Refractive Index Copolysiloxanes. *J. Therm. Anal. Calorim.* **2014**, *117* (2), 875–883. https://doi.org/10.1007/s10973-014-3780-9.
- (198) Hook, R. J. A ²⁹Si NMR Study of the Sol-Gel Polymerisation Rates of Substituted Ethoxysilanes. *J. Non-Cryst. Solids* **1996**, 195 (1–2), 1–15. https://doi.org/10.1016/0022-3093(95)00508-0.
- (199) Cella, J. A.; Cargioli, J. D.; Williams, E. A. ²⁹Si NMR OF FIVE- AND SIX-COORDINATE ORGANOSILICON COMPLEXES. *J. Organomet. Chem.* **1980**, *18*6, 13–17. https://doi.org/10.1016/S0022-328X(00)93813-0.
- (200) Fyfe, C. A.; Aroca, P. P. Quantitative Kinetic Analysis by High-Resolution ²⁹Si NMR Spectroscopy of the Initial Stages in the Sol-Gel Formation of Silica Gel from Tetraethoxysilane. *Chem. Mater.* **1995**, *7*, 1800–1806.
- (201) Pouxviel, J. C.; Boilot, J. P.; Beloeil, J. C.; Lallemand, J. Y. NMR Study of the Sol/Gel Polymerization. *J. Non-Cryst. Solids* **1987**, 89 (3), 345–360. https://doi.org/10.1016/S0022-3093(87)80277-6.
- (202) Mazúr, M.; Mlynárik, V.; Valko, M.; Pelikán, P. The Time Evolution of the Sol-Gel

- Process: ²⁹Si NMR Study of the Hydrolysis and Condensation Reactions of Tetraethoxysilane. *Appl. Magn. Reson.* **2000**, *18*, 187–197. https://doi.org/10.1007/BF03162110.
- (203) Depla, A.; Lesthaeghe, D.; van Erp, T. S.; Aerts, A.; Houthoofd, K.; Fan, F.; Li, C.; Van Speybroeck, V.; Waroquier, M.; Kirschhock, C. E. A.; others. ²⁹Si NMR and UV-Raman Investigation of Initial Oligomerization Reaction Pathways in Acid-Catalyzed Silica Sol-Gel Chemistry. *J. Phys. Chem. C* **2011**, *115* (9), 3562–3571. https://doi.org/10.1021/jp109901v.
- (204) Bernards, T. N. M.; Van Bommel, M. J.; Boonstra, A. H. Hydrolysis-Condensation Processes of the Tetra-Alkoxysilanes TPOS, TEOS and TMOS in Some Alcoholic Solvents. *J. Non-Cryst. Solids* **1991**, *134* (1–2), 1–13. https://doi.org/10.1016/0022-3093(91)90005-Q.
- (205) Hunter, B. K.; Reeves, L. W. Chemical Shifts for Compounds of the Group IV Elements Silicon and Tin. *Can. J. Chem.* **1968**, *46* (8), 1399–1414. https://doi.org/10.1139/v68-229.
- (206) Oberhammer, H.; Boggs, J. E. Importance of $(p-d)\pi$ Bonding in the Siloxane Bond. J. Am. Chem. Soc. **1980**, 102, 7241–7244.
- (207) Beckmann, J.; Dakternieks, D.; Duthie, A.; Larchin, M. L.; Tiekink, E. R. T. Tert-Butoxysilanols as Model Compounds for Labile Key Intermediates of the Sol-Gel Process: Crystal and Molecular Structures of (t-BuO)₃SiOH and HO[(t-BuO)₂SiO]₂H. *Appl. Organometal. Chem.* **2003**, *17* (1), 52–62. https://doi.org/10.1002/aoc.380.
- (208) Janeta, M.; John, Ł.; Ejfler, J.; Szafert, S. Novel Organic-Inorganic Hybrids Based on T₈ and T₁₀ Silsesquioxanes: Synthesis, Cage-Rearrangement and Properties. *RSC Adv.* **2015**, *5* (88), 72340–72351. https://doi.org/10.1039/c5ra10136k.
- (209) Bassindale, A. R.; Pannell, K. H. Molecular Motion in Cyclic Siloxanes Studied by ¹⁷O, ²⁹Si, and ¹³C Nuclear Magnetic Resonance Spectroscopy. *J. Chem. Soc., Perkin Trans. 2* **1990**, No. 11, 1801–1804. https://doi.org/10.1039/P29900001801.
- (210) Criado, M.; Sobrados, I.; Sanz, J. Polysiloxane Hybrids via Sol-Gel Process: Effect of Temperature on Network Formation. *Coatings* **2020**, *10* (7), 677. https://doi.org/10.3390/coatings10070677.
- (211) Schmid, N.; Bruderer, S.; Paruzzo, F.; Fischetti, G.; Toscano, G.; Graf, D.; Fey, M.; Henrici, A.; Ziebart, V.; Heitmann, B.; others. Deconvolution of 1D NMR Spectra: A Deep Learning-Based Approach. *J. Magn. Reson.* **2023**, *347*, 107357. https://doi.org/10.1016/j.jmr.2022.107357.
- (212) Murray, D. K. Differentiating and Characterizing Geminal Silanols in Silicas by ²⁹Si NMR Spectroscopy. *J. Colloid. Interface Sci.* **2010**, *352* (1), 163–170. https://doi.org/10.1016/j.jcis.2010.08.045.
- (213) Cabrera, Y.; Cabrera, A.; Larsen, F. H.; Felby, C. Solid-State ²⁹Si NMR and FTIR Analyses of Lignin-Silica Coprecipitates. *Holzforschung* **2016**, *70* (8), 709–718. https://doi.org/10.1515/hf-2015-0165.
- (214) Jitianu, A.; Cadars, S.; Zhang, F.; Rodriguez, G.; Picard, Q.; Aparicio, M.; Mosa, J.;

- Klein, L. C. ²⁹Si NMR and SAXS Investigation of the Hybrid Organic-Inorganic Glasses Obtained by Consolidation of the Melting Gels. *Dalton Trans.* **2017**, *46* (11), 3729–3741. https://doi.org/10.1039/c6dt04394a.
- (215) Gong, S.; Epasinghe, D. J.; Zhang, W.; Zhou, B.; Niu, L.; Ryou, H.; Eid, A. A.; Frassetto, A.; Yiu, C. K. Y.; Arola, D. D.; others. Synthesis of Antimicrobial Silsesquioxane-Silica Hybrids by Hydrolytic Co-Condensation of Alkoxysilanes. *Polym. Chem.* **2014**, *5* (2), 454–462. https://doi.org/10.1039/c3py00635b.
- (216) Protsak, I. S.; Morozov, Y. M.; Dong, W.; Le, Z.; Zhang, D.; Henderson, I. M. A ²⁹Si, ¹H, and ¹³C Solid-State NMR Study on the Surface Species of Various Depolymerized Organosiloxanes at Silica Surface. *Nanoscale Res. Lett.* **2019**, *14* (160), 1–15. https://doi.org/10.1186/s11671-019-2982-2.
- (217) Romeo, H. E.; Fanovich, M. A.; Williams, R. J. J.; Matějka, L.; Pleštil, J.; Brus, J. Self-Assembly of a Bridged Silsesquioxane Containing a Pendant Hydrophobic Chain in the Organic Bridge. *Macromolecules* **2007**, *40* (5), 1435–1443. https://doi.org/10.1021/ma062091b.
- (218) Sawvel, A. M.; Crowhurst, J. C.; Mason, H. E.; Oakdale, J. S.; Ruelas, S.; Eshelman, H. V; Maxwell, R. S. Spectroscopic Signatures of MQ-Resins in Silicone Elastomers. *Macromolecules* **2021**, *54* (9), 4300–4312. https://doi.org/10.1021/acs.macromol.1c00086.
- (219) Vasil'ev, S. G.; Volkov, V. I.; Tatarinova, E. A.; Muzafarov, A. M. A Solid-State NMR Investigation of MQ Silicone Copolymers. *Appl. Magn. Reson.* **2013**, *44*, 1015–1025. https://doi.org/10.1007/s00723-013-0456-8.
- (220) Engelhardt, G.; Jancke, H.; Lippmaa, E.; Samoson, A. Structure Investigations of Solid Organosilicon Polymers by High Resolution Solid State ²⁹Si NMR. *J. Organomet. Chem.* **1981**, *210* (3), 295–301. https://doi.org/10.1016/S0022-328X(00)80888-8.
- (221) Metz, G.; Ziliox, M.; Smith, S. O. Towards Quantitative CP-MAS NMR. *Solid State Nucl. Magn. Reson.* **1996**, *7* (3), 155–160. https://doi.org/10.1016/S0926-2040(96)01257-X.
- (222) Fyfe, C. A.; Gobbi, G. C.; Kennedy, G. J. Quantitatively Reliable Silicon-29 Magic-Angle Spinning Nuclear Magnetic Resonance Spectra of Surfaces and Surface-Immobilized Species at High Field Using a Conventional High-Resolution Spectrometer. *J. Phys. Chem.* **1985**, 89 (2), 277–281.
- (223) Zhao, X. S.; Lu, G. Q.; Whittaker, A. K.; Millar, G. J.; Zhu, H. Y. Comprehensive Study of Surface Chemistry of MCM-41 Using ²⁹Si CP/MAS NMR, FTIR, Pyridine-TPD, and TGA. *J. Phys. Chem. B.* **1997**, 101 (33), 6525–6531. https://doi.org/10.1021/jp971366+.
- (224) Hilbig, H.; Köhler, F. H.; Schießl, P. Quantitative ²⁹Si MAS NMR Spectroscopy of Cement and Silica Fume Containing Paramagnetic Impurities. *Cem. Concr. Res.* **2006**, 36 (2), 326–329. https://doi.org/10.1016/j.cemconres.2005.03.017.
- (225) Pan, Z.; Zhu, S.; Huang, B.; Kang, Y.; Zhu, L. Synthesis of High-Refractive-Index Epoxy-Modified Vinyl Methyl Phenyl Silicone Resins for Encapsulation of LEDs. J.

- Electron. Mater. **2019**, 48, 2865–2875. https://doi.org/10.1007/s11664-019-07015-x.
- (226) Yang, X.; Shao, Q.; Yang, L.; Zhu, X.; Hua, X.; Zheng, Q.; Song, G.; Lai, G. Preparation and Performance of High Refractive Index Silicone Resin-Type Materials for the Packaging of Light-Emitting Diodes. *J. Appl. Polym. Sci.* **2013**, *127* (3), 1717–1724. https://doi.org/10.1002/app.37897.
- (227) Chen, X.; Eldred, D.; Liu, J.; Chiang, H.; Wang, X.; Rickard, M. A.; Tu, S.; Cui, L.; LaBeaume, P.; Skinner, K. Simultaneous In Situ Monitoring of Trimethoxysilane Hydrolysis Reactions Using Raman, Infrared, and Nuclear Magnetic Resonance (NMR) Spectroscopy Aided by Chemometrics and Ab Initio Calculations. *Appl. Spectrosc.* **2018**, *72* (9), 1404–1415. https://doi.org/10.1177/0003702818774570.
- (228) Loy, D. A.; Carpenter, J. P.; Alam, T. M.; Shaltout, R.; Dorhout, P. K.; Greaves, J.; Small, J. H.; Shea, K. J. Cyclization Phenomena in the Sol-Gel Polymerization of α,ω-Bis(Triethoxysilyl)Alkanes and Incorporation of the Cyclic Structures into Network Silsesquioxane Polymers. *J. Am. Chem. Soc.* **1999**, *121* (23), 5413–5425. https://doi.org/10.1021/ja982751v.
- (229) Grill, A.; Neumayer, D. A. Structure of Low Dielectric Constant to Extreme Low Dielectric Constant SiCOH Films: Fourier Transform Infrared Spectroscopy Characterization. *J. Appl. Phys.* **2003**, *94* (10), 6697–6707. https://doi.org/10.1063/1.1618358.
- (230) Ueda, N.; Gunji, T.; Abe, Y. Syntheses of Linear Ethoxysiloxanes by the Oxidative Condensation of Triethoxysilane. *J. Sol-Gel Sci. Technol.* **2008**, *48*, 163–167. https://doi.org/10.1007/s10971-008-1808-y.
- (231) Laird, M.; Herrmann, N.; Ramsahye, N.; Totée, C.; Carcel, C.; Unno, M.; Bartlett, J. R.; Wong Chi Man, M. Large Polyhedral Oligomeric Silsesquioxane Cages: The Isolation of Functionalized POSS with an Unprecedented Si₁₈O₂₇ Core. *Angew. Chem. Int. Ed.* **2021**, 60 (6), 3022–3027. https://doi.org/10.1002/anie.202010458.
- (232) Qin, Z.-L.; Yang, R.-J.; Zhang, W.-C.; Jiao, Q.-J. Mechanistic Insights into the Synthesis of Fully Condensed Polyhedral Octaphenylsilsesquioxane. *Chin. J. Chem.* **2019**, *37* (10), 1051–1056. https://doi.org/10.1002/cjoc.201900170.
- (233) Frye, C. L.; Collins, W. T. The Oligomeric Silsesquioxanes, (HSiO_{3/2})_N. *J. Am. Chem.* Soc. **1970**, 92 (19), 5586–5588.
- (234) Park, E. S.; Ro, H. W.; Nguyen, C. V.; Jaffe, R. L.; Yoon, D. Y. Infrared Spectroscopy Study of Microstructures of Poly(Silsesquioxane)S. *Chem. Mater.* **2008**, *20* (4), 1548–1554. https://doi.org/10.1021/cm071575z.
- (235) Yoshino, H.; Kamiya, K.; Nasu, H. IR Study on the Structural Evolution of Sol-Gel Derived SiO₂ Gels in the Early Stage of Conversion to Glasses. *J. Non-Cryst. Solids* **1990**, *126* (1–2), 68–78. https://doi.org/10.1016/0022-3093(90)91024-L.
- (236) Capozzi, C. A.; Pye, L. D.; Condrate Sr, R. A. Vibrational Spectral/Structural Changes from the Hydrolysis/Polycondensation of Methyl-Modified Silicates. I. Comparisons for Single Monomer Condensates. *Mater. Lett.* **1992**, *15* (1–2), 130–136. https://doi.org/10.1016/0167-577X(92)90028-I.

- (237) Kamiya, K.; Yoko, T.; Tanaka, K.; Takeuchi, M. Thermal Evolution of Gels Derived from $CH_3Si(OC_2H_5)_3$ by the Sol-Gel Method. *J. Non-Cryst. Solids* **1990**, *121* (1–3), 182–187. https://doi.org/10.1016/0022-3093(90)90128-9.
- (238) Dumitriu, A.-M.-C.; Cazacu, M.; Bargan, A.; Balan, M.; Vornicu, N.; Varganici, C.-D.; Shova, S. Full Functionalized Silica Nanostructure with Well-Defined Size and Functionality: Octakis(3-Mercaptopropyl)Octasilsesquioxane. *J. Organomet. Chem.* 2015, 799–800, 195–200. https://doi.org/10.1016/j.jorganchem.2015.09.025.
- (239) Kowalewska, A.; Nowacka, M.; Maniukiewicz, W. Octa(3-Mercaptopropyl)Octasilsesquioxane A Reactive Nanocube of Unique Self-Assembled Packing Morphology. *J. Organomet. Chem.* **2016**, *810*, 15–24. https://doi.org/10.1016/j.jorganchem.2016.02.040.
- (240) Warring, S. L.; Beattie, D. A.; McQuillan, A. J. Surficial Siloxane-to-Silanol Interconversion during Room-Temperature Hydration/Dehydration of Amorphous Silica Films Observed by ATR-IR and TIR-Raman Spectroscopy. *Langmuir* **2016**, *32* (6), 1568–1576. https://doi.org/10.1021/acs.langmuir.5b04506.
- (241) Davis, K. M.; Tomozawa, M. An Infrared Spectroscopic Study of Water-Related Species in Silica Glasses. *J. Non-Cryst. Solids* **1996**, *201* (3), 177–198. https://doi.org/10.1016/0022-3093(95)00631-1.
- (242) Mori, T.; Kuroda, Y.; Yoshikawa, Y.; Nagao, M.; Kittaka, S. Preparation of a Water-Resistant Siliceous MCM-41 Sample, through Improvement of Crystallinity, and Its Prominent Adsorption Features. *Langmuir* **2002**, *18* (5), 1595–1603. https://doi.org/10.1021/la011019y.
- (243) Liu, F.; Zeng, X.; Lai, X.; Li, H. Synthesis and Characterization of Polyphenylsilsesquioxane Terminated with Methyl and Vinyl Groups Low-Melting Glass. *J. Adhes. Sci. Technol.* **2017**, *31* (22), 2399–2409. https://doi.org/10.1080/01694243.2017.1302699.
- (244) Crowe-Willoughby, J. A.; Weiger, K. L.; Özçam, A. E.; Genzer, J. Formation of Silicone Elastomer Networks Films with Gradients in Modulus. *Polymer* **2010**, *51* (3), 763–773. https://doi.org/10.1016/j.polymer.2009.11.070.
- (245) Kargarfard, N.; Simon, F.; Schlenstedt, K.; Ulischberger, L.; Voit, B.; Gedan-Smolka, M.; Zimmerer, C. Self-Stratifying Powder Coatings Based on Eco-Friendly, Solvent-Free Epoxy/Silicone Technology for Simultaneous Corrosion and Weather Protection. *Prog. Org. Coat.* **2021**, *161*, 106443. https://doi.org/10.1016/j.porgcoat.2021.106443.
- (246) Jurásková, A.; Dam-Johansen, K.; Olsen, S. M.; Skov, A. L. Factors Influencing Mechanical Long-Term Stability of Condensation Curing Silicone Elastomers. *J. Polym. Res.* **2020**, *27* (341). https://doi.org/10.1007/s10965-020-02272-5.
- (247) Wu, Y.; Liu, J.; Cheng, F.; Jiao, X.; Fan, Y.; Lai, G.; Luo, M.; Yang, X. Fabrication of Transparent UV-Cured Coatings with Allyl-Terminated Hyperbranched Polycarbosilanes and Thiol Silicone Resins. *ACS Omega* **2020**, *5* (25), 15311–15316. https://doi.org/10.1021/acsomega.0c01338.

- (248) Li, H.; Ai, J.; Wang, C.; Nie, X.; Liu, B.; Liu, J.; Zhao, Z. Synthesis and Properties of Silicone-Epoxy Polymer with Long Silicone Chain. *J. Appl. Polym. Sci.* **2023**, *140* (25), e53971. https://doi.org/10.1002/app.53971.
- (249) Kuo, C.-F. J.; Chen, J.-B. Study on the Synthesis and Application of Silicone Resin Containing Phenyl Group. *J. Sol-Gel Sci. Technol.* **2015**, *76*, 66–73. https://doi.org/10.1007/s10971-015-3752-y.
- (250) He, X. W.; Widmaier, J. M.; Herz, J. E.; Meyer, G. C. Competition between Polycondensation of α,ω-Dihydroxy Polydimethylsiloxane and Its Condensation with Alkoxy Silane: A Kinetic Approach. *Eur. Polym. J.* **1988**, *24* (12), 1145–1148.
- (251) Chan-Park, M. B.; Katsoulis, D. E.; Baney, R. H. Characterization of a Rigid Silicone Resin. *Polym. Compos.* **2003**, *24* (1), 13–23. https://doi.org/10.1002/pc.10001.
- (252) Nair, S.; Aswathy, U. V; Mathew, A.; Raghavan, R. Studies on the Thermal Properties of Silicone Polymer Based Thermal Protection Systems for Space Applications. *J. Therm. Anal. Calorim.* **2017**, *128*, 1731–1741. https://doi.org/10.1007/s10973-016-6025-2.
- (253) Qian, H.; Jiang, B. Silicone Resin Applications for Heat-Resistant Coatings: A Review. *Polym. Sci. Ser. C* **2023**, 65, 206–219. https://doi.org/10.1134/S1811238223700443.
- (254) Koh, K.; Sohn, H. Fast Curable Polysiloxane-Silphenylene Hybrimer with High Transparency and Refractive Index for Optical Applications. *Polymers* **2021**, *13* (4), 515. https://doi.org/10.3390/polym13040515.
- (255) Chen, M.; Zhang, G.; Liang, X.; Zhang, W.; Zhou, L.; He, B.; Song, P.; Yuan, X.; Zhang, C.; Zhang, L.; Yu, H.; Yang, H. Thermally Stable Transparent Sol-Gel Based Active Siloxane-Oligomer Materials with Tunable High Refractive Index and Dual Reactive Groups. *RSC Adv.* **2016**, 6 (75), 70825–70831. https://doi.org/10.1039/c6ra13164f.
- (256) Kim, J.-S.; Yang, S.; Bae, B.-S. Thermally Stable Transparent Sol Gel Based Siloxane Hybrid Material with High Refractive Index for Light Emitting Diode (LED) Encapsulation. *Chem. Mater.* **2010**, *22* (11), 3549–3555. https://doi.org/10.1021/cm100903b.
- (257) Zhang, H.; Yan, Z.; Yang, Z.; Yao, J.; Mu, Q.; Peng, D.; Zhao, H. Study on the Synthesis and Thermal Stability of Silicone Resins Reinforced by Si-O-Ph Cross-Linking. *RSC Adv.* **2021**, *11* (49), 30971–30979. https://doi.org/10.1039/d1ra05524k.
- (258) Klein, L. C.; McClarren, B.; Jitianu, A. Silica-Containing Hybrid Nanocomposite "Melting Gels." *Mater. Sci. Forum* **2014**, *783–786*, 1432–1437. https://doi.org/10.4028/www.scientific.net/msf.783-786.1432.
- (259) Chang, L.-B.; Pan, K.-W.; Yen, C.-Y.; Jeng, M.-J.; Wu, C.-T.; Hu, S.-C.; Kuo, Y.-K. Comparison of Silicone and Spin-on Glass Packaging Materials for Light-Emitting Diode Encapsulation. *Thin Solid Films* **2014**, *570* (Part B), 496–499. https://doi.org/10.1016/j.tsf.2014.03.033.
- (260) Antosik, A. K.; Bednarczyk, P.; Czech, Z. Aging of Silicone Pressure-Sensitive

- Adhesives. *Polym. Bull.* **2018**, *75*, 1141–1147. https://doi.org/10.1007/s00289-017-2083-2.
- (261) Kim, J.-S.; Yang, S. C.; Kwak, S.-Y.; Choi, Y.; Paik, K.-W.; Bae, B.-S. High Performance Encapsulant for Light-Emitting Diodes (LEDs) by a Sol-Gel Derived Hydrogen Siloxane Hybrid. *J. Mater. Chem.* **2012**, *22* (16), 7954–7960. https://doi.org/10.1039/c2jm16907j.
- (262) Lee, S.-A.; Kim, Y. J. Novel Silicone Laminating Materials for Improved Index Matching in Automotive Display Applications. *J. Soc. Inf. Disp.* **2021**, *29* (8), 608–619. https://doi.org/10.1002/jsid.1003.
- (263) Ke, Q.; Dai, Z.; Chen, X. Fluorosilicone Resin as a High Ultraviolet Transmittance Optical Material. *J. Appl. Polym. Sci.* **2020**, *137* (37), 49102. https://doi.org/10.1002/app.49102.
- (264) Wu, Y.; Liu, J.; Jiao, X.; Cheng, F.; Lai, G.; Yang, X. UV-Cured Transparent Flexible Silicone Materials with High Tensile Strength. *ACS Omega* **2020**, *5* (11), 6199–6206. https://doi.org/10.1021/acsomega.0c00401.
- (265) Liu, J.; He, N.; Shen, J.; Gong, Z.; Fan, Y.; Li, M.; Song, Y.; Yang, X. UV Cured Silicon-Containing Polyurethane-Acrylate Coatings with Non-Traditional Fluorescence and Temperature-Sensitive Transparency. *Prog. Org. Coat.* **2021**, *161*, 106513. https://doi.org/10.1016/j.porgcoat.2021.106513.
- (266) Chen, H.; Wang, Y.; Lin, J.; Shuai, M.; Zhu, H.; Zhang, W.; Ling, Q. Transparent Red-Emitting Silicone Resin for Color Conversion and Encapsulation of NUV Light-Emitting Diodes. *J. Am. Ceram. Soc.* **2019**, *102* (5), 2718–2726. https://doi.org/10.1111/jace.16140.
- (267) Wu, J.; Xin, W.; Wu, Y.; Zhan, Y.; Li, J.; Wang, J.; Huang, S.; Wang, X. Solid-State Photoluminescent Silicone-Carbon Dots/Dendrimer Composites for Highly Efficient Luminescent Solar Concentrators. *Chem. Eng. J.* **2021**, *422*, 130158. https://doi.org/10.1016/j.cej.2021.130158.
- (268) Reis, J. C. R.; Lampreia, I. M. S.; Santos, Â. F. S.; Moita, M. L. C. J.; Douhéret, G. Refractive Index of Liquid Mixtures: Theory and Experiment. *ChemPhysChem* **2010**, 11 (17), 3722–3733. https://doi.org/10.1002/cphc.201000566.
- (269) Tan, C. Z. Dependence of the Refractive Index on Density, Temperature, and the Wavelength of the Incident Light. *Eur. Phys. J. B* **2021**, 94, 139. https://doi.org/10.1140/epjb/s10051-021-00147-2.
- (270) Thormählen, I.; Straub, J.; Grigull, U. Refractive Index of Water and Its Dependence on Wavelength, Temperature, and Density. *J. Phys. Chem. Ref. data* **1985**, *14* (4), 933–945. https://doi.org/10.1063/1.555743.
- (271) Jellison Jr, G. E.; Burke, H. H. The Temperature Dependence of the Refractive Index of Silicon at Elevated Temperatures at Several Laser Wavelengths. *J. Appl. Phys.* **1986**, 60 (2), 841–843. https://doi.org/10.1063/1.337386.
- (272) Tan, C. Z.; Arndt, J. Temperature Dependence of Refractive Index of Glassy SiO₂ in the Infrared Wavelength Range. J. Phys. Chem. Solids 2000, 61 (8), 1315–1320.

- https://doi.org/10.1016/S0022-3697(99)00411-4.
- (273) Kohjiya, S.; Maeda, K.; Yamashita, S.; Shibata, Y. Chemical Modification of Silicone Elastomers for Optics. *J. Mater. Sci.* **1990**, *25*, 3368–3374. https://doi.org/10.1007/BF00587699.
- (274) Zhuo, Y.; Li, H.; Xu, X.; Chen, M.; Xiong, D.; Long, Y.; Chen, S.; Li, R.; Liu, Z. Enhanced Luminous Efficiency of Multilayer Gradient Refractive Index Phosphor in P₂O₅-ZnO-B₂O₃-BaO Glass for White Light-Emitting Diode Packages. *J. Non-Cryst. Solids* **2017**, *471*, 215–221. https://doi.org/10.1016/j.jnoncrysol.2017.05.042.
- (275) Xu, X.; Li, H.; Zhuo, Y.; Li, R.; Tian, P.; Xiong, D.; Chen, M. High Refractive Index Coating of Phosphor-in-Glass for Enhanced Light Extraction Efficiency of White LEDs. *J. Mater. Sci.* **2018**, *53*, 1335–1345. https://doi.org/10.1007/s10853-017-1571-y.
- (276) Lee, S.; Shin, H.-J.; Yoon, S.-M.; Yi, D. K.; Choi, J.-Y.; Paik, U. Refractive Index Engineering of Transparent ZrO₂- Polydimethylsiloxane Nanocomposites. *J. Mater. Chem.* **2008**, *18* (15), 1751–1755. https://doi.org/10.1039/b715338d.
- (277) Chen, X.; Fang, L.; Wang, J.; He, F.; Chen, X.; Wang, Y.; Zhou, J.; Tao, Y.; Sun, J.; Fang, Q. Intrinsic High Refractive Index Siloxane-Sulfide Polymer Networks Having High Thermostability and Transmittance via Thiol-Ene Cross-Linking Reaction. *Macromolecules* 2018, 51 (19), 7567–7573. https://doi.org/10.1021/acs.macromol.8b01586.
- (278) Lee, L.-H.; Chen, W.-C. High-Refractive-Index Thin Films Prepared from Trialkoxysilane-Capped Poly(Methylmethacrylate) Titania Materials. *Chem. Mater.* **2001**, *13* (3), 1137–1142. https://doi.org/10.1021/cm000937z.
- (279) Matsuda, T.; Funae, Y.; Yoshida, M.; Yamamoto, T.; Takaya, T. Optical Material of High Refractive Index Resin Composed of Sulfur-Containing Aliphatic and Alicyclic Methacrylates. *J. Appl. Polym. Sci.* **2000**, *76* (1), 45–49. https://doi.org/10.1002/(SICI)1097-4628(20000404)76:1<45::AID-APP6>3.0.CO;2-M.
- (280) Macdonald, E. K.; Shaver, M. P. Intrinsic High Refractive Index Polymers. *Polym. Int.* **2015**, *64*, 6–14. https://doi.org/10.1002/pi.4821.
- (281) Ramachandran, S.; Cohen, D. A.; Quist, A. P.; Lal, R. High Performance, LED Powered, Waveguide Based Total Internal Reflection Microscopy. *Sci. Rep.* **2013**, 3. https://doi.org/10.1038/srep02133.
- (282) Yang, J. S.; Park, J.-H.; O, B.-H.; Park, S.-G.; Lee, S. G. Design Method for a Total Internal Reflection LED Lens with Double Freeform Surfaces for Narrow and Uniform Illumination. *J. Opt. Soc. Korea* **2016**, *20* (5), 614–622. https://doi.org/10.3807/JOSK.2016.20.5.614.
- (283) Chang, M.-H.; Das, D.; Varde, P. V; Pecht, M. Light Emitting Diodes Reliability Review. *Microelectron. Reliab.* **2012**, 52 (5), 762–782. https://doi.org/10.1016/j.microrel.2011.07.063.
- (284) Mont, F. W.; Kim, J. K.; Schubert, M. F.; Schubert, E. F.; Siegel, R. W. High-

- Refractive-Index TiO₂-Nanoparticle-Loaded Encapsulants for Light-Emitting Diodes. *J. Appl. Phys.* **2008**, *103* (8), 083120. https://doi.org/10.1063/1.2903484.
- (285) Das, S.; Lenka, T. R.; Talukdar, F. A.; Velpula, R. T.; Nguyen, H. P. T. Design and Analysis of Novel High-Performance III-Nitride MQW-Based Nanowire White-LED Using HfO2/SiO2 Encapsulation. *Opt. Quant. Electron.* **2023**, *55*, 67. https://doi.org/10.1007/s11082-022-04350-y.
- (286) Allen, S. C.; Steckl, A. J. A Nearly Ideal Phosphor-Converted White Light-Emitting Diode. *Appl. Phys. Lett.* **2008**, *92* (14), 143309. https://doi.org/10.1063/1.2901378.
- (287) Badur, T.; Dams, C.; Hampp, N. High Refractive Index Polymers by Design. *Macromolecules* **2018**, *51* (11), 4220–4228. https://doi.org/10.1021/acs.macromol.8b00615.
- (288) Huang, J.-H.; Li, C.-P.; Chang-Jian, C.-W.; Lee, K.-C.; Huang, J.-H. Preparation and Characterization of High Refractive Index Silicone/TiO₂ Nanocomposites for LED Encapsulants. *J. Taiwan Inst. Chem. Eng.* **2015**, *46*, 168–175. https://doi.org/10.1016/j.jtice.2014.09.008.
- (289) Huang, P.; Shi, H.-Q.; Xiao, H.-M.; Li, Y.-Q.; Hu, N.; Fu, S.-Y. High Performance Surface-Modified $TiO_2/Silicone$ Nanocomposite. *Sci. Rep.* **2017**, *7*, 1–7. https://doi.org/10.1038/s41598-017-05166-7.
- (290) He, X.; Pu, Y.; Wang, J.-X.; Wang, D.; Chen, J.-F. Surface Engineering of Titanium Dioxide Nanoparticles for Silicone-Based Transparent Hybrid Films with Ultrahigh Refractive Indexes. *Langmuir* **2021**, *37* (8), 2707–2713. https://doi.org/10.1021/acs.langmuir.0c03377.
- (291) Huang, Y.; Feng, Y.; Sun, X.; Han, Y.; Liu, D.; Tan, X. Preparation of ZrO₂/Silicone Hybrid Materials for LED Encapsulation via in Situ Sol-Gel Reaction. *Polym. Adv. Technol.* **2019**, *30* (7), 1818–1824. https://doi.org/10.1002/pat.4614.
- (292) Lu, Y.; Zhao, Z.; Fan, X.; Cao, X.; Hai, M.; Yang, Z.; Zheng, K.; Lu, J.; Zhang, J.; Ma, Y.; Zhang, R.; Fang, S. Zirconia/Phenylsiloxane Nano-Composite for LED Encapsulation with High and Stable Light Extraction Efficiency. *RSC Adv.* **2021**, *11* (30), 18326–18332. https://doi.org/10.1039/d1ra02230j.
- (293) Rubinsztajn, S.; Chojnowski, J.; Cypryk, M.; Mizerska, U.; Uznański, P.; Walkiewicz-Pietrzykowska, A. Reactions of Titanium Alkoxide with SiH Containing Polymers as a Route to Titanium/Siloxane Hybrid Materials with Enhanced Refractive Index. *Appl. Organometal. Chem.* **2020**, *34* (5), e5571. https://doi.org/10.1002/aoc.5571.
- (294) Chen, J.; Fu, Z.; Huang, H.; Chen, Z.; Zeng, X. A Facile Route to Prepare Homogeneous Silicone Resin Doped with Titanium. *J. Appl. Polym. Sci.* **2019**, *136* (32), 47834. https://doi.org/10.1002/app.47834.
- (295) Zhao, D.; Shan, S.-X.; Zhang, M.; Zhang, X.-A.; Jiang, S.-L.; Lyu, Y.-F. Preparation of Titanium-Silphenylene-Siloxane Hybrid Polymers with High Refractive Index, Transmittance, and Thermal Stability. *Chin. J. Polym. Sci.* **2020**, *38*, 973–982. https://doi.org/10.1007/s10118-020-2398-6.
- (296) Bae, J.-Y.; Yang, S.; Jin, J. H.; Jung, K.; Kim, J.-S.; Bae, B.-S. Fabrication of

- Transparent Methacrylate Zirconium Siloxane Hybrid Materials Using Sol-Gel Synthesized Oligosiloxane Resin. *J. Sol-Gel Sci. Technol.* **2011**, *58*, 114–120. https://doi.org/10.1007/s10971-010-2363-x.
- (297) Xu, J.; Zhu, W.; Jiang, L.; Xu, J.; Zhang, Y.; Cui, Y. Carbazole-Grafted Silicone Hydrogel with a High Refractive Index for Intraocular Lens. *RSC Adv.* **2015**, *5* (89), 72736–72744. https://doi.org/10.1039/c5ra10614a.
- (298) Mosley, D. W.; Khanarian, G.; Conner, D. M.; Thorsen, D. L.; Zhang, T.; Wills, M. High Refractive Index Thermally Stable Phenoxyphenyl and Phenylthiophenyl Silicones for Light-Emitting Diode Applications. *J. Appl. Polym. Sci.* **2014**, *131* (3). https://doi.org/10.1002/app.39824.
- (299) Lemonier, S.; Marty, J.-D.; Fitremann, J. Polysiloxanes Modified by Thiol-Ene Reaction and Their Interaction with Gold Nanoparticles. *Helv. Chim. Acta* **2019**, *102* (11), e1900180. https://doi.org/10.1002/hlca.201900180.
- (300) Li, H. H. Refractive Index of Silicon and Germanium and Its Wavelength and Temperature Derivatives. *J. Phys. Chem. Ref. Data* **1980**, 9 (3), 561–658. https://doi.org/10.1063/1.555624.
- (301) Cai, D.; Neyer, A.; Kuckuk, R.; Heise, H. M. Raman, Mid-Infrared, near-Infrared and Ultraviolet-Visible Spectroscopy of PDMS Silicone Rubber for Characterization of Polymer Optical Waveguide Materials. *J. Mol. Struct.* **2010**, *976* (1–3), 274–281. https://doi.org/10.1016/j.molstruc.2010.03.054.
- (302) Lai, Y.; Jin, L.; Hang, J.; Sun, X.; Shi, L. Highly Transparent Thermal Stable Silicone/Titania Hybrids with High Refractive Index for LED Encapsulation. *J. Coat. Technol. Res.* **2015**, *12*, 1185–1192. https://doi.org/10.1007/s11998-015-9681-4.
- (303) Hu, X.; Yao, B.; Liu, J.; Liu, J.; Chen, K.; Yan, M.; Wang, L. Preparation and Properties of High Refractive Index UV-Cured Titanium Hybrid Optical Materials. *Mater. Lett.* **2020**, *2*65, 127466. https://doi.org/10.1016/j.matlet.2020.127466.
- (304) Ryan, J. W. Redistribution and Reduction Reactions of Alkoxysilanes. *J. Am. Chem.* Soc. **1962**, *84* (24), 4730–4734. https://doi.org/10.1021/ja00883a024.
- (305) Methyltrimethoxysilane (Sigma-Aldrich). https://www.sigmaaldrich.com/DE/de/product/aldrich/440175?srsltid=AfmBOop f09im84UDP1F0JDXBebZheayELgQuv1J-dHVDji1MYEkOyb5E, accessed: 20250326.
- (306) Dimethoxydimethylsilane (Sigma-Aldrich). https://www.sigmaaldrich.com/DE/de/product/aldrich/104906, accessed: 20250326.
- (307) Phenylmethyldimethoxysilane (Gelest). https://www.gelest.com/product/SIP6740.0/ accessed: 20250326.
- (308) Diphenyldimethoxysilane (Gelest). https://www.gelest.com/product/SID4535.0/accessed: 20250326.
- (309) Phenyltrimethoxysilane (Gelest). https://www.gelest.com/product/SIP6822.0/accessed: 20250326.

- (310) Phenyltriethoxysilane (Gelest). https://www.gelest.com/product/SIP6821.0/accessed: 20250326.
- (311) Phenyltrichlorosilane (Sigma-Aldrich). https://www.sigmaaldrich.com/DE/de/product/sial/440108?srsltid=AfmBOoqz9g jR48zBIMPTaiHimpjdc8nooqJEDYE71PjaXt0Z1HtoJyvY, access:20250326.
- (312) Silanol Terminated Polydimethylsiloxane, 35-45 CSt (Gelest). https://www.gelest.com/product/DMS-S14/accessed:20250326.
- (313) Silanol Terminated Polydimethylsiloxane, 3,500 CSt (Gelest). https://www.gelest.com/product/DMS-S33/accessed: 20250326.
- (314) Poly(Methylphenylsiloxane), 450-550 CSt (Sigma-Aldrich). https://www.sigmaaldrich.com/DE/de/product/aldrich/378496?srsltid=AfmBOop QmnIre5ofvWy4U7tkW4XwQ9REzpPK2nqOJ_xpXMP7WHtSpfxL, accessed:20250326.
- (315) Schraub, M.; Soll, S.; Hampp, N. High Refractive Index Coumarin-Based Photorefractive Polysiloxanes. *Eur. Polym. J.* **2013**, *4*9 (6), 1714–1721. https://doi.org/10.1016/j.eurpolymj.2013.03.021.
- (316) Shang, X. X.; Duan, S.; Zhang, M.; Cao, X. Y.; Zheng, K.; Zhang, J. N.; Ma, Y. M.; Zhang, R. B. UV-Curable Ladder-like Diphenylsiloxane-Bridged Methacryl-Phenyl-Siloxane for High Power LED Encapsulation. *RSC Adv.* **2018**, 8 (17), 9049–9056. https://doi.org/10.1039/c8ra00063h.
- (317) Legrand, S.; Hannu-Kuure, M.; Kärkkäinen, A. Design, Preparation, and Characterization of New High-Refractive Index Hybrid Organic–Inorganic Polysiloxanes: Innovative Coatings for Optoelectronic Applications. *J. Appl. Polym. Sci.* **2021**, *138* (8), 49877. https://doi.org/10.1002/app.49877.
- (318) Nakamura, T.; Fujii, H.; Juni, N.; Tsutsumi, N. Enhanced Coupling of Light from Organic Electroluminescent Device Using Diffusive Particle Dispersed High Refractive Index Resin Substrate. *Opt. Rev.* **2006**, *13*, 104–110. https://doi.org/10.1007/s10043-006-0104-8.
- (319) Krogman, K. C.; Druffel, T.; Sunkara, M. K. Anti-Reflective Optical Coatings Incorporating Nanoparticles. *Nanotechnology* **2005**, *16*, 338–343. https://doi.org/10.1088/0957-4484/16/7/005.
- (320) Sanders, D. P. Advances in Patterning Materials for 193 Nm Immersion Lithography. *Chem. Rev.* **2010**, *110* (1), 321–360. https://doi.org/10.1021/cr900244n.
- (321) Sergienko, N.; Godovsky, D.; Zavin, B.; Lee, M.; Ko, M. Nanocomposites of ZnS and Poly-(Dimethyl)-Block-(Phenyl)Siloxane as a New High-Refractive-Index Polymer Media. *Nanoscale Res. Lett.* **2012**, *7*, 181. https://doi.org/10.1186/1556-276X-7-181.
- (322) Zhao, M.; Feng, Y.; Li, G.; Li, Y.; Wang, Y.; Han, Y.; Sun, X.; Tan, X. Synthesis of an Adhesion-Enhancing Polysiloxane Containing Epoxy Groups for Addition-Cure Silicone Light Emitting Diodes Encapsulant. *Polym. Adv. Technol.* **2014**, *25* (9),

- 927-933. https://doi.org/10.1002/pat.3327.
- (323) Liu, J.; Ueda, M. High Refractive Index Polymers: Fundamental Research and Practical Applications. *J. Mater. Chem.* **2009**, *19* (47), 8907–8919. https://doi.org/10.1039/b909690f.
- (324) Javadi, A.; Abouzari-Lotf, E.; Mehdipour-Ataei, S.; Zakeri, M.; Nasef, M. M.; Ahmad, A.; Ripin, A. High Refractive Index Materials: A Structural Property Comparison of Sulfide- and Sulfoxide-Containing Polyamides. *J. Polym. Sci., Part A: Polym. Chem.* **2015**, *53* (24), 2867–2877. https://doi.org/10.1002/pola.27764.
- (325) Javadi, A.; Najjar, Z.; Bahadori, S.; Vatanpour, V.; Malek, A.; Abouzari-Lotf, E.; Shockravi, A. High Refractive Index and Low-Birefringence Polyamides Containing Thiazole and Naphthalene Units. *RSC Adv.* **2015**, *5* (111), 91670–91682. https://doi.org/10.1039/c5ra18898a.
- (326) McGrath, J. E.; Rasmussen, L.; Shultz, A. R.; Shobha, H. K.; Sankarapandian, M.; Glass, T.; Long, T. E.; Pasquale, A. J. Novel Carbazole Phenoxy-Based Methacrylates to Produce High-Refractive Index Polymers. *Polymer* **2006**, *47* (11), 4042–4057. https://doi.org/10.1016/j.polymer.2006.02.030.
- (327) Nakano, K.; Tatsumi, G.; Nozaki, K. Synthesis of Sulfur-Rich Polymers: Copolymerization of Episulfide with Carbon Disulfide by Using [PPN]Cl/(Salph)Cr(III)Cl System. *J. Am. Chem. Soc.* **2007**, *129* (49), 15116–15117. https://doi.org/10.1021/ja076056b.
- (328) Paquet, C.; Cyr, P. W.; Kumacheva, E.; Manners, I. Polyferrocenes: Metallopolymers with Tunable and High Refractive Indices. *Chem. Commun.* **2004**, No. 2, 234–235. https://doi.org/10.1039/b311934c.
- (329) Matsumoto, K.; Costner, E. A.; Nishimura, I.; Ueda, M.; Willson, C. G. High Index Resist for 193 Nm Immersion Lithography. *Macromolecules* **2008**, *41* (15), 5674–5680. https://doi.org/10.1021/ma800295s.
- (330) Steinbrück, N.; Kickelbick, G. Perylene Polyphenylmethylsiloxanes for Optoelectronic Applications. *J. Polym. Sci., Part B: Polym. Phys.* **2019**, 57 (16), 1062–1073. https://doi.org/10.1002/polb.24861.
- (331) Hu, H.; Ma, J.; Li, X.; Yin, Q.; Fan, L.; Wei, X.; Peng, Q.; Yang, J. Benzocyclobutene-Functional Double-Decker Silsesquioxane: Self-Assembled Hybrid Resin for High-Performance Dielectrics and LED Encapsulants. *Polym. Chem.* **2019**, *10* (33), 4551–4560. https://doi.org/10.1039/c9py00719a.
- (332) Ma, M.; Mont, F. W.; Yan, X.; Cho, J.; Schubert, E. F.; Kim, G. B.; Sone, C. Effects of the Refractive Index of the Encapsulant on the Light-Extraction Efficiency of Light-Emitting Diodes. *Opt. Express* **2011**, *19* (S5), A1135–A1140. https://doi.org/10.1364/oe.19.0a1135.
- (333) Boyer, R. F. A Statistical Theory of Discoloration for Halogen-Containing Polymers and Copolymers. *J. Phys. Chem.* **1947**, *51* (1), 80–106. https://doi.org/10.1021/j150451a006.
- (334) Pohl, S.; Janka, O.; Füglein, E.; Kickelbick, G. Thermoplastic Silsesquioxane Hybrid

- Polymers with a Local Ladder-Type Structure. *Macromolecules* **2021**, *54* (8), 3873–3885. https://doi.org/10.1021/acs.macromol.1c00310.
- (335) Steinbrück, N.; Pohl, S.; Kickelbick, G. Platinum Free Thermally Curable Siloxanes for Optoelectronic Application-Synthesis and Properties. *RSC Adv.* **2019**, 9 (4), 2205–2216. https://doi.org/10.1039/c8ra09801h.
- (336) Atkins, G. R.; Maryla Krolikowska, R.; Samoc, A. Optical Properties of an Ormosil System Comprising Methyl- and Phenyl-Substituted Silica. *J. Non-Cryst. Solids* **2000**, *265* (3), 210–220. https://doi.org/10.1016/S0022-3093(00)00008-9.
- (337) Ojima, Y.; Yamaguchi, K.; Mizuno, N. An Efficient Solvent-Free Route to Silyl Esters and Silyl Ethers. *Adv. Synth. Catal.* **2009**, *351* (9), 1405–1411. https://doi.org/10.1002/adsc.200900230.
- (338) Kim, W.-S.; Kim, K.-S.; Eo, Y.-J.; Yoon, K. B.; Bae, B.-S. Synthesis of Fluorinated Hybrid Material for UV Embossing of a Large Core Optical Waveguide Structure. *J. Mater. Chem.* **2005**, *15* (4), 465–469. https://doi.org/10.1039/b412419g.
- (339) Wen, R.; Huo, J.; Lv, J.; Liu, Z.; Yu, Y. Effect of Silicone Resin Modification on the Performance of Epoxy Materials for LED Encapsulation. *J. Mater. Sci.: Mater. Electron.* **2017**, *28*, 14522–14535. https://doi.org/10.1007/s10854-017-7316-5.
- (340) Launer, P. J.; Arkles, B. Infrared Analysis of Orgaonsilicon Compounds: Spectra-Structure Correlations. In *Silicon Compounds: Silanes and Silicones*; **2013**; pp 175–178.
- (341) Li, Y.-S.; Wang, Y.; Ceesay, S. Vibrational Spectra of Phenyltriethoxysilane, Phenyltrimethoxysilane and Their Sol-Gels. *Spectrochim. Acta A: Mol. Biomol. Spectrosc.* **2009**, *71* (5), 1819–1824. https://doi.org/10.1016/j.saa.2008.04.027.
- (342) Imoto, H.; Wada, S.; Yumura, T.; Naka, K. Transition-Metal-Catalyzed Direct Arylation of Caged Silsesquioxanes: Substrate Scope and Mechanistic Study. *Eur. J. Inorg. Chem.* **2019**, *2019* (16), 2202–2207. https://doi.org/10.1002/ejic.201900126.
- (343) Masrat, R.; Maswal, M.; Dar, A. A. Competitive Solubilization of Naphthalene and Pyrene in Various Micellar Systems. *J. Hazard. Mater.* **2013**, *244–245*, 662–670. https://doi.org/10.1016/j.jhazmat.2012.10.057.
- (344) Mousset, E.; Oturan, N.; Van Hullebusch, E. D.; Guibaud, G.; Esposito, G.; Oturan, M. A. A New Micelle-Based Method to Quantify the Tween 80° Surfactant for Soil Remediation. *Agron. Sustain. Dev.* **2013**, 33, 839–846. https://doi.org/10.1007/s13593-013-0140-2.
- (345) Fox, R. B.; Price, T. R.; Cozzens, R. F.; McDonald, J. R. Photophysical Processes in Polymers. IV. Excimer Formation in Vinylaromatic Polymers and Copolymers. *J. Chem. Phys.* **1972**, *57* (1), 534–541. https://doi.org/10.1063/1.1677997.
- (346) Bricks, J. L.; Slominskii, Y. L.; Panas, I. D.; Demchenko, A. P. Fluorescent J-Aggregates of Cyanine Dyes: Basic Research and Applications Review. *Methods Appl. Fluoresc.* **2018**, 6, 012001. https://doi.org/10.1088/2050-6120/aa8d0d.
- (347) Deng, Y.; Yuan, W.; Jia, Z.; Liu, G. H- and J Aggregation of Fluorene-Based

- Chromophores. *J. Phys. Chem. B.* **2014**, *118* (49), 14536–14545. https://doi.org/dx.doi.org/10.1021/jp510520m.
- (348) Ramamurthy, V.; Shailaja, J.; Kaanumalle, L. S.; Sunoj, R. B.; Chandrasekhar, J. Controlling Chemistry with Cations: Photochemistry within Zeolites. *Chem. Commun.* **2003**, No. 16, 1987–1999. https://doi.org/10.1039/b212741e.
- (349) Fukami, T.; Yamaguchi, K.; Tozuka, Y.; Moribe, K.; Oguchi, T.; Yamamoto, K. Novel Channel Structure of Bile Acid-Guest Inclusion Complex Formed between Ursodeoxycholic Acid and Phenanthrene. *Chem. Pharm. Bull.* **2003**, *51* (2), 227–229. https://doi.org/10.1248/cpb.51.227.
- (350) Regan, J.; Dolores, J.; Lepore, M.; Gualano, M.; Badson, J.; Zimnoch, A.; Capitani, J. F.; Fan, J. Modified Silica Gels as Recyclable Adsorbents of Aqueous Polycyclic Aromatic Hydrocarbons. *Green Chem. Lett. Rev.* **2019**, *12* (4), 435–443. https://doi.org/10.1080/17518253.2019.1687760.
- (351) Benkenfoud, K.; Harrane, A.; Belbachir, M. Ring Opening Polymerization of Tetrahydrofuran Catalysed by Maghnite-H+. *Chin. J. Polym. Sci.* **2012**, *30*, 56–62. https://doi.org/10.1007/s10118-012-1094-6.
- (352) Morikawa, A.; Kakimoto, M.; Imai, Y. Convergent Synthesis of Siloxane Starburst Dendrons and Dendrimers via Hydrosilylation. *Macromolecules* **1992**, *25*, 3247–3253.
- (353) Smaihi, M.; Jermoumi, T.; Marignan, J. Structural Study of Poly (Phenylsilsesquioxane) Sol-Gel Materials. *Chem. Mater.* **1995**, *7*, 2293–2299.
- (354) Jitianu, A.; Gonzalez, G.; Klein, L. C. Hybrid Sol-Gel Glasses with Glass-Transition Temperatures below Room Temperature. *J. Am. Ceram. Soc.* **2015**, 98 (12), 3673–3679. https://doi.org/10.1111/jace.13798.
- (355) Hu, N.; Rao, Y.; Sun, S.; Hou, L.; Wu, P.; Fan, S.; Ye, B. Structural Evolution of Silica Gel and Silsesquioxane Upon Thermal Curing. *Appl. Spectrosc.* **2016**, *70* (8), 1–11. https://doi.org/10.1177/0003702816654063.
- (356) Lei, I.-A.; Lai, D.-F.; Don, T.-M.; Chen, W.-C.; Yu, Y.-Y.; Chiu, W.-Y. Silicone Hybrid Materials Useful for the Encapsulation of Light-Emitting Diodes. *Mater. Chem. Phys.* **2014**, 144 (1–2), 41–48. https://doi.org/10.1016/j.matchemphys.2013.12.009.
- (357) Nishihara, T.; Kaneko, M. The Dependence of Excimer Formation of Polystyrene Solutions on Solvent and Concentration. *Macromol. Chem. Phys.* **1969**, *124* (1), 84–90. https://doi.org/10.1002/macp.1969.021240109.
- (358) Polacka, B. Prompt and Delayed Excimer Fluorescence of Naphthalene in Poly(Methylmethacrylate) Matrix. *J. Photochem.* **1987**, 36 (2), 205–210. https://doi.org/10.1016/0047-2670(87)87077-6.
- (359) Aladekomo, J. B.; Birks, J. B. "Excimer" Fluorescence. VII. Spectral Studies of Naphthalene and Its Derivatives. *Proc. R. Soc. Lond. A* **1965**, *284* (1399), 551–565. https://doi.org/10.1098/rspa.1965.0080.
- (360) Cao, T.; Zhang, X.; Qian, R. Excimer Fluorescence of Poly(Polyoxytetramethylene-

- Glycol Naphthalene-2,6-Dicarboxylate). *Polym. J.* **1989**, *21* (6), 489–497. https://doi.org/10.1295/polymj.21.489.
- (361) Ghosh, M.; Nath, S.; Hajra, A.; Sinha, S. Fluorescence Self-Quenching of Tetraphenylporphyrin in Liquid Medium. *J. Lumin.* **2013**, *141*, 87–92. https://doi.org/10.1016/j.jlumin.2013.03.025.
- (362) Gao, Y.; Liu, H.; Zhang, S.; Gu, Q.; Shen, Y.; Ge, Y.; Yang, B. Excimer Formation and Evolution of Excited State Properties in Discrete Dimeric Stacking of an Anthracene Derivative: A Computational Investigation. *Phys. Chem. Chem. Phys.* **2018**, *20* (17), 12129–12137. https://doi.org/10.1039/c8cp00834e.
- (363) Förster, T. Formation and Dissociation of Excited Dimers. *Pure Appl. Chem.* **1963**, 7(1), 73–78. https://doi.org/10.1351/pac196307010073.
- (364) Zhu, H. D.; Kantor, S. W.; MacKnight, W. J. Thermally Stable Silphenylene Vinyl Siloxane Elastomers and Their Blends. *Macromolecules* **1998**, *31* (3), 850–856. https://doi.org/10.1021/ma970455h.
- (365) Dvornic, P. R.; Lenz, R. W. Exactly Alternating Silarylene-Siloxane Polymers. 9. Relationships between Polymer Structure and Glass Transition Temperature. *Macromolecules* **1992**, *25*, 3769–3778.
- (366) Nordin, N. H.; Ramli, M. R.; Othman, N.; Ahmad, Z. Synthesis of Carbazole-Substituted Poly(Dimethylsiloxane) and Its Improved Refractive Index. *J. Appl. Polym. Sci.* **2015**, *132* (11), 1–9. https://doi.org/10.1002/app.41654.
- (367) Yi, M.; Chen, X.; Wu, S.; Ge, J.; Zhou, X.; Yin, G. Fabrication of Reactive Poly(Phenyl-Substituted Siloxanes/Silsesquioxanes) with Si-H and Alkoxy Functional Groups via the Piers-Rubinsztajn Reaction. *Polymers* **2018**, *10* (9), 1006. https://doi.org/10.3390/polym10091006.
- (368) Schneider, A. F.; Lu, E. K.; Lu, G.; Brook, M. A. Facile Synthesis of Phenyl-Rich Functional Siloxanes from Simple Silanes. *J. Polym. Sci.* **2020**, *58* (21), 3095–3106. https://doi.org/10.1002/pol.20200527.
- (369) Natali, M.; Kenny, J. M.; Torre, L. Science and Technology of Polymeric Ablative Materials for Thermal Protection Systems and Propulsion Devices: A Review. *Prog. Mater. Sci.* **2016**, *84*, 192–275. https://doi.org/10.1016/j.pmatsci.2016.08.003.
- (370) Coates, J. Interpretation of Infrared Spectra, A Practical Approach. In *Encyclopedia* of *Analytical Chemistry*; John Wiley & Sons Ltd, Chichester, **2000**; pp 10815–10837.
- (371) Liang, C. Y.; Krimm, S. Infrared Spectra of High Polymers. VI. Polystyrene. *J. Polym. Sci.* **1958**, *27* (115), 241–254. https://doi.org/10.1002/pol.1958.1202711520.
- (372) Pimentel, G. C.; McClellan, A. L. The Infrared Spectra of Naphthalene Crystals, Vapor, and Solutions. *J. Chem. Phys.* **1952**, *20* (2), 270–277. https://doi.org/10.1063/1.1700390.
- (373) Person, W. B.; Pimentel, G. C.; Schnepp, O. Infrared Studies of Naphthalene and Naphthalene-d₈. *J. Chem. Phys.* **1955**, *23* (2), 230–233. https://doi.org/10.1063/1.1741945.

- (374) Zhou, W.; Yang, H.; Guo, X.; Lu, J. Thermal Degradation Behaviors of Some Branched and Linear Polysiloxanes. *Polym. Degrad. Stab.* **2006**, *91* (7), 1471–1475. https://doi.org/10.1016/j.polymdegradstab.2005.10.005.
- (375) Fina, A.; Tabuani, D.; Carniato, F.; Frache, A.; Boccaleri, E.; Camino, G. Polyhedral Oligomeric Silsesquioxanes (POSS) Thermal Degradation. *Thermochim. Acta* **2006**, 440 (1), 36–42. https://doi.org/10.1016/j.tca.2005.10.006.
- (376) Zha, C.; Hemley, R. J.; Mao, H.; Duffy, T. S.; Meade, C. Acoustic Velocities and Refractive Index of SiO₂ Glass to 57.5 GPa by Brillouin Scattering. *Phys. Rev. B* **1994**, *50* (18), 13105–13112. https://doi.org/10.1103/PhysRevB.50.13105.
- (377) You, N.-H.; Suzuki, Y.; Higashihara, T.; Ando, S.; Ueda, M. Synthesis and Characterization of Highly Refractive Polyimides Derived from 2,7-Bis(4'-Aminophenylenesulfanyl)Thianthrene-5,5,10,10-Tetraoxide and Aromatic Dianhydrides. *Polymer* **2009**, *50* (3), 789–795. https://doi.org/10.1016/j.polymer.2008.12.001.
- (378) Terraza, C. A.; Liu, J.-G.; Nakamura, Y.; Shibasaki, Y.; Ando, S.; Ueda, M. Synthesis and Properties of Highly Refractive Polyimides Derived from Fluorene-Bridged Sulfur-Containing Dianhydrides and Diamines. *J. Polym. Sci., Part A: Polym. Chem.* **2008**, *4*6 (4), 1510–1520. https://doi.org/10.1002/pola.22492.
- (379) Pan, Z.; Zhu, S.; Zhu, L.; Kang, Y.; Huang, B. Synthesis of High Refractive Index Epoxy Modified Methyl Phenyl Silicone Resin and Amine Phenyl Silicone Resin for LEDs Packaging. *Silicon* **2020**, *12*, 1379–1389. https://doi.org/10.1007/s12633-019-00231-4.
- (380) Bhagat, S. D.; Chatterjee, J.; Chen, B.; Stiegman, A. E. High Refractive Index Polymers Based on Thiol-Ene Cross-Linking Using Polarizable Inorganic/Organic Monomers. *Macromolecules* **2012**, *45* (3), 1174–1181. https://doi.org/10.1021/ma202467a.
- (381) Chevalier, P. M.; Ou, D. L. Novel Organosilanes for the Preparation of High Refractive Index Silicone Coatings. *MRS Proceedings* **2004**, *847*, EE1.2. https://doi.org/10.1557/PROC-847-EE1.2.
- (382) Shuto, K.; Kato, T.; Nagasawa, T. Polymerizable Silane Compound, WO 2017/208748. **2019**.
- (383) Briesenick, M.; Gallei, M.; Kickelbick, G. High-Refractive-Index Polysiloxanes Containing Naphthyl and Phenanthrenyl Groups and Their Thermally Cross-Linked Resins. *Macromolecules* **2022**, *55* (11), 4675–4691. https://doi.org/10.1021/acs.macromol.2c00265.
- (384) Li, Y.; Zhang, L.; Li, C. Highly Transparent and Scratch Resistant Polysiloxane Coatings Containing Silica Nanoparticles. *J. Colloid. Interface Sci.* **2020**, 559, 273–281. https://doi.org/10.1016/j.jcis.2019.09.031.
- (385) Lee, A. S.; Choi, S.-S.; Baek, K.-Y.; Hwang, S. S. Hydrolysis Kinetics of a Sol-Gel Equilibrium Yielding Ladder-like Polysilsesquioxanes. *Inorg. Chem. Commun.* **2016**, *73*, 7–11. https://doi.org/10.1016/j.inoche.2016.09.004.

- (386) Handke, M.; Sitarz, M.; Długoń, E. Amorphous SiC_xO_y Coatings from Ladder-like Polysilsesquioxanes. *J. Mol. Struct.* **2011**, 993 (1–3), 193–197. https://doi.org/10.1016/j.molstruc.2010.12.017.
- (387) Kim, Y. H.; Lim, Y.-W.; Lee, D.; Kim, Y. H.; Bae, B.-S. A Highly Adhesive Siloxane LED Encapsulant Optimized for High Thermal Stability and Optical Efficiency. *J. Mater. Chem. C* **2016**, *4* (46), 10791–10796. https://doi.org/10.1039/c6tc04305d.
- (388) Khandekar, S.; Sahu, G.; Muralidhar, K.; Gatapova, E. Y.; Kabov, O. A.; Hu, R.; Luo, X.; Zhao, L. Cooling of High-Power LEDs by Liquid Sprays: Challenges and Prospects. *Appl. Therm. Eng.* **2021**, 184, 115640. https://doi.org/10.1016/j.applthermaleng.2020.115640.
- (389) Jitianu, M.; Jitianu, A.; Stamper, M.; Aboagye, D.; Klein, L. C. Melting Gel Films for Low Temperature Seals. *MRS Online Proceedings Library* **2013**, *1547*, 81–86. https://doi.org/10.1557/opl.2013.506.
- (390) Cervantes, J.; Zárraga, R.; Salazar-Hernández, C. Organotin Catalysts in Organosilicon Chemistry. *Appl. Organometal. Chem.* **2012**, *26* (4), 157–163. https://doi.org/10.1002/aoc.2832.
- (391) van Der Weij, F. W. The Action of Tin Compounds in Condensation-type RTV Silicone Rubbers. *Macromol. Chem. Phys.* **1980**, *181* (12), 2541–2548. https://doi.org/10.1002/macp.1980.021811211.
- (392) Werlang, M. M.; Yoshida, I. V. P.; de Araújo, M. A. Silphenylene and Silphenylene-Siloxane Oligomers: Structure-Property Relationships. *J. Inorg. Organomet. Polym.* **1995**, *5* (1), 75–85. https://doi.org/10.1007/BF01157524.
- (393) Matsumoto, K.; Shimada, S.; Sato, K. Sequence-Controlled Catalytic One-Pot Synthesis of Siloxane Oligomers. *Chem. Eur. J.* **2019**, *25* (4), 920–928. https://doi.org/10.1002/chem.201803565.
- (394) Matsumoto, K.; Sajna, K. V.; Satoh, Y.; Sato, K.; Shimada, S. By-Product-Free Siloxane-Bond Formation and Programmed One-Pot Oligosiloxane Synthesis. *Angew. Chem., Int. Ed.* **2017**, 56 (12), 3168–3171. https://doi.org/10.1002/anie.201611623.
- (395) Klein, L. C.; Al-Marzoki, K.; Jitianu, A.; Rodriguez, G. Effect of Tetraethoxysilane (TEOS) on Melting Gel Behavior. *J. Am. Ceram. Soc.* **2020**, *103* (8), 4140–4149. https://doi.org/10.1111/jace.17106.
- (396) Klein, L. C.; Jitianu, A. Erratum to: Organic-Inorganic Hybrid Melting Gels. *J. Sol-Gel Sci. Technol.* **2011**, 59, 424–431. https://doi.org/10.1007/s10971-011-2414-y.
- (397) Song, J.; Chen, G.; Wu, G.; Cai, C.; Liu, P.; Li, Q. Thermal and Dynamic Mechanical Properties of Epoxy Resin/Poly(Urethane-Imide)/Polyhedral Oligomeric Silsesquioxane Nanocomposites. *Polym. Adv. Technol.* **2011**, *22* (12), 2069–2074. https://doi.org/10.1002/pat.1722.
- (398) Al-Hartomy, O. A.; Ibrahim, M. A.; Al-Ghamdi, A.; Dishovsky, N.; Ivanov, M.; Mihaylov, M.; El-Tantawy, F. Dynamic Mechanical Thermal Analysis and Dielectric Thermal Analysis of Siloxane Rubber-Based Composites Filled with Carbon Black.

- *J. Compos. Mater.* **2012**, 46 (14), 1765–1770. https://doi.org/10.1177/0021998311425619.
- (399) Ioan, S.; Grigorescu, G.; Stanciu, A. Dynamic-Mechanical and Differential Scanning Calorimetry Measurements on Crosslinked Poly(Ester-Siloxane)-Urethanes. *Polymer* **2001**, *42* (8), 3633–3639. https://doi.org/10.1016/S0032-3861(00)00747-3.
- (400) Chiu, Y.-C.; Huang, C.-C.; Tsai, H.-C. Synthesis, Characterization, and Thermo Mechanical Properties of Siloxane-Modified Epoxy-Based Nano Composite. *J. Appl. Polym. Sci.* **2014**, *131* (21), 1–7. https://doi.org/10.1002/app.40984.
- (401) Lee, K. S.; Chang, Y.-W. Thermal and Mechanical Properties of Poly(ε-Caprolactone)/Polyhedral Oligomeric Silsesquioxane Nanocomposites. *Polym. Int.* **2013**, 62 (1), 64–70. https://doi.org/10.1002/pi.4309.
- (402) Džunuzović, J. V.; Pergal, M. V.; Poręba, R.; Vodnik, V. V.; Simonović, B. R.; Špírková, M.; Jovanović, S. Analysis of Dynamic Mechanical, Thermal and Surface Properties of Poly(Urethane-Ester-Siloxane) Networks Based on Hyperbranched Polyester. *J. Non-Cryst.* Solids **2012**, 358 (23), 3161–3169. https://doi.org/10.1016/j.jnoncrysol.2012.09.013.
- (403) Ni, Y.; Zheng, S.; Nie, K. Morphology and Thermal Properties of Inorganic-Organic Hybrids Involving Epoxy Resin and Polyhedral Oligomeric Silsesquioxanes. *Polymer* **2004**, *45* (16), 5557–5568. https://doi.org/10.1016/j.polymer.2004.06.008.
- (404) Wang, Y.; Wang, S.; Bian, C.; Zhong, Y.; Jing, X. Effect of Chemical Structure and Cross-Link Density on the Heat Resistance of Phenolic Resin. *Polym. Degrad. Stab.* **2015**, *111*, 239–246. https://doi.org/10.1016/j.polymdegradstab.2014.11.016.
- (405) Chou, C.; Yang, M.-H. Structural Effects on the Thermal Properties of PDPS/PDMS Copolymers. *J. Therm. Anal.* **1993**, *40*, 657–667. https://doi.org/10.1007/BF02546637.
- (406) Englert, M.; Minister, F.; Moussaoui, A.; Pisula, W. Mechanical Properties of Thermo-Oxidative Aged Silicone Rubber Thermally Stabilized by Titanium Oxide Based Fillers. *Polym. Test.* **2022**, *115*, 107726. https://doi.org/10.1016/j.polymertesting.2022.107726.
- (407) Li, Z.; Wang, Z.; Qiu, X.; Bai, L.; Zheng, J. Effect of Acid-Treated Multi-Walled Carbon Nanotubes on Thermo-Oxidative Stability and Degradation Behavior of Silicone Rubber. *J. Therm. Anal. Calorim.* **2018**, *133*, 1353–1364. https://doi.org/10.1007/s10973-018-7214-y.
- (408) Li, R.; Zhang, B.; Sun, Y.; Liu, B.; Wang, G. Synthesis of Vinylphenyl Oligomeric Silsesquioxane Based on MQ Silicone Resin. *Asian J. Chem.* **2013**, *25* (5), 2541–2546. https://doi.org/10.14233/ajchem.2013.13448.
- (409) Arkles, B.; Larson, G. Dvornic, Petar R, High Temperature Stability of Polysiloxanes. In *Silicon Compounds: Silanes and Silicones*; Gelest Inc.: Morrisville, PA, **2008**; pp 419–431.

- (410) Feher, F. J.; Terroba, R.; Ziller, J. W. Base-Catalyzed Cleavage and Homologation of Polyhedral Oligosilsesquioxanes. *Chem. Commun.* **1999**, No. 21, 2153–2154. https://doi.org/10.1039/a906397h.
- (411) Choi, S.-S.; Lee, A. S.; Lee, H. S.; Jeon, H. Y.; Baek, K.-Y.; Choi, D. H.; Hwang, S. S. Synthesis and Characterization of UV-Curable Ladder-like Polysilsesquioxane. *J. Polym. Sci., Part A: Polym. Chem.* **2011**, 49 (23), 5012–5018. https://doi.org/10.1002/pola.24942.
- (412) Liu, C.; Liu, Y.; Shen, Z.; Xie, P.; Dai, D.; Zhang, R.; He, C.; Chung, T. Synthesis and Characterization of Novel Alcohol-Soluble Ladderlike Poly(Silsesquioxane)s Containing Side-Chain Hydroxy Groups. *Macromol. Chem. Phys.* **2001**, *202* (9), 1576–1580. https://doi.org/10.1002/1521-3935(20010601)202:9<1576::AID-MACP1576>3.0.CO;2-E.
- (413) Majka, T. M.; Raftopoulos, K. N.; Pielichowski, K. The Influence of POSS Nanoparticles on Selected Thermal Properties of Polyurethane-Based Hybrids. *J. Therm. Anal. Calorim.* **2018**, *133*, 289–301. https://doi.org/10.1007/s10973-017-6942-8.
- (414) Jalarvo, N.; Gourdon, O.; Ehlers, G.; Tyagi, M.; Kumar, S. K.; Dobbs, K. D.; Smalley, R. J.; Guise, W. E.; Ramirez-Cuesta, A.; Wildgruber, C.; Crawford, M. K. Structure and Dynamics of Octamethyl-POSS Nanoparticles. *J. Phys. Chem. C* **2014**, *118* (10), 5579–5592. https://doi.org/10.1021/jp412228r.
- (415) Mya, K. Y.; Gose, H. B.; Pretsch, T.; Bothe, M.; He, C. Star-Shaped POSS-Polycaprolactone Polyurethanes and Their Shape Memory Performance. *J. Mater. Chem.* **2011**, *21* (13), 4827–4836. https://doi.org/10.1039/c0jm04459h.
- (416) Bothe, M.; Mya, K. Y.; Jie Lin, E. M.; Yeo, C. C.; Lu, X.; He, C.; Pretsch, T. Triple-Shape Properties of Star-Shaped POSS-Polycaprolactone Polyurethane Networks. *Soft Matter* **2012**, *8* (4), 965–972. https://doi.org/10.1039/c1sm06474f.
- (417) Schwab, J. J.; Lichtenhan, J. D. Polyhedral Oligomeric Silsesquioxane (POSS)-Based Polymers. *Appl. Organometal. Chem.* **1998**, *12* (10–11), 707–713. https://doi.org/10.1002/(SICI)1099-0739(199810/11)12:10/11<707::AID-AOC776>3.0.CO;2-1.
- (418) Mohamed, M. G.; Kuo, S.-W. Polybenzoxazine/Polyhedral Oligomeric Silsesquioxane (POSS) Nanocomposites. *Polymers* **2016**, *8* (6), 225. https://doi.org/10.3390/polym8060225.
- (419) Tunstall-Garcia, H.; Charles, B. L.; Evans, R. C. The Role of Polyhedral Oligomeric Silsesquioxanes in Optical Applications. *Adv. Photonics Res.* **2021**, *2* (6), 2000196. https://doi.org/10.1002/adpr.202000196.
- (420) Raut, H. K.; Dinachali, S. S.; He, A. Y.; Ganesh, V. A.; Saifullah, M. S. M.; Law, J.; Ramakrishna, S. Robust and Durable Polyhedral Oligomeric Silsesquioxane-Based Anti-Reflective with Broadband Quasi-Omnidirectional Nanostructures Properties. Energy Environ. Sci. 2013, 1929-1937. 6 (6),https://doi.org/10.1039/c3ee24037a.
- (421) Ramirez, N. V.; Sanchez-Soto, M. Effects of POSS Nanoparticles on ABS-g-Ma

- Thermo Oxidation Resistance. *Polym. Compos.* **2012**, *33* (10), 1707–1718. https://doi.org/10.1002/pc.22304.
- (422) Bandyopadhyay, P.; Banerjee, S. Synthesis, Characterization and Gas Transport Properties of Polyamide-Tethered Polyhedral Oligomeric Silsesquioxane (POSS) Nanocomposites. *Ind. Eng. Chem. Res.* **2014**, *53* (47), 18273–18282. https://doi.org/10.1021/ie503475k.
- (423) Zheng, L.; Farris, R. J.; Coughlin, E. B. Novel Polyolefin Nanocomposites: Synthesis and Characterizations of Metallocene-Catalyzed Polyolefin Polyhedral Oligomeric Silsesquioxane Copolymers. *Macromolecules* **2001**, *34* (23), 8034–8039. https://doi.org/10.1021/ma0110094.
- (424) Ma, L.; Geng, H.; Song, J.; Li, J.; Chen, G.; Li, Q. Hierarchical Self-Assembly of Polyhedral Oligomeric Silsesquioxane End-Capped Stimuli-Responsive Polymer: From Single Micelle to Complex Micelle. *J. Phys. Chem. B* **2011**, *115* (36), 10586–10591. https://doi.org/10.1021/jp203782g.
- (425) McCusker, C.; Carroll, J. B.; Rotello, V. M. Cationic Polyhedral Oligomeric Silsesquioxane (POSS) Units as Carriers for Drug Delivery Processes. *Chem. Commun.* **2005**, No. 8, 996–998. https://doi.org/10.1039/b416266h.
- (426) Janaszewska, A.; Gradzinska, K.; Marcinkowska, M.; Klajnert-Maculewicz, B.; Stanczyk, W. A. In Vitro Studies of Polyhedral Oligo Silsesquioxanes: Evidence for Their Low Cytotoxicity. *Materials* 2015, 8 (9), 6062–6070. https://doi.org/10.3390/ma8095291.
- (427) Carroll, J. B.; Waddon, A. J.; Nakade, H.; Rotello, V. M. "Plug and Play" Polymers. Thermal and X-Ray Characterizations of Noncovalently Grafted Polyhedral Oligomeric Silsesquioxane (POSS)-Polystyrene Nanocomposites. *Macromolecules* **2003**, 36 (17), 6289–6291. https://doi.org/10.1021/ma034652u.
- (428) Zheng, L.; Kasi, R. M.; Farris, R. J.; Bryan Coughlin, E. Synthesis and Thermal Properties of Hybrid Copolymers of Syndiotactic Polystyrene and Polyhedral Oligomeric Silsesquioxane. *J. Polym. Sci., Part A: Polym. Chem.* **2002**, *40* (7), 885–891. https://doi.org/10.1002/pola.10175.
- (429) Li, M.; Zhang, H.; Wu, W.; Li, M.; Xu, Y.; Chen, G.; Dai, L. A Novel POSS-Based Copolymer Functionalized Graphene: An Effective Flame Retardant for Reducing the Flammability of Epoxy Resin. *Polymers* **2019**, *11* (2), 241. https://doi.org/10.3390/polym11020241.
- (430) Zhou, H.; Ye, Q.; Xu, J. Polyhedral Oligomeric Silsesquioxane-Based Hybrid Materials and Their Applications. *Mater. Chem. Front.* **2017**, *1* (2), 212–230. https://doi.org/10.1039/c6qm00062b.
- (431) Tanaka, K.; Kitamura, N.; Naka, K.; Morita, M.; Inubushi, T.; Chujo, M.; Nagao, M.; Chujo, Y. Improving Proton Relaxivity of Dendritic MRI Contrast Agents by Rigid Silsesquioxane Core. *Polym. J.* **2009**, *41*, 287–292. https://doi.org/10.1295/polymj.PJ2008274.
- (432) Tanaka, K.; Inafuku, K.; Naka, K.; Chujo, Y. Enhancement of Entrapping Ability of Dendrimers by a Cubic Silsesquioxane Core. *Org. Biomol. Chem.* **2008**, 6 (21),

- 3899–3901. https://doi.org/10.1039/b812349g.
- (433) Tanaka, K.; Chujo, Y. Advanced Functional Materials Based on Polyhedral Oligomeric Silsesquioxane (POSS). *J. Mater. Chem.* **2012**, *22* (5), 1733–1746. https://doi.org/10.1039/c1jm14231c.
- (434) Yandek, G. R.; Moore, B. M.; Ramirez, S. M.; Mabry, J. M. Effects of Peripheral Architecture on the Properties of Aryl Polyhedral Oligomeric Silsesquioxanes. *J. Phys. Chem. C* **2012**, *116* (31), 16755–16765. https://doi.org/10.1021/jp3039708.
- (435) Feng, X.; Zhu, S.; Yue, K.; Su, H.; Guo, K.; Wesdemiotis, C.; Zhang, W.-B.; Cheng, S. Z. D.; Li, Y. T₁₀ Polyhedral Oligomeric Silsesquioxane-Based Shape Amphiphiles with Diverse Head Functionalities via "Click" Chemistry. *ACS Macro Lett.* **2014**, *3* (9), 900–905. https://doi.org/10.1021/mz500422g.
- (436) Heeley, E. L.; Hughes, D. J.; El Aziz, Y.; Taylor, P. G.; Bassindale, A. R. Linear Long Alkyl Chain Substituted POSS Cages: The Effect of Alkyl Chain Length on the Self-Assembled Packing Morphology. *Macromolecules* **2013**, *4*6 (12), 4944–4954. https://doi.org/10.1021/ma400635e.
- (437) Qi, Z.; Zhang, W.; He, X.; Yang, R. High-Efficiency Flame Retardency of Epoxy Resin Composites with Perfect T₈ Caged Phosphorus Containing Polyhedral Oligomeric Silsesquioxanes (P-POSSs). *Compos. Sci. Technol.* **2016**, *127*, 8–19. https://doi.org/10.1016/j.compscitech.2016.02.026.
- (438) Lin, X.; Deng, Y.-Y.; Zhang, Q.; Han, D.; Fu, Q. Effect of POSS Size on the Porosity and Adsorption Performance of Hybrid Porous Polymers. *Macromolecules* **2023**, 56 (3), 1243–1252. https://doi.org/10.1021/acs.macromol.2c02486.
- (439) Kim, S. G.; Choi, J.; Tamaki, R.; Laine, R. M. Synthesis of Amino-Containing Oligophenylsilsesquioxanes. *Polymer* **2005**, *46* (12), 4514–4524. https://doi.org/10.1016/j.polymer.2005.02.036.
- (440) Zhang, D.; Zhou, H.; Yang, R.; Zhang, W.; Li, L. Analysis on the Caged Structure of Polyhedral Oligomeric Dodecaphenyl Silsesquioxane and Its Condensation Mechanism. *J. Mol. Struct.* **2023**, *1280*, 135024. https://doi.org/10.1016/j.molstruc.2023.135024.
- (441) Bolln, C.; Tsuchida, A.; Frey, H.; Mülhaupt, R. Thermal Properties of the Homologous Series of 8-Fold Alkyl-Substituted Octasilsesquioxanes. *Chem. Mater.* **1997**, 9 (6), 1475–1479. https://doi.org/10.1021/cm970090f.
- (442) Clarke, D.; Mathew, S.; Matisons, J.; Simon, G.; Skelton, B. W. Synthesis and Characterization of a Range of POSS Imides. *Dyes Pigments* **2012**, 92 (1), 659–667. https://doi.org/10.1016/j.dyepig.2011.05.028.
- (443) Du, F.; Tian, J.; Wang, H.; Liu, B.; Jin, B.; Bai, R. Synthesis and Luminescence of POSS-Containing Perylene Bisimide-Bridged Amphiphilic Polymers. *Macromolecules* **2012**, *45* (7), 3086–3093. https://doi.org/10.1021/ma300100s.
- (444) Liu, J.; Gao, S.-Y.; Zhang, X.-Y.; Feng, Y.; Wu, H.-C.; Chen, Z.; Bermeshev, M. V; Ren, X.-K. POSS-Containing Polynorbornene with Pendant Perylene Diimide: From a Unique Supramolecular Structure to Tunable Luminescence Properties. *J. Mater.*

- Chem. C 2022, 10 (22), 8791-8796. https://doi.org/10.1039/d2tc01487d.
- (445) Foorginezhad, S.; Zerafat, M. M. Preparation of Highly Crystalline Octavinyl Silsesquioxane Building Blocks via Sol-Gel Technique. *Nanochem Res* **2020**, *5* (1), 14–24. https://doi.org/10.22036/ncr.2020.01.002.
- (446) Gravel, M.-C.; Zhang, C.; Dinderman, M.; Laine, R. M. Octa(3-Chloroammoniumpropyl) Octasilsesquioxane. *Appl. Organometal. Chem.* **1999**, 13 (4), 329–336. https://doi.org/10.1002/(SICI)1099-0739(199904)13:4<329::AID-AOC870>3.0.CO;2-V.
- (447) Tanaka, K.; Adachi, S.; Chujo, Y. Structure-Property Relationship of Octa-Substituted POSS in Thermal and Mechanical Reinforcements of Conventional Polymers. *J. Polym. Sci., Part A: Polym. Chem.* **2009**, *47* (21), 5690–5697. https://doi.org/10.1002/pola.23612.
- (448) Feher, F. J.; Newman, D. A.; Walzer, J. F. Silsesquioxanes as Models for Silica Surfaces. *J. Am. Chem. Soc.* **1989**, *111* (5), 1741–1748. https://doi.org/10.1021/ja00187a028.
- (449) Haddad, T. S.; Lichtenhan, J. D. Hybrid Organic Inorganic Thermoplastics: Styryl-Based Polyhedral Oligomeric Silsequioxane Polymers. *Macromolecules* **1996**, *29* (22), 7302–7304. https://doi.org/10.1021/ma960609d.
- (450) Pyun, J.; Matyjaszewski, K. The Synthesis of Hybrid Polymers Using Atom Transfer Radical Polymerization: Homopolymers and Block Copolymers from Polyhedral Oligomeric Silsesquioxane Monomers. *Macromolecules* **2000**, *33* (1), 217–220. https://doi.org/10.1021/ma9910787.
- (451) Mather, P. T.; Jeon, H. G.; Romo-Uribe, A.; Haddad, T. S.; Lichtenhan, J. D. Mechanical Relaxation and Microstructure of Poly(Norbornyl-POSS) Copolymers. *Macromolecules* **1999**, *32* (4), 1194–1203. https://doi.org/10.1021/ma981210n.
- (452) Ramesh, S.; Kim, J.; Kim, J.-H. Characteristic of Hybrid Cellulose-Amino Functionalized POSS-Silica Nanocomposite and Antimicrobial Activity. *J. Nanomater.* **2015**, *2015*, 1–9. https://doi.org/10.1155/2015/936590.
- (453) Rakesh, S.; Sakthi Dharan, C. P.; Selladurai, M.; Sudha, V.; Sundararajan, P. R.; Sarojadevi, M. Thermal and Mechanical Properties of POSS-Cyanate Ester/Epoxy Nanocomposites. *High Perform. Polym.* **2012**, *25* (1), 87–96. https://doi.org/10.1177/0954008312457192.
- (454) Dhanapal, D.; Srinivasan, A. K.; Ramalingam, N. Role of POSS as Coupling Agent for DGEBA/GF Reinforced Nanocomposites. *Silicon* **2018**, *10*, 537–546. https://doi.org/10.1007/s12633-016-9487-8.
- (455) Song, K.; Jiang, Y.; Zou, Z. Effect of Vesicle Structure on Catalytic Activity of Suzuki-Miyaura Cross-Coupling Reaction: Impact of Framework and Morphology. *ChemistrySelect* **2020**, 5 (37), 11438–11445. https://doi.org/10.1002/slct.202003233.
- (456) Furgal, J. C.; Goodson III, T.; Laine, R. M. D_{5h} [PhSiO_{1.5}]₁₀ Synthesis via F⁻ Catalyzed Rearrangement of [PhSiO_{1.5}]_n. An Experimental/Computational Analysis of Likely

- Reaction Pathways. *Dalton Trans.* **2016**, *45* (3), 1025–1039. https://doi.org/10.1039/c5dt04182a.
- (457) Liotta, C. L.; Harris, H. P. The Chemistry of "Naked" Anions. I. Reactions of the 18-Crown-6 Complex of Potassium Fluoride with Organic Substrates in Aprotic Organic Solvents. J. Am. Chem. Soc. **1974**, 96 (7), 2250–2252.
- (458) Mataga, N.; Tomura, M.; Nishimura, H. Fluorescence Decay Times of Naphthalene and Naphthalene Excimers. *Mol. Phys.* **1965**, 9 (4), 367–375. https://doi.org/10.1080/00268976500100501.
- (459) Maeda, H.; Maeda, T.; Mizuno, K. Absorption and Fluorescence Spectroscopic Properties of 1- and 1,4-Silyl-Substituted Naphthalene Derivatives. *Molecules* **2012**, *17* (5), 5108–5125. https://doi.org/10.3390/molecules17055108.
- (460) Sau, S.; Solanki, B.; Orprecio, R.; Van Stam, J.; Evans, C. H. Higher-Order Cyclodextrin Complexes: The Naphthalene System. *J. Incl. Phenom.* **2004**, *48* (3/4), 173–180. https://doi.org/10.1023/B:JIPH.0000022556.47230.c8.
- (461) Kumar, V. B.; Fleming, C. L.; Murali, S. S.; Hume, P. A.; Davis, N. J. L. K.; Söhnel, T.; Leitao, E. M. The Photophysical Properties of Naphthalene Bridged Disilanes. *RSC Adv.* **2021**, *11* (35), 21343–21350. https://doi.org/10.1039/D1RA02961D.
- (462) Van Duuren, B. L. Effects of the Environment on the Fluorescence of Aromatic Compounds in Solution. *Chem. Rev.* **1963**, 63 (4), 325–354.
- (463) Zhang, Y.; Wang, L.; Liu, P.; Li, Y.; Zhan, R.; Huang, Z.; Lin, H. Measurement and Extrapolation Modeling of PAH Laser-Induced Fluorescence Spectra at Elevated Temperatures. *Appl. Phys. B* **2019**, *125* (6). https://doi.org/10.1007/s00340-018-7115-6.
- (464) Aguiar, M.; Fugihara, M. C.; Hümmelgen, I. A.; Péres, L. O.; Garcia, J. R.; Gruber, J.; Akcelrud, L. Interchain Luminescence in Poly(Acetoxy-p-Phenylene Vinylene). *J. Lumin.* **2002**, 96 (2–4), 219–225. https://doi.org/10.1016/S0022-2313(01)00235-6.
- (465) Appiarius, Y.; Gliese, P. J.; Segler, S. A. W.; Rusch, P.; Zhang, J.; Gates, P. J.; Pal, R.; Malaspina, L. A.; Sugimoto, K.; Neudecker, T.; others. BN-Substitution in Dithienylpyrenes Prevents Excimer Formation in Solution and in the Solid State. J. Phys. Chem. C 2022, 126 (9), 4563–4576. https://doi.org/10.1021/acs.jpcc.1c08812.
- (466) Hayashi, H.; Kawasaki, S.; Kobori, K.; Koyama, Y.; Asai, S.; Takata, T. Synthesis and Properties of Polysiloxanes Possessing 9,9-Diarylfluorene Structure in the Main Chain. *Polym. J.* **2009**, *41*, 272–278. https://doi.org/10.1295/polymj.PJ2008241.
- (467) Melendez-Zamudio, M.; Silverthorne, K. E. C.; Brook, M. A. High Refractive Index, Enantiopure Silicones Based on BINOL. *Macromol. Rapid Commun.* **2022**, *43* (9), 2200022. https://doi.org/10.1002/marc.202200022.
- (468) Kota, A. K.; Kwon, G.; Tuteja, A. The Design and Applications of Superomniphobic Surfaces. *NPG Asia Mater.* **2014**, 6, e109. https://doi.org/10.1038/am.2014.34.
- (469) Chen, Q.; Xue, F.; DIng, E. Preparation of POSS-Triol/Wollastonite Composite Particles by Liquid Phase Mechanochemical Method and Its Application in UV

- Curable Coatings. *Sci. Eng. Compos. Mater.* **2019**, *26* (1), 183–196. https://doi.org/10.1515/secm-2019-0001.
- (470) Ye, M.; Wu, Y.; Zhang, W.; Yang, R. Synthesis of Incompletely Caged Silsesquioxane (T₇-POSS) Compounds via a Versatile Three-Step Approach. *Res. Chem. Intermed.* **2018**, *44*, 4277–4294. https://doi.org/10.1007/s11164-018-3368-2.
- (471) Roll, M. F.; Kampf, J. W.; Kim, Y.; Yi, E.; Laine, R. M. Nano Building Blocks via Iodination of $[PhSiO_{1.5}]_n$, Forming $[p-I-C_6H_4SiO_{1.5}]_n$ (n = 8, 10, 12), and a New Route to High-Surface-Area, Thermally Stable, Microporous Materials via Therm. *J. Am. Chem. Soc.* **2010**, *132* (29), 10171–10183. https://doi.org/10.1021/ja102453s.
- (472) Brown, Jr., J. F.; Vogt, Jr., L. H.; Prescott, P. I. Preparation and Characterization of the Lower Equilibrated Phenylsilsesquioxanes. *J. Am. Chem. Soc.* **1964**, *86* (6), 1120–1125. https://doi.org/10.1021/ja01060a033.
- (473) Su, C.-H.; Chiu, Y.-P.; Teng, C.-C.; Chiang, C.-L. Preparation, Characterization and Thermal Properties of Organic-Inorganic Composites Involving Epoxy and Polyhedral Oligomeric Silsesquioxane (POSS). *J. Polym. Res.* **2010**, *17*, 673–681. https://doi.org/10.1007/s10965-009-9355-y.
- (474) Ahn, S. H.; Park, K. M.; Moon, J. H.; Lee, S. H.; Kim, M. S. Quantification of Carbohydrates and Related Materials Using Sodium Ion Adducts Produced by Matrix-Assisted Laser Desorption Ionization. *J. Am. Soc. Mass Spectrom.* **2016**, *27*, 1887–1890. https://doi.org/10.1007/s13361-016-1495-9.
- (475) Chimjarn, S.; Kunthom, R.; Chancharone, P.; Sodkhomkhum, R.; Sangtrirutnugul, P.; Ervithayasuporn, V. Synthesis of Aromatic Functionalized Cage-Rearranged Silsesquioxanes (T₈, T₁₀, and T₁₂) via Nucleophilic Substitution Reactions. *Dalton Trans.* **2015**, *44* (3), 916–919. https://doi.org/10.1039/c4dt02941k.
- (476) Leong, F. Y.; Low, L. E.; Chew, I. M. L. Theoretical Analysis of Substituent-and Cage-Dependent Electronic Properties of POSS. *AIP Advances* **2023**, *13* (6), 065216. https://doi.org/10.1063/5.0150173.
- (477) Yuan, H.; Li, Q.; Zuo, Y.; Zhang, H.; Zhang, J.; Liu, H.; Xie, J. New Insight into the Structural Stability of Large POSS by Quantum Chemistry Calculation. *Inorg. Chem. Commun.* **2025**, 172, 113761. https://doi.org/10.1016/j.inoche.2024.113761.
- (478) Chinnam, P. R.; Gau, M. R.; Schwab, J.; Zdilla, M. J.; Wunder, S. L. The Polyoctahedral Silsesquioxane (POSS) 1,3,5,7,9,11,13,15-Octaphenylpentacyclo[9.5.1.1^{3,9}.1^{5,15}.1^{7,13}]Octasiloxane (Octaphenyl-POSS). *Acta crystallogr.*, *C Struct. chem.* **2014**, *C70*, 971–974. https://doi.org/10.1107/S2053229614019834.
- (479) Clegg, W.; Sheldrick, G. M.; Vater, N. Dodeca(Phenylsilasesquioxane). *Acta Crystallogr. B Struct. Sci. Cryst. Eng. Mater.* **1980**, *B36*, 3162–3164. https://doi.org/10.1107/S0567740880011156.
- (480) Bassindale, A. R.; Pourny, M.; Taylor, P. G.; Hursthouse, M. B.; Light, M. E. Fluoride-Ion Encapsulation within a Silsesquioxane Cage. *Angew. Chem., Int. Ed.* **2003**, *42*, 3488–3490. https://doi.org/10.1002/anie.200351249.

- (481) Fan, H.; Yang, R. Thermal Decomposition of Polyhedral Oligomeric Octaphenyl, Octa(Nitrophenyl), and Octa(Aminophenyl) Silsesquioxanes. *J. Therm. Anal. Calorim.* **2014**, *116*, 349–357. https://doi.org/10.1007/s10973-013-3554-9.
- (482) Zhang, D.; Yang, R.; Qin, Z.; Zhang, W. Study on the Thermal Behaviors of Polyhedral Oligomeric Octaphenylsilsesquioxane (OPS). *J. Therm. Anal. Calorim.* **2023**, *148*, 2345–2355. https://doi.org/10.1007/s10973-022-11887-3.
- (483) Sheldrick, G. M. SHELXT Integrated Space-Group and Crystal-Structure Determination. *Acta Crystallogr. A: Found. Adv.* **2015**, *71* (1), 3–8. https://doi.org/10.1107/S2053273314026370.
- (484) Sheldrick, G. M. Crystal Structure Refinement with SHELXL. *Acta crystallogr., C Struct. chem.* **2015**, *71* (1), 3–8. https://doi.org/10.1107/S2053229614024218.
- (485) Hübschle, C. B.; Sheldrick, G. M.; Dittrich, B. ShelXle: A Qt Graphical User Interface for SHELXL. *J. Appl. Crystallogr.* **2011**, *44* (6), 1281–1284. https://doi.org/10.1107/S0021889811043202.

6 Supporting Information

- 6.1 High-Refractive-Index Polysiloxanes Containing Naphthyl and Phenanthrenyl Groups and their Thermally Cross-Linked Resins
- 6.1.1 Dialkoxysilanes
- 6.1.1.1 Nuclear Magnetic Resonance (NMR) Spectroscopy
- 1-NaphPhSi(OMe)₂

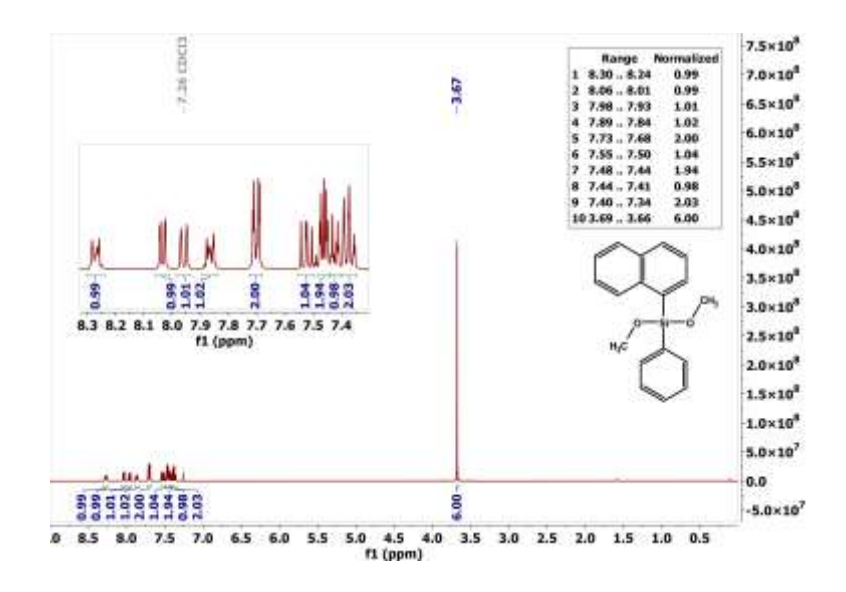


Figure S 1: ¹H NMR spectrum (CDCl₃, 400 MHz) of dimethoxyphenyl-(1-naphthyl)silane.

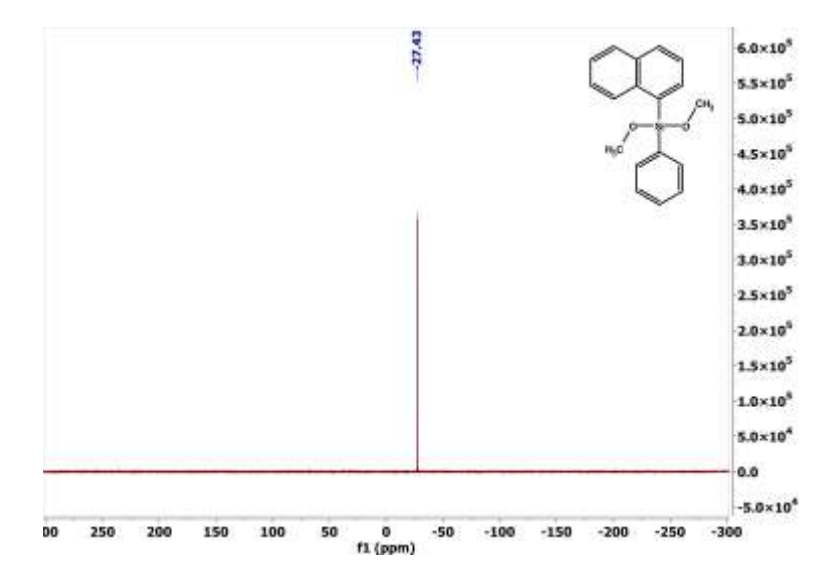


Figure S 2: ²⁹Si NMR spectrum (CDCl₃, 79 MHz) of dimethoxyphenyl-(1-naphthyl)silane.

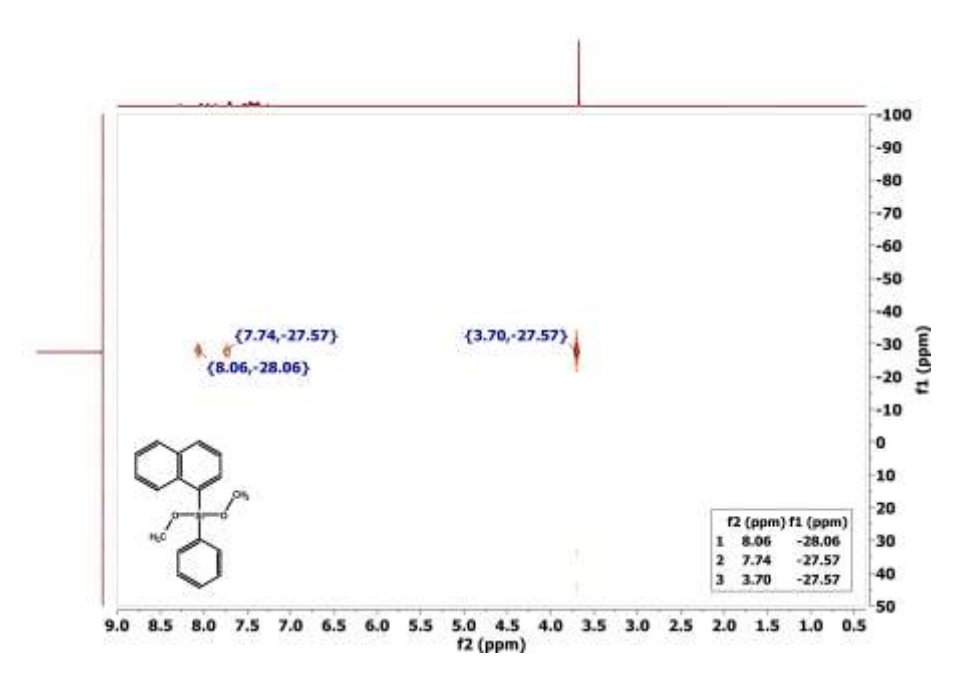


Figure S 3: ¹H, ²⁹Si HMBC spectrum (CDCl₃, 400 MHz; 79 MHz) of dimethoxyphenyl-(1-naphthyl)silane.

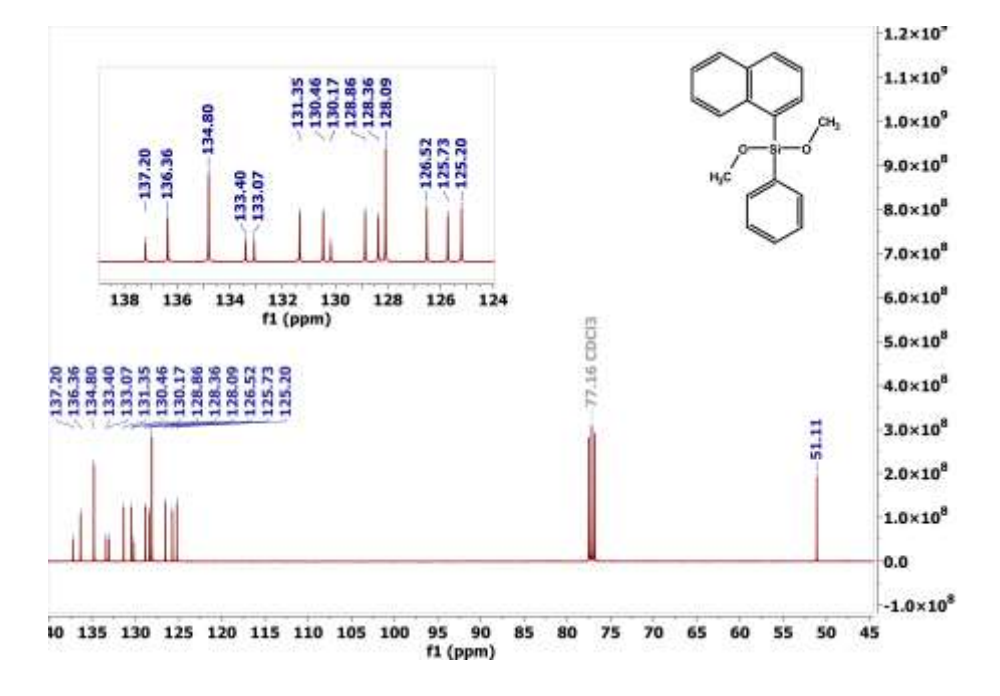


Figure S 4: ¹³C NMR spectrum (CDCl₃, 101 MHz) of dimethoxyphenyl-(1-naphthyl)silane.

2-NaphPhSi(OMe)₂

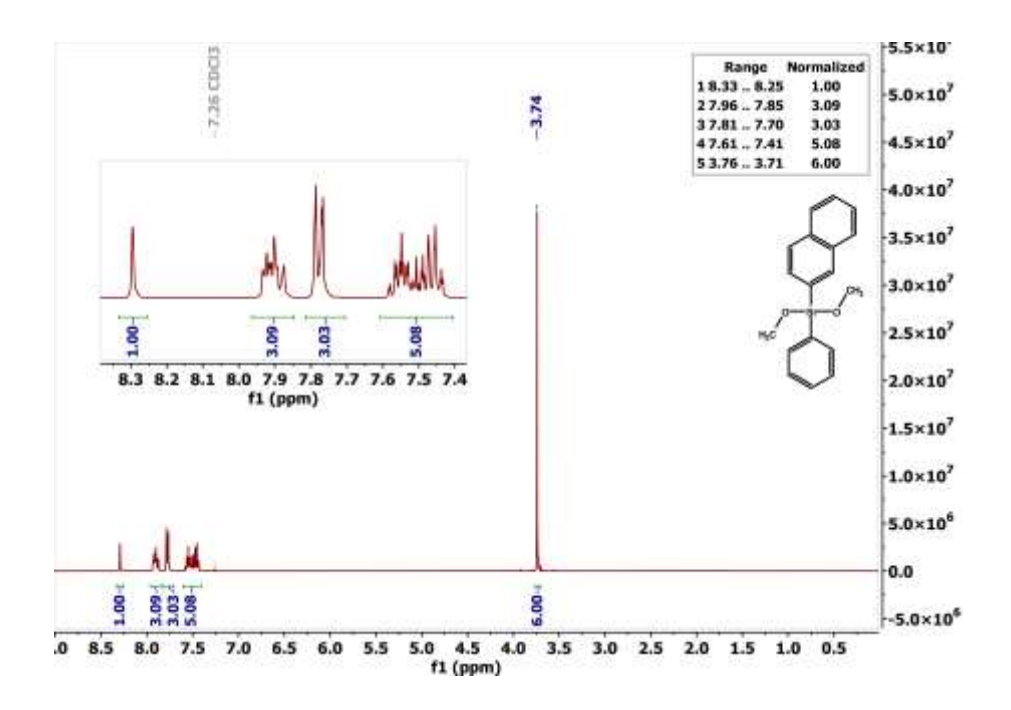


Figure S 5: ¹H NMR spectrum (CDCl₃, 400 MHz) of dimethoxyphenyl-(2-naphthyl)silane.

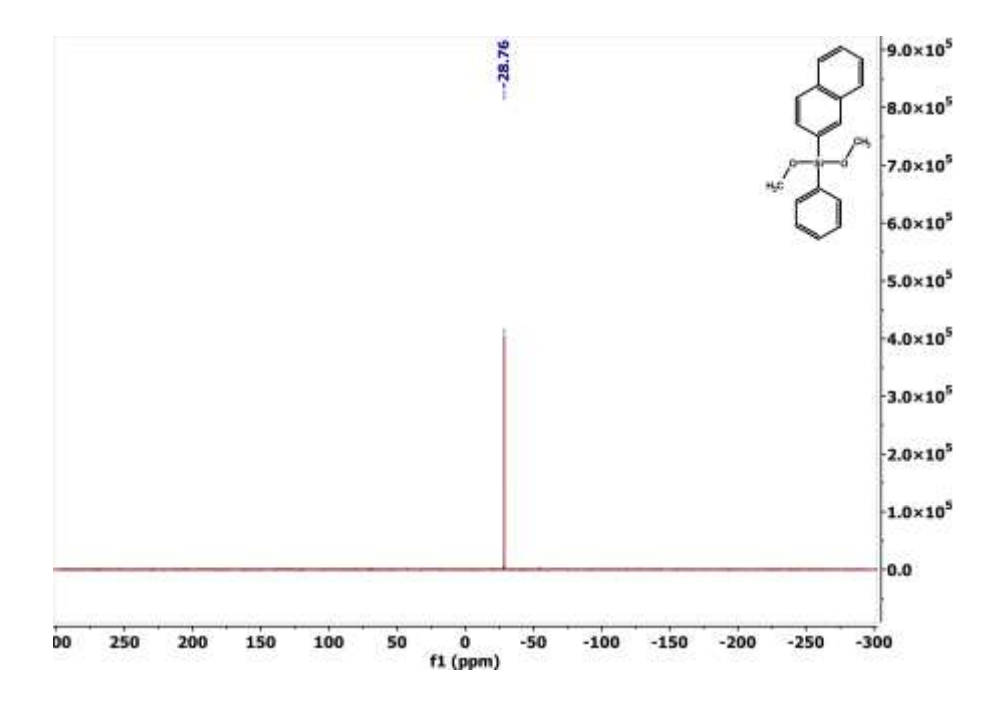


Figure S 6: ²⁹Si NMR spectrum (CDCl₃, 79 MHz) of dimethoxyphenyl-(2-naphthyl)silane.

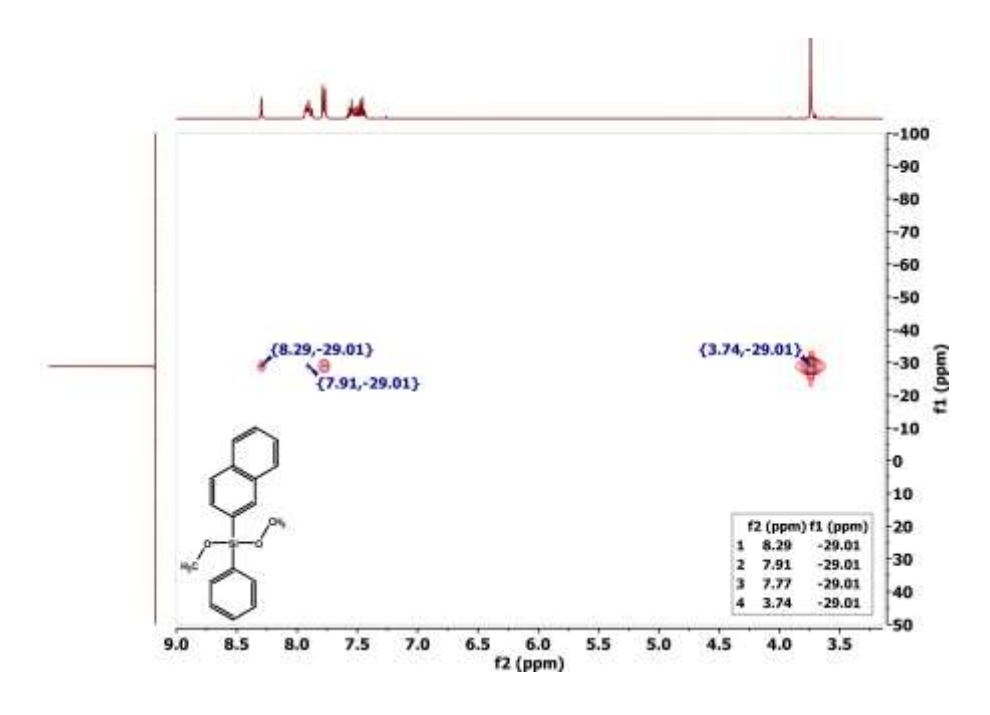


Figure S 7: ¹H, ²⁹Si HMBC spectrum (CDCl₃, 400 MHz; 79 MHz) of dimethoxyphenyl-(2-naphthyl)silane.

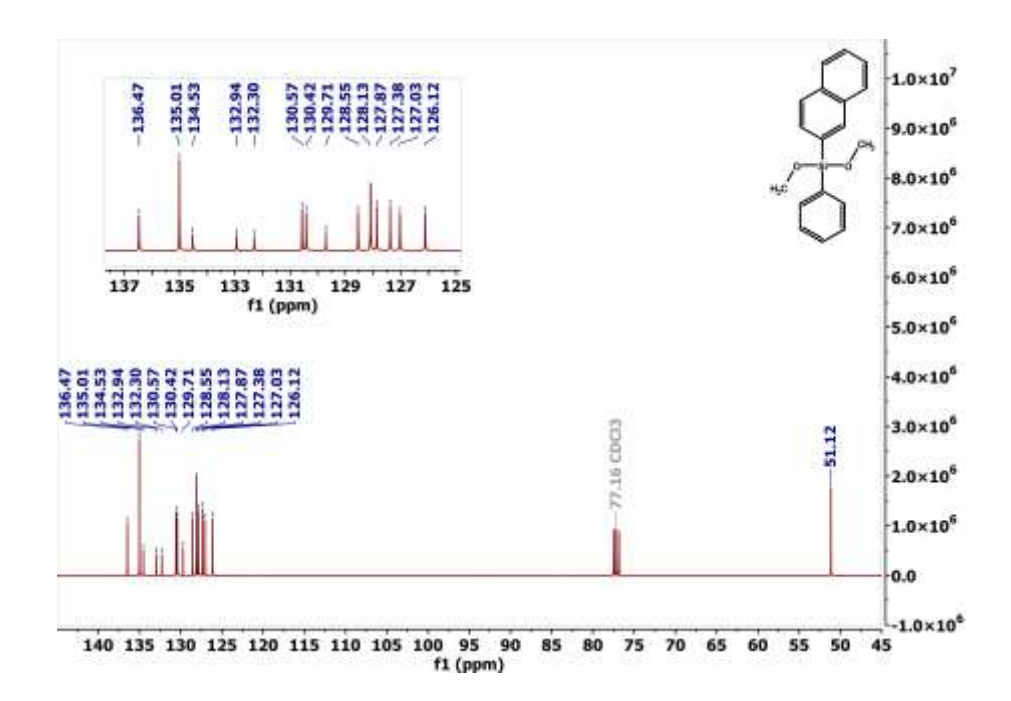


Figure S 8: ¹³C NMR spectrum (CDCl₃, 101 MHz) of dimethoxyphenyl-(2-naphthyl)silane.

9-PhenPhSi(OMe)₂

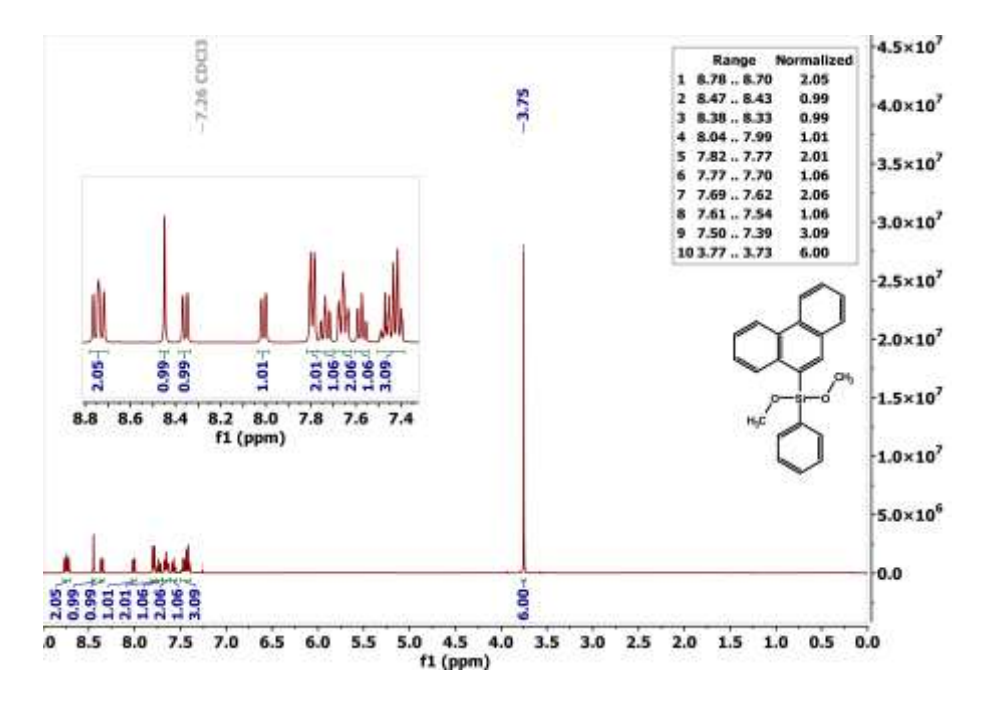


Figure S 9: ¹H NMR spectrum (CDCl₃, 400 MHz) of dimethoxyphenyl-(9-phenanthrenyl)silane.

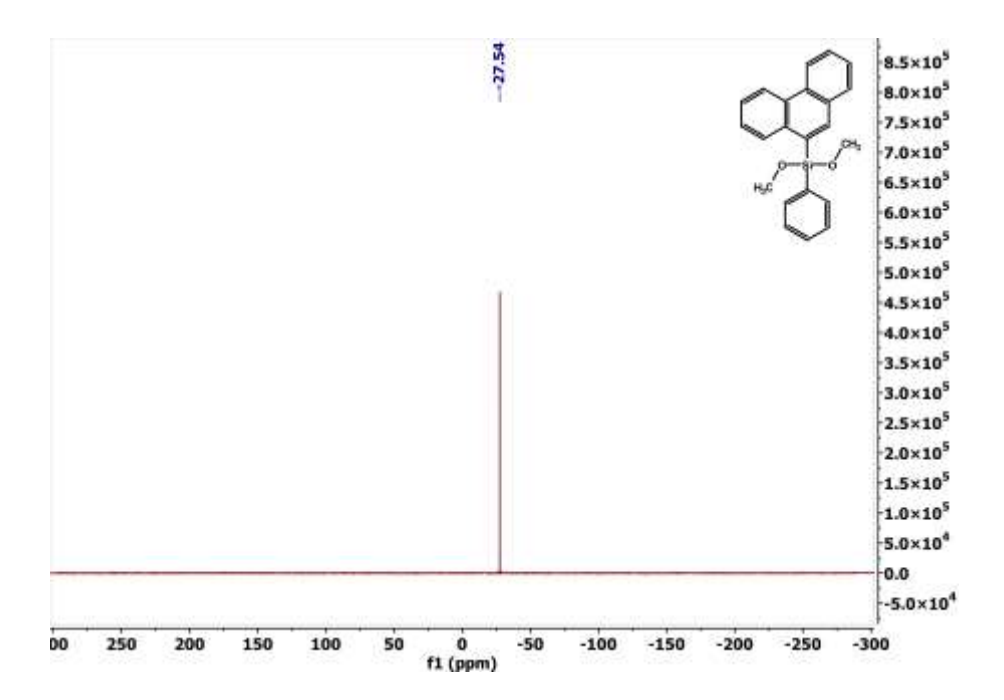


Figure S 10: ²⁹Si NMR spectrum (CDCl₃, 79 MHz) of dimethoxyphenyl-(9-phenanthrenyl)silane.

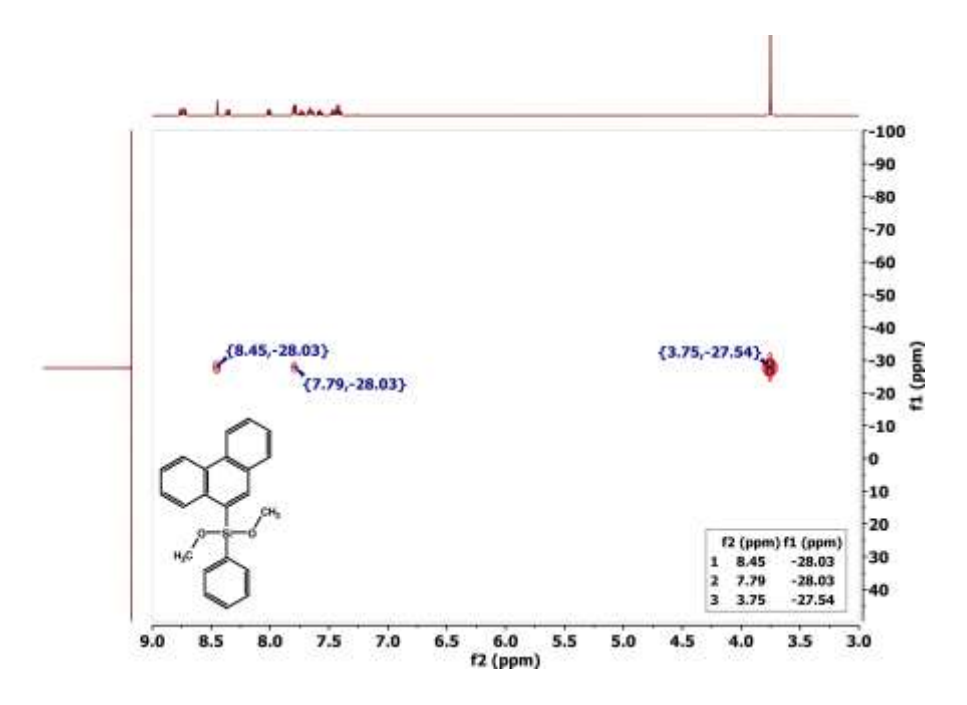


Figure S 11: ¹H, ²⁹Si HMBC spectrum (CDCl₃, 400 MHz; 79 MHz) of dimethoxyphenyl-(9-phenanthrenyl)silane.

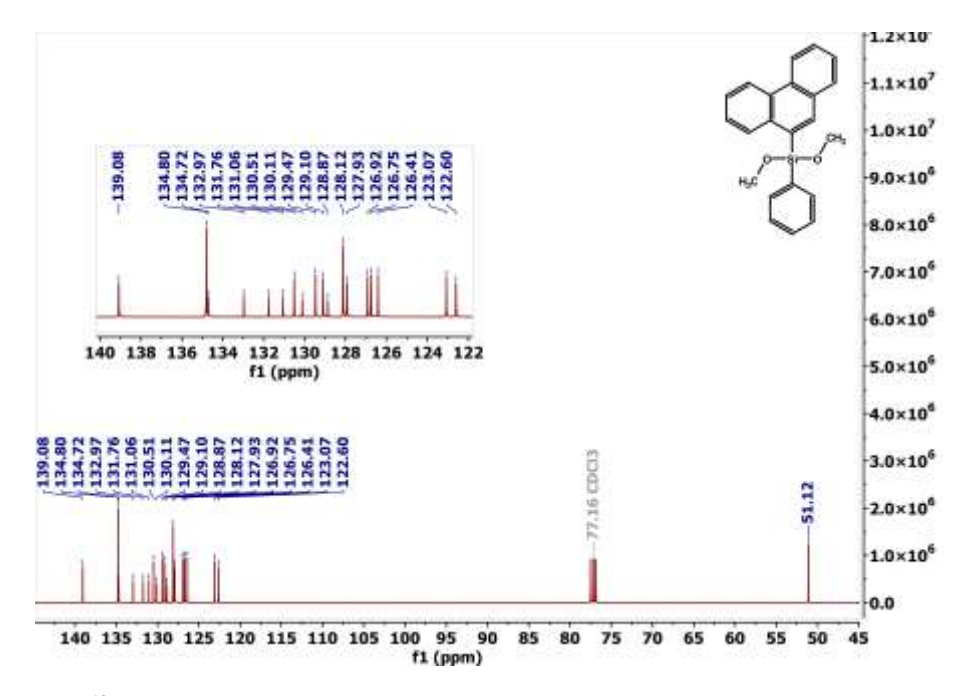


Figure S 12: ¹³C NMR spectrum (CDCl₃, 101 MHz) of dimethoxyphenyl-(9-phenanthrenyl)silane.

6.1.1.2 Fourier Transform Infrared (FTIR) Spectroscopy

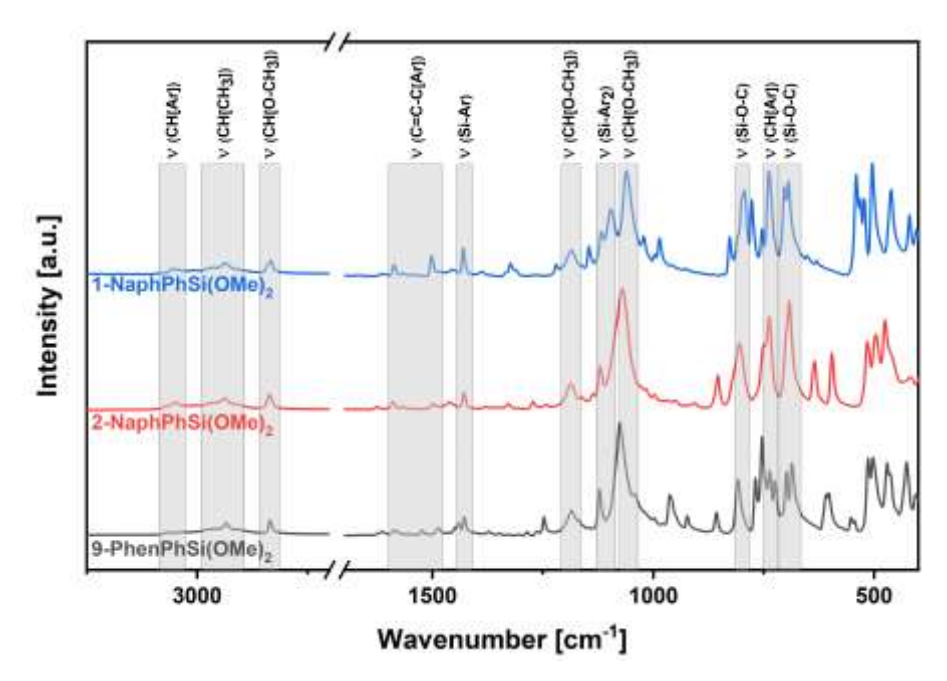


Figure S 13: FTIR spectra of 1-NaphPhSi(OMe)₂ (blue), 2-NaphPhSi(OMe)₂ (red) and 9-PhenPhSi(OMe)₂ (black).

FTIR: 3060 cm⁻¹ (v(CH)_{Ar}), 2937 cm⁻¹ (v(CH₃)), 2828 cm⁻¹ (v(O-CH₃)), 1586 cm⁻¹ (v(C=C-C)_{Ar}), 1503 cm⁻¹ (v(C=C-C)_{Ar}), 1434 cm⁻¹ (v(Si-Ar)), 1187 cm⁻¹ (v(CH_{OCH3})), 1097 cm⁻¹ (v(Ar-Si-Ar)), 1059 cm⁻¹ (v(CH_{OCH3})), 792 cm⁻¹ (v(Si-O-C)), 736 cm⁻¹ (v(CH)_{Ar}), 690 cm⁻¹ (v(Si-O-C))

6.1.1.3 Elemental Analysis

Table S 1: Elemental analysis of 1-NaphPhSi(OMe)₂, 2-NaphPhSi(OMe)₂ and 9-PhenPhSi(OMe)₂.

	C (calc.)	C (found)	H (calc.)	H (found)	ΔC	ΔΗ
	[%]	[%]	[%]	[%]	[%]	[%]
1-NaphPhSi(OMe) ₂	73.43	73.21	6.16	5.78	0.22	0.38
2-NaphPhSi(OMe) ₂	73.43	73.30	6.16	6.39	0.13	0.23
9-PhenPhSi(OMe) ₂	76.71	76.07	5.85	5.68	0.64	0.17

6.1.1.4 Ultraviolet-visible (UV-vis) Spectroscopy

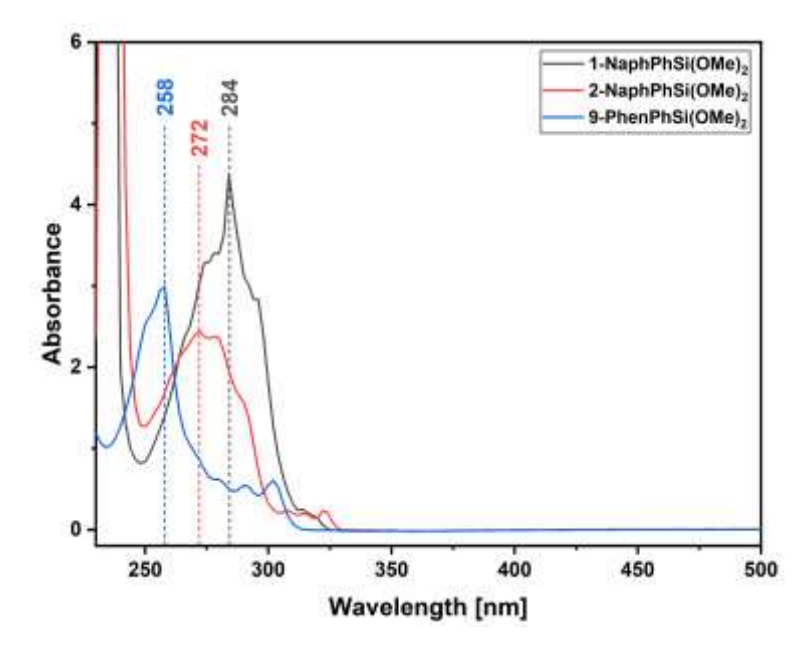


Figure S 14: UV-vis spectra of 1-NaphPhSi(OMe)₂ (black), 2-NaphPhSi(OMe)₂ (red) and 9-PhenPhSi(OMe)₂ (blue).

6.1.1.5 Fluorescence Spectroscopy

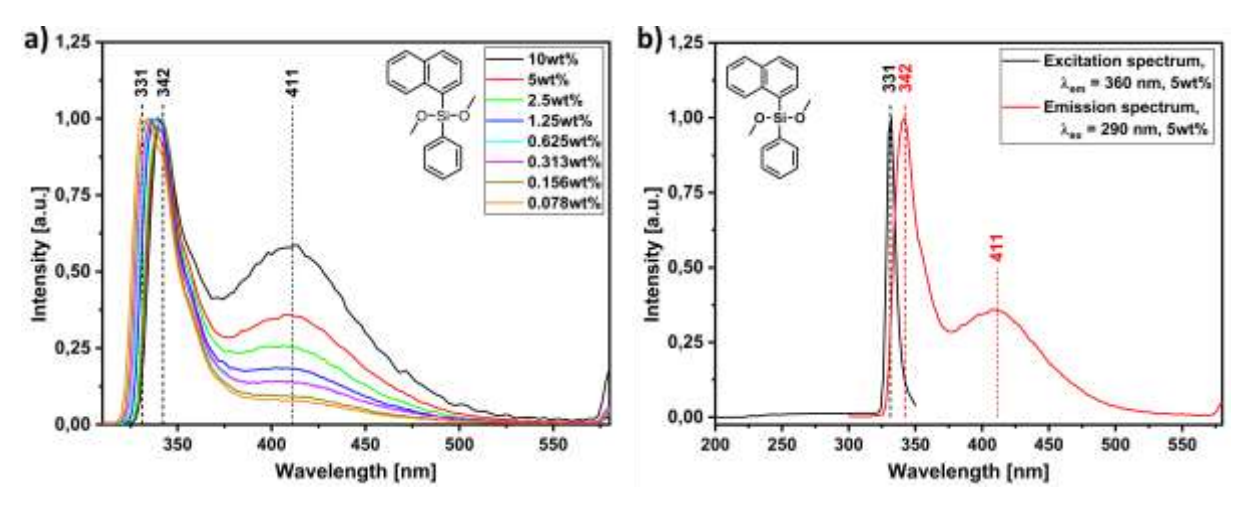


Figure S 15: a) Fluorescence spectra of a dilution series of 1-NaphPhSi(OMe)₂ in DCM with λ_{ex} = 290 nm and b) emission and excitation spectra of a 5wt% solution of 1-NaphPhSi(OMe)₂.

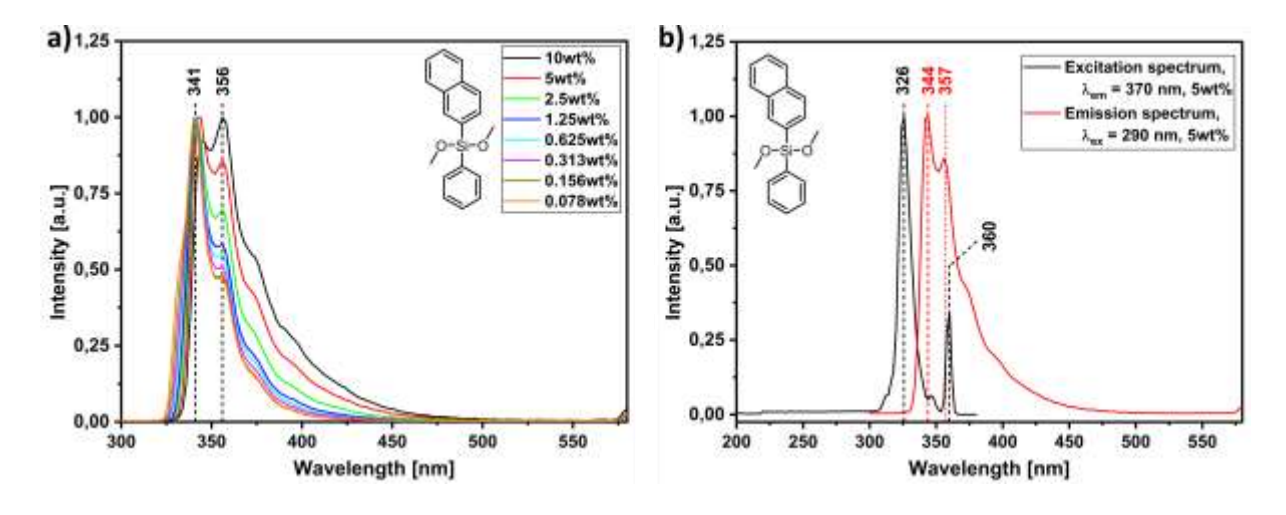


Figure S 16: a) Fluorescence spectra of a dilution series of 2-NaphPhSi(OMe)₂ in DCM with λ_{ex} = 290 nm and b) emission and excitation spectra of a 5wt% solution of 2-NaphPhSi(OMe)₂.

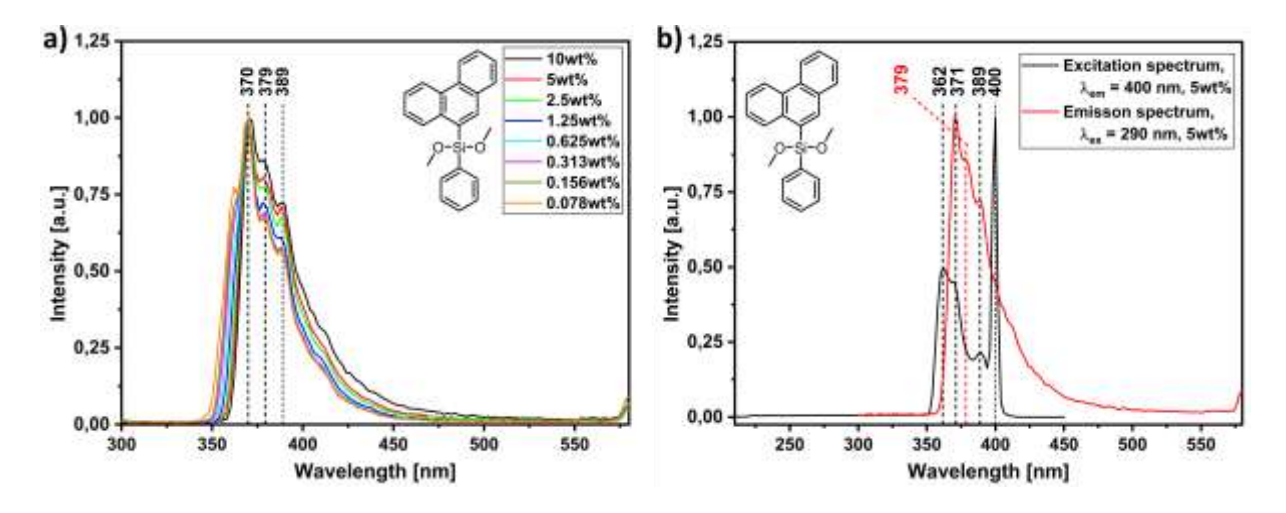


Figure S 17: a) Fluorescence spectra of a dilution series of 9-PhenPhSi(OMe)₂ in DCM with λ_{ex} = 290 nm and b) emission and excitation spectra of a 5wt% solution of 9-PhenPhSi(OMe)₂.

6.1.1.6 Refractive Index (RI)

For solid samples and soluble polysiloxanes, the RI is determined using a calibration method. Each of the samples is diluted in toluene to yield a solution with 22.5 wt%. After the RI of the initial solution is determined it is further diluted in fixed steps of 2.5 wt% up to 7.5 wt%. After all measurements have been made the RI is plotted against the dilution and a linear regression is applied. To simulate the undiluted sample, 100 is used for x and the equation is solved. An evaluation of this method was done by comparing the average RI of 2-NaphPhSi(OMe)₂ measured three times directly and by the described method. Both RIs only vary by 0.004 (see **Figure S 18**) which shows that this method is well suited to obtain the refractive index of solids.

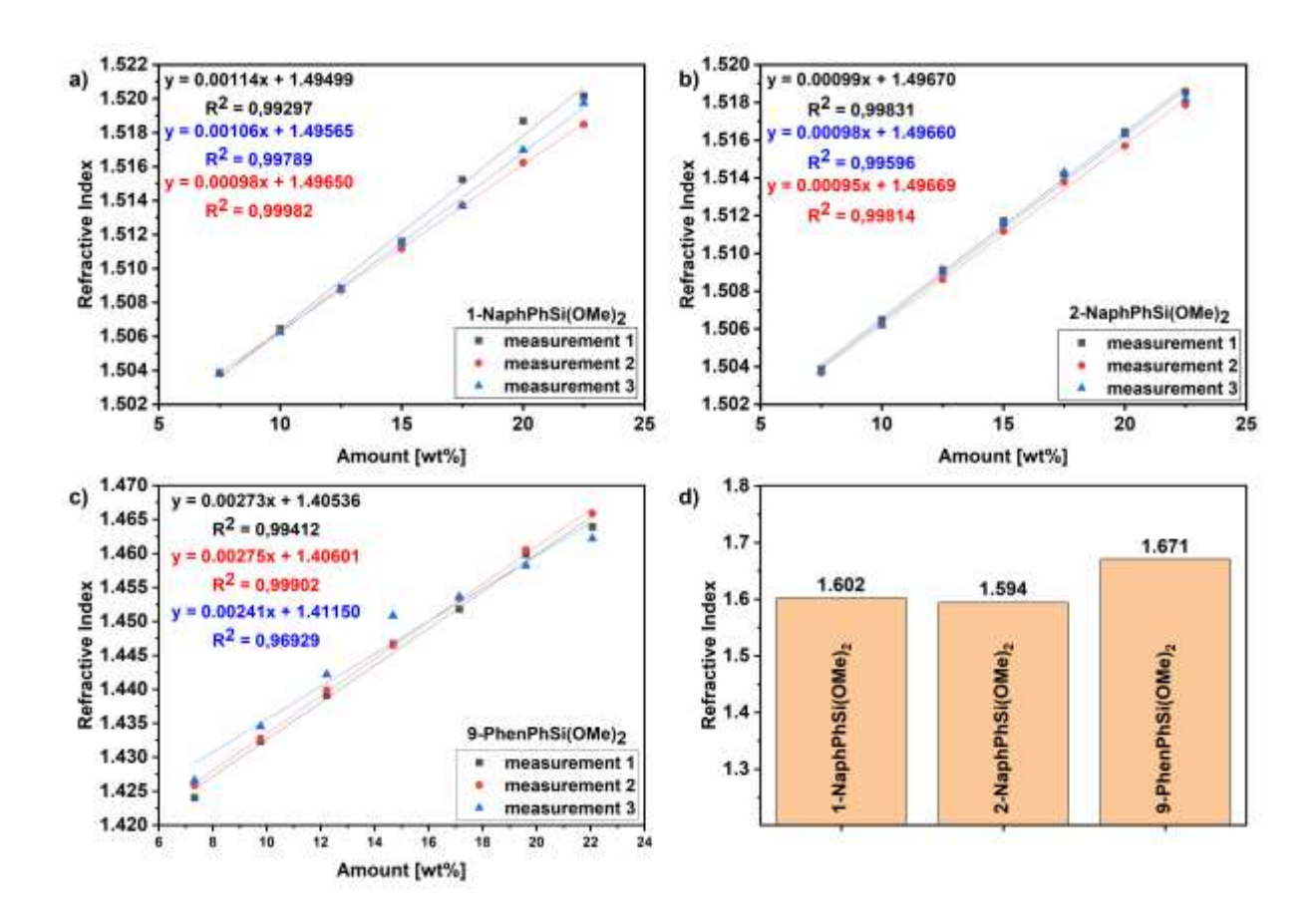


Figure S 18: Calibration curve of a) 1-NaphPhSi(OMe)₂, b) 2-NaphPhSi(OMe)₂ and c) 9-PhenPhSi(OMe)₂ diluted in different amounts of toluene; d) summary of all RIs.

$$RI_{1,a} = 0.00114 \cdot 100 + 1.49499 = 1.609$$

 $RI_{2,a} = 0.00106 \cdot 100 + 1.49565 = 1.602$
 $RI_{3,a} = 0.00098 \cdot 100 + 1.49650 = 1.595$
 $RI_{av,a} = 1.602$

$$RI_{1,b} = 0.00099 \cdot 100 + 1.49670 = 1.596$$

 $RI_{2,b} = 0.00098 \cdot 100 + 1.49660 = 1.595$
 $RI_{3,b} = 0.00095 \cdot 100 + 1.49669 = 1.592$

$$RI_{av,b} = 1.594$$

$$RI_{1,c} = 0.00273 \cdot 100 + 1.40536 = 1.678$$

 $RI_{2,c} = 0.00275 \cdot 100 + 1.40601 = 1.681$
 $RI_{3,c} = 0.00241 \cdot 100 + 1.41150 = 1.653$
 $RI_{av,c} = 1.671$

Table S 2: Refractive indices of 1-NaphPhSi(OMe)₂, 2-NaphPhSi(OMe)₂ and 9-PhenPhSi(OMe)₂.

Compound	Average of calibration curves	Average of direct measurements
1-NaphPhSi(OMe) ₂	1.602 ± 0.006	
2-NaphPhSi(OMe) ₂	1.594 ± 0.002	1.598 ± 0.000
9-PhenPhSi(OMe) ₂	1.671 ± 0.013	

6.1.2 Polysiloxanes/Silsesquioxanes

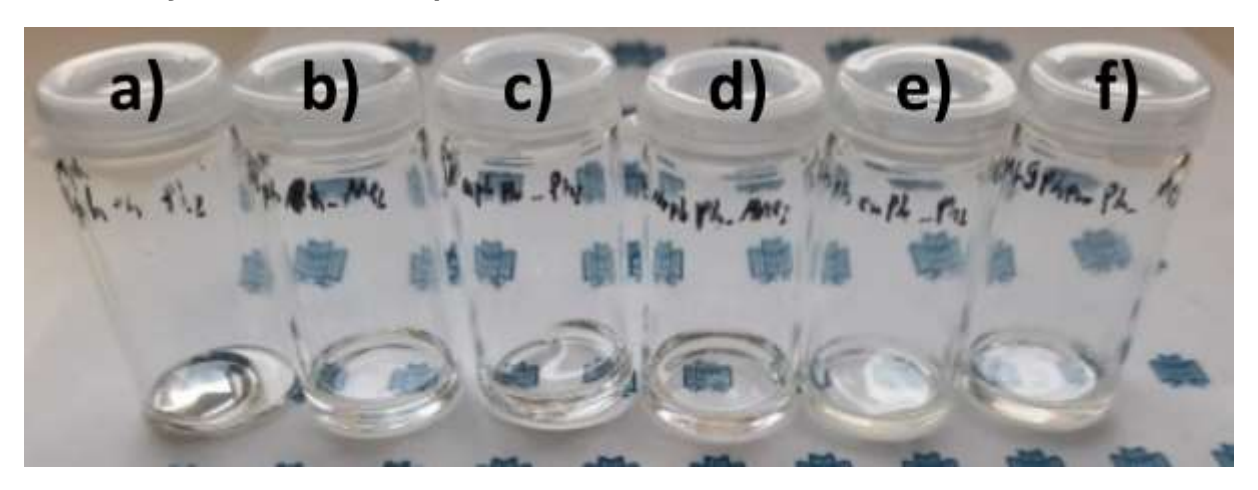


Figure S 19: Polysiloxanes before consolidation. a) MGNaph1_Ph_Ph₂, b) MGNaph1_Ph_Me₂, c) MGNaph2_Ph_Ph₂, d) MGNaph2_Ph_Me₂, e) MGPhen9_Ph_Ph₂, f) MGPhen9_Ph_Me₂.

6.1.2.1 Nuclear Magnetic Resonance (NMR) Spectroscopy

MGNaph1_Ph_Ph2

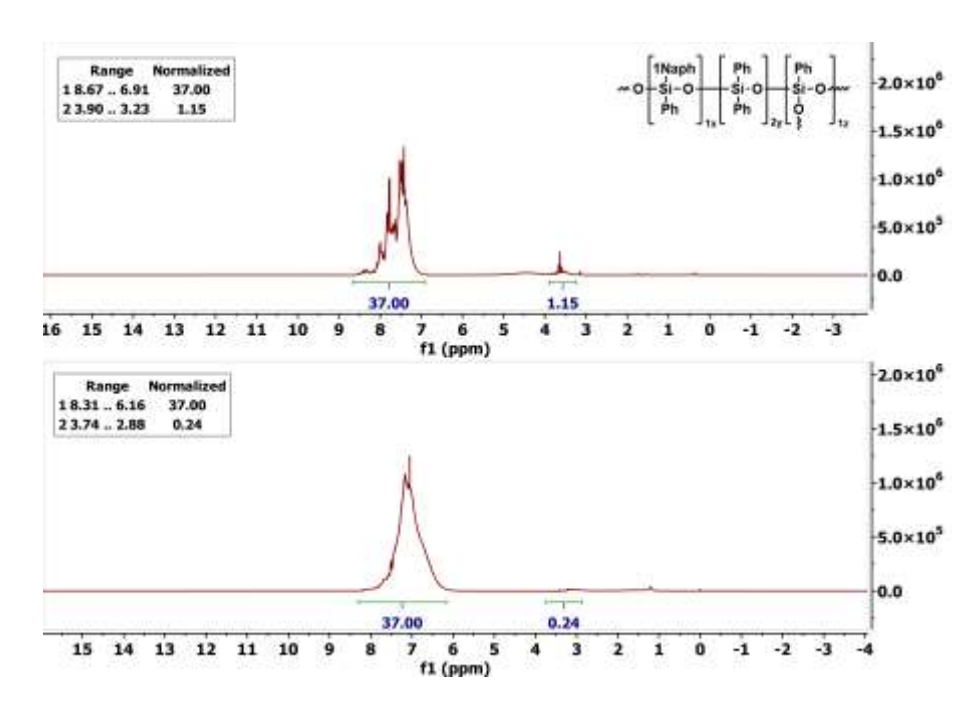


Figure S 20: ¹H NMR spectrum (CDCl₃, 400 MHz) of MGNaph1_Ph_Ph₂ unconsolidated (top) and consolidated (bottom).

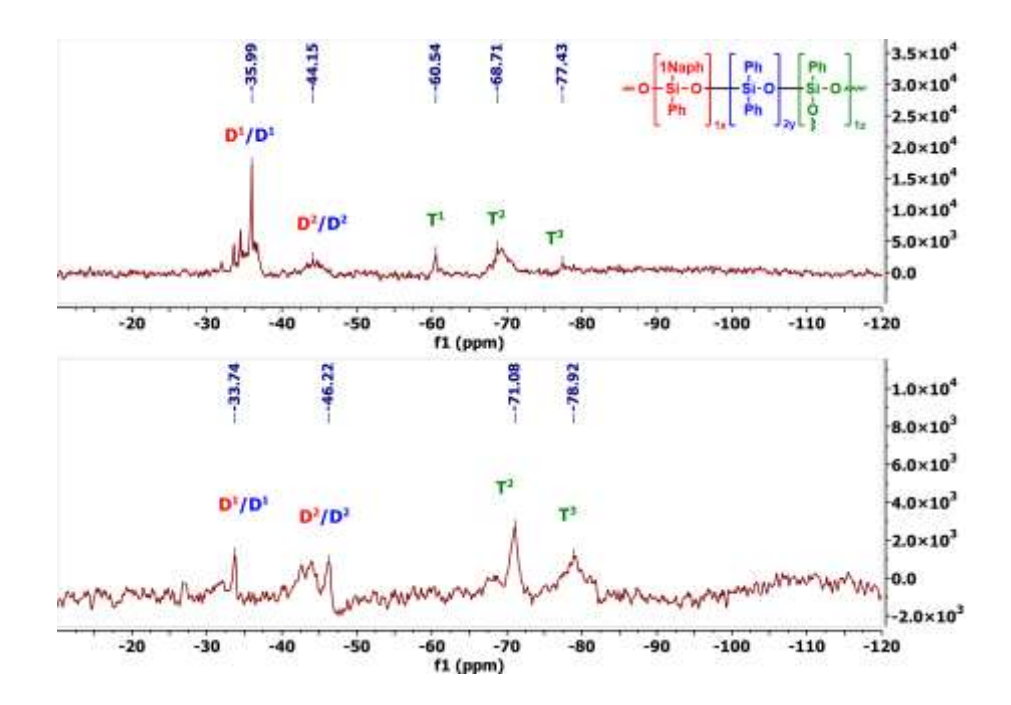


Figure S 21: ²⁹Si NMR spectrum (CDCl₃, 79 MHz) of MGNaph1_Ph_Ph₂ unconsolidated (top) and consolidated (bottom).

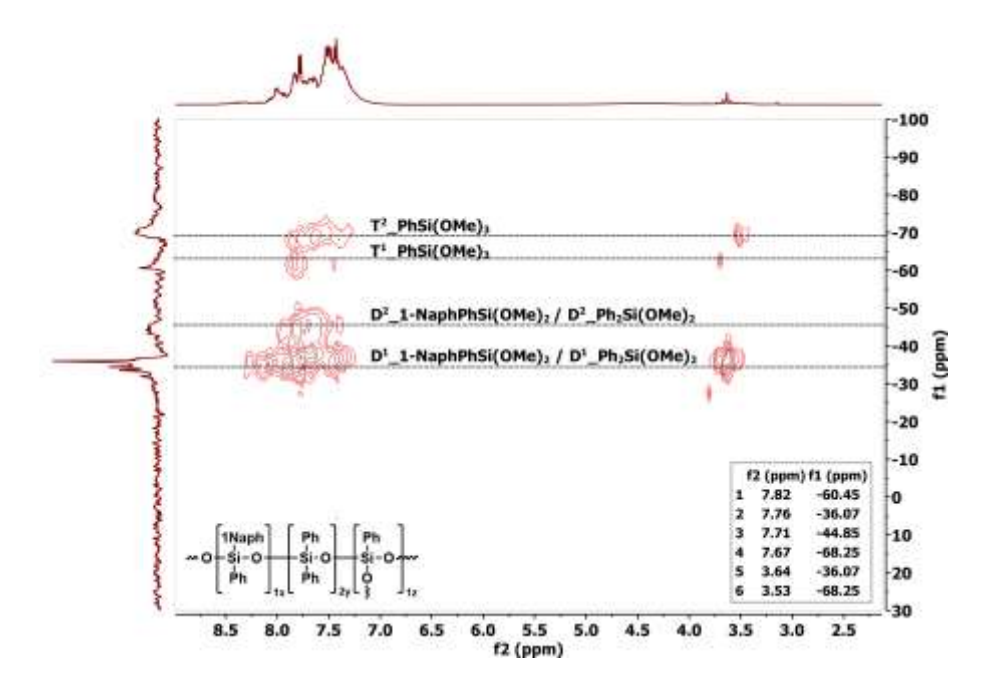


Figure S 22: ¹H, ²⁹Si HMBC spectrum (CDCl₃, 400 MHz; 79 MHz) of the unconsolidated MGNaph1_Ph_Ph₂.

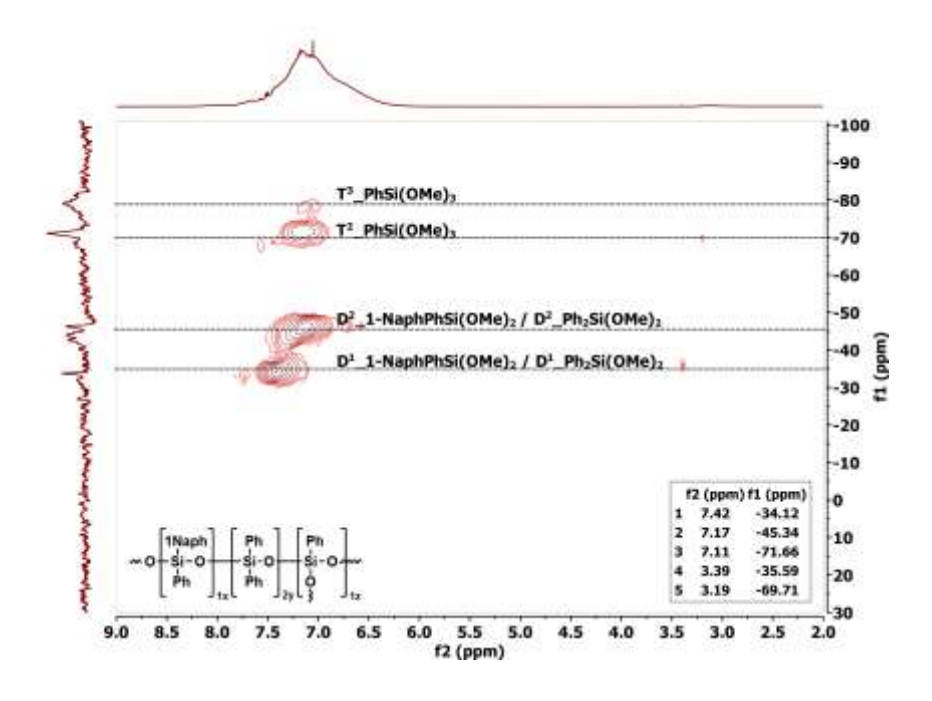


Figure S 23: ¹H, ²⁹Si HMBC spectrum (CDCl₃, 400 MHz; 79 MHz) of the consolidated MGNaph1_Ph_Ph₂.

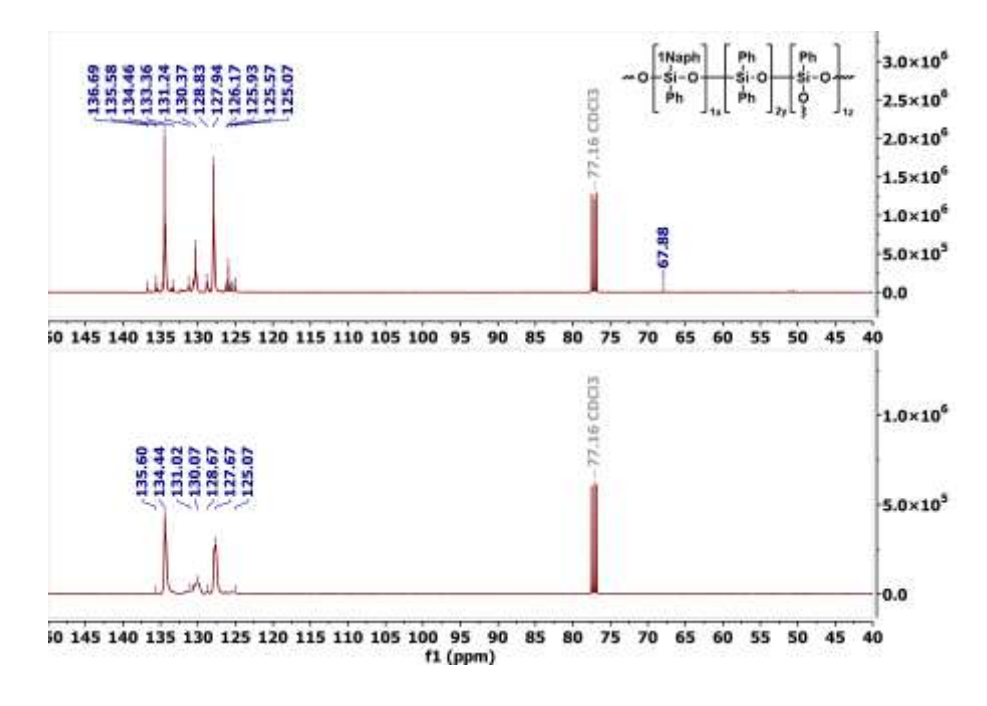


Figure S 24: ¹³C NMR spectrum (CDCl₃, 101 MHz) of MGNaph1_Ph_Ph₂ unconsolidated (top) and consolidated (bottom).

MGNaph1_Ph_Me2

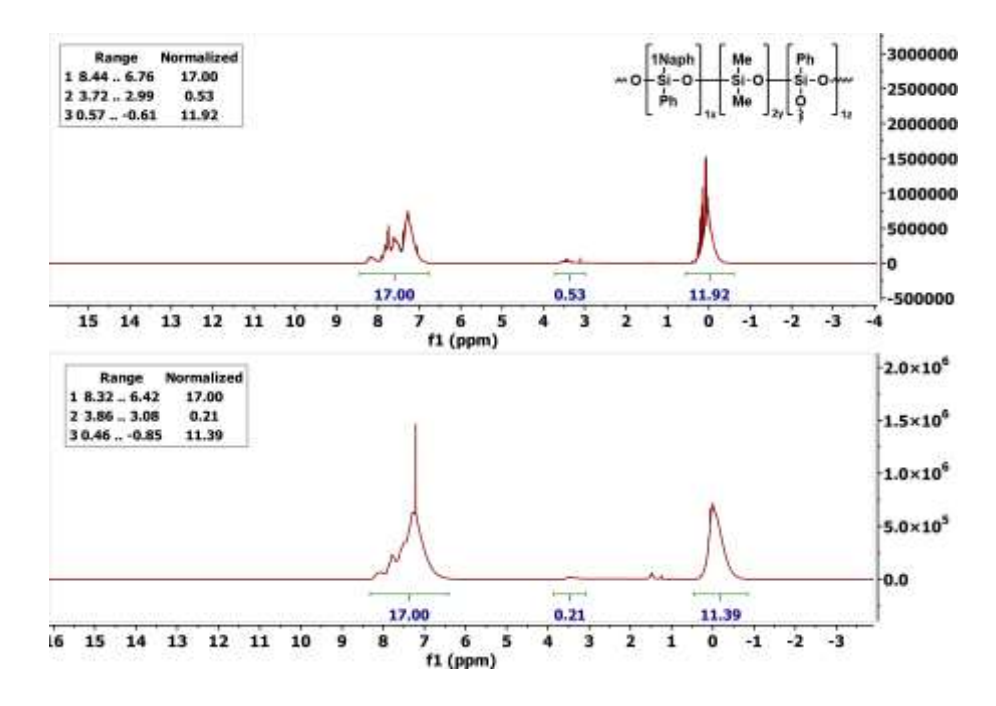


Figure S 25: ¹H NMR spectrum (CDCl₃, 400 MHz) of MGNaph1_Ph_Me₂ unconsolidated (top) and consolidated (bottom).

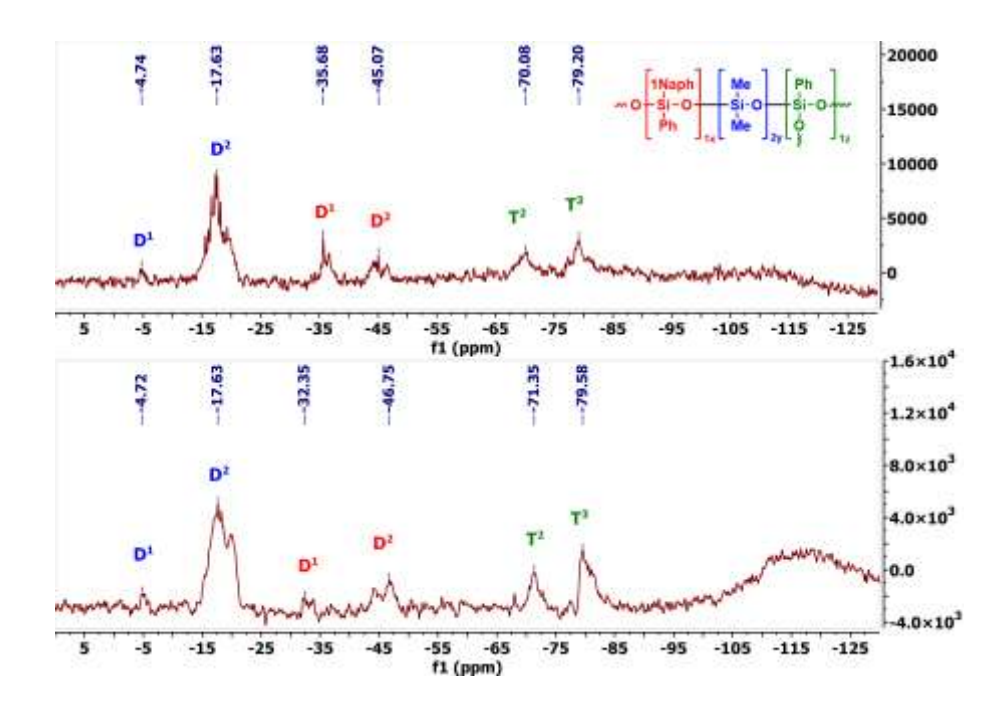


Figure S 26: ²⁹Si NMR spectrum (CDCl₃, 79 MHz) of MGNaph1_Ph_Me₂ unconsolidated (top) and consolidated (bottom).

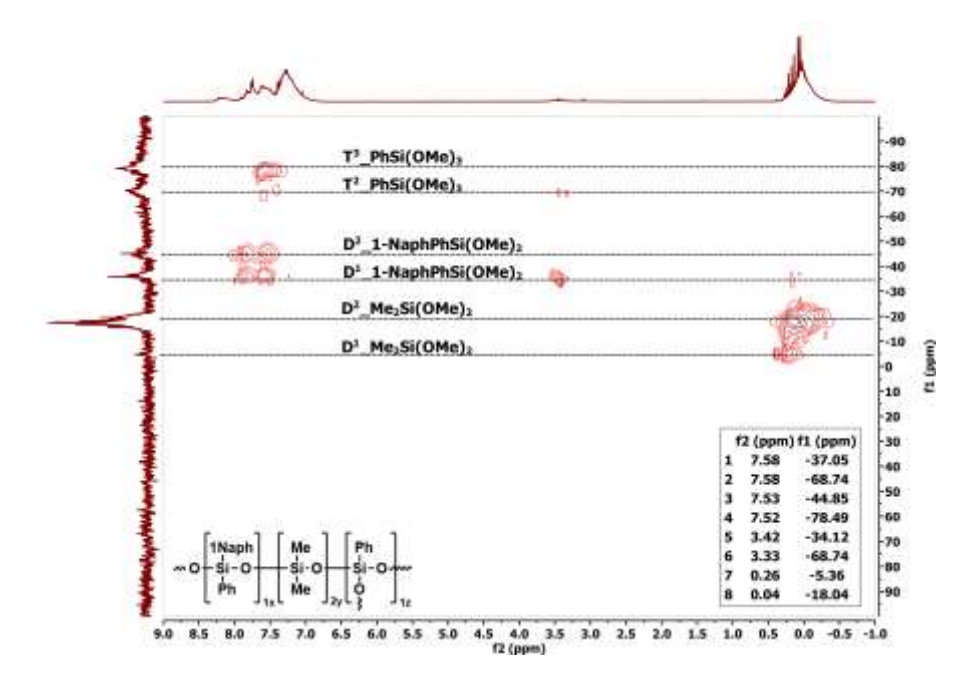


Figure S 27: ¹H, ²⁹Si HMBC spectrum (CDCl₃, 400 MHz; 79 MHz) of the unconsolidated MGNaph1_Ph_Me₂.

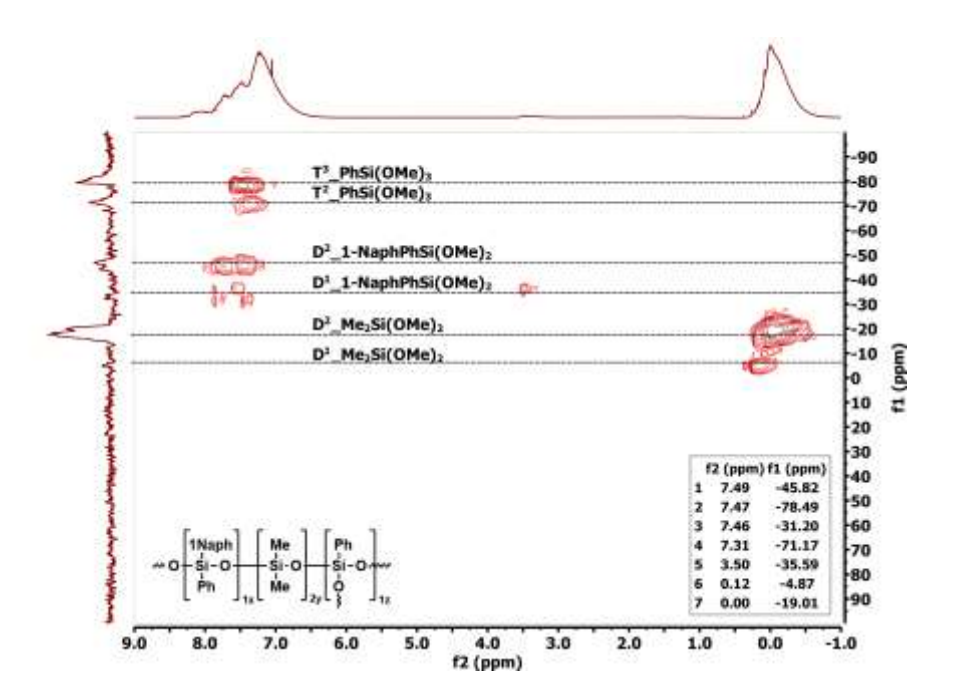


Figure S 28: ¹H, ²⁹Si HMBC spectrum (CDCl₃, 400 MHz; 79 MHz) of the consolidated MGNaph1_Ph_Me₂.

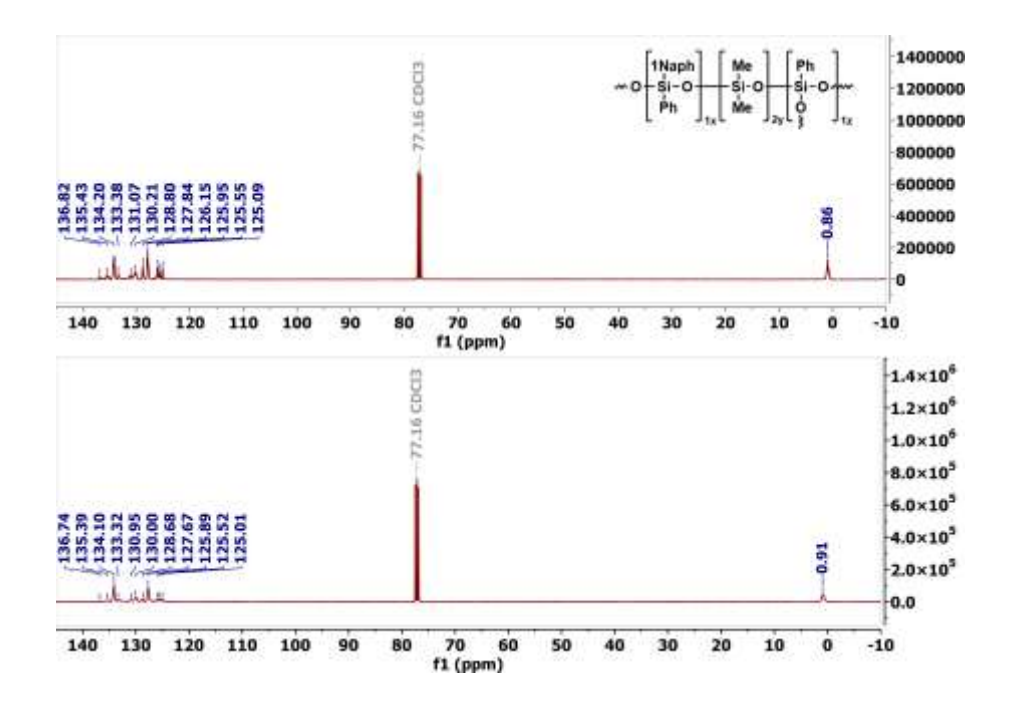


Figure S 29: ¹³C NMR spectrum (CDCl₃, 101 MHz) of MGNaph1_Ph_Me₂ unconsolidated (top) and consolidated (bottom).

MGNaph2_Ph_Ph2

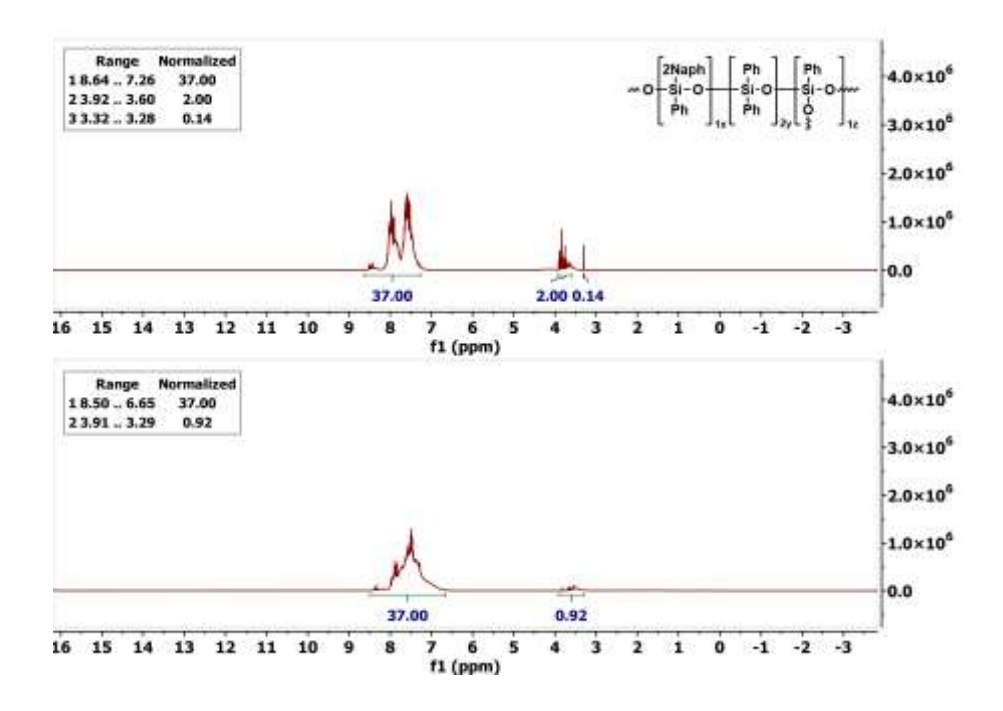


Figure S 30: ¹H NMR spectrum (CDCl₃, 400 MHz) of MGNaph2_Ph_Ph₂ unconsolidated (top) and consolidated (bottom).

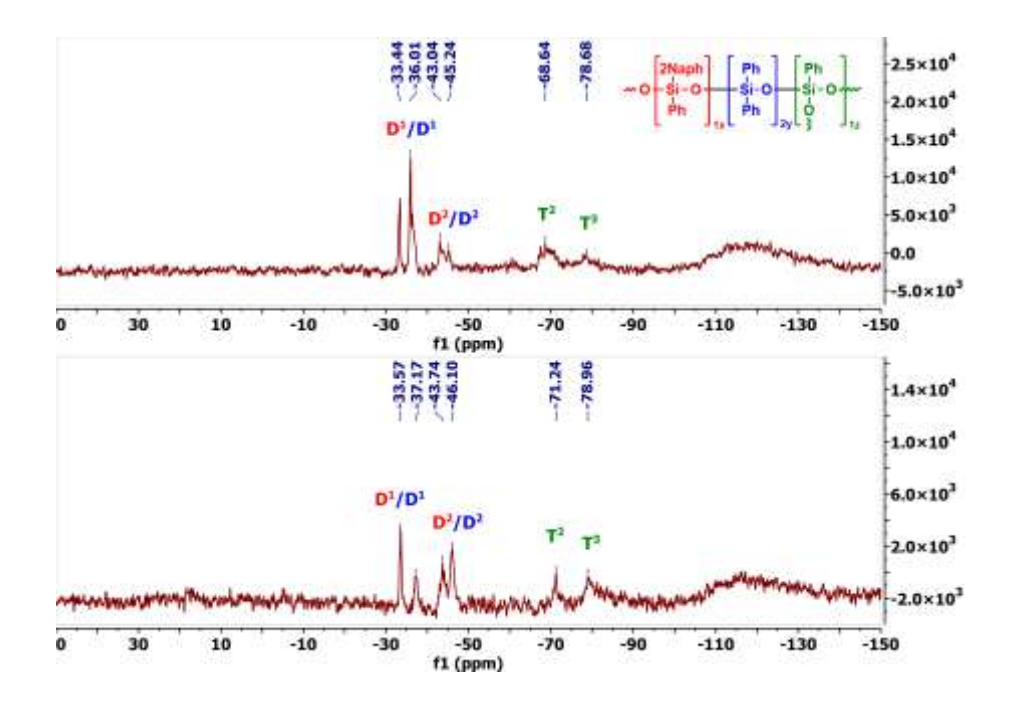


Figure S 31: ²⁹Si NMR spectrum (CDCl₃, 79 MHz) of MGNaph2_Ph_Ph₂ unconsolidated (top) and consolidated (bottom).

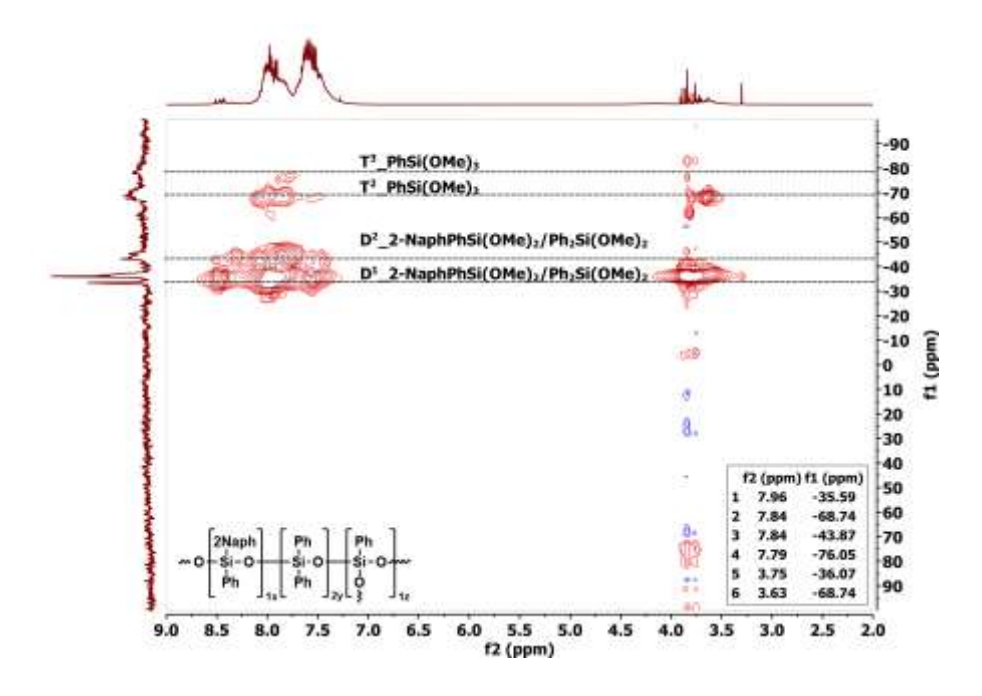


Figure S 32: ¹H, ²⁹Si HMBC spectrum (CDCl₃, 400 MHz; 79 MHz) of the unconsolidated MGNaph2_Ph_Ph₂.

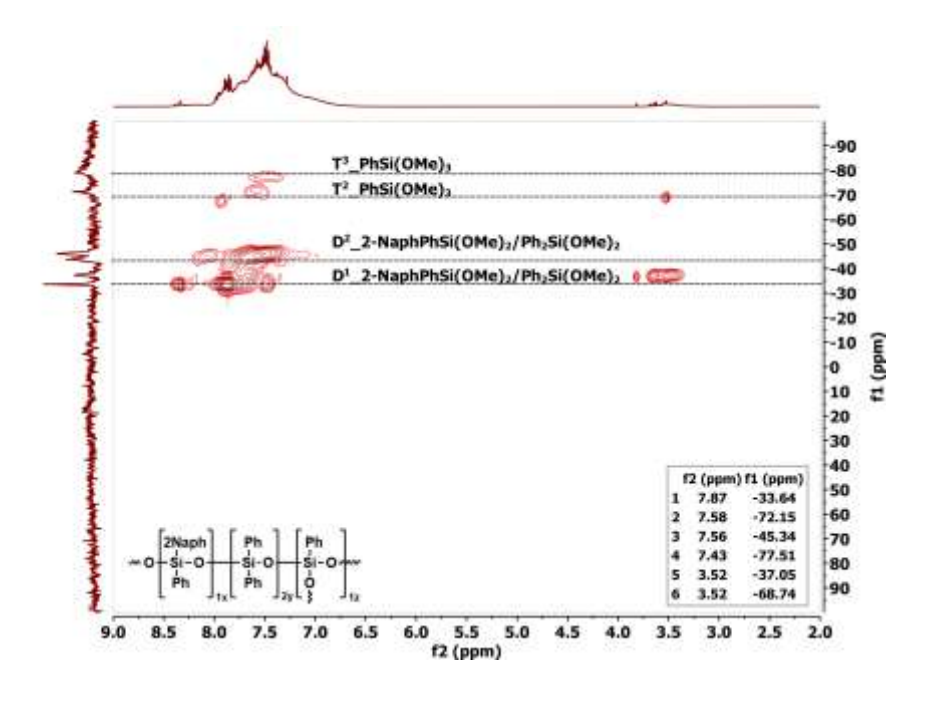


Figure S 33: ¹H, ²⁹Si HMBC spectrum (CDCl₃, 400 MHz; 79 MHz) of the consolidated MGNaph2_Ph_Ph₂.

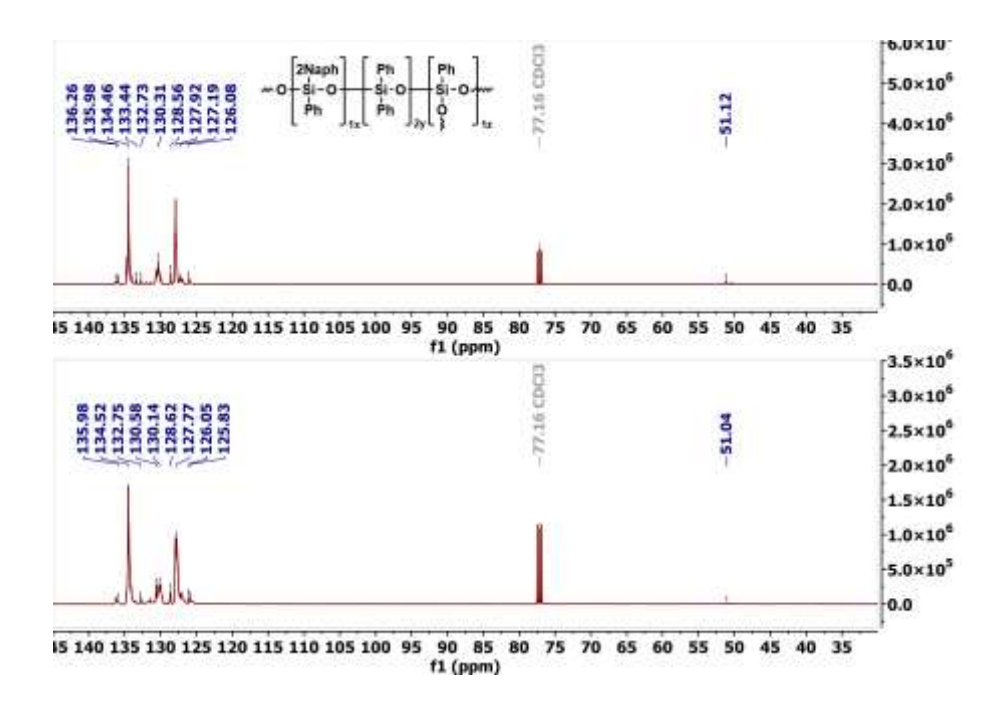


Figure S 34: ¹³C NMR spectrum (CDCl₃, 101 MHz) of MGNaph2_Ph_Ph₂ unconsolidated (top) and consolidated (bottom).

MGNaph2_Ph_Me2

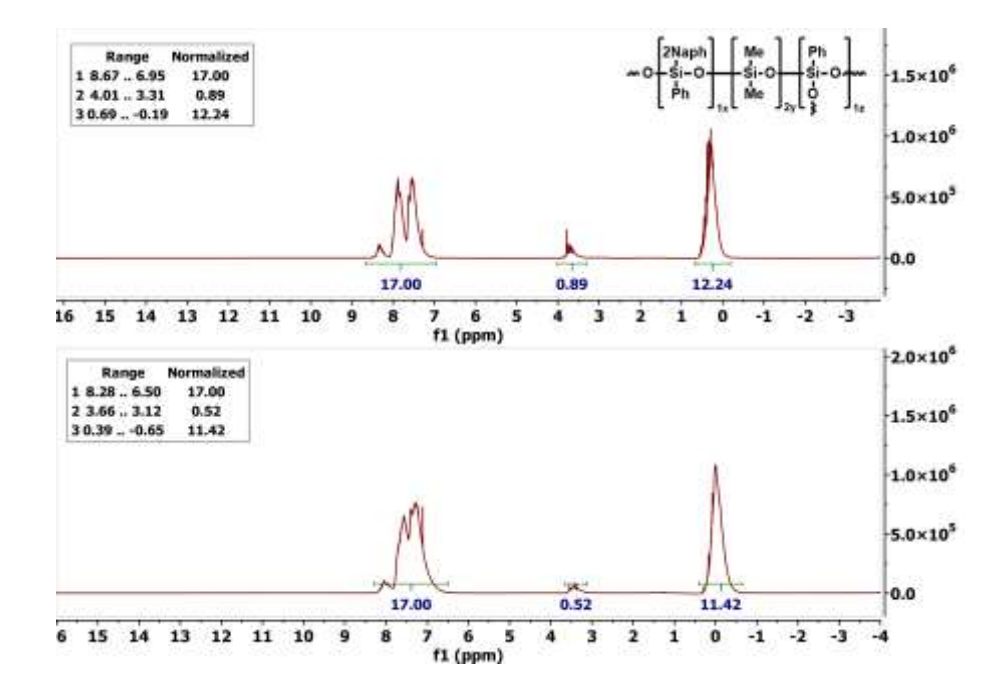


Figure S 35: ¹H NMR spectrum (CDCl₃, 400 MHz) of MGNaph2_Ph_Me₂ unconsolidated (top) and consolidated (bottom).

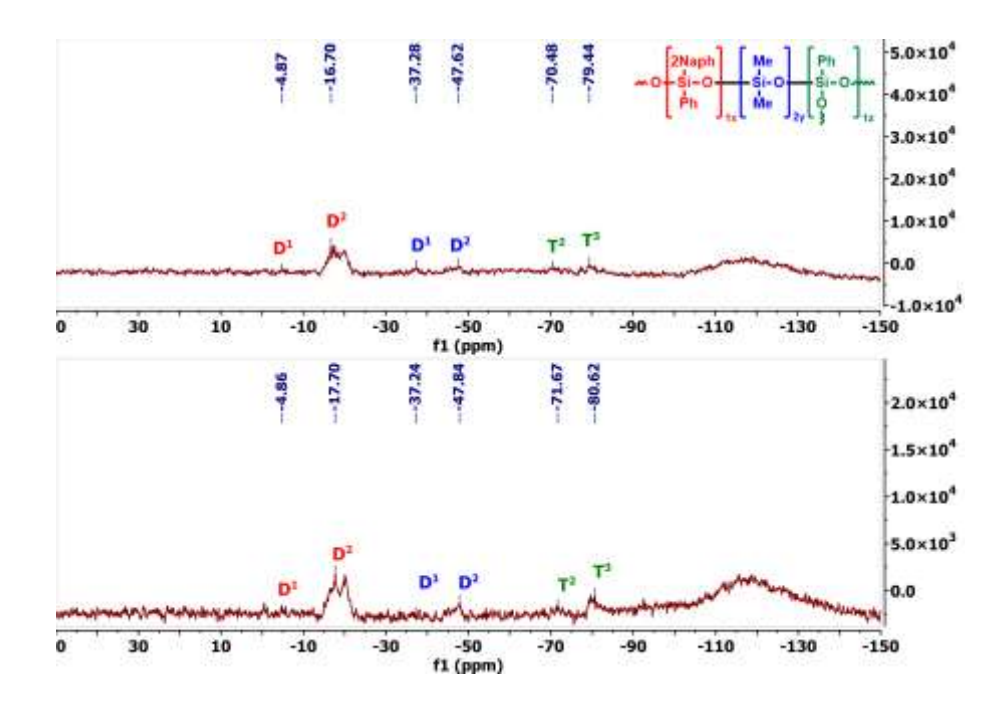


Figure S 36: ²⁹Si NMR spectrum (CDCl₃, 79 MHz) of MGNaph2_Ph_Me₂ unconsolidated (top) and consolidated (bottom).

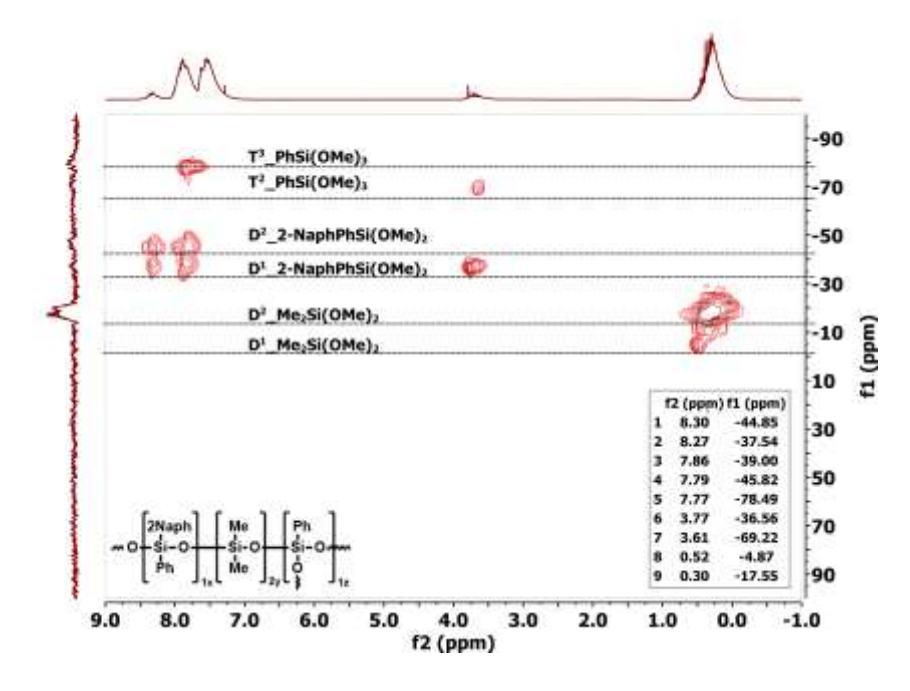


Figure S 37: ¹H, ²⁹Si HMBC spectrum (CDCl₃, 400 MHz; 79 MHz) of the unconsolidated MGNaph2_Ph_Me₂.

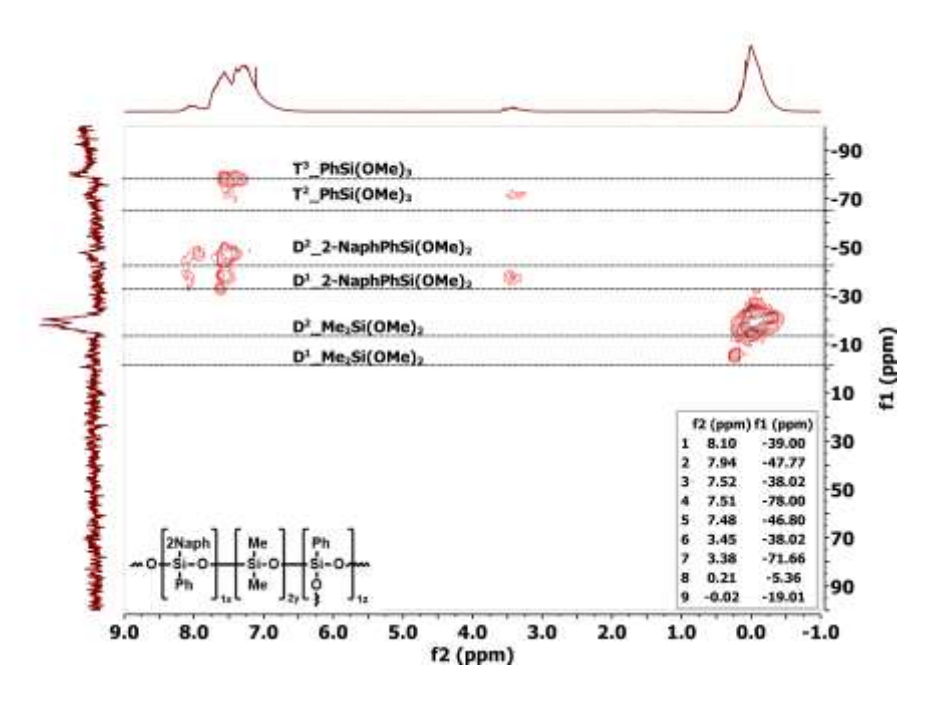


Figure S 38: ¹H, ²⁹Si HMBC spectrum (CDCl₃, 400 MHz; 79 MHz) of the consolidated MGNaph2_Ph_Me₂.

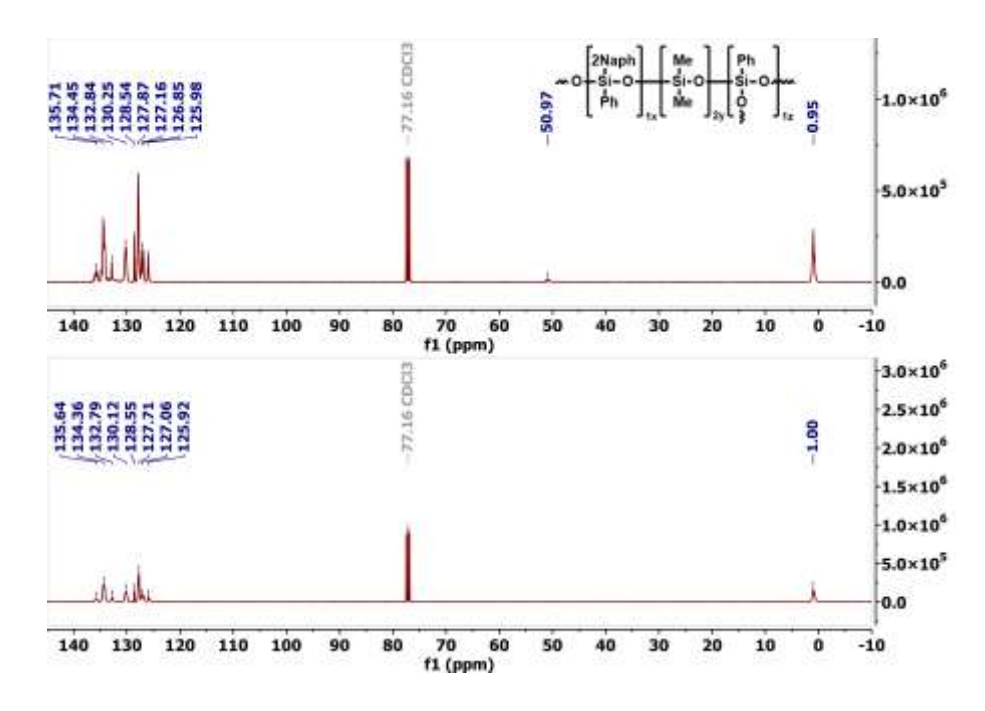


Figure S 39: ¹³C NMR spectrum (CDCl₃, 101 MHz) of MGNaph2_Ph_Me₂ unconsolidated (top) and consolidated (bottom).

MGPhen9_Ph_Ph2

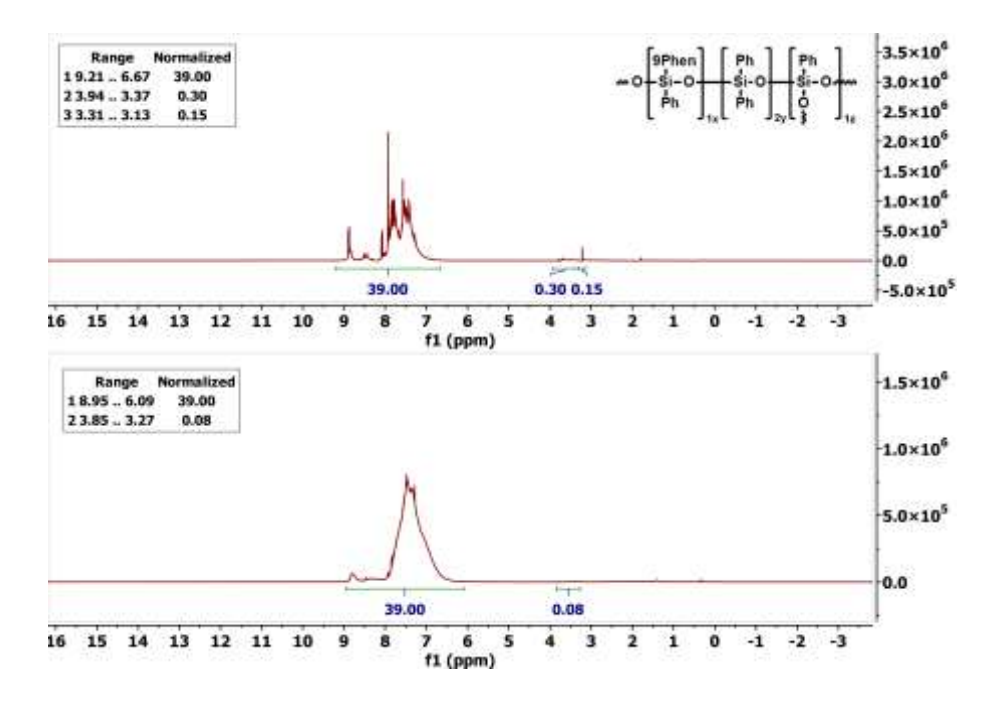


Figure S 40: ¹H NMR spectrum (CDCl₃, 400 MHz) of MGPhen9_Ph_Ph₂ unconsolidated (top) and consolidated (bottom).

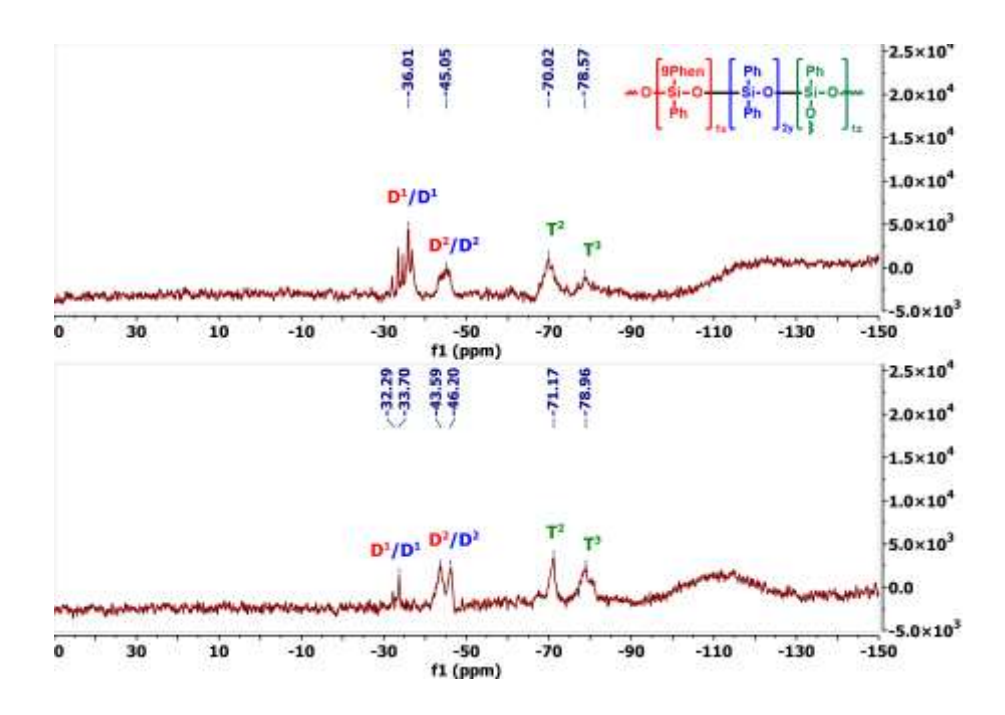


Figure S 41: ²⁹Si NMR spectrum (CDCl₃, 79 MHz) of MGPhen9_Ph_Ph₂ unconsolidated (top) and consolidated (bottom).

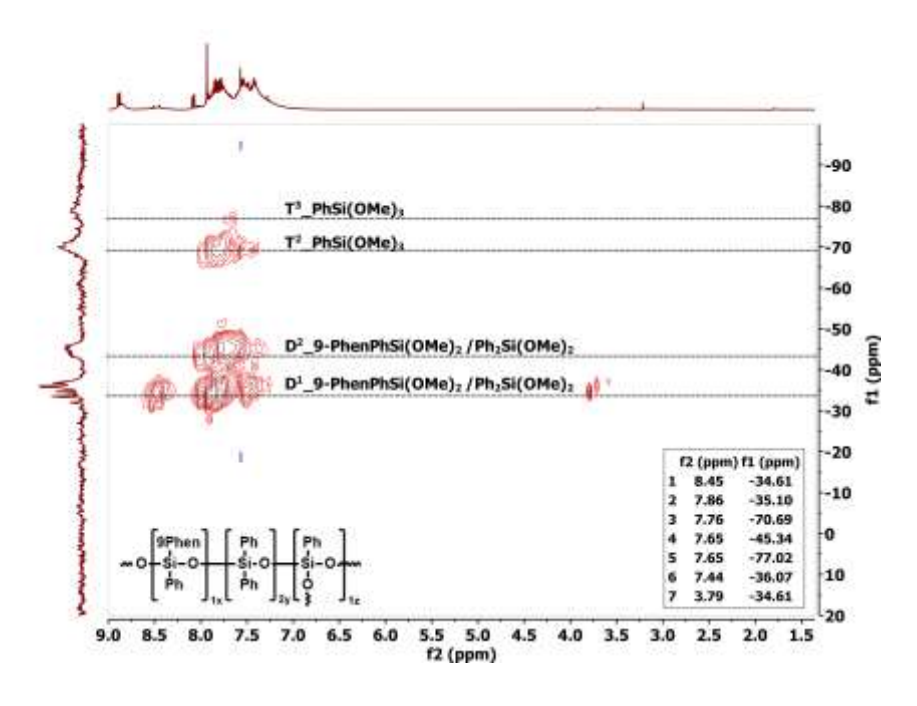


Figure S 42: ¹H, ²⁹Si HMBC spectrum (CDCl₃, 400 MHz; 79 MHz) of the unconsolidated MGPhen9_Ph_Ph₂.

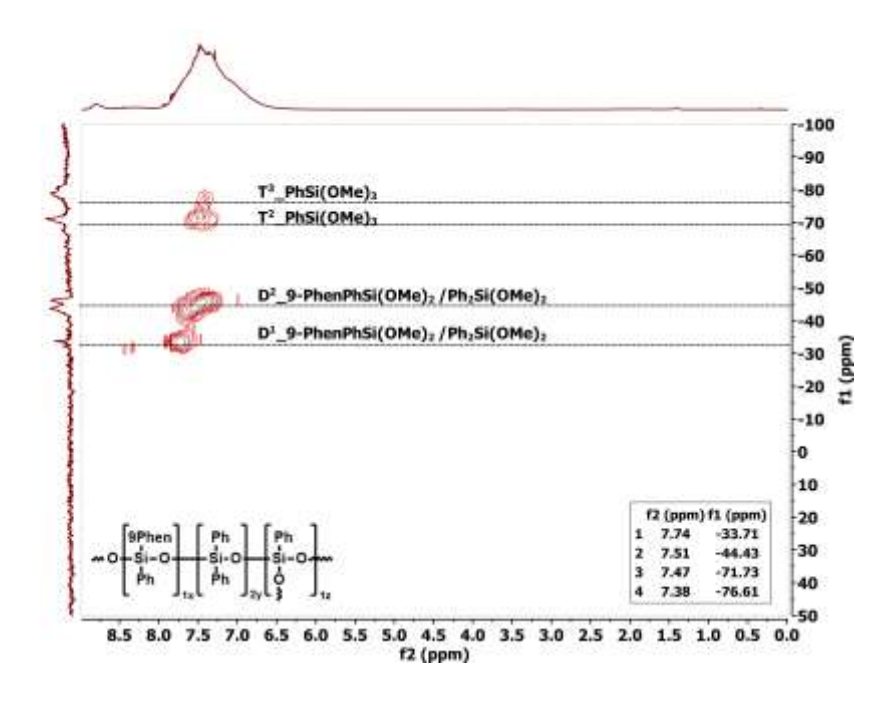


Figure S 43: ¹H, ²⁹Si HMBC spectrum (CDCl₃, 400 MHz; 79 MHz) of the consolidated MGPhen9_Ph_Ph₂.

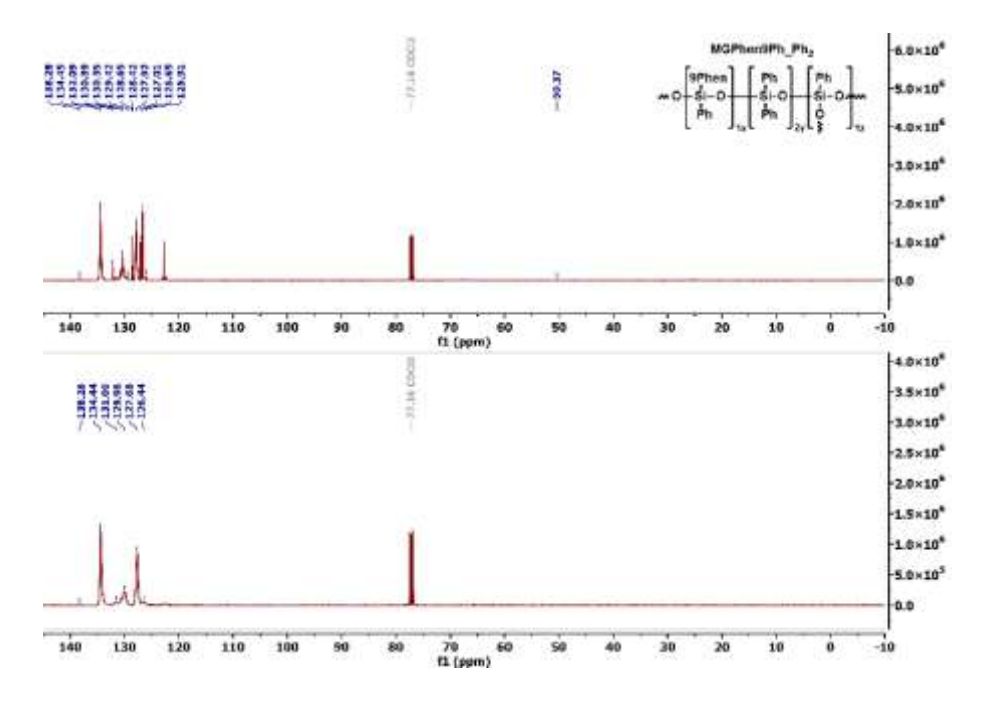


Figure S 44: ¹³C NMR spectrum (CDCl₃, 101 MHz) of MGPhen9_Ph_Ph₂ unconsolidated (top) and consolidated (bottom).

MGPhen9_Ph_Me2

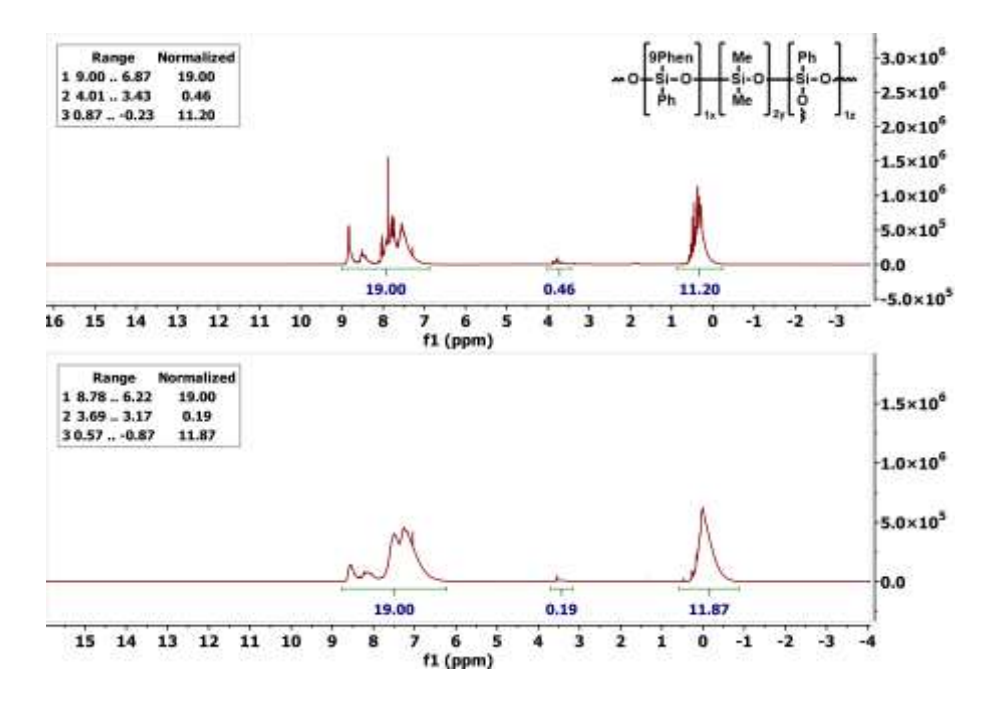


Figure S 45: ¹H NMR spectrum (CDCl₃, 400 MHz) of MGPhen9_Ph_Me₂ unconsolidated (top) and consolidated (bottom).

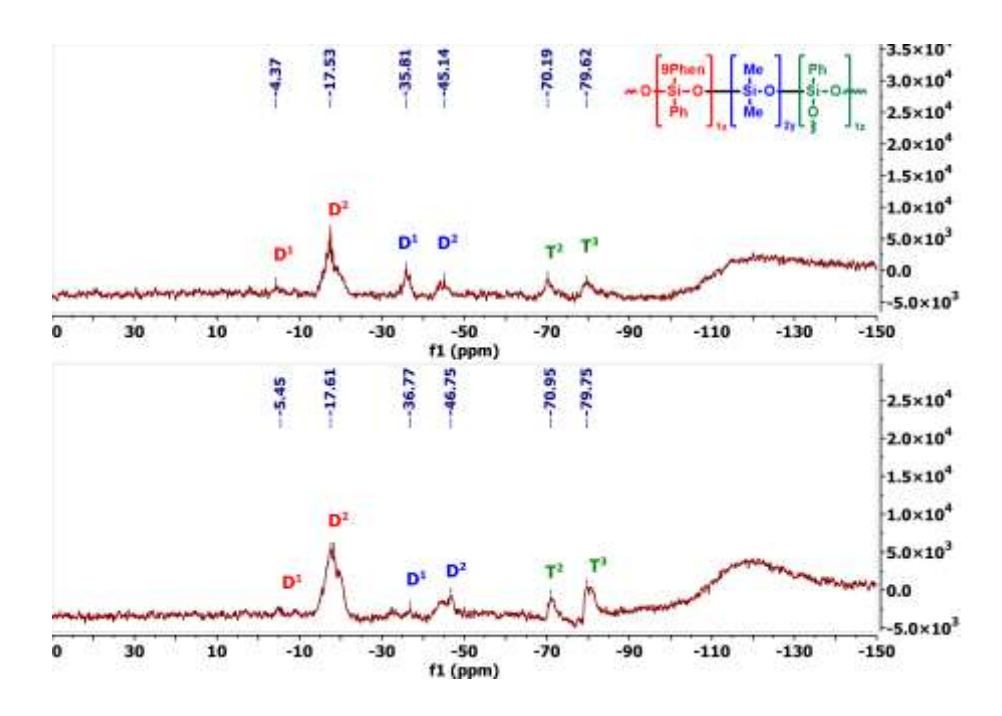


Figure S 46: ²⁹Si NMR spectrum (CDCl₃, 79 MHz) of MGPhen9_Ph_Me₂ unconsolidated (top) and consolidated (bottom).

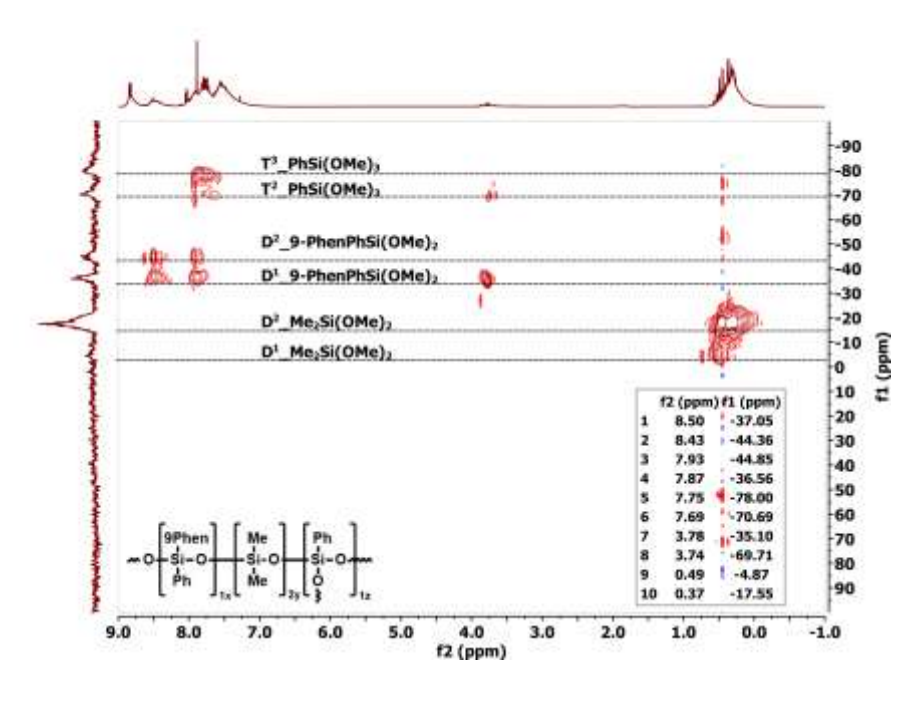


Figure S 47: ¹H, ²⁹Si HMBC spectrum (CDCl₃, 400 MHz; 79 MHz) of the unconsolidated MGPhen9_Ph_Me₂.

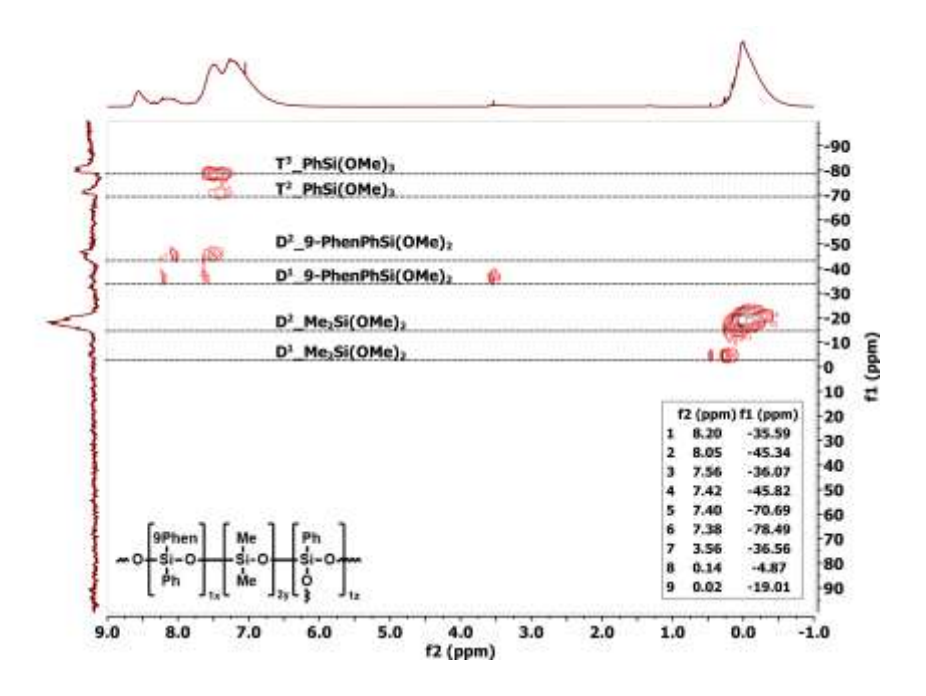


Figure S 48: ¹H, ²⁹Si HMBC spectrum (CDCl₃, 400 MHz; 79 MHz) of the consolidated MGPhen9_Ph_Me₂.

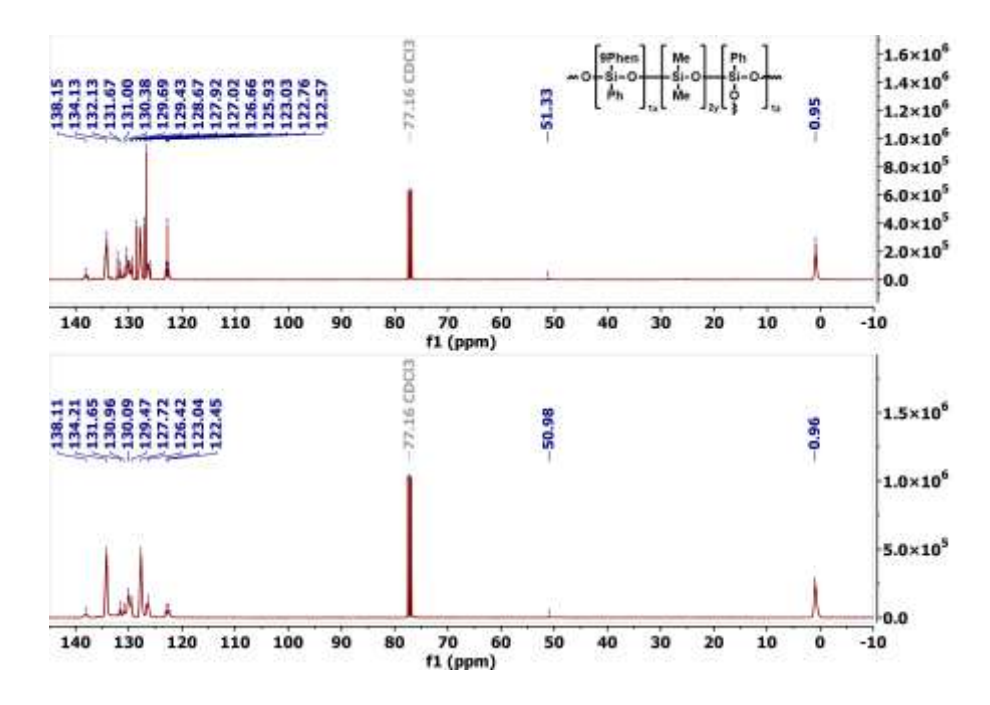


Figure S 49: ¹³C NMR spectrum (CDCl₃, 101 MHz) of MGPhen9_Ph_Me₂ unconsolidated (top) and consolidated (bottom).

CP-MAS NMR Spectroscopy

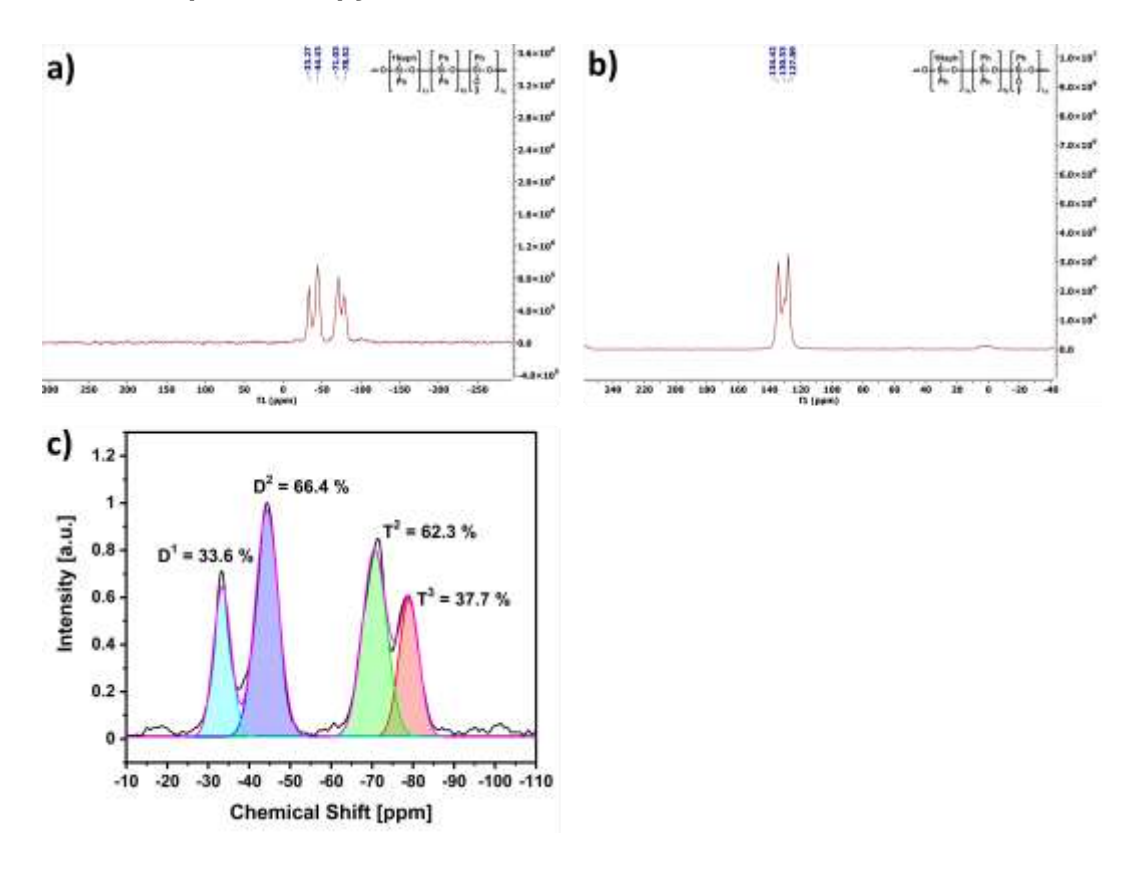


Figure S 50: CP-MAS NMR of MGNaph1_Ph_Ph₂. a) ²⁹Si NMR, b) ¹³C NMR, c) integrated ²⁹Si NMR.

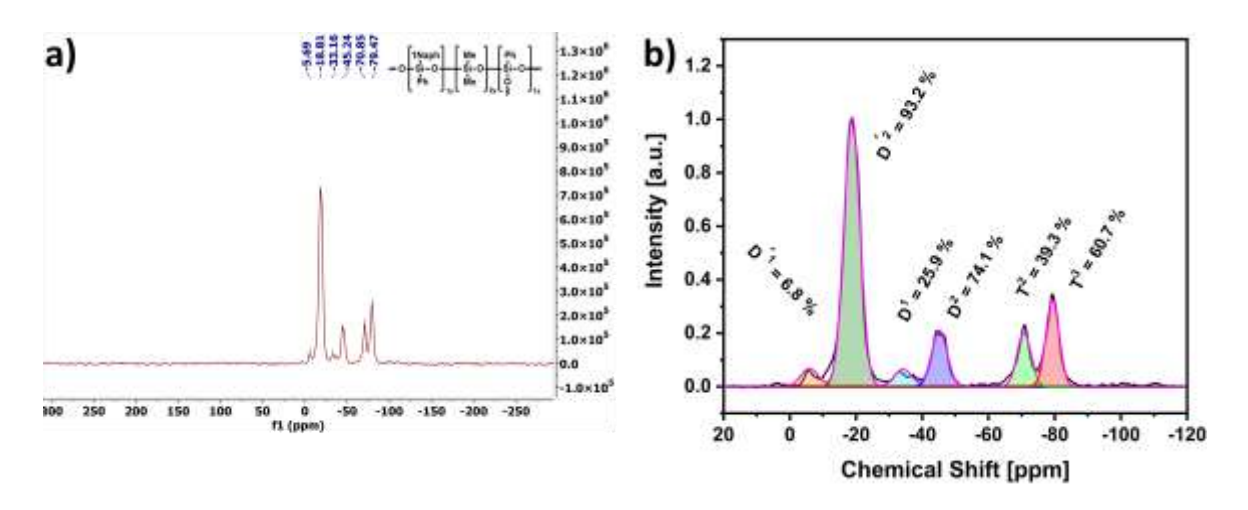


Figure S 51: CP-MAS NMR of MGNaph1_Ph_Me₂. a) ²⁹Si NMR, b) integrated ²⁹Si NMR.

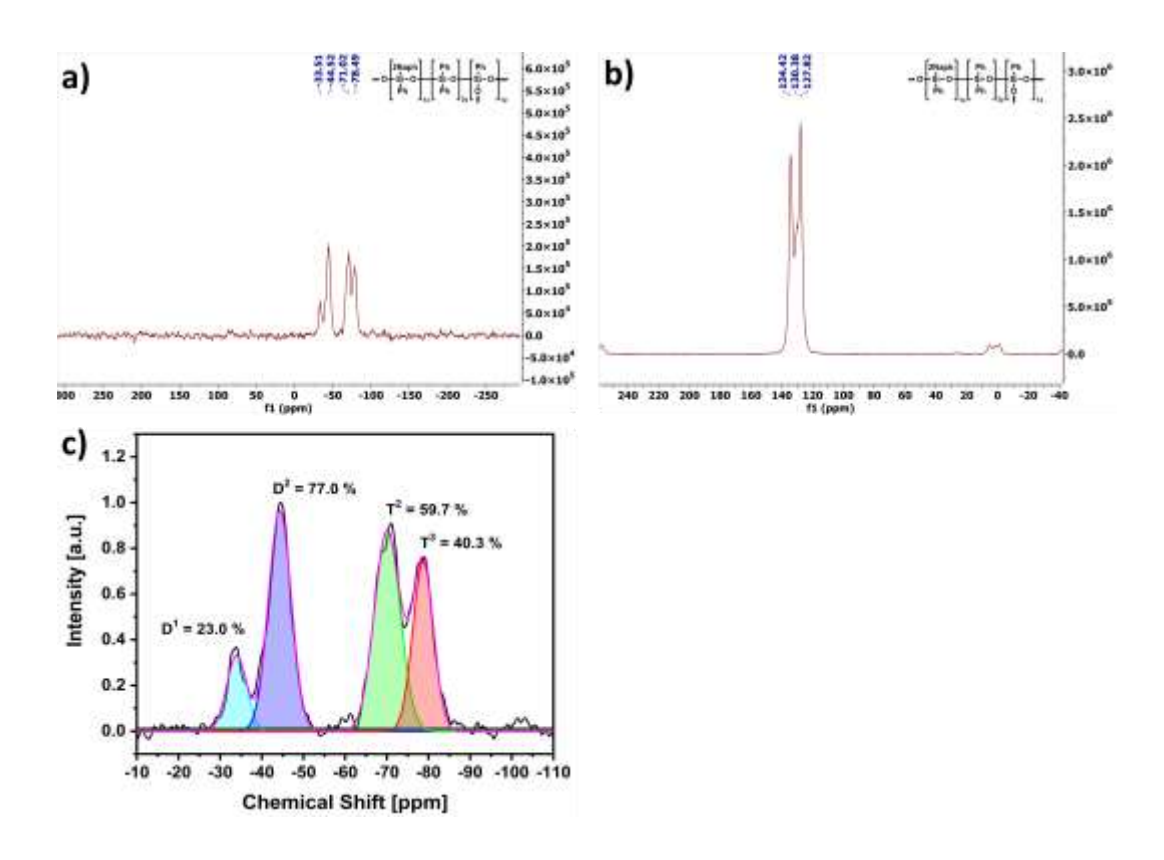


Figure S 52: CP-MAS NMR of MGNaph2_Ph_Ph₂. a) ²⁹Si NMR, b) ¹³C NMR, c) integrated ²⁹Si NMR.

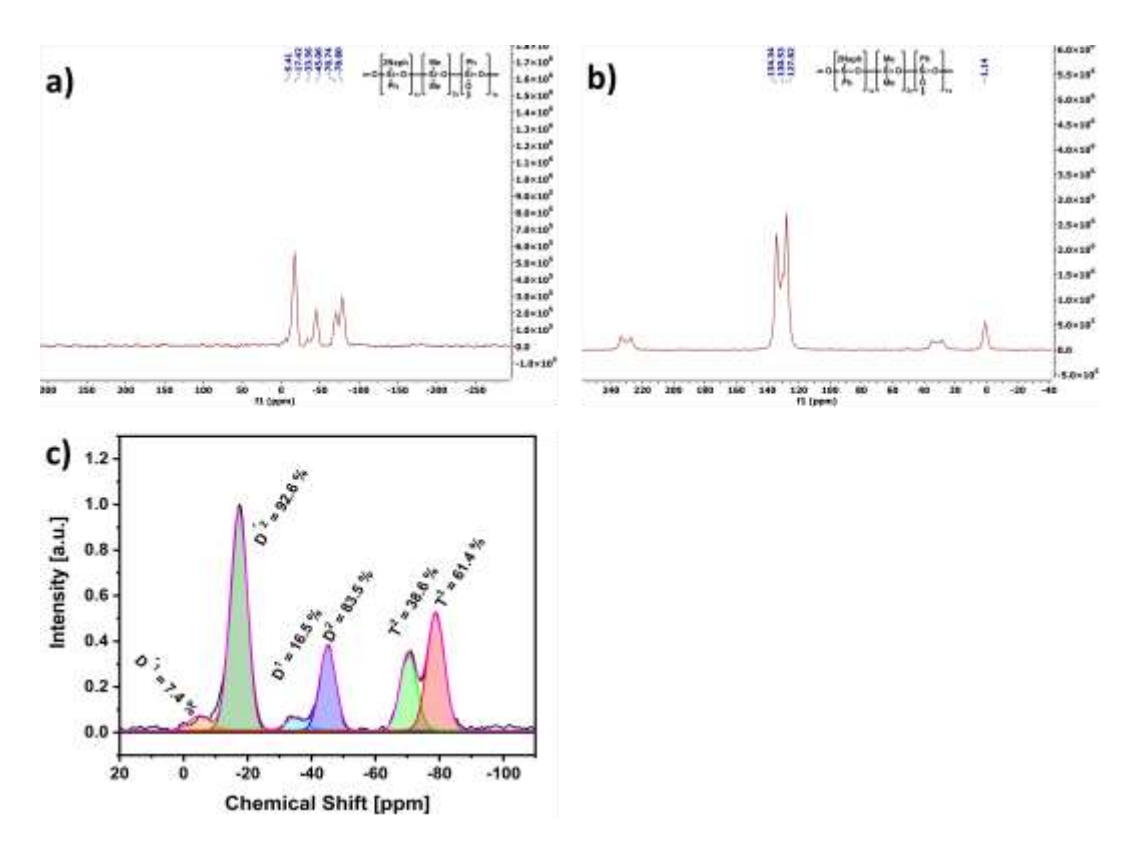


Figure S 53: CP-MAS NMR of MGNaph2_Ph_Me₂. a) ²⁹Si NMR, b) ¹³C NMR, c) integrated ²⁹Si NMR.

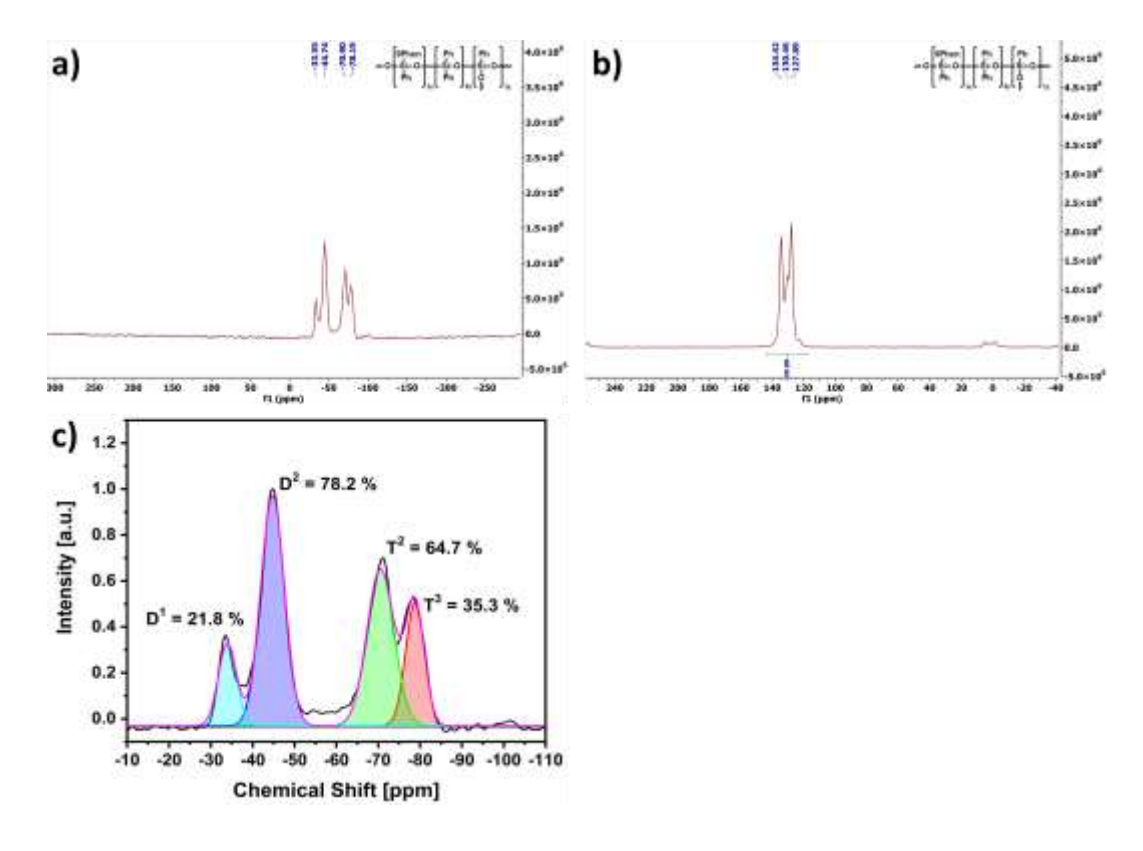


Figure S 54: CP-MAS NMR of MGPhen9_Ph_Ph₂. a) ²⁹Si NMR, b) ¹³C NMR, c) integrated ²⁹Si NMR.

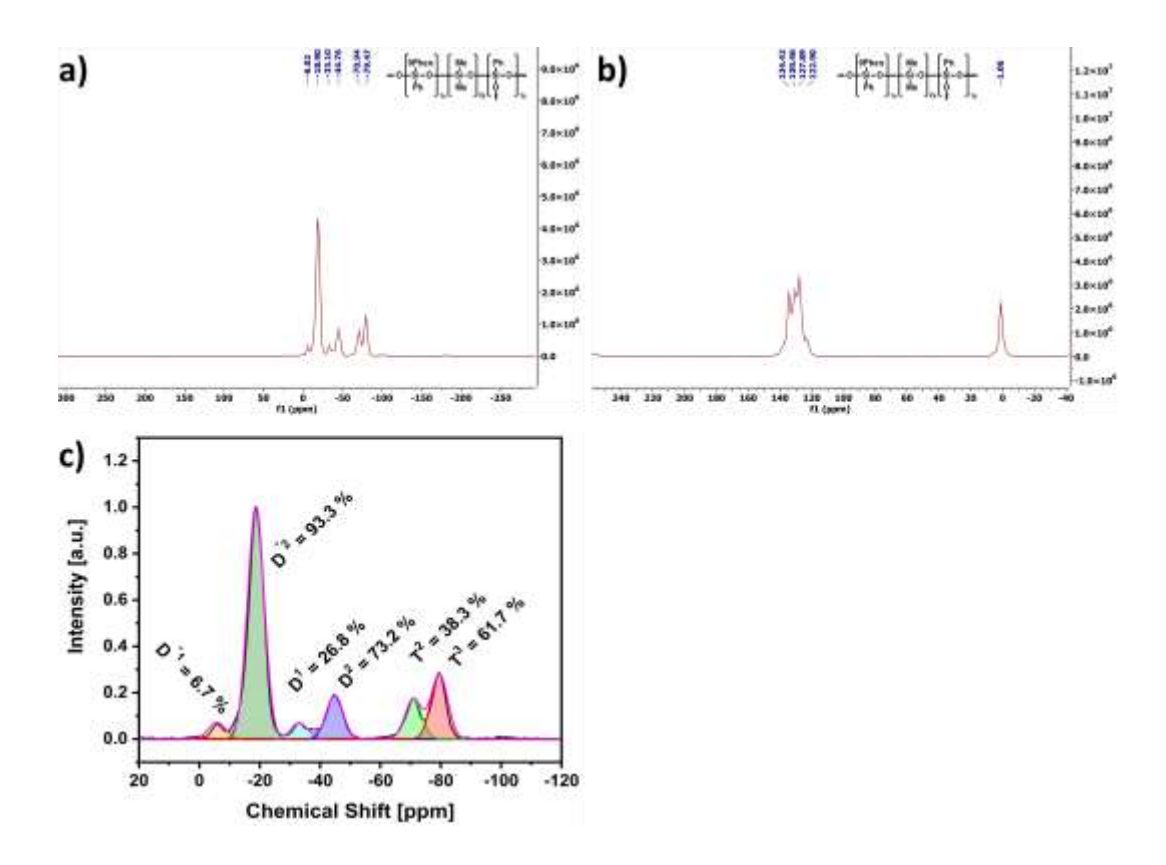


Figure S 55: CP-MAS NMR of MGPhen9_Ph_Me₂. a) ²⁹Si NMR, b) ¹³C NMR, c) integrated ²⁹Si NMR.

Degree of Condensation (DOC)

Table S 3: Degree of condensation of all oligosiloxanes after consolidation.

Oligomer	D′1/%	D´²/%	D1/%	D ² /%	T1/%	T ² /%	T³/%	DOC/%
MGNaph1_Ph_Ph₂			33.6	66.4		62.3	37.7	80.8
MGNaph1_Ph_Me₂	6.8	93.2	25.9	74.1		39.3	60.7	89.7
MGNaph2_Ph_Ph₂			23.0	77.0		59.7	40.3	83.5
MGNaph2_Ph_Me₂	7.4	92.6	16.5	83.5		38.6	61.4	91.1
MGPhen9_Ph_Ph2			21.8	78.2		64.7	35.3	82.7
MGPhen9_Ph_Me ₂	6.7	93.3	26.8	73.2		38.3	61.7	89.7

6.1.2.2 Powder X-ray Diffraction (PXRD)

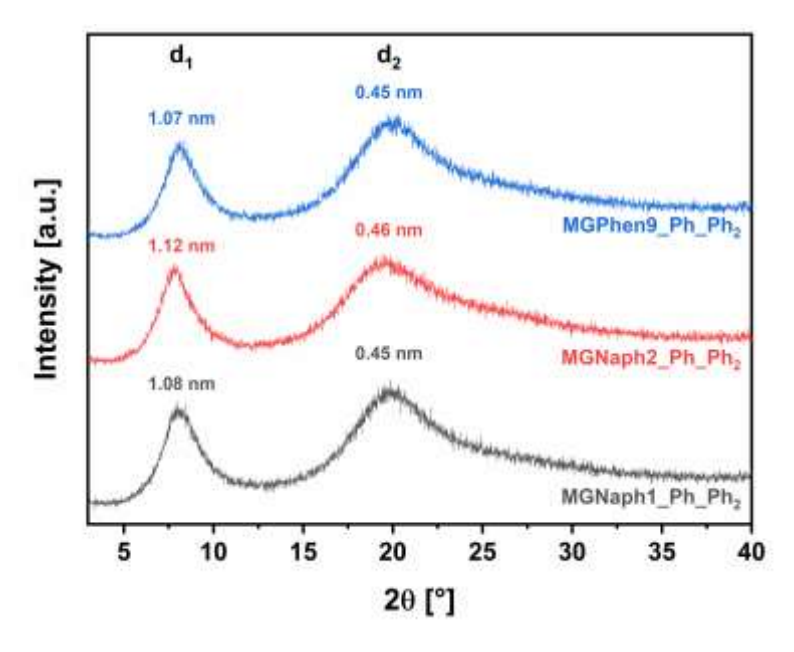


Figure S 56: PXRD pattern of MGNaph1_Ph_Ph₂ (grey), MGNaph2_Ph_Ph₂ (red) and MGPhen9_Ph_Ph₂ (blue) after consolidation.

Table S 4: Listing of the PXRD parameters for the three measured oligosiloxanes.

Compound	d₁[nm]	d ₂ [nm]	20 d ₁ /d ₂ [°]	Intensity d ₁ /d ₂ [a.u]
MGNaph1_Ph_Ph ₂	1.08	0.45	8.2/19.8	618/718
MGNaph2_Ph_Ph₂	1.12	0.46	7.9/19.3	607/652
MGPhen9_Ph_Ph ₂	1.07	0.45	8.2/19.8	583/726

6.1.2.3 Fourier Transform Infrared (FTIR) Spectroscopy

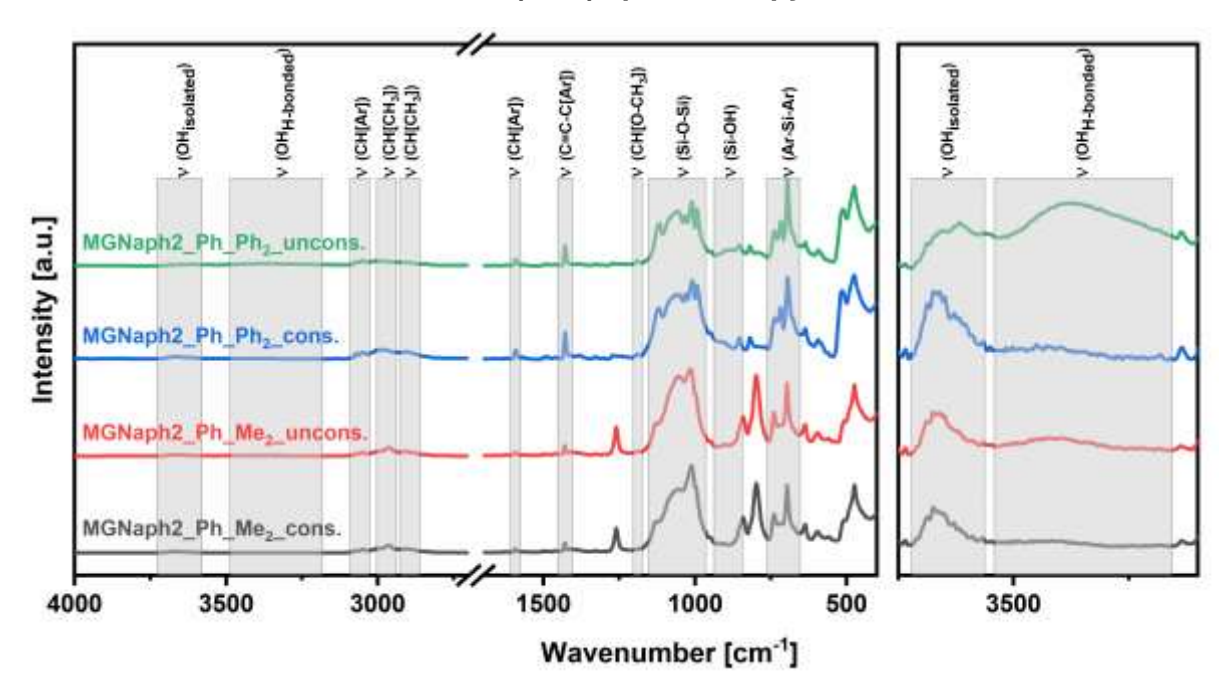


Figure S 57: FTIR spectra of both MGNaph2_Ph_Me₂ before (red) and after (black) and MGNaph2_Ph_Ph₂ before (green) and after (blue) consolidation.

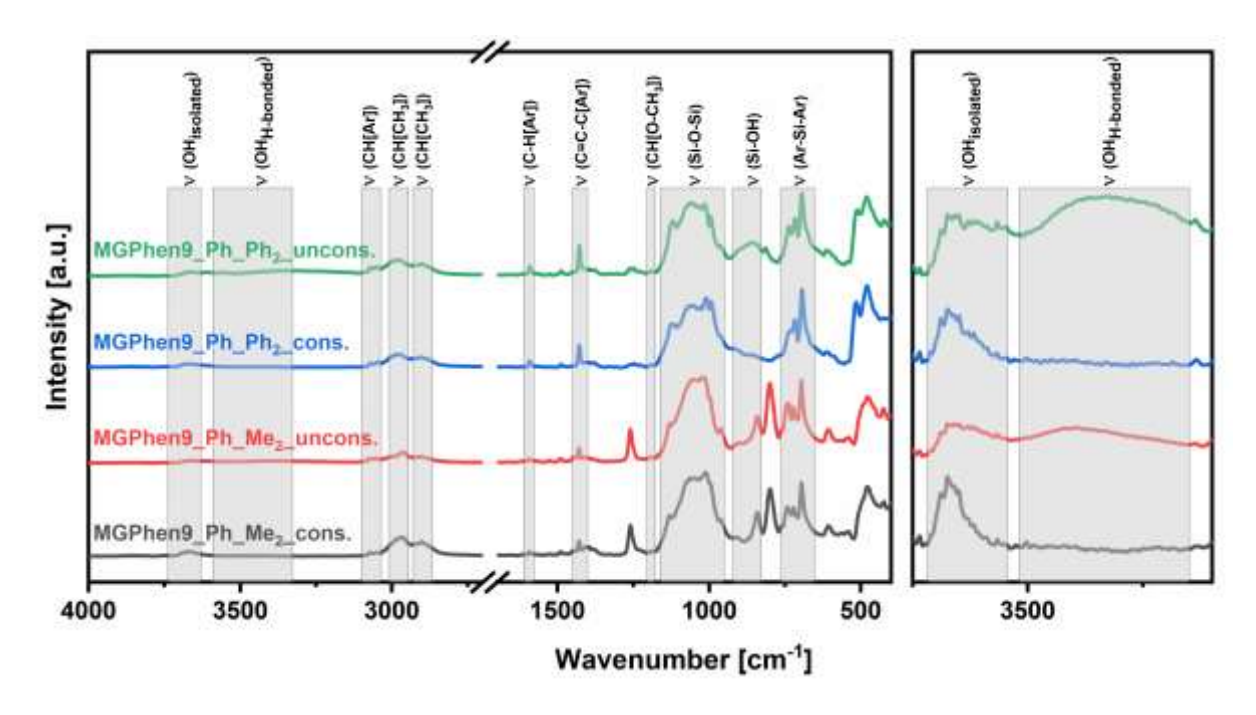


Figure S 58: FTIR spectra of both MGPhen9_Ph_Me₂ before (red) and after (black) and MGPhen9_Ph_Ph₂ before (green) and after (blue) consolidation.

6.1.2.4 Ultraviolet-visible (UV-vis) Spectroscopy

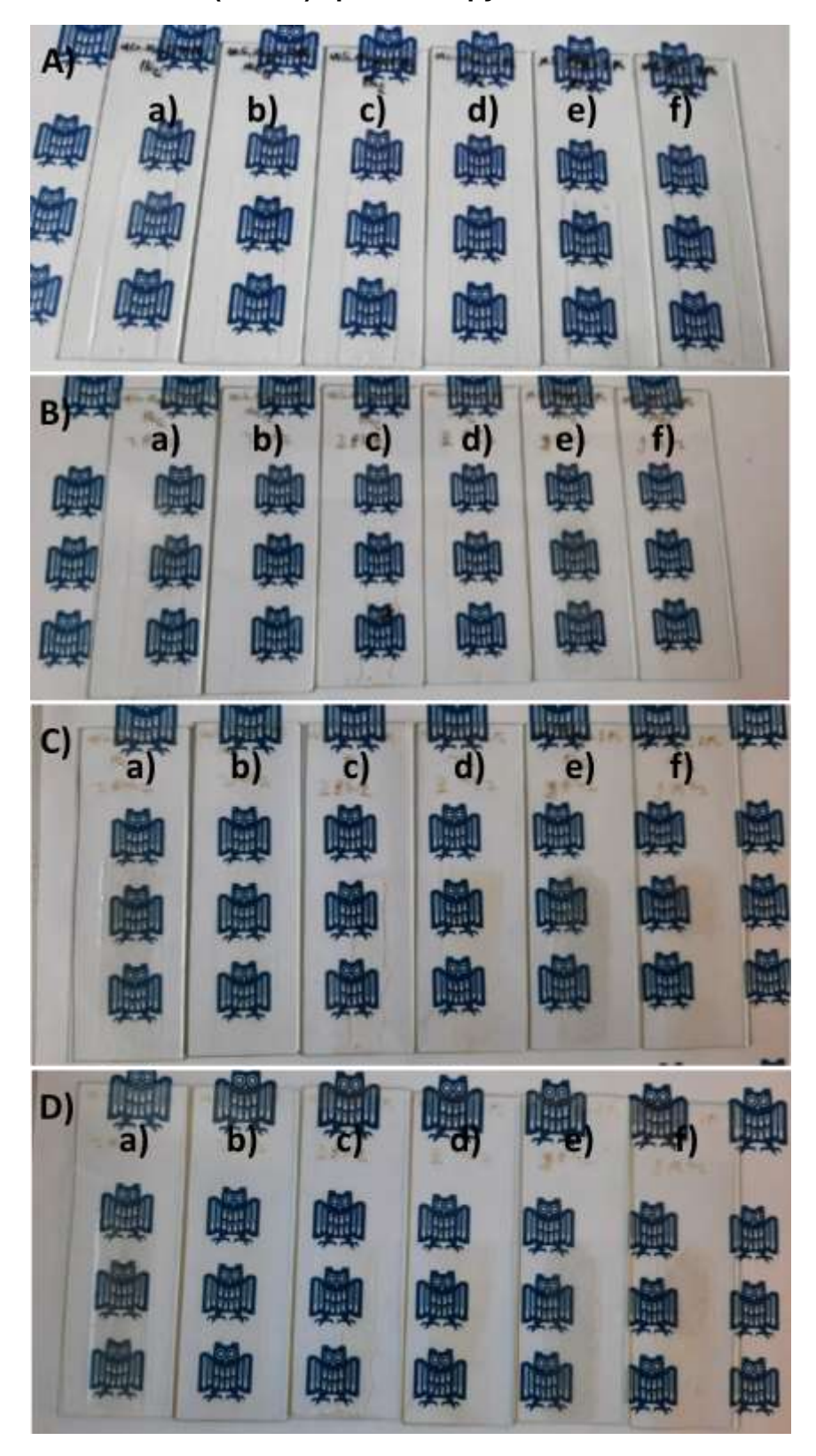


Figure S 59: Oligosiloxanes doctor bladed onto glass slides. A) before, B) after consolidation, C) after 3 d at 200 °C, D) after 7 d at 200 °C. a) MGNaph1_Ph_Ph_2, b) MGNaph1_Ph_Me_2, c) MGNaph2_Ph_Ph_2, d) MGNaph2_Ph_Me_2, e) MGPhen9_Ph_Ph_2, f) MGPhen9_Ph_Me_2.

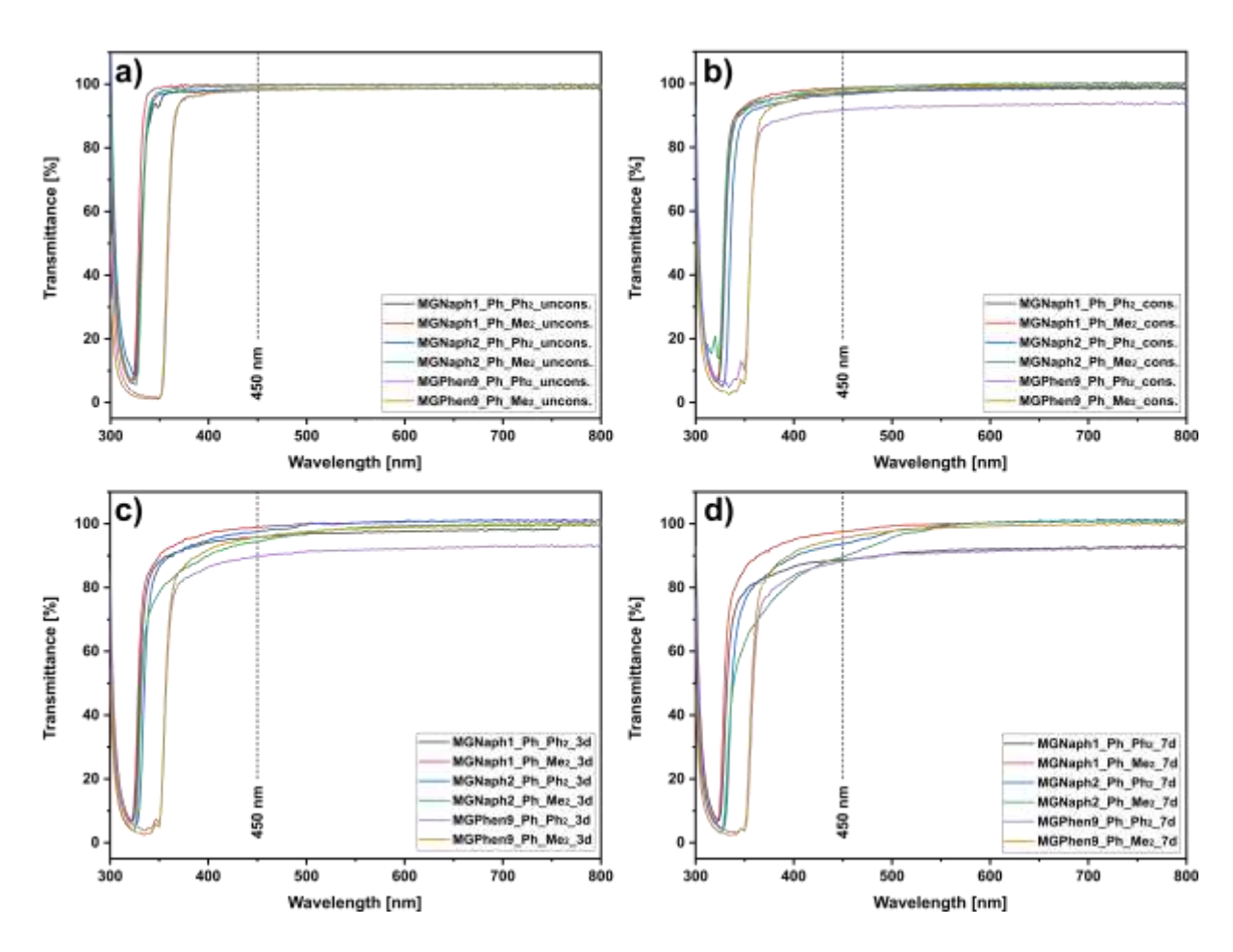


Figure S 60: UV-vis spectra of all oligosiloxanes. a) after condensation, b) after consolidation, c) after 3 d at 200 °C, d) after 7 d at 200 °C.

6.1.2.5 Fluorescence Spectroscopy

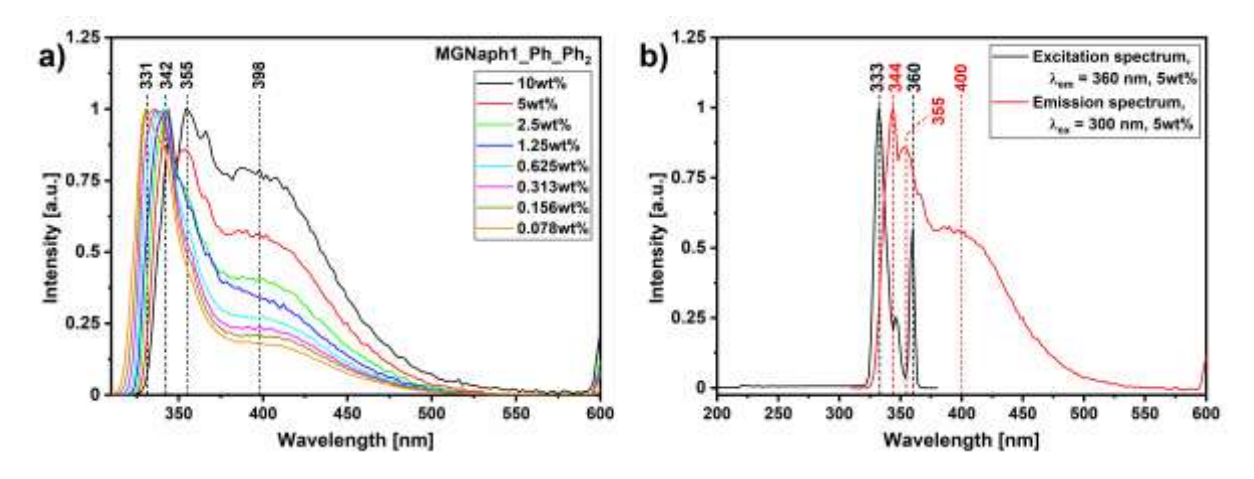


Figure S 61: a) Fluorescence spectra of a dilution series of MGNaph1_Ph_Ph2 in DCM with λ_{ex} = 300 nm and b) emission and excitation spectra of a 5wt% solution of MGNaph1_Ph_Ph2.

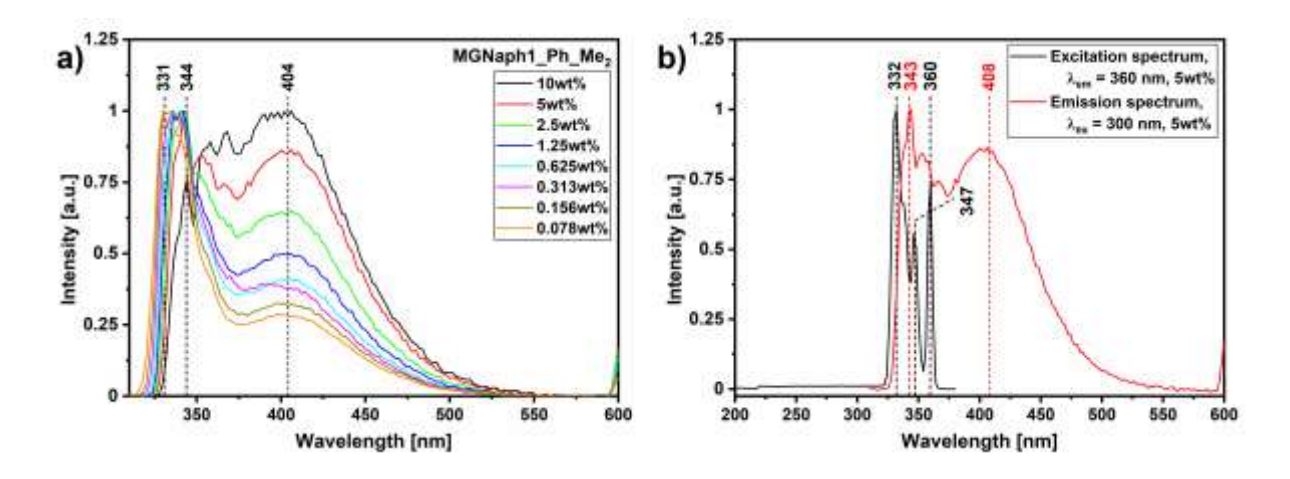


Figure S 62: a) Fluorescence spectra of a dilution series of MGNaph1_Ph_Me₂ in DCM with λ_{ex} = 300 nm and b) emission and excitation spectra of a 5wt% solution of MGNaph1_Ph_Me₂.

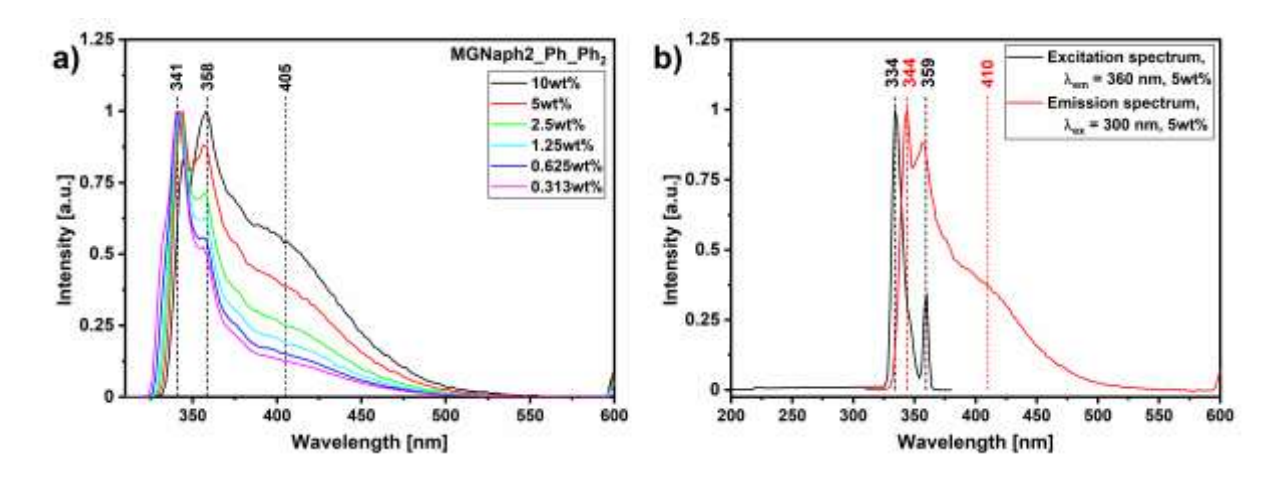


Figure S 63: a) Fluorescence spectra of a dilution series of MGNaph2_Ph_Ph₂ in DCM with λ_{ex} = 300 nm and b) emission and excitation spectra of a 5wt% solution of MGNaph2_Ph_Ph₂.

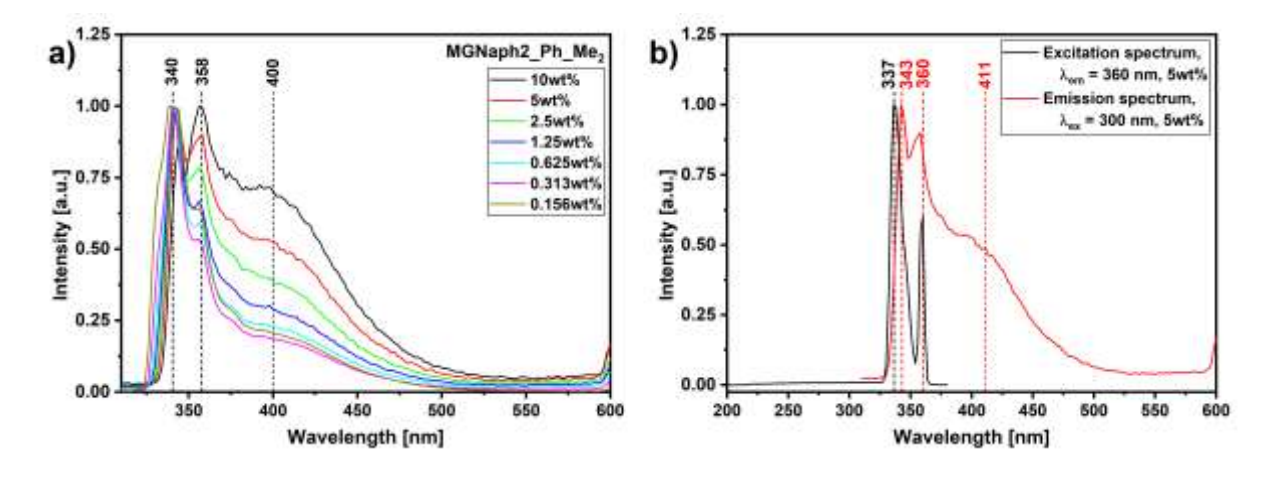


Figure S 64: a) Fluorescence spectra of a dilution series of MGNaph2_Ph_Me₂ in DCM with λ_{ex} = 300 nm and b) emission and excitation spectra of a 5wt% solution of MGNaph2_Ph_Me₂.

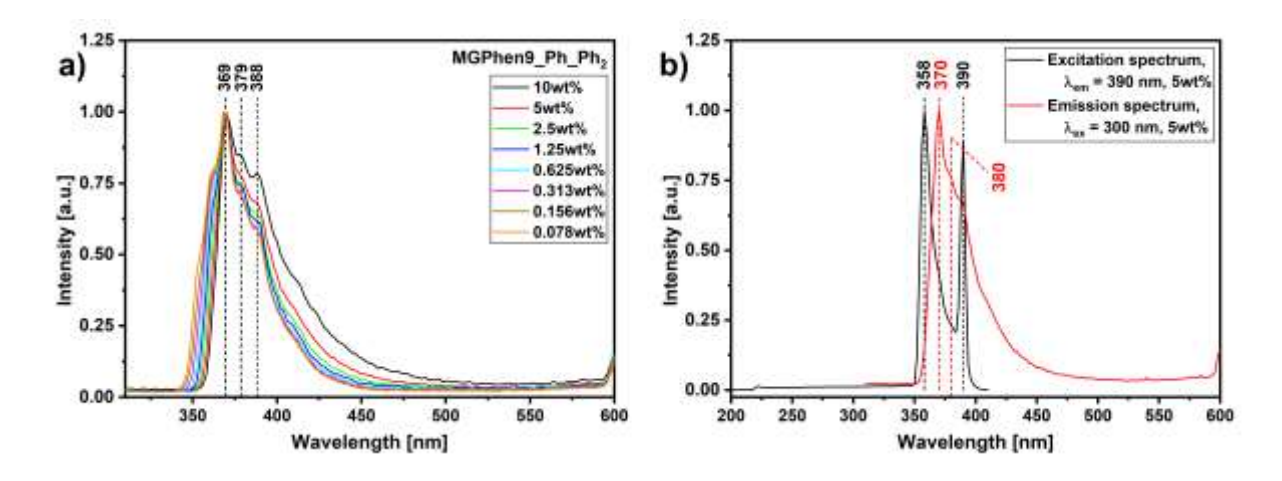


Figure S 65: a) Fluorescence spectra of a dilution series of MGPhen9_Ph_Ph₂ in DCM with λ_{ex} = 300 nm and b) emission and excitation spectra of a 5wt% solution of MGPhen9_Ph_Ph₂.

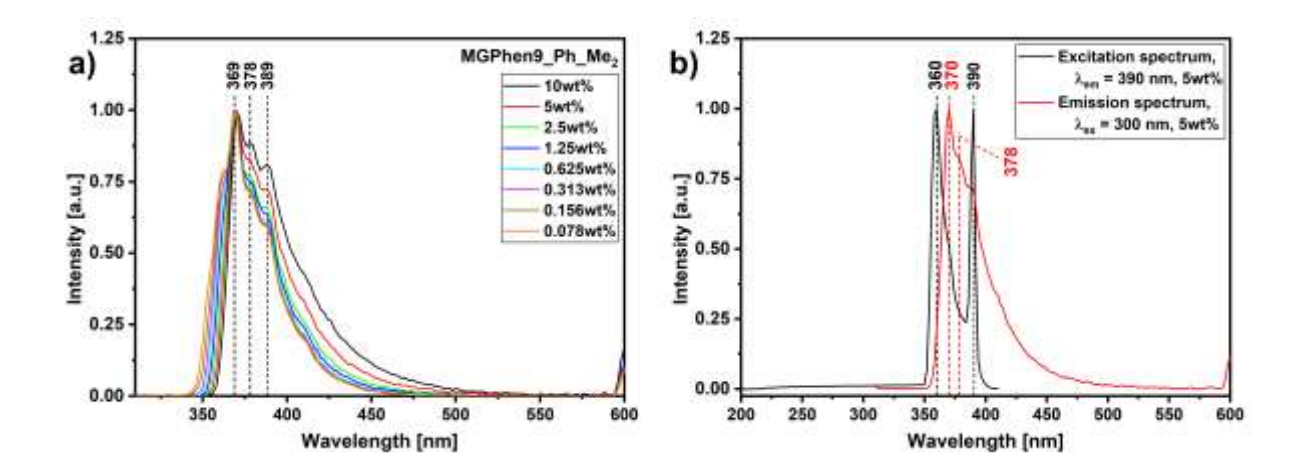


Figure S 66: a) Fluorescence spectra of a dilution series of MGPhen9_Ph_Me $_2$ in DCM with λ_{ex} = 300 nm and b) emission and excitation spectra of a 5wt% solution of MGPhen9_Ph_Me $_2$.

6.1.2.6 Matrix-Assisted Laser Desorption/Ionization Time of Flight (MALDI-TOF)

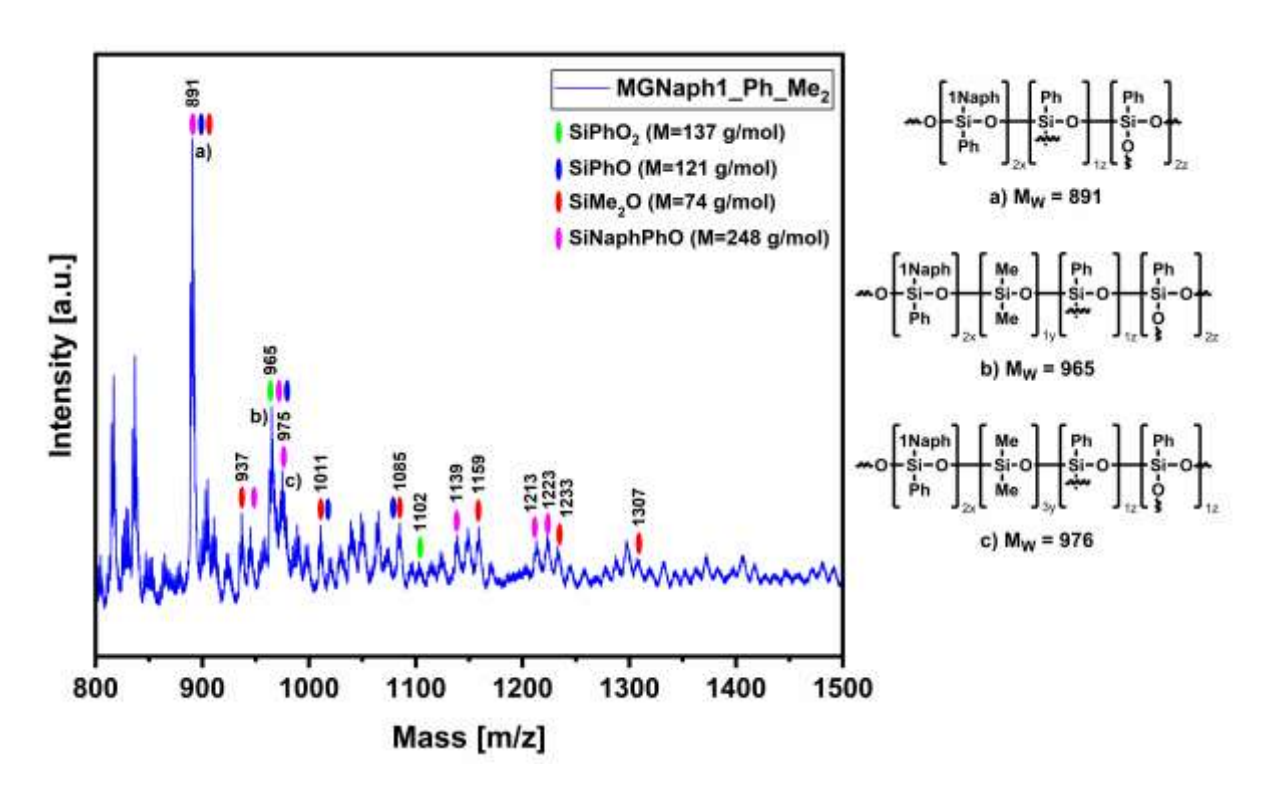


Figure S 67: MALDI-TOF measurement of MGNaph1_Ph_Me₂, its fragments and possible structures.

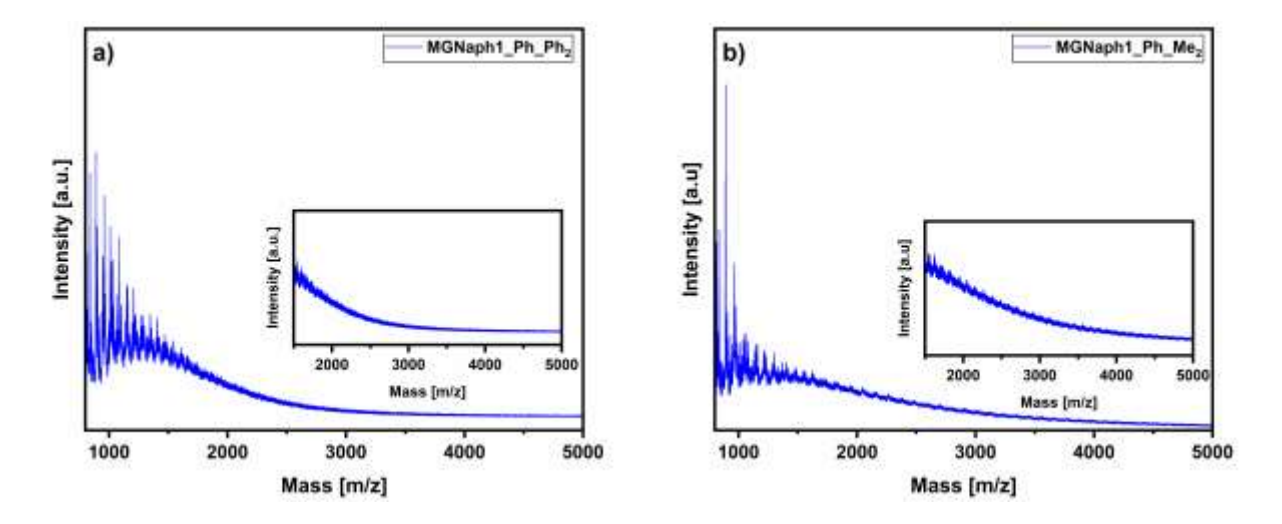


Figure S 68: Complete measuring range of a) MGNaph1_Ph_Ph2 and b) MGNaph1_Ph_Me2.

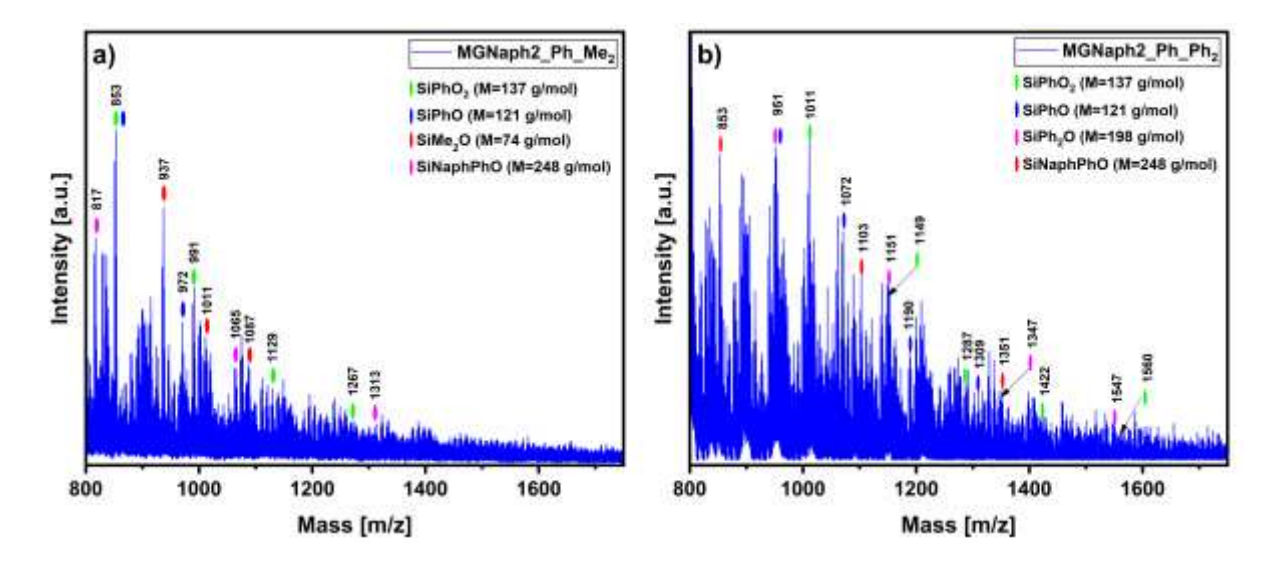


Figure S 69: MALDI-TOF measurement of a) MGNaph2_Ph_Me₂ and b) MGNaph2_Ph_Ph₂ and their fragments.

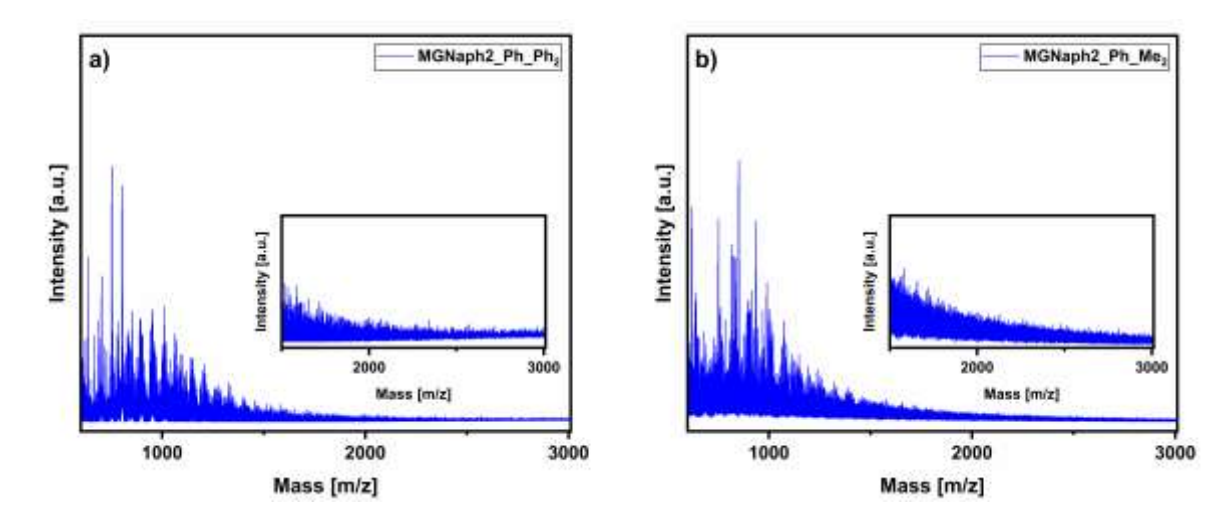


Figure S 70: Complete measuring range of a) MGNaph2_Ph_Ph2 and b) MGNaph2_Ph_Me2.

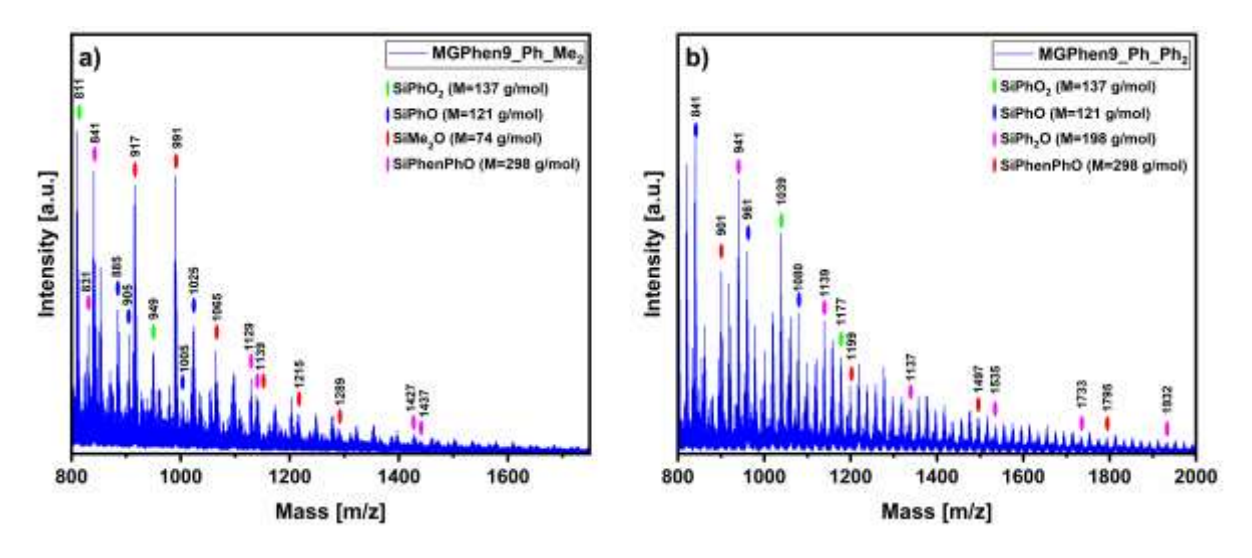


Figure S 71: MALDI-TOF measurement of a) MGPhen9_Ph_Me₂ and b) MGPhen9_Ph_Ph₂ and their fragments.

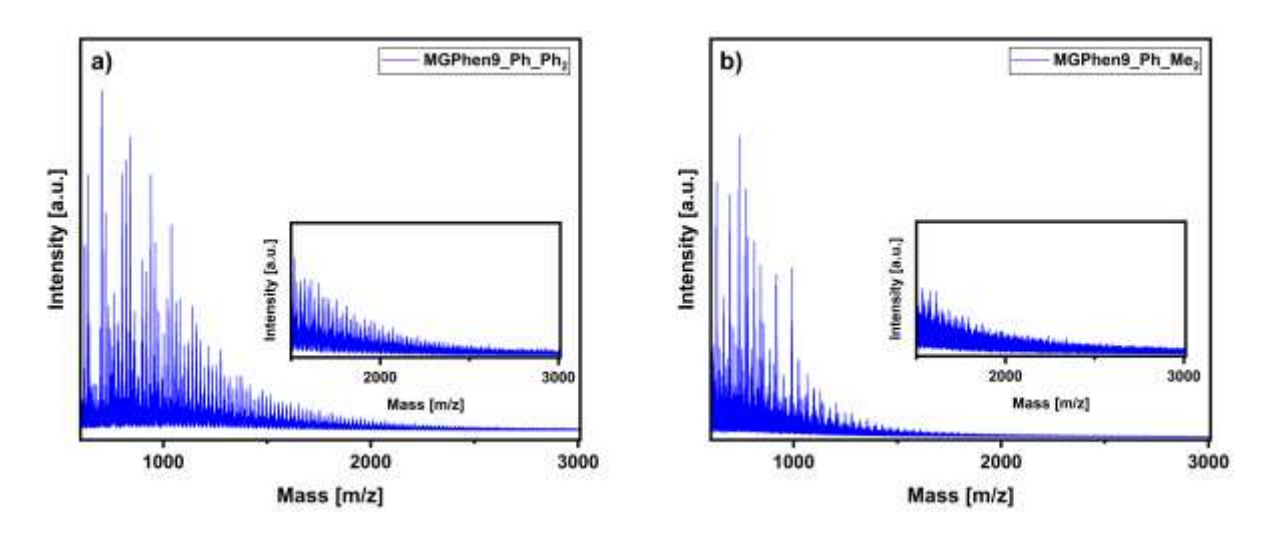


Figure S 72: Complete measuring range of a) MGPhen9_Ph_Ph2 and b) MGPhen9_Ph_Me2.

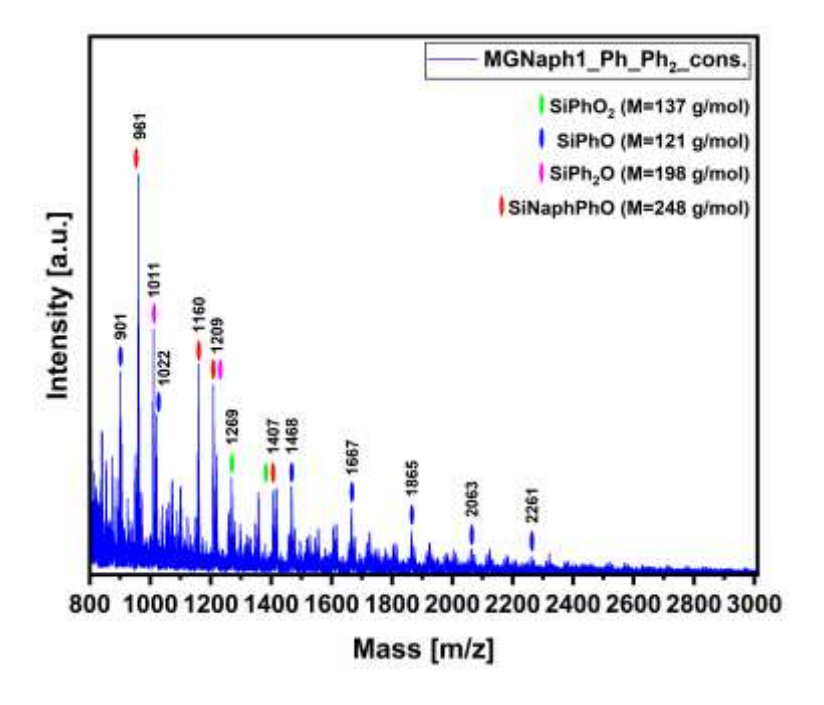


Figure S 73: MALDI-TOF measurement of MGNaph1_Ph_Ph2_cons. and its fragments.

6.1.2.7 Size Exclusion Chromatography (SEC)

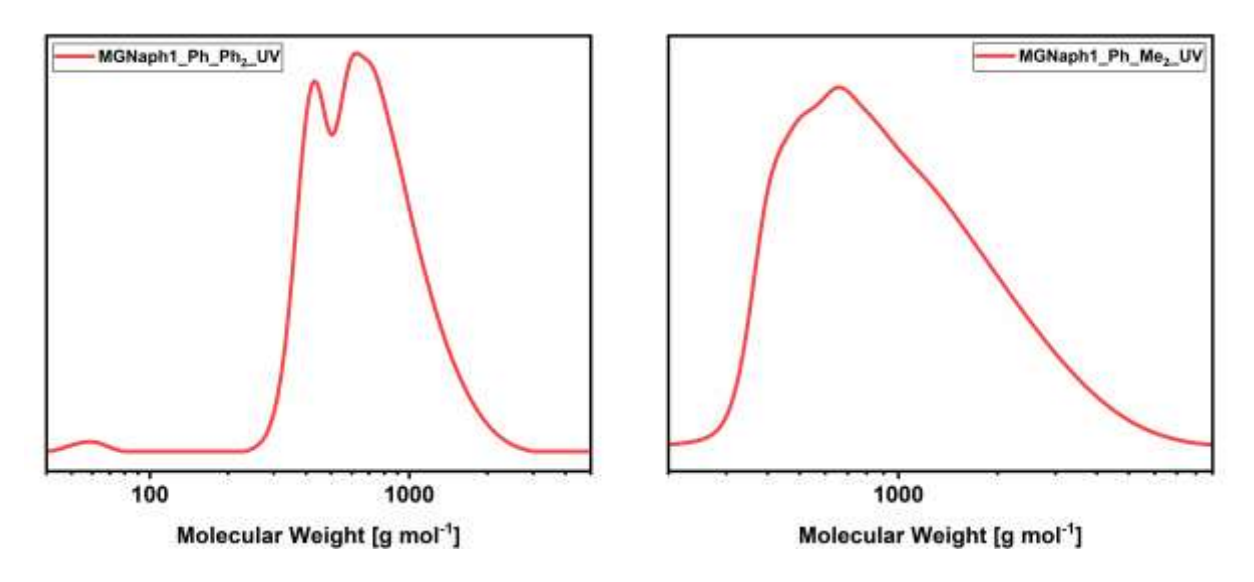


Figure S 74: SEC profiles for a) MGNaph1_Ph_Ph2 and b) MGNaph1_Ph_Me2 measured on a UV detector.

Table S 5: SEC results of both oligosiloxanes measured in THF and detected via UV.

	MGNaph1_Ph_Ph₂	MGNaph1_Ph_Me ₂
	UV	UV
Mn	673	849
M _w	790	1212
Mz	948	1845
PDI	1.174	1.428

6.1.2.8 Refractive Index (RI)

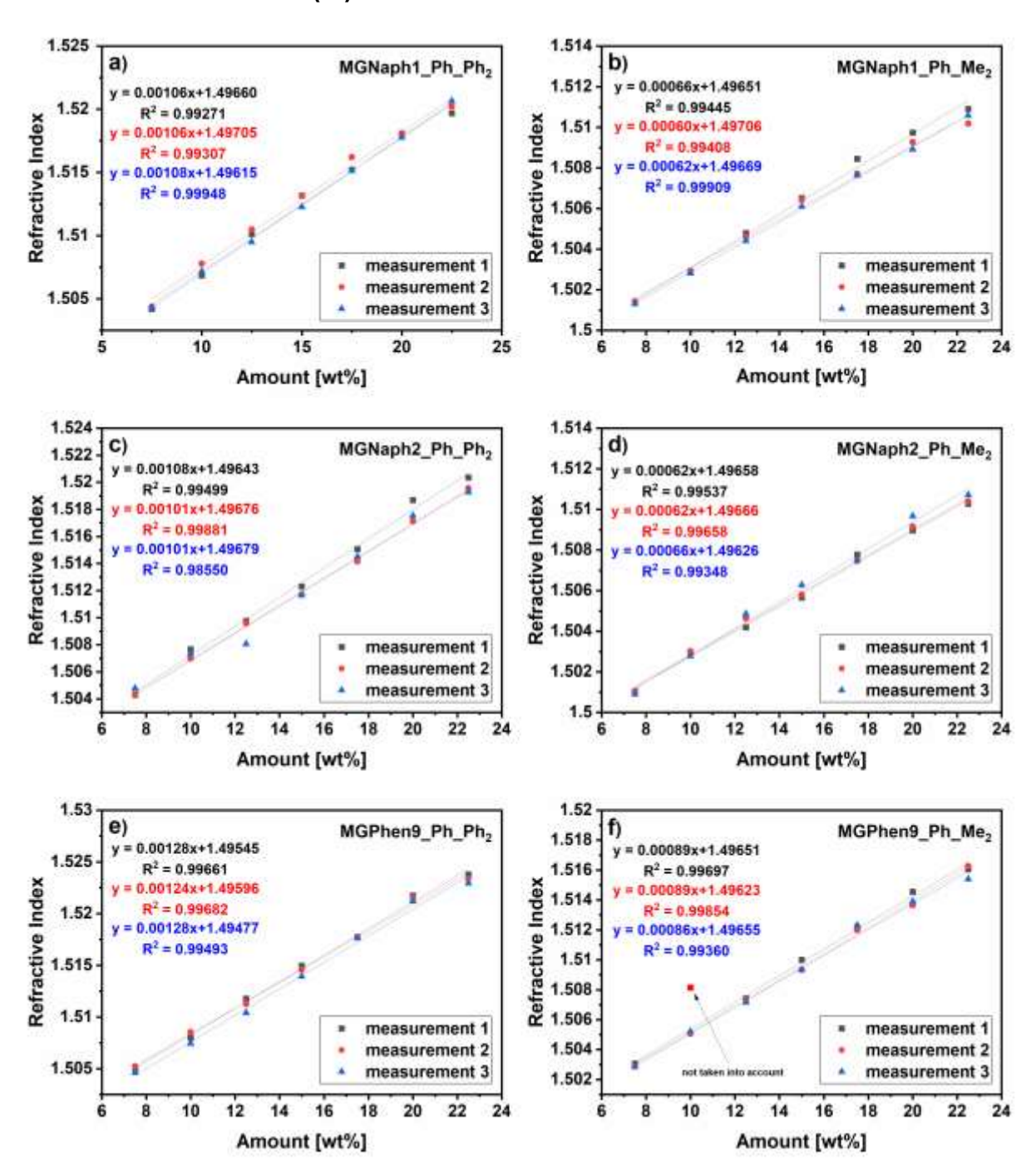


Figure S 75: Refractive index measurements of the unconsolidated polysiloxanes via calibration curve.

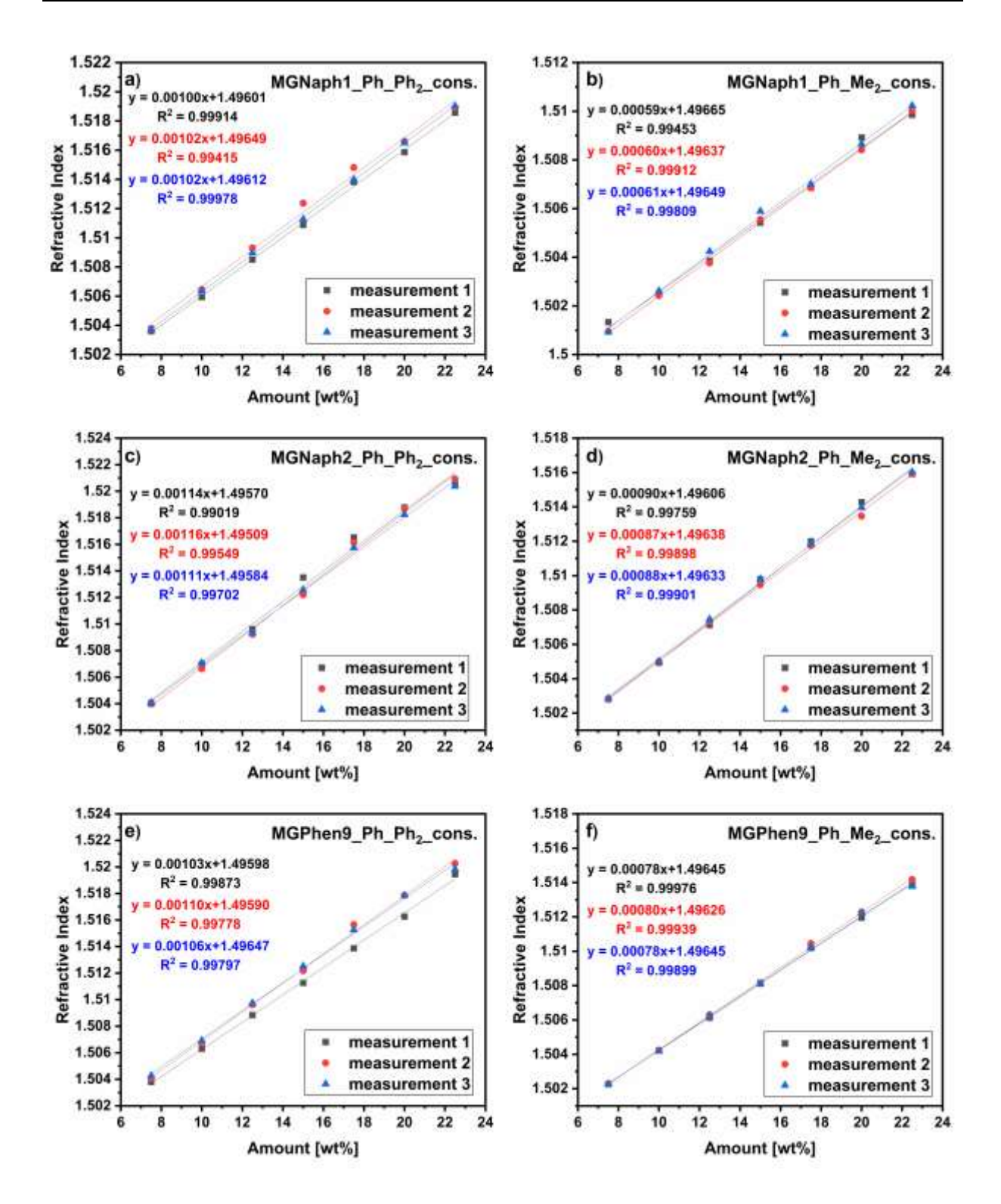


Figure S 76: Refractive index measurements of the consolidated polysiloxanes via calibration curve.

6.2 Post-Cross-Linking of Siloxane/Silsesquioxane Mixtures Containing Polycyclic Aromatic Groups to Modify their Softening Behavior for Usage in High-Temperature Applications

6.2.1 Synthesis of Dimethoxyphenyl-(1-naphthyl)silane

Scheme S 1: Synthesis of 1-NaphPhSi(OMe)₂ using a Grignard reaction.

The synthesis of dimethoxyphenyl-(1-naphthyl)silane was done according to our previous publication using a Grignard reaction.³⁸³

To a 1000 mL three-necked round bottom flask, which was equipped with a reflux condenser, a dropping funnel and a gas inlet and was flame-dried under vacuum and back-filled with argon magnesium chips (12.37 g, 508.8 mmol, 1.5 eq) and 400 mL abs THF were added and heated to 45 °C. 1-bromonaphthalene (70.39 g, 339.9 mmol, 1 eq) was diluted with 60 mL of abs THF in a dropping funnel an added dropwise over 30 minutes. After the addition the reaction mixture was stirred at 60 °C for 2 h. To a 1000 mL Schlenk flask, which was flame-dried under vacuum and back-filled with argon phenyltrimethoxysilane (203.4 g, 1025.7 mmol, 3 eq) was added and cooled to -10 °C in an ethanol/nitrogen bath. The hot reaction mixture was added to the cooled phenyltrimethoxysilane via cannula in one swoop while stirring, allowed to warm to room temperature and stirred overnight.

After the solvent was removed under vacuum 400 mL n-hexane were added, refluxed for 10 minutes, allowed to cool to room temperature and decanted. 200 mL n-hexane were added to the remaining solid, refluxed again for 10 minutes and filtered while hot. The solvent of the combined organic layers was removed under vacuum and the remaining solution was distillated: 1. Fraction (1.3x10⁻² mbar, 80 °C) was excess phenyltrimethoxysilane, 2. Fraction (1.3x10⁻² mbar, 170 °C) was the desired product. The product solidified overnight, was mortared, washed with cold ethanol, and also precipitated from said ethanol. Dimethoxyphenyl-(1-naphthyl)silane was obtained with a yield of 74.3 g (74 %) as a white powder.

6.2.2 Differential Scanning Calorimetry (DSC)

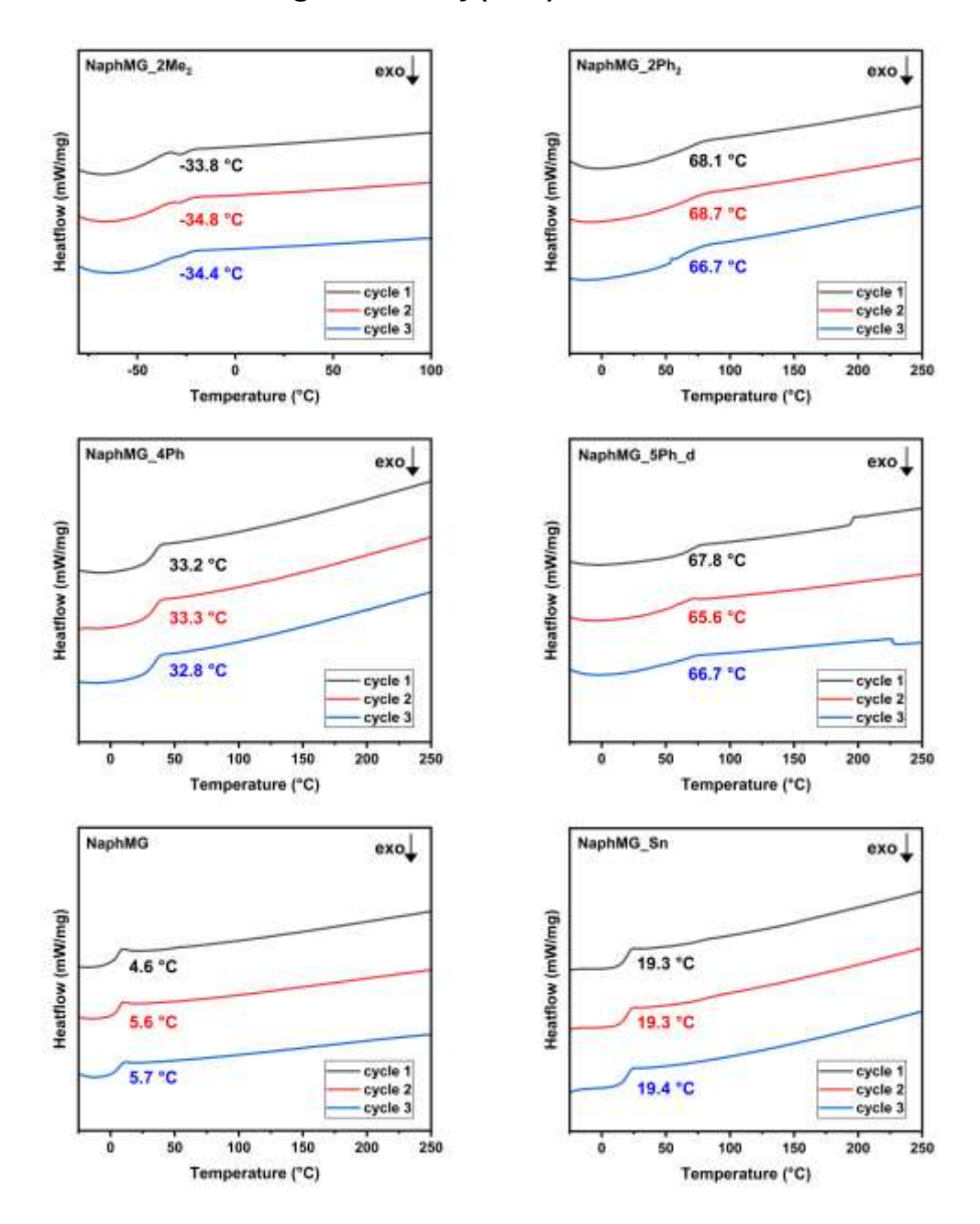


Figure S 77: DSC measurements of all siloxanes after consolidation. Each sample was measured three times.

6.2.3 Thermal Treatment Experiment

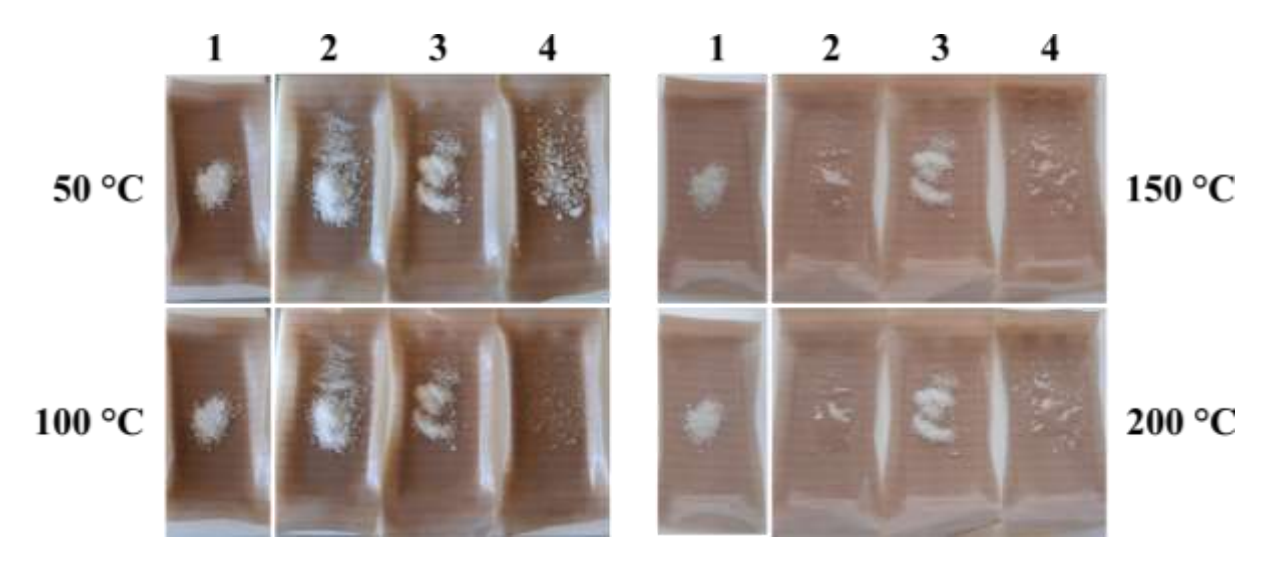


Figure S 78: Thermal treatment experiments of all solid siloxane samples at different temperatures (only temperatures are shown at which samples turned liquid). 1) NaphMG_2Ph₂, 2) NaphMG_5Ph_d, 3) NaphMG_4Ph, 4) NaphMG_Sn.

6.2.4 Dynamic Mechanical Analysis (DMA)

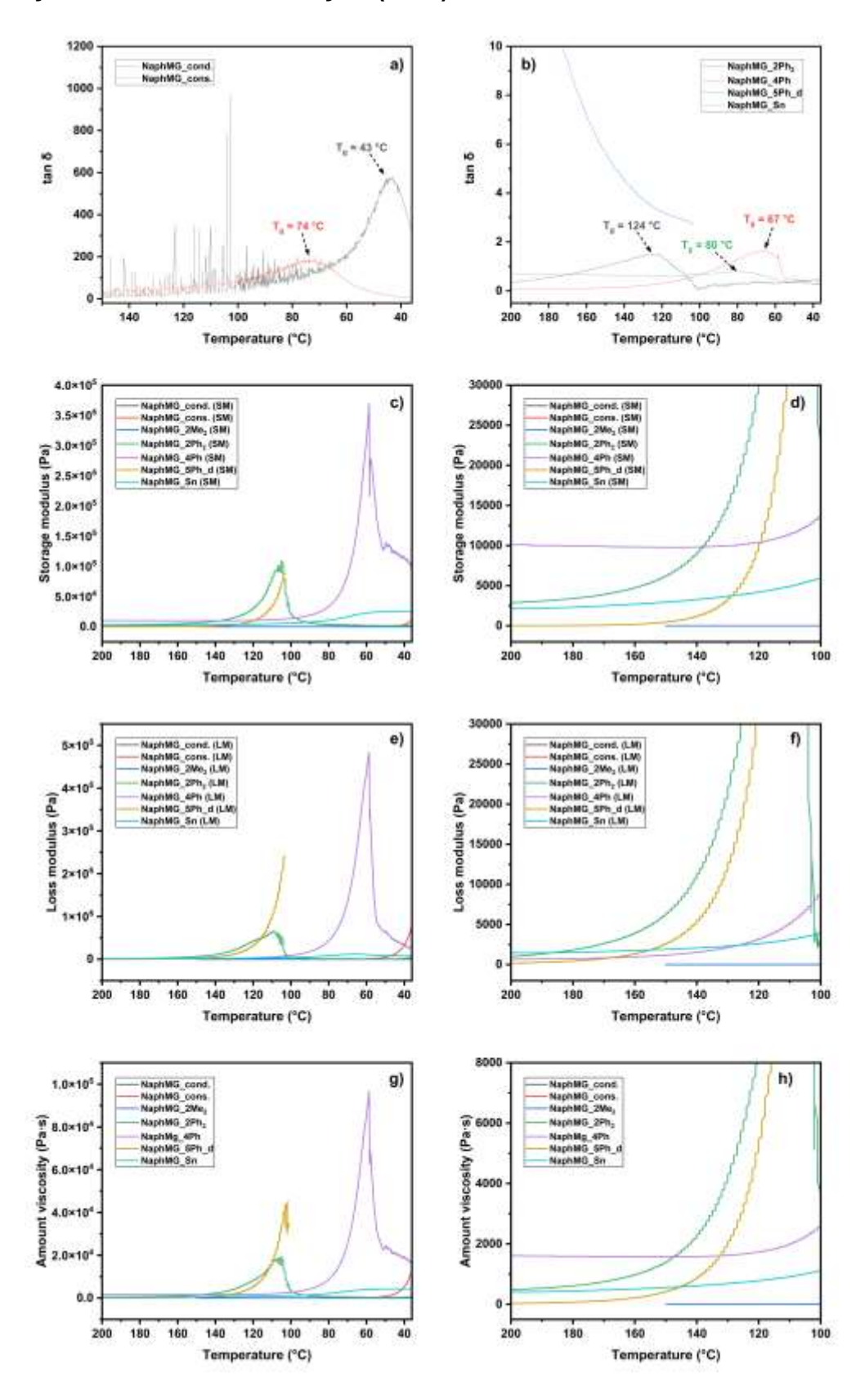


Figure S 79: Dynamic mechanical analysis of all siloxanes. a) $\tan \delta$, b) $\tan \delta$ (zoomed in), c) storage modulus, d) storage modulus (zoomed in), e) loss modulus, f) loss modulus (zoomed in), g) viscosity, h) viscosity (zoomed in).

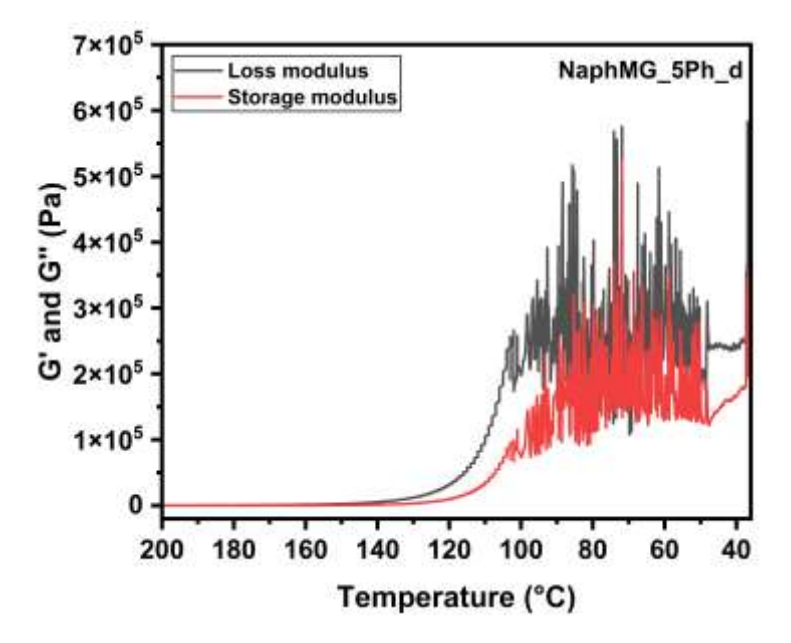


Figure S 80: Storage (G') and loss modulus (G'') of NaphMG_5Ph_d across the whole temperature range.

Table S 6: Viscosities of all siloxanes. a) not measured due to viscosity being too high and therefore risk of breakage, b) not measured due to viscosity being too low and therefore risk of loss of contact between both plates. c) Viscosities are not reliable due to cracking/breaking of the sample.

Amount viscosity (mPa·s)										
	50	100	150	200 150		100	50			
	°C	°C	°C	°C	°C	°C	°C			
NaphMG	3350	229	55.4	b	b	233	3490			
_2Me ₂										
NaphMG	а	а	а	479000	1400000	3430000°)	260000°)			
_2Ph ₂										
NaphMG	а	а	а	1610000	1570000	2590000	2.41E7 ^{c)}			
_4Ph										
NaphMG	а	а	395000	26800	417000	3.38E7 ^{c)}	4.03E7c)			
_5Ph_d										
NaphMG	18200	338	58.7	b	b	416	43500			
_cond.										
NaphMG	654000	2930	322	b	b	3190	733000			
_cons.										
NaphMG	а	а	510000	416000	557000	1130000	4220000			
_Sn										

6.2.5 Nuclear Magnetic Resonance (NMR) Spectroscopy

Besides ²⁹Si- and ¹³C CP-MAS NMR spectroscopy we also applied ²⁹Si- and ¹³C SP-MAS spectroscopy as a comparison because the former tends to underestimate the amount of highly cross-linked species. ^{221–223} Since these two techniques can only be applied to solid samples, the viscous sample NaphMG_2Me₂ could not be measured like this. The solid NaphMG could also not be measured using solid state NMR since the pulverized sample did not rotate properly in the NMR due to being sticky at room temperature and a stationary measurement showed only very broad and overlapping signals that could not be analyzed properly. Therefore, ²⁹Si solution NMR measurements were conducted to these two samples using chromium(III)acetylacetonate as a relaxation agent. ^{198–200} Unfortunately, NaphMG_Sn did show the same problems in the solid state NMR and also did not sufficiently dissolve in any NMR solvent, leading to no measurement available.

The DOC of all samples was calculated according to equation (1'). 291

$$DOC = \frac{D^{1} + 2D^{2} + D^{1'} + 2D^{2'} + T^{1} + 2T^{2} + 3T^{3}}{2 \cdot (D^{1} + D^{2} + D^{1'} + D^{2'}) + 3 \cdot (T^{1} + T^{2} + T^{3})}$$
(1')

NaphMG

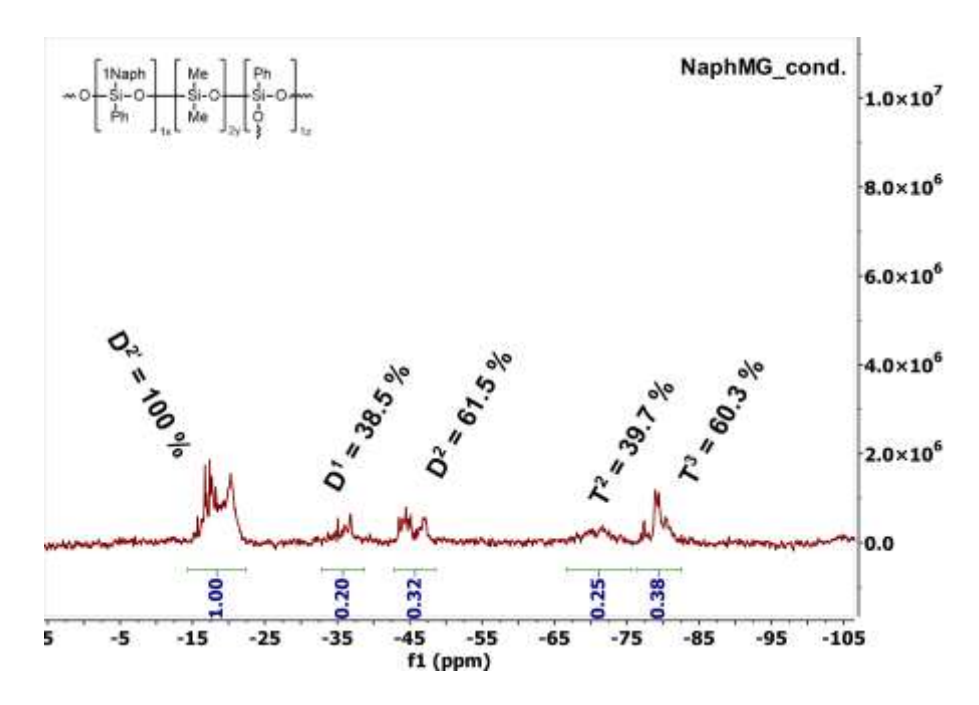


Figure S 81: ²⁹Si NMR spectrum (CDCl₃, 59.63 MHz, liquid) of NaphMG before consolidation.

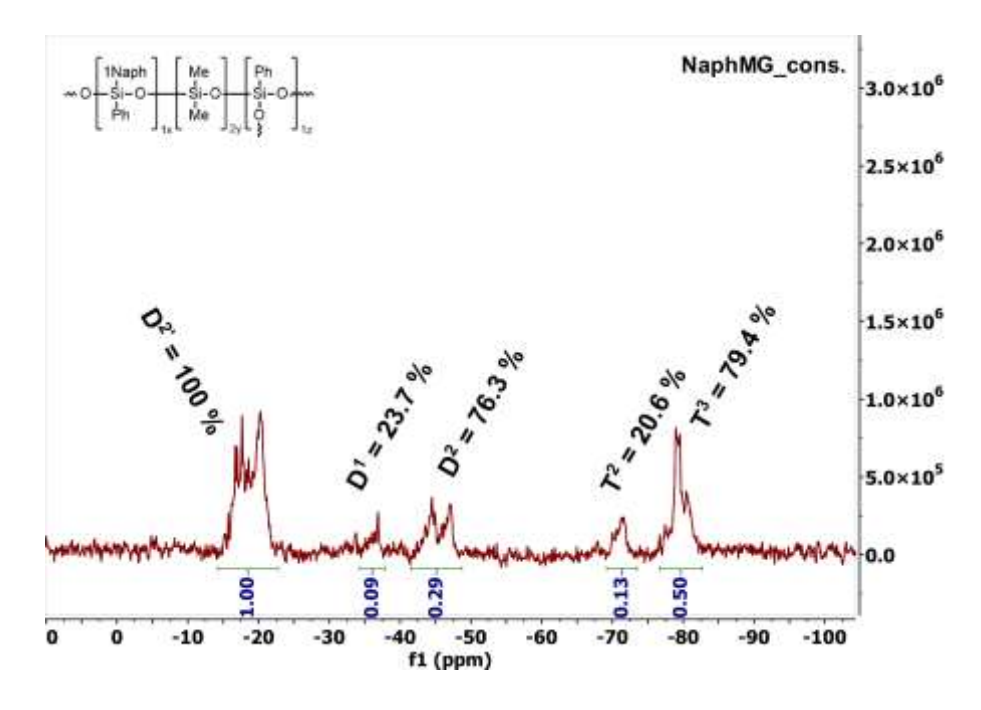
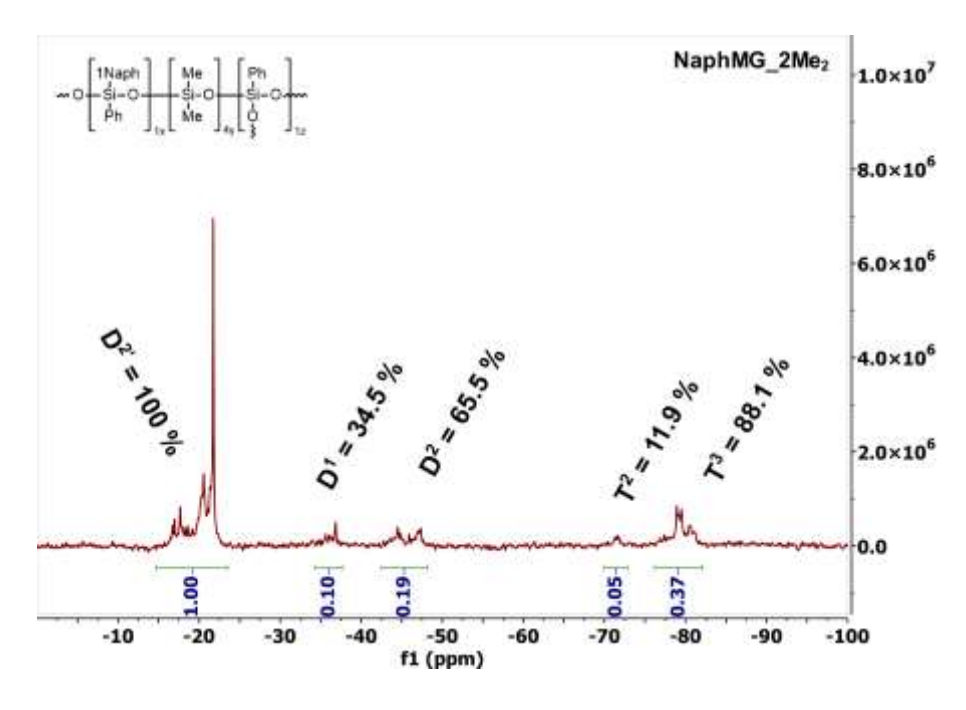


Figure S 82: 29 Si NMR spectrum (CDCl₃, 59.63 MHz, liquid) of NaphMG after consolidation.

NaphMG_2Me₂



 $\textbf{Figure S 83:} \ ^{29}\text{Si NMR spectrum (CDCl}_3, 59.63 \ \text{MHz, liquid) of NaphMG}_2\text{Me}_2 \ \text{after consolidation.}$

NaphMG_2Ph₂

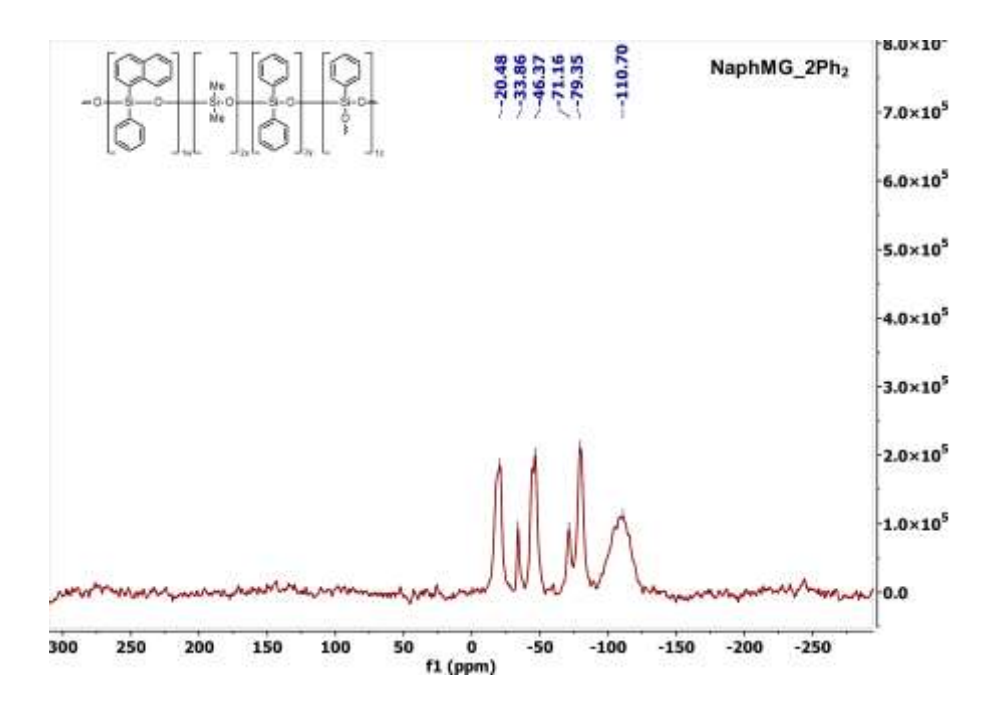


Figure S 84: ²⁹Si MAS spectrum of NaphMG_2Ph₂ after consolidation.

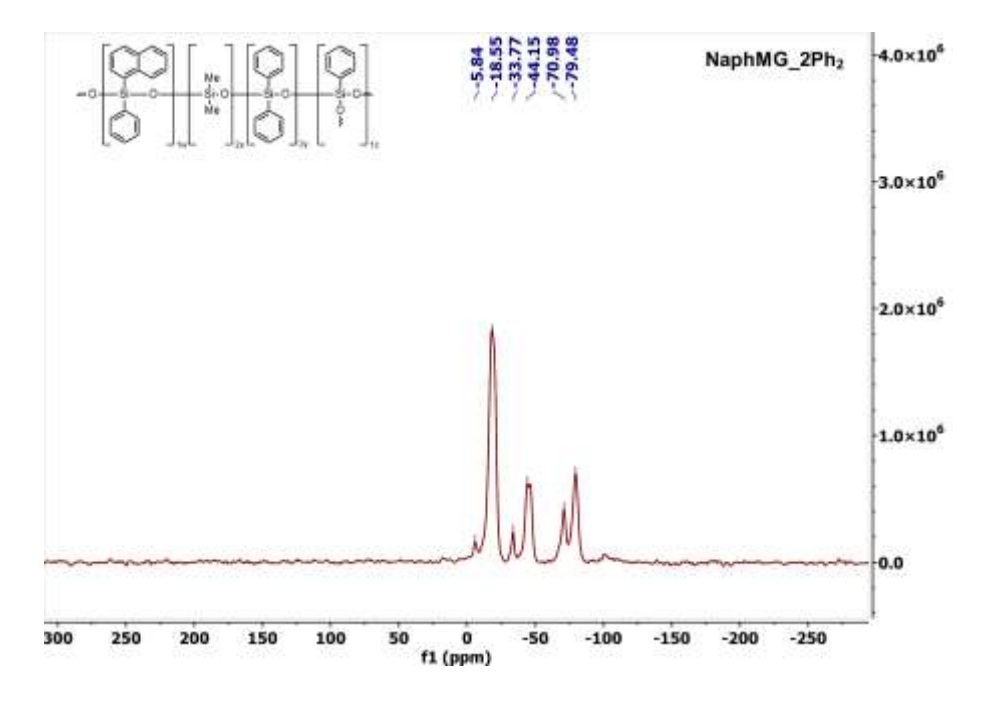


Figure S 85: ²⁹Si CP-MAS spectrum of NaphMG_2Ph₂ after consolidation.

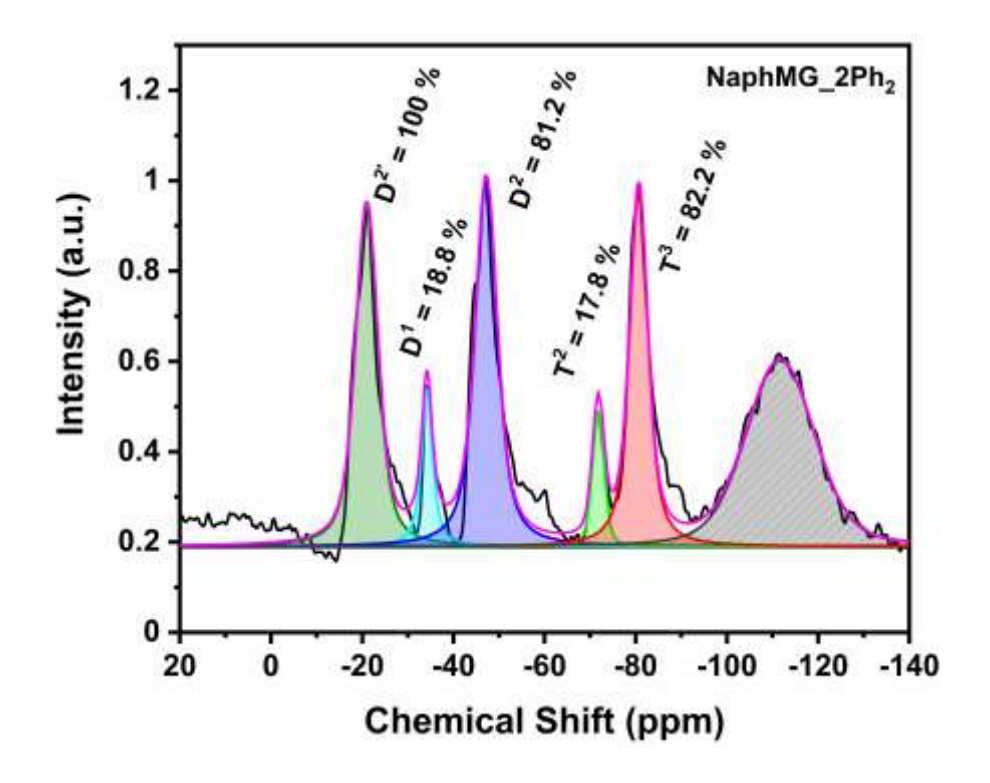


Figure S 86: Integrated ²⁹Si MAS spectrum of NaphMG_2Ph₂ after consolidation.

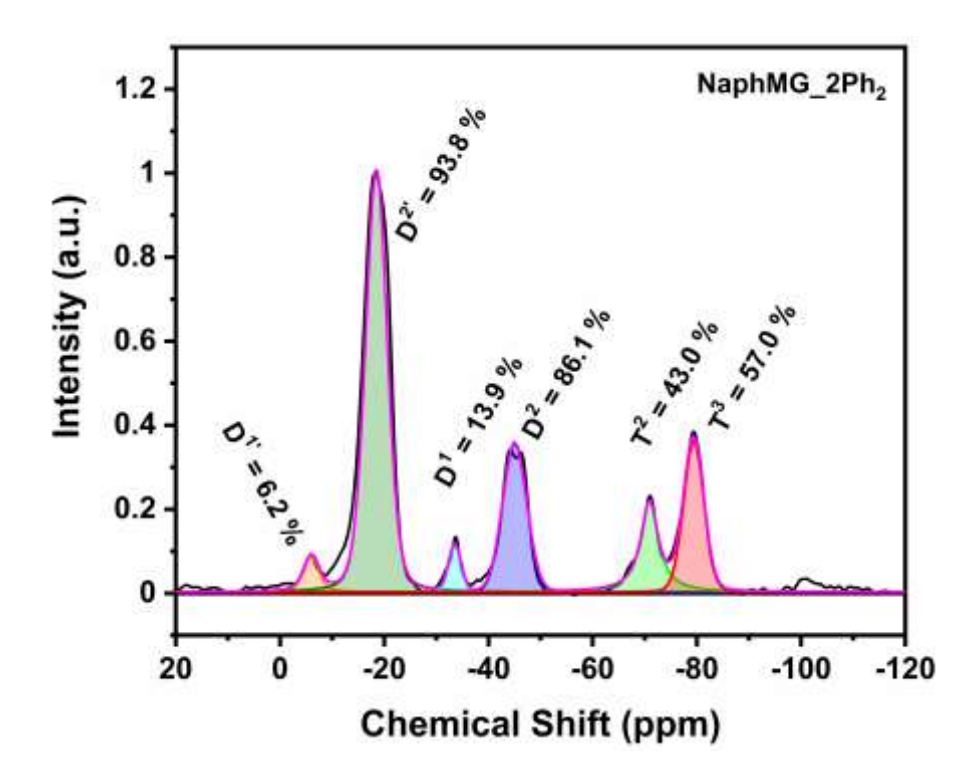


Figure S 87: Integrated ²⁹Si CP-MAS spectrum of NaphMG_2Ph₂ after consolidation.

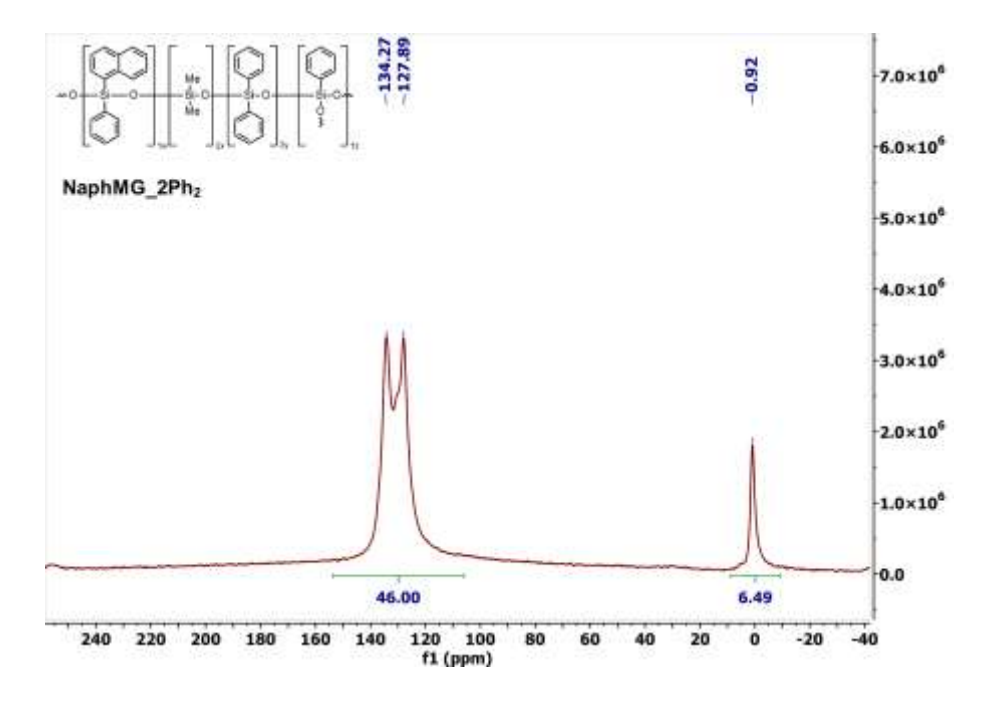


Figure S 88: ¹³C MAS spectrum of NaphMG_2Ph₂ after consolidation.

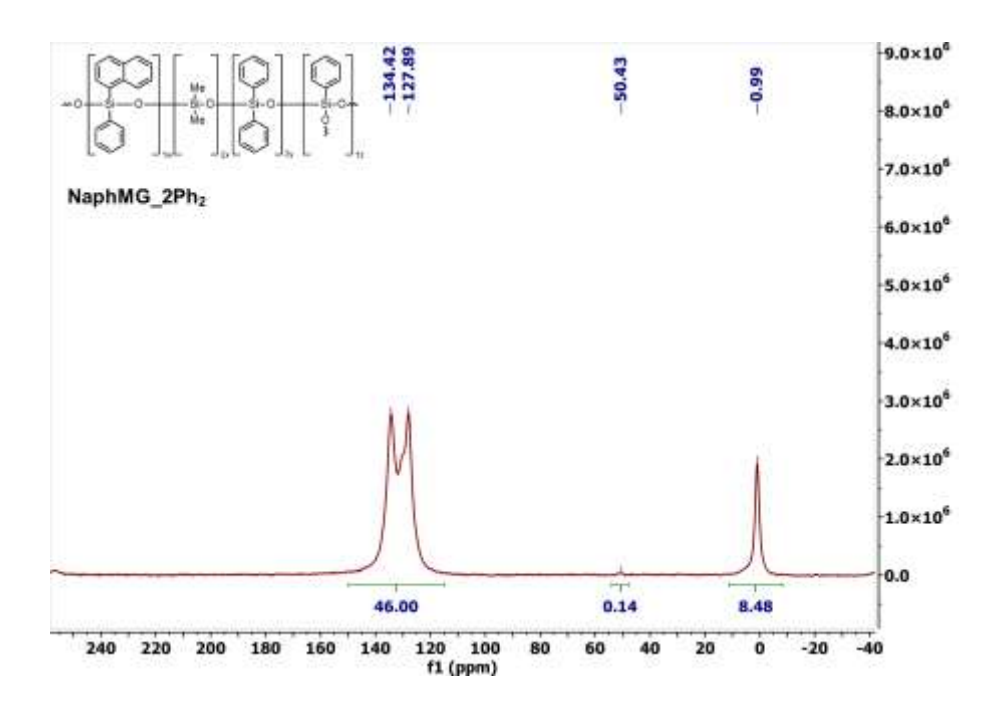


Figure S 89: ¹³C CP-MAS spectrum of NaphMG_2Ph₂ after consolidation.

NaphMG_4Ph

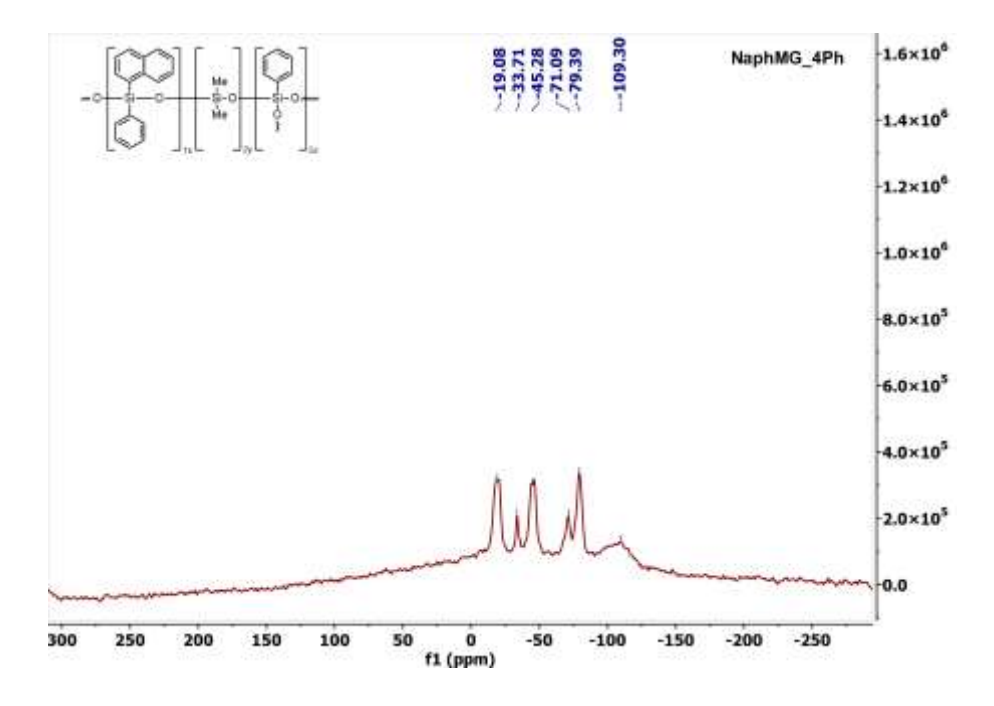


Figure S 90: ²⁹Si MAS spectrum of NaphMG_4Ph after consolidation.

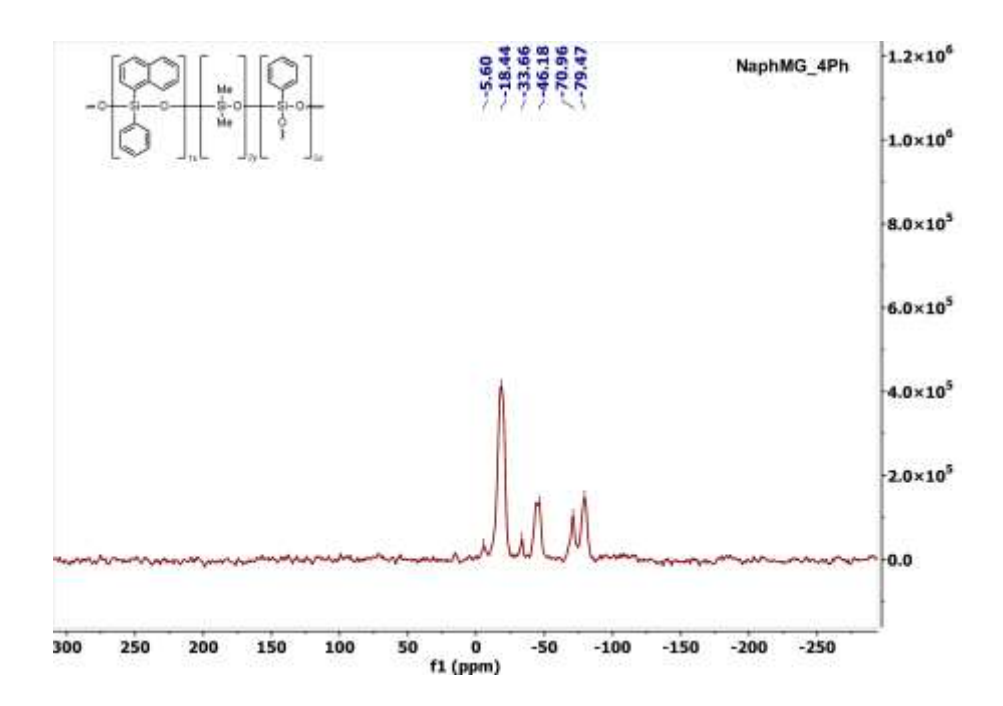


Figure S 91: ²⁹Si CP-MAS spectrum of NaphMG_4Ph after consolidation.

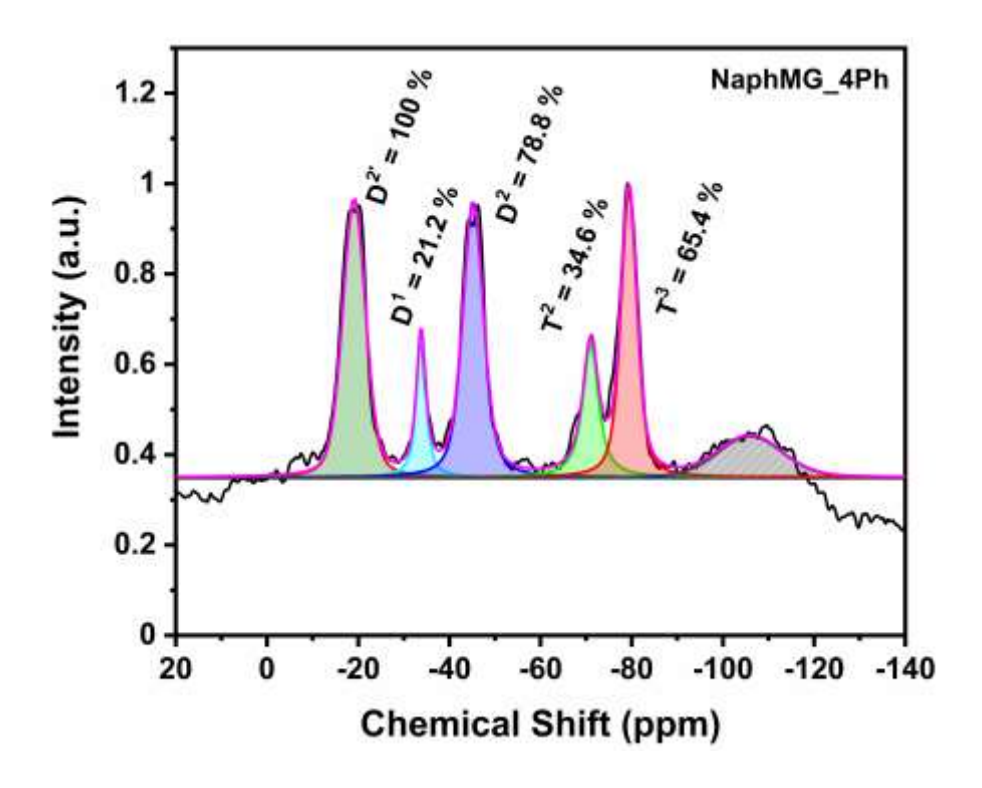


Figure S 92: Integrated ²⁹Si MAS spectrum of NaphMG_4Ph after consolidation.

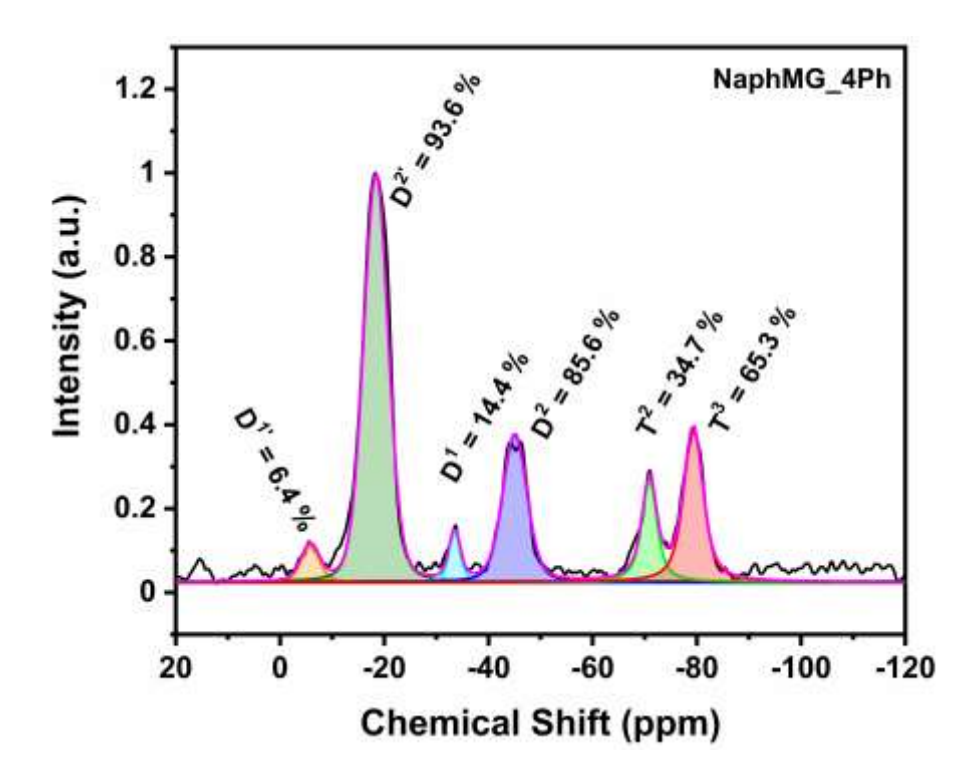


Figure S 93: Integrated ²⁹Si CP-MAS spectrum of NaphMG_4Ph after consolidation.

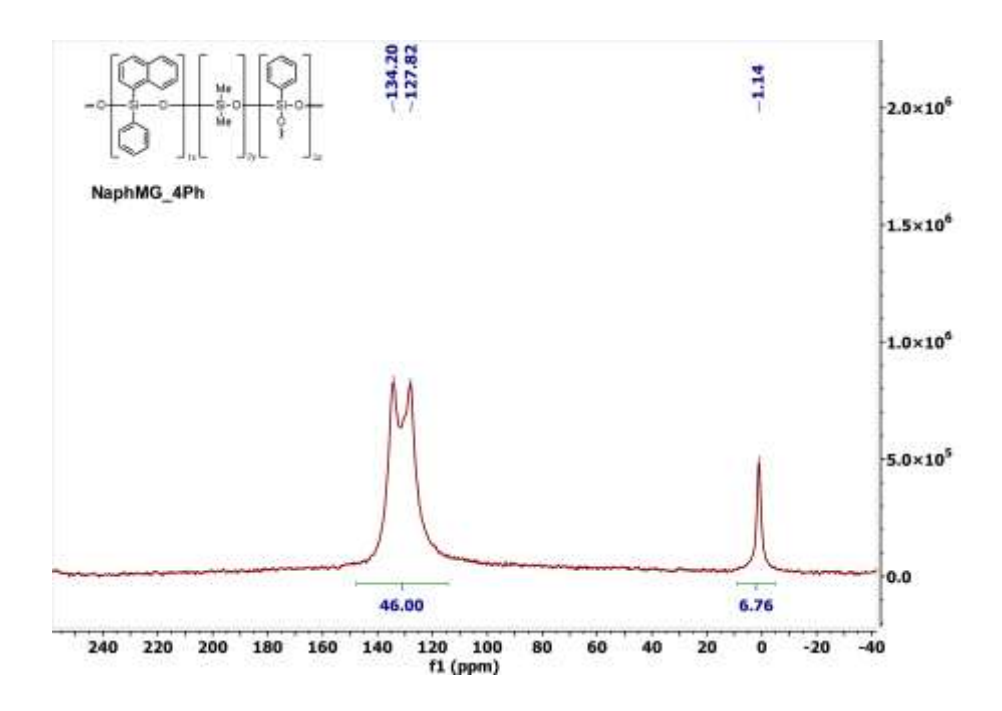


Figure S 94: ¹³C MAS spectrum of NaphMG_4Ph after consolidation.

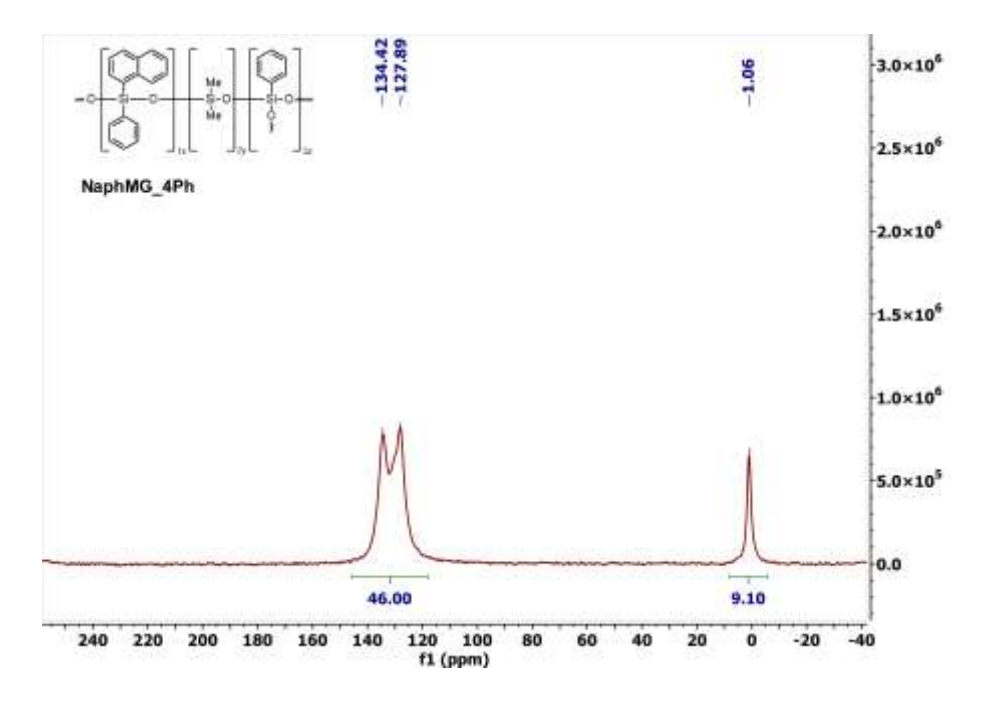


Figure S 95: ¹³C CP-MAS spectrum of NaphMG_4Ph after consolidation.

NaphMG_5Ph_d

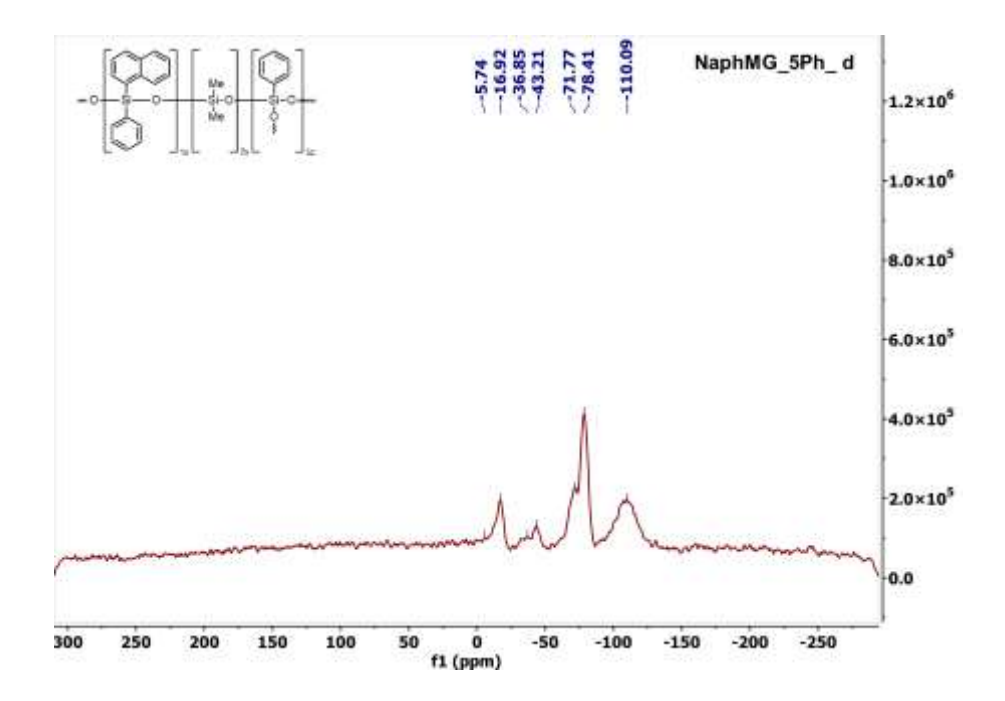


Figure S 96: ²⁹Si MAS spectrum of NaphMG_5Ph_d after consolidation.

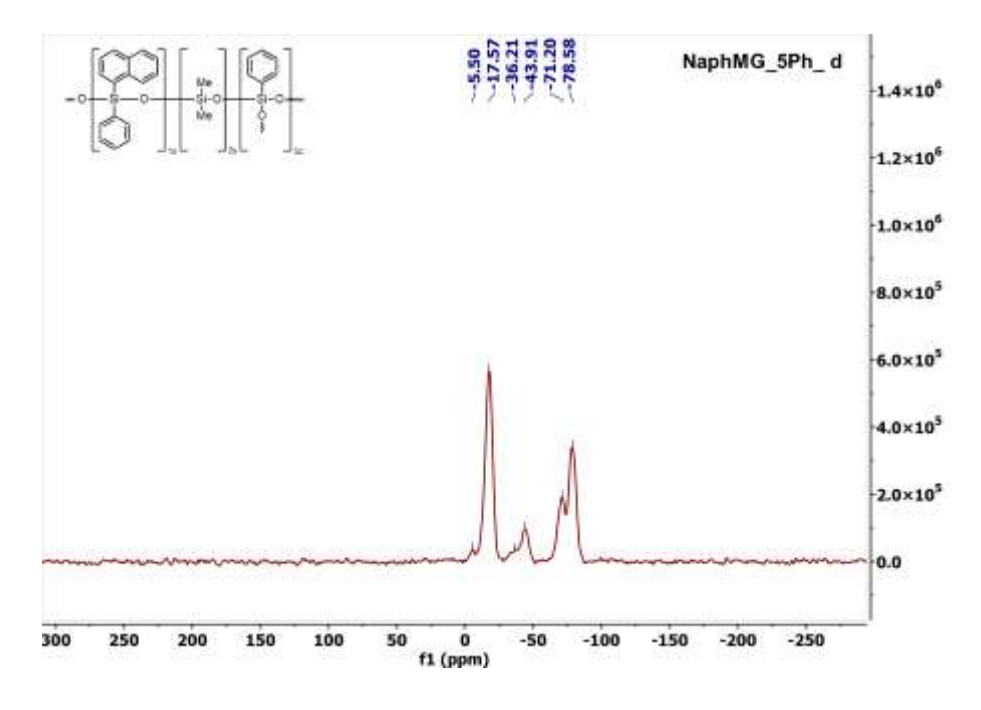


Figure S 97: ²⁹Si CP-MAS spectrum of NaphMG_5Ph_d after consolidation.

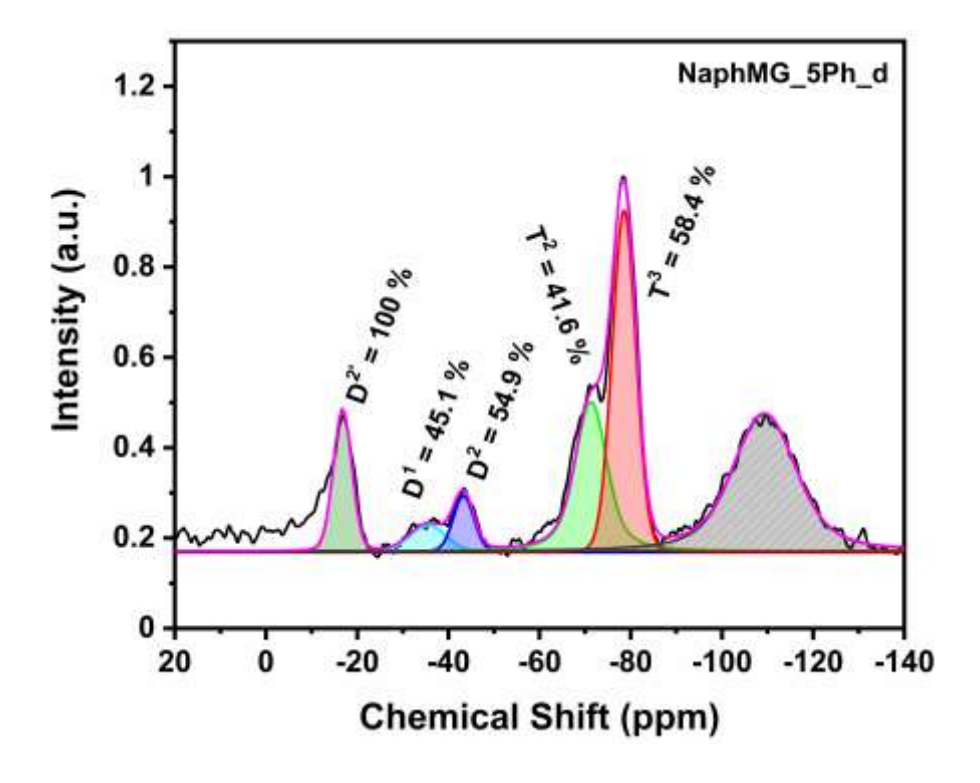


Figure S 98: Integrated ²⁹Si MAS spectrum of NaphMG_5Ph_d after consolidation.

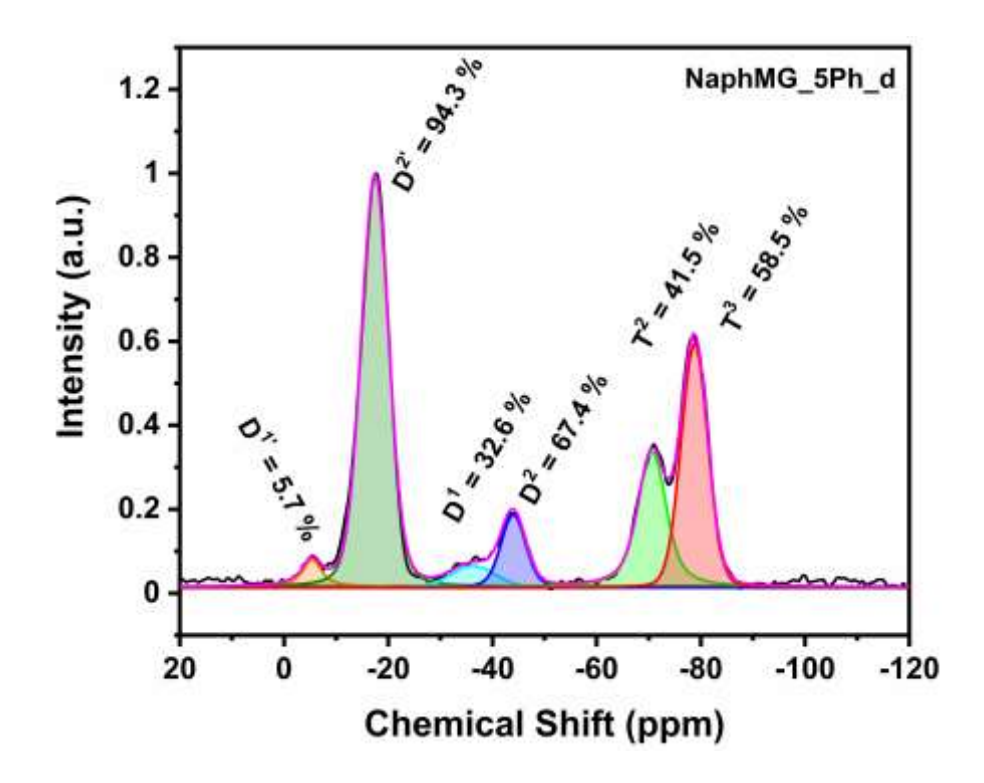


Figure S 99: Integrated ²⁹Si CP-MAS spectrum of NaphMG_5Ph_d after consolidation.

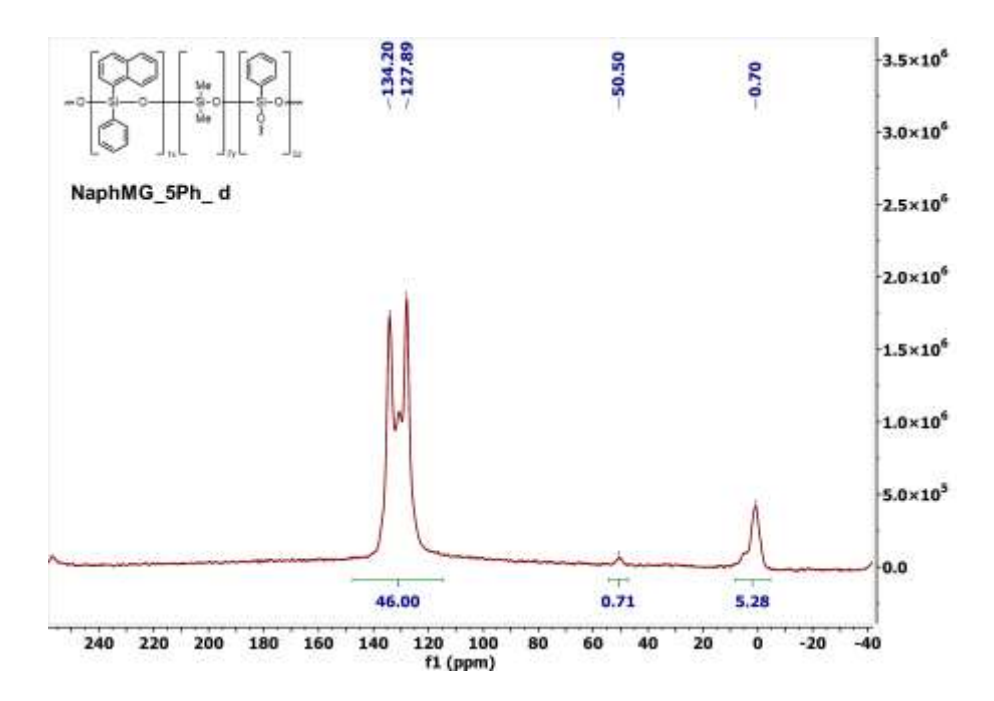


Figure S 100: ¹³C MAS spectrum of NaphMG_5Ph_d after consolidation.

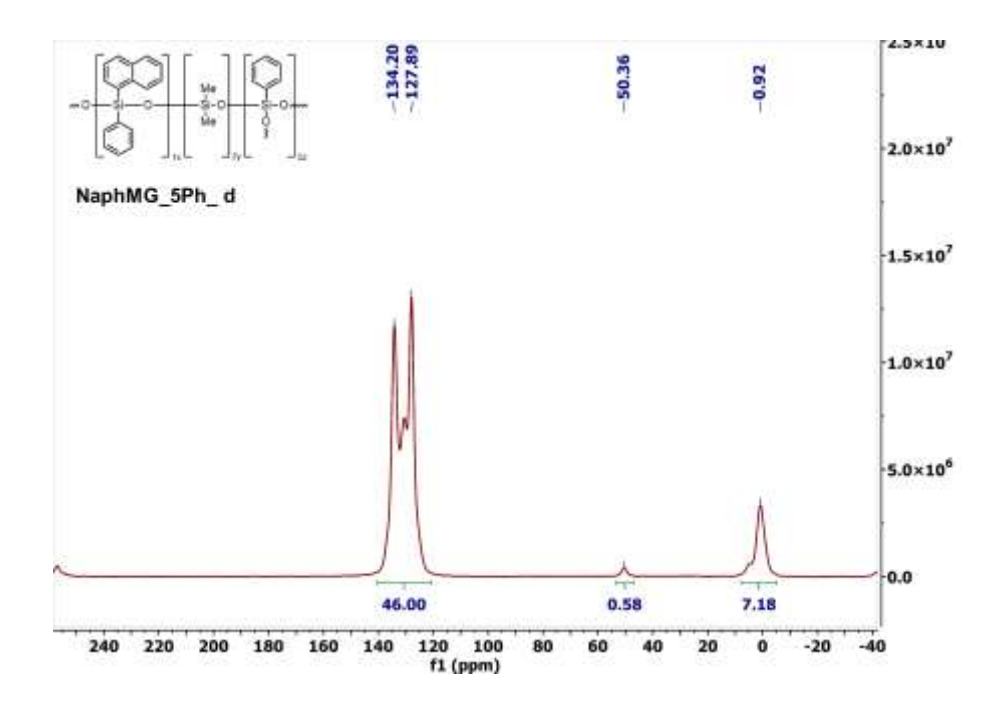


Figure S 101: ¹³C CP-MAS spectrum of NaphMG_5Ph_d after consolidation.

Table S 7: Summary of the results of all ²⁹Si liquid, ²⁹Si CP-MAS and ²⁹Si MAS NMR measurements including D- and T-signals as well as DOC.

	NMR	D1' /%	D ² /%	D¹ /%	D ² /%	T ² /%	T³ /%	DOC/%
NaphMG_cond.	Liquid	0	100	38.5	61.5	39.7	60.3	88.8
NaphMG_cons.	Liquid	0	100	23.7	76.3	20.6	79.4	93.7
NaphMG_2Me₂	Liquid	0	100	34.5	65.5	11.9	88.1	93.4
NaphMG_2Ph ₂	CPMAS	6.2	93.8	13.9	86.1	43.0	57.0	91.0
	MAS	0	100	18.8	81.2	17.8	82.2	94.8
NaphMG_4Ph	CPMAS	6.4	93.6	14.4	85.6	34.7	65.3	92.1
	MAS	0	100	21.2	78.8	34.6	65.4	92.0
NaphMG_5Ph_d	CPMAS	5.7	94.3	32.6	67.4	41.5	58.5	88.6
	MAS	0	100	45.1	54.9	41.6	58.4	87.6

6.2.6 Fourier Transform Infrared (FTIR) Spectroscopy

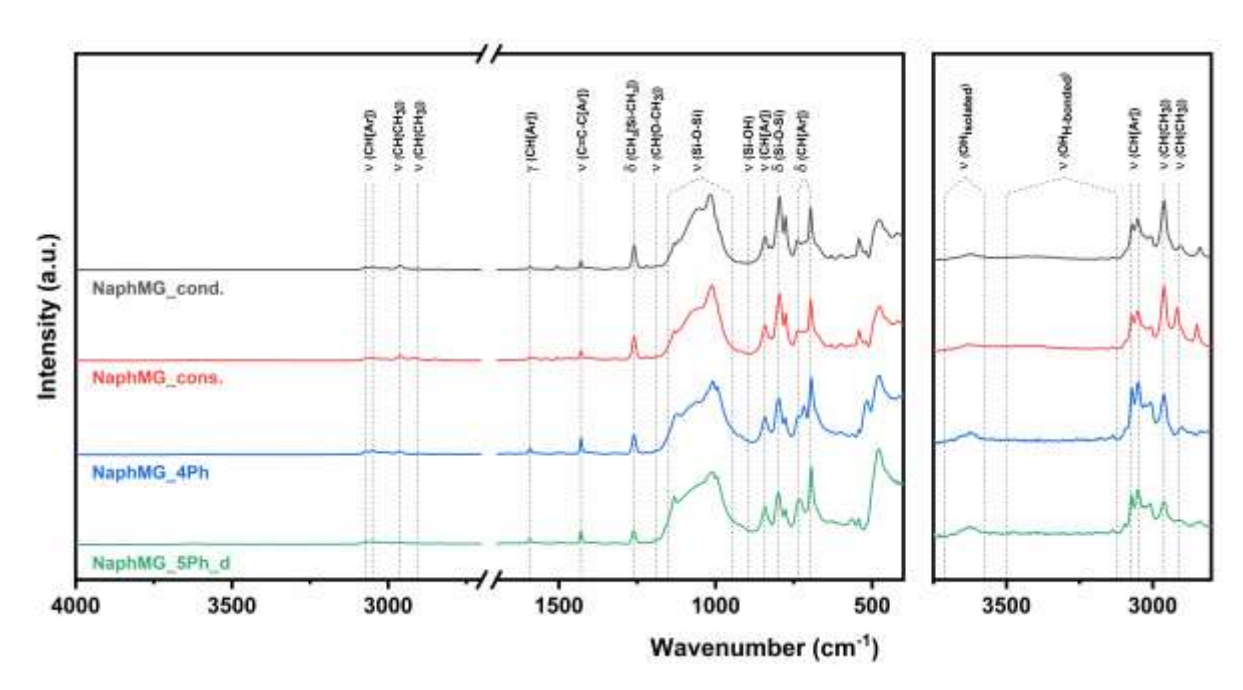


Figure S 102: FTIR spectra of NaphMG_cond. (black), NaphMG_cons. (red), as well as the consolidated samples NaphMG_4Ph (blue) and NaphMG_5Ph_d (green). Left: full spectrum, right: enlarged area.

Table S 8: FTIR absorption bands of all samples. 99,341,354,355

Absorption band	Wavenumber		
Aryl	3073 cm ⁻¹ (v _{asym} CH), 3049 cm ⁻¹ (v _{sym} CH), 1591 cm ⁻¹ (γ CH _{Ar}),		
	1429 cm ⁻¹ (v C-C _{Ar}), 845 cm ⁻¹ (δ CH), 735 cm ⁻¹ (δ CH),		
	698 cm ⁻¹ (δ CH)		
Methyl	2962 cm $^{\text{-1}}$ (v _{asym} CH $_{\text{3}}$), 2904 cm $^{\text{-1}}$ (v _{sym} CH $_{\text{3}}$) and 1259 cm $^{\text{-1}}$		
	$(\delta_s CH_3 (Si-CH_3))$		
Si-O-Si	1131 – 996 cm ⁻¹ , 798 cm ⁻¹		
$OH_{isolated}$	3712 – 3575 cm ⁻¹		
$OH_{H ext{-}bonded}$	3500 – 3120 cm ⁻¹		
Si-OH	920 – 890 cm ⁻¹		

6.2.7 Powder X-ray Diffraction (PXRD)

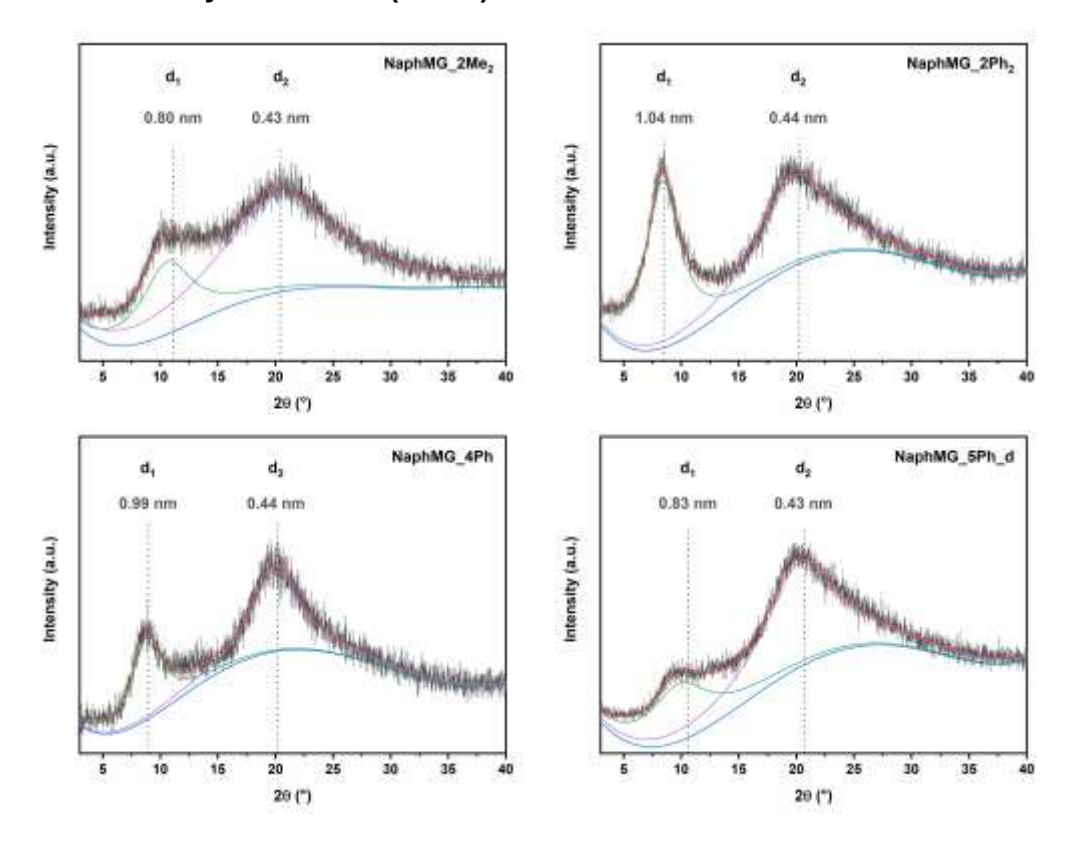


Figure S 103: PXRD spectra of NaphMG_2Me₂, NaphMG_2Ph₂, NaphMG_4Ph and NaphMG_5Ph_d. All samples were measured as tablets.

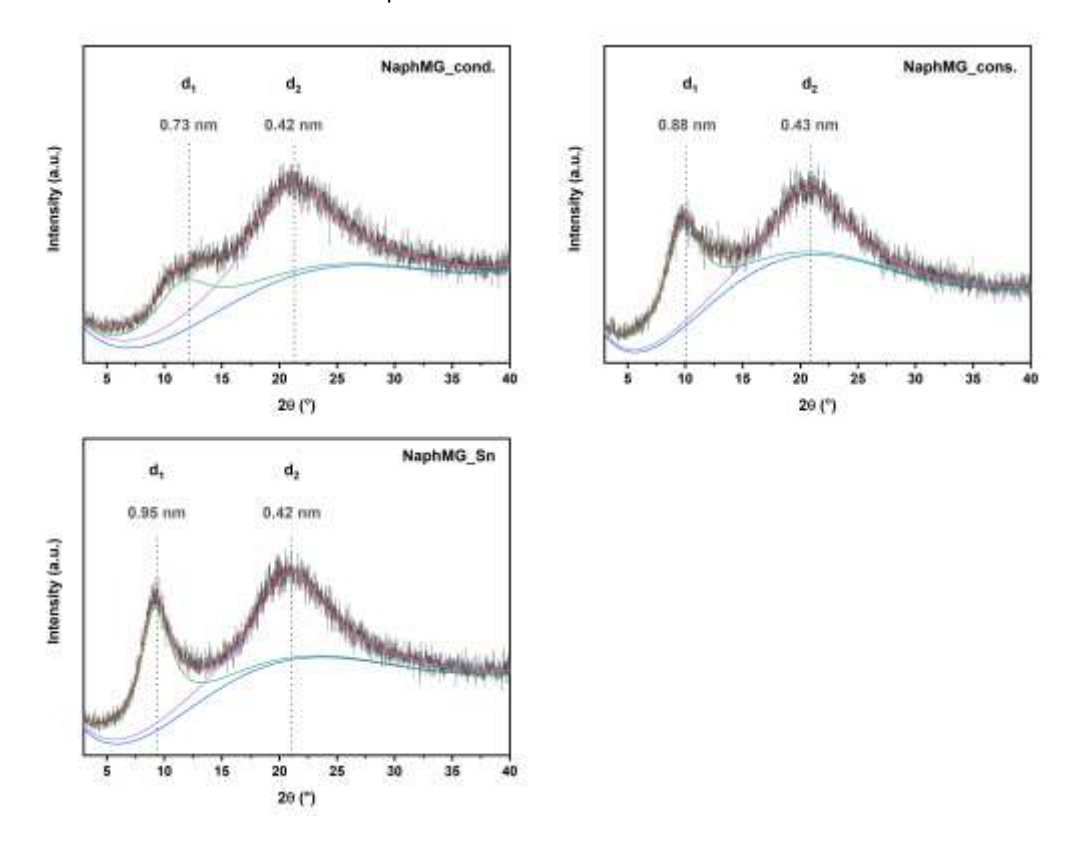


Figure S 104: PXRD spectra of NaphMG_cond., NaphMG_cons. and NaphMG_Sn. All samples were measured as tablets.

6.2.8 Ultraviolet-visible (UV-vis) Spectroscopy

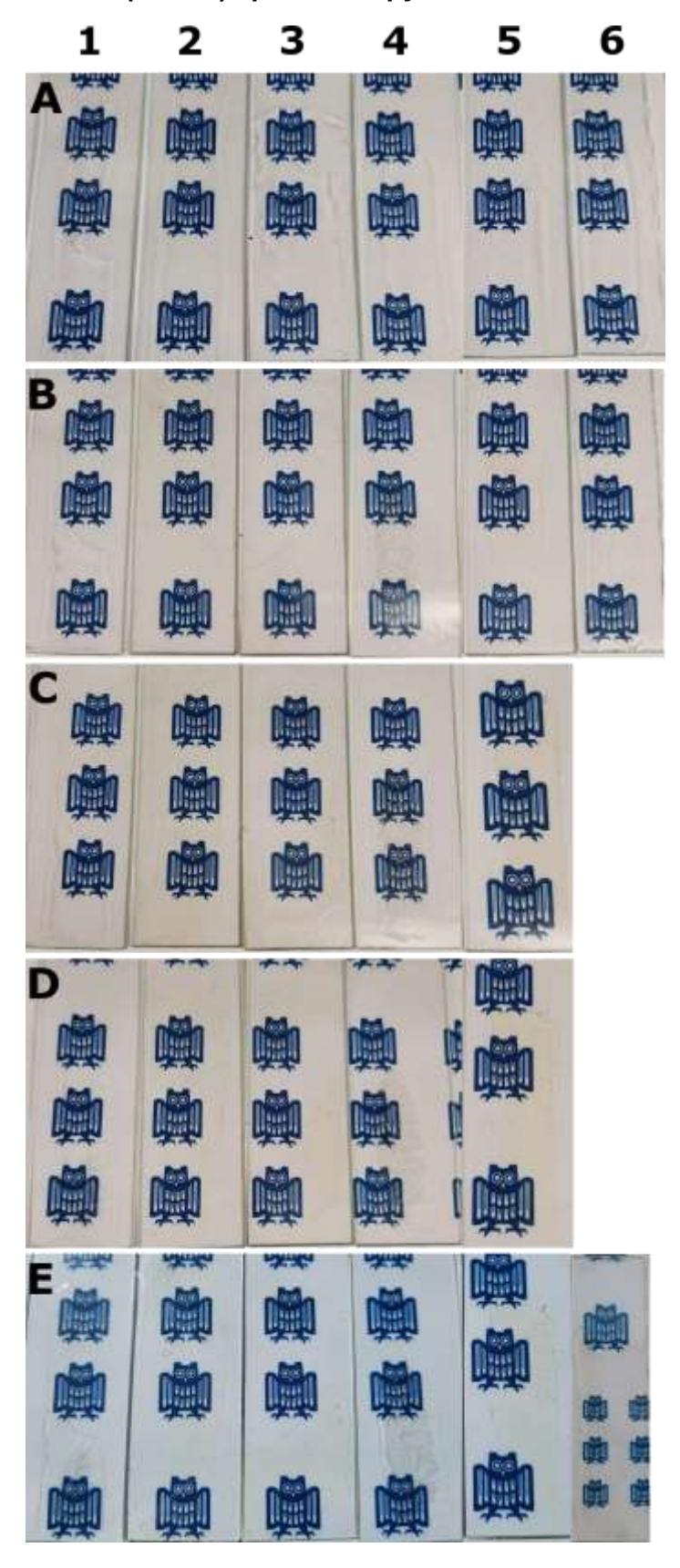


Figure S 105: Siloxanes doctor bladed onto glass slides. A) before consolidation, B) after consolidation, C) after 3 d at 200 °C D) after 7 d at 200 °C, E) after 7 d at 200 °C, different lighting. 1) NaphMG_2Ph₂, 2) NaphMG_2Me₂, 3) NaphMG_4Ph, 4) NaphMG_5Ph_d, 5) NaphMG, 6) NaphMG_Sn.

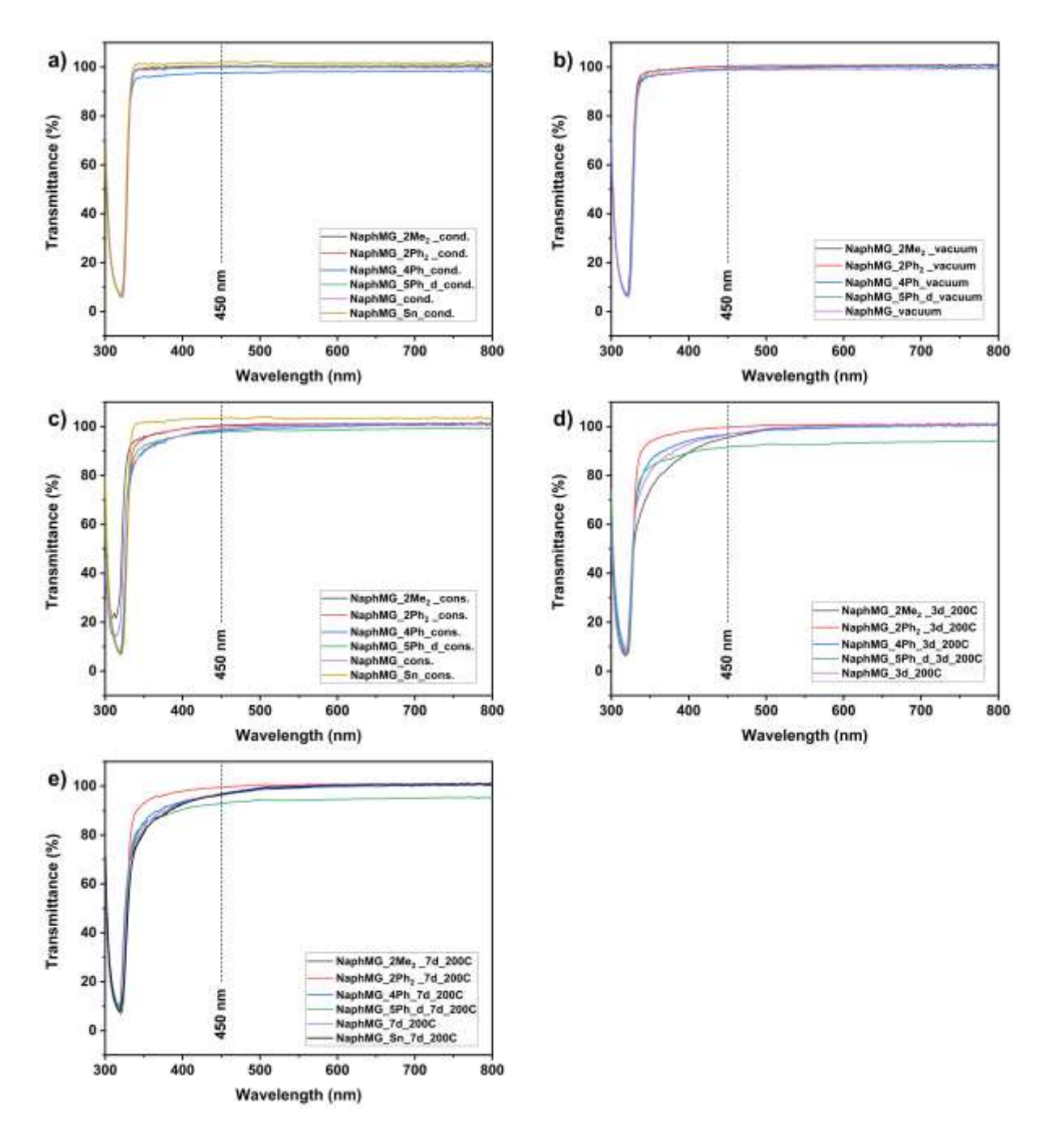


Figure S 106: UV-vis measurements of all samples. a) after condensation, b) after 24 h under vacuum at 110 °C, c) after consolidation (72 h, 200 °C), d) after 3 d at 200 °C, e) after 7 d at 200 °C.

6.3 Synthesis of Polyhedral Oligomeric Silsesquioxanes (POSS) Containing Polycyclic Aryl Groups

6.3.1 Trialkoxysilanes

6.3.1.1 Nuclear Magnetic Resonance (NMR) Spectroscopy

1-NaphSi(OMe)₃

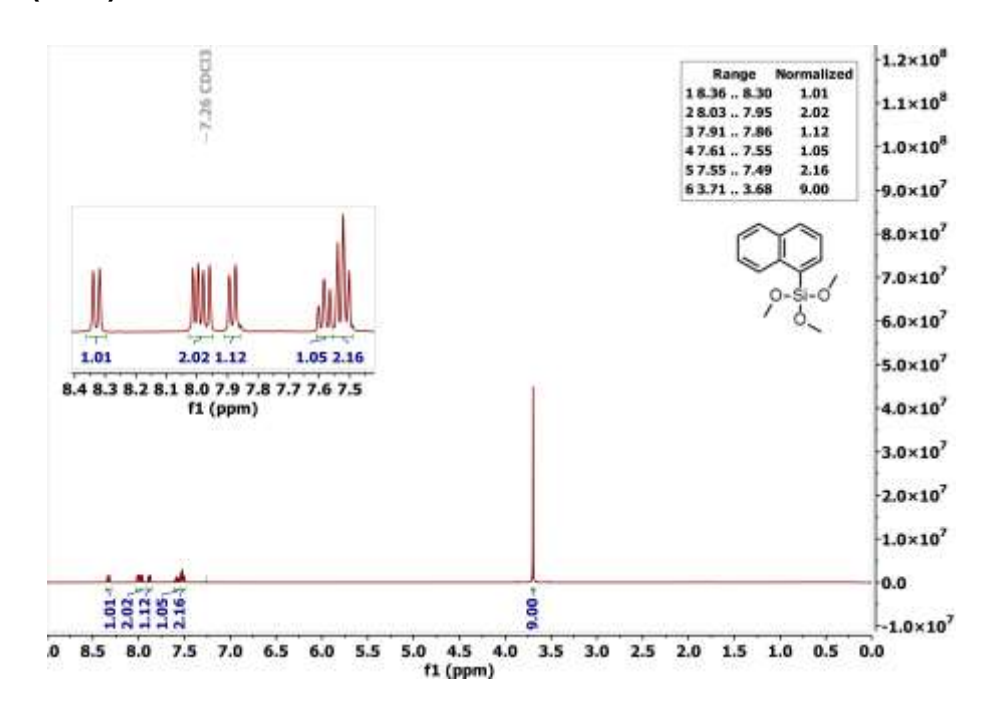


Figure S 107: ¹H NMR spectrum (CDCl₃, 400.13 MHz) of trimethoxy-(1-naphthyl)silane.

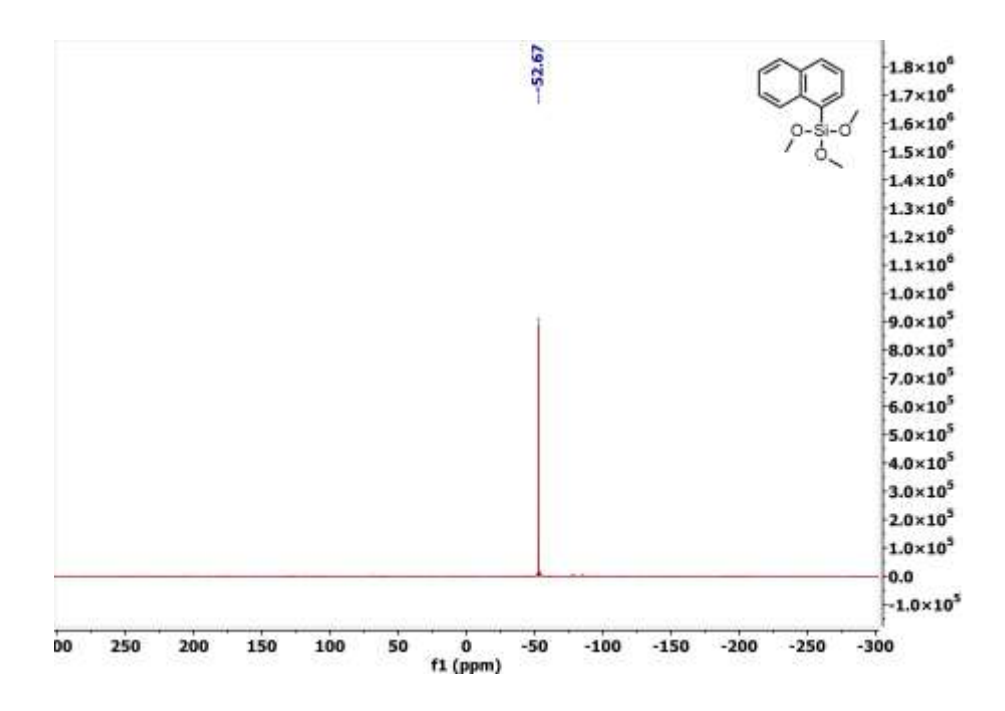


Figure S 108: ²⁹Si NMR spectrum (CDCl₃, 79.49 MHz) of trimethoxy-(1-naphthyl)silane.

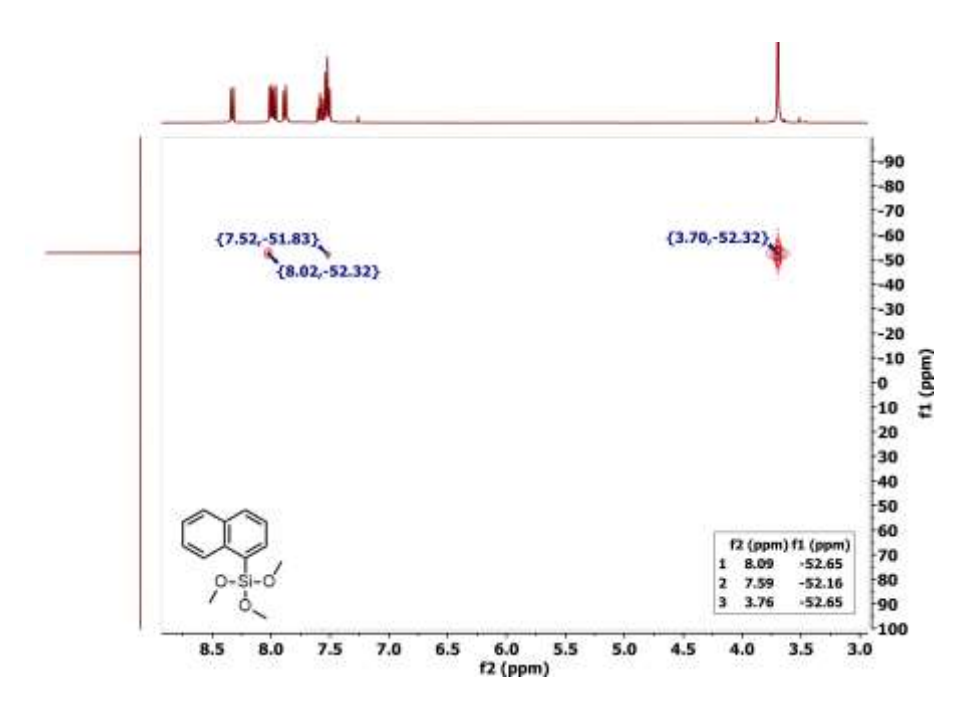


Figure S 109: ¹H, ²⁹Si HMBC spectrum (CDCl₃, 400.13 MHz; 79.49 MHz) of trimethoxy-(1-naphthyl)silane.

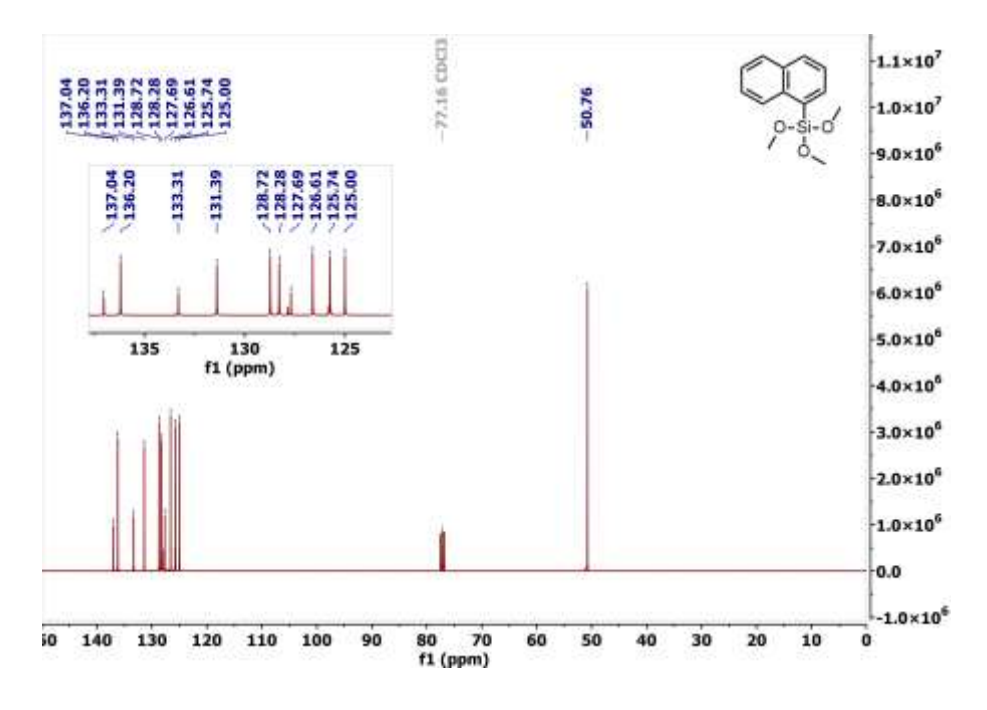


Figure S 110: ¹³C NMR spectrum (CDCl₃, 100.62 MHz) of trimethoxy-(1-naphthyl)silane.

2-NaphSi(OMe)₃

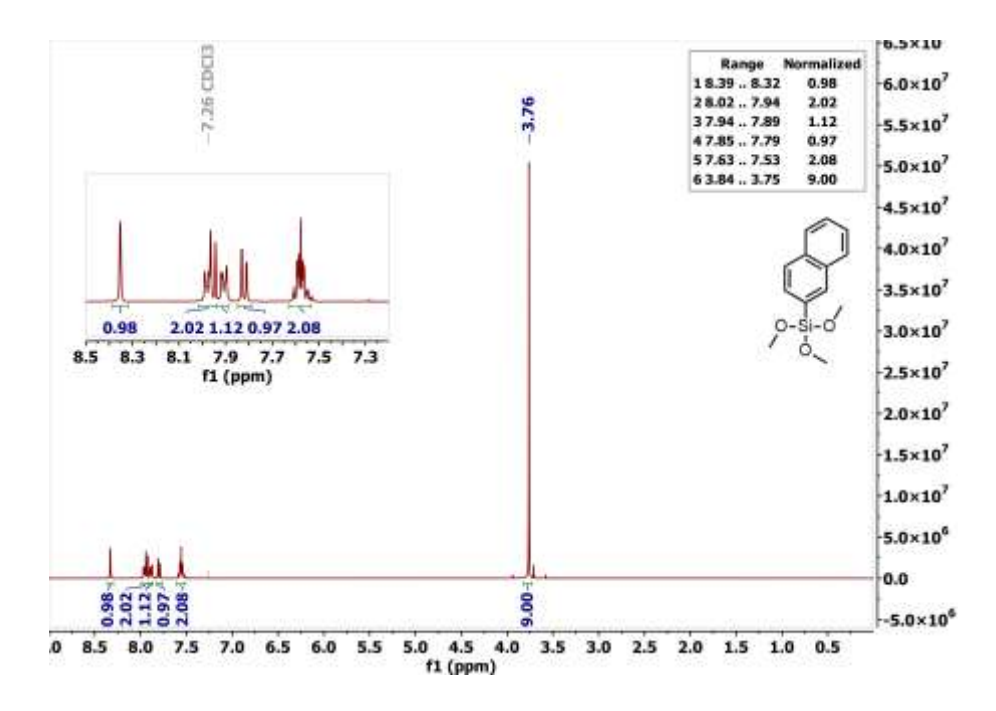


Figure S 111: ¹H NMR spectrum (CDCl₃, 400.13 MHz) of trimethoxy-(2-naphthyl)silane.

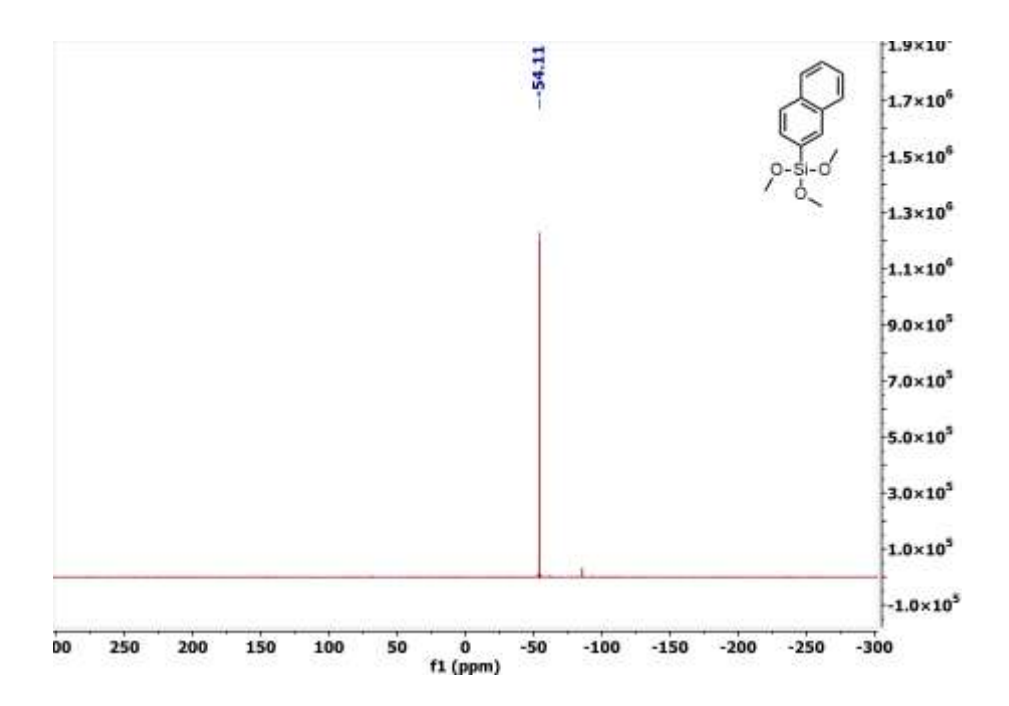


Figure S 112: ²⁹Si NMR spectrum (CDCl₃, 79.49 MHz) of trimethoxy-(2-naphthyl)silane.

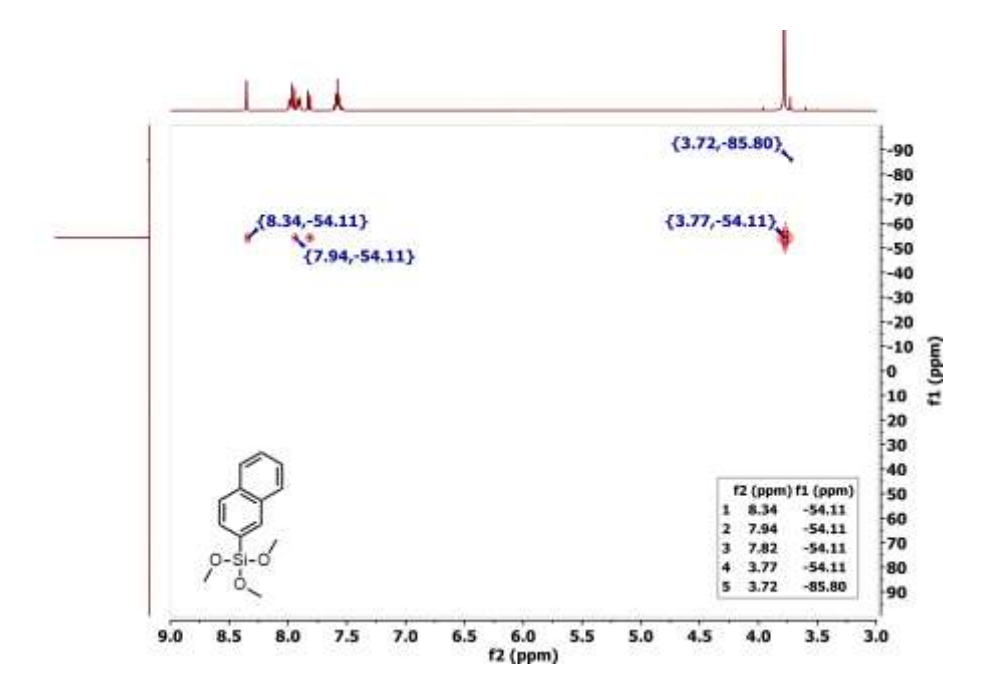


Figure S 113: ¹H, ²⁹Si HMBC spectrum (CDCl₃, 400.13 MHz; 79.49 MHz) of trimethoxy-(2-naphthyl)silane.

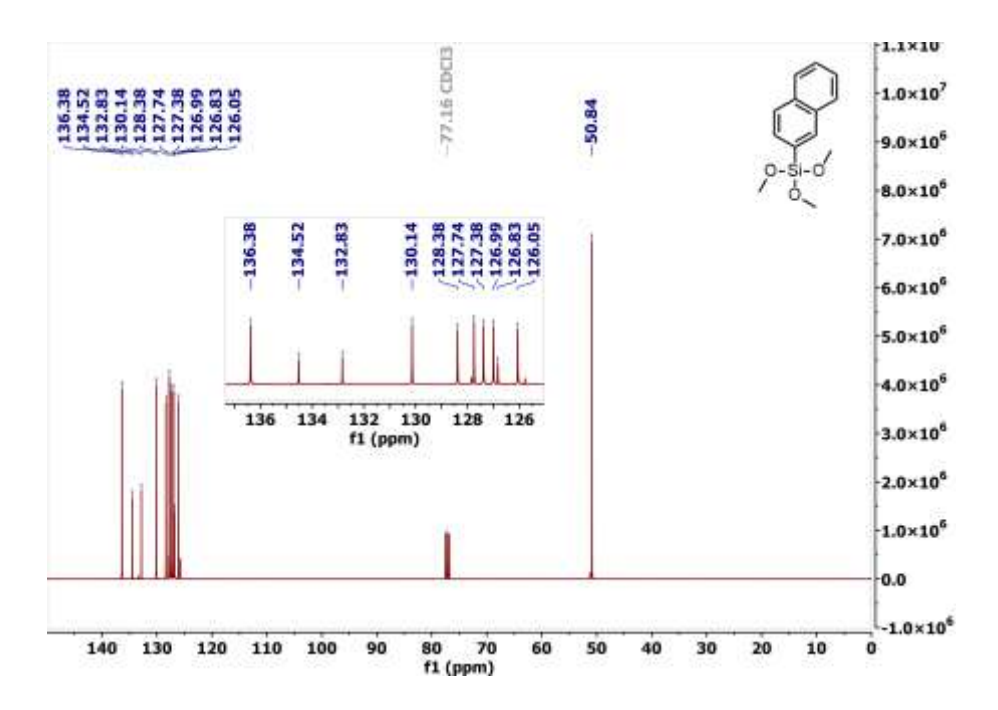


Figure S 114: ¹³C NMR spectrum (CDCl₃, 100.62 MHz) of trimethoxy-(2-naphthyl)silane.

9-PhenSi(OMe)₃

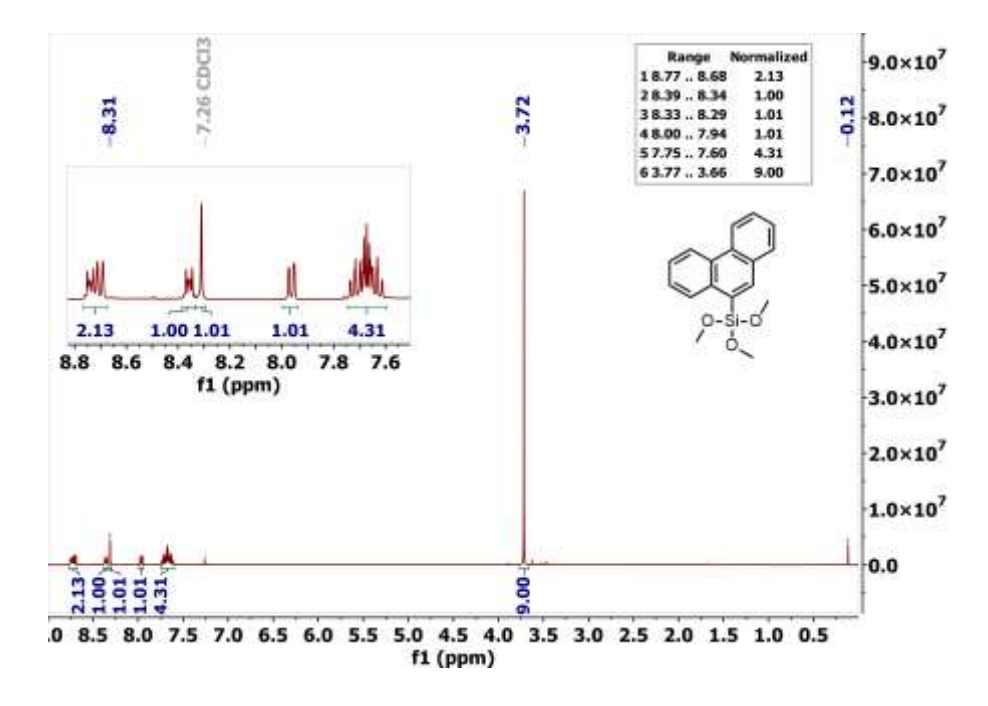


Figure S 115: ¹H NMR spectrum (CDCl₃, 400.13 MHz) of trimethoxy-(9-phenanthrenyl)silane.

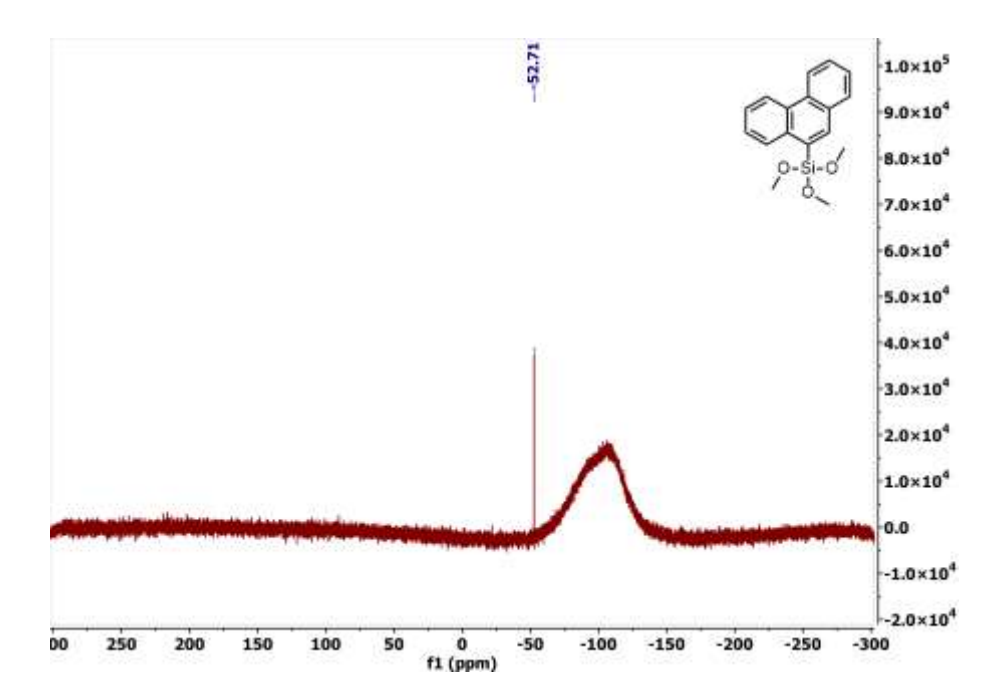


Figure S 116: ²⁹Si NMR spectrum (CDCl₃, 79.49 MHz) of trimethoxy-(9-phenanthrenyl)silane.

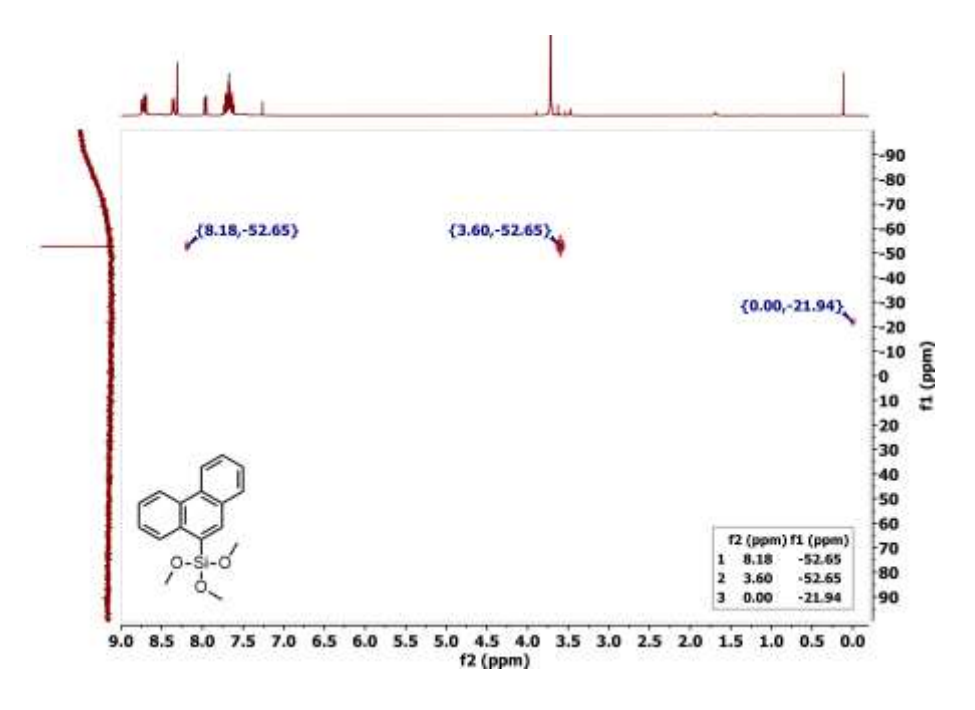


Figure S 117: ¹H, ²⁹Si HMBC spectrum (CDCl₃, 400.13 MHz; 79.49 MHz) of trimethoxy-(9-phenanthrenyl)silane.

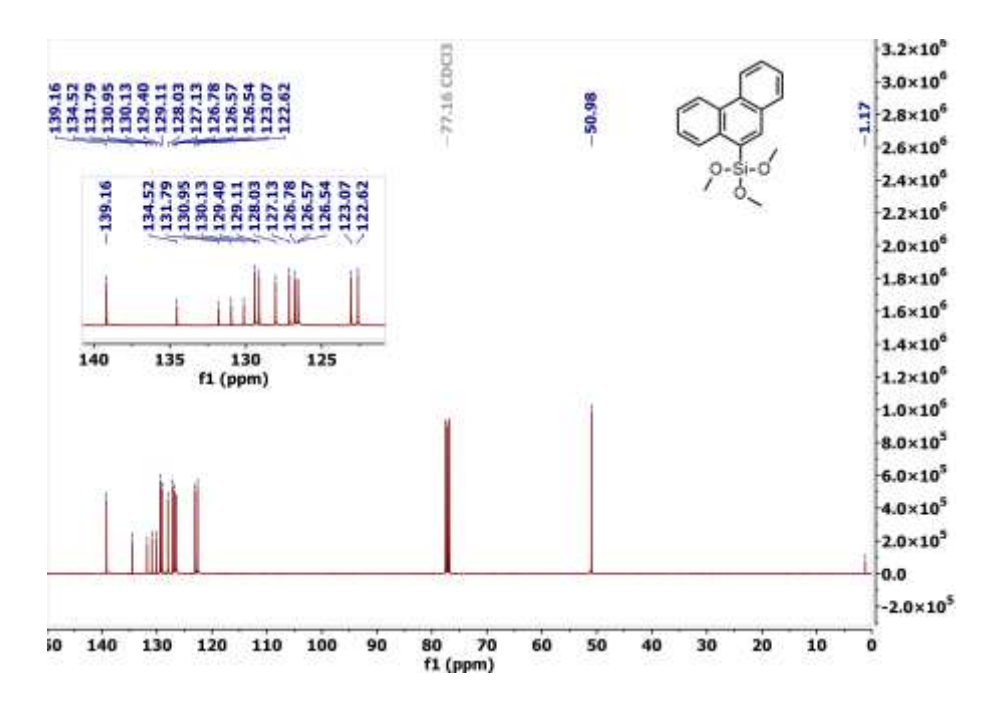


Figure S 118: ¹³C NMR spectrum (CDCl₃, 100.62 MHz) of trimethoxy-(9-phenanthrenyl)silane.

6.3.1.2 Elemental Analysis

	C (calc.)	C (found)	H (calc.)	H (found)	ΔC	ΔΗ
	[%]	[%]	[%]	[%]	[%]	[%]
1-NaphSi(OMe)₃	62.87	62.70	6.49	5.53	0.17	0.96
2-NaphSi(OMe)₃	62.87	63.28	6.49	5.88	0.41	0.61
9-PhenSi(OMe)₃	68.42	67.73	6.08	5.45	0.69	0.63

6.3.1.3 Fourier Transform Infrared (FTIR) Spectroscopy

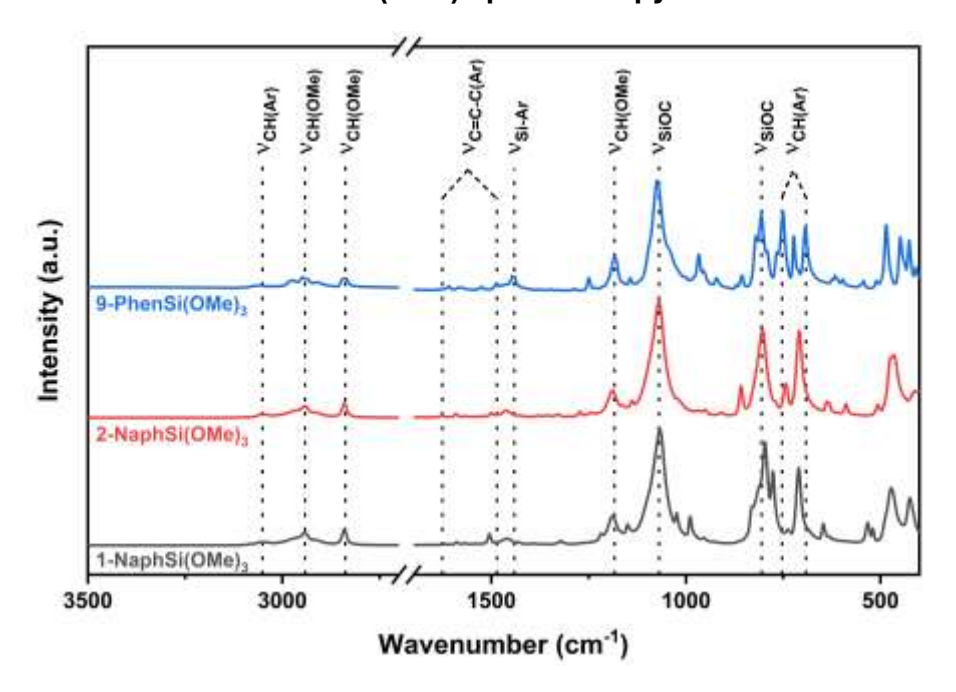


Figure S 119: FTIR spectra of 1-NaphSi(OMe)₃ (black), 2-NaphSi(OMe)₃ (red) and 9-PhenSi(OMe)₃ (blue).

FTIR: 3052 cm^{-1} (v(CH)_{Ar}), 2942 cm^{-1} (v(CH_{OMe})), 2836 cm^{-1} (v(CH_{OMe})), $1626 - 1486 \text{ cm}^{-1}$ (v(CC)_{Ar}), 1442 cm^{-1} (v(Si-Ar)), 1183 cm^{-1} (v(CH_{OMe})), 1097 cm^{-1} (v(SiOC)), 806 cm^{-1} (v(SiOC), $750 - 692 \text{ cm}^{-1}$ (v(CH)_{Ar}).

6.3.1.4 Ultraviolet-visible (UV-vis) Spectroscopy

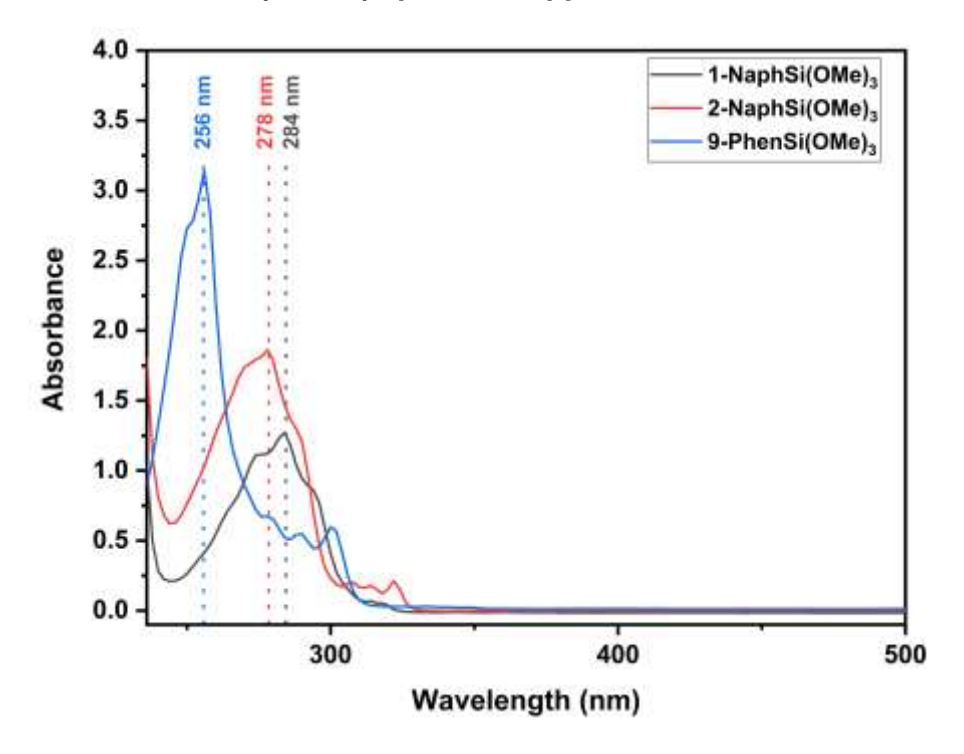


Figure S 120: UV-vis spectra of 1-NaphSi(OMe)₃ (black), 2-NaphSi(OMe)₃ (red) and 9-PhenSi(OMe)₃ (blue).

6.3.1.5 Fluorescence Spectroscopy

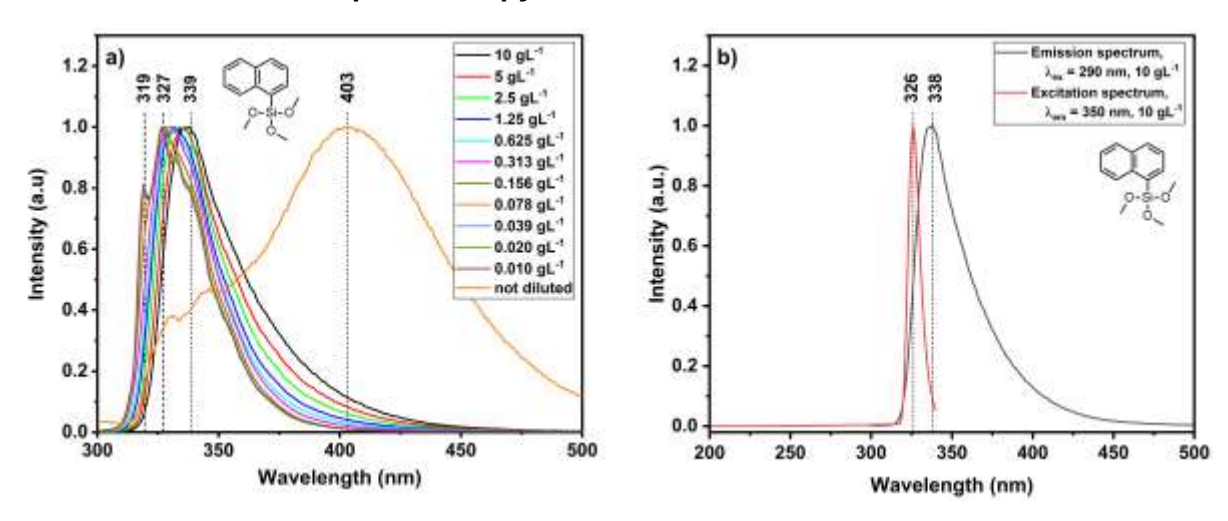


Figure S 121: Fluorescence spectra of a dilution series of 1-NaphSi(OMe)₃ in DCM. a) Emission spectra at λ_{Ex} = 290 nm, b) emission and excitation spectra of a solution in DCM.

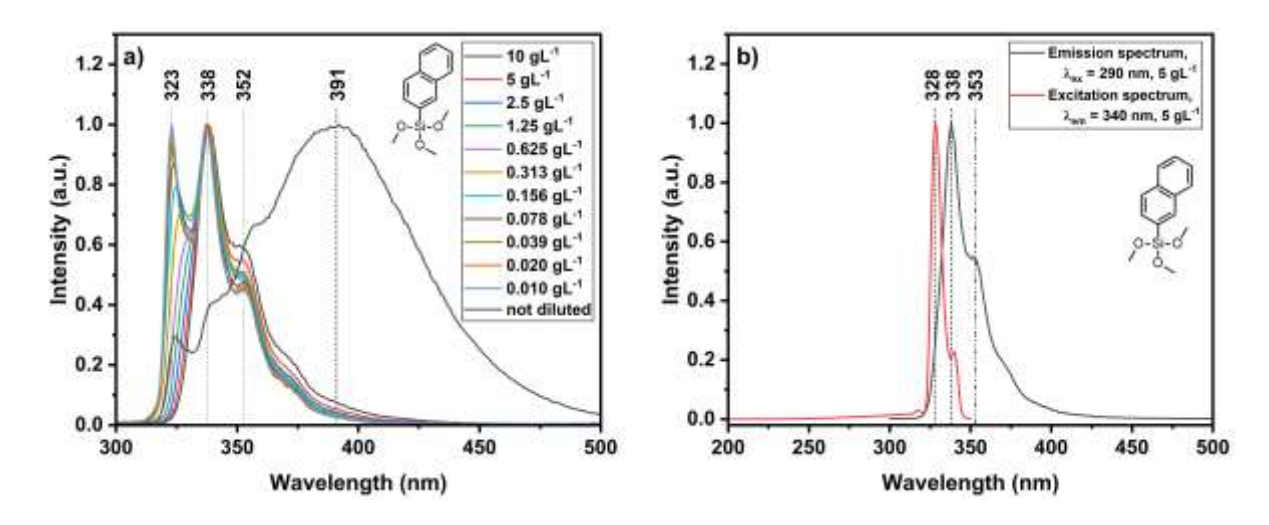


Figure S 122: Fluorescence spectra of a dilution series of 2-NaphSi(OMe)₃ in DCM. a) Emission spectra at λ_{Ex} = 290 nm, b) emission and excitation spectra of a solution in DCM.

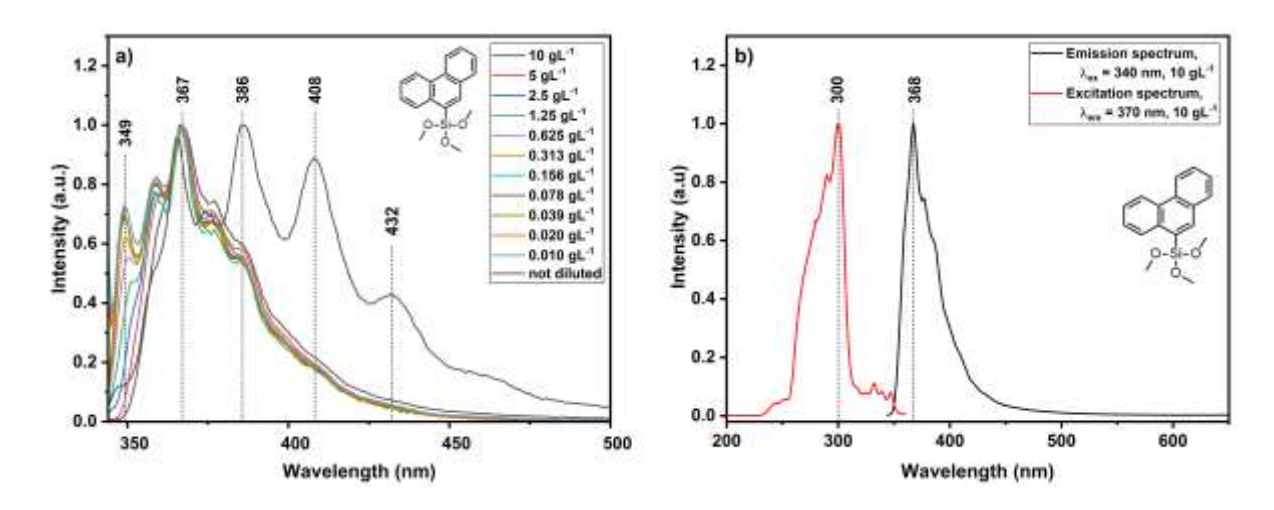


Figure S 123: Fluorescence spectra of a dilution series of 9-PhenSi(OMe)₃ in DCM. a) Emission spectra at λ_{Ex} = 340 nm, b) emission and excitation spectra of a solution in DCM.

6.3.1.6 Differential Scanning Calorimetry (DSC)

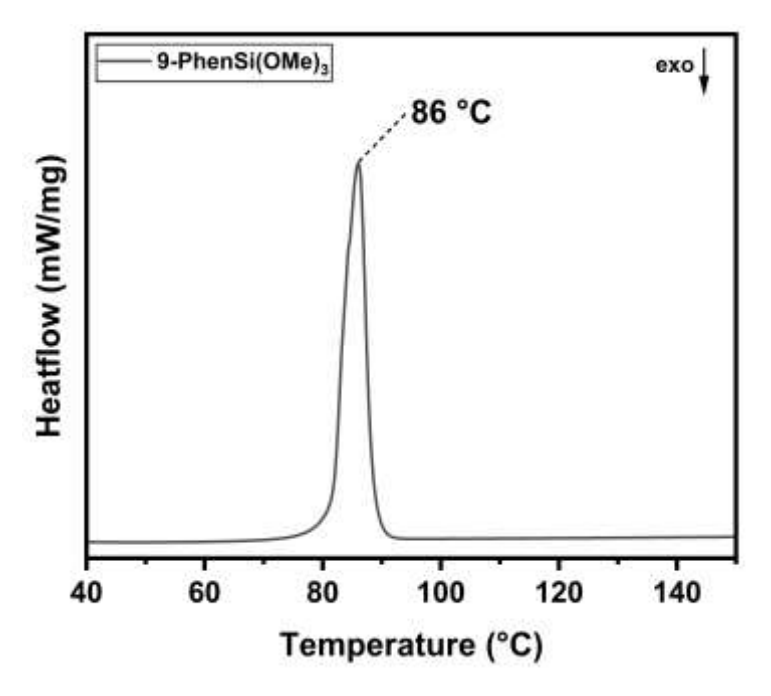


Figure S 124: DSC measurement of 9-PhenSi(OMe)₃.

6.3.1.7 Refractive Index (RI)

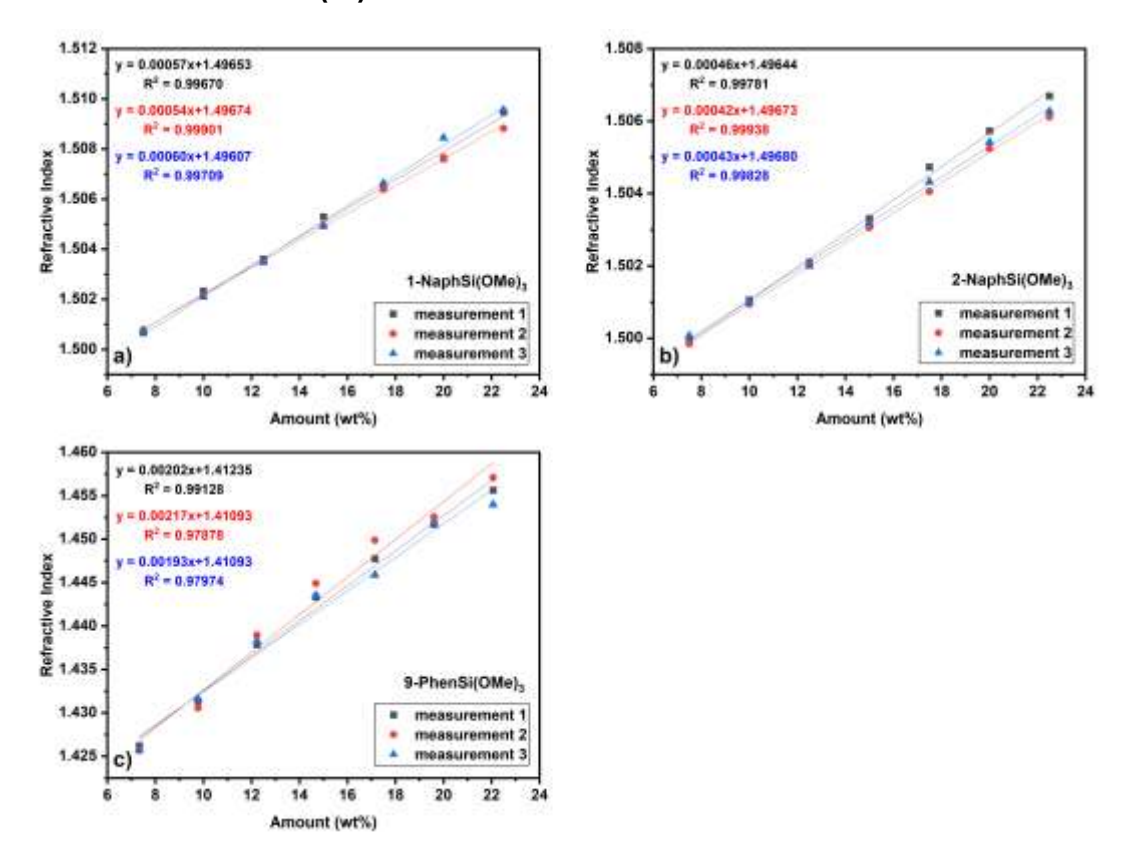


Figure S 125: Calibration curves for the refractive indices of all three trialkoxysilanes, measured three times each. a) 1-NaphSi(OMe)₃, b) 2-NaphSi(OMe)₃, c) 9-PhenSi(OMe)₃.

$$RI_{1Naph,a} = 0.00057 \cdot 100 + 1.49653 = 1.554$$

 $RI_{1Naph,b} = 0.00054 \cdot 100 + 1.49674 = 1.551$
 $RI_{1Naph,c} = 0.00060 \cdot 100 + 1.49607 = 1.556$
 $RI_{1Naph,av} = 1.554$

$$RI_{2Naph,a} = 0.00046 \cdot 100 + 1.49644 = 1.542$$

 $RI_{2Naph,b} = 0.00042 \cdot 100 + 1.49673 = 1.540$
 $RI_{2Naph,c} = 0.00043 \cdot 100 + 1.49680 = 1.541$
 $RI_{2Naph,av} = 1.541$

$$RI_{9Phen,a} = 0.00202 \cdot 100 + 1.41235 = 1.614$$

 $RI_{9Phen,b} = 0.00217 \cdot 100 + 1.41093 = 1.628$
 $RI_{9Phen,c} = 0.00193 \cdot 100 + 1.41093 = 1.604$
 $RI_{9Phen,av} = 1.615$

Table S 10: Determined refractive indices of all three trialkoxysilanes via calibration curve method, three times each and their average.

	1-NaphSi(OMe)₃	2-NaphSi(OMe)₃	9-PhenSi(OMe) ₃
RI₁	1.554	1.542	1.614
RI_2	1.551	1.540	1.628
RI ₃	1.556	1.541	1.604
Average	1.554	1.541	1.615

6.3.2 Silsesquioxanes

6.3.2.1 Nuclear Magnetic Resonance (NMR) Spectroscopy

1-Naph_POSS_KOH

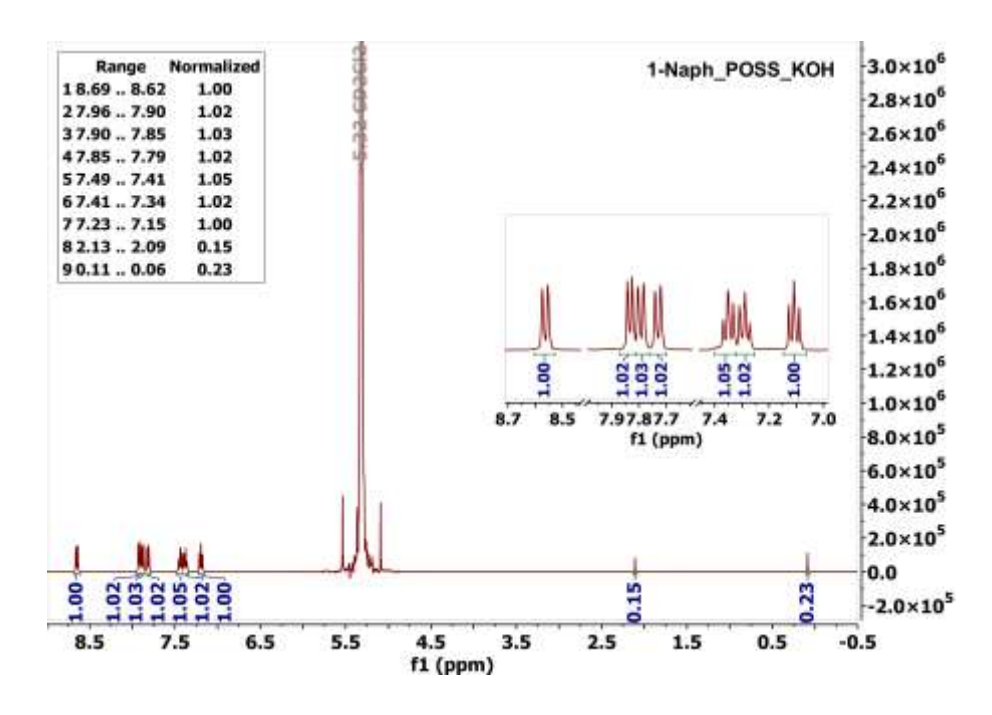


Figure S 126: ¹H NMR spectrum (CD₂Cl₂, 400.13 MHz) of 1-Naph_POSS synthesized with KOH.

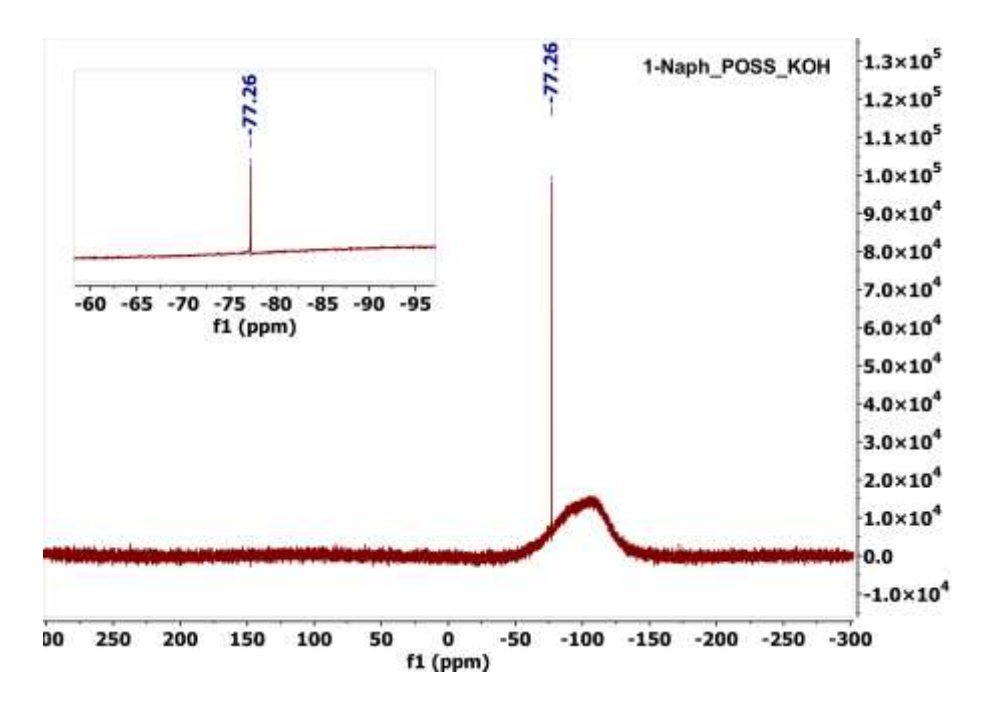


Figure S 127: ²⁹Si NMR spectrum (CD₂Cl₂, 79.49 MHz) of 1-Naph_POSS synthesized with KOH.

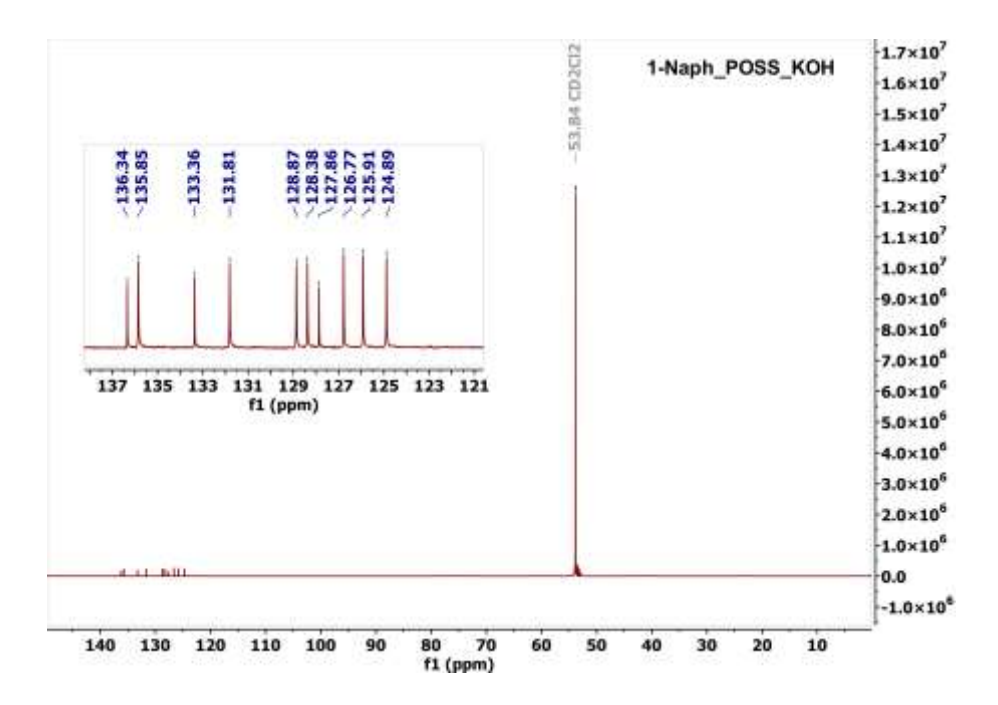


Figure S 128: ¹³C NMR spectrum (CD₂Cl₂, 100.62 MHz) of 1-Naph_POSS synthesized with KOH.

1-Naph_POSS_TBAF

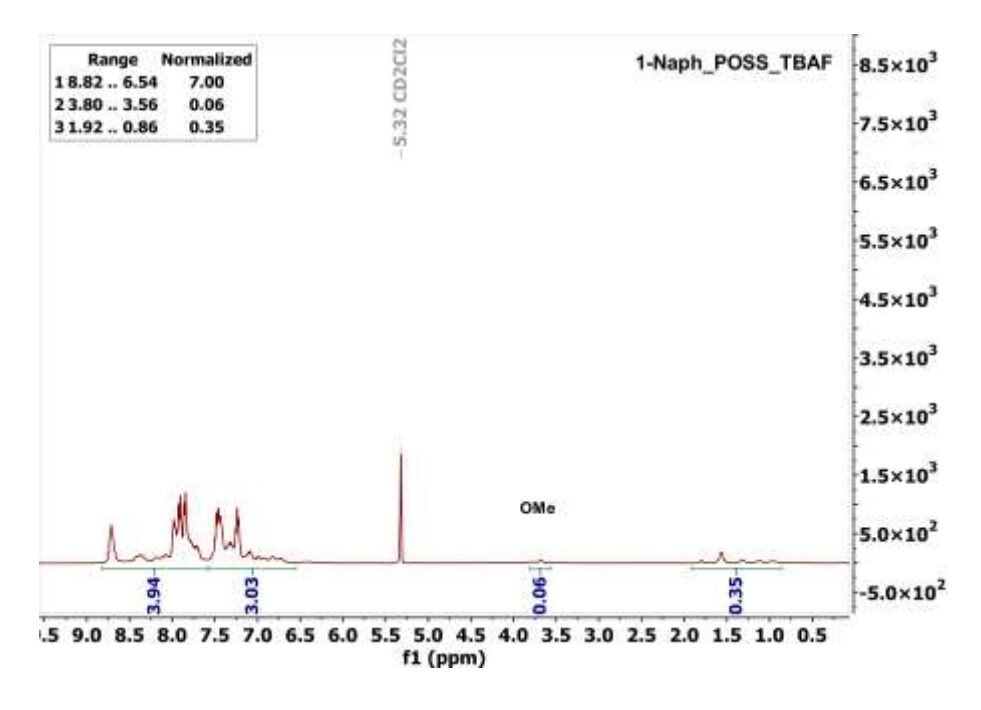


Figure S 129: ¹H NMR spectrum (CD₂Cl₂, 400.13 MHz) of 1-Naph_POSS synthesized with TBAF.

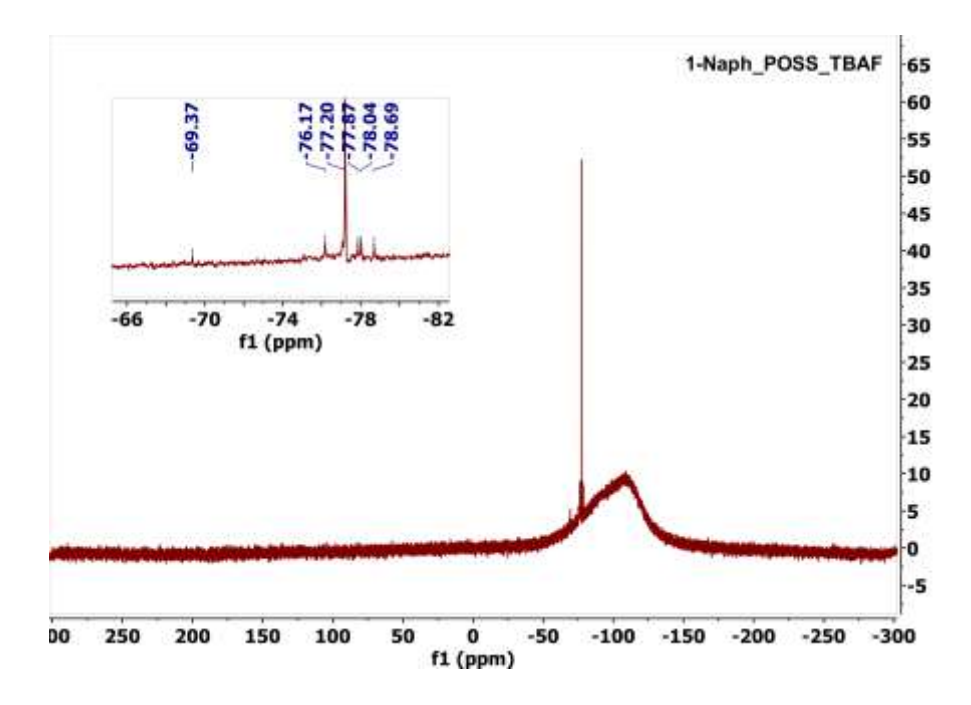


Figure S 130: ²⁹Si NMR spectrum (CD₂Cl₂, 79.49 MHz) of 1-Naph_POSS synthesized with TBAF.

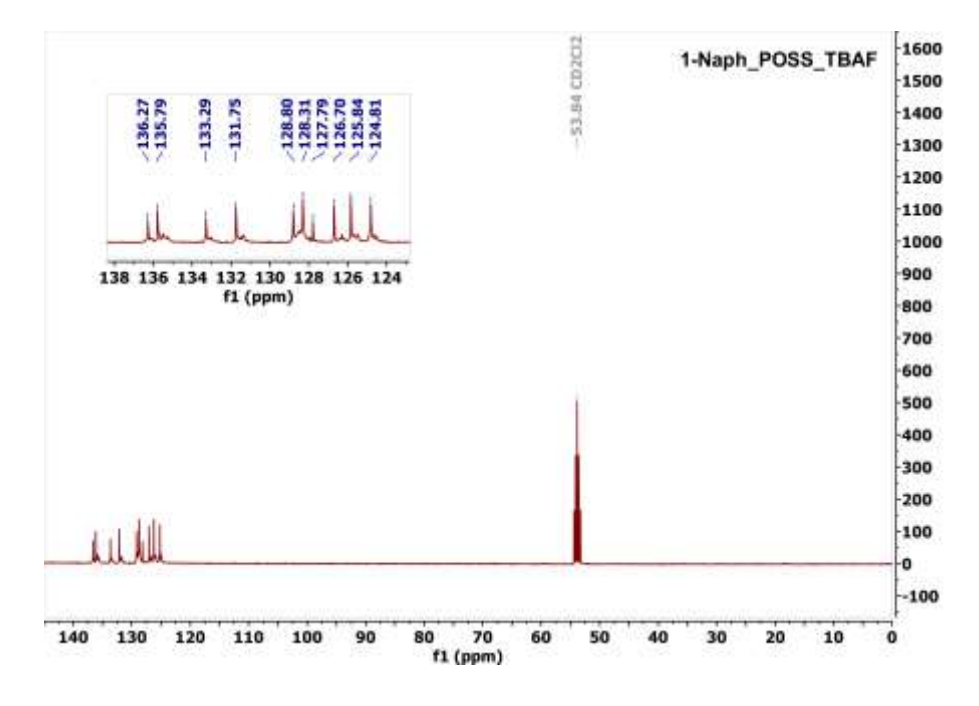


Figure S 131: ¹³C NMR spectrum (CD₂Cl₂, 100.62 MHz) of 1-Naph_POSS synthesized with TBAF.

2-Naph_POSS_KOH

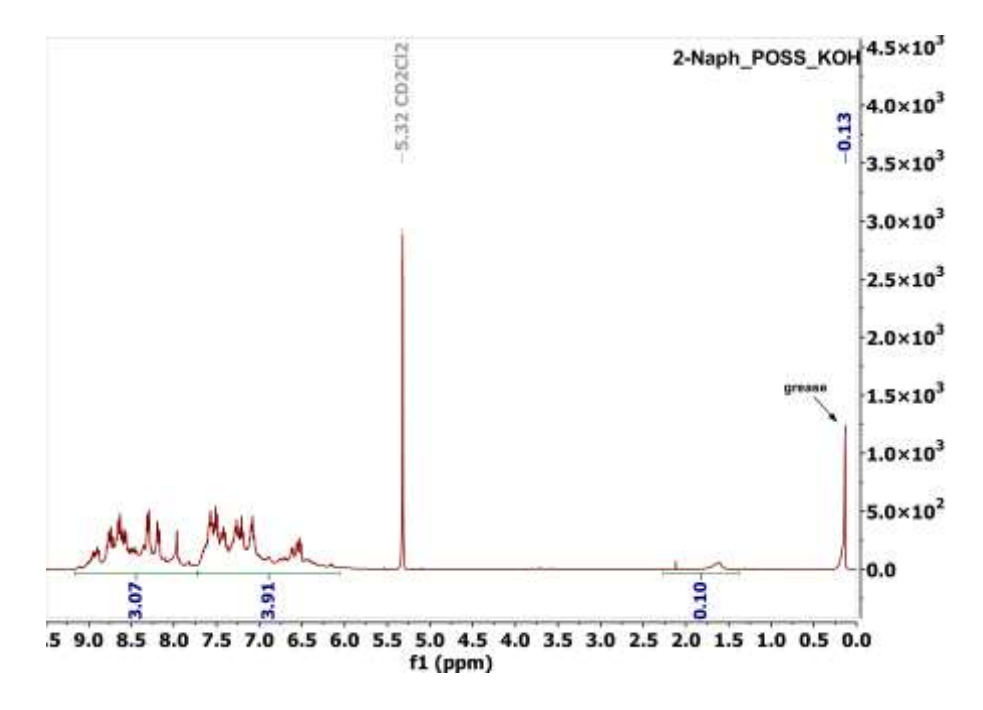


Figure S 132: ¹H NMR spectrum (CD₂Cl₂, 400.13 MHz) of 2-Naph_POSS synthesized with KOH.

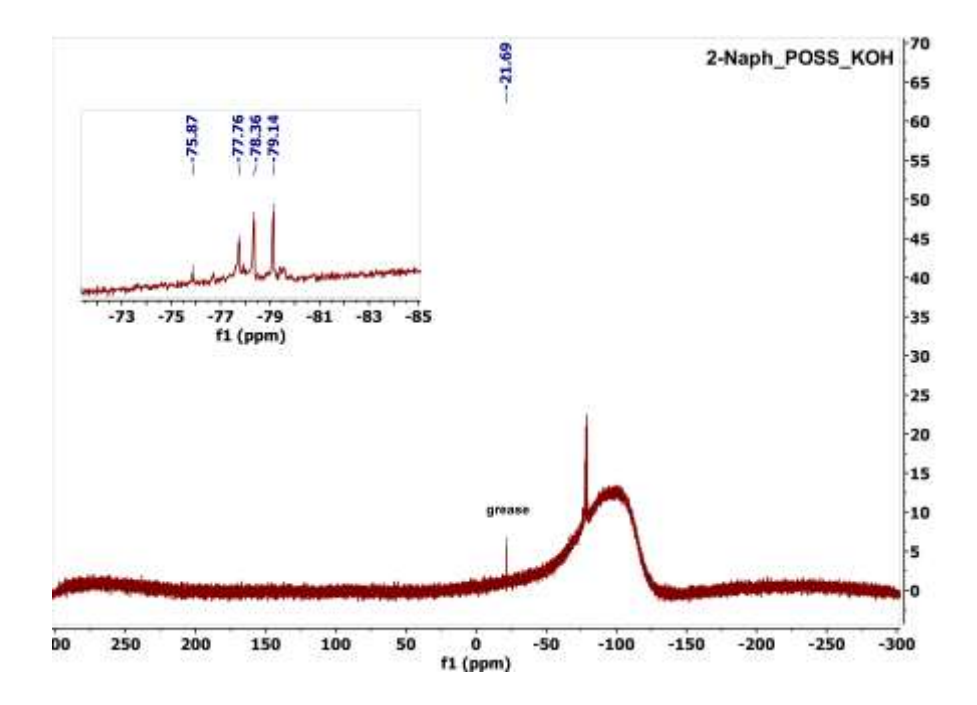


Figure S 133: ²⁹Si NMR spectrum (CD₂Cl₂, 79.49 MHz) of 2-Naph_POSS synthesized with KOH.

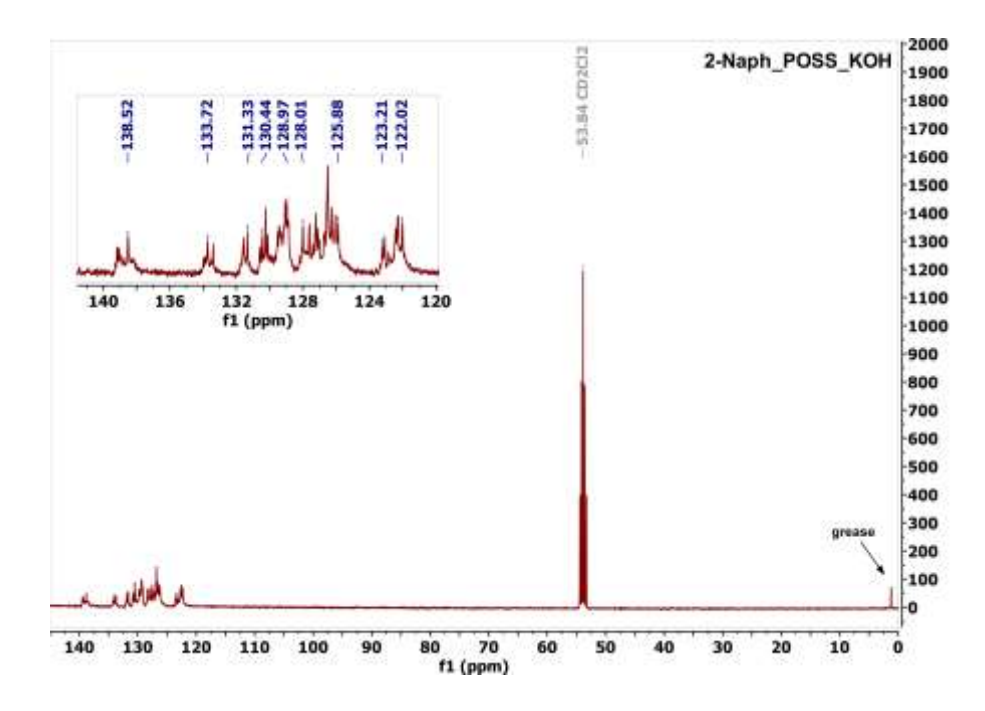


Figure S 134: ¹³C NMR spectrum (CD₂Cl₂, 100.62 MHz) of 2-Naph_POSS synthesized with KOH.

2-Naph_POSS_TBAF

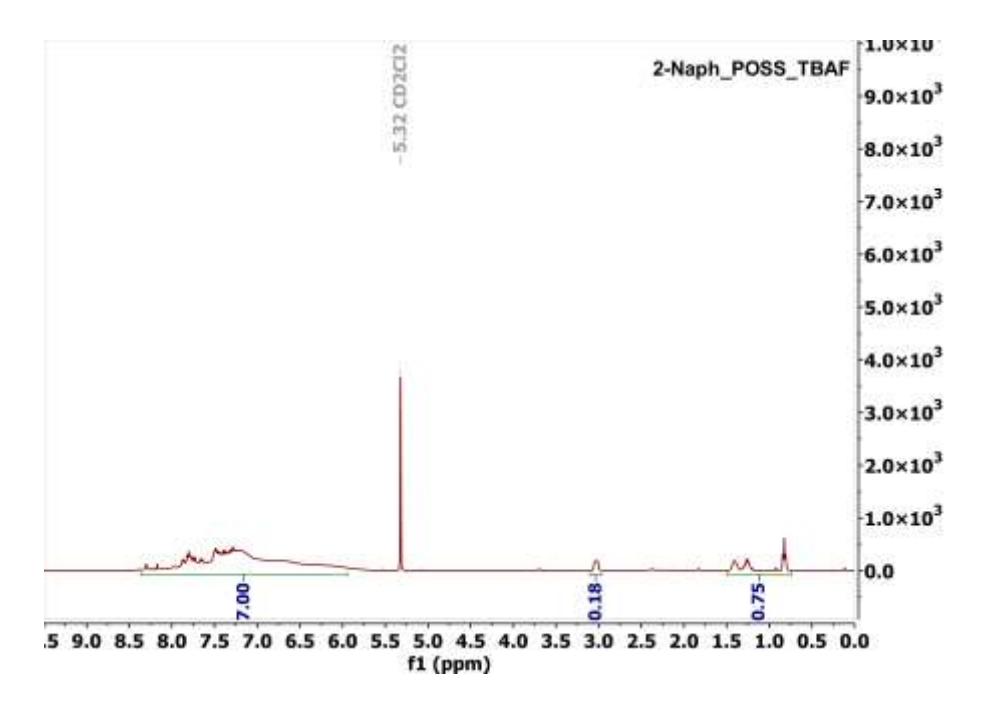


Figure S 135: 1 H NMR spectrum (CD $_2$ Cl $_2$, 400.13 MHz) of 2-Naph_POSS synthesized with TBAF.

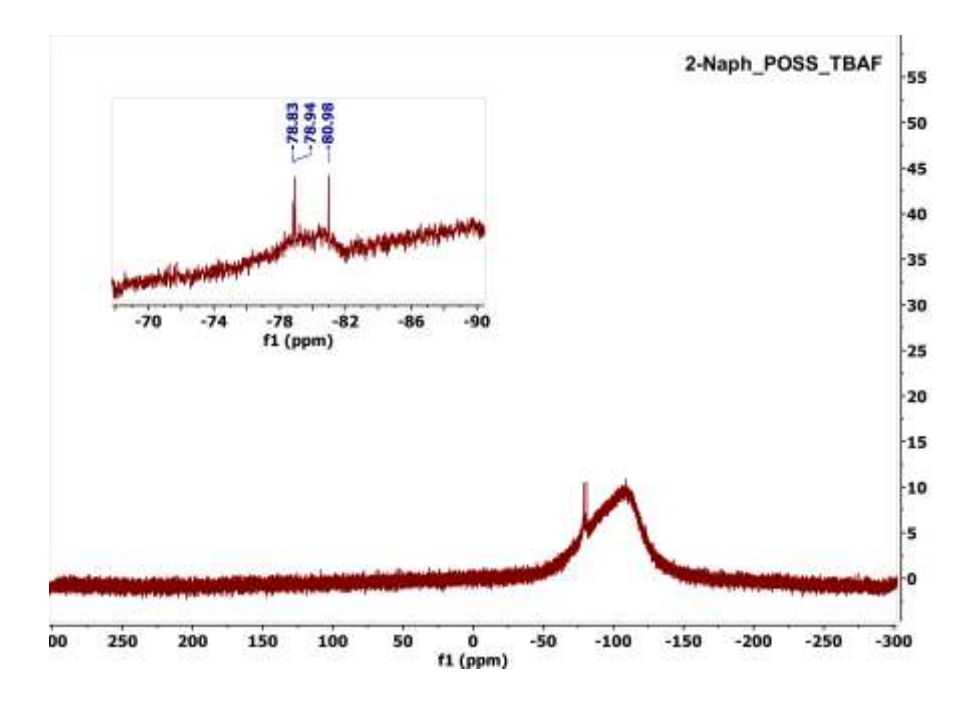


Figure S 136: ²⁹Si NMR spectrum (CD₂Cl₂, 79.49 MHz) of 2-Naph_POSS synthesized with TBAF.

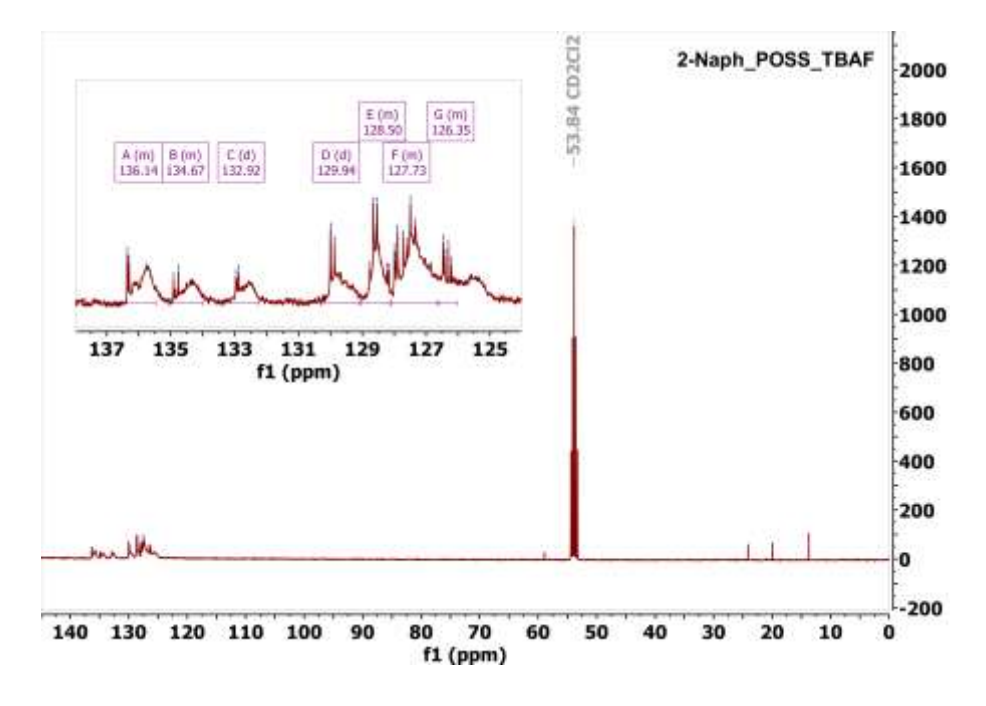


Figure S 137: ¹³C NMR spectrum (CD₂Cl₂, 100.62 MHz) of 2-Naph_POSS synthesized with TBAF.

9-Phen_POSS_KOH

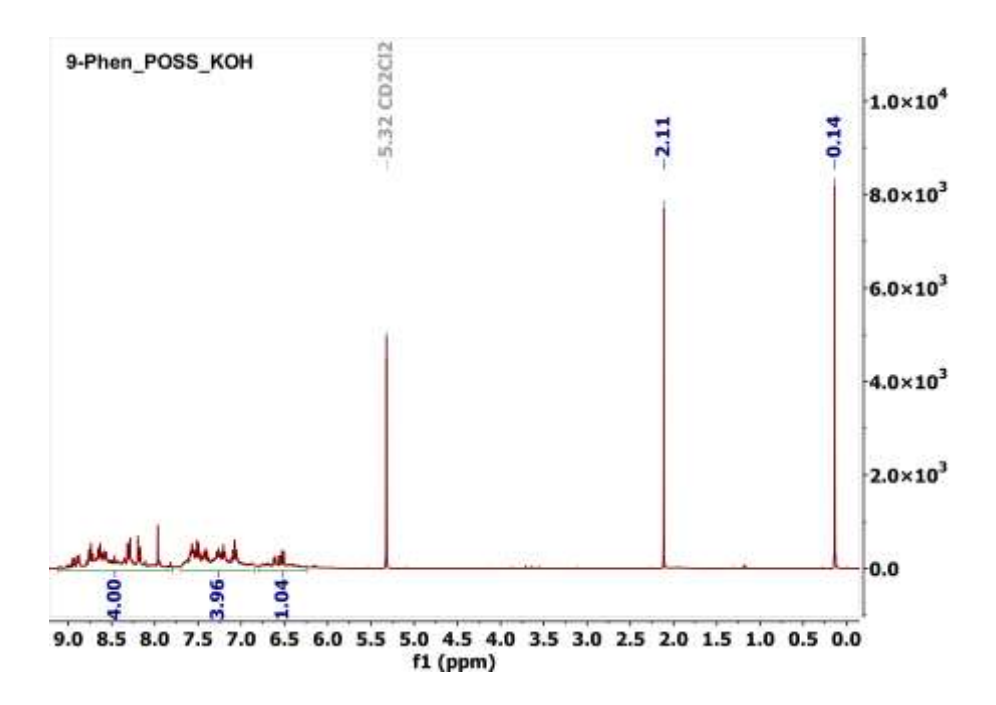


Figure S 138: ¹H NMR spectrum (CD₂Cl₂, 400.13 MHz) of 9-Phen_POSS synthesized with KOH.

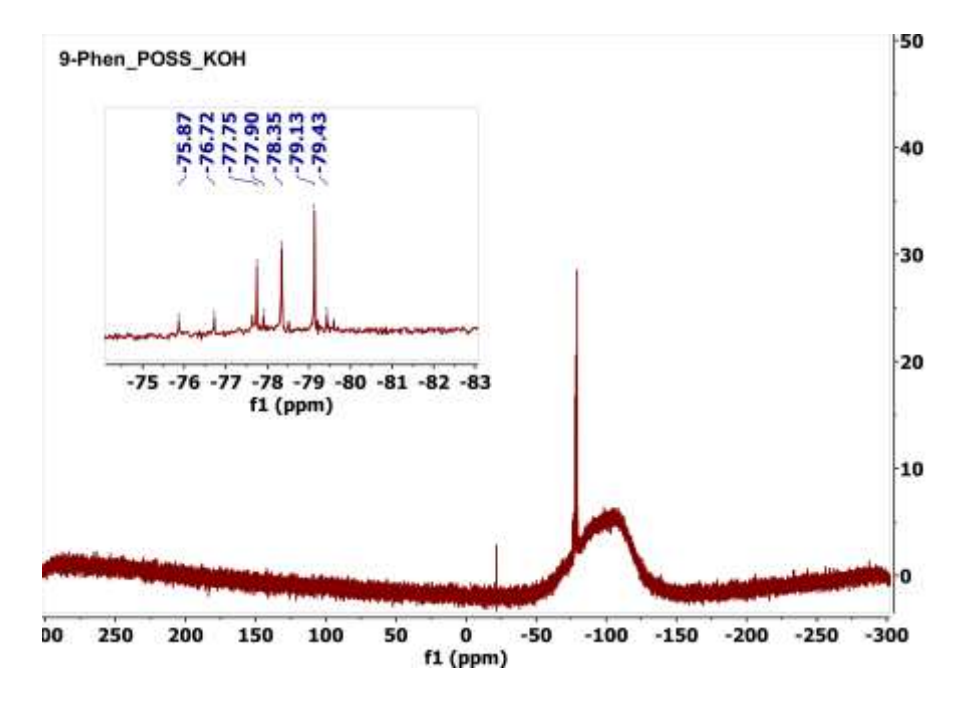


Figure S 139: ²⁹Si NMR spectrum (CD₂Cl₂, 79.49 MHz) of 9-Phen_POSS synthesized with KOH.

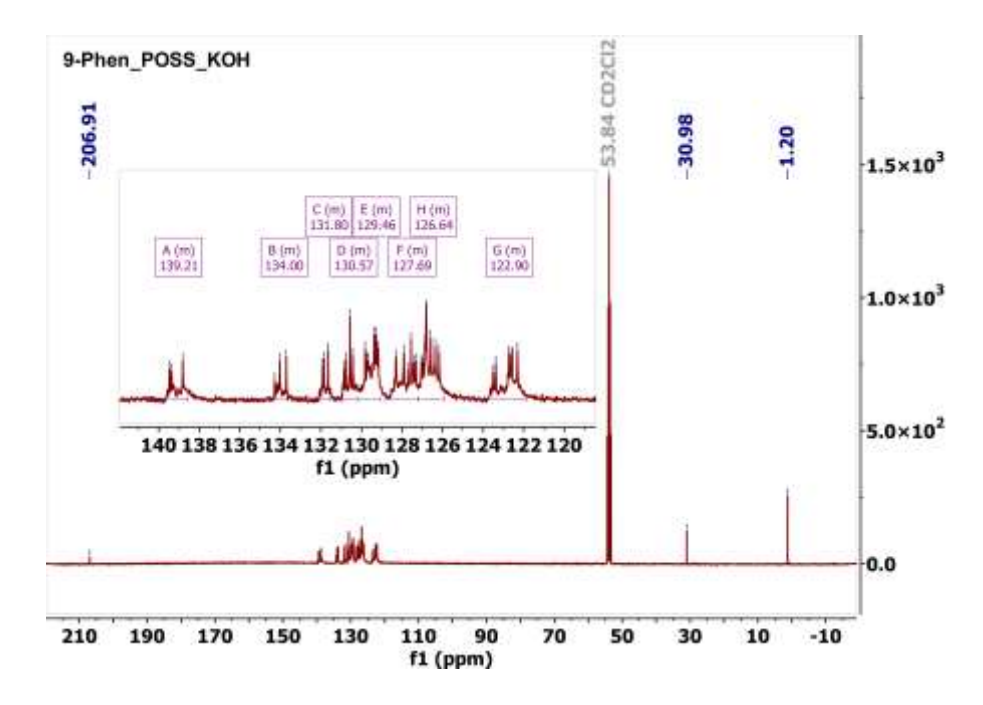


Figure S 140: 13 C NMR spectrum (CD₂Cl₂, 100.62 MHz) of 9-Phen_POSS synthesized with KOH.

9-Phen_POSS_TBAF

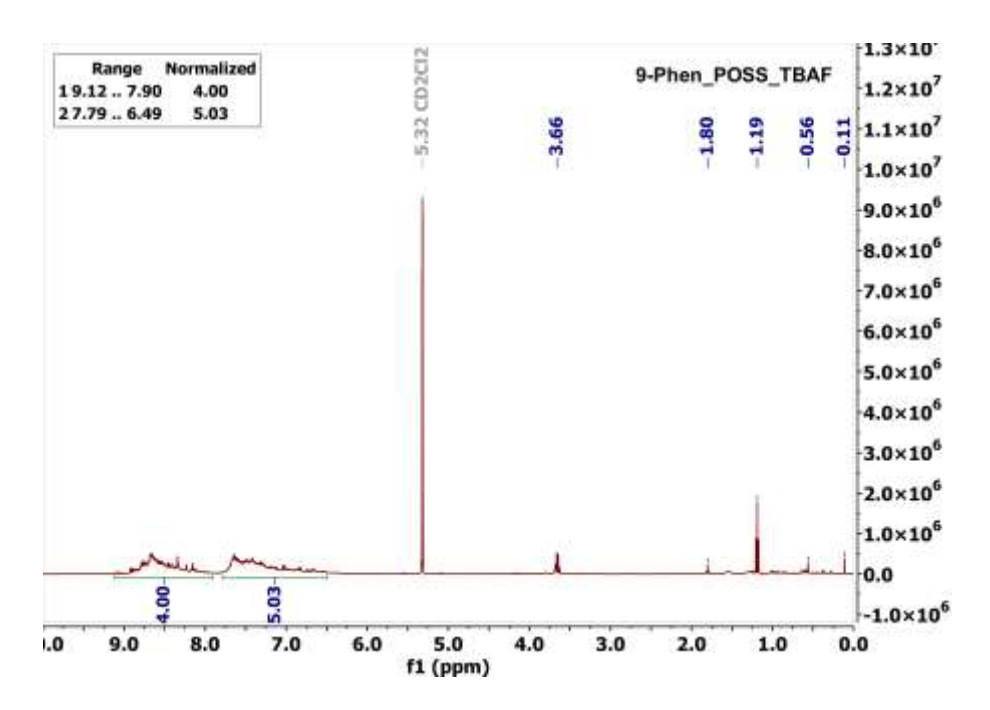


Figure S 141: ¹H NMR spectrum (CD₂Cl₂, 400.13 MHz) of 9-Phen_POSS synthesized with TBAF.

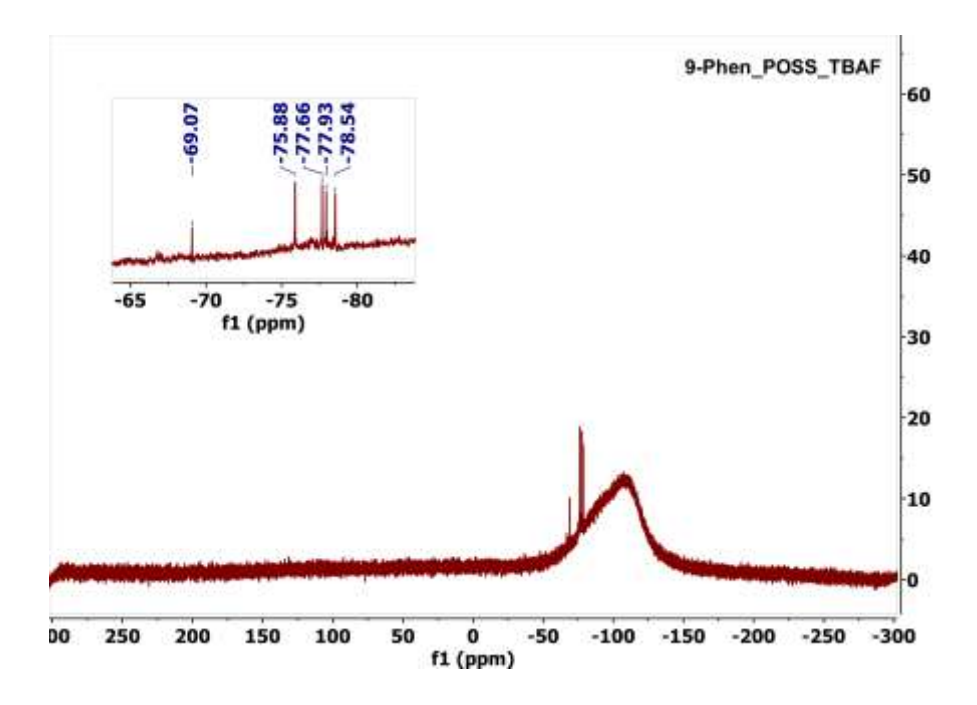


Figure S 142: ²⁹Si NMR spectrum (CD₂Cl₂, 79.49 MHz) of 9-Phen_POSS synthesized with TBAF.

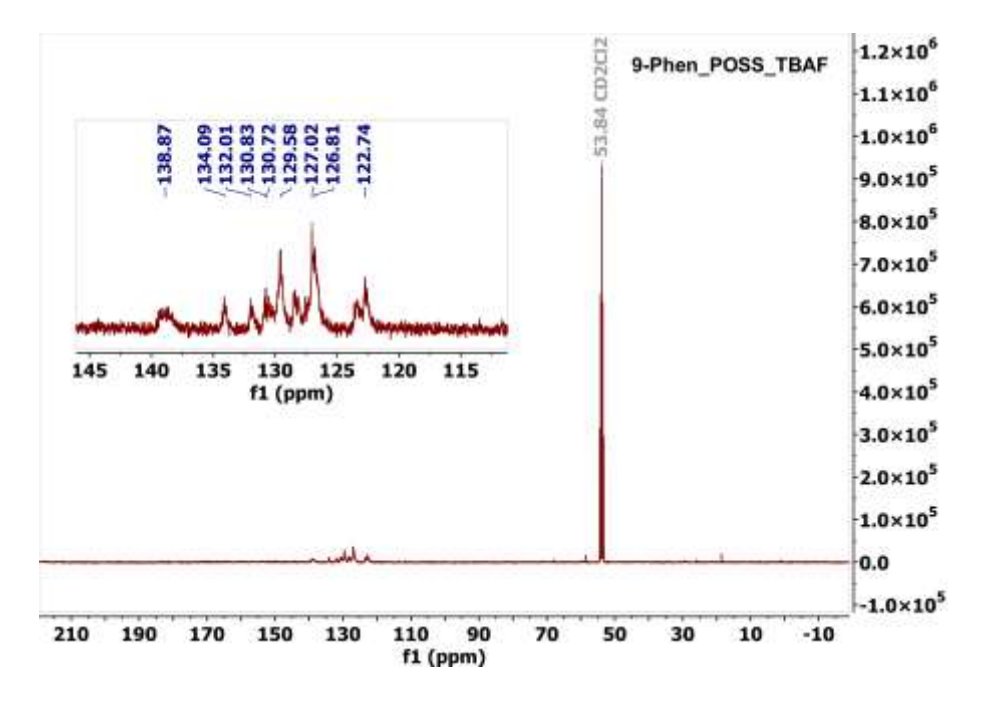


Figure S 143: ¹³C NMR spectrum (CD₂Cl₂, 100.62 MHz) of 9-Phen_POSS synthesized with TBAF.

6.3.2.2 Single Crystal X-ray Crystallography

Table S 11: Crystal data and structure refinement for 1-Naph_POSS_KOH.

Empirical formula $C_{82}H_{60}C_{l4}O_{12}Si_8$ Formula weight $1603.82~g~mol^{-1}$

Temperature 133(2) K

Wavelength Mo $K_{\alpha,1}$, 71.073 pm

Crystal system triclinic Space group $P\overline{1}$

Unit cell dimensions a = 1539.31(8) pm $\alpha = 113.503(2)^{\circ}$

b = 1564.66(8) pm $\beta = 93.273(2)^{\circ}$

c = 1928.57(9) pm $\gamma = 111.374(2)^{\circ}$

Volume 3.8536(3) nm³

Z 2

Density (calculated) $1.38 \, \mathrm{g \, cm^{-3}}$ Absorption coefficient $0.3 \, \mathrm{mm^{-1}}$ F(000) 1656

Crystal size $0.220 \times 0.155 \times 0.060 \text{ mm}^3$

Theta range for data collection 2.22 to 27.91°.

Index ranges $h = \pm 20, k = \pm 20, l = \pm 25$

Reflections collected 168440

Independent reflections 18407 [$R_{int} = 0.0541$]

Completeness to theta = 25.242° 99.6 %

Absorption correction Semi-empirical from equivalents

Max. and min. transmission 0.7440 and 0.7233

Refinement method Full-matrix least-squares on F^2

Data / restraints / parameters 18407 / 1161 / 1065

Goodness-of-fit on F^2 1.024

Extinction coefficient n/a

Largest diff. peak and hole $0.77 \text{ and } -0.79 \text{ e.Å}^{-3}$

Table S 12: Atomic coordinates (x 10⁴) and equivalent isotropic displacement parameters (\mathring{A}^2x 10³) for 1-Naph_POSS_KOH. U_{eq} is defined as one third of the trace of the orthogonalized U_{ij} tensor.

	X	У	Z	U_{eq}
Si(1)	8065(1)	4027(1)	-371(1)	22(1)
Si(2)	9284(1)	5687(1)	-871(1)	22(1)
Si(3)	10567(1)	7049(1)	808(1)	22(1)
Si(4)	9345(1)	5389(1)	1308(1)	21(1)
Si(5)	3826(1)	5527(1)	4329(1)	20(1)
Si(6)	5088(1)	6816(1)	6043(1)	20(1)
Si(7)	6814(1)	6437(1)	5434(1)	19(1)
Si(8)	5546(1)	5141(1)	3718(1)	20(1)
O(1)	8444(1)	4841(1)	-720(1)	31(1)
O(2)	9917(1)	6646(1)	-40(1)	31(1)
O(3)	9933(1)	6419(1)	1227(1)	31(1)
O(4)	8434(1)	4624(1)	567(1)	31(1)
O(5)	8493(1)	3180(1)	-710(1)	30(1)
O(6)	9968(1)	5184(1)	-1302(1)	31(1)
O(7)	4317(1)	6339(1)	5237(1)	28(1)
O(8)	6132(1)	6953(1)	5861(1)	26(1)
O(9)	6395(1)	5890(1)	4503(1)	27(1)
O(10)	4652(1)	5443(1)	3865(1)	30(1)
O(11)	3194(1)	4425(1)	4300(1)	26(1)
O(12)	4779(1)	6040(1)	6433(1)	26(1)
C(1)	6738(1)	3424(1)	-654(1)	27(1)
C(2)	6286(1)	3744(2)	-1074(1)	37(1)
C(3)	5276(2)	3343(2)	-1296(1)	51(1)
C(4)	4721(1)	2633(2)	-1083(1)	48(1)
C(5)	5135(1)	2280(1)	-646(1)	35(1)
C(6)	6154(1)	2666(1)	-436(1)	28(1)
C(7)	6550(1)	2281(1)	-13(1)	34(1)
C(8)	5972(2)	1576(2)	204(1)	44(1)
C(9)	4966(2)	1212(2)	4(1)	48(1)
C(10)	4561(2)	1550(2)	-411(1)	44(1)
C(11)	8797(1)	6135(1)	-1481(1)	27(1)
C(12)	9212(1)	6171(1)	-2090(1)	33(1)
C(13)	8914(2)	6526(2)	-2582(1)	45(1)
C(14)	8201(2)	6836(2)	-2467(1)	48(1)
C(15)	7746(2)	6823(2)	-1857(1)	42(1)
C(16)	8044(1)	6469(1)	-1349(1)	32(1)
C(17)	7575(2)	6454(2)	-743(1)	44(1)
C(18)	6848(2)	6767(2)	-648(2)	58(1)

C(19)	6562(2)	7116(2)	-1150(2)	64(1)
C(20)	6995(2)	7144(2)	-1731(2)	59(1)
C(21)	10955(1)	8439(1)	1396(1)	28(1)
C(22)	11916(2)	9048(1)	1735(1)	42(1)
C(23)	12264(2)	10118(2)	2205(2)	59(1)
C(24)	11649(2)	10565(2)	2329(1)	60(1)
C(25)	10657(2)	9992(2)	1991(1)	46(1)
C(26)	10296(1)	8909(1)	1521(1)	34(1)
C(27)	9298(2)	8350(2)	1187(1)	43(1)
C(28)	8694(2)	8829(2)	1300(2)	57(1)
C(29)	9059(2)	9898(2)	1765(2)	66(1)
C(30)	10011(2)	10460(2)	2098(2)	62(1)
C(31)	8970(1)	5763(1)	2232(1)	22(1)
C(32)	9166(1)	6785(1)	2671(1)	26(1)
C(33)	8917(1)	7132(1)	3395(1)	30(1)
C(34)	8484(1)	6458(1)	3677(1)	31(1)
C(35)	8263(1)	5402(1)	3255(1)	27(1)
C(36)	8502(1)	5043(1)	2522(1)	24(1)
C(37)	8260(1)	3978(1)	2107(1)	34(1)
C(38)	7813(2)	3311(2)	2402(1)	44(1)
C(39)	7586(2)	3678(2)	3131(1)	44(1)
C(40)	7807(1)	4693(2)	3543(1)	36(1)
C(41)	3101(1)	5965(1)	3877(1)	24(1)
C(42)	3369(1)	6210(1)	3286(1)	30(1)
C(43)	2837(2)	6541(2)	2915(1)	38(1)
C(44)	2021(2)	6597(2)	3120(1)	38(1)
C(45)	1700(1)	6341(1)	3712(1)	31(1)
C(46)	2253(1)	6041(1)	4106(1)	25(1)
C(47)	1932(1)	5819(1)	4713(1)	32(1)
C(48)	1095(1)	5852(2)	4899(1)	42(1)
C(49)	534(1)	6107(2)	4485(1)	46(1)
C(50)	837(1)	6360(2)	3914(1)	42(1)
C(51)	5144(1)	8073(1)	6726(1)	28(1)
C(52)	5042(2)	8232(2)	7467(1)	44(1)
C(53)	5125(2)	9191(2)	8033(1)	64(1)
C(54)	5323(2)	9985(2)	7860(2)	63(1)
C(55)	5432(2)	9878(2)	7111(1)	46(1)
C(56)	5326(1)	8904(1)	6530(1)	32(1)
C(57)	5404(1)	8810(2)	5778(1)	36(1)
C(58)	5595(2)	9629(2)	5617(2)	51(1)
C(59)	5721(2)	10589(2)	6201(2)	64(1)

C(61) 8076(1) 7380(1) 5682(1) 24(1) C(62A) 8742(8) 7019(10) 5788(5) 26(2) C(63A) 9718(10) 7612(9) 5870(8) 34(2) C(64A) 10023(7) 8527(7) 5843(5) 41(2) C(65A) 9366(7) 8924(6) 5741(5) 42(2) C(66A) 8381(8) 8357(11) 5704(17) 35(2) C(67A) 7727(10) 8748(10) 5591(12) 44(2) C(68A) 8016(7) 9681(8) 5570(6) 55(2) C(69A) 8987(5) 10241(6) 5628(6) 63(2) C(70A) 9639(5) 9878(6) 5718(6) 56(2) C(62B) 8820(9) 7105(10) 5794(5) 26(2) C(62B) 9804(10) 7750(9) 5980(8) 34(2) C(66B) 9351(8) 8710(7) 6051(6) 41(2) C(66B) 3351(8) 8390(11) 5724(17) 34(2) C(67B) 7704(9)	C(60)	5640(2)	10706(2)	6923(2)	62(1)
C(62A) 8742(8) 7019(10) 5788(5) 26(2) C(63A) 9718(10) 7612(9) 5870(8) 34(2) C(64A) 10023(7) 8527(7) 5843(5) 41(2) C(65A) 9366(7) 8924(6) 5741(5) 42(2) C(66A) 8381(8) 8357(11) 5704(17) 35(2) C(67A) 7727(10) 8748(10) 5591(12) 44(2) C(68A) 8016(7) 9681(8) 5570(6) 55(2) C(69A) 8987(5) 10241(6) 5628(6) 63(2) C(70A) 9639(5) 9878(6) 5718(6) 56(2) C(69A) 8987(5) 10241(6) 5628(6) 63(2) C(70A) 9639(5) 9878(6) 5718(6) 56(2) C(62B) 8820(9) 7105(10) 5794(5) 26(2) C(62B) 8820(9) 7105(10) 5794(5) 26(2) C(68B) 9360(7) 9063(6) 5943(6) 41(2) C(66B) 8351(8)					
C(63A) 9718(10) 7612(9) 5870(8) 34(2) C(64A) 10023(7) 8527(7) 5843(5) 41(2) C(65A) 9366(7) 8924(6) 5741(5) 42(2) C(66A) 8381(8) 8357(11) 5704(17) 35(2) C(67A) 7727(10) 8748(10) 5591(12) 44(2) C(68A) 8016(7) 9681(8) 5570(6) 55(2) C(69A) 8987(5) 10241(6) 5628(6) 63(2) C(70A) 9639(5) 9878(6) 5718(6) 56(2) C(62B) 820(9) 7105(10) 5794(5) 26(2) C(63B) 9804(10) 7750(9) 5980(8) 34(2) C(64B) 10058(8) 8710(7) 6051(6) 41(2) C(64B) 9360(7) 963(6) 5943(6) 41(2) C(66B) 3351(8) 839(11) 5724(17) 34(2) C(66B) 3028(7) 9839(7) 5825(6) 51(2) C(67B) 7004(9)					
C(64A) 10023(7) 8527(7) 5843(5) 41(2) C(65A) 9366(7) 8924(6) 5741(5) 42(2) C(66A) 8381(8) 8357(11) 5704(17) 35(2) C(67A) 7727(10) 8748(10) 5591(12) 44(2) C(68A) 8016(7) 9681(8) 5570(6) 55(2) C(69A) 8887(5) 10241(6) 5628(6) 63(2) C(70A) 9639(5) 9878(6) 5718(6) 56(2) C(62B) 8820(9) 7105(10) 5794(5) 26(2) C(63B) 8804(10) 7750(9) 5980(8) 34(2) C(64B) 10058(8) 8710(7) 6051(6) 41(2) C(65B) 9360(7) 9963(6) 5943(6) 41(2) C(66B) 8351(8) 8390(11) 5724(17) 34(2) C(66B) 3851(8) 8390(11) 5724(17) 34(2) C(67B) 7704(9) 8832(10) 5685(11) 38(2) C(68B) 9028(7) </td <td></td> <td></td> <td></td> <td></td> <td></td>					
C(65A) 9366(7) 8924(6) 5741(5) 42(2) C(66A) 8381(8) 8357(11) 5704(17) 35(2) C(67A) 7727(10) 8748(10) 5591(12) 44(2) C(68A) 8016(7) 9681(8) 5570(6) 55(2) C(69A) 8987(5) 10241(6) 5628(6) 63(2) C(70A) 9639(5) 9878(6) 5718(6) 56(2) C(62B) 8820(9) 7105(10) 5794(5) 26(2) C(63B) 9804(10) 7750(9) 5980(8) 34(2) C(64B) 10058(8) 8710(7) 6051(6) 41(2) C(65B) 9360(7) 9063(6) 5943(6) 41(2) C(66B) 8351(8) 8390(11) 5724(17) 34(2) C(66B) 8351(8) 8390(11) 5724(17) 34(2) C(67B) 7704(9) 8832(10) 5685(11) 38(2) C(68B) 8028(7) 9839(7) 5825(6) 51(2) C(69B) 9004(5) <td></td> <td></td> <td></td> <td></td> <td></td>					
C(66A) 8381(8) 8357(11) 5704(17) 35(2) C(67A) 7727(10) 8748(10) 5591(12) 44(2) C(68A) 8016(7) 9681(8) 5570(6) 55(2) C(69A) 8987(5) 10241(6) 5628(6) 63(2) C(70A) 9639(5) 9878(6) 5718(6) 56(2) C(62B) 8820(9) 7105(10) 5794(5) 26(2) C(63B) 9804(10) 7750(9) 5980(8) 34(2) C(64B) 10058(8) 8710(7) 6051(6) 41(2) C(65B) 9360(7) 9063(6) 5943(6) 41(2) C(66B) 8351(8) 8390(11) 5724(17) 34(2) C(67B) 7704(9) 8832(10) 5685(11) 38(2) C(67B) 7704(9) 8832(10) 5685(11) 38(2) C(68B) 8028(7) 9839(7) 5825(6) 51(2) C(69B) 9004(5) 10460(6) 5999(6) 60(2) C(69B) 9059(1) </td <td></td> <td></td> <td></td> <td></td> <td></td>					
C(67A) 7727(10) 8748(10) 5591(12) 44(2) C(68A) 8016(7) 9681(8) 5570(6) 55(2) C(69A) 8987(5) 10241(6) 5628(6) 63(2) C(70A) 9639(5) 9878(6) 5718(6) 56(2) C(62B) 8820(9) 7105(10) 5794(5) 26(2) C(63B) 9804(10) 7750(9) 5980(8) 34(2) C(64B) 10058(8) 8710(7) 6051(6) 41(2) C(65B) 9360(7) 9063(6) 5943(6) 41(2) C(66B) 8351(8) 8390(11) 5724(17) 34(2) C(66B) 8351(8) 8390(11) 5724(17) 34(2) C(67B) 7704(9) 8832(10) 5685(11) 38(2) C(68B) 8028(7) 9839(7) 5825(6) 51(2) C(69B) 9004(5) 10460(6) 5999(6) 60(2) C(70B) 9659(5) 10090(6) 6064(6) 56(2) C(71) 5937(1) <td></td> <td></td> <td></td> <td></td> <td></td>					
C(68A) 8016(7) 9681(8) 5570(6) 55(2) C(69A) 8987(5) 10241(6) 5628(6) 63(2) C(70A) 9639(5) 9878(6) 5718(6) 56(2) C(62B) 8820(9) 7105(10) 5794(5) 26(2) C(63B) 9804(10) 7750(9) 5980(8) 34(2) C(64B) 10058(8) 8710(7) 6051(6) 41(2) C(65B) 9360(7) 9063(6) 5943(6) 41(2) C(66B) 8351(8) 8390(11) 5724(17) 34(2) C(67B) 7704(9) 8832(10) 5685(11) 38(2) C(67B) 7704(9) 8832(10) 5685(11) 38(2) C(68B) 8028(7) 9839(7) 5825(6) 51(2) C(69B) 9004(5) 10460(6) 5999(6) 60(2) C(70B) 9659(5) 10090(6) 6064(6) 56(2) C(71) 5937(1) 5268(1) 2864(1) 25(1) C(72) 5837(1)					
C(69A) 8987(5) 10241(6) 5628(6) 63(2) C(70A) 9639(5) 9878(6) 5718(6) 56(2) C(62B) 8820(9) 7105(10) 5794(5) 26(2) C(63B) 9804(10) 7750(9) 5980(8) 34(2) C(64B) 10058(8) 8710(7) 6051(6) 41(2) C(65B) 9360(7) 9063(6) 5943(6) 41(2) C(66B) 8351(8) 8390(11) 5724(17) 34(2) C(66B) 8351(8) 8390(11) 5724(17) 34(2) C(66B) 8351(8) 8390(11) 5724(17) 34(2) C(67B) 7704(9) 8832(10) 5685(11) 38(2) C(68B) 8028(7) 9839(7) 5825(6) 51(2) C(69B) 9004(5) 10460(6) 5999(6) 60(2) C(70B) 9659(5) 10090(6) 6064(6) 56(2) C(771) 5937(1) 5268(1) 2864(1) 25(1) C(72) 5837(1)					
C(70A) 9639(5) 9878(6) 5718(6) 56(2) C(62B) 8820(9) 7105(10) 5794(5) 26(2) C(63B) 9804(10) 7750(9) 5980(8) 34(2) C(64B) 10058(8) 8710(7) 6051(6) 41(2) C(65B) 9360(7) 9063(6) 5943(6) 41(2) C(66B) 8351(8) 8390(11) 5724(17) 34(2) C(66B) 8351(8) 8390(11) 5724(17) 34(2) C(66B) 8351(8) 8390(11) 5724(17) 34(2) C(67B) 7704(9) 8832(10) 5685(11) 38(2) C(68B) 8028(7) 9839(7) 5825(6) 51(2) C(68B) 9004(5) 10460(6) 5999(6) 60(2) C(69B) 9004(5) 10460(6) 5999(6) 60(2) C(70B) 9659(5) 10090(6) 6064(6) 56(2) C(71) 5937(1) 5268(1) 2864(1) 25(1) C(72) 5837(1)					
C(62B) 8820(9) 7105(10) 5794(5) 26(2) C(63B) 9804(10) 7750(9) 5980(8) 34(2) C(64B) 10058(8) 8710(7) 6051(6) 41(2) C(65B) 9360(7) 9063(6) 5943(6) 41(2) C(66B) 8351(8) 8390(11) 5724(17) 34(2) C(67B) 7704(9) 8832(10) 5685(11) 38(2) C(68B) 8028(7) 9839(7) 5825(6) 51(2) C(69B) 9004(5) 10460(6) 5999(6) 60(2) C(70B) 9659(5) 10090(6) 6064(6) 56(2) C(71) 5937(1) 5268(1) 2864(1) 25(1) C(72) 5837(1) 4395(2) 2226(1) 34(1) C(73) 6145(2) 4425(2) 1557(1) 45(1) C(74) 6571(2) 5334(2) 1538(1) 45(1) C(75) 6703(1) 6259(2) 2172(1) 37(1) C(76) 6367(1) <					
C(63B) 9804(10) 7750(9) 5980(8) 34(2) C(64B) 10058(8) 8710(7) 6051(6) 41(2) C(65B) 9360(7) 9063(6) 5943(6) 41(2) C(66B) 8351(8) 8390(11) 5724(17) 34(2) C(67B) 7704(9) 8832(10) 5685(11) 38(2) C(68B) 8028(7) 9839(7) 5825(6) 51(2) C(69B) 9004(5) 10460(6) 5999(6) 60(2) C(70B) 9659(5) 10090(6) 6064(6) 56(2) C(71) 5937(1) 5268(1) 2864(1) 25(1) C(72) 5837(1) 4395(2) 2226(1) 34(1) C(73) 6145(2) 4425(2) 1557(1) 45(1) C(74) 6571(2) 5334(2) 1538(1) 45(1) C(75) 6703(1) 6259(2) 2172(1) 37(1) C(76) 6367(1) 6234(1) 2842(1) 30(1) C(77) 6498(2) <td< td=""><td></td><td></td><td></td><td></td><td></td></td<>					
C(64B) 10058(8) 8710(7) 6051(6) 41(2) C(65B) 9360(7) 9063(6) 5943(6) 41(2) C(66B) 8351(8) 8390(11) 5724(17) 34(2) C(67B) 7704(9) 8832(10) 5685(11) 38(2) C(68B) 8028(7) 9839(7) 5825(6) 51(2) C(69B) 9004(5) 10460(6) 5999(6) 60(2) C(70B) 9659(5) 10090(6) 6064(6) 56(2) C(71) 5937(1) 5268(1) 2864(1) 25(1) C(72) 5837(1) 4395(2) 2226(1) 34(1) C(73) 6145(2) 4425(2) 1557(1) 45(1) C(74) 6571(2) 5334(2) 1538(1) 45(1) C(75) 6703(1) 6259(2) 2172(1) 37(1) C(76) 6367(1) 6234(1) 2842(1) 30(1) C(77) 6498(2) 7173(2) 3462(1) 44(1) C(78) 6953(2) 8					
C(65B) 9360(7) 9063(6) 5943(6) 41(2) C(66B) 8351(8) 8390(11) 5724(17) 34(2) C(67B) 7704(9) 8832(10) 5685(11) 38(2) C(68B) 8028(7) 9839(7) 5825(6) 51(2) C(69B) 9004(5) 10460(6) 5999(6) 60(2) C(70B) 9659(5) 10090(6) 6064(6) 56(2) C(71) 5937(1) 5268(1) 2864(1) 25(1) C(72) 5837(1) 4395(2) 2226(1) 34(1) C(73) 6145(2) 4425(2) 1557(1) 45(1) C(74) 6571(2) 5334(2) 1538(1) 45(1) C(74) 6571(2) 5334(2) 1538(1) 45(1) C(75) 6703(1) 6259(2) 2172(1) 37(1) C(76) 6367(1) 6234(1) 2842(1) 30(1) C(77) 6498(2) 7173(2) 3462(1) 44(1) C(78) 7303(2) 810	C(64B)				
C(67B) 7704(9) 8832(10) 5685(11) 38(2) C(68B) 8028(7) 9839(7) 5825(6) 51(2) C(69B) 9004(5) 10460(6) 5999(6) 60(2) C(70B) 9659(5) 10090(6) 6064(6) 56(2) C(71) 5937(1) 5268(1) 2864(1) 25(1) C(72) 5837(1) 4395(2) 2226(1) 34(1) C(73) 6145(2) 4425(2) 1557(1) 45(1) C(73) 6145(2) 4425(2) 1538(1) 45(1) C(74) 6571(2) 5334(2) 1538(1) 45(1) C(75) 6703(1) 6259(2) 2172(1) 37(1) C(76) 6367(1) 6234(1) 2842(1) 30(1) C(77) 6498(2) 7173(2) 3462(1) 44(1) C(78) 6953(2) 8086(2) 3434(2) 62(1) C(79) 7303(2) 8104(2) 2777(2) 63(1) C(80) 7177(2) 7221(2)	C(65B)		9063(6)	5943(6)	
C(68B) 8028(7) 9839(7) 5825(6) 51(2) C(69B) 9004(5) 10460(6) 5999(6) 60(2) C(70B) 9659(5) 10090(6) 6064(6) 56(2) C(71) 5937(1) 5268(1) 2864(1) 25(1) C(72) 5837(1) 4395(2) 2226(1) 34(1) C(73) 6145(2) 4425(2) 1557(1) 45(1) C(74) 6571(2) 5334(2) 1538(1) 45(1) C(75) 6703(1) 6259(2) 2172(1) 37(1) C(76) 6367(1) 6234(1) 2842(1) 30(1) C(77) 6498(2) 7173(2) 3462(1) 44(1) C(78) 6953(2) 8086(2) 3434(2) 62(1) C(79) 7303(2) 8104(2) 2777(2) 63(1) C(80) 7177(2) 7221(2) 2170(2) 51(1) C(81) 7065(3) 1376(3) 3998(3) 112(2) Cl(1) 7415(1) 949(1) 4603(1) 111(1) C(82A) 9168(5) 10962(5)	C(66B)	8351(8)	8390(11)	5724(17)	34(2)
C(69B) 9004(5) 10460(6) 5999(6) 60(2) C(70B) 9659(5) 10090(6) 6064(6) 56(2) C(71) 5937(1) 5268(1) 2864(1) 25(1) C(72) 5837(1) 4395(2) 2226(1) 34(1) C(73) 6145(2) 4425(2) 1557(1) 45(1) C(74) 6571(2) 5334(2) 1538(1) 45(1) C(75) 6703(1) 6259(2) 2172(1) 37(1) C(76) 6367(1) 6234(1) 2842(1) 30(1) C(77) 6498(2) 7173(2) 3462(1) 44(1) C(78) 6953(2) 8086(2) 3434(2) 62(1) C(79) 7303(2) 8104(2) 2777(2) 63(1) C(80) 7177(2) 7221(2) 2170(2) 51(1) C(81) 7065(3) 1376(3) 3998(3) 112(2) Cl(1) 7471(1) 1086(1) 3155(1) 124(1) Cl(2) 7415(1) 949(1) <td>C(67B)</td> <td>7704(9)</td> <td>8832(10)</td> <td>5685(11)</td> <td>38(2)</td>	C(67B)	7704(9)	8832(10)	5685(11)	38(2)
C(70B) 9659(5) 10090(6) 6064(6) 56(2) C(71) 5937(1) 5268(1) 2864(1) 25(1) C(72) 5837(1) 4395(2) 2226(1) 34(1) C(73) 6145(2) 4425(2) 1557(1) 45(1) C(74) 6571(2) 5334(2) 1538(1) 45(1) C(75) 6703(1) 6259(2) 2172(1) 37(1) C(76) 6367(1) 6234(1) 2842(1) 30(1) C(77) 6498(2) 7173(2) 3462(1) 44(1) C(78) 6953(2) 8086(2) 3434(2) 62(1) C(79) 7303(2) 8104(2) 2777(2) 63(1) C(80) 7177(2) 7221(2) 2170(2) 51(1) C(81) 7065(3) 1376(3) 3998(3) 112(2) Cl(1) 7471(1) 1086(1) 3155(1) 124(1) Cl(2) 7415(1) 949(1) 4603(1) 111(1) C(82A) 9168(5) 10962(5) </td <td>C(68B)</td> <td>8028(7)</td> <td>9839(7)</td> <td>5825(6)</td> <td>51(2)</td>	C(68B)	8028(7)	9839(7)	5825(6)	51(2)
C(71) 5937(1) 5268(1) 2864(1) 25(1) C(72) 5837(1) 4395(2) 2226(1) 34(1) C(73) 6145(2) 4425(2) 1557(1) 45(1) C(74) 6571(2) 5334(2) 1538(1) 45(1) C(75) 6703(1) 6259(2) 2172(1) 37(1) C(76) 6367(1) 6234(1) 2842(1) 30(1) C(77) 6498(2) 7173(2) 3462(1) 44(1) C(78) 6953(2) 8086(2) 3434(2) 62(1) C(79) 7303(2) 8104(2) 2777(2) 63(1) C(80) 7177(2) 7221(2) 2170(2) 51(1) C(81) 7065(3) 1376(3) 3998(3) 112(2) Cl(1) 7471(1) 1086(1) 3155(1) 124(1) Cl(2) 7415(1) 949(1) 4603(1) 111(1) C(82A) 9168(5) 10962(5) 358(5) 95(2) Cl(3A) 8476(1) 11562(1) <td>C(69B)</td> <td>9004(5)</td> <td>10460(6)</td> <td>5999(6)</td> <td>60(2)</td>	C(69B)	9004(5)	10460(6)	5999(6)	60(2)
C(72) 5837(1) 4395(2) 2226(1) 34(1) C(73) 6145(2) 4425(2) 1557(1) 45(1) C(74) 6571(2) 5334(2) 1538(1) 45(1) C(75) 6703(1) 6259(2) 2172(1) 37(1) C(76) 6367(1) 6234(1) 2842(1) 30(1) C(77) 6498(2) 7173(2) 3462(1) 44(1) C(78) 6953(2) 8086(2) 3434(2) 62(1) C(79) 7303(2) 8104(2) 2777(2) 63(1) C(80) 7177(2) 7221(2) 2170(2) 51(1) C(81) 7065(3) 1376(3) 3998(3) 112(2) Cl(1) 7471(1) 1086(1) 3155(1) 124(1) Cl(2) 7415(1) 949(1) 4603(1) 111(1) C(82A) 9168(5) 10962(5) 358(5) 95(2) Cl(3A) 8476(1) 11562(1) 786(1) 104(1) Cl(4A) 8603(2) 9700(1) -264(1) 127(1) Cl(3B) 7599(4) 10199(6)	C(70B)	9659(5)	10090(6)	6064(6)	56(2)
C(73) 6145(2) 4425(2) 1557(1) 45(1) C(74) 6571(2) 5334(2) 1538(1) 45(1) C(75) 6703(1) 6259(2) 2172(1) 37(1) C(76) 6367(1) 6234(1) 2842(1) 30(1) C(77) 6498(2) 7173(2) 3462(1) 44(1) C(78) 6953(2) 8086(2) 3434(2) 62(1) C(79) 7303(2) 8104(2) 2777(2) 63(1) C(80) 7177(2) 7221(2) 2170(2) 51(1) C(81) 7065(3) 1376(3) 3998(3) 112(2) Cl(1) 7471(1) 1086(1) 3155(1) 124(1) Cl(2) 7415(1) 949(1) 4603(1) 111(1) C(82A) 9168(5) 10962(5) 358(5) 95(2) Cl(3A) 8476(1) 11562(1) 786(1) 104(1) Cl(4A) 8603(2) 9700(1) -264(1) 127(1) Cl(3B) 7599(4) 10102(14) -137(12) 114(5)	C(71)	5937(1)	5268(1)	2864(1)	25(1)
C(74) 6571(2) 5334(2) 1538(1) 45(1) C(75) 6703(1) 6259(2) 2172(1) 37(1) C(76) 6367(1) 6234(1) 2842(1) 30(1) C(77) 6498(2) 7173(2) 3462(1) 44(1) C(78) 6953(2) 8086(2) 3434(2) 62(1) C(79) 7303(2) 8104(2) 2777(2) 63(1) C(80) 7177(2) 7221(2) 2170(2) 51(1) C(81) 7065(3) 1376(3) 3998(3) 112(2) Cl(1) 7471(1) 1086(1) 3155(1) 124(1) Cl(2) 7415(1) 949(1) 4603(1) 111(1) C(82A) 9168(5) 10962(5) 358(5) 95(2) Cl(3A) 8476(1) 11562(1) 786(1) 104(1) Cl(4A) 8603(2) 9700(1) -264(1) 127(1) Cl(3B) 7599(4) 10199(6) 65(5) 148(2)	C(72)	5837(1)	4395(2)	2226(1)	34(1)
C(75) 6703(1) 6259(2) 2172(1) 37(1) C(76) 6367(1) 6234(1) 2842(1) 30(1) C(77) 6498(2) 7173(2) 3462(1) 44(1) C(78) 6953(2) 8086(2) 3434(2) 62(1) C(79) 7303(2) 8104(2) 2777(2) 63(1) C(80) 7177(2) 7221(2) 2170(2) 51(1) C(81) 7065(3) 1376(3) 3998(3) 112(2) Cl(1) 7471(1) 1086(1) 3155(1) 124(1) Cl(2) 7415(1) 949(1) 4603(1) 111(1) C(82A) 9168(5) 10962(5) 358(5) 95(2) Cl(3A) 8476(1) 11562(1) 786(1) 104(1) Cl(4A) 8603(2) 9700(1) -264(1) 127(1) Cl(3B) 7599(4) 10199(6) 65(5) 148(2)	C(73)	6145(2)	4425(2)	1557(1)	45(1)
C(76) 6367(1) 6234(1) 2842(1) 30(1) C(77) 6498(2) 7173(2) 3462(1) 44(1) C(78) 6953(2) 8086(2) 3434(2) 62(1) C(79) 7303(2) 8104(2) 2777(2) 63(1) C(80) 7177(2) 7221(2) 2170(2) 51(1) C(81) 7065(3) 1376(3) 3998(3) 112(2) Cl(1) 7471(1) 1086(1) 3155(1) 124(1) Cl(2) 7415(1) 949(1) 4603(1) 111(1) C(82A) 9168(5) 10962(5) 358(5) 95(2) Cl(3A) 8476(1) 11562(1) 786(1) 104(1) Cl(4A) 8603(2) 9700(1) -264(1) 127(1) Cl(3B) 8654(12) 10102(14) -137(12) 114(5) Cl(3B) 7599(4) 10199(6) 65(5) 148(2)	C(74)	6571(2)	5334(2)	1538(1)	45(1)
C(77) 6498(2) 7173(2) 3462(1) 44(1) C(78) 6953(2) 8086(2) 3434(2) 62(1) C(79) 7303(2) 8104(2) 2777(2) 63(1) C(80) 7177(2) 7221(2) 2170(2) 51(1) C(81) 7065(3) 1376(3) 3998(3) 112(2) Cl(1) 7471(1) 1086(1) 3155(1) 124(1) Cl(2) 7415(1) 949(1) 4603(1) 111(1) C(82A) 9168(5) 10962(5) 358(5) 95(2) Cl(3A) 8476(1) 11562(1) 786(1) 104(1) Cl(4A) 8603(2) 9700(1) -264(1) 127(1) C(82B) 8654(12) 10102(14) -137(12) 114(5) Cl(3B) 7599(4) 10199(6) 65(5) 148(2)	C(75)	6703(1)	6259(2)	2172(1)	37(1)
C(78) 6953(2) 8086(2) 3434(2) 62(1) C(79) 7303(2) 8104(2) 2777(2) 63(1) C(80) 7177(2) 7221(2) 2170(2) 51(1) C(81) 7065(3) 1376(3) 3998(3) 112(2) Cl(1) 7471(1) 1086(1) 3155(1) 124(1) Cl(2) 7415(1) 949(1) 4603(1) 111(1) C(82A) 9168(5) 10962(5) 358(5) 95(2) Cl(3A) 8476(1) 11562(1) 786(1) 104(1) Cl(4A) 8603(2) 9700(1) -264(1) 127(1) C(82B) 8654(12) 10102(14) -137(12) 114(5) Cl(3B) 7599(4) 10199(6) 65(5) 148(2)	C(76)	6367(1)	6234(1)	2842(1)	30(1)
C(79) 7303(2) 8104(2) 2777(2) 63(1) C(80) 7177(2) 7221(2) 2170(2) 51(1) C(81) 7065(3) 1376(3) 3998(3) 112(2) Cl(1) 7471(1) 1086(1) 3155(1) 124(1) Cl(2) 7415(1) 949(1) 4603(1) 111(1) C(82A) 9168(5) 10962(5) 358(5) 95(2) Cl(3A) 8476(1) 11562(1) 786(1) 104(1) Cl(4A) 8603(2) 9700(1) -264(1) 127(1) C(82B) 8654(12) 10102(14) -137(12) 114(5) Cl(3B) 7599(4) 10199(6) 65(5) 148(2)	C(77)	6498(2)	7173(2)	3462(1)	44(1)
C(80) 7177(2) 7221(2) 2170(2) 51(1) C(81) 7065(3) 1376(3) 3998(3) 112(2) Cl(1) 7471(1) 1086(1) 3155(1) 124(1) Cl(2) 7415(1) 949(1) 4603(1) 111(1) C(82A) 9168(5) 10962(5) 358(5) 95(2) Cl(3A) 8476(1) 11562(1) 786(1) 104(1) Cl(4A) 8603(2) 9700(1) -264(1) 127(1) C(82B) 8654(12) 10102(14) -137(12) 114(5) Cl(3B) 7599(4) 10199(6) 65(5) 148(2)	C(78)	6953(2)	8086(2)	3434(2)	62(1)
C(81) 7065(3) 1376(3) 3998(3) 112(2) Cl(1) 7471(1) 1086(1) 3155(1) 124(1) Cl(2) 7415(1) 949(1) 4603(1) 111(1) C(82A) 9168(5) 10962(5) 358(5) 95(2) Cl(3A) 8476(1) 11562(1) 786(1) 104(1) Cl(4A) 8603(2) 9700(1) -264(1) 127(1) C(82B) 8654(12) 10102(14) -137(12) 114(5) Cl(3B) 7599(4) 10199(6) 65(5) 148(2)	C(79)	7303(2)	8104(2)	2777(2)	63(1)
Cl(1) 7471(1) 1086(1) 3155(1) 124(1) Cl(2) 7415(1) 949(1) 4603(1) 111(1) C(82A) 9168(5) 10962(5) 358(5) 95(2) Cl(3A) 8476(1) 11562(1) 786(1) 104(1) Cl(4A) 8603(2) 9700(1) -264(1) 127(1) C(82B) 8654(12) 10102(14) -137(12) 114(5) Cl(3B) 7599(4) 10199(6) 65(5) 148(2)	C(80)	7177(2)	7221(2)	2170(2)	51(1)
Cl(2) 7415(1) 949(1) 4603(1) 111(1) C(82A) 9168(5) 10962(5) 358(5) 95(2) Cl(3A) 8476(1) 11562(1) 786(1) 104(1) Cl(4A) 8603(2) 9700(1) -264(1) 127(1) C(82B) 8654(12) 10102(14) -137(12) 114(5) Cl(3B) 7599(4) 10199(6) 65(5) 148(2)	C(81)	7065(3)	1376(3)	3998(3)	112(2)
C(82A) 9168(5) 10962(5) 358(5) 95(2) Cl(3A) 8476(1) 11562(1) 786(1) 104(1) Cl(4A) 8603(2) 9700(1) -264(1) 127(1) C(82B) 8654(12) 10102(14) -137(12) 114(5) Cl(3B) 7599(4) 10199(6) 65(5) 148(2)	Cl(1)	7471(1)	1086(1)	3155(1)	124(1)
Cl(3A) 8476(1) 11562(1) 786(1) 104(1) Cl(4A) 8603(2) 9700(1) -264(1) 127(1) C(82B) 8654(12) 10102(14) -137(12) 114(5) Cl(3B) 7599(4) 10199(6) 65(5) 148(2)	Cl(2)	7415(1)	949(1)	4603(1)	111(1)
Cl(4A) 8603(2) 9700(1) -264(1) 127(1) C(82B) 8654(12) 10102(14) -137(12) 114(5) Cl(3B) 7599(4) 10199(6) 65(5) 148(2)	C(82A)	9168(5)	10962(5)	358(5)	95(2)
C(82B) 8654(12) 10102(14) -137(12) 114(5) Cl(3B) 7599(4) 10199(6) 65(5) 148(2)	Cl(3A)	8476(1)	11562(1)	786(1)	104(1)
Cl(3B) 7599(4) 10199(6) 65(5) 148(2)	Cl(4A)	8603(2)	9700(1)	-264(1)	127(1)
	C(82B)	8654(12)	10102(14)	-137(12)	114(5)
Cl(4B) 9636(5) 11198(6) 443(4) 105(2)	Cl(3B)	7599(4)	10199(6)	65(5)	148(2)
	Cl(4B)	9636(5)	11198(6)	443(4)	105(2)

 $\textbf{Table S 13:} \ \mathsf{Bond} \ \mathsf{lengths} \ \mathsf{[pm]} \ \mathsf{for} \ \mathsf{1-Naph_POSS_KOH}.$

Bond	Length [pm]	Bond	Length [pm]
Si(1)-O(1)	161.34(12)	Si(1)-O(5)	161.57(12)
Si(1)-O(4)	161.60(12)	Si(1)-C(1)	184.97(17)
Si(2)-O(6)	161.32(12)	Si(2)-O(2)	161.44(12)
Si(2)-O(1)	161.56(12)	Si(2)-C(11)	183.85(16)
Si(3)-O(3)	161.18(12)	Si(3)-O(2)	161.47(12)
Si(3)-O(5)#1	161.76(12)	Si(3)-C(21)	183.94(16)
Si(4)-O(3)	161.01(12)	Si(4)-O(6)#1	161.39(12)
Si(4)-O(4)	162.01(12)	Si(4)-C(31)	183.92(15)
Si(5)-O(10)	161.02(12)	Si(5)-O(11)	161.83(12)
Si(5)-O(7)	162.08(12)	Si(5)-C(41)	184.26(16)
Si(6)-O(7)	161.31(12)	Si(6)-O(12)	161.71(12)
Si(6)-O(8)	162.11(11)	Si(6)-C(51)	184.64(16)
Si(7)-O(9)	161.65(11)	Si(7)-O(8)	161.85(11)
Si(7)-O(11)#2	161.99(12)	Si(7)-C(61)	184.97(16)
Si(8)-O(10)	161.53(12)	Si(8)-O(9)	161.72(12)
Si(8)-O(12)#2	162.13(12)	Si(8)-C(71)	184.40(16)
C(1)-C(2)	137.8(2)	C(1)-C(6)	143.4(2)
C(2)-C(3)	141.2(3)	C(3)-C(4)	135.8(3)
C(4)-C(5)	141.1(3)	C(5)-C(10)	141.7(3)
C(5)-C(6)	142.5(2)	C(6)-C(7)	141.5(3)
C(7)-C(8)	137.1(3)	C(8)-C(9)	140.9(3)
C(9)-C(10)	135.2(3)	C(11)-C(12)	138.1(2)
C(11)-C(16)	143.1(2)	C(12)-C(13)	140.6(2)
C(13)-C(14)	134.8(3)	C(14)-C(15)	140.7(3)
C(15)-C(20)	141.5(3)	C(15)-C(16)	143.0(3)
C(16)-C(17)	141.2(3)	C(17)-C(18)	137.0(3)
C(18)-C(19)	140.7(4)	C(19)-C(20)	134.4(4)
C(21)-C(22)	137.4(3)	C(21)-C(26)	143.5(2)
C(22)-C(23)	141.1(3)	C(23)-C(24)	134.9(4)
C(24)-C(25)	140.8(4)	C(25)-C(30)	141.5(3)
C(25)-C(26)	142.6(3)	C(26)-C(27)	141.3(3)
C(27)-C(28)	136.8(3)	C(28)-C(29)	140.7(4)
C(29)-C(30)	135.5(4)	C(31)-C(32)	138.0(2)
C(31)-C(36)	143.5(2)	C(32)-C(33)	141.4(2)
C(33)-C(34)	135.6(3)	C(34)-C(35)	141.3(3)
C(35)-C(40)	141.5(2)	C(35)-C(36)	142.3(2)

C(38)-C(39) 140.9(3) C(39)-C(40) 135.6(3) C(41)-C(42) 138.0(2) C(41)-C(46) 143.1(2) C(42)-C(43) 141.0(2) C(43)-C(44) 136.0(3) C(44)-C(45) 141.3(3) C(45)-C(50) 141.2(3) C(45)-C(46) 142.3(2) C(46)-C(47) 141.5(2) C(47)-C(48) 137.0(2) C(48)-C(49) 140.3(3) C(49)-C(50) 136.3(3) C(51)-C(52) 137.9(3) C(51)-C(56) 143.2(2) C(52)-C(53) 141.3(3) C(53)-C(54) 134.8(4) C(54)-C(55) 141.3(4) C(56)-C(50) 141.4(3) C(55)-C(56) 142.9(2) C(56)-C(57) 141.4(3) C(57)-C(58) 137.0(3) C(58)-C(59) 140.6(4) C(59)-C(60) 135.0(4) C(61)-C(62A) 137.8(10) C(61)-C(62B) 139.4(9) C(61)-C(66A) 140.8(9) C(61)-C(66B) 144.6(8) C(62A)-C(63A) 140.8(10) C(63A)-C(64A) 135.9(9) C(64A)-C(65A) 143.1(10) C(66A)-C(67A)				
C(42)-C(43) 141.0(2) C(43)-C(44) 136.0(3) C(44)-C(45) 141.3(3) C(45)-C(50) 141.2(3) C(45)-C(46) 142.3(2) C(46)-C(47) 141.5(2) C(47)-C(48) 137.0(2) C(48)-C(49) 140.3(3) C(49)-C(50) 136.3(3) C(51)-C(52) 137.9(3) C(51)-C(56) 143.2(2) C(52)-C(53) 141.3(3) C(53)-C(54) 134.8(4) C(54)-C(55) 141.3(4) C(55)-C(60) 141.4(3) C(55)-C(56) 142.9(2) C(56)-C(57) 141.4(3) C(57)-C(58) 137.0(3) C(58)-C(59) 140.6(4) C(59)-C(60) 135.0(4) C(61)-C(62A) 137.8(10) C(61)-C(62B) 139.4(9) C(61)-C(66A) 140.8(9) C(61)-C(66B) 144.6(8) C(62A)-C(63A) 140.8(10) C(63A)-C(64A) 135.9(9) C(64A)-C(65A) 140.7(9) C(65A)-C(70A) 141.6(8) C(65A)-C(66A) 143.1(10) C(66A)-C(67A) 140.1(10) C(67A)-C(68A) 138.1(10) C(66B)-C(6	C(38)-C(39)	140.9(3)	C(39)-C(40)	135.6(3)
C(44)-C(45) 141.3(3) C(45)-C(50) 141.2(3) C(45)-C(46) 142.3(2) C(46)-C(47) 141.5(2) C(47)-C(48) 137.0(2) C(48)-C(49) 140.3(3) C(49)-C(50) 136.3(3) C(51)-C(52) 137.9(3) C(51)-C(56) 143.2(2) C(52)-C(53) 141.3(3) C(53)-C(54) 134.8(4) C(54)-C(55) 141.3(4) C(55)-C(60) 141.4(3) C(55)-C(56) 142.9(2) C(56)-C(57) 141.4(3) C(57)-C(58) 137.0(3) C(58)-C(59) 140.6(4) C(59)-C(60) 135.0(4) C(61)-C(62A) 137.8(10) C(61)-C(62B) 139.4(9) C(61)-C(66A) 140.8(9) C(61)-C(66B) 144.6(8) C(62A)-C(63A) 140.8(10) C(63A)-C(64A) 135.9(9) C(64A)-C(65A) 140.7(9) C(65A)-C(70A) 141.6(8) C(65A)-C(66A) 143.1(10) C(66A)-C(67A) 140.1(10) C(67A)-C(68A) 138.1(10) C(66A)-C(67B) 140.5(9) C(69A)-C(64B) 135.2(9) C(64B)	C(41)-C(42)	138.0(2)	C(41)-C(46)	143.1(2)
C(45)-C(46) 142.3(2) C(46)-C(47) 141.5(2) C(47)-C(48) 137.0(2) C(48)-C(49) 140.3(3) C(49)-C(50) 136.3(3) C(51)-C(52) 137.9(3) C(51)-C(56) 143.2(2) C(52)-C(53) 141.3(3) C(53)-C(54) 134.8(4) C(54)-C(55) 141.3(4) C(55)-C(60) 141.4(3) C(55)-C(56) 142.9(2) C(56)-C(57) 141.4(3) C(57)-C(58) 137.0(3) C(58)-C(59) 140.6(4) C(59)-C(60) 135.0(4) C(61)-C(62A) 137.8(10) C(61)-C(62B) 139.4(9) C(61)-C(66A) 140.8(9) C(61)-C(66B) 144.6(8) C(62A)-C(63A) 140.8(10) C(63A)-C(64A) 135.9(9) C(64A)-C(65A) 140.7(9) C(65A)-C(70A) 141.6(8) C(65A)-C(66A) 143.1(10) C(66A)-C(67A) 140.1(10) C(67A)-C(66A) 135.1(10) C(66A)-C(67A) 140.1(10) C(67A)-C(66B) 135.2(9) C(64B)-C(65B) 140.5(9) C(69B)-C(70B) 141.4(8) C	C(42)-C(43)	141.0(2)	C(43)-C(44)	136.0(3)
C(47)-C(48) 137.0(2) C(48)-C(49) 140.3(3) C(49)-C(50) 136.3(3) C(51)-C(52) 137.9(3) C(51)-C(56) 143.2(2) C(52)-C(53) 141.3(3) C(53)-C(54) 134.8(4) C(54)-C(55) 141.3(4) C(55)-C(60) 141.4(3) C(55)-C(56) 142.9(2) C(56)-C(57) 141.4(3) C(57)-C(58) 137.0(3) C(58)-C(59) 140.6(4) C(59)-C(60) 135.0(4) C(58)-C(59) 140.6(4) C(59)-C(60) 135.0(4) C(61)-C(62A) 137.8(10) C(61)-C(62B) 139.4(9) C(61)-C(66A) 140.8(9) C(61)-C(66B) 144.6(8) C(62A)-C(63A) 140.8(10) C(63A)-C(64A) 135.9(9) C(64A)-C(65A) 143.1(10) C(66A)-C(67A) 140.1(10) C(67A)-C(66A) 138.1(10) C(66A)-C(67A) 140.1(10) C(67A)-C(66A) 138.1(10) C(66B)-C(65B) 140.2(9) C(63B)-C(64B) 135.2(9) C(62B)-C(63B) 140.6(9) C(65B)-C(66B) 141.4(8)	C(44)-C(45)	141.3(3)	C(45)-C(50)	141.2(3)
C(49)-C(50) 136.3(3) C(51)-C(52) 137.9(3) C(51)-C(56) 143.2(2) C(52)-C(53) 141.3(3) C(53)-C(54) 134.8(4) C(54)-C(55) 141.3(4) C(55)-C(60) 141.4(3) C(55)-C(56) 142.9(2) C(56)-C(57) 141.4(3) C(57)-C(58) 137.0(3) C(58)-C(59) 140.6(4) C(59)-C(60) 135.0(4) C(61)-C(62A) 137.8(10) C(61)-C(62B) 139.4(9) C(61)-C(66A) 140.8(9) C(61)-C(66B) 144.6(8) C(62A)-C(63A) 140.8(10) C(63A)-C(64A) 135.9(9) C(64A)-C(65A) 143.1(10) C(66A)-C(67A) 141.6(8) C(65A)-C(66A) 143.1(10) C(66A)-C(67A) 140.1(10) C(67A)-C(68A) 138.1(10) C(66A)-C(67A) 140.2(9) C(69A)-C(60B) 135.5(8) C(62B)-C(63B) 140.6(9) C(63B)-C(60B) 135.2(9) C(64B)-C(65B) 141.4(8) C(65B)-C(70B) 141.4(8) C(65B)-C(66B) 144.2(9) C(66B)-C(67B) 141.7(9)	C(45)-C(46)	142.3(2)	C(46)-C(47)	141.5(2)
C(51)-C(56) 143.2(2) C(52)-C(53) 141.3(3) C(53)-C(54) 134.8(4) C(54)-C(55) 141.3(4) C(55)-C(60) 141.4(3) C(55)-C(56) 142.9(2) C(56)-C(57) 141.4(3) C(57)-C(58) 137.0(3) C(58)-C(59) 140.6(4) C(59)-C(60) 135.0(4) C(61)-C(62A) 137.8(10) C(61)-C(62B) 139.4(9) C(61)-C(66A) 140.8(9) C(61)-C(66B) 144.6(8) C(62A)-C(63A) 140.8(10) C(63A)-C(64A) 135.9(9) C(64A)-C(65A) 140.7(9) C(65A)-C(70A) 141.6(8) C(65A)-C(66A) 143.1(10) C(66A)-C(67A) 140.1(10) C(67A)-C(68A) 138.1(10) C(66B)-C(67A) 140.2(9) C(69A)-C(70A) 135.5(8) C(62B)-C(63B) 140.6(9) C(63B)-C(64B) 135.2(9) C(64B)-C(65B) 141.4(8) C(65B)-C(70B) 141.4(8) C(65B)-C(66B) 144.2(9) C(66B)-C(67B) 141.7(9) C(67B)-C(68B) 137.0(9) C(68B)-C(69B) 139.0(8)	C(47)-C(48)	137.0(2)	C(48)-C(49)	140.3(3)
C(53)-C(54) 134.8(4) C(54)-C(55) 141.3(4) C(55)-C(60) 141.4(3) C(55)-C(56) 142.9(2) C(56)-C(57) 141.4(3) C(57)-C(58) 137.0(3) C(58)-C(59) 140.6(4) C(59)-C(60) 135.0(4) C(61)-C(62A) 137.8(10) C(61)-C(62B) 139.4(9) C(61)-C(66A) 140.8(9) C(61)-C(66B) 144.6(8) C(62A)-C(63A) 140.8(10) C(63A)-C(64A) 135.9(9) C(64A)-C(65A) 140.7(9) C(65A)-C(70A) 141.6(8) C(65A)-C(66A) 143.1(10) C(66A)-C(67A) 140.1(10) C(67A)-C(68A) 138.1(10) C(66A)-C(69A) 140.2(9) C(69A)-C(70A) 135.5(8) C(62B)-C(63B) 140.6(9) C(63B)-C(64B) 135.2(9) C(64B)-C(65B) 141.4(8) C(65B)-C(70B) 141.4(8) C(65B)-C(66B) 144.2(9) C(66B)-C(67B) 141.7(9) C(67B)-C(68B) 137.0(9) C(68B)-C(69B) 139.0(8) C(69B)-C(70B) 135.5(8) C(71)-C(72) 137.4(2)	C(49)-C(50)	136.3(3)	C(51)-C(52)	137.9(3)
C(55)-C(60) 141.4(3) C(55)-C(56) 142.9(2) C(56)-C(57) 141.4(3) C(57)-C(58) 137.0(3) C(58)-C(59) 140.6(4) C(59)-C(60) 135.0(4) C(61)-C(62A) 137.8(10) C(61)-C(62B) 139.4(9) C(61)-C(66A) 140.8(9) C(61)-C(66B) 144.6(8) C(62A)-C(63A) 140.8(10) C(63A)-C(64A) 135.9(9) C(64A)-C(65A) 140.7(9) C(65A)-C(67A) 141.6(8) C(65A)-C(66A) 143.1(10) C(66A)-C(67A) 140.1(10) C(67A)-C(68A) 138.1(10) C(68A)-C(69A) 140.2(9) C(63B)-C(68B) 135.5(8) C(62B)-C(63B) 140.6(9) C(63B)-C(64B) 135.2(9) C(64B)-C(65B) 141.4(8) C(65B)-C(64B) 135.2(9) C(64B)-C(65B) 141.4(8) C(65B)-C(67B) 141.7(9) C(65B)-C(66B) 144.2(9) C(66B)-C(67B) 141.7(9) C(67B)-C(68B) 135.5(8) C(71)-C(72) 137.4(2) C(71)-C(76) 143.1(2) C(72)-C(73) 141.1(2)	C(51)-C(56)	143.2(2)	C(52)-C(53)	141.3(3)
C(56)-C(57) 141.4(3) C(57)-C(58) 137.0(3) C(58)-C(59) 140.6(4) C(59)-C(60) 135.0(4) C(61)-C(62A) 137.8(10) C(61)-C(62B) 139.4(9) C(61)-C(66A) 140.8(9) C(61)-C(66B) 144.6(8) C(62A)-C(63A) 140.8(10) C(63A)-C(64A) 135.9(9) C(64A)-C(65A) 140.7(9) C(65A)-C(70A) 141.6(8) C(65A)-C(66A) 143.1(10) C(66A)-C(67A) 140.1(10) C(67A)-C(68A) 138.1(10) C(68A)-C(69A) 140.2(9) C(69A)-C(70A) 135.5(8) C(62B)-C(63B) 140.6(9) C(63B)-C(64B) 135.2(9) C(64B)-C(65B) 141.4(8) C(65B)-C(70B) 141.4(8) C(65B)-C(66B) 144.2(9) C(66B)-C(67B) 141.7(9) C(67B)-C(68B) 137.0(9) C(68B)-C(69B) 139.0(8) C(69B)-C(70B) 135.5(8) C(71)-C(72) 137.4(2) C(71)-C(76) 143.1(2) C(72)-C(73) 141.1(2) C(73)-C(74) 135.0(3) C(75)-C(76) 142.9(2)	C(53)-C(54)	134.8(4)	C(54)-C(55)	141.3(4)
C(58)-C(59) 140.6(4) C(59)-C(60) 135.0(4) C(61)-C(62A) 137.8(10) C(61)-C(62B) 139.4(9) C(61)-C(66A) 140.8(9) C(61)-C(66B) 144.6(8) C(62A)-C(63A) 140.8(10) C(63A)-C(64A) 135.9(9) C(64A)-C(65A) 140.7(9) C(65A)-C(70A) 141.6(8) C(65A)-C(66A) 143.1(10) C(66A)-C(67A) 140.1(10) C(67A)-C(68A) 138.1(10) C(68A)-C(69A) 140.2(9) C(69A)-C(70A) 135.5(8) C(62B)-C(63B) 140.6(9) C(63B)-C(64B) 135.2(9) C(64B)-C(65B) 141.4(8) C(65B)-C(70B) 141.4(8) C(65B)-C(66B) 144.2(9) C(66B)-C(67B) 141.7(9) C(67B)-C(68B) 137.0(9) C(68B)-C(69B) 139.0(8) C(69B)-C(70B) 135.5(8) C(71)-C(72) 137.4(2) C(71)-C(76) 143.1(2) C(72)-C(73) 141.1(2) C(73)-C(74) 135.0(3) C(75)-C(76) 142.9(2) C(75)-C(80) 141.5(3) C(77)-C(78) 136.7(3)	C(55)-C(60)	141.4(3)	C(55)-C(56)	142.9(2)
C(61)-C(62A) 137.8(10) C(61)-C(62B) 139.4(9) C(61)-C(66A) 140.8(9) C(61)-C(66B) 144.6(8) C(62A)-C(63A) 140.8(10) C(63A)-C(64A) 135.9(9) C(64A)-C(65A) 140.7(9) C(65A)-C(70A) 141.6(8) C(65A)-C(66A) 143.1(10) C(66A)-C(67A) 140.1(10) C(67A)-C(68A) 138.1(10) C(68A)-C(69A) 140.2(9) C(69A)-C(70A) 135.5(8) C(62B)-C(63B) 140.6(9) C(63B)-C(64B) 135.2(9) C(64B)-C(65B) 141.4(8) C(65B)-C(70B) 141.4(8) C(65B)-C(66B) 144.2(9) C(66B)-C(67B) 141.7(9) C(67B)-C(68B) 137.0(9) C(68B)-C(69B) 139.0(8) C(69B)-C(70B) 135.5(8) C(71)-C(72) 137.4(2) C(71)-C(76) 143.1(2) C(72)-C(73) 141.1(2) C(73)-C(74) 135.0(3) C(74)-C(75) 140.5(3) C(75)-C(80) 141.5(3) C(75)-C(76) 142.9(2) C(76)-C(77) 140.9(3) C(77)-C(78) 136.7(3)	C(56)-C(57)	141.4(3)	C(57)-C(58)	137.0(3)
C(61)-C(66A) 140.8(9) C(61)-C(66B) 144.6(8) C(62A)-C(63A) 140.8(10) C(63A)-C(64A) 135.9(9) C(64A)-C(65A) 140.7(9) C(65A)-C(70A) 141.6(8) C(65A)-C(66A) 143.1(10) C(66A)-C(67A) 140.1(10) C(67A)-C(68A) 138.1(10) C(68A)-C(69A) 140.2(9) C(69A)-C(70A) 135.5(8) C(62B)-C(63B) 140.6(9) C(63B)-C(64B) 135.2(9) C(64B)-C(65B) 141.4(8) C(65B)-C(70B) 141.4(8) C(65B)-C(66B) 144.2(9) C(66B)-C(67B) 141.7(9) C(67B)-C(68B) 137.0(9) C(68B)-C(69B) 139.0(8) C(69B)-C(70B) 135.5(8) C(71)-C(72) 137.4(2) C(71)-C(76) 143.1(2) C(72)-C(73) 141.1(2) C(73)-C(74) 135.0(3) C(75)-C(76) 142.9(2) C(75)-C(80) 141.5(3) C(75)-C(76) 142.9(2) C(76)-C(77) 140.9(3) C(77)-C(78) 136.7(3) C(78)-C(79) 141.0(4) C(79)-C(80) 134.4(4)	C(58)-C(59)	140.6(4)	C(59)-C(60)	135.0(4)
C(62A)-C(63A) 140.8(10) C(63A)-C(64A) 135.9(9) C(64A)-C(65A) 140.7(9) C(65A)-C(70A) 141.6(8) C(65A)-C(66A) 143.1(10) C(66A)-C(67A) 140.1(10) C(67A)-C(68A) 138.1(10) C(68A)-C(69A) 140.2(9) C(69A)-C(70A) 135.5(8) C(62B)-C(63B) 140.6(9) C(63B)-C(64B) 135.2(9) C(64B)-C(65B) 141.4(8) C(65B)-C(70B) 141.4(8) C(65B)-C(66B) 144.2(9) C(66B)-C(67B) 141.7(9) C(67B)-C(68B) 137.0(9) C(68B)-C(69B) 139.0(8) C(69B)-C(70B) 135.5(8) C(71)-C(72) 137.4(2) C(71)-C(76) 143.1(2) C(72)-C(73) 141.1(2) C(73)-C(74) 135.0(3) C(74)-C(75) 140.5(3) C(75)-C(80) 141.5(3) C(75)-C(76) 142.9(2) C(76)-C(77) 140.9(3) C(77)-C(78) 136.7(3) C(78)-C(79) 141.0(4) C(79)-C(80) 134.4(4) C(81)-Cl(2) 170.6(5) C(82A)-Cl(4A) 168.3(7)	C(61)-C(62A)	137.8(10)	C(61)-C(62B)	139.4(9)
C(64A)-C(65A) 140.7(9) C(65A)-C(70A) 141.6(8) C(65A)-C(66A) 143.1(10) C(66A)-C(67A) 140.1(10) C(67A)-C(68A) 138.1(10) C(68A)-C(69A) 140.2(9) C(69A)-C(70A) 135.5(8) C(62B)-C(63B) 140.6(9) C(63B)-C(64B) 135.2(9) C(64B)-C(65B) 141.4(8) C(65B)-C(70B) 141.4(8) C(65B)-C(66B) 144.2(9) C(66B)-C(67B) 141.7(9) C(67B)-C(68B) 137.0(9) C(68B)-C(69B) 139.0(8) C(69B)-C(70B) 135.5(8) C(71)-C(72) 137.4(2) C(71)-C(76) 143.1(2) C(72)-C(73) 141.1(2) C(73)-C(74) 135.0(3) C(74)-C(75) 140.5(3) C(75)-C(80) 141.5(3) C(75)-C(76) 142.9(2) C(76)-C(77) 140.9(3) C(77)-C(78) 136.7(3) C(78)-C(79) 141.0(4) C(79)-C(80) 134.4(4) C(81)-Cl(2) 170.6(5) C(81)-Cl(1) 172.5(5) C(82A)-Cl(4A) 168.3(7) C(82A)-Cl(3A) 170.5(7)	C(61)-C(66A)	140.8(9)	C(61)-C(66B)	144.6(8)
C(65A)-C(66A) 143.1(10) C(66A)-C(67A) 140.1(10) C(67A)-C(68A) 138.1(10) C(68A)-C(69A) 140.2(9) C(69A)-C(70A) 135.5(8) C(62B)-C(63B) 140.6(9) C(63B)-C(64B) 135.2(9) C(64B)-C(65B) 141.4(8) C(65B)-C(70B) 141.4(8) C(65B)-C(66B) 144.2(9) C(66B)-C(67B) 141.7(9) C(67B)-C(68B) 137.0(9) C(68B)-C(69B) 139.0(8) C(69B)-C(70B) 135.5(8) C(71)-C(72) 137.4(2) C(71)-C(76) 143.1(2) C(72)-C(73) 141.1(2) C(73)-C(74) 135.0(3) C(74)-C(75) 140.5(3) C(75)-C(80) 141.5(3) C(75)-C(76) 142.9(2) C(76)-C(77) 140.9(3) C(77)-C(78) 136.7(3) C(78)-C(79) 141.0(4) C(79)-C(80) 134.4(4) C(81)-Cl(2) 170.6(5) C(81)-Cl(1) 172.5(5) C(82A)-Cl(4A) 168.3(7) C(82A)-Cl(3A) 170.5(7) C(82B)-Cl(4B) 169.3(16)	C(62A)-C(63A)	140.8(10)	C(63A)-C(64A)	135.9(9)
C(67A)-C(68A) 138.1(10) C(68A)-C(69A) 140.2(9) C(69A)-C(70A) 135.5(8) C(62B)-C(63B) 140.6(9) C(63B)-C(64B) 135.2(9) C(64B)-C(65B) 141.4(8) C(65B)-C(70B) 141.4(8) C(65B)-C(66B) 144.2(9) C(66B)-C(67B) 141.7(9) C(67B)-C(68B) 137.0(9) C(68B)-C(69B) 139.0(8) C(69B)-C(70B) 135.5(8) C(71)-C(72) 137.4(2) C(71)-C(76) 143.1(2) C(72)-C(73) 141.1(2) C(73)-C(74) 135.0(3) C(74)-C(75) 140.5(3) C(75)-C(80) 141.5(3) C(75)-C(76) 142.9(2) C(76)-C(77) 140.9(3) C(77)-C(78) 136.7(3) C(78)-C(79) 141.0(4) C(79)-C(80) 134.4(4) C(81)-Cl(2) 170.6(5) C(81)-Cl(1) 172.5(5) C(82A)-Cl(4A) 168.3(7) C(82A)-Cl(3A) 170.5(7) C(82B)-Cl(4B) 169.3(16)	C(64A)-C(65A)	140.7(9)	C(65A)-C(70A)	141.6(8)
C(69A)-C(70A) 135.5(8) C(62B)-C(63B) 140.6(9) C(63B)-C(64B) 135.2(9) C(64B)-C(65B) 141.4(8) C(65B)-C(70B) 141.4(8) C(65B)-C(66B) 144.2(9) C(66B)-C(67B) 141.7(9) C(67B)-C(68B) 137.0(9) C(68B)-C(69B) 139.0(8) C(69B)-C(70B) 135.5(8) C(71)-C(72) 137.4(2) C(71)-C(76) 143.1(2) C(72)-C(73) 141.1(2) C(73)-C(74) 135.0(3) C(74)-C(75) 140.5(3) C(75)-C(80) 141.5(3) C(75)-C(76) 142.9(2) C(76)-C(77) 140.9(3) C(77)-C(78) 136.7(3) C(78)-C(79) 141.0(4) C(79)-C(80) 134.4(4) C(81)-Cl(2) 170.6(5) C(81)-Cl(1) 172.5(5) C(82A)-Cl(4A) 168.3(7) C(82A)-Cl(3A) 170.5(7) C(82B)-Cl(4B) 169.3(16)	C(65A)-C(66A)	143.1(10)	C(66A)-C(67A)	140.1(10)
C(63B)-C(64B) 135.2(9) C(64B)-C(65B) 141.4(8) C(65B)-C(70B) 141.4(8) C(65B)-C(66B) 144.2(9) C(66B)-C(67B) 141.7(9) C(67B)-C(68B) 137.0(9) C(68B)-C(69B) 139.0(8) C(69B)-C(70B) 135.5(8) C(71)-C(72) 137.4(2) C(71)-C(76) 143.1(2) C(72)-C(73) 141.1(2) C(73)-C(74) 135.0(3) C(74)-C(75) 140.5(3) C(75)-C(80) 141.5(3) C(75)-C(76) 142.9(2) C(76)-C(77) 140.9(3) C(77)-C(78) 136.7(3) C(78)-C(79) 141.0(4) C(79)-C(80) 134.4(4) C(81)-Cl(2) 170.6(5) C(81)-Cl(1) 172.5(5) C(82A)-Cl(4A) 168.3(7) C(82A)-Cl(3A) 170.5(7) C(82B)-Cl(4B) 169.3(16)	C(67A)-C(68A)	138.1(10)	C(68A)-C(69A)	140.2(9)
C(65B)-C(70B) 141.4(8) C(65B)-C(66B) 144.2(9) C(66B)-C(67B) 141.7(9) C(67B)-C(68B) 137.0(9) C(68B)-C(69B) 139.0(8) C(69B)-C(70B) 135.5(8) C(71)-C(72) 137.4(2) C(71)-C(76) 143.1(2) C(72)-C(73) 141.1(2) C(73)-C(74) 135.0(3) C(74)-C(75) 140.5(3) C(75)-C(80) 141.5(3) C(75)-C(76) 142.9(2) C(76)-C(77) 140.9(3) C(77)-C(78) 136.7(3) C(78)-C(79) 141.0(4) C(79)-C(80) 134.4(4) C(81)-Cl(2) 170.6(5) C(81)-Cl(1) 172.5(5) C(82A)-Cl(4A) 168.3(7) C(82A)-Cl(3A) 170.5(7) C(82B)-Cl(4B) 169.3(16)	C(69A)-C(70A)	135.5(8)	C(62B)-C(63B)	140.6(9)
C(66B)-C(67B) 141.7(9) C(67B)-C(68B) 137.0(9) C(68B)-C(69B) 139.0(8) C(69B)-C(70B) 135.5(8) C(71)-C(72) 137.4(2) C(71)-C(76) 143.1(2) C(72)-C(73) 141.1(2) C(73)-C(74) 135.0(3) C(74)-C(75) 140.5(3) C(75)-C(80) 141.5(3) C(75)-C(76) 142.9(2) C(76)-C(77) 140.9(3) C(77)-C(78) 136.7(3) C(78)-C(79) 141.0(4) C(79)-C(80) 134.4(4) C(81)-Cl(2) 170.6(5) C(81)-Cl(1) 172.5(5) C(82A)-Cl(4A) 168.3(7) C(82A)-Cl(3A) 170.5(7) C(82B)-Cl(4B) 169.3(16)	C(63B)-C(64B)	135.2(9)	C(64B)-C(65B)	141.4(8)
C(68B)-C(69B) 139.0(8) C(69B)-C(70B) 135.5(8) C(71)-C(72) 137.4(2) C(71)-C(76) 143.1(2) C(72)-C(73) 141.1(2) C(73)-C(74) 135.0(3) C(74)-C(75) 140.5(3) C(75)-C(80) 141.5(3) C(75)-C(76) 142.9(2) C(76)-C(77) 140.9(3) C(77)-C(78) 136.7(3) C(78)-C(79) 141.0(4) C(79)-C(80) 134.4(4) C(81)-Cl(2) 170.6(5) C(81)-Cl(1) 172.5(5) C(82A)-Cl(4A) 168.3(7) C(82A)-Cl(3A) 170.5(7) C(82B)-Cl(4B) 169.3(16)	C(65B)-C(70B)	141.4(8)	C(65B)-C(66B)	144.2(9)
C(71)-C(72) 137.4(2) C(71)-C(76) 143.1(2) C(72)-C(73) 141.1(2) C(73)-C(74) 135.0(3) C(74)-C(75) 140.5(3) C(75)-C(80) 141.5(3) C(75)-C(76) 142.9(2) C(76)-C(77) 140.9(3) C(77)-C(78) 136.7(3) C(78)-C(79) 141.0(4) C(79)-C(80) 134.4(4) C(81)-Cl(2) 170.6(5) C(81)-Cl(1) 172.5(5) C(82A)-Cl(4A) 168.3(7) C(82A)-Cl(3A) 170.5(7) C(82B)-Cl(4B) 169.3(16)	C(66B)-C(67B)	141.7(9)	C(67B)-C(68B)	137.0(9)
C(72)-C(73) 141.1(2) C(73)-C(74) 135.0(3) C(74)-C(75) 140.5(3) C(75)-C(80) 141.5(3) C(75)-C(76) 142.9(2) C(76)-C(77) 140.9(3) C(77)-C(78) 136.7(3) C(78)-C(79) 141.0(4) C(79)-C(80) 134.4(4) C(81)-Cl(2) 170.6(5) C(81)-Cl(1) 172.5(5) C(82A)-Cl(4A) 168.3(7) C(82A)-Cl(3A) 170.5(7) C(82B)-Cl(4B) 169.3(16)	C(68B)-C(69B)	139.0(8)	C(69B)-C(70B)	135.5(8)
C(74)-C(75) 140.5(3) C(75)-C(80) 141.5(3) C(75)-C(76) 142.9(2) C(76)-C(77) 140.9(3) C(77)-C(78) 136.7(3) C(78)-C(79) 141.0(4) C(79)-C(80) 134.4(4) C(81)-Cl(2) 170.6(5) C(81)-Cl(1) 172.5(5) C(82A)-Cl(4A) 168.3(7) C(82A)-Cl(3A) 170.5(7) C(82B)-Cl(4B) 169.3(16)	C(71)-C(72)	137.4(2)	C(71)-C(76)	143.1(2)
C(75)-C(76) 142.9(2) C(76)-C(77) 140.9(3) C(77)-C(78) 136.7(3) C(78)-C(79) 141.0(4) C(79)-C(80) 134.4(4) C(81)-Cl(2) 170.6(5) C(81)-Cl(1) 172.5(5) C(82A)-Cl(4A) 168.3(7) C(82A)-Cl(3A) 170.5(7) C(82B)-Cl(4B) 169.3(16)	C(72)-C(73)	141.1(2)	C(73)-C(74)	135.0(3)
C(77)-C(78) 136.7(3) C(78)-C(79) 141.0(4) C(79)-C(80) 134.4(4) C(81)-Cl(2) 170.6(5) C(81)-Cl(1) 172.5(5) C(82A)-Cl(4A) 168.3(7) C(82A)-Cl(3A) 170.5(7) C(82B)-Cl(4B) 169.3(16)	C(74)-C(75)	140.5(3)	C(75)-C(80)	141.5(3)
C(79)-C(80) 134.4(4) C(81)-Cl(2) 170.6(5) C(81)-Cl(1) 172.5(5) C(82A)-Cl(4A) 168.3(7) C(82A)-Cl(3A) 170.5(7) C(82B)-Cl(4B) 169.3(16)	C(75)-C(76)	142.9(2)	C(76)-C(77)	140.9(3)
C(81)-Cl(1) 172.5(5) C(82A)-Cl(4A) 168.3(7) C(82A)-Cl(3A) 170.5(7) C(82B)-Cl(4B) 169.3(16)	C(77)-C(78)	136.7(3)	C(78)-C(79)	141.0(4)
C(82A)-Cl(3A) 170.5(7) C(82B)-Cl(4B) 169.3(16)	C(79)-C(80)	134.4(4)	C(81)-Cl(2)	170.6(5)
	C(81)-Cl(1)	172.5(5)	C(82A)-Cl(4A)	168.3(7)
C(82B)-Cl(3B) 173.8(17)	C(82A)-Cl(3A)	170.5(7)	C(82B)-Cl(4B)	169.3(16)
	C(82B)-Cl(3B)	173.8(17)		

Symmetry transformations used to generate equivalent atoms:

#1 - x + 2, -y + 1, -z #2 - x + 1, -y + 1, -z + 1

Table S 14: Bond angles [°] for 1-Naph_POSS_KOH

Bond	Angle [°]	Bond	Angle [°]
O(1)-Si(1)-O(5)	109.33(7)	O(1)-Si(1)-O(4)	109.42(7)
O(5)-Si(1)-O(4)	108.83(7)	O(1)-Si(1)-C(1)	107.77(7)
O(5)-Si(1)-C(1)	111.38(7)	O(4)-Si(1)-C(1)	110.10(7)
O(6)-Si(2)-O(2)	108.66(7)	O(6)-Si(2)-O(1)	109.05(7)
O(2)-Si(2)-O(1)	108.60(7)	O(6)-Si(2)-C(11)	108.71(7)
O(2)-Si(2)-C(11)	109.88(7)	O(1)-Si(2)-C(11)	111.88(7)
O(3)-Si(3)-O(2)	107.75(7)	O(3)-Si(3)-O(5)#1	109.19(7)
O(2)-Si(3)-O(5)#1	109.36(7)	O(3)-Si(3)-C(21)	110.64(7)
O(2)-Si(3)-C(21)	111.05(7)	O(5)#1-Si(3)-C(21)	108.82(7)
O(3)-Si(4)-O(6)#1	109.07(7)	O(3)-Si(4)-O(4)	109.07(7)
O(6)#1-Si(4)-O(4)	108.27(7)	O(3)-Si(4)-C(31)	108.05(7)
O(6)#1-Si(4)-C(31)	110.46(6)	O(4)-Si(4)-C(31)	111.89(7)
O(10)-Si(5)-O(11)	109.57(6)	O(10)-Si(5)-O(7)	109.50(7)
O(11)-Si(5)-O(7)	106.94(6)	O(10)-Si(5)-C(41)	107.59(7)
O(11)-Si(5)-C(41)	112.46(7)	O(7)-Si(5)-C(41)	110.76(7)
O(7)-Si(6)-O(12)	109.59(6)	O(7)-Si(6)-O(8)	108.85(6)
O(12)-Si(6)-O(8)	108.98(6)	O(7)-Si(6)-C(51)	110.32(7)
O(12)-Si(6)-C(51)	109.21(7)	O(8)-Si(6)-C(51)	109.87(7)
O(9)-Si(7)-O(8)	108.90(6)	O(9)-Si(7)-O(11)#2	109.04(6)
O(8)-Si(7)-O(11)#2	109.06(6)	O(9)-Si(7)-C(61)	109.29(6)
O(8)-Si(7)-C(61)	112.85(7)	O(11)#2-Si(7)-C(61)	107.63(7)
O(10)-Si(8)-O(9)	107.17(6)	O(10)-Si(8)-O(12)#2	109.08(6)
O(9)-Si(8)-O(12)#2	108.92(6)	O(10)-Si(8)-C(71)	110.77(7)
O(9)-Si(8)-C(71)	111.79(7)	O(12)#2-Si(8)-C(71)	109.05(7)
Si(1)-O(1)-Si(2)	152.67(8)	Si(2)-O(2)-Si(3)	147.77(8)
Si(4)-O(3)-Si(3)	153.82(8)	Si(1)-O(4)-Si(4)	146.61(8)
Si(1)-O(5)-Si(3)#1	147.53(8)	Si(2)-O(6)-Si(4)#1	148.76(8)
Si(6)-O(7)-Si(5)	152.47(8)	Si(7)-O(8)-Si(6)	149.04(8)
Si(7)-O(9)-Si(8)	153.38(8)	Si(5)-O(10)-Si(8)	150.29(8)
Si(5)-O(11)-Si(7)#2	146.05(8)	Si(6)-O(12)-Si(8)#2	145.01(7)
C(2)-C(1)-C(6)	118.30(16)	C(2)-C(1)-Si(1)	118.44(13)
C(6)-C(1)-Si(1)	123.22(12)	C(1)-C(2)-C(3)	122.03(18)
C(4)-C(3)-C(2)	119.83(19)	C(3)-C(4)-C(5)	121.17(18)
C(4)-C(5)-C(10)	121.57(18)	C(4)-C(5)-C(6)	119.07(17)
C(10)-C(5)-C(6)	119.35(18)	C(7)-C(6)-C(5)	117.92(16)
C(7)-C(6)-C(1)	122.51(15)	C(5)-C(6)-C(1)	119.57(16)
C(8)-C(7)-C(6)	121.10(18)	C(7)-C(8)-C(9)	120.4(2)

C(10)-C(9)-C(8)	120.19(19)	C(9)-C(10)-C(5)	121.04(19)
C(12)-C(11)-C(16)	118.97(15)	C(12)-C(11)-Si(2)	116.71(13)
C(16)-C(11)-Si(2)	124.29(13)	C(11)-C(12)-C(13)	121.58(18)
C(14)-C(13)-C(12)	120.0(2)	C(13)-C(14)-C(15)	121.56(18)
C(14)-C(15)-C(20)	122.1(2)	C(14)-C(15)-C(16)	119.18(18)
C(20)-C(15)-C(16)	118.7(2)	C(17)-C(16)-C(15)	118.41(18)
C(17)-C(16)-C(11)	122.88(16)	C(15)-C(16)-C(11)	118.70(18)
C(18)-C(17)-C(16)	120.7(2)	C(17)-C(18)-C(19)	120.4(2)
C(20)-C(19)-C(18)	120.5(2)	C(19)-C(20)-C(15)	121.3(2)
C(22)-C(21)-C(26)	118.88(16)	C(22)-C(21)-Si(3)	118.43(14)
C(26)-C(21)-Si(3)	122.69(14)	C(21)-C(22)-C(23)	121.6(2)
C(24)-C(23)-C(22)	119.9(2)	C(23)-C(24)-C(25)	121.6(2)
C(24)-C(25)-C(30)	122.0(2)	C(24)-C(25)-C(26)	118.9(2)
C(30)-C(25)-C(26)	119.1(2)	C(27)-C(26)-C(25)	117.91(18)
C(27)-C(26)-C(21)	123.04(16)	C(25)-C(26)-C(21)	119.04(19)
C(28)-C(27)-C(26)	121.4(2)	C(27)-C(28)-C(29)	120.1(3)
C(30)-C(29)-C(28)	120.2(2)	C(29)-C(30)-C(25)	121.2(2)
C(32)-C(31)-C(36)	118.76(14)	C(32)-C(31)-Si(4)	118.37(12)
C(36)-C(31)-Si(4)	122.86(12)	C(31)-C(32)-C(33)	121.53(15)
C(34)-C(33)-C(32)	120.10(16)	C(33)-C(34)-C(35)	121.08(15)
C(34)-C(35)-C(40)	121.42(15)	C(34)-C(35)-C(36)	119.25(15)
C(40)-C(35)-C(36)	119.33(16)	C(37)-C(36)-C(35)	117.92(15)
C(37)-C(36)-C(31)	122.80(14)	C(35)-C(36)-C(31)	119.28(15)
C(38)-C(37)-C(36)	121.24(17)	C(37)-C(38)-C(39)	120.24(19)
C(40)-C(39)-C(38)	120.08(17)	C(39)-C(40)-C(35)	121.19(17)
C(42)-C(41)-C(46)	118.43(15)	C(42)-C(41)-Si(5)	119.19(12)
C(46)-C(41)-Si(5)	122.37(12)	C(41)-C(42)-C(43)	121.63(16)
C(44)-C(43)-C(42)	120.28(17)	C(43)-C(44)-C(45)	120.83(16)
C(50)-C(45)-C(44)	121.70(16)	C(50)-C(45)-C(46)	119.27(17)
C(44)-C(45)-C(46)	119.02(16)	C(47)-C(46)-C(45)	117.95(15)
C(47)-C(46)-C(41)	122.29(14)	C(45)-C(46)-C(41)	119.76(15)
C(48)-C(47)-C(46)	121.24(16)	C(47)-C(48)-C(49)	120.35(19)
C(50)-C(49)-C(48)	119.99(18)	C(49)-C(50)-C(45)	121.12(17)
C(52)-C(51)-C(56)	118.54(16)	C(52)-C(51)-Si(6)	118.48(14)
C(56)-C(51)-Si(6)	122.94(13)	C(51)-C(52)-C(53)	121.7(2)
C(54)-C(53)-C(52)	120.2(2)	C(53)-C(54)-C(55)	121.28(19)
C(54)-C(55)-C(60)	121.8(2)	C(54)-C(55)-C(56)	118.9(2)
C(60)-C(55)-C(56)	119.3(2)	C(57)-C(56)-C(55)	117.65(18)
C(57)-C(56)-C(51)	123.01(16)	C(55)-C(56)-C(51)	119.34(18)

C(58)-C(57)-C(56)	121.21(19)	C(57)-C(58)-C(59)	120.5(2)
C(60)-C(59)-C(58)	120.1(2)	C(59)-C(60)-C(55)	121.3(2)
C(62A)-C(61)-C(66A)	120.0(8)	C(62B)-C(61)-C(66B)	116.7(8)
C(62A)-C(61)-Si(7)	114.1(6)	C(62B)-C(61)-Si(7)	119.8(6)
C(66A)-C(61)-Si(7)	125.6(5)	C(66B)-C(61)-Si(7)	123.5(5)
C(61)-C(62A)-C(63A)	119.1(11)	C(64A)-C(63A)-C(62A)	121.9(11)
C(63A)-C(64A)-C(65A)	120.6(8)	C(64A)-C(65A)-C(70A)	123.4(8)
C(64A)-C(65A)-C(66A)	117.8(8)	C(70A)-C(65A)-C(66A)	118.7(7)
C(67A)-C(66A)-C(61)	121.8(9)	C(67A)-C(66A)-C(65A)	117.6(9)
C(61)-C(66A)-C(65A)	120.1(8)	C(68A)-C(67A)-C(66A)	122.2(10)
C(67A)-C(68A)-C(69A)	119.5(9)	C(70A)-C(69A)-C(68A)	120.1(7)
C(69A)-C(70A)-C(65A)	121.7(6)	C(61)-C(62B)-C(63B)	125.1(11)
C(64B)-C(63B)-C(62B)	118.0(11)	C(63B)-C(64B)-C(65B)	121.4(8)
C(70B)-C(65B)-C(64B)	119.4(7)	C(70B)-C(65B)-C(66B)	119.9(7)
C(64B)-C(65B)-C(66B)	120.6(7)	C(67B)-C(66B)-C(65B)	116.6(8)
C(67B)-C(66B)-C(61)	124.6(9)	C(65B)-C(66B)-C(61)	118.0(8)
C(68B)-C(67B)-C(66B)	121.2(10)	C(67B)-C(68B)-C(69B)	121.1(9)
C(70B)-C(69B)-C(68B)	120.4(6)	C(69B)-C(70B)-C(65B)	120.6(6)
C(72)-C(71)-C(76)	118.44(15)	C(72)-C(71)-Si(8)	118.27(13)
C(76)-C(71)-Si(8)	123.26(12)	C(71)-C(72)-C(73)	122.07(18)
C(74)-C(73)-C(72)	119.99(19)	C(73)-C(74)-C(75)	120.96(17)
C(74)-C(75)-C(80)	121.64(19)	C(74)-C(75)-C(76)	119.50(18)
C(80)-C(75)-C(76)	118.9(2)	C(77)-C(76)-C(75)	117.99(17)
C(77)-C(76)-C(71)	123.01(16)	C(75)-C(76)-C(71)	118.98(17)
C(78)-C(77)-C(76)	121.2(2)	C(77)-C(78)-C(79)	120.4(2)
C(80)-C(79)-C(78)	120.0(2)	C(79)-C(80)-C(75)	121.5(2)
Cl(2)-C(81)-Cl(1)	114.7(2)	Cl(4A)-C(82A)-Cl(3A)	117.3(4)
Cl(4B)-C(82B)-Cl(3B)	111.8(12)		

Symmetry transformations used to generate equivalent atoms:

#1-x+2,-y+1,-z #2-x+1,-y+1,-z+1

Table S 15: Hydrogen coordinates (\times 10⁴) and isotropic displacement parameters ($\mathring{A}^2 \times$ 10³) for 1-Naph_POSS_KOH.

	Х	У	Z	$U_{ m eq}$
H(2)	6666	4250	-1218	44
H(3)	4985	3569	-1594	61
H(4)	4041	2369	-1232	57
H(7)	7226	2516	123	41

H(8)	6252	1330	490	53
H(9)	4571	729	161	57
H(10)	3882	1294	-548	53
H(12)	9712	5950	-2180	40
H(13)	9214	6548	-2996	53
H(14)	8002	7069	-2806	58
H(17)	7765	6226	-397	53
H(18)	6535	6749	-240	70
H(19)	6058	7334	-1078	77
H(20)	6795	7385	-2064	70
H(22)	12356	8742	1651	50
H(23)	12932	10523	2434	71
H(24)	11891	11285	2653	72
H(27)	9040	7626	878	52
H(28)	8027	8438	1064	68
H(29)	8637	10227	1845	79
H(30)	10249	11182	2410	75
H(32)	9476	7266	2483	31
H(33)	9054	7838	3684	36
H(34)	8326	6700	4167	37
H(37)	8410	3720	1616	41
H(38)	7657	2599	2115	52
H(39)	7278	3214	3334	52
H(40)	7652	4933	4035	44
H(42)	3927	6155	3125	36
H(43)	3049	6725	2521	45
H(44)	1663	6811	2861	45
H(47)	2304	5643	4997	38
H(48)	893	5701	5309	50
H(49)	-58	6104	4603	56
H(50)	463	6552	3648	51
H(52)	4912	7683	7601	53
H(53)	5040	9275	8537	76
H(54)	5391	10630	8249	75
H(57)	5322	8166	5377	44
H(58)	5644	9547	5108	62
H(59)	5863	11156	6087	77
H(60)	5724	11358	7313	75
H(62A)	8545	6379	5804	32

H(63A)	10177	7366	5947	41	
H(64A)	10686	8902	5893	49	
H(67A)	7064	8357	5526	52	
H(68A)	7559	9941	5518	66	
H(69A)	9188	10877	5603	76	
H(70A)	10296	10274	5767	67	
H(62B)	8648	6430	5740	31	
H(63B)	10276	7519	6055	41	
H(64B)	10719	9157	6175	49	
H(67B)	7032	8422	5560	46	
H(68B)	7579	10118	5803	62	
H(69B)	9214	11148	6073	71	
H(70B)	10324	10525	6193	68	
H(72)	5552	3751	2235	40	
H(73)	6052	3806	1121	54	
H(74)	6784	5350	1088	54	
H(77)	6267	7173	3908	53	
H(78)	7034	8710	3858	75	
H(79)	7627	8741	2764	75	
H(80)	7412	7244	1730	62	
H(81A)	7298	2132	4286	134	
H(81B)	6354	1074	3856	134	
H(82A)	9529	11324	74	114	
H(82B)	9646	11049	776	114	
H(82C)	8691	9524	-63	137	
H(82D)	8646	9949	-688	137	

Table S 16: Torsion angles [°] for 1-Naph_POSS_KOH.

Bond	Angle [°]	Bond	Angle [°]
O(5)-Si(1)-O(1)-Si(2)	-57.2(2)	O(4)-Si(1)-O(1)-Si(2)	61.9(2)
C(1)-Si(1)-O(1)-Si(2)	-178.40(18)	O(6)-Si(2)-O(1)-Si(1)	56.4(2)
O(2)-Si(2)-O(1)-Si(1)	-61.8(2)	C(11)-Si(2)-O(1)-Si(1)	176.71(18)
O(6)-Si(2)-O(2)-Si(3)	-61.94(18)	O(1)-Si(2)-O(2)-Si(3)	56.56(18)
C(11)-Si(2)-O(2)-Si(3)	179.23(15)	O(3)-Si(3)-O(2)-Si(2)	-56.20(18)
O(5)#1-Si(3)-O(2)-Si(2)	62.37(18)	C(21)-Si(3)-O(2)-Si(2)	-177.52(15)
O(6)#1-Si(4)-O(3)-Si(3)	54.9(2)	O(4)-Si(4)-O(3)-Si(3)	-63.2(2)
C(31)-Si(4)-O(3)-Si(3)	174.97(19)	O(2)-Si(3)-O(3)-Si(4)	63.2(2)
O(5)#1-Si(3)-O(3)-Si(4)	-55.5(2)	C(21)-Si(3)-O(3)-Si(4)	-175.21(19)
O(1)-Si(1)-O(4)-Si(4)	-53.78(17)	O(5)-Si(1)-O(4)-Si(4)	65.63(17)
		282	

C(1)-Si(1)-O(4)-Si(4)	-172.04(15)	O(3)-Si(4)-O(4)-Si(1)	53.39(17)
O(6)#1-Si(4)-O(4)-Si(1)	-65.17(17)	C(31)-Si(4)-O(4)-Si(1)	172.87(14)
O(1)-Si(1)-O(5)-Si(3)#1	57.42(17)	O(4)-Si(1)-O(5)-Si(3)#1	-62.04(17)
C(1)-Si(1)-O(5)-Si(3)#1	176.40(15)	O(2)-Si(2)-O(6)-Si(4)#1	61.99(19)
O(1)-Si(2)-O(6)-Si(4)#1	-56.23(19)	C(11)-Si(2)-O(6)-Si(4)#1	-178.45(16)
O(12)-Si(6)-O(7)-Si(5)	-73.43(19)	O(8)-Si(6)-O(7)-Si(5)	45.7(2)
C(51)-Si(6)-O(7)-Si(5)	166.29(17)	O(10)-Si(5)-O(7)-Si(6)	-45.4(2)
O(11)-Si(5)-O(7)-Si(6)	73.28(19)	C(41)-Si(5)-O(7)-Si(6)	-163.86(17)
O(9)-Si(7)-O(8)-Si(6)	62.87(17)	O(11)#2-Si(7)-O(8)-Si(6)	-56.02(17)
C(61)-Si(7)-O(8)-Si(6)	-175.58(15)	O(7)-Si(6)-O(8)-Si(7)	-62.43(17)
O(12)-Si(6)-O(8)-Si(7)	57.05(17)	C(51)-Si(6)-O(8)-Si(7)	176.67(15)
O(8)-Si(7)-O(9)-Si(8)	-49.9(2)	O(11)#2-Si(7)-O(9)-Si(8)	68.97(19)
C(61)-Si(7)-O(9)-Si(8)	-173.61(17)	O(10)-Si(8)-O(9)-Si(7)	49.4(2)
O(12)#2-Si(8)-O(9)-Si(7)	-68.46(19)	C(71)-Si(8)-O(9)-Si(7)	170.96(17)
O(11)-Si(5)-O(10)-Si(8)	-53.29(19)	O(7)-Si(5)-O(10)-Si(8)	63.71(19)
C(41)-Si(5)-O(10)-Si(8)	-175.84(17)	O(9)-Si(8)-O(10)-Si(5)	-63.90(19)
O(12)#2-Si(8)-O(10)-Si(5)	53.87(19)	C(71)-Si(8)-O(10)-Si(5)	173.91(17)
O(10)-Si(5)-O(11)-Si(7)#2	65.91(15)	O(7)-Si(5)-O(11)-Si(7)#2	-52.68(15)
C(41)-Si(5)-O(11)-Si(7)#2	-174.48(13)	O(7)-Si(6)-O(12)-Si(8)#2	49.76(15)
O(8)-Si(6)-O(12)-Si(8)#2	-69.26(15)	C(51)-Si(6)-O(12)-Si(8)#2	170.72(13)
O(1)-Si(1)-C(1)-C(2)	-1.60(16)	O(5)-Si(1)-C(1)-C(2)	-121.50(14)
O(4)-Si(1)-C(1)-C(2)	117.68(14)	O(1)-Si(1)-C(1)-C(6)	-179.35(13)
O(5)-Si(1)-C(1)-C(6)	60.74(15)	O(4)-Si(1)-C(1)-C(6)	-60.07(15)
C(6)-C(1)-C(2)-C(3)	-0.5(3)	Si(1)-C(1)-C(2)-C(3)	-178.33(17)
C(1)-C(2)-C(3)-C(4)	1.2(4)	C(2)-C(3)-C(4)-C(5)	-0.4(4)
C(3)-C(4)-C(5)-C(10)	179.1(2)	C(3)-C(4)-C(5)-C(6)	-1.0(3)
C(4)-C(5)-C(6)-C(7)	-178.53(18)	C(10)-C(5)-C(6)-C(7)	1.3(2)
C(4)-C(5)-C(6)-C(1)	1.7(3)	C(10)-C(5)-C(6)-C(1)	-178.38(16)
C(2)-C(1)-C(6)-C(7)	179.29(17)	Si(1)-C(1)-C(6)-C(7)	-3.0(2)
C(2)-C(1)-C(6)-C(5)	-1.0(2)	Si(1)-C(1)-C(6)-C(5)	176.76(12)
C(5)-C(6)-C(7)-C(8)	-1.4(3)	C(1)-C(6)-C(7)-C(8)	178.34(17)
C(6)-C(7)-C(8)-C(9)	0.4(3)	C(7)-C(8)-C(9)-C(10)	0.7(3)
C(8)-C(9)-C(10)-C(5)	-0.7(3)	C(4)-C(5)-C(10)-C(9)	179.5(2)
C(6)-C(5)-C(10)-C(9)	-0.3(3)	O(6)-Si(2)-C(11)-C(12)	-12.38(16)
O(2)-Si(2)-C(11)-C(12)	106.42(14)	O(1)-Si(2)-C(11)-C(12)	-132.87(13)
O(6)-Si(2)-C(11)-C(16)	169.39(14)	O(2)-Si(2)-C(11)-C(16)	-71.82(16)
O(1)-Si(2)-C(11)-C(16)	48.90(16)	C(16)-C(11)-C(12)-C(13)	0.0(3)
Si(2)-C(11)-C(12)-C(13)	-178.35(15)	C(11)-C(12)-C(13)-C(14)	-0.4(3)
C(12)-C(13)-C(14)-C(15)	0.5(3)	C(13)-C(14)-C(15)-C(20)	-179.9(2)

C(13)-C(14)-C(15)-C(16)	-0.2(3)	C(14)-C(15)-C(16)-C(17)	-179.60(19)
C(20)-C(15)-C(16)-C(17)	0.1(3)	C(14)-C(15)-C(16)-C(11)	-0.2(3)
C(20)-C(15)-C(16)-C(11)	179.45(18)	C(12)-C(11)-C(16)-C(17)	179.68(18)
Si(2)-C(11)-C(16)-C(17)	-2.1(3)	C(12)-C(11)-C(16)-C(15)	0.3(2)
Si(2)-C(11)-C(16)-C(15)	178.53(13)	C(15)-C(16)-C(17)-C(18)	0.4(3)
C(11)-C(16)-C(17)-C(18)	-179.0(2)	C(16)-C(17)-C(18)-C(19)	-0.5(4)
C(17)-C(18)-C(19)-C(20)	0.2(4)	C(18)-C(19)-C(20)-C(15)	0.2(4)
C(14)-C(15)-C(20)-C(19)	179.3(2)	C(16)-C(15)-C(20)-C(19)	-0.4(3)
O(3)-Si(3)-C(21)-C(22)	112.37(15)	O(2)-Si(3)-C(21)-C(22)	-128.02(15)
O(5)#1-Si(3)-C(21)-C(22)	-7.59(17)	O(3)-Si(3)-C(21)-C(26)	-66.86(15)
O(2)-Si(3)-C(21)-C(26)	52.75(15)	O(5)#1-Si(3)-C(21)-C(26)	173.18(13)
C(26)-C(21)-C(22)-C(23)	0.5(3)	Si(3)-C(21)-C(22)-C(23)	-178.80(19)
C(21)-C(22)-C(23)-C(24)	-0.1(4)	C(22)-C(23)-C(24)-C(25)	-0.9(4)
C(23)-C(24)-C(25)-C(30)	-178.0(3)	C(23)-C(24)-C(25)-C(26)	1.5(4)
C(24)-C(25)-C(26)-C(27)	180.0(2)	C(30)-C(25)-C(26)-C(27)	-0.5(3)
C(24)-C(25)-C(26)-C(21)	-1.1(3)	C(30)-C(25)-C(26)-C(21)	178.42(19)
C(22)-C(21)-C(26)-C(27)	179.04(18)	Si(3)-C(21)-C(26)-C(27)	-1.7(2)
C(22)-C(21)-C(26)-C(25)	0.2(3)	Si(3)-C(21)-C(26)-C(25)	179.39(14)
C(25)-C(26)-C(27)-C(28)	0.9(3)	C(21)-C(26)-C(27)-C(28)	-178.0(2)
C(26)-C(27)-C(28)-C(29)	-0.9(4)	C(27)-C(28)-C(29)-C(30)	0.5(4)
C(28)-C(29)-C(30)-C(25)	-0.1(4)	C(24)-C(25)-C(30)-C(29)	179.6(3)
C(26)-C(25)-C(30)-C(29)	0.1(4)	O(3)-Si(4)-C(31)-C(32)	4.20(14)
O(6)#1-Si(4)-C(31)-C(32)	123.43(13)	O(4)-Si(4)-C(31)-C(32)	-115.88(13)
O(3)-Si(4)-C(31)-C(36)	-174.40(12)	O(6)#1-Si(4)-C(31)-C(36)	-55.17(14)
O(4)-Si(4)-C(31)-C(36)	65.52(14)	C(36)-C(31)-C(32)-C(33)	0.0(2)
Si(4)-C(31)-C(32)-C(33)	-178.68(12)	C(31)-C(32)-C(33)-C(34)	0.7(2)
C(32)-C(33)-C(34)-C(35)	-0.7(3)	C(33)-C(34)-C(35)-C(40)	-179.69(16)
C(33)-C(34)-C(35)-C(36)	0.0(2)	C(34)-C(35)-C(36)-C(37)	-179.15(15)
C(40)-C(35)-C(36)-C(37)	0.6(2)	C(34)-C(35)-C(36)-C(31)	0.6(2)
C(40)-C(35)-C(36)-C(31)	-179.64(15)	C(32)-C(31)-C(36)-C(37)	179.14(16)
Si(4)-C(31)-C(36)-C(37)	-2.3(2)	C(32)-C(31)-C(36)-C(35)	-0.6(2)
Si(4)-C(31)-C(36)-C(35)	177.96(11)	C(35)-C(36)-C(37)-C(38)	-0.3(3)
C(31)-C(36)-C(37)-C(38)	179.96(18)	C(36)-C(37)-C(38)-C(39)	-0.1(3)
C(37)-C(38)-C(39)-C(40)	0.2(3)	C(38)-C(39)-C(40)-C(35)	0.2(3)
C(34)-C(35)-C(40)-C(39)	179.19(18)	C(36)-C(35)-C(40)-C(39)	-0.5(3)
O(10)-Si(5)-C(41)-C(42)	-4.00(15)	O(11)-Si(5)-C(41)-C(42)	-124.75(13)
O(7)-Si(5)-C(41)-C(42)	115.66(13)	O(10)-Si(5)-C(41)-C(46)	174.72(12)
O(11)-Si(5)-C(41)-C(46)	53.97(15)	O(7)-Si(5)-C(41)-C(46)	-65.63(14)
C(46)-C(41)-C(42)-C(43)	0.7(3)	Si(5)-C(41)-C(42)-C(43)	179.46(14)

C(41)-C(42)-C(43)-C(44)	-1.9(3)	C(42)-C(43)-C(44)-C(45) 0.9(3)
C(43)-C(44)-C(45)-C(50)	-177.77(19)	C(43)-C(44)-C(45)-C(46) 1.2(3)
C(50)-C(45)-C(46)-C(47)	-2.8(2)	C(44)-C(45)-C(46)-C(47) 178.11(17)
C(50)-C(45)-C(46)-C(41)	176.61(16)	C(44)-C(45)-C(46)-C(41) -2.4(2)
C(42)-C(41)-C(46)-C(47)	-179.10(16)	Si(5)-C(41)-C(46)-C(47) 2.2(2)
C(42)-C(41)-C(46)-C(45)	1.5(2)	Si(5)-C(41)-C(46)-C(45) -177.25(12)
C(45)-C(46)-C(47)-C(48)	2.4(3)	C(41)-C(46)-C(47)-C(48) -177.02(18)
C(46)-C(47)-C(48)-C(49)	0.1(3)	C(47)-C(48)-C(49)-C(50) -2.4(3)
C(48)-C(49)-C(50)-C(45)	1.9(3)	C(44)-C(45)-C(50)-C(49) 179.8(2)
C(46)-C(45)-C(50)-C(49)	0.7(3)	O(7)-Si(6)-C(51)-C(52) 127.90(16)
O(12)-Si(6)-C(51)-C(52)	7.38(17)	O(8)-Si(6)-C(51)-C(52) -112.10(16)
O(7)-Si(6)-C(51)-C(56)	-54.59(16)	O(12)-Si(6)-C(51)-C(56) -175.11(13)
O(8)-Si(6)-C(51)-C(56)	65.42(15)	C(56)-C(51)-C(52)-C(53) -0.8(3)
Si(6)-C(51)-C(52)-C(53)	176.8(2)	C(51)-C(52)-C(53)-C(54) -1.0(4)
C(52)-C(53)-C(54)-C(55)	1.4(5)	C(53)-C(54)-C(55)-C(60) 180.0(3)
C(53)-C(54)-C(55)-C(56)	0.2(4)	C(54)-C(55)-C(56)-C(57) 177.7(2)
C(60)-C(55)-C(56)-C(57)	-2.1(3)	C(54)-C(55)-C(56)-C(51) -2.0(3)
C(60)-C(55)-C(56)-C(51)	178.1(2)	C(52)-C(51)-C(56)-C(57) -177.38(18)
Si(6)-C(51)-C(56)-C(57)	5.1(2)	C(52)-C(51)-C(56)-C(55) 2.3(3)
Si(6)-C(51)-C(56)-C(55)	-175.17(14)	C(55)-C(56)-C(57)-C(58) 1.4(3)
C(51)-C(56)-C(57)-C(58)	-178.83(19)	C(56)-C(57)-C(58)-C(59) 0.1(3)
C(57)-C(58)-C(59)-C(60)	-0.9(4)	C(58)-C(59)-C(60)-C(55) 0.2(4)
C(54)-C(55)-C(60)-C(59)	-178.5(3)	C(56)-C(55)-C(60)-C(59) 1.3(4)
O(9)-Si(7)-C(61)-C(62A)	-98.4(4)	O(8)-Si(7)-C(61)-C(62A) 140.3(4)
O(11)#2-Si(7)-C(61)-C(62A)	19.9(4)	O(9)-Si(7)-C(61)-C(62B) -97.5(4)
O(8)-Si(7)-C(61)-C(62B)	141.2(4)	O(11)#2-Si(7)-C(61)-C(62B) 20.8(4)
O(9)-Si(7)-C(61)-C(66A)	76.2(15)	O(8)-Si(7)-C(61)-C(66A) -45.2(15)
O(11)#2-Si(7)-C(61)-C(66A)	-165.5(15)	O(9)-Si(7)-C(61)-C(66B) 78.6(14)
O(8)-Si(7)-C(61)-C(66B)	-42.8(14)	O(11)#2-Si(7)-C(61)-C(66B) -163.1(14)
C(66A)-C(61)-C(62A)-C(63A)	-3.7(14)	Si(7)-C(61)-C(62A)-C(63A) 171.1(4)
C(61)-C(62A)-C(63A)-C(64A)	-0.5(8)	C(62A)-C(63A)-C(64A)-C(65A) 0.9(12)
C(63A)-C(64A)-C(65A)-C(70A)	179.1(8)	C(63A)-C(64A)-C(65A)-C(66A) 2.9(17)
C(62A)-C(61)-C(66A)-C(67A)	179.3(17)	Si(7)-C(61)-C(66A)-C(67A) 5(3)
C(62A)-C(61)-C(66A)-C(65A)	8(3)	Si(7)-C(61)-C(66A)-C(65A) -166.7(12)
C(64A)-C(65A)-C(66A)-C(67A)	-179.1(16)	C(70A)-C(65A)-C(66A)-C(67A) 4(3)
C(64A)-C(65A)-C(66A)-C(61)	-7(3)	C(70A)-C(65A)-C(66A)-C(61) 176.5(15)
C(61)-C(66A)-C(67A)-C(68A)	-176.5(18)	C(65A)-C(66A)-C(67A)-C(68A) -5(3)
C(66A)-C(67A)-C(68A)-C(69A)	3(2)	C(67A)-C(68A)-C(69A)-C(70A) -1.3(13)
C(68A)-C(69A)-C(70A)-C(65A)	1.3(11)	C(64A)-C(65A)-C(70A)-C(69A) -179.2(7)

C(66A)-C(65A)-C(70A)-C(69A)	-3.0(16)	C(66B)-C(61)-C(62B)-C(63B) 3.3(13)
Si(7)-C(61)-C(62B)-C(63B)	179.7(4)	C(61)-C(62B)-C(63B)-C(64B) -0.7(8)
C(62B)-C(63B)-C(64B)-C(65B)	0.1(12)	C(63B)-C(64B)-C(65B)-C(70B) 176.5(9)
C(63B)-C(64B)-C(65B)-C(66B)	-2.4(17)	C(70B)-C(65B)-C(66B)-C(67B) -3(3)
C(64B)-C(65B)-C(66B)-C(67B)	175.5(15)	C(70B)-C(65B)-C(66B)-C(61) -173.9(14)
C(64B)-C(65B)-C(66B)-C(61)	5(3)	C(62B)-C(61)-C(66B)-C(67B) -175.0(18)
Si(7)-C(61)-C(66B)-C(67B)	9(3)	C(62B)-C(61)-C(66B)-C(65B) -5(3)
Si(7)-C(61)-C(66B)-C(65B)	178.5(12)	C(65B)-C(66B)-C(67B)-C(68B) 2(3)
C(61)-C(66B)-C(67B)-C(68B)	171.8(19)	C(66B)-C(67B)-C(68B)-C(69B) 1(2)
C(67B)-C(68B)-C(69B)-C(70B)	-2.6(13)	C(68B)-C(69B)-C(70B)-C(65B) 1.2(11)
C(64B)-C(65B)-C(70B)-C(69B)	-177.0(7)	C(66B)-C(65B)-C(70B)-C(69B) 1.9(17)
O(10)-Si(8)-C(71)-C(72)	-115.14(14)	O(9)-Si(8)-C(71)-C(72) 125.41(13)
O(12)#2-Si(8)-C(71)-C(72)	4.91(15)	O(10)-Si(8)-C(71)-C(76) 66.98(15)
O(9)-Si(8)-C(71)-C(76)	-52.48(15)	O(12)#2-Si(8)-C(71)-C(76) -172.97(13)
C(76)-C(71)-C(72)-C(73)	0.0(3)	Si(8)-C(71)-C(72)-C(73) -177.94(15)
C(71)-C(72)-C(73)-C(74)	1.4(3)	C(72)-C(73)-C(74)-C(75) -0.9(3)
C(73)-C(74)-C(75)-C(80)	177.8(2)	C(73)-C(74)-C(75)-C(76) -1.1(3)
C(74)-C(75)-C(76)-C(77)	-179.02(18)	C(80)-C(75)-C(76)-C(77) 2.0(3)
C(74)-C(75)-C(76)-C(71)	2.5(2)	C(80)-C(75)-C(76)-C(71) -176.45(16)
C(72)-C(71)-C(76)-C(77)	179.64(18)	Si(8)-C(71)-C(76)-C(77) -2.5(2)
C(72)-C(71)-C(76)-C(75)	-2.0(2)	Si(8)-C(71)-C(76)-C(75) 175.89(12)
C(75)-C(76)-C(77)-C(78)	-1.5(3)	C(71)-C(76)-C(77)-C(78) 176.9(2)
C(76)-C(77)-C(78)-C(79)	0.0(4)	C(77)-C(78)-C(79)-C(80) 1.0(4)
C(78)-C(79)-C(80)-C(75)	-0.4(4)	C(74)-C(75)-C(80)-C(79) 180.0(2)
C(76)-C(75)-C(80)-C(79)	-1.1(3)	

Symmetry transformations used to generate equivalent atoms:

#1 -x+2,-y+1,-z #2 -x+1,-y+1,-z+1

6.3.2.3 Further Purification and Separation Attempts

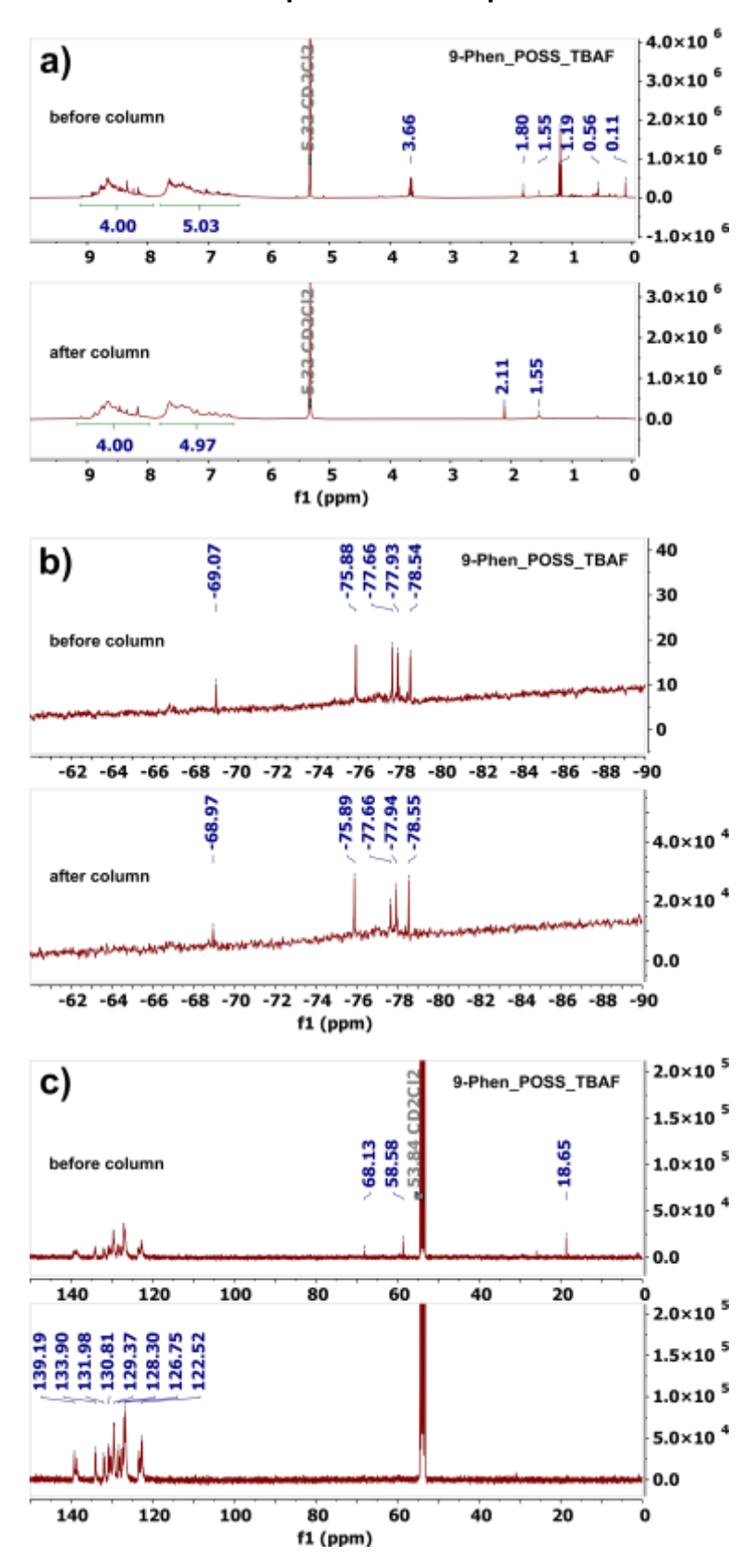


Figure S 144: NMR characterization of 9-Phen_POSS_TBAF (CD_2Cl_2) before and after column chromatography. a) ¹H NMR, b) ²⁹Si NMR, c) ¹³C NMR.

6.3.2.4 Fluorescence Spectroscopy

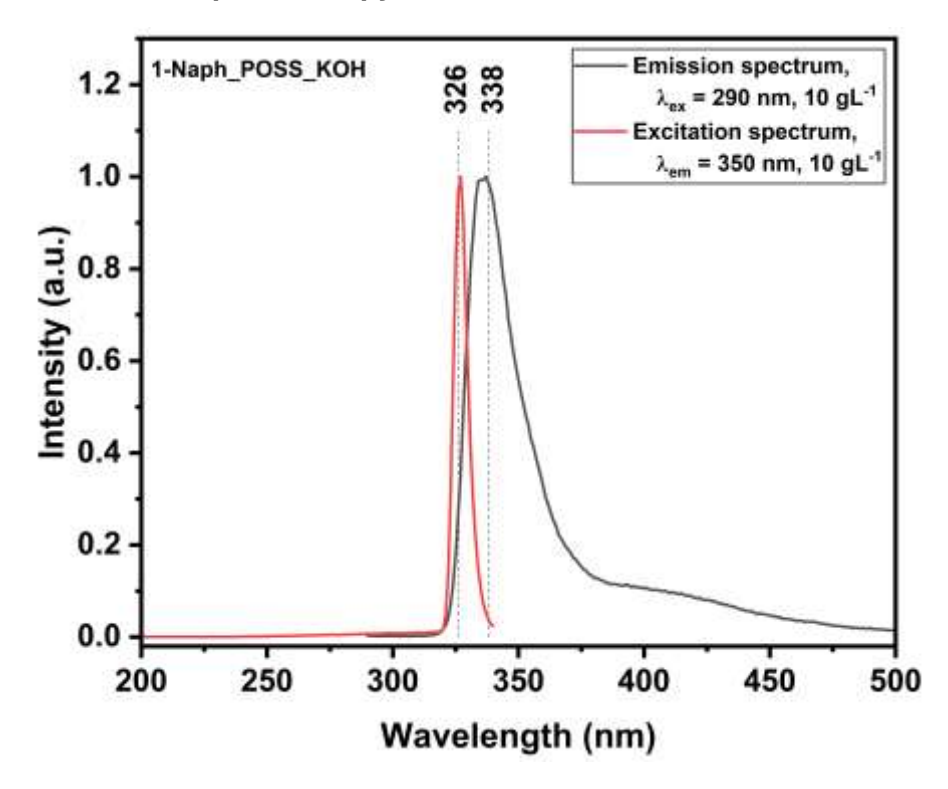


Figure S 145: Emission and excitation spectra of a solution of 1-Naph_POSS_KOH in DCM.